

4

AD-A208 564

DTIC
ELECTE
MAY 24 1989
D

Technical Document 1532
April 1989

DARPA Review on EHF Devices

Defense Advanced
Research Projects Agency
Joint Contractor Review

Held at Naval Ocean Systems Center
San Diego, California 92152-5000 on
24-25 January 1989



Approved for public release; distribution is unlimited.

The views and conclusions contained in this report are those of the contractors and should not be interpreted as representing the official policies, either expressed or implied, of the Naval Ocean Systems Center or the U.S. Government.

NAVAL OCEAN SYSTEMS CENTER
San Diego, California 92152-5000

E. G. SCHWEIZER, CAPT, USN
Commander

R. M. HILLYER
Technical Director

ADMINISTRATIVE INFORMATION

This document is a compilation of the papers delivered at the Defense Advanced Research Projects Agency (DARPA) Review of EHF Devices. This review was held at the Naval Ocean Systems Center, San Diego, California, on 24 and 25 January 1989.

Released by
L. J. Messick
Material and Device
Technology Branch

Under authority of
H. E. Rast, Head
Electronic Material
Sciences Division

CONTENTS

	PAGE NO.
Agenda.....	1
Attendance List.....	3
Overview of Millimeter Wave Components and Systems for Army Military Applications.....	7
Ballistic Transport in the Vertical and Lateral Domains.....	33 35
Permeable Base Transistor and Regrowth FET Development.....	70 75
Transport Considerations for EHF Devices.....	101
GaAlAs/GaAs Heterojunction Bipolar Transistors for mm-Wave Applications.....	150 157
Heterojunction Power FET Technology.....	185 195
Molecular Beam Epitaxy and Resonant Tunneling Devices.....	220 231
Array Applications.....	250 261
mm-Wave Phased-Array Antenna Concepts.....	280 299
Materials Choice for Ballistic and Drift Transport Devices.....	327
AlInAs-GaInAs HEMTs FOR HIGH SPEED APPLICATIONS.....	345
Measurement of Response of High Speed Tunneling Devices.....	370 383
EHF HBT Development.....	441
On Wafer Characterization of High Speed Circuits.....	465



Checked by For	
DATE	✓
TIME	G

A-1

AGENDA

DARPA REVIEW ON EHF DEVICES

NOSC Meeting Coordinator
Kitty Pitts
Code 032

NOSC Host
Louis Messick
Code 561

TUESDAY, 24 JANUARY

0745 Late Registration at the LaJolla Village Inn,
Torry & Sorrento Rooms

0815 Introductory Remarks

JAMES MURPHY
DARPA

0830 Requirements for 94 GHz 3-Terminal Circuit
Technology

JOHN ARMATA
Army LABCOM

0910 Ballistic Transport in the Vertical and Lateral
Dimensions

MORDEHI HEIBLUM
IBM

0950 Break

1010 Permeable Base and Vertical Transistors

MARK HOLLIS
MIT Lincoln Lab

1050 Transport Considerations in EHF Devices

HAL GRUBIN
Scientific Research
Associates

1130 GaAlAs/GaAs HBTs for mm-Wave Applications

PETER ASBECK
Rockwell Interna'l

1215 Lunch in University Room

1330 Heterojunction Power FET Technology

BUMAN KIM
Texas Instruments

1410 Resonant Tunnelling Structures

JAMES HARRIS
Stanford University

1450 Array Applications

JAMES BALLINGAL
General Electric

1530 Break

1550 mm-Wave Phased Array Antennas

CHARLES LIECHTI
Rockwell Interna'l

1630 Round Table Discussion: Promising Directions in
mm-Wave Device Technology for Phased Array Applications

1830 Buffet Dinner

WEDNESDAY, 25 JANUARY

0800	Materials Engineering for Ballistic Transport and Drift Devices	S. KRISHNAMURPHY SRI International
0840	mm-Wave Performance of InGaAs/InAlAs HEMT	UMESH MISHRA North Carolina State University
0920	Break	
0940	Measurement of Response of High Speed Tunneling Devices	TOM MCGILL Cal. Tech.
1020	EHF HBT Development	B. BAYRAKTAROGLU Texas Instruments
1100	On Wafer Characterization of High Speed Circuits	DAVID BLOOM Stanford University
1140	End Review	

ATTENDANCE LIST

Dr. Peter M. Asbeck
High Speed Electronics,
Rockwell International Science
Center
1049 Camino Dos Rios
Thousand Oaks, CA 91360

Dr. Burhan Bayraktaroglu
Texas Instruments
P. O. Box 655936, M/S 134
Dallas, TX 75265

Dr. John J. Berenz
TRW Electronic Systems Group
One Space Park, M5-2174E
Redondo Beach, CA 90278

Mr. Robert W. Bierig
Raytheon Company
Research Division
131 Spring Street
Lexington, MA 02173

Steven C. Binari (Code 6852)
Naval Research Laboratory
4555 Overlook Ave., SW
Washington, DC 20375

Mr. Brad Boos (Code 6852)
Naval Research Laboratory
4555 Overlook Ave., SW
Washington, DC 20375

Dr. Carl O. Bozler
MIT Lincoln Laboratory (Group 87)
244 Wood State
Lexington, MA 02173

John Carson (Code 753)
Naval Ocean Systems Center
San Diego, CA 92152-5000

Dr. P. C. Chao
General Electric Company
EP3-115
Syracuse, NY 13221

Daniel R. Ch'en
Microwave Monolithics Incorporated
465 E. Easy Street
Simi Valley, CA 93065

Dr. Derek T. Cheung
High Speed Electronics
Rockwell International Science
Center
1049 Camino Dos Rios
Thousand Oaks, CA 91360

Arthur R. Clawson (Code 561)
Naval Ocean Systems Center
San Diego, CA 92152-5000

Dr. Lester F. Eastman
Cornell University
425 Phillips Hall
Ithaca, NY 14850

Doris I. Elder (Code 561)
Naval Ocean Systems Center
San Diego, CA 92152-5000

Dr. H. L. Grubin
Scientific Research Associates,
Inc.
P. O. Box 1058
Glastonbury, CT 06033

Dr. Cynthia M. Hanson (Code 561)
Naval Ocean Systems Center
San Diego, CA 92152-5000

Dr. James S. Harris
Stanford University
McCullough 208
Stanford, CA 94305

Mordehai Heiblum
IBM
P. O. Box 218
Yorktown Heights, NY 10598

Dr. John Aiden Higgins
Rockwell International Science
Center
1049 Camino Dos Rios, A16
Thousand Oaks, CA 91360

Mark A. Hollis (Group 87)
MIT-Lincoln Laboratory
244 Wood Street, E-124F
Lexington, MA 02173

James A. Hutchby
Research Triangle Institute
P. O. Box 12194
Research Triangle Park, NC 27709

Bumman R. Kim
Texas Instruments
P. O. Box 655936, M/S 134
Dallas, TX 75265

Mr. Thomas Koscica
U.S. Army Electronics Technology
& Devices Laboratory
Fort Monmouth, NJ 07703-5000

Srinivasan Krishnamurthy
Stanford Research Institute
International (SRI)
333 Ravenswood Avenue, 41029
Menlo Park, CA 94025

Dr. Regis F. Leonard
National Aeronautics & Space
Administration
Lewis Research Center
Mail Stop 54-5
21000 Brookpark Road
Cleveland, OH 44135

Howard Lessoff (Code 6820)
Naval Research Laboratory
4555 Overlook Ave., SW
Washington, DC 20375

Dr. Charles A. Liechti
Rockwell International Science
Center
P. O. Box 1085
Thousand Oaks, CA 91360

Dr. Louis J. Messick (Code 561)
Naval Ocean Systems Center
San Diego, CA 92152-5000

Dr. James Murphy
Defense Advanced Research Projects
Agency
Defense Sciences Office
1400 Wilson Blvd.
Arlington, VA 22209/2308

Dr. R. Allen Murphy
MIT Lincoln Laboratory
244 Wood Street
Lexington, MA 02173

Richard Nguyen (Code 561)
Naval Ocean Systems Center
San Diego, CA 92152-5000

Dr. Howard E. Rast (Code 56)
Naval Ocean Systems Center
San Diego, CA 92152-5000

Victor Rehn (Code 3813)
Naval Weapons Center
China Lake, CA 93555

A. Landis Riley
Jet Propulsion Laboratory
4800 Oak Grove Dr., M/S 161-213
Pasadena, CA 91109

David Rubin (Code 753)
Naval Ocean Systems Center
San Diego, CA 92152-5000

Dr. Paul Saunier
Texas Instruments, Inc.
P. O. Box 655936, M/S 134
Dallas, TX 75265

Arden Sher
Stanford Research Institute
International (SRI)
333 Ravenswood Ave., 41042
Menlo Park, CA 94025

Ken Slegler (Code 6852)
Naval Research Laboratory
4555 Overlook Ave., SW
Washington, DC 20375-5000

Dr. Phillip M. Smith
General Electric Company
EP3-115 Electronics Park
Syracuse, NY 13221

Dr. Alan W. Swanson
General Electric Company
Electronics Laboratory
EP #3-115 Electronics Park
Syracuse, NY 13221

Marylin J. Taylor (Code 561)
Naval Ocean Systems Center
San Diego, CA 92152-5000

Norman Tien
University of California
Department of ECE, R-007
LaJolla, CA 92092-0407

Hua Quen Tserng
Texas Instruments
P. O. Box 655936, M/S 134
Dallas, TX 75265

Thao T. Vu (Code 561)
Naval Ocean Systems Center
San Diego, CA 92152-5000

Mr. Richard T. Webster
Rome Air Development Center
RADC/EEAC
Hanscom AFB, MA 01731

H. H. Wieder
University of California, San
Diego
Department of Electrical
Engineering & Computer Sciences
R-007
LaJolla, CA 92093

Gerald L. Witt
Air Force Office of Scientific
Research
AFOSR/NE
Bolling AFB, DC 20332-6448

Huan-Chun Yen
TRW
1 Space Park
Redondo Beach, CA 90278

Dr. Jim Zeidler (Code 7601)
Naval Ocean Systems Center
San Diego, CA 92152-5000

Dr. Carl R. Zeisse (Code 561)
Naval Ocean Systems Center
San Diego, CA 92152-5000

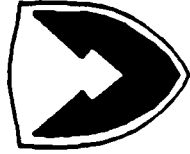
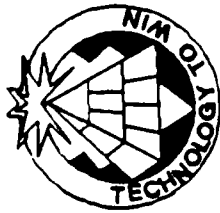
Overview of Millimeter Wave Components and Systems for Army Military Applications
and
Requirements for 94 GHz Phased Arrays

John F. Armata, Jr.

and

Thomas Kostica

U.S. Army Electronics Technology & Devices Laboratory
Ft. Monmouth, NJ



US ARMY
LABORATORY COMMAND

ELECTRONICS TECHNOLOGY and DEVICES LABORATORY

***OVERVIEW OF MILLIMETER WAVE COMPONENTS AND SYSTEMS
FOR ARMY MILITARY APPLICATIONS
AND
REQUIREMENTS FOR 94 GHz PHASED ARRAYS***

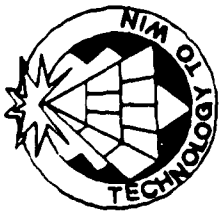
JOHN F. ARMATA, JR.

and

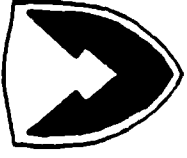
THOMAS KOSCICA

**U.S. ARMY ELECTRONICS TECHNOLOGY AND DEVICES LABORATORY
FORT MONMOUTH, NEW JERSEY**

JCOV#52



AGENDA



US ARMY
LABORATORY COMMAND

ELECTRONICS TECHNOLOGY and DEVICES LABORATORY

RADAR COMPONENTS DEVELOPED UNDER FORT MONMOUTH SPONSORSHIP

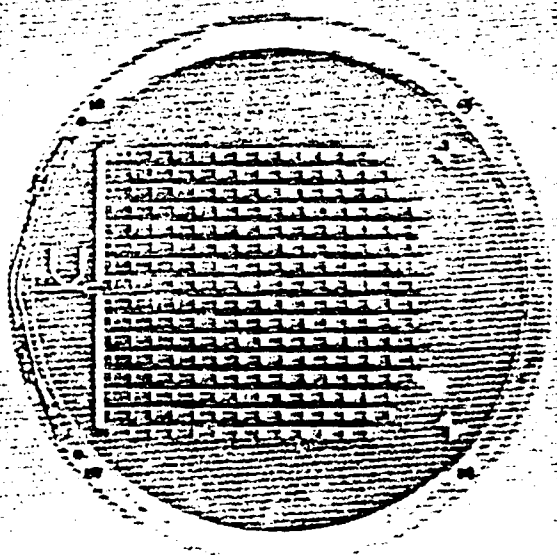
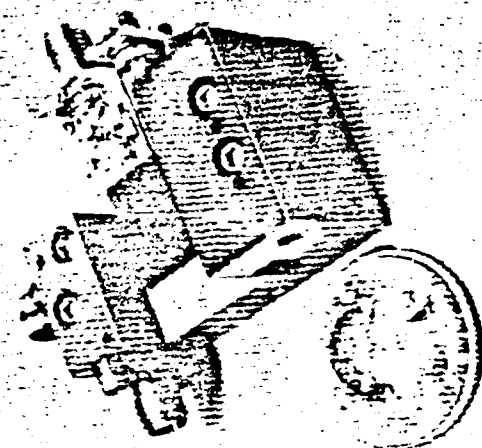
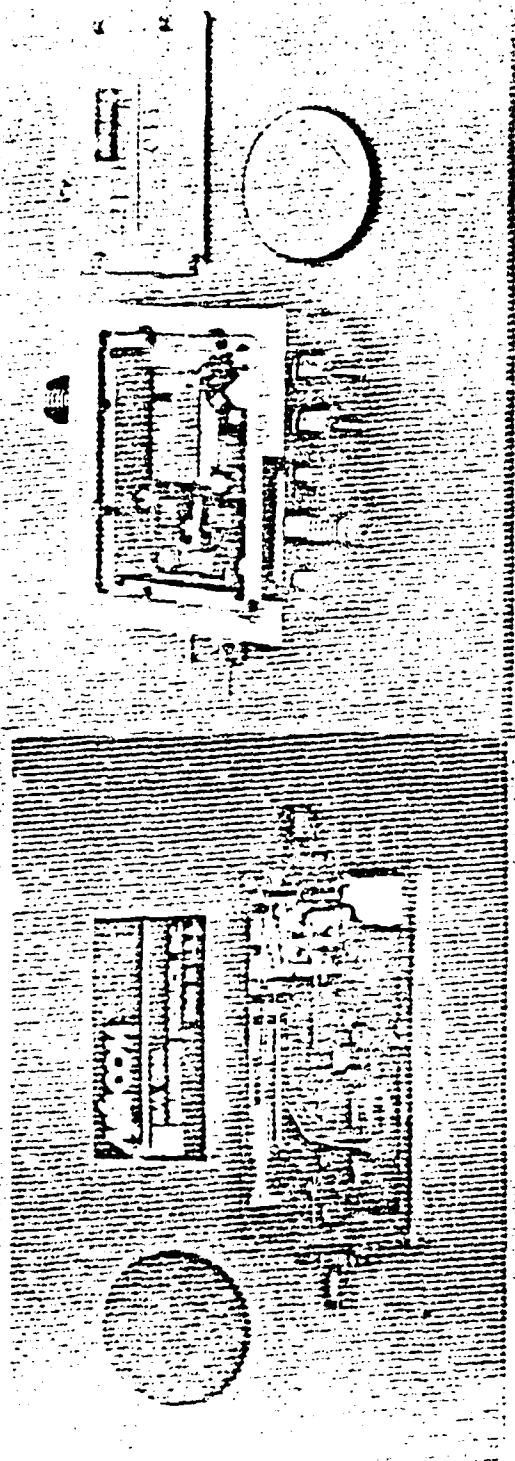
° REVIEW OF SOME SYSTEM APPLICATIONS AND REQUIREMENTS

SADARM

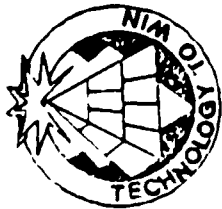
SCOTT

MLRS-TGW

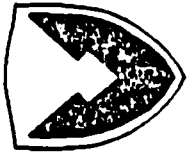
ACTIVE TANK DEFENSE



35 GHz TRANSCIEVER COMPONENTS

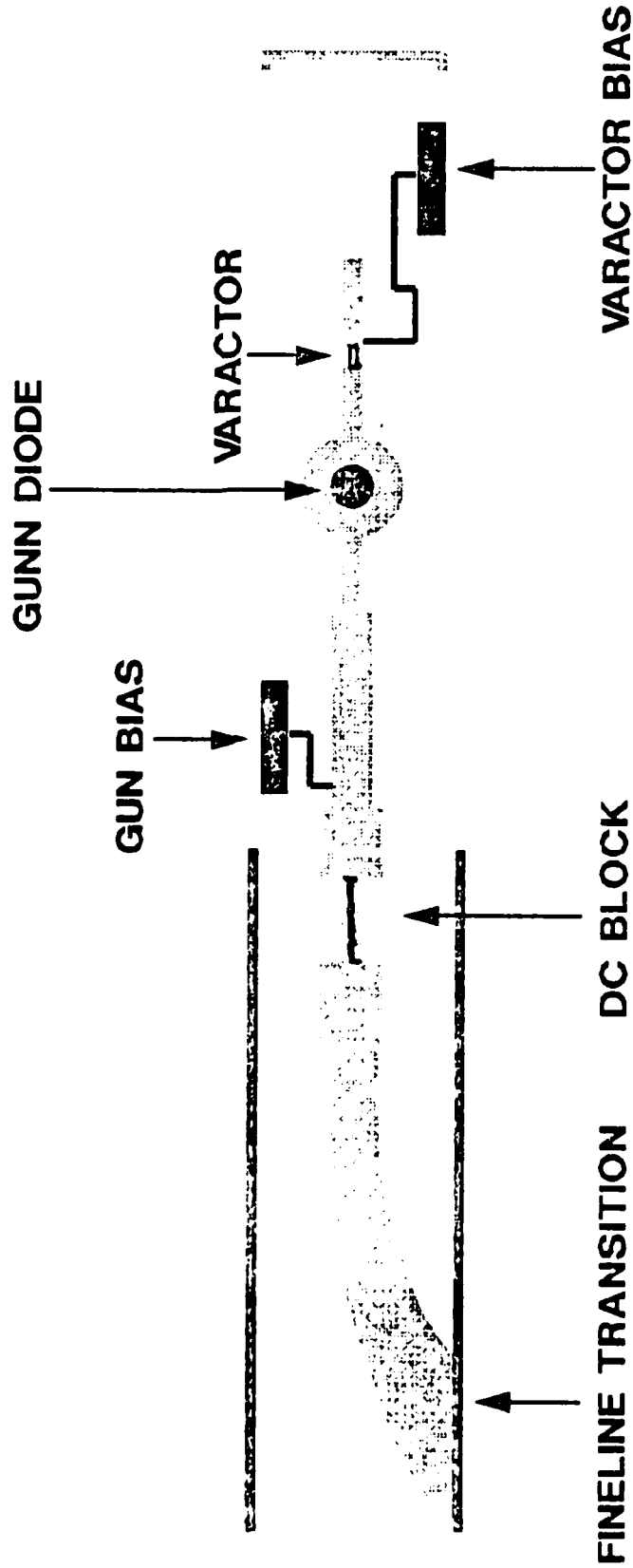


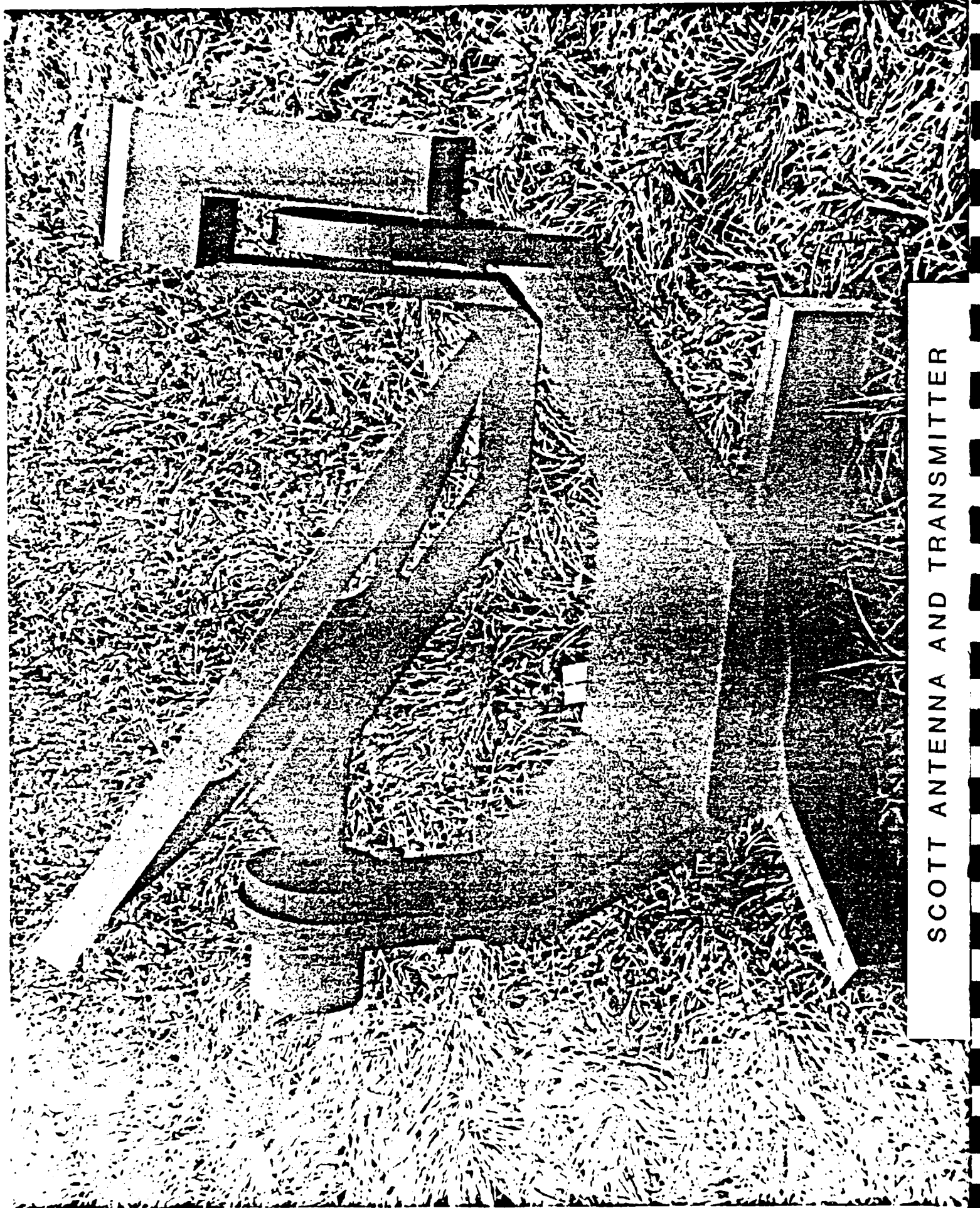
Ka-BAND MICROSTRIP VCO CIRCUIT



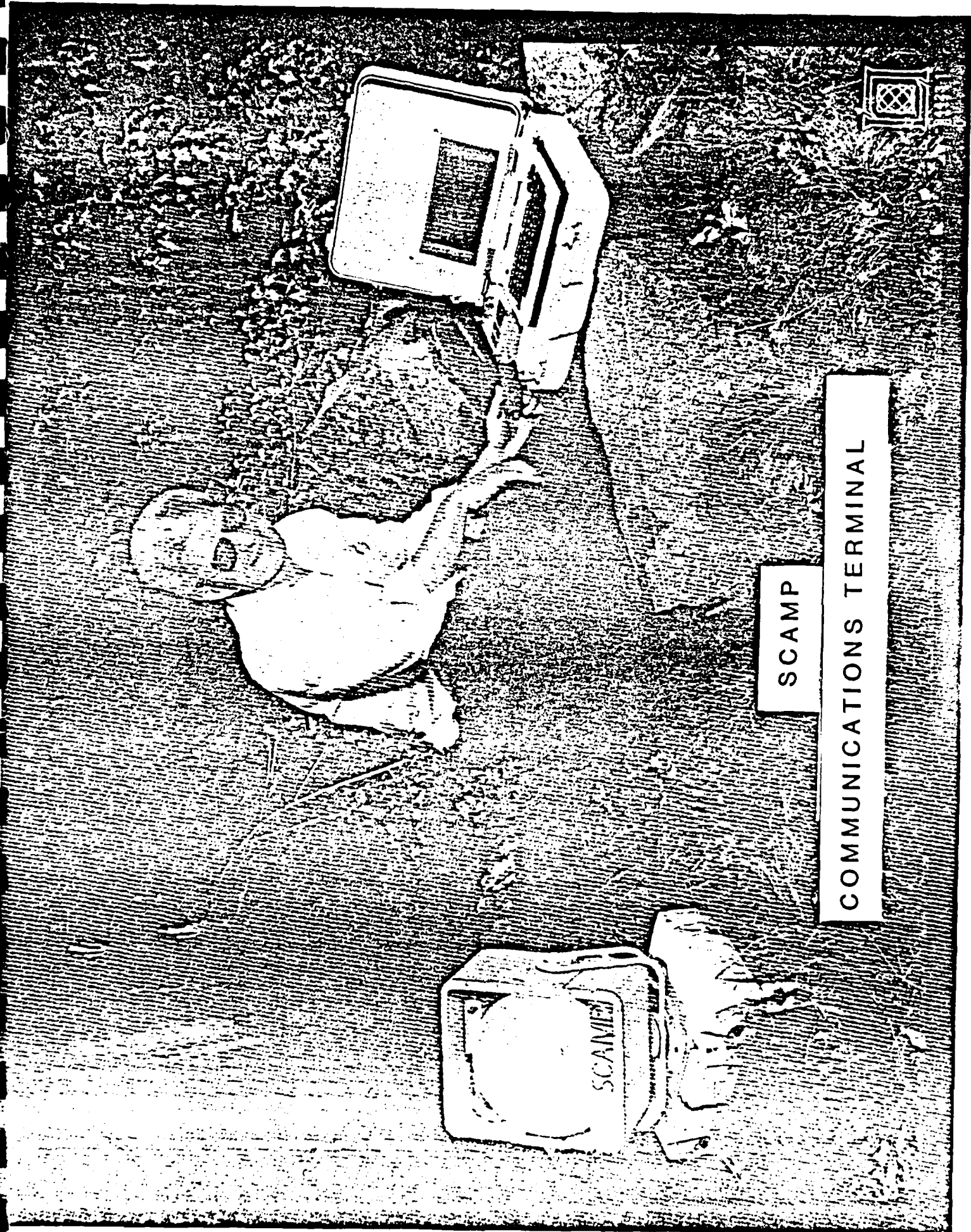
US ARMY
LABORATORY COMMAND

ELECTRONICS TECHNOLOGY and DEVICES LABORATORY



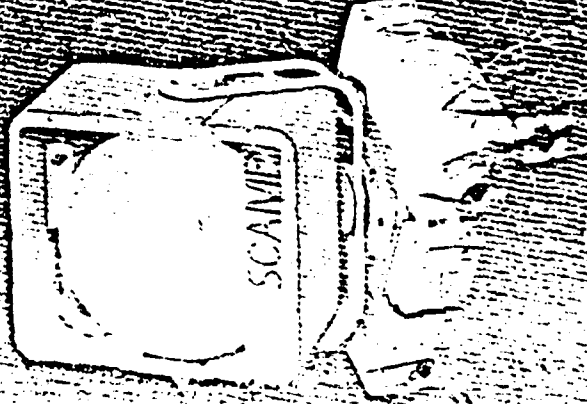


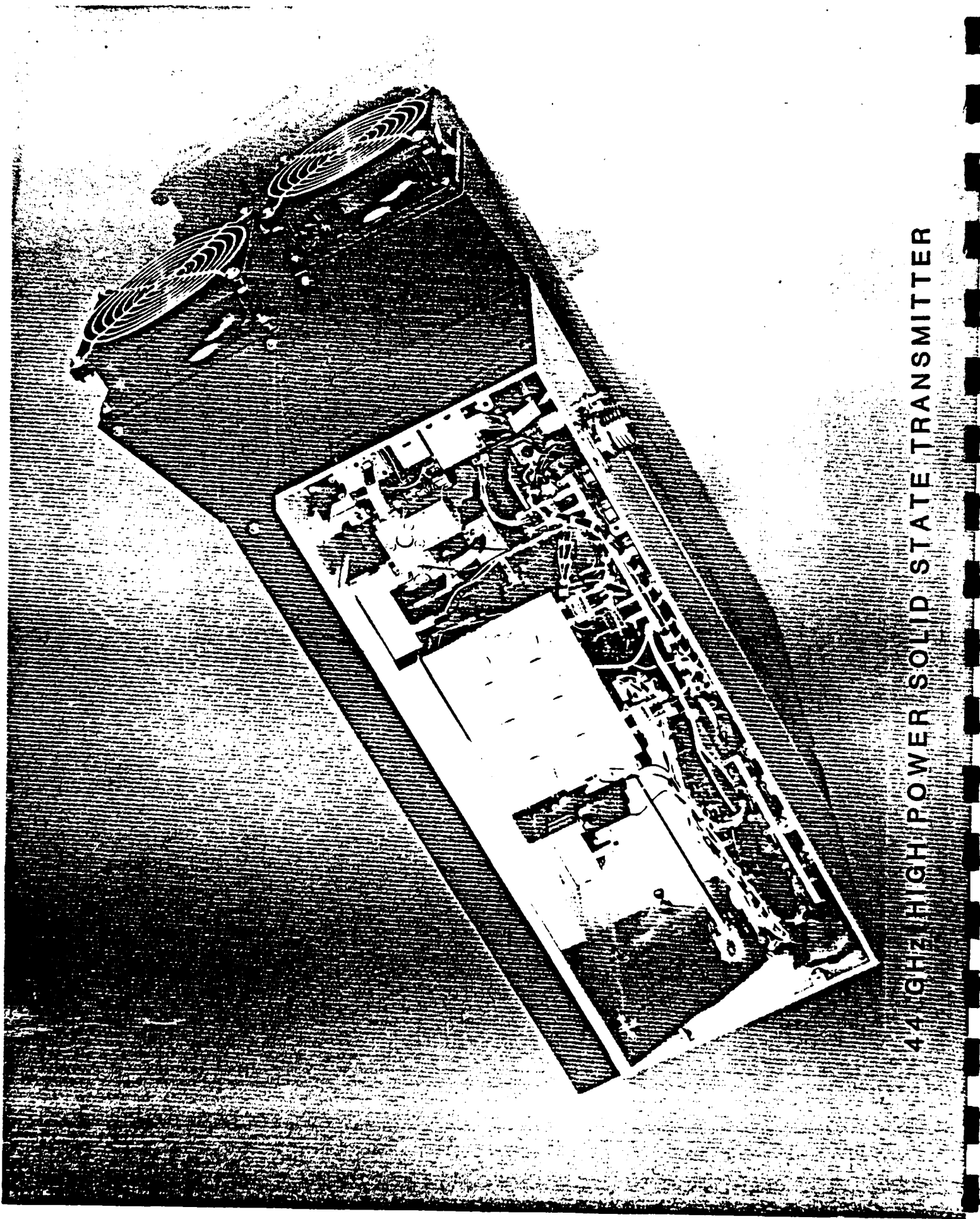
SCOTT ANTENNA AND TRANSMITTER



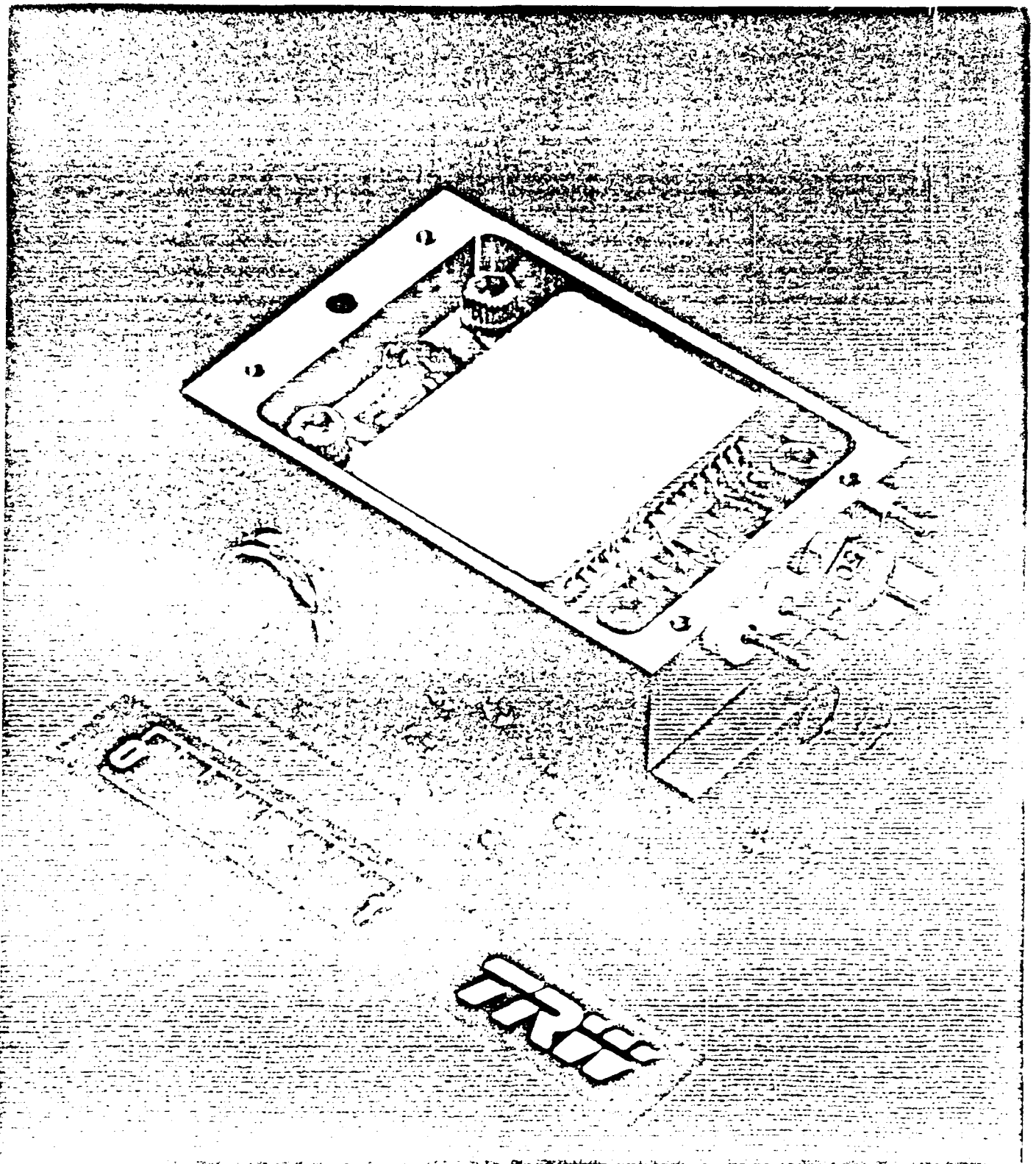
SCAMP

COMMUNICATIONS TERMINAL

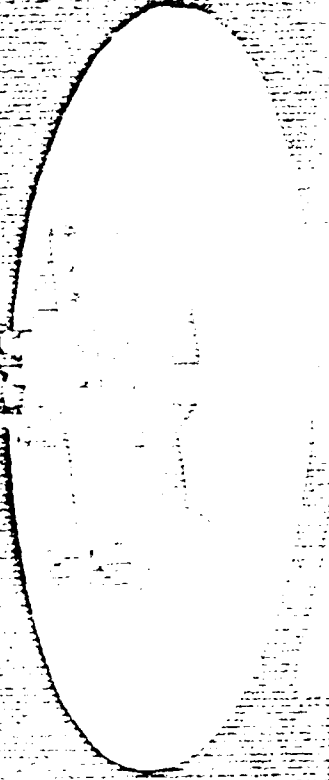




44 GHz HIGH POWER SOLID STATE TRANSMITTER

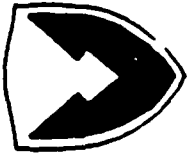


SECRET





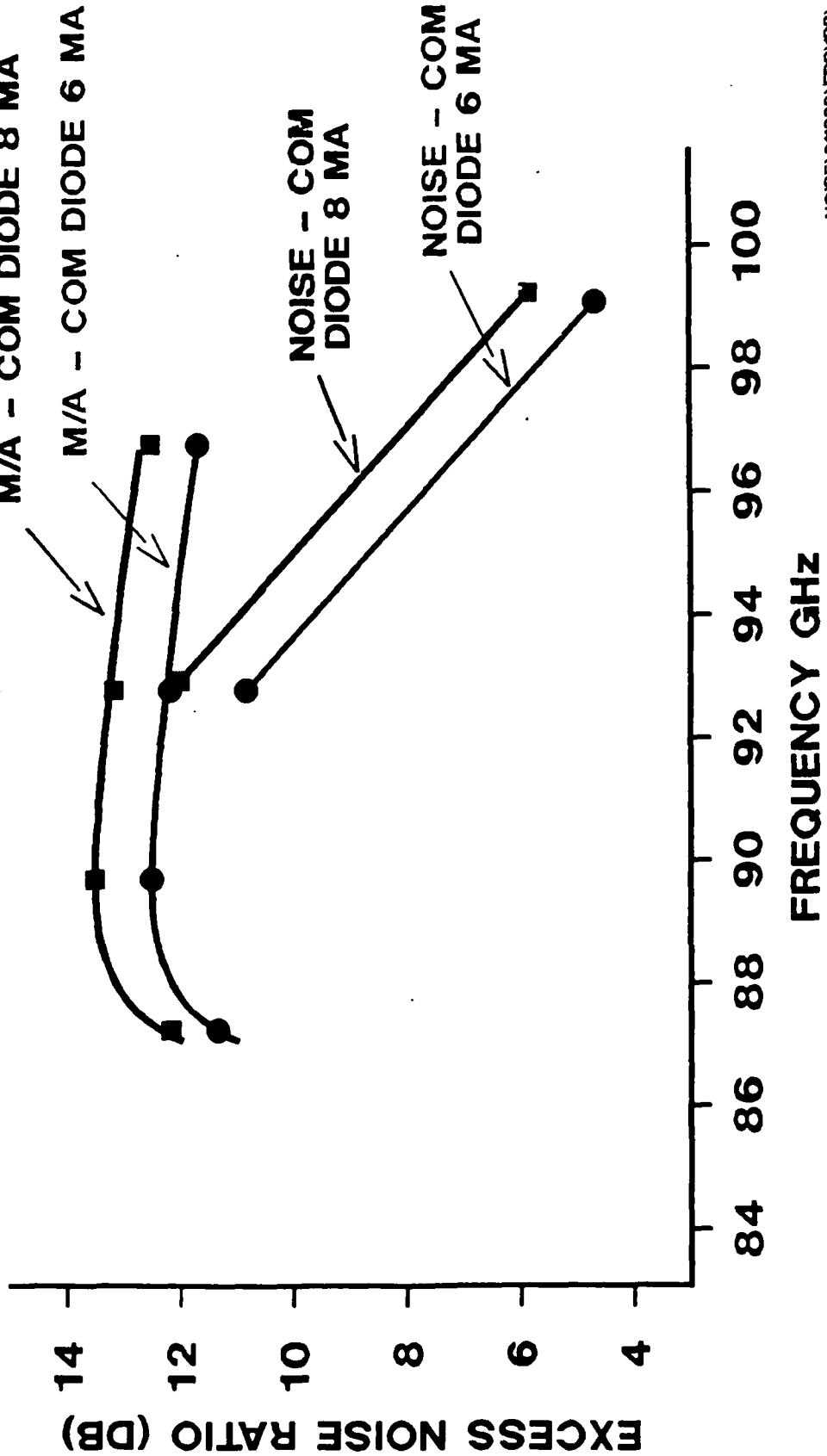
NOISE COM INC - NOSIE SOURCE P/N 12473, S/N 001



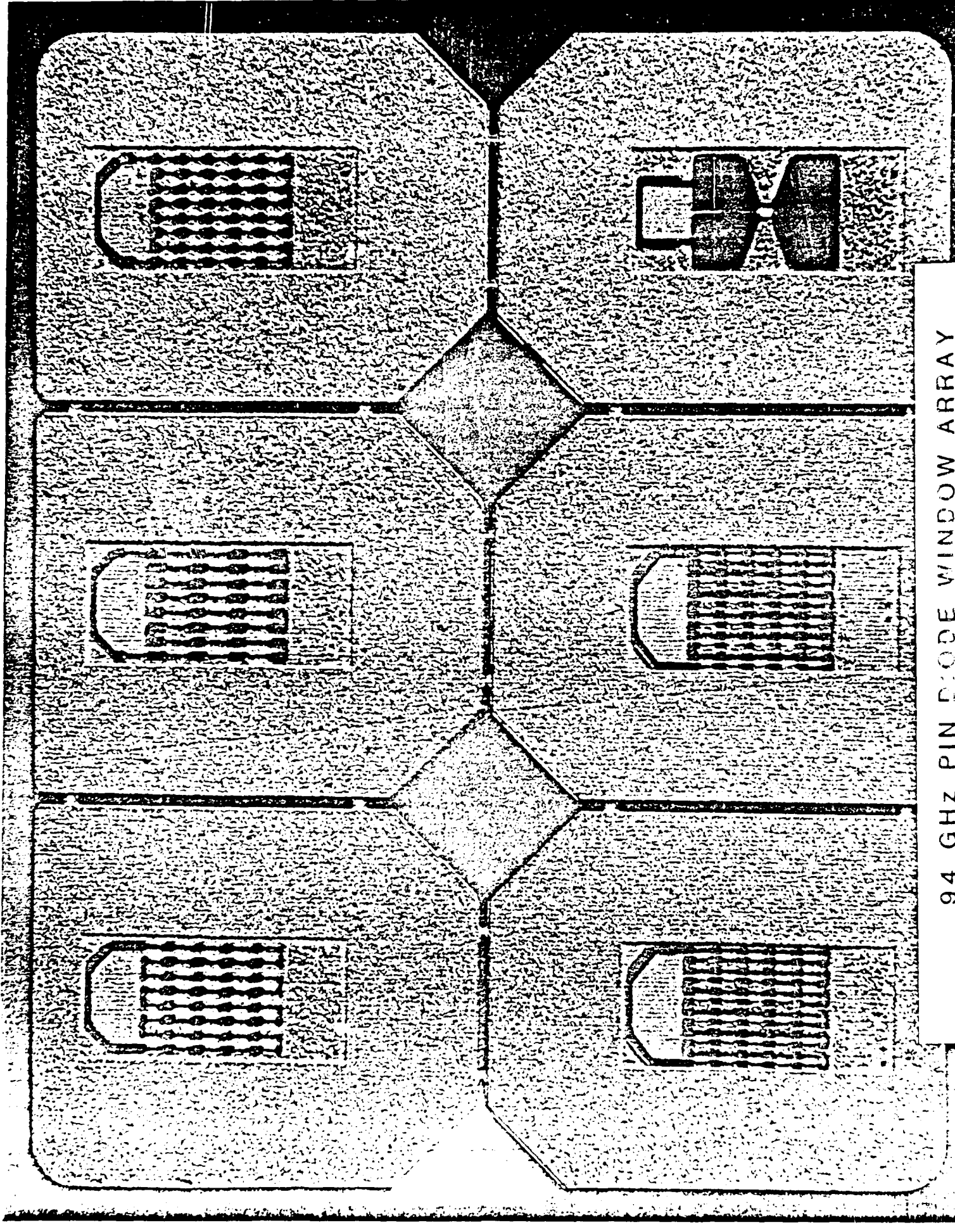
US ARMY
LABORATORY COMMAND

ENR (DB) VS. FREQUENCY

ELECTRONICS TECHNOLOGY and DEVICES LABORATORY

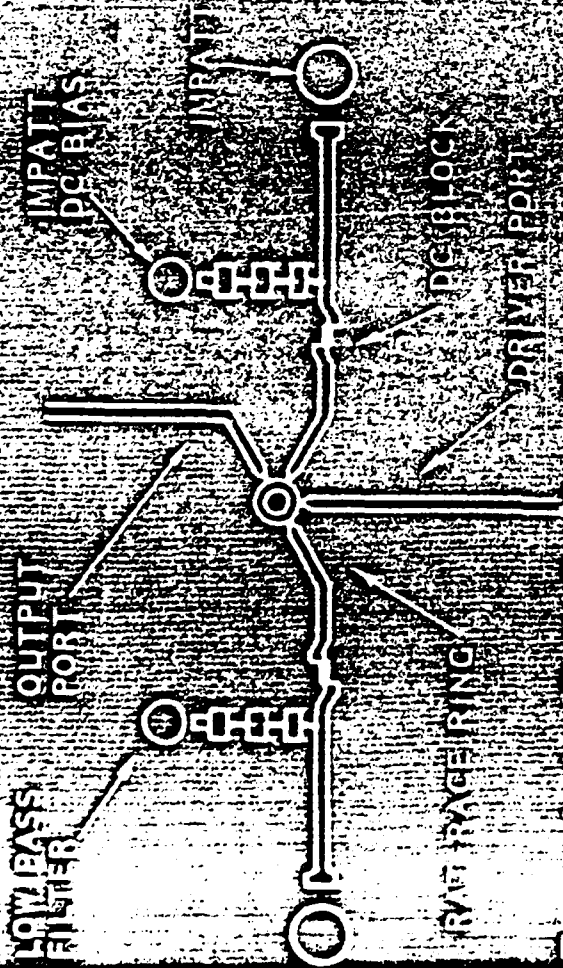


NOISE\011889\EP8\088\62\A.M.F

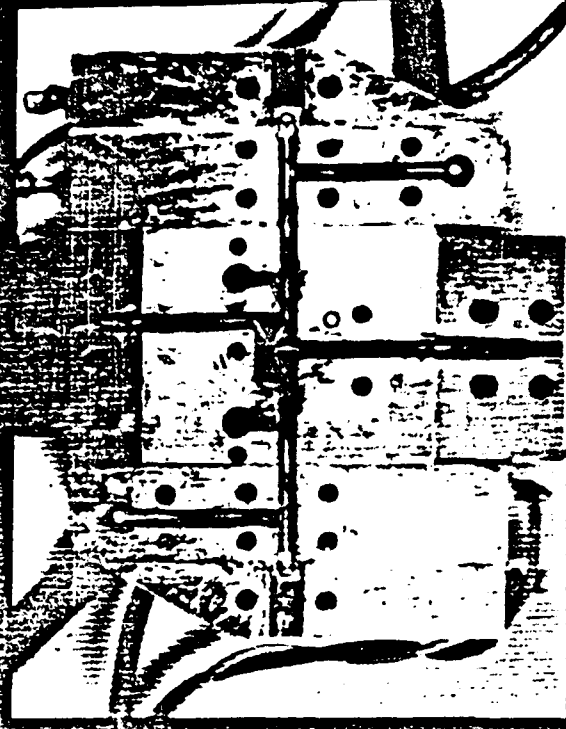


94 GHz PIN DIODE WINDOW ARRAY

W-Band MIC High Power Pulse Combiner



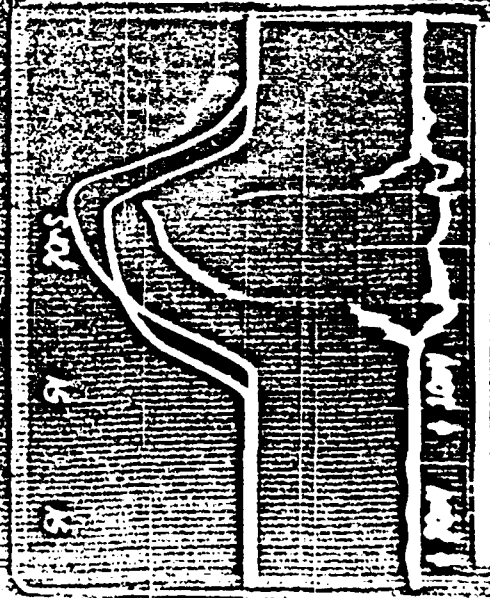
Transmission Type Rat-Race Combiner

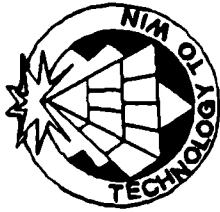


MIC Short Pulse Rat-Race Combiner

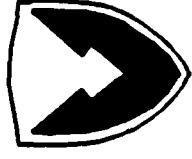
FEATURES

- RAT RACE RING HYBRID POWER COMBINER
- 20W PEAK PULSED POWER NEAR 96 GHz
- 150MHz FREQUENCY/CHIRPING
- OVER 80% COMBINING EFFICIENCY
- ISOLATION BETWEEN INPUT AND OUTPUT PORTS IS > 18 dB
- MICROSTRIP CONSTRUCTION LENDS ITSELF TO SMALL SIZE, LOW COST, AND COMPATIBILITY WITH MONOLITHIC IMPLEMENTATION





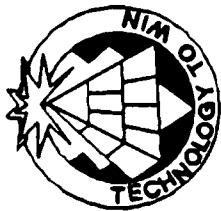
PROBLEMS WITH IMPATT AMPLIFIERS FOR 44 GHZ



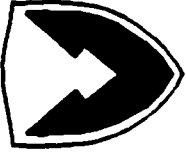
**US ARMY
LABORATORY COMMAND**

ELECTRONICS TECHNOLOGY and DEVICES LABORATORY

- 1. COMPLEX CIRCUITRY**
- 2. LARGE PHYSICAL SIZE**
- 3. LOW EFFICIENCY (APPROXIMATELY 5-6%)**
- 4. DIODE SELECTION PROBLEMS**
- 5. IMPATTs OPERATE AT HIGH TEMPERATURES (RELIABILITY)**
- 6. COSTLY**



PROBLEMS WITH PRESENT MLRS-TGW RADAR



**US ARMY
LABORATORY COMMAND**

ELECTRONICS TECHNOLOGY and DEVICES LABORATORY

POWER, GIMBAL ANTENNA

WAVEGUIDE AND MICROSTRIP LOSS

LOSSY COMPARATOR, FREQUENCY STABILITY

HIGH COST, HIGH NOISE FIGURE

LARGE VOLUME REQUIREMENTS

ET&D LAB

FT. MONMOUTH, NJ

JOHN ARMATA

(ELECTRONIC COMPONENTS &
SUB-SYSTEM DEVELOPER)

EW LAB

FT. MONMOUTH, NJ

RICK IVONE

(RADIATION DETECTION AND ECM)

7

TACOM

WARREN, MI

KENNETH LIM

(TANK COMMAND -
SYSTEM INTEGRATOR & USER)

TRW INC.

REDONDO BEACH, CA

FRANK STODDARD

(RADAR SYSTEM DESIGN & EVAL.)

PSI INC.

MANASQUAN, NJ

WILLIAM CAVE

(DYNAMIC SYSTEM GRAPHICS
AND MODELING)

**ACTIVE TANK DEFENSE
COOPERATIVE TEAM**

MYK INC.

INDUSTRY CITY, CA

Dr. YUEN CHANG

(RADAR SENSORS & CONCEPTS)

BALL AEROSPACE

BOULDER, CO

ROBERT MONSON

(CONFORMAL ANTENNAS)

TEXAS INST. INC.

DALLAS, TX

Dr. BURHAN BAYRAKTARGOLU

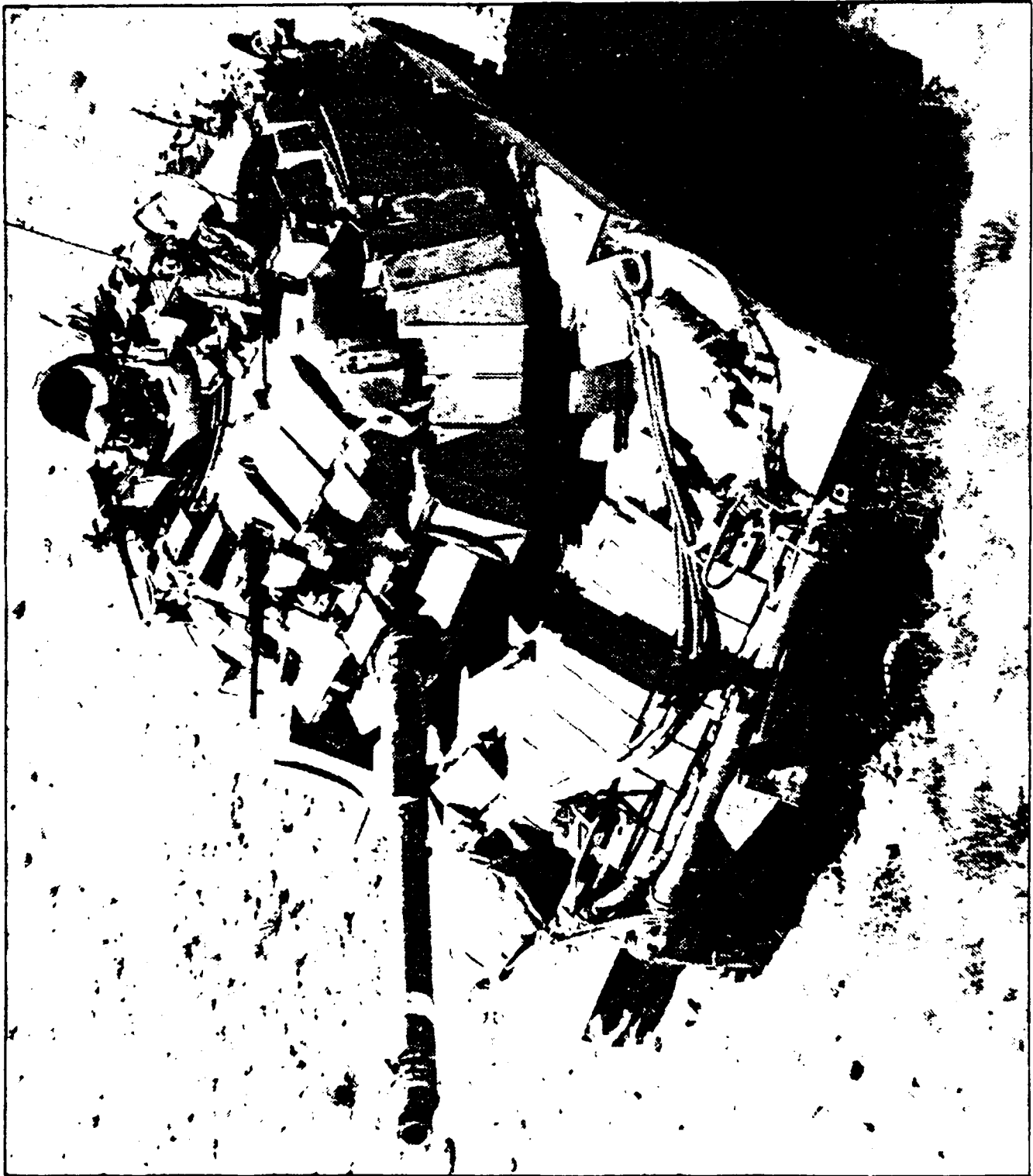
(MONOLITHIC RADAR CHIPS)

MILLITECH CORP.

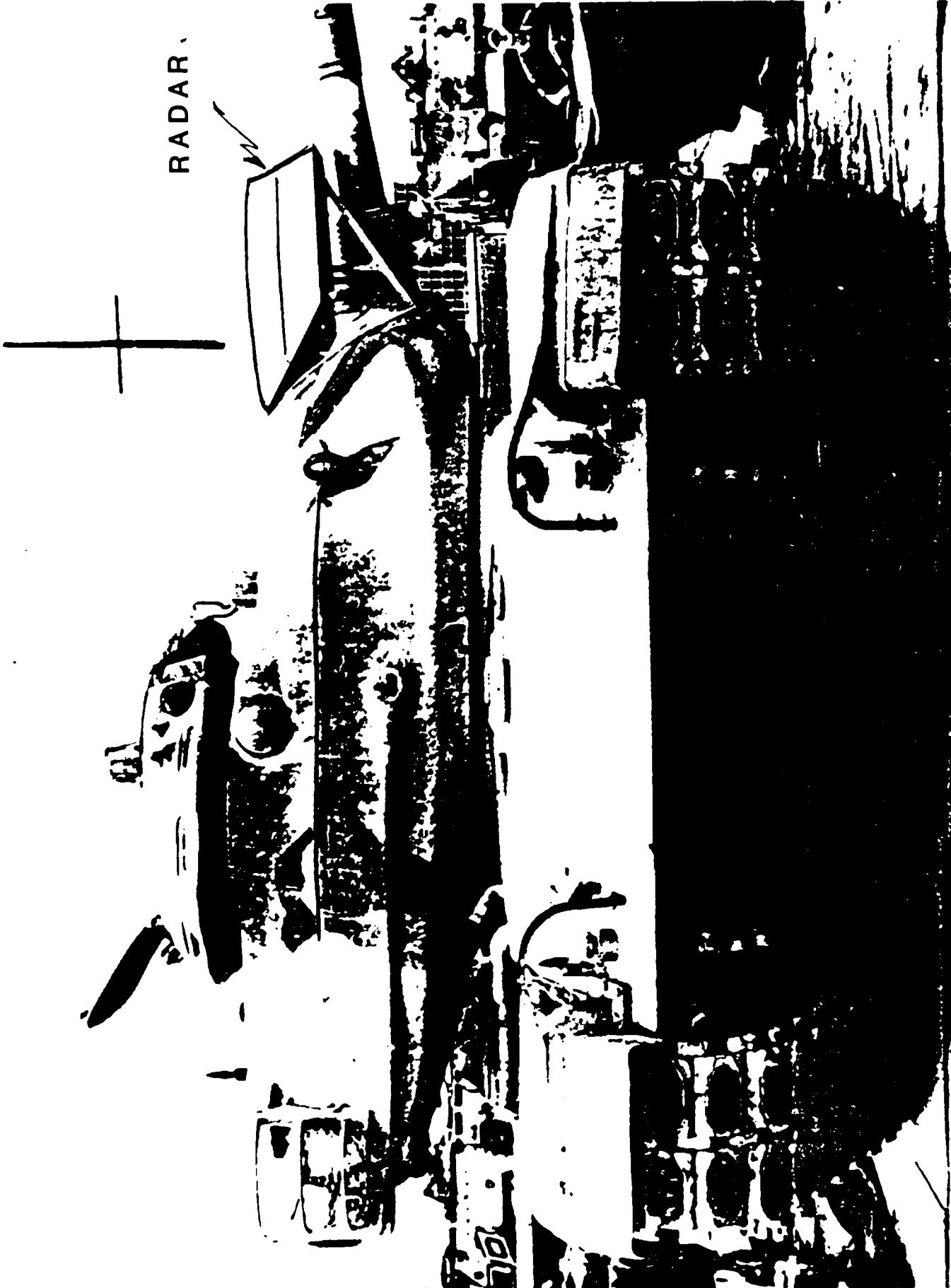
SOUTH DEERFIELD, MA

DANA WHEELER

(MILLIMETER RADAR FUSING)

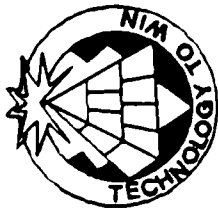


▲ The countermeasure, reactive armour, reduces penetration by exploding outward when hit

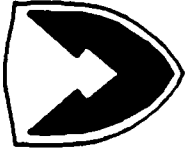


RADAR

EARLY VERSION OF MMW TARGET ACQUISITION RADAR FOR TANKS



SAMPLE TANK THREATS



US ARMY
LABORATORY COMMAND

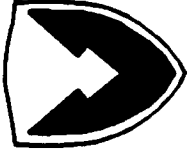
ELECTRONICS TECHNOLOGY and DEVICES LABORATORY

<i>TYPE</i>	<i>SAMPLE SYSTEM</i>	<i>RADAR CROSS-SECTION</i>	<i>SPEED</i>
OVERHEAD ATTACK	SADARM, MERLIN	MEDIUM	LOW
GUIDED MISSILE	TOW	LARGE	MEDIUM
HOMING MISSILE	MLRS, HELLFIRE	MEDIUM	MEDIUM
HEAT SEEKING MISSILE	HELLFIRE, STINGER	MEDIUM	MEDIUM
HEAT ROUND	GUN FIRED (105-135 MM)	SMALL	HIGH
LONG ROD PENETRATOR	GUN FIRED (105-135 MM)	V. SMALL	V. HIGH

STT\011989\EP5\198\#62\MJR



WHAT MAKES SENSE



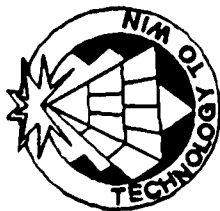
US ARMY
LABORATORY COMMAND

ELECTRONICS TECHNOLOGY and DEVICES LABORATORY

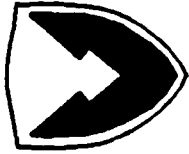
**SURVIVABILITY OF TANK AND ARMORED
PERSONNEL CARRIER CAN NO LONGER
DEPEND ON HEAVIER COMPLEX ARMOR.**

PROBLEMS: COST, WEIGHT, LOSS OF SPEED, FUEL REQUIREMENTS, ETC.

**SOLUTION: REQUIRES NEW LEVEL OF ELECTRONIC TECHNOLOGY TO
PROVIDE THE DEGREE OF PROTECTION REQUIRED IN
BATTLEFIELD OF THE FUTURE.**



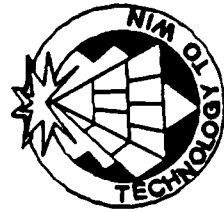
MAJOR TANK DEFENSE PHASED ARRAY REQUIREMENTS



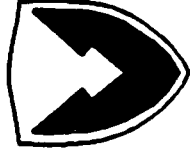
US ARMY
LABORATORY COMMAND

ELECTRONICS TECHNOLOGY and DEVICES LABORATORY

- HIGH RESOLUTION
- MULTIPLE BEAM
- HEMISPHERICAL COVERAGE
- COVERTNESS
- HIGH ANGULAR RESOLUTION
- LOW TO MEDIUM POWER
- HIGH BEAM SCAN
- LOW SIDELOBES
- CONFORMAL
- AFFORDABLE



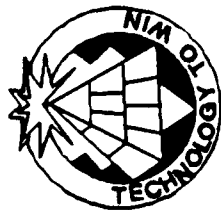
POTENTIAL MILITARY SYSTEMS CANDIDATES FOR PHASED ARRAYS



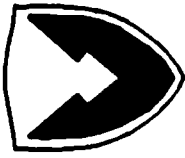
US ARMY
LABORATORY COMMAND

ELECTRONICS TECHNOLOGY and DEVICES LABORATORY

- 60GHZ SPACE COMMUNICATIONS, SDI SABIR
- 35, 60, 94 GHZ SMART MUNITIONS MLRS, HELLFIRE
- 94 GHZ ACQUISITION RADAR ETAS (STARTLE)
TACTICAL AIR
- 44, 60 GHZ COMMUNICATIONS SPACE, HELICOPTER,
TANKS
- 60, 94 GHZ TANK DEFENSE DETECTION OF
MISSILE & GUN
FIRED PROJECTILES

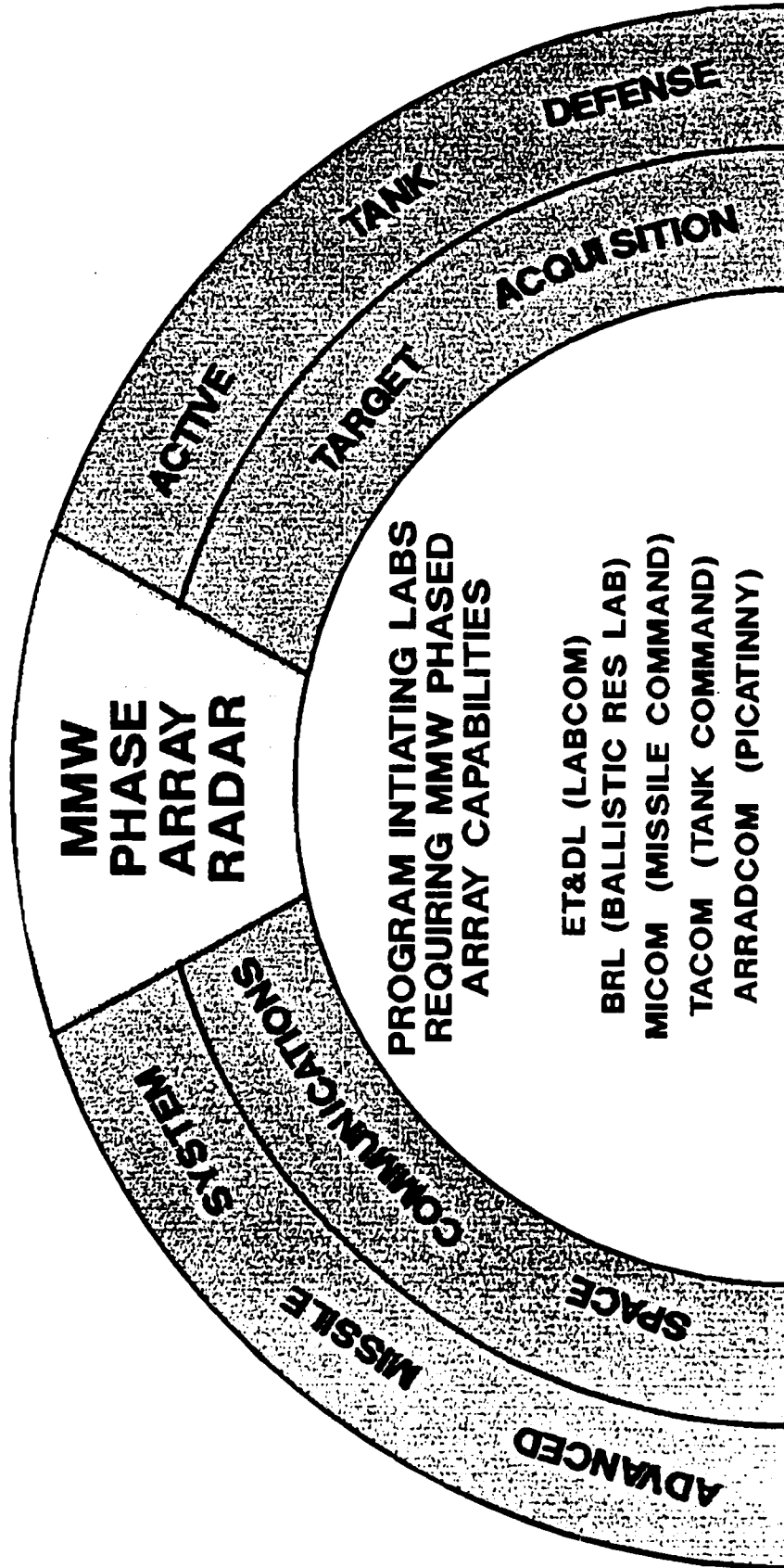


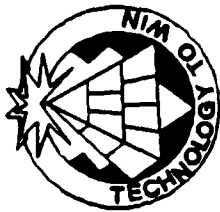
**THE KEY ELEMENT
FOR
CRITICAL FUTURE MILITARY SYSTEMS**



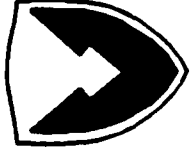
**US ARMY
LABORATORY COMMAND**

ELECTRONICS TECHNOLOGY and DEVICES LABORATORY



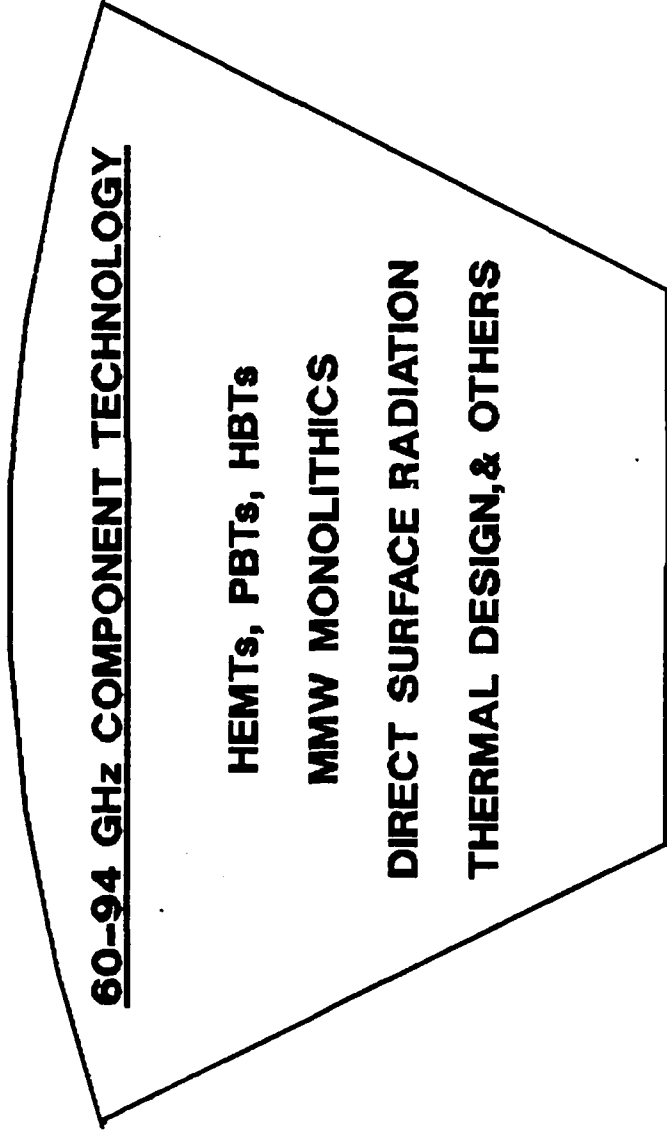


CRITICAL KEY AREAS FOR R&D



US ARMY
LABORATORY COMMAND

ELECTRONICS TECHNOLOGY and DEVICES LABORATORY



(AT 44 GHz EHF ARRAY PROGRAM HAS MADE A SIGNIFICANT IMPACT.)

REQUIRE ANOTHER CONCENTRATED EFFORT TO DESIGN AND DEVELOP A NEW

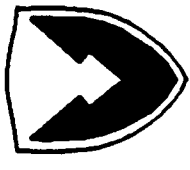
GENERATION OF DEVICES AND CIRCUITS FOR 94 GHz TO MEET DOD NEEDS.

(MIMIC PROGRAM WILL NOT ADDRESS THESE AREAS)

CKAFR1ADY-20-89\EP3Y196Y\#63\SP



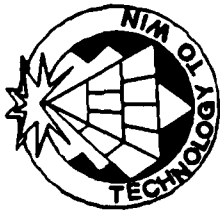
**POTENTIAL CANDIDATES 3-TERMINAL
DEVICES FOR MILLIMETER WAVE
PHASED ARRAY CIRCUIT ELEMENTS**



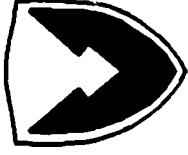
**US ARMY
LABORATORY COMMAND**

ELECTRONICS TECHNOLOGY and DEVICES LABORATORY

- **MESFETS**
- **PSEUDOMORPHIC HEMTS**
- **HETEROJUNCTION BIPOLAR**
- **PERMEABLE BASE TRANSISTOR**
- **INDIUM PHOSPHIDE FETS**



FORT MONMOUTH PROGRAMS



US ARMY
LABORATORY COMMAND

ELECTRONICS TECHNOLOGY and DEVICES LABORATORY

1. PSEUDOMORPHIC HEMT (POWER) FOR SCOTT

FUNDED \approx 175 IN FY89

TOTAL \approx 900K

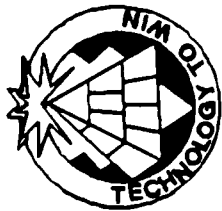
2. HBT FOR POWER AND EFFICIENCY (MMW)

3. MULTI BEAM PHASED ARRAY

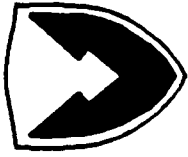
STUDY FOR TANK DEFENSE



POTENTIAL NEW STARTS
FOR FY89 IF FUNDING IS
AVAILABLE AT THE
PRESENT TIME.



EHF DARPA ARRAY PROGRAM IMPACT



**US ARMY
LABORATORY COMMAND**

ELECTRONICS TECHNOLOGY and DEVICES LABORATORY

- **LEADING THE DEVELOPMENT OF MILLIMETER WAVE DEVICES FOR HIGHER POWERS.**
- **HEMTs, HBTs, PBTs ARE ALL POTENTIAL CANDIDATES FOR REPLACEMENTS IN NEAR FUTURE.**
- *** PRESENTLY, Ft. MONMOUTH HAS A PROGRAM TO DEVELOP A 44 GHZ 1/2 WATT DEVICE AND A 1 WATT MODULE TO REPLACE THE IMPATT BASED AMPLIFIER.**
- **PROJECT THAT WITHIN 3 YEARS-USING POWER DEVICE, THE IMPATT AMPLIFIER WILL BE REPLACED WITH MMW TRANSISTOR WHICH WILL ALLOW SMALL, EFFICIENT, COST EFFECTIVE AMPLIFIER.**

33/34

Ballistic Transport in the Vertical and Lateral Domains

Mordehai Heiblum

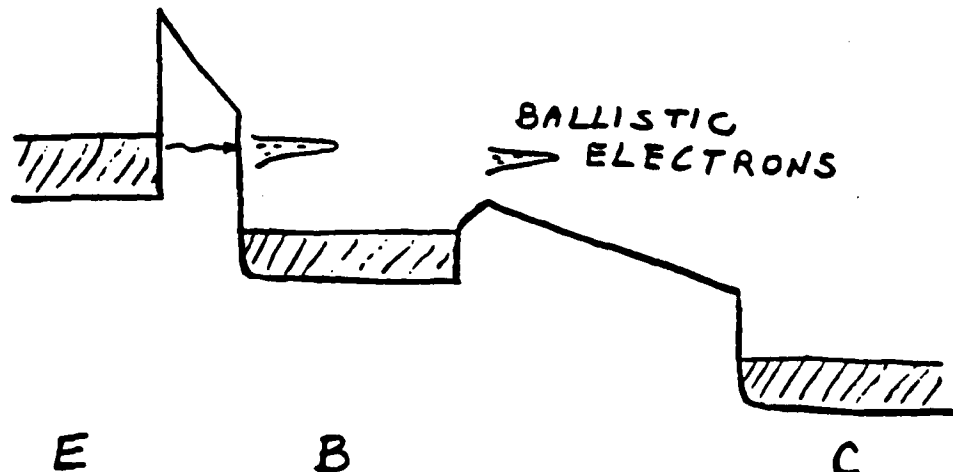
*IBM
Yorktown Heights, NY*

BALLISTIC TRANSPORT IN THE VERTICAL AND LATERAL DOMAINS

M. Heiblum

K. Seo, A. Palevski, C. Umbach, M. Weckwerth, D. Galbi,
L. Osterling, C. Knoedler, and P. Bhattacharya

- Making High Gain THETA Devices
 1. All GaAs Device
 2. Strained Base Device
- A Lateral Ballistic Device
- Physics of Ballistic Transport: Single Phonon Emission

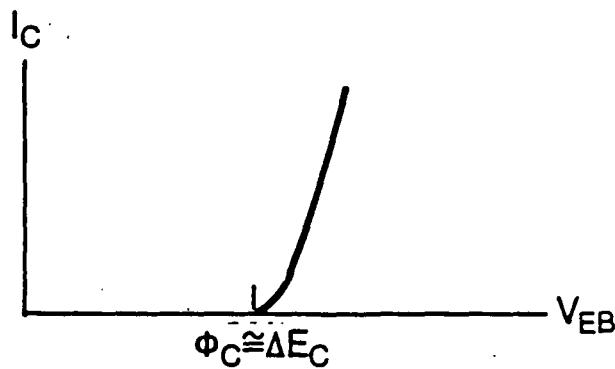


DEVICE POTENTIAL

- No Minority Carriers Storage Effects

- Threshold Type Device

Threshold Determined by AIAs Mole-Fraction



- Transit Time is < 0.2 pS

For $J \cong 10^5$ A/cm²
0.25 μ m Geometry } $\Delta t < 1$ ps
 $\Delta V = 0.1$ V

TECHNOLOGICAL PROBLEMS WITH THE THETA DEVICE

- **Low Gain**
- **Low Current Density**
- **High Base Resistance**
- **Poor Ohmic Contact to Base**

**Low Gain.....Is it an inherent problem in Ballistic
Devices ?**

CURRENT GAIN IN GaAs THETA DEVICES

Record Value Achieved for Base Doping of
 $8 \times 10^{17} \text{ cm}^{-3}$:

$$\alpha=0.9$$

$$\beta=9 \text{ at } 77 \text{ K}$$

Questions Asked:

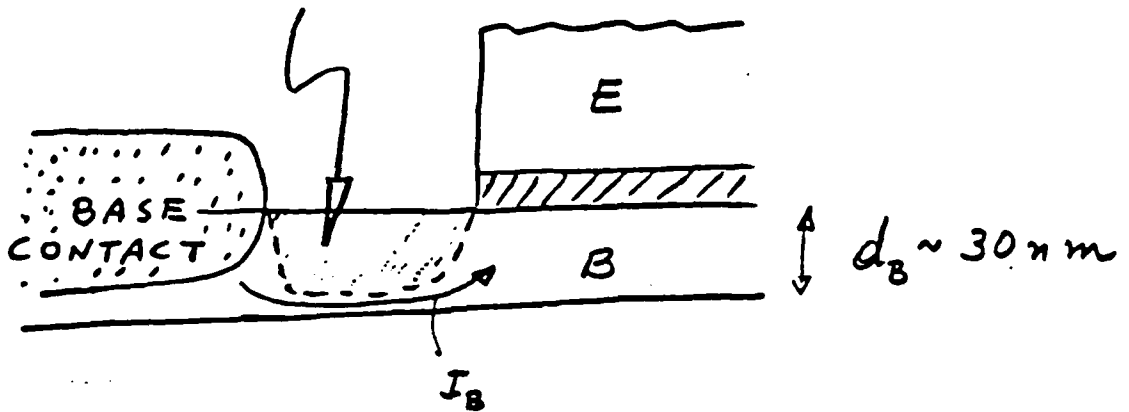
- What is the Ultimate Gain in GaAs Base Devices?
- Can the Gain be Increased with Different Base Materials?

FACT : As the Doping Decreases the Gain Goes up !

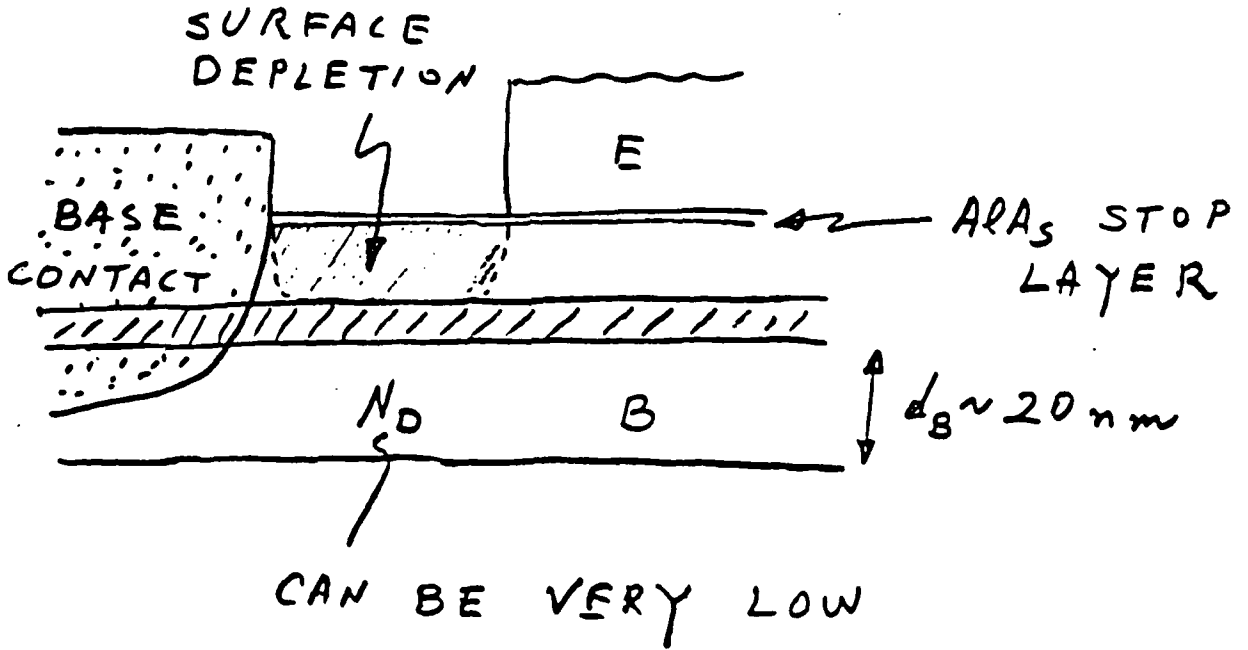
The Base Depletion Problem

For $N_D = 4 \times 10^{17} \text{ cm}^{-3}$

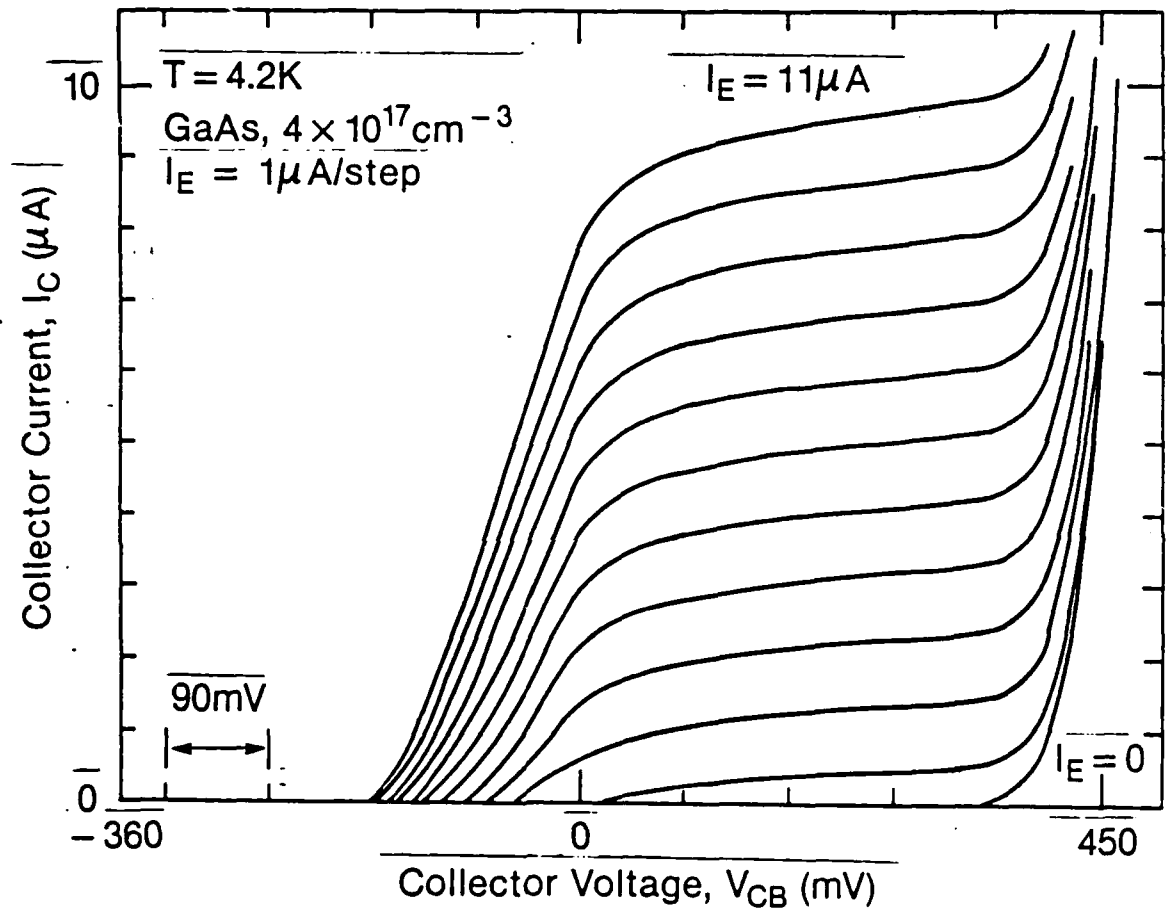
SURFACE DEPLETION



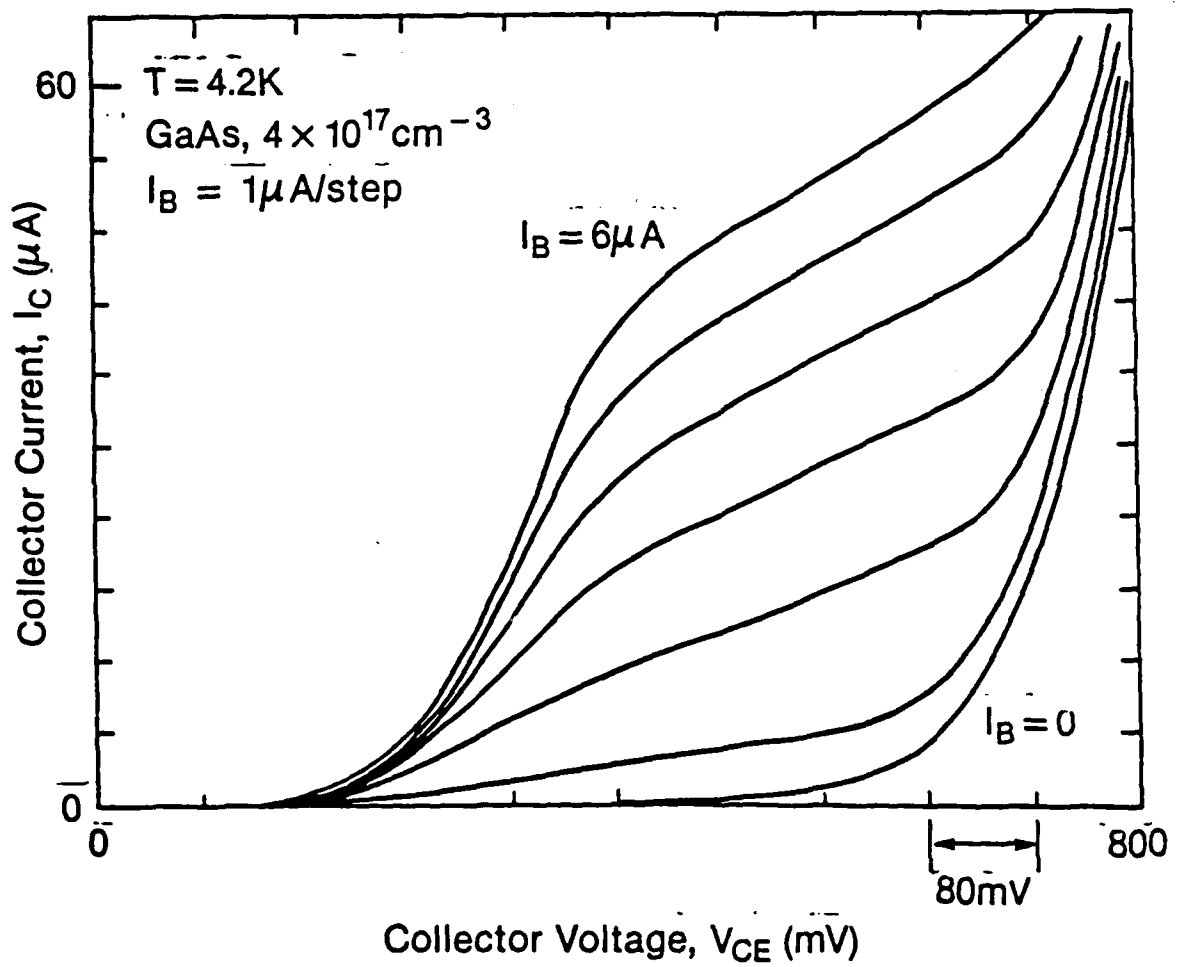
A Modified Design to Prevent Base Depletion



Common Base Characteristics



Common Emitter Configuration

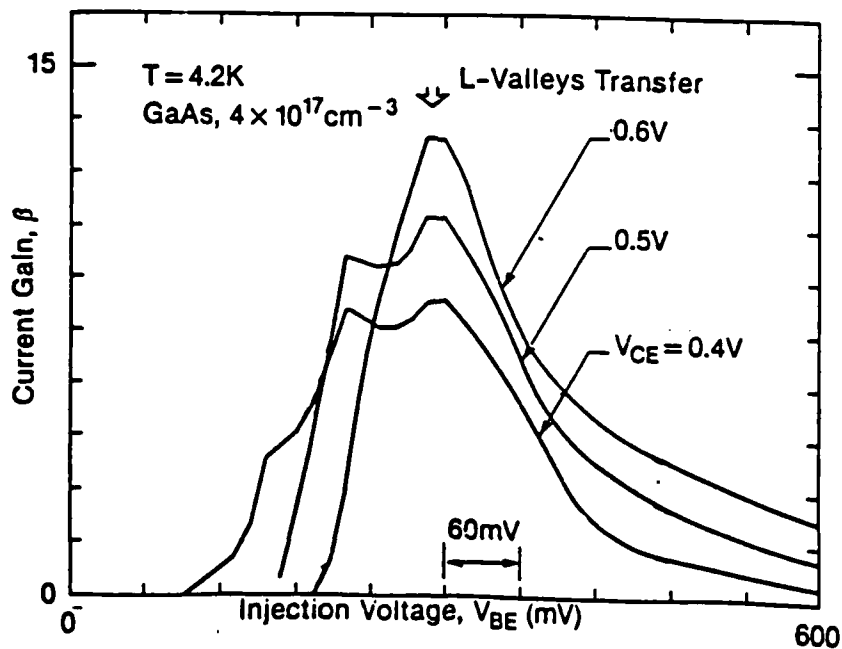


HIGHER GAIN RESULTS

$$\alpha_{\text{max}} = 0.93$$

$$\beta_{\text{max}} = 13 \text{ at } 77 \text{ K}$$

$$L_{\text{mfp}} > 300 \text{ nm}$$

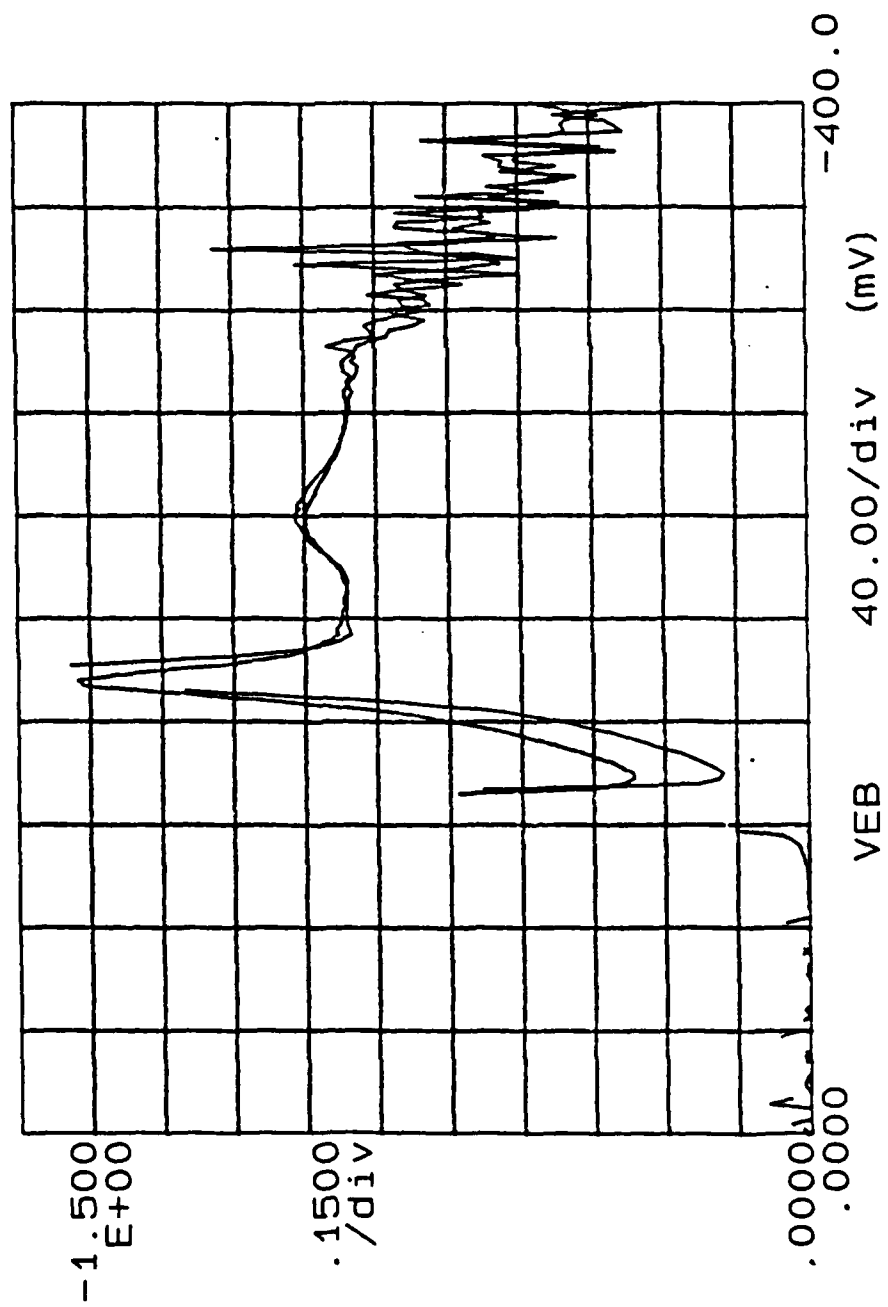


The Limiting Factor is L Valleys Transfer !

***** GRAPHICS PLOT *****

AL ()

843



Variable1:
 VEB -Ch1
 Linear sweep
 Start .0000V
 Stop .4000V
 Step .0020V

Variable2:
 VCB -Ch3
 Start .3000V
 Stop .2990V
 Step .1000V

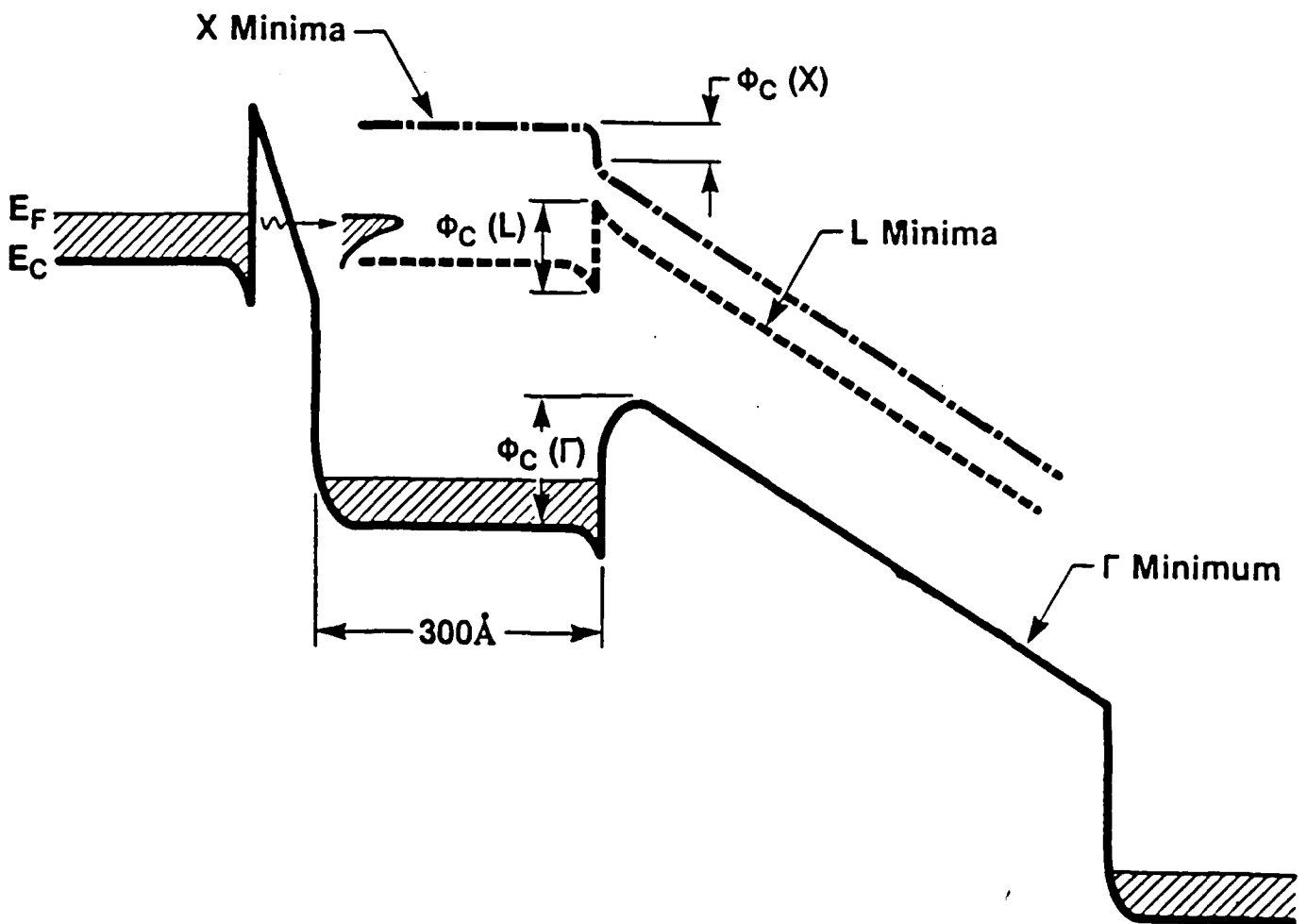
Constants:
 VB1 -Ch2 .0000V
 VB2 -Ch4 .0000V

+

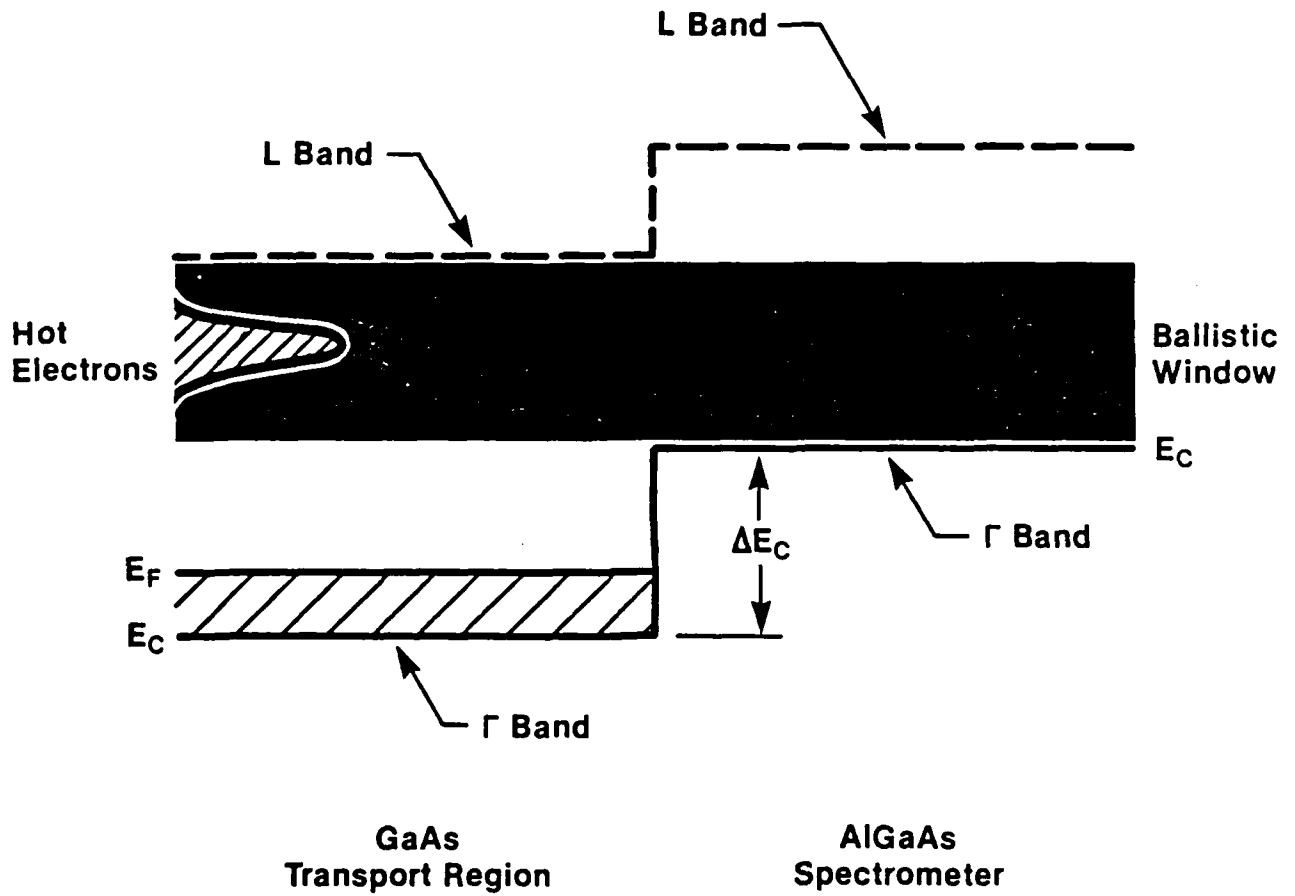
+

AL () = ΔIC/ΔIE
 SAL () = IC/IE

THE PROBLEM OF L VALLEYS TRANSFER



Window for Ballistic Transport



InGaAs PSEUDOMORPHIC BASE THETA DEVICE

(A) The Γ - L Separation in InAs is $E_{TL} = 1.16$ eV

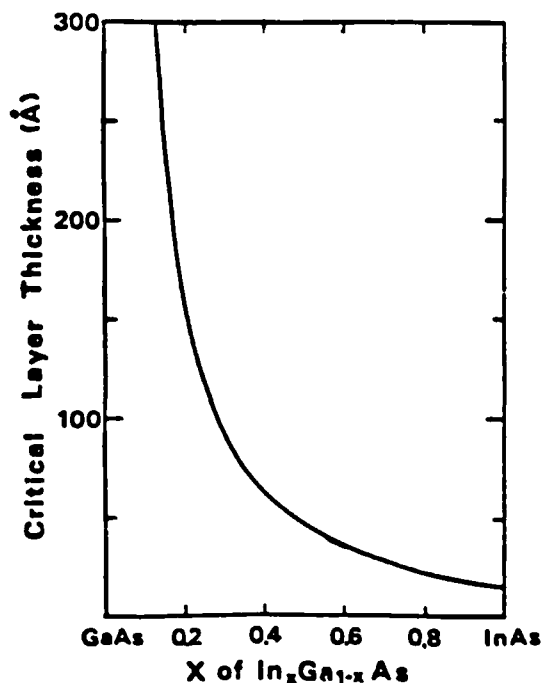
In InGaAs: 0.29 eV $< E_{TL} < 1.16$ eV

(B) There is a band discontinuity ΔE_c to GaAs

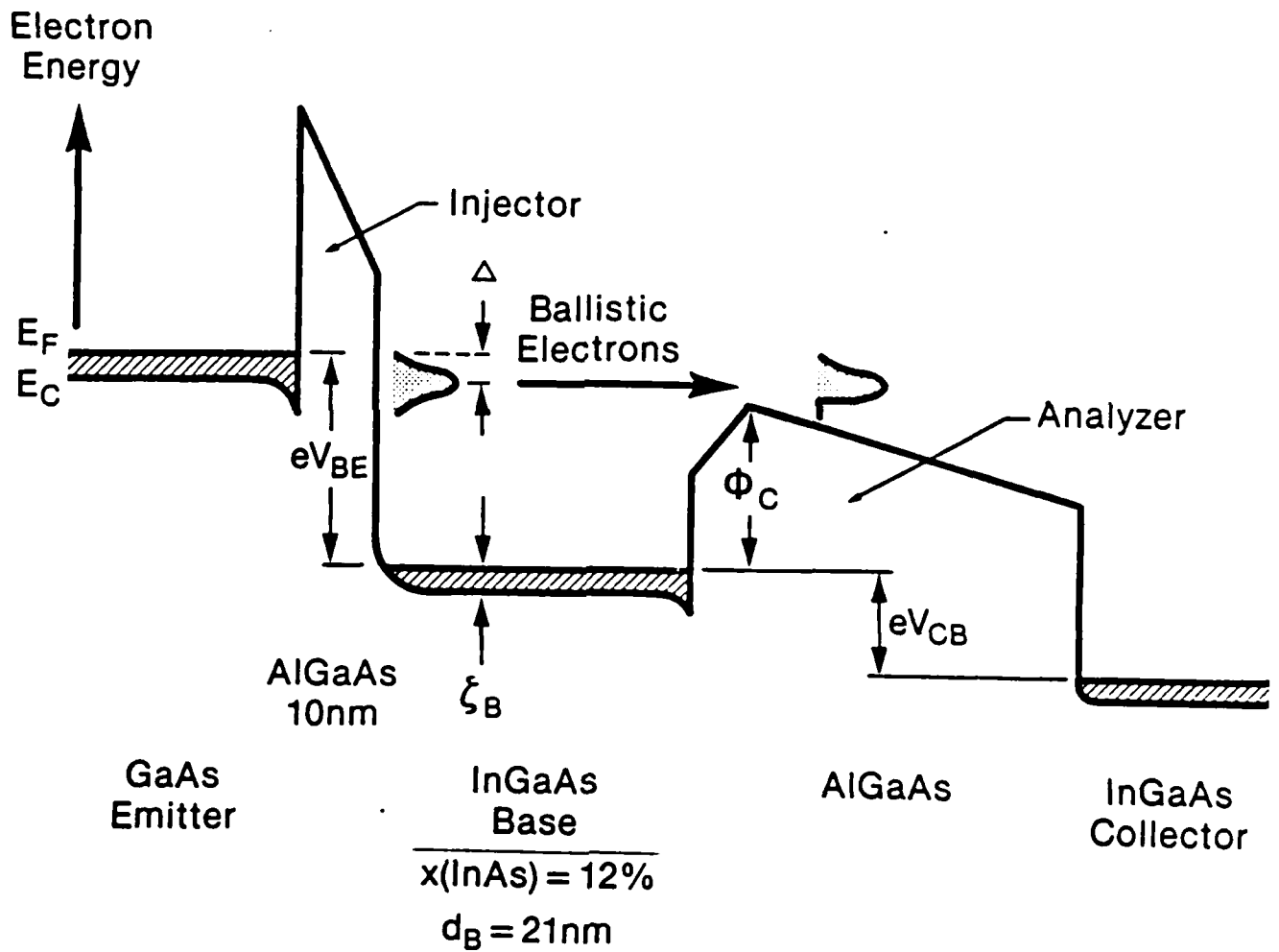
(C) InAs has a lattice constant 7% larger than GaAs.

For $In_xGa_{1-x}As$, $x=14\%$, 1% Lattice Mismatch

CRITICAL THICKNESS for each InAs mole fraction.
Below the CT Layers Can Grow
PSEUDOMORPHIC

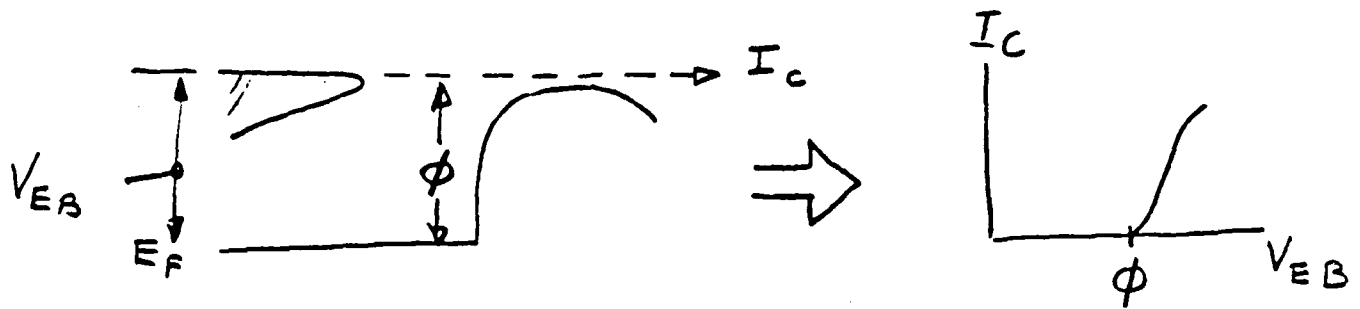


Pseudomorphic Base THETA



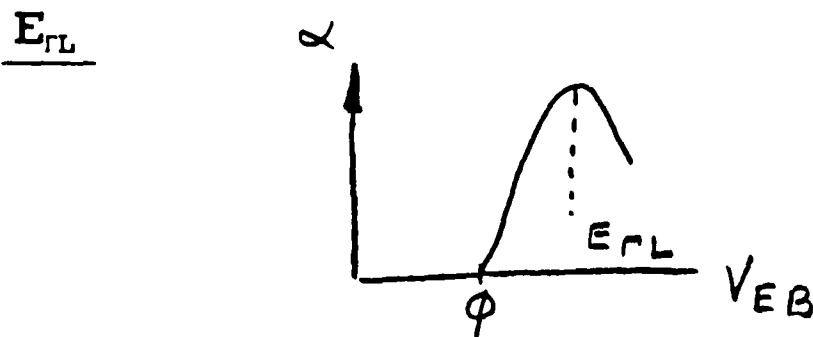
CHARACTERISTICS OF InGaAs BASE DEVICE

The Extra Band Discontinuity

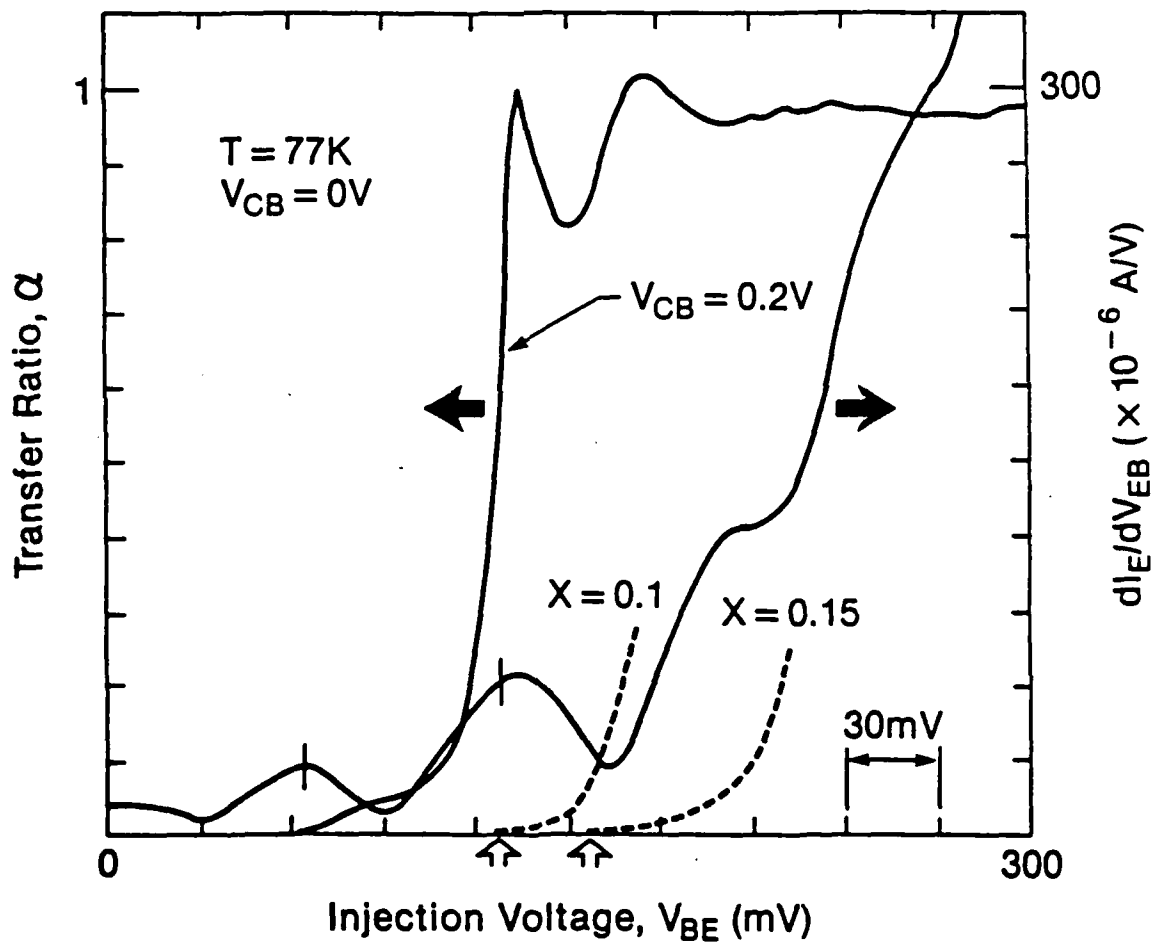


$$\Delta E_C(\text{GaAs} - \text{In}_x\text{Ga}_{1-x}\text{As}) = 7.5 \text{ meV}/1\%$$

$$\text{For } x=15\% \dots \dots \dots \Delta E_C = 110 \text{ meV}$$

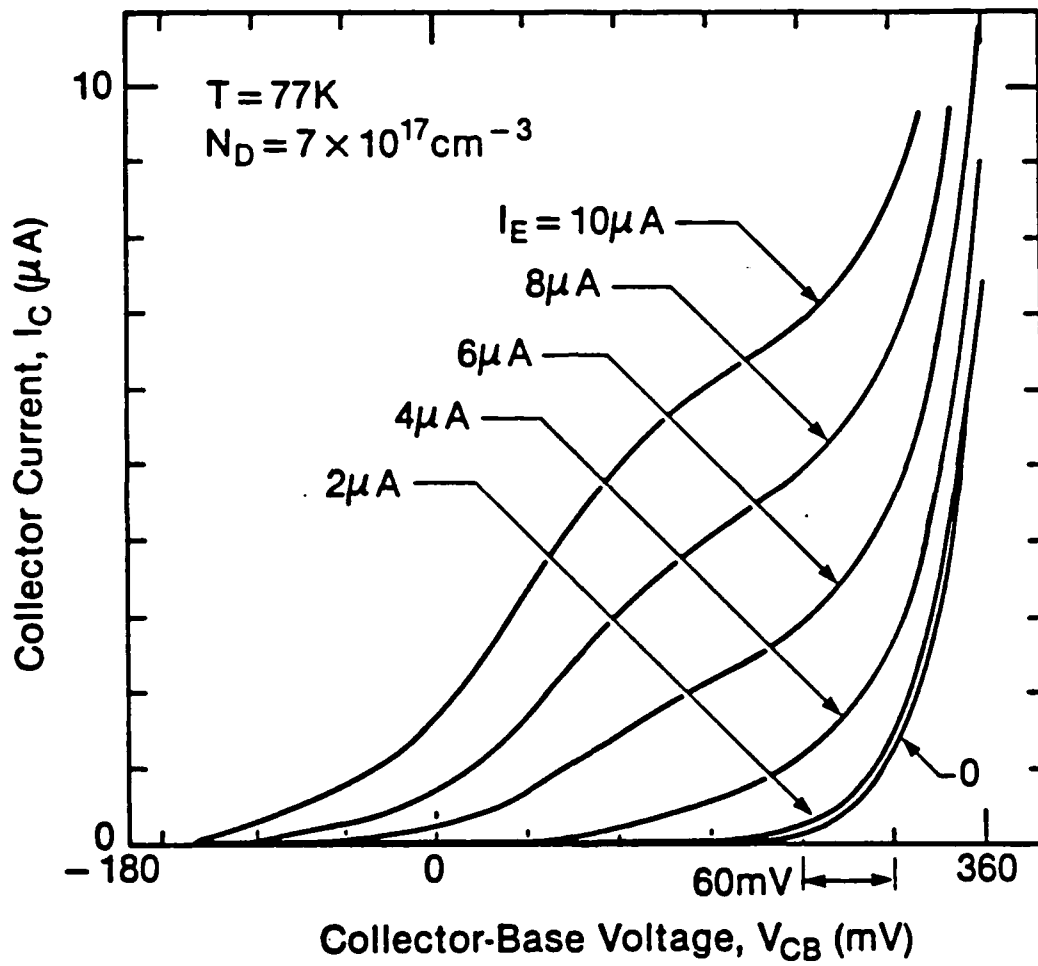


$x=0$	$\dots \dots \dots E_{TL} = 0.29 \text{ eV}$
$x=0.12$	$\dots \dots \dots E_{TL} = 0.38 \text{ eV}$
$x=0.15$	$\dots \dots \dots E_{TL} = 0.41 \text{ eV}$



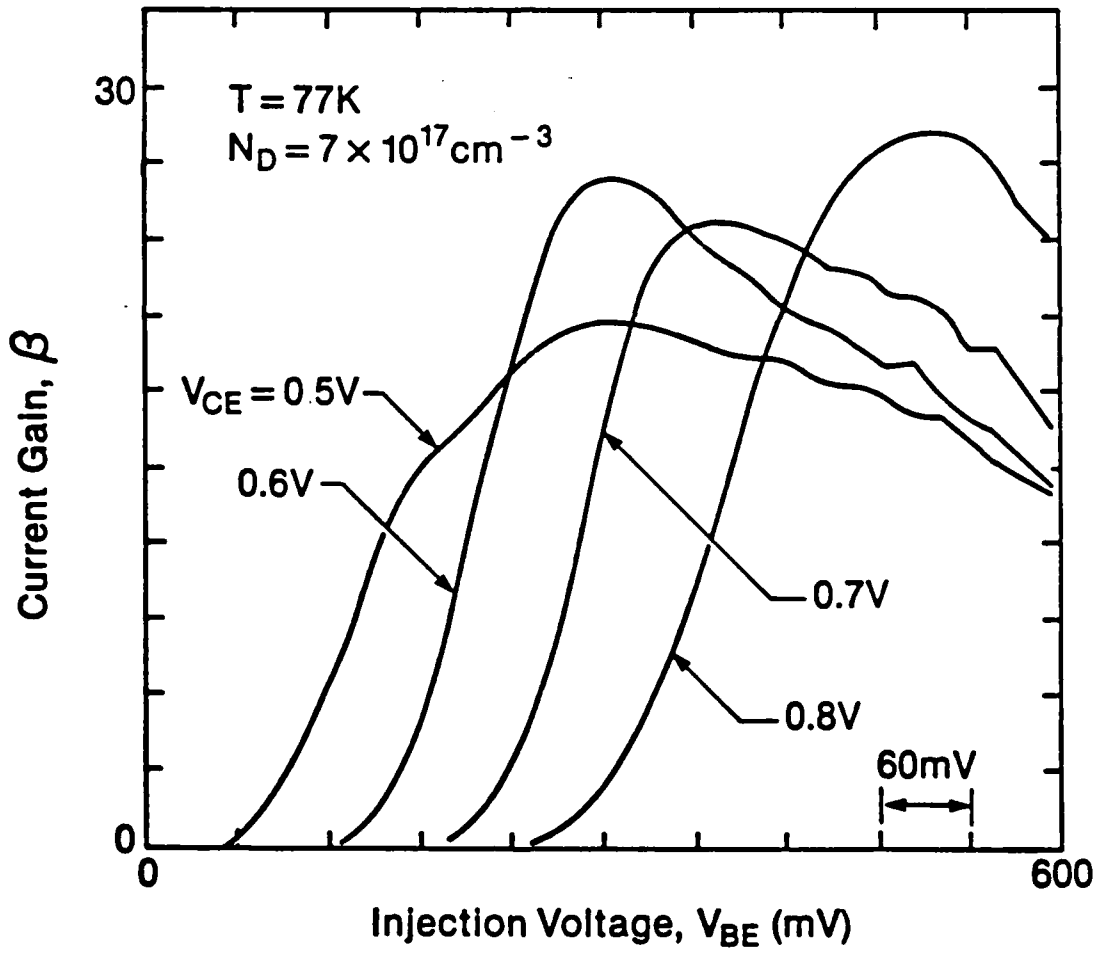
(b)

InGaAs Base, CBC



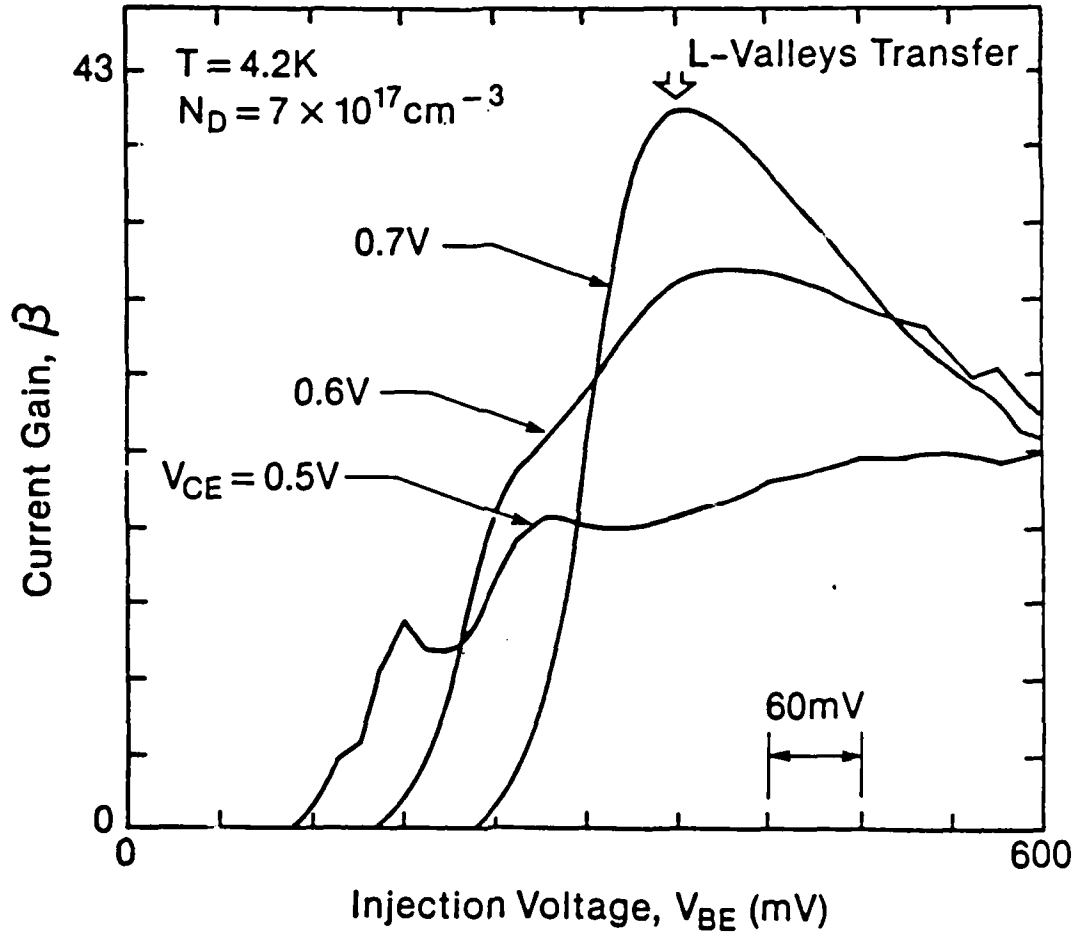
InGaAs Base

CEC, Current Gain at 77K



InGaAs Base

CEC, Current Gain at 4.2K



$$\alpha_{\max} = 0.975$$

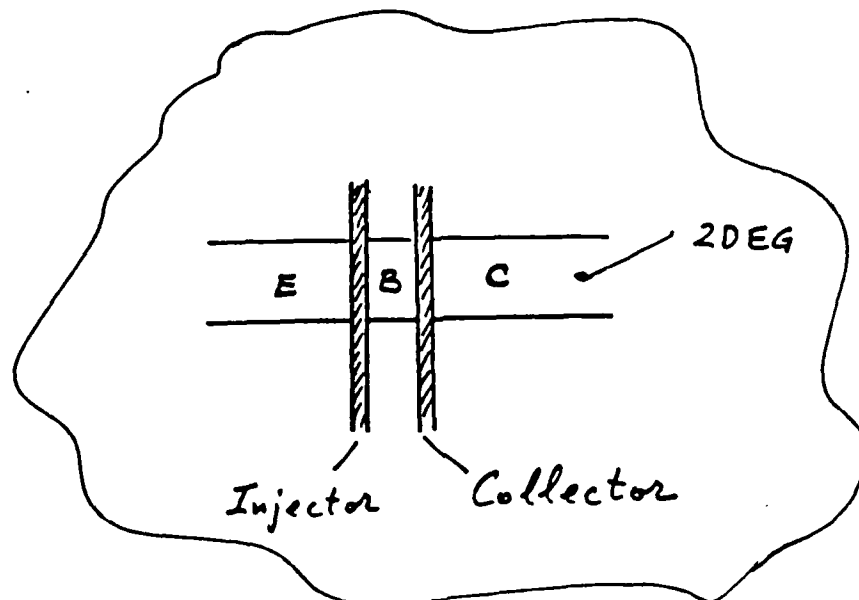
$$L_{\text{mfp}} > 800 \text{ nm}$$

Device Achievements

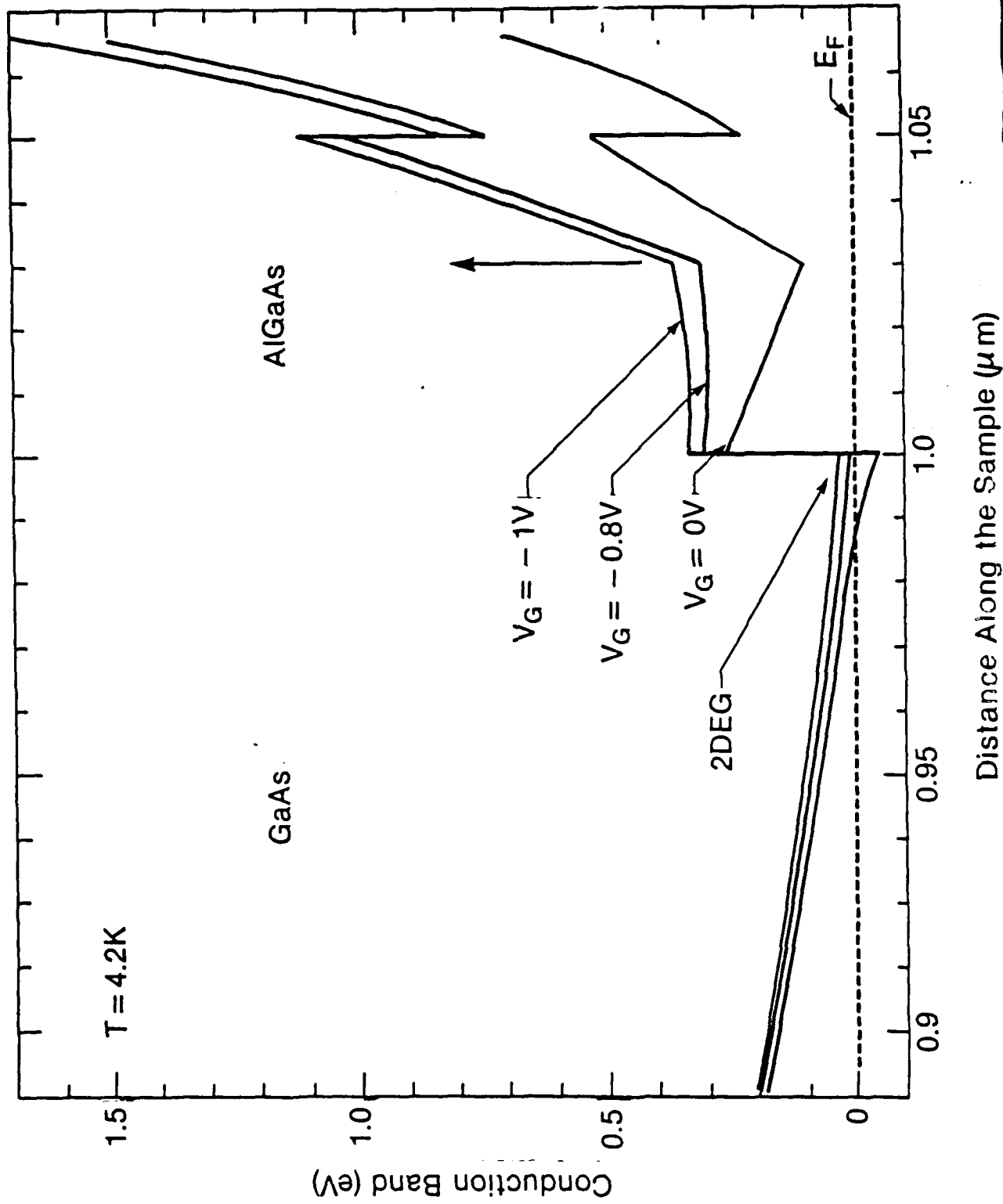
- Until Recently : $\beta_{\max} \cong 9$
- Reduced Base Doping $\rightarrow 4 \times 10^{17} \text{cm}^{-3}$
 $d_B \cong 250 \text{\AA}$
 $\beta_{\max} \cong 13 (4.2\text{K})$
- Increase Γ -L Valleys Separation by an InGaAs Pseudomorphic Base
 $\beta_{\max} \cong 40 (4.2\text{K})$
 $\beta_{\max} \cong 30 (77\text{K})$

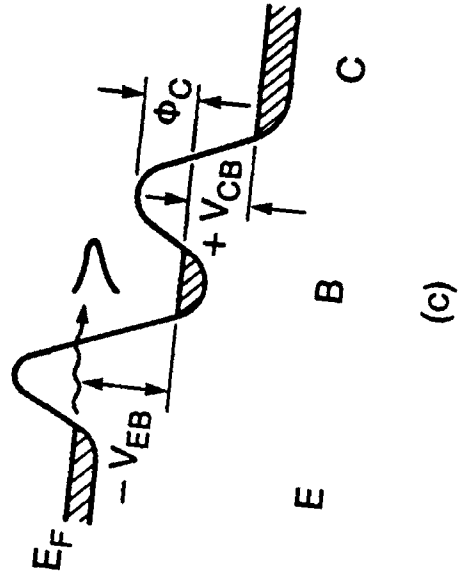
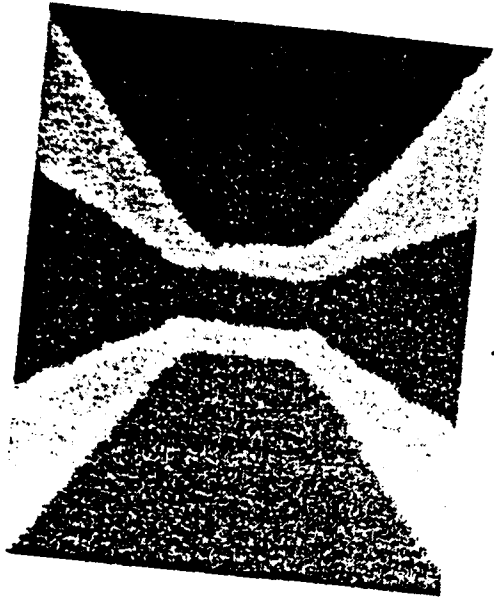
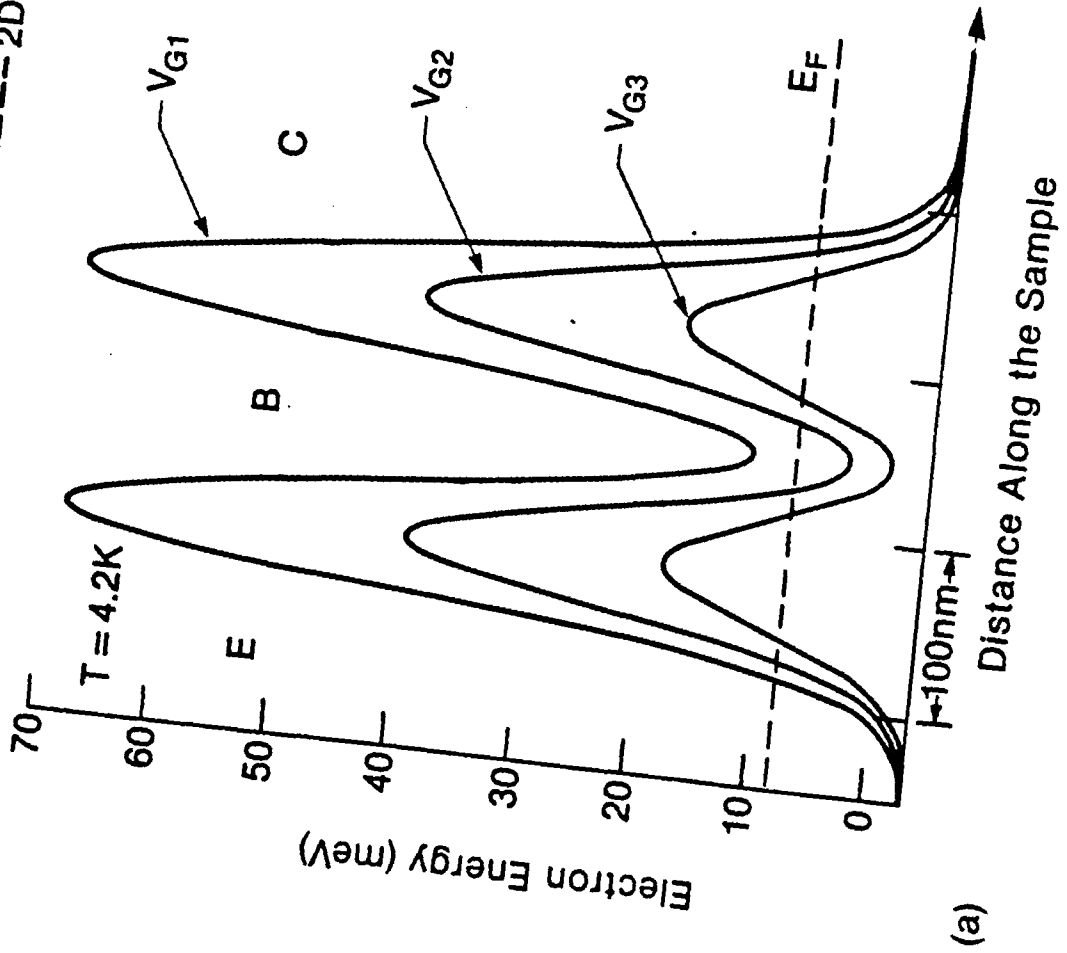
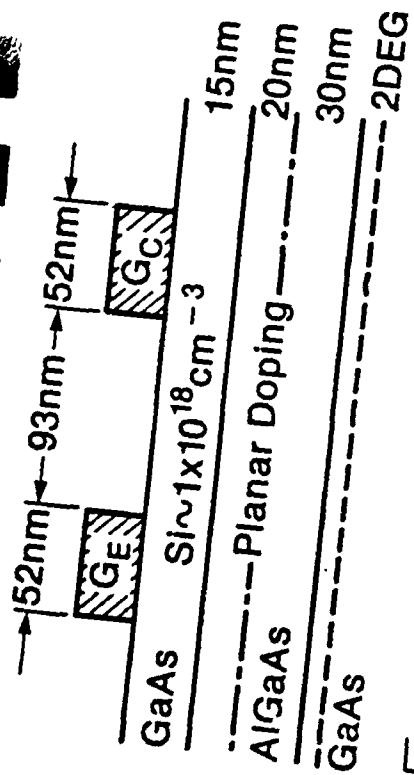
A LATERAL BALLISTIC DEVICE

- Easy Contacting to Regions of the Device
- Using 2DEG as the Medium for Transport - Long Ballistic mfp
- An Added Lateral Dimension - Possibility of Stirring Electrons in the Plane



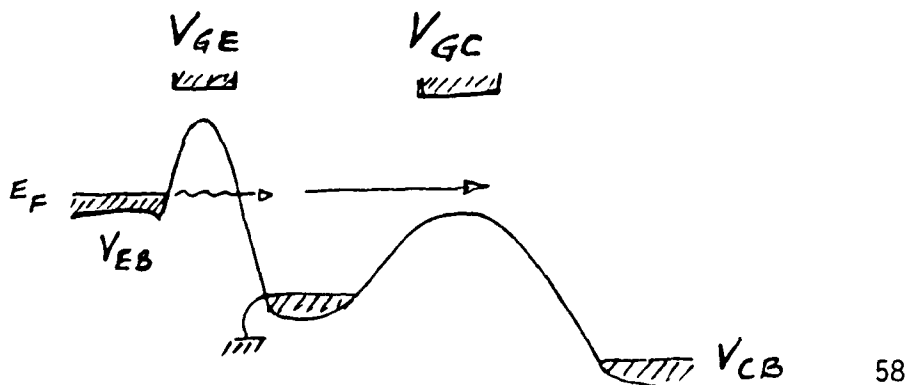
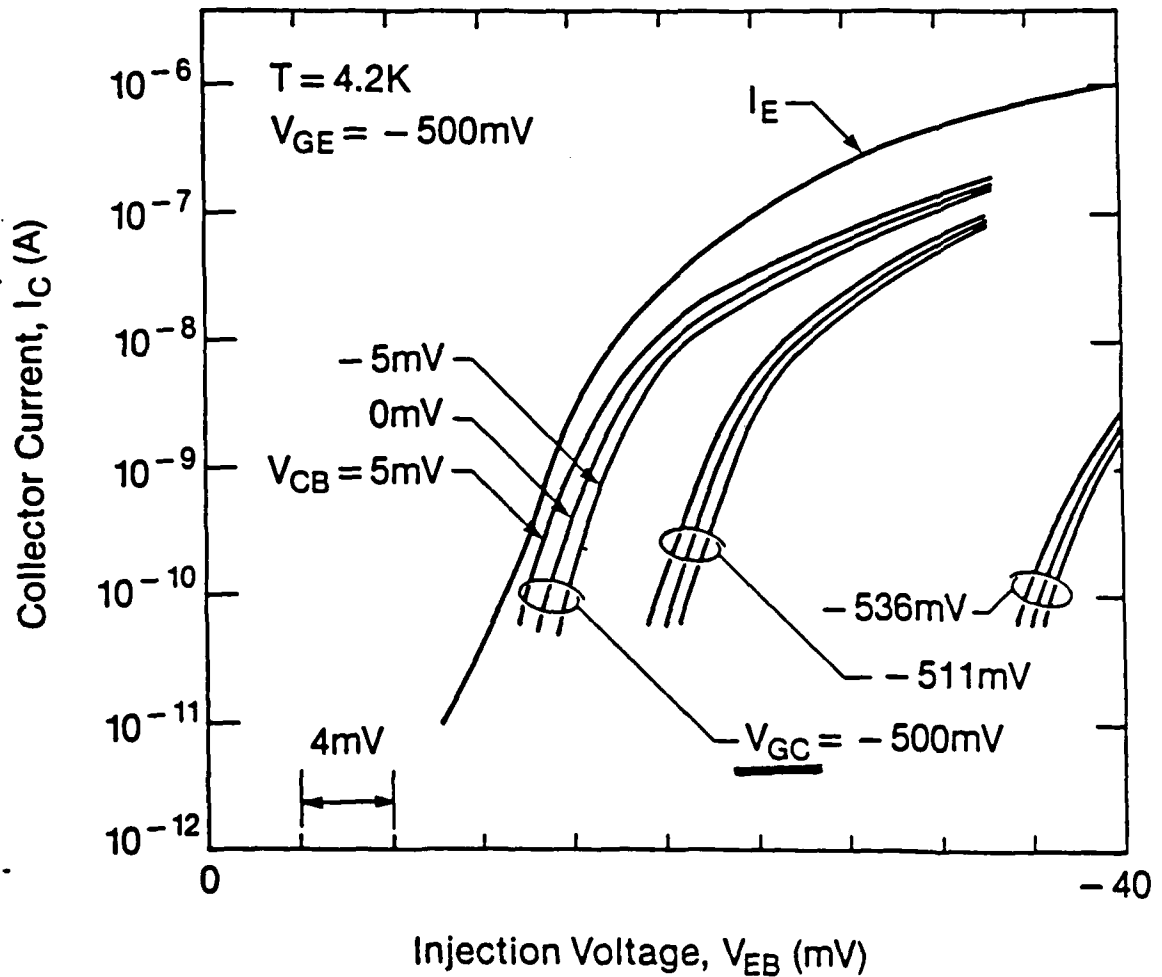
Biasing a 2DEG with a Gate



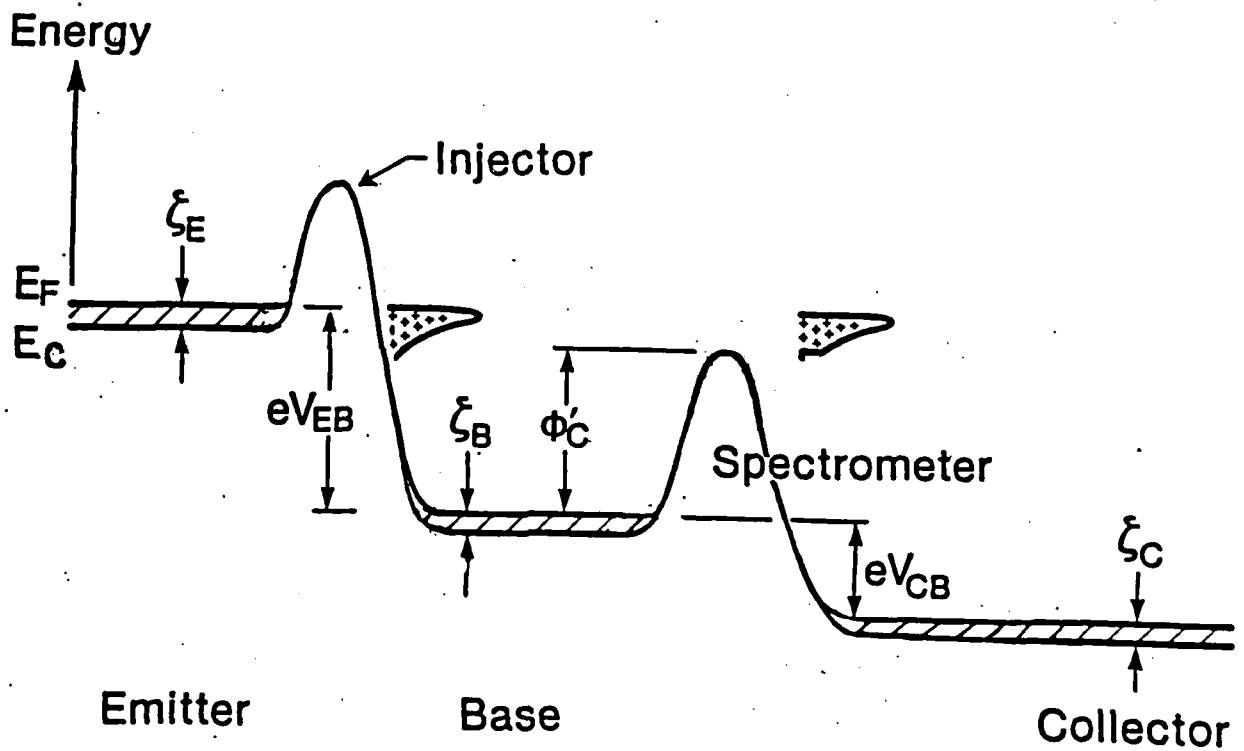


Collector Current Onset Changes

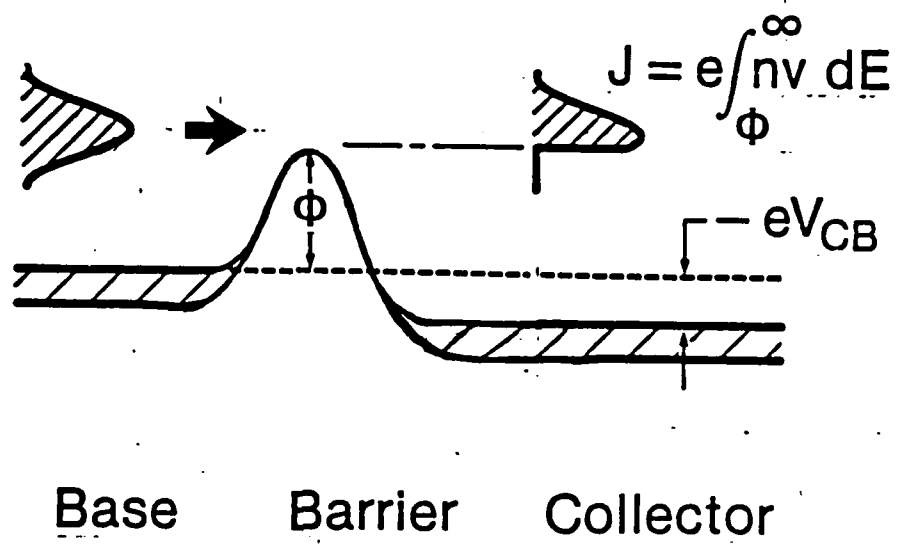
PROOF OF ELASTIC TUNNELING



Ballistic Transport and Spectroscopy in Lateral THETA Device



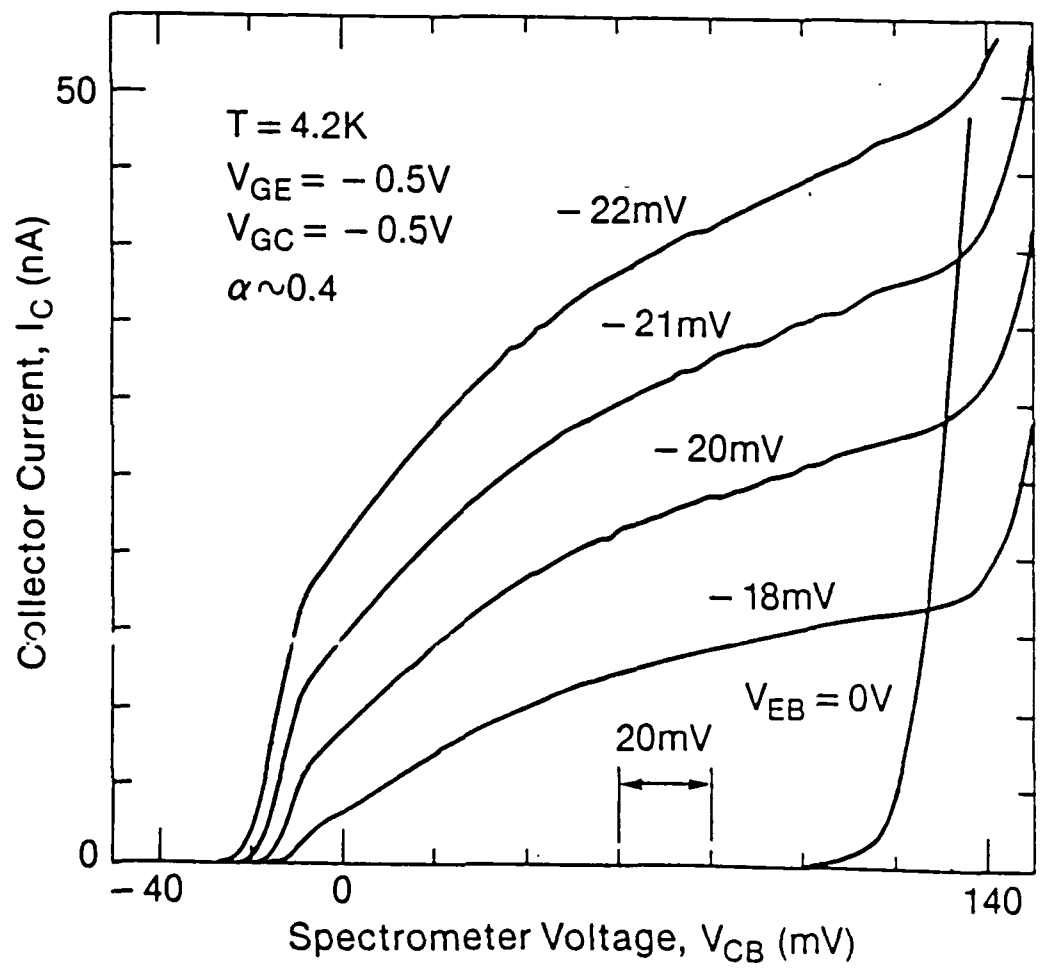
Spectroscopy of Ballistic Electrons



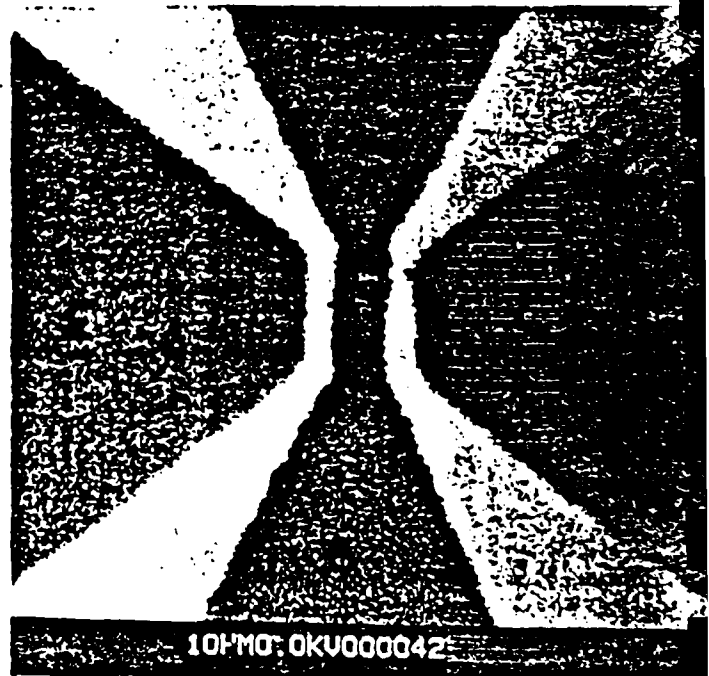
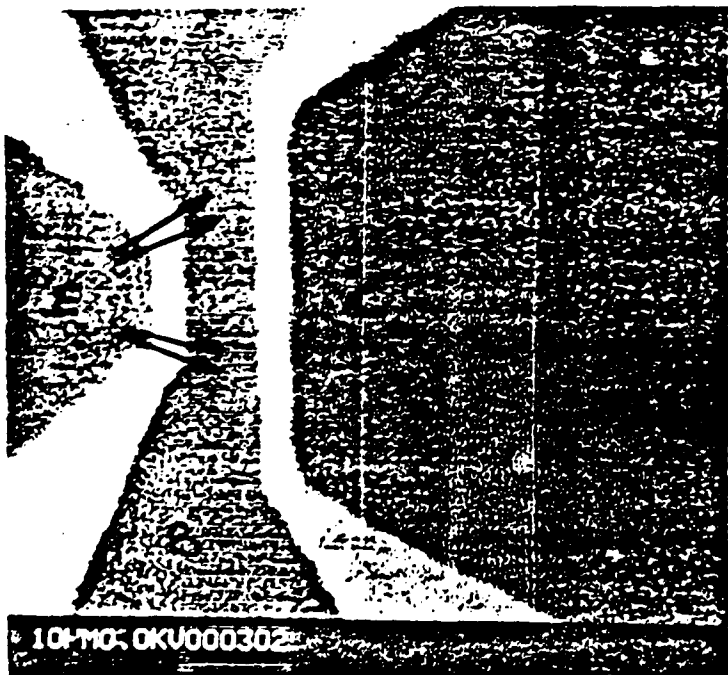
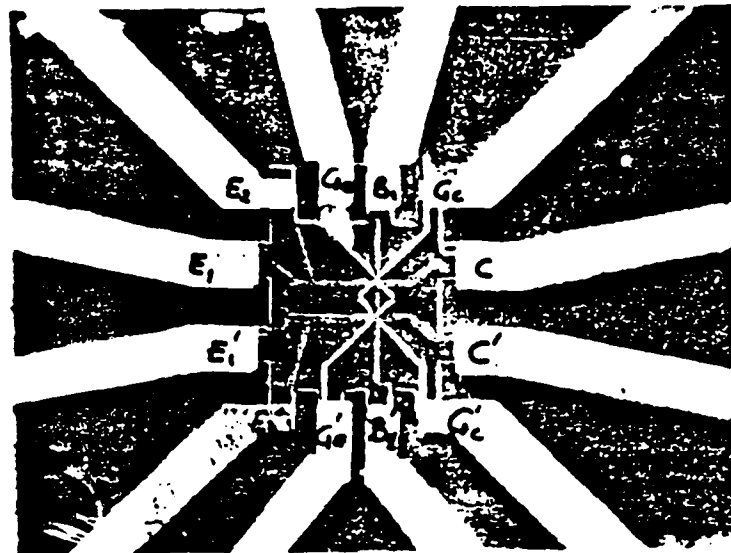
$$nv \sim \frac{dJ}{d\phi} = \frac{\frac{dJ}{dV_{CB}}}{\frac{d\phi}{dV_{CB}}}$$

Measured

Output Characteristics in a Common Base Configuration

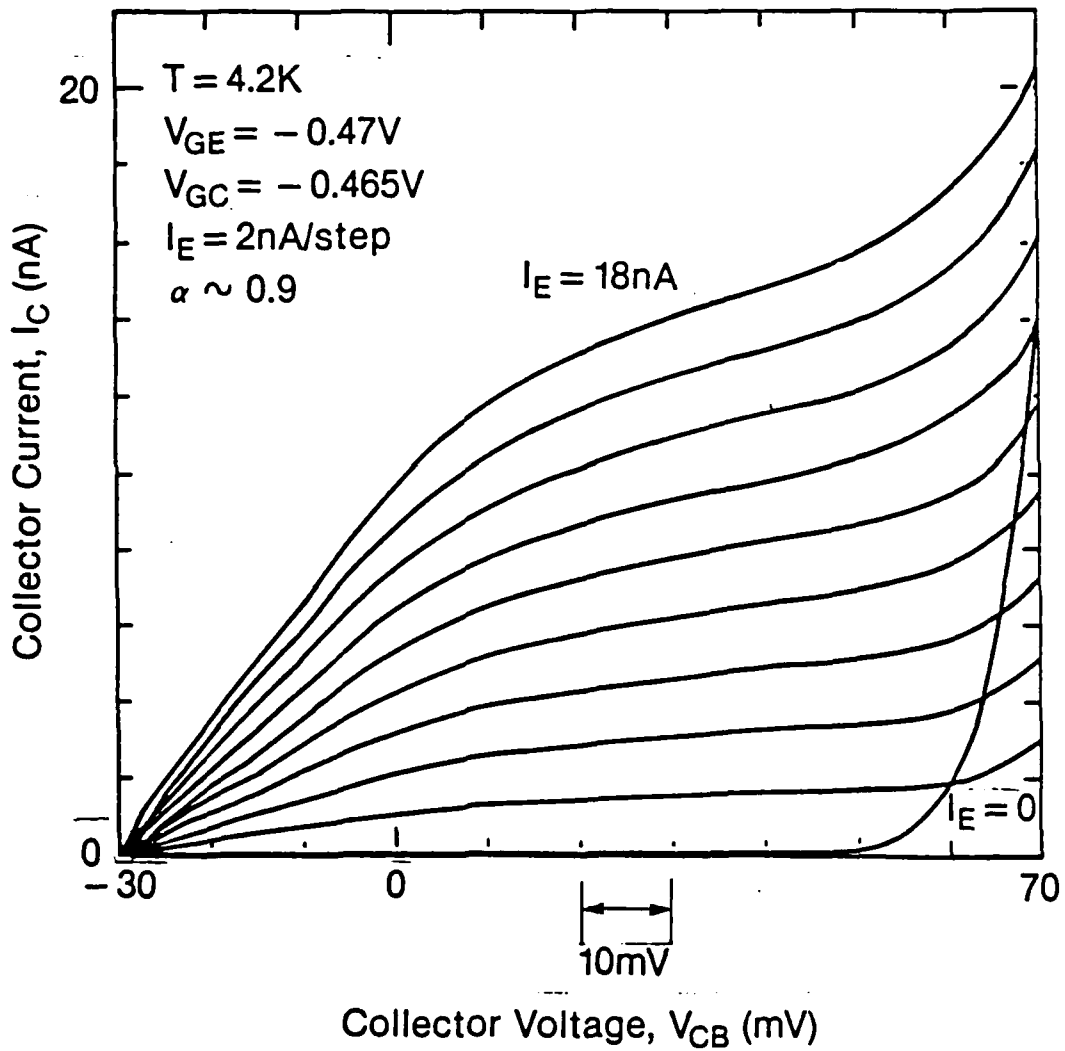


Geometry of the Gates and Formation of Ohmic Contact to a Base.

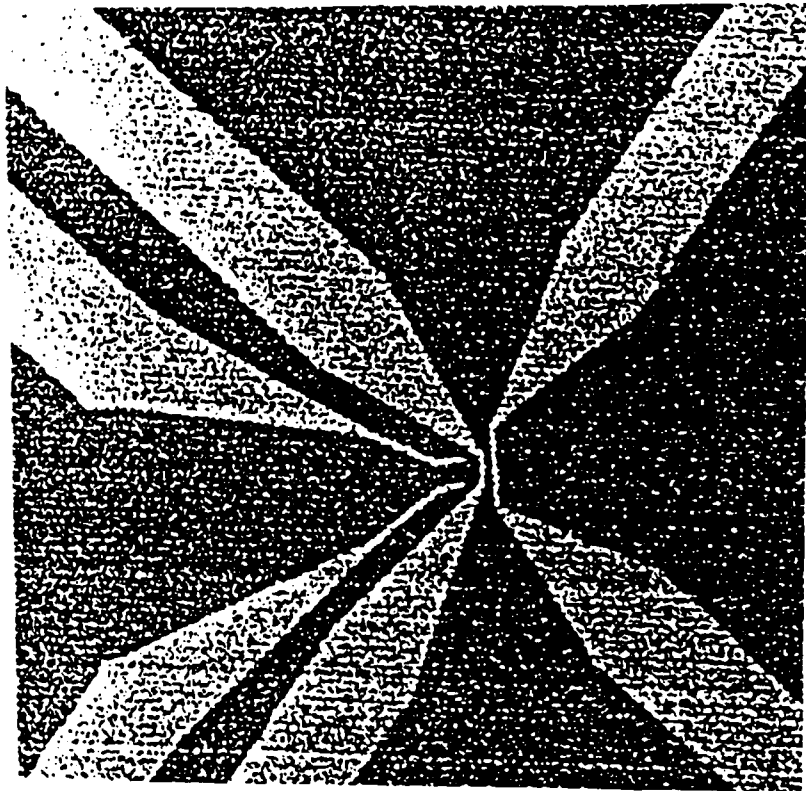


Common Base Configuration

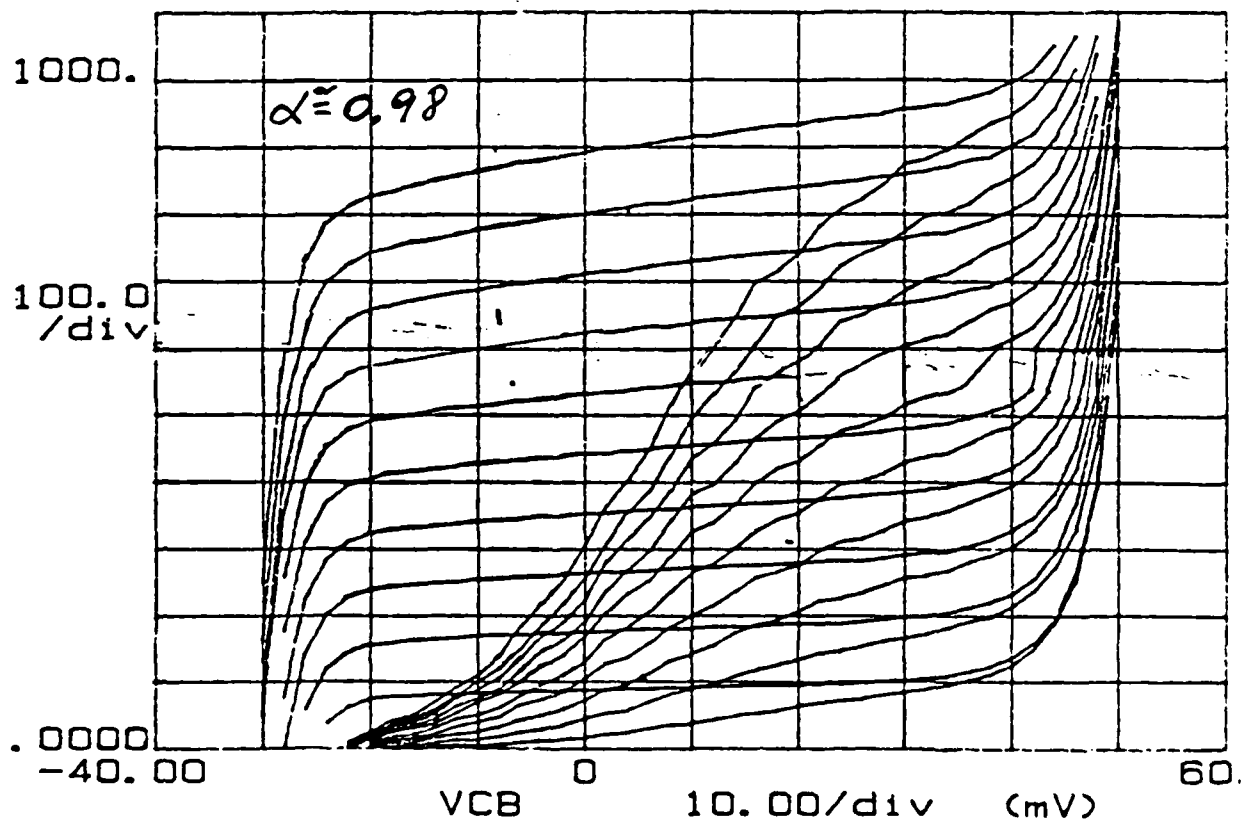
LATERAL THETA



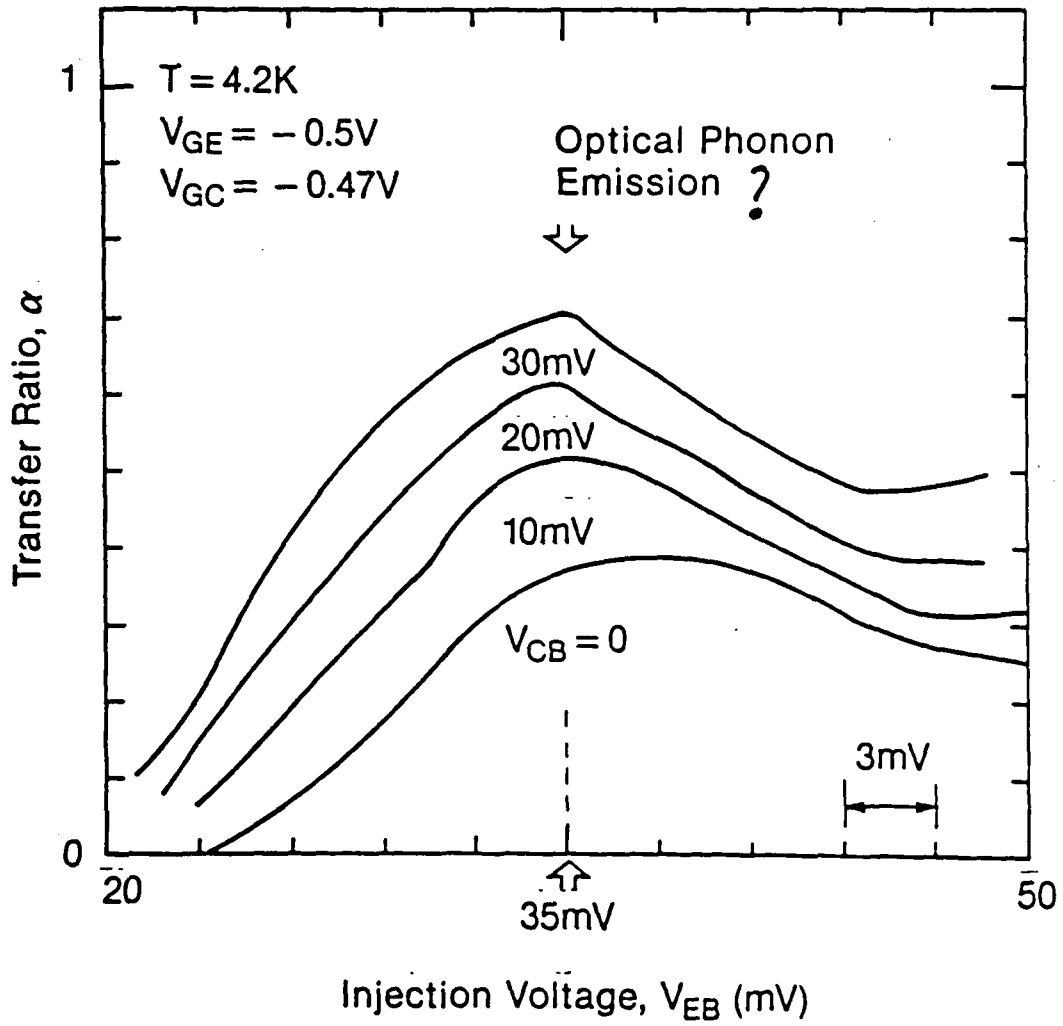
$$\alpha \approx 0.9$$



IC
(pA)



Optical Phonon Emission



$$\alpha = \exp\left(-\frac{d_E}{\lambda}\right) = .7$$

$$\lambda \approx 480 \text{ nm}$$

Conclusions

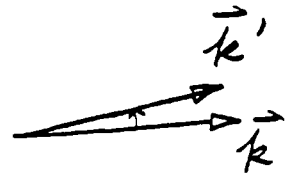
- Proof of Lateral Tunneling through a Wide Barrier
- Proof of Lateral Ballistic Transport with a Long Mean Free Path
- Possible High Gain THETA device.
- New Experimental Tool for Studying Quantum Properties of Electron Transport

PHYSICS WITH THE THETA DEVICE

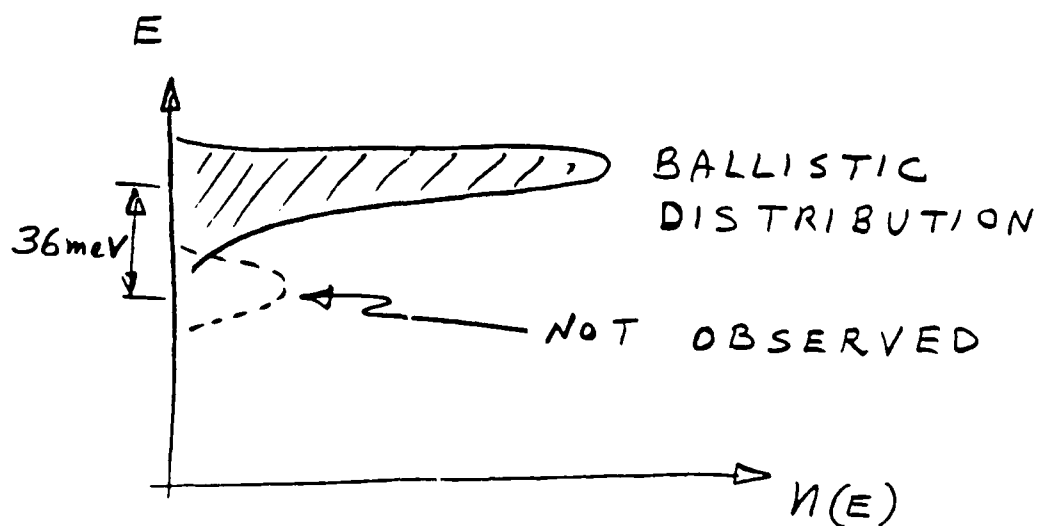
- Observation of Ballistic Transport
(Electrons and Holes)
- Observation of Quantum Interference Effects
(Electrons and Holes)
- Observation of L Valleys Transfer
- Measuring Band Discontinuities
- Observation of a Single Phonon Emission

PHONON EMISSION

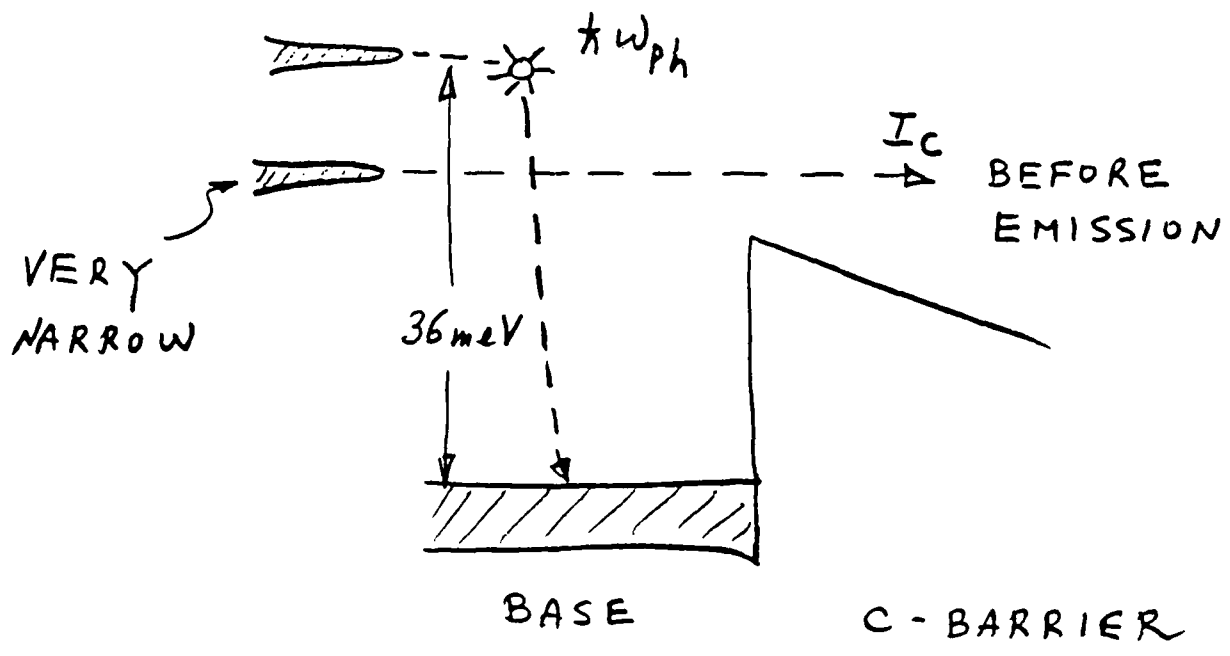
- Dominant Phonon Scattering is due to LO Phonons in GaAs.
- Scattering $\sim |\vec{k} - \vec{k}'|^{-2}$,
Small Angle Scattering is Preferred
- Phonon Energy in Unscreened GaAs, $\hbar\omega_{LO} = 36 \text{ meV}$
- At Low Temperatures Only Phonon Emission Dominates



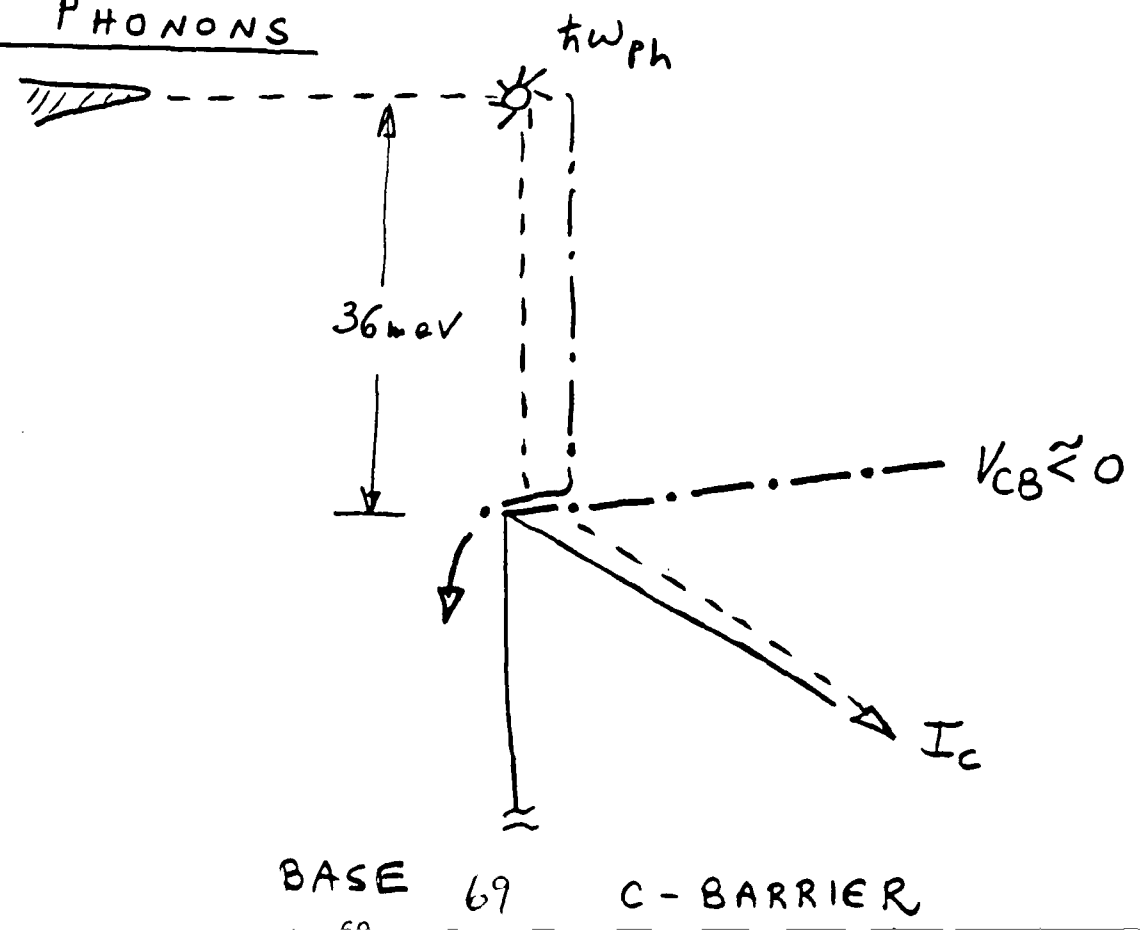
Experimentally: We did not Observe Phonon Emission via Spectroscopy



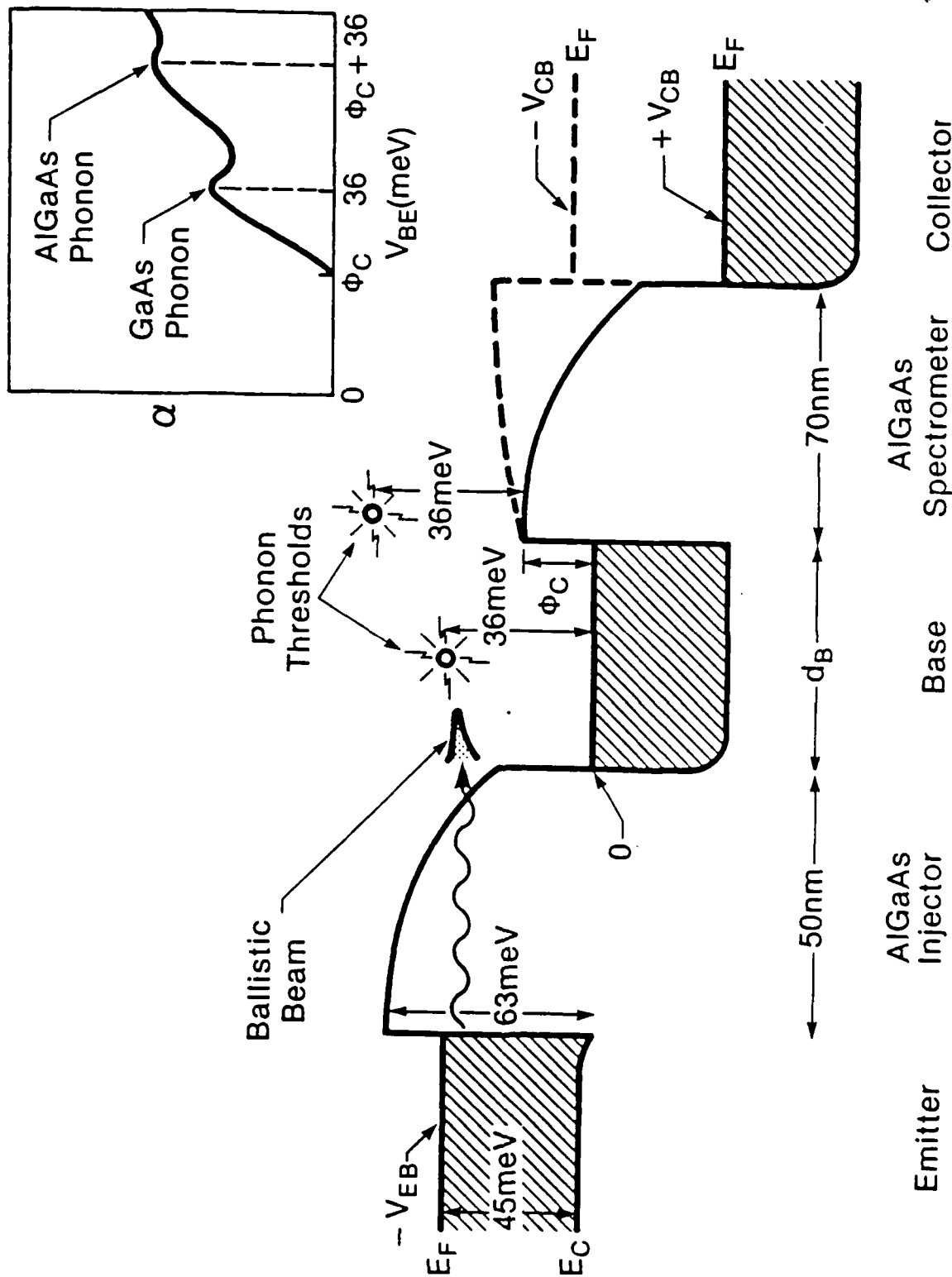
GaAs PHONONS



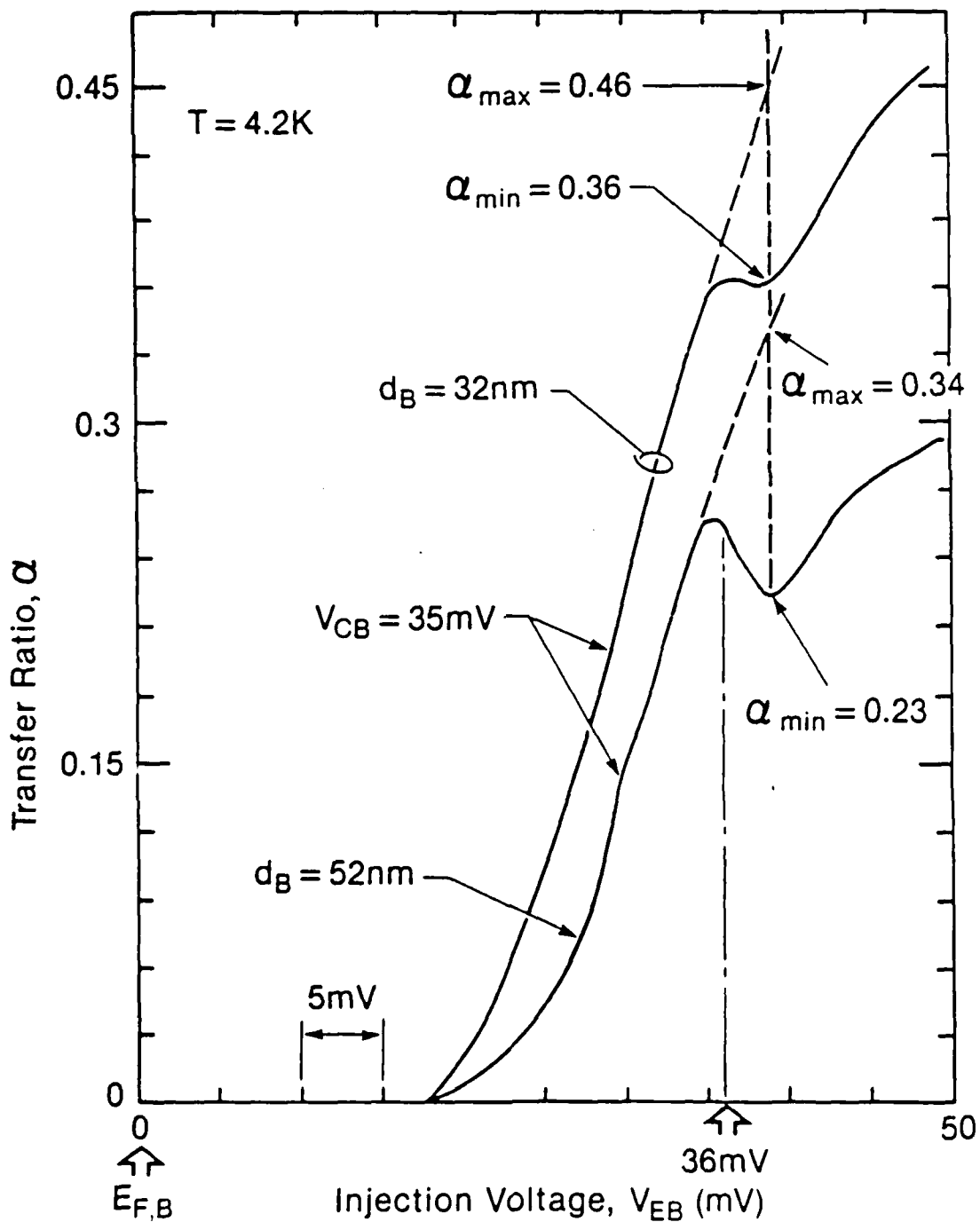
AlGaAs PHONONS



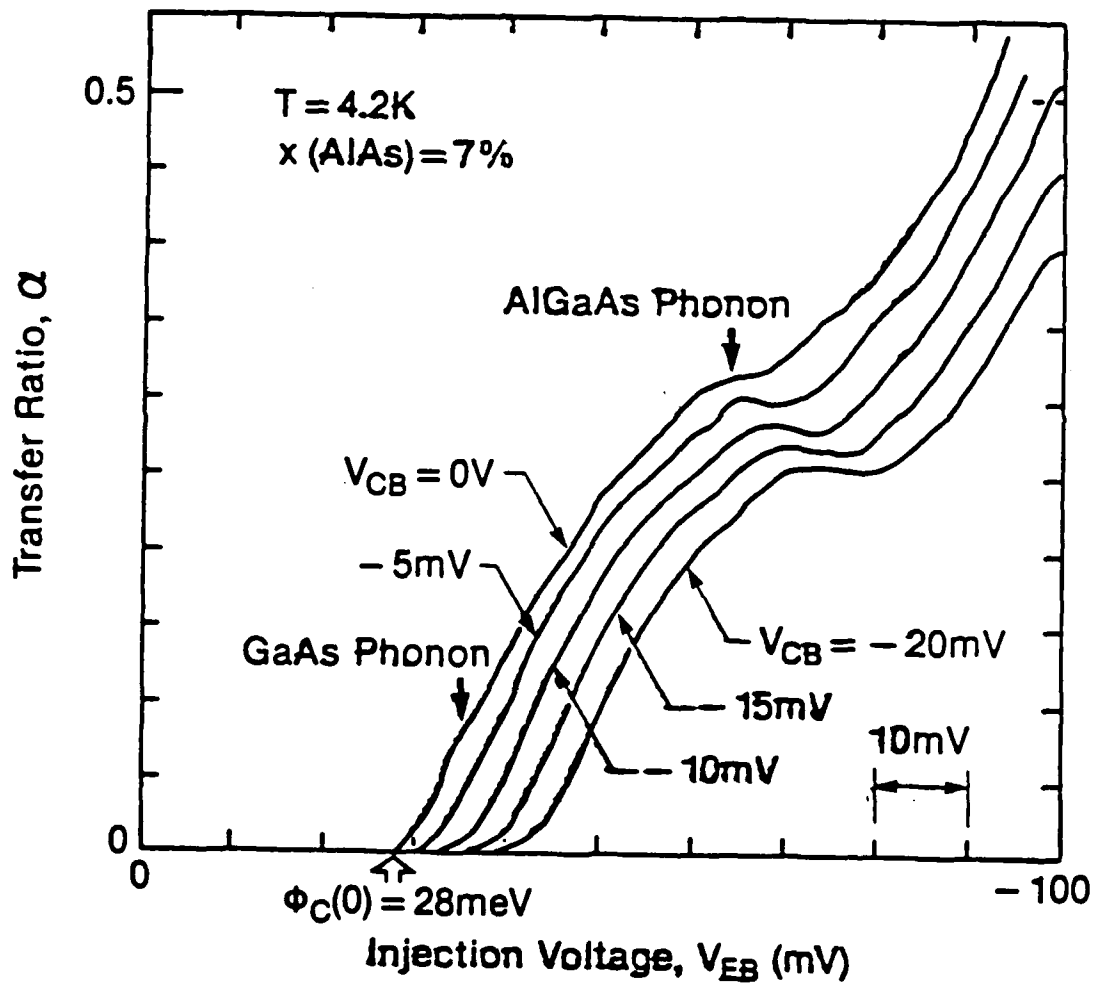
Ballistic Electrons Emitting Phonons



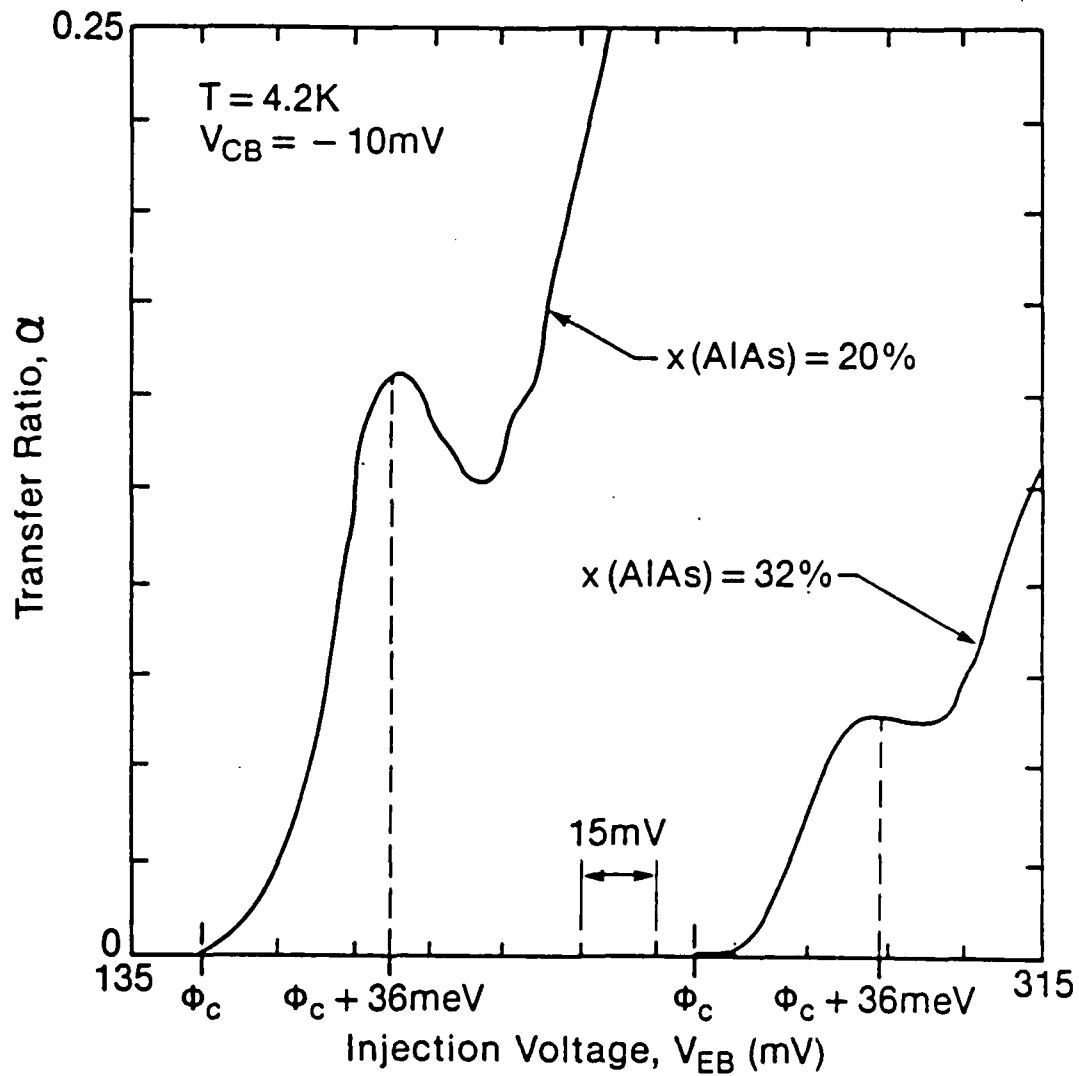
Observation of Single Phonon Emission in GaAs



$$l_{\text{mfp}} \approx 130 \text{ nm}$$



Observation of Single Phonon Emission in AlGaAs



Permeable Base Transistor and Regrowth FET Development

Mark A. Hollis

*MIT Lincoln Laboratory
Lexington, MA*

PBT AND REGROWTH FET DEVELOPMENT

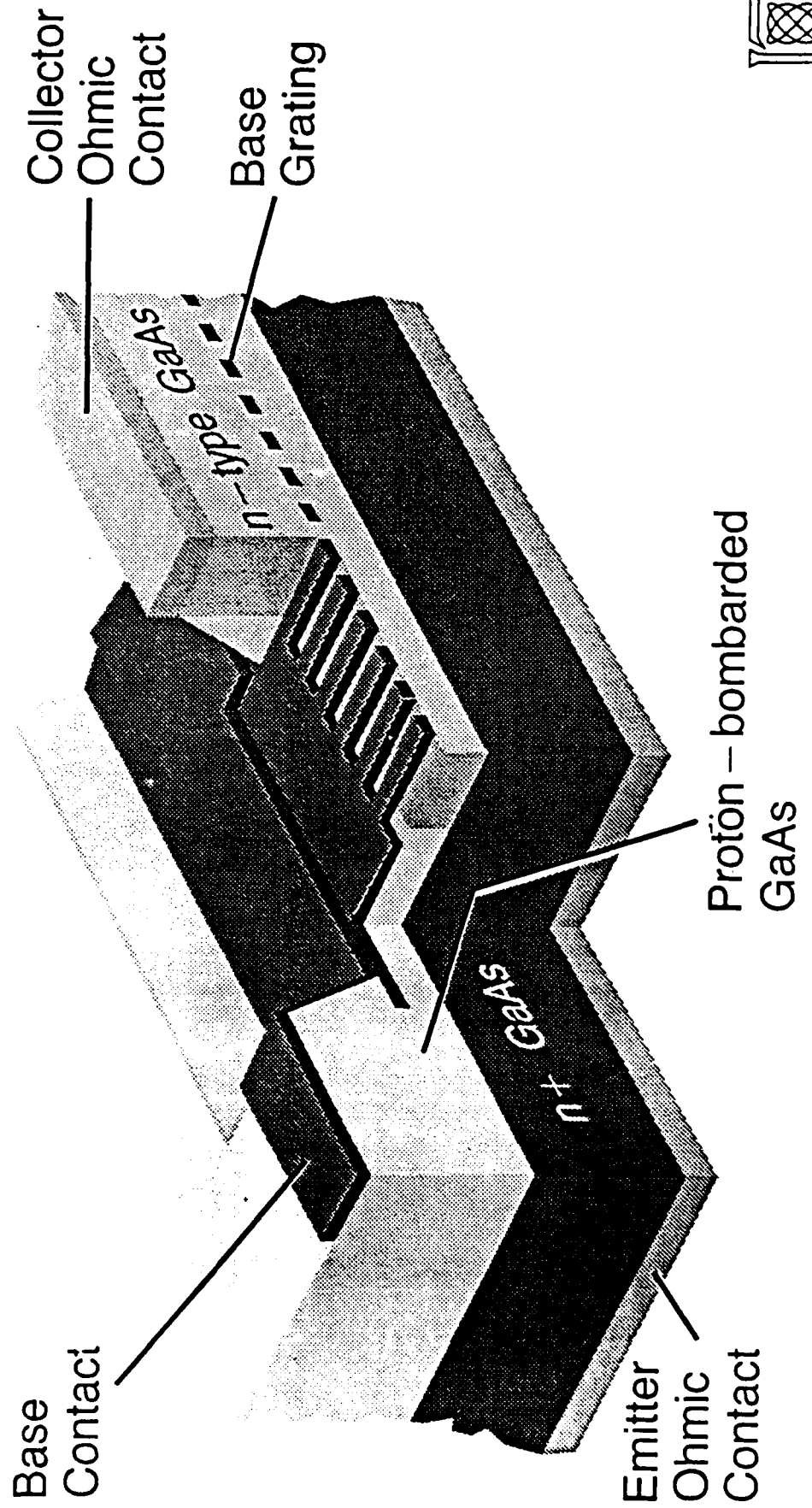
MARK A. HOLLIS

MIT LINCOLN LABORATORY

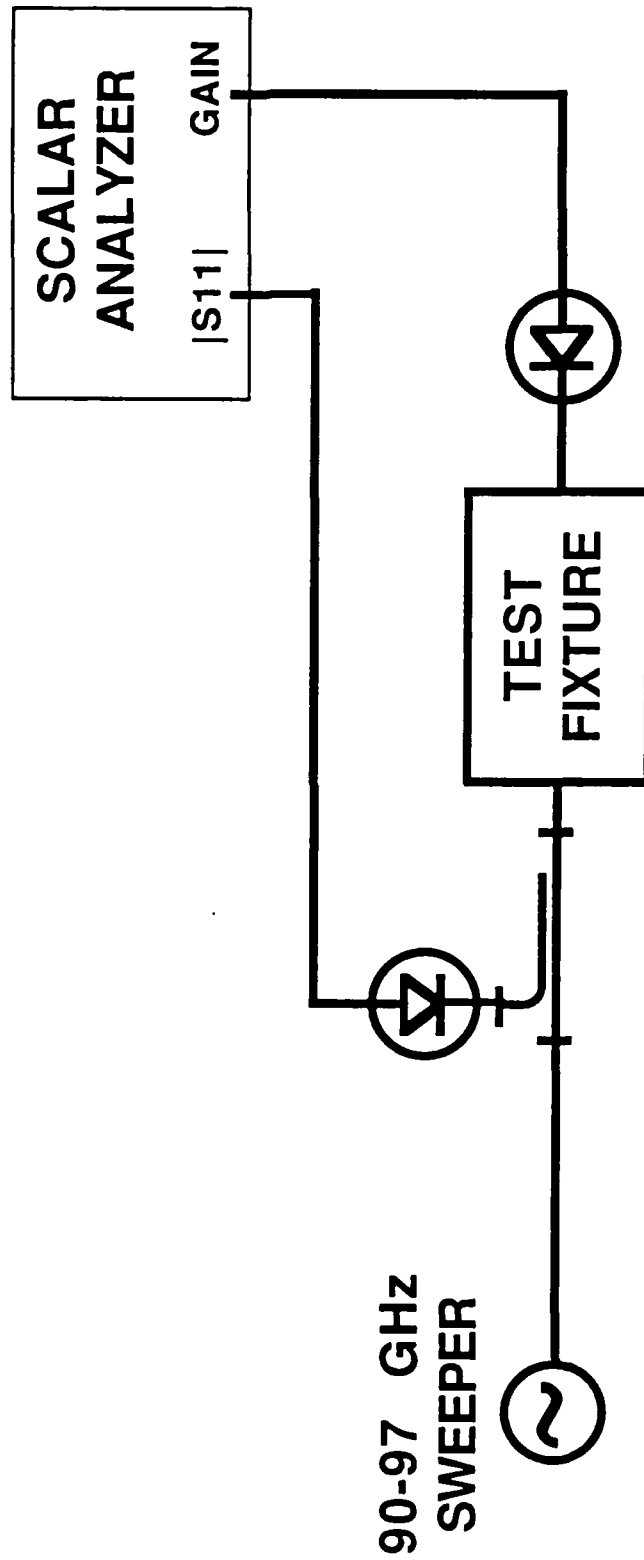
- **PERMEABLE BASE TRANSISTOR**
 - **94 GHz PERFORMANCE**
 - **PBTs ON SEMI-INSULATING SUBSTRATES**
 - **REDUCED-PERIODICITY PBT**
 - **PBT PERFORMANCE DATA**
 - **YIELD AND MANUFACTURABILITY**
 - **SUMMARY**

- **REGROWTH FIELD-EFFECT TRANSISTOR**
 - **BASIC STRUCTURE**
 - **FABRICATION SEQUENCE**
 - **PROCESS DEVELOPMENT**
 - **SUMMARY**

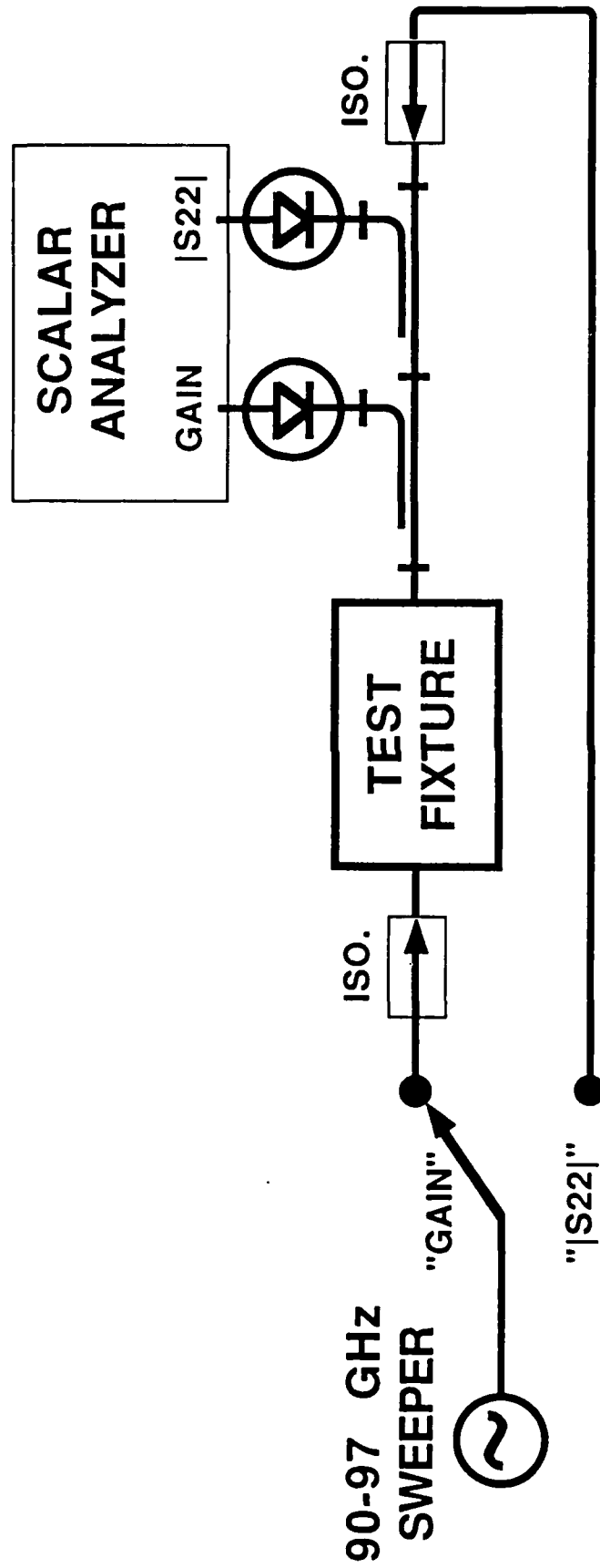
PERMEABLE BASE TRANSISTOR



90-97 GHz Scalar Test Set

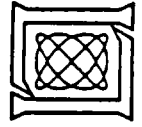
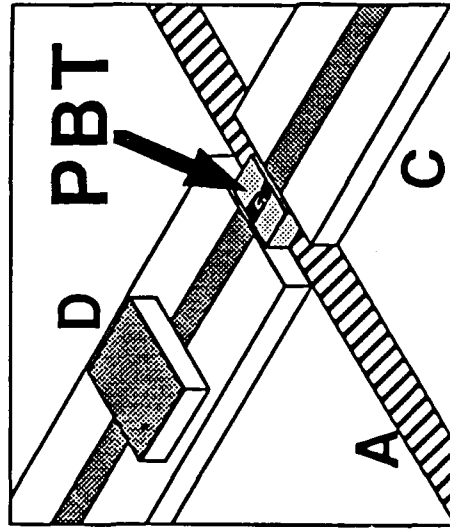
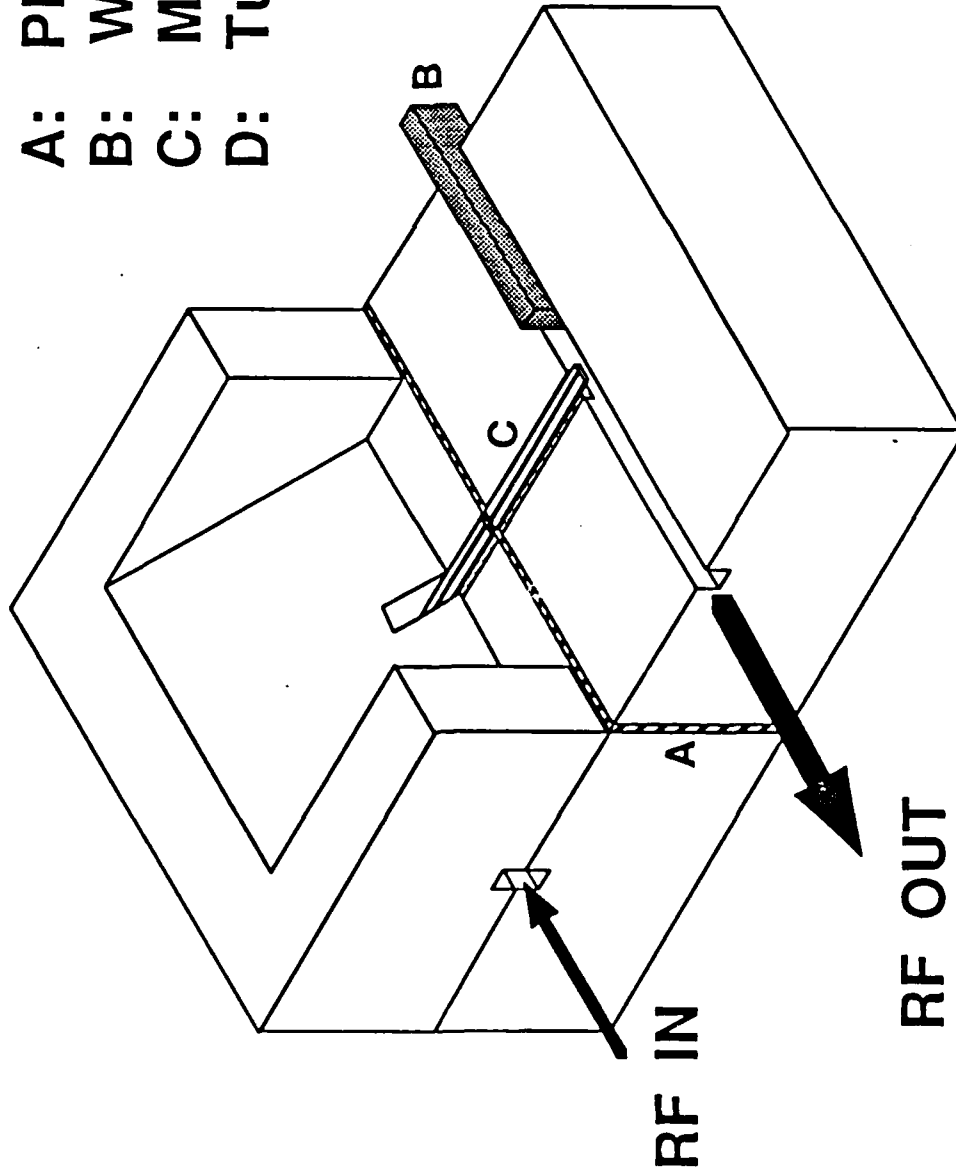


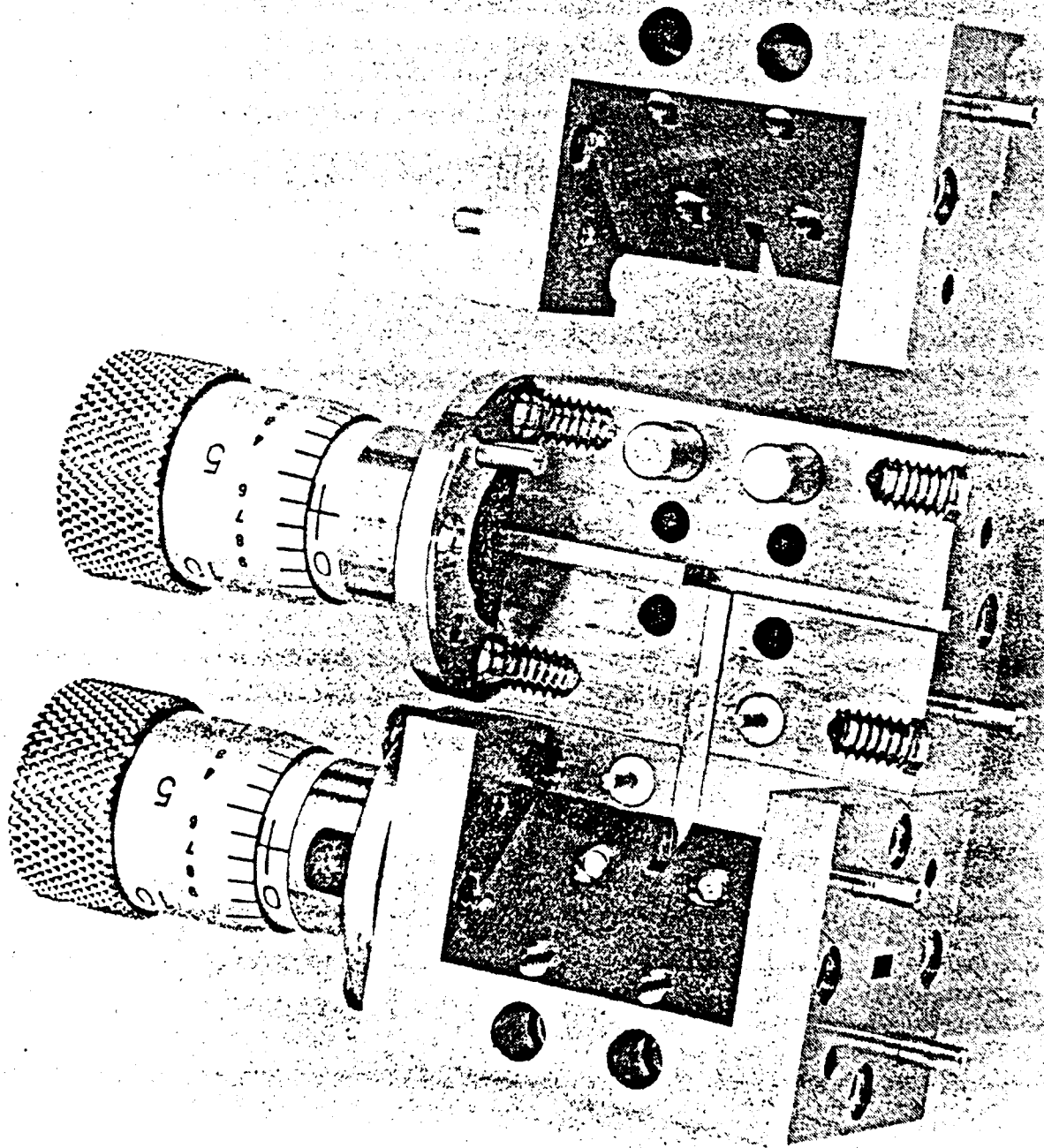
90-97 GHz Scalar Test Set



94-GHz Test Fixture

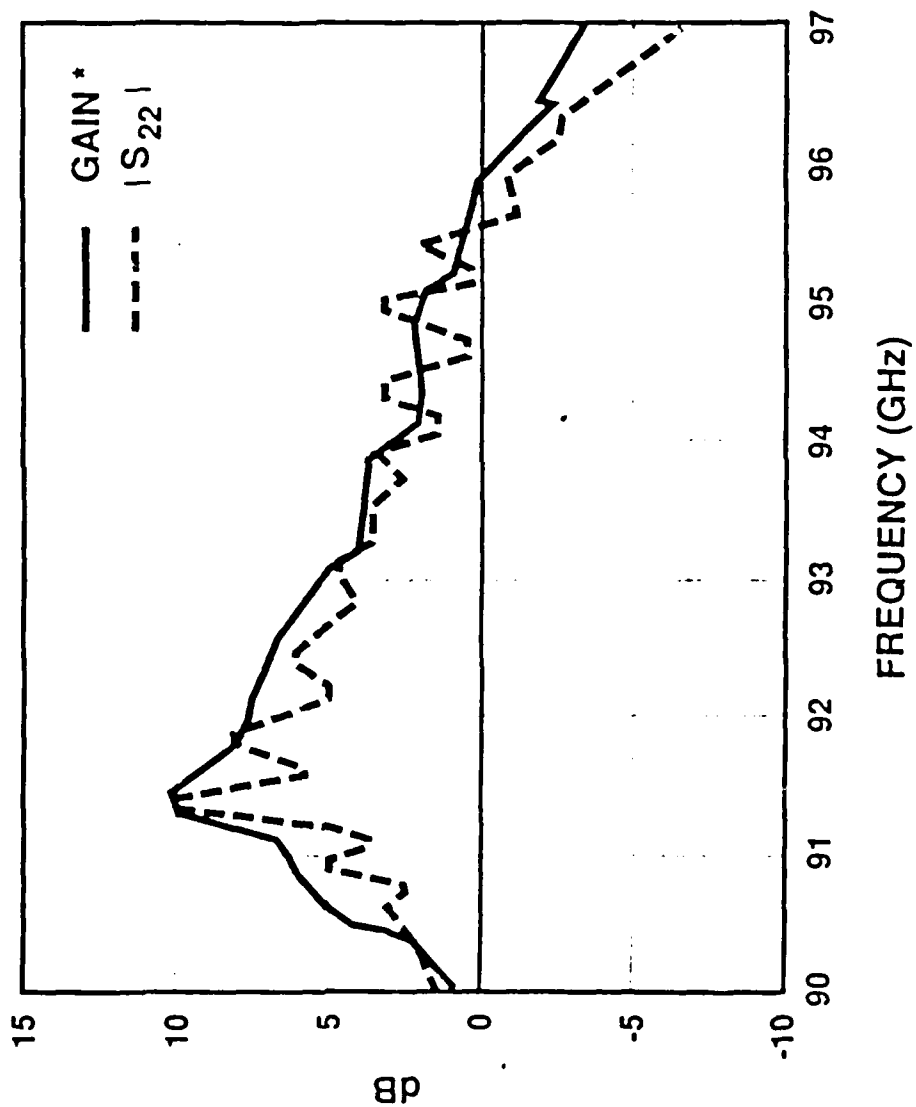
- A: PBT Carrier
- B: Waveguide Short
- C: Microstrip Carrier
- D: Tuning Chip





PBT SINGLE-STAGE HYBRID AMPLIFIER

REGENERATIVE TUNING



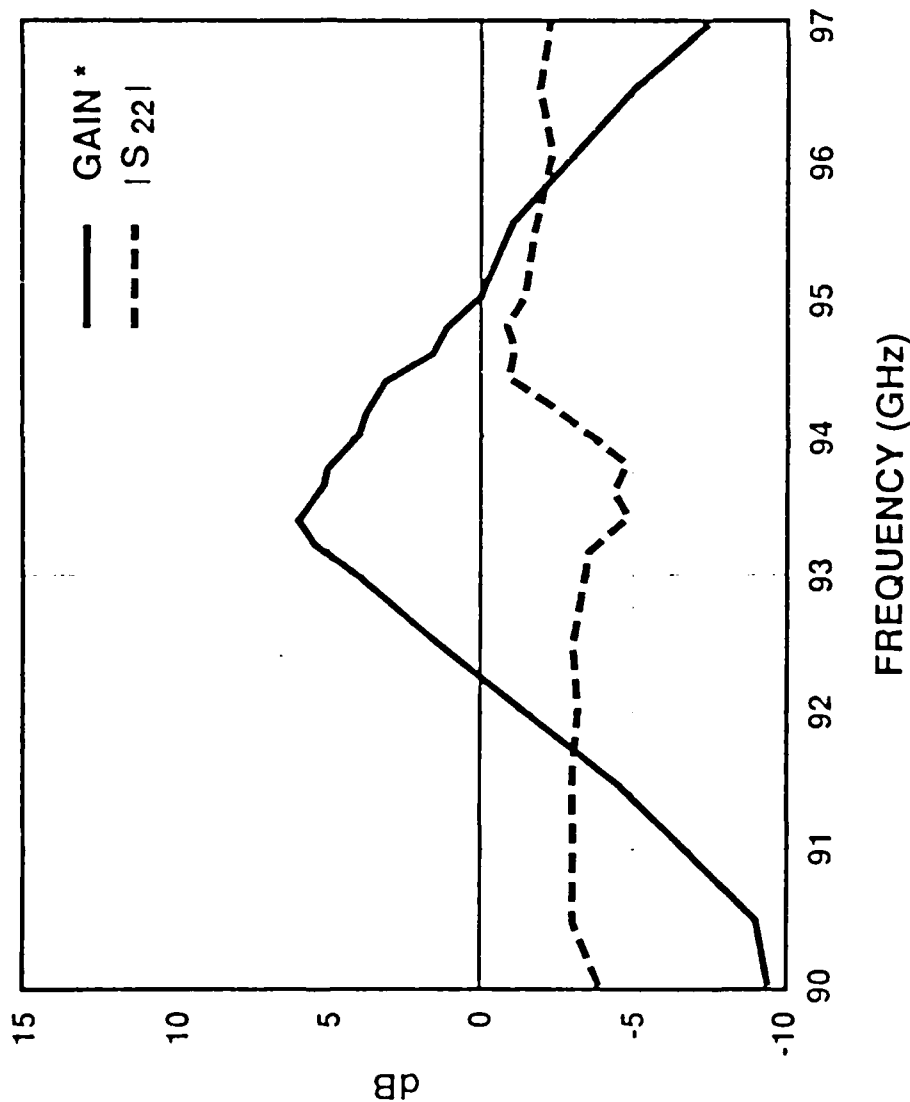
* CORRECTED FOR FIXTURE LOSSES



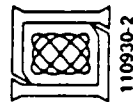
1109306-1

PBT SINGLE-STAGE HYBRID AMPLIFIER

NON-REGENERATIVE TUNING

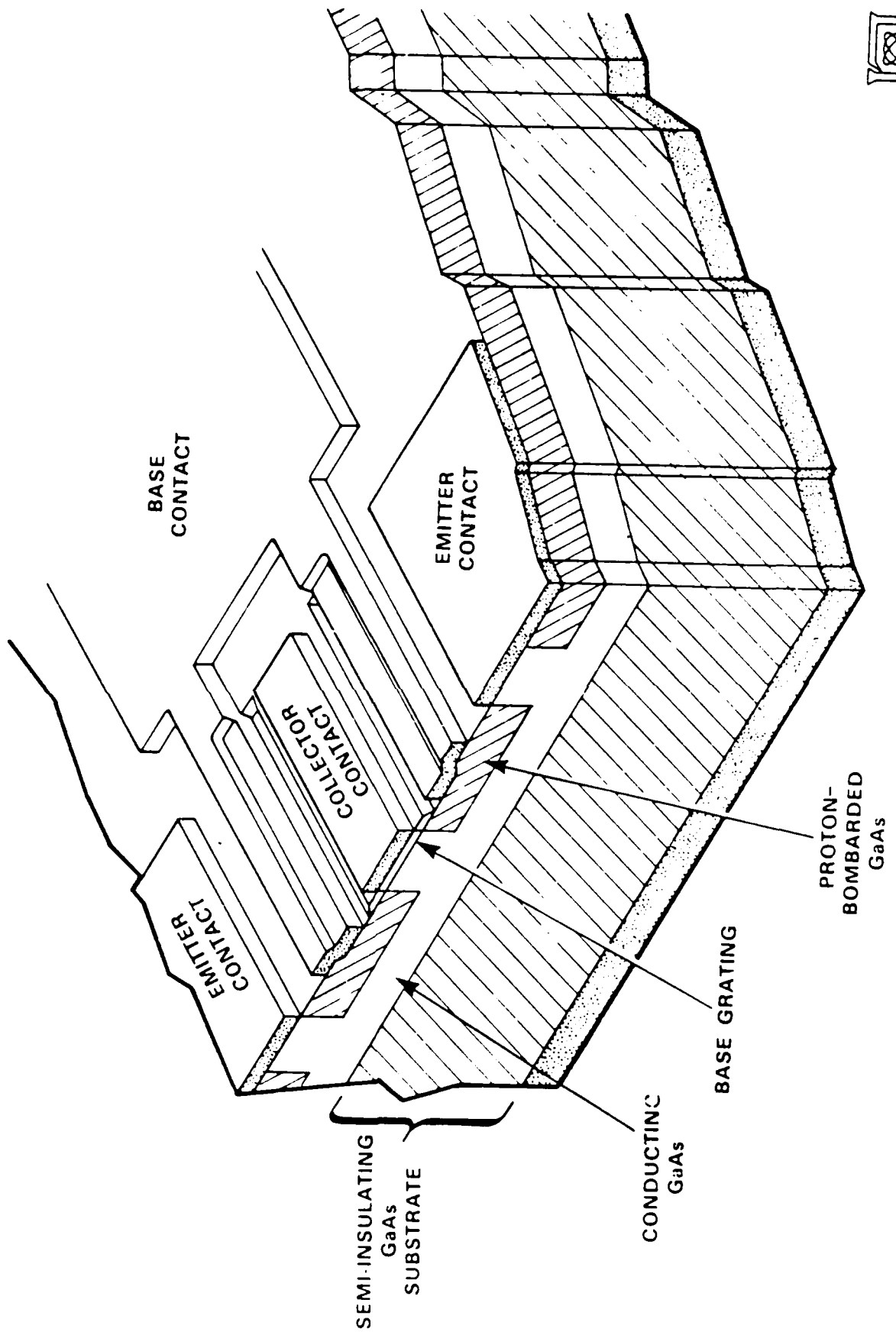


* CORRECTED FOR FIXTURE LOSSES



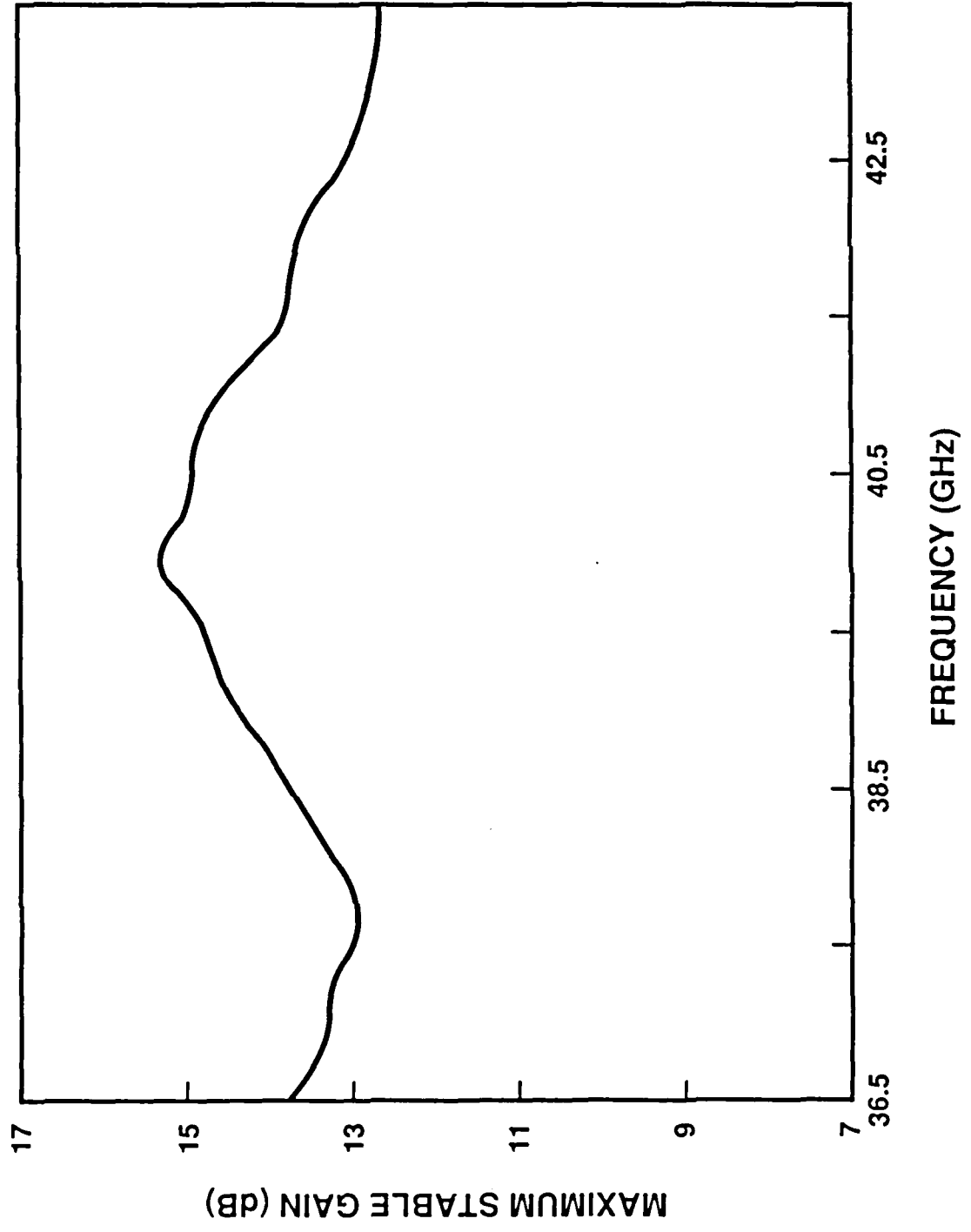
110930-2

PBT ON SEMI-INSULATING SUBSTRATE

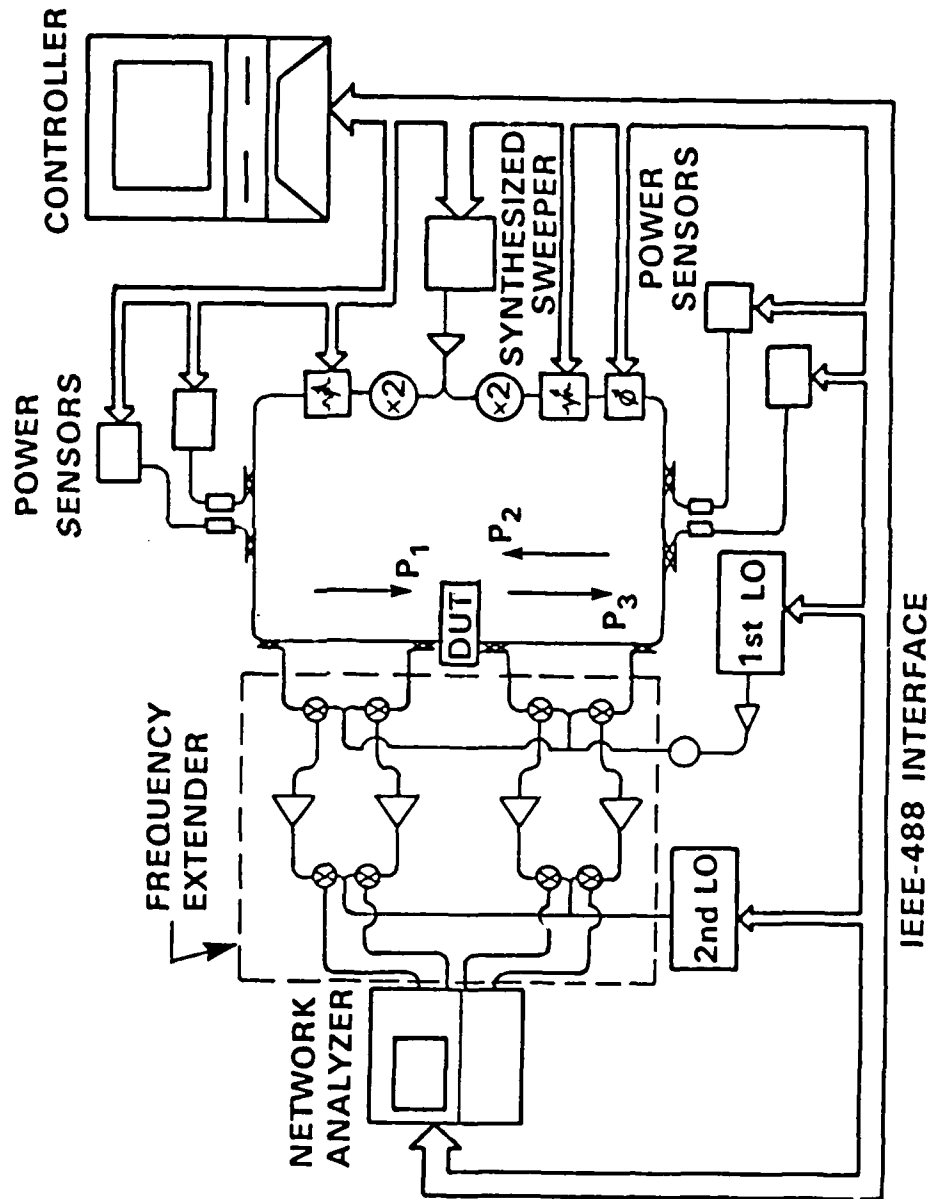


956

GAIN OF PBT ON SEMI-INSULATING SUBSTRATE

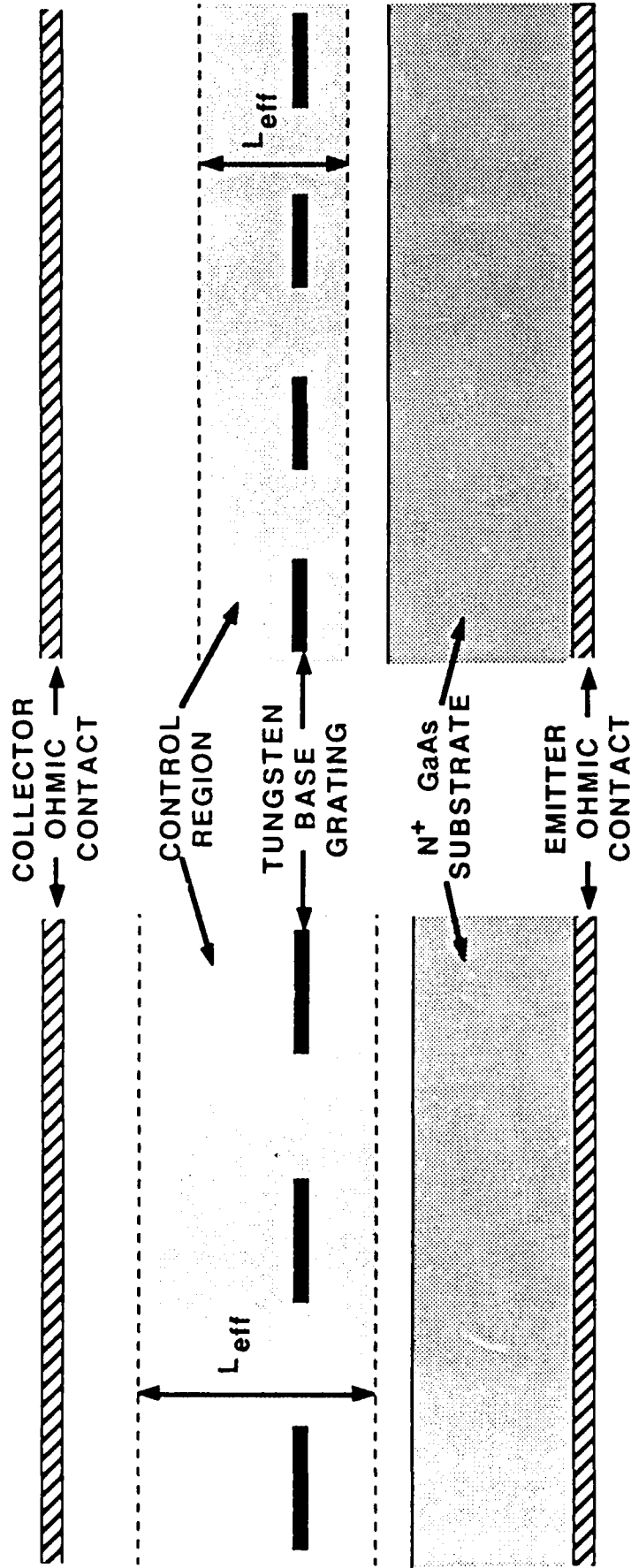


EHF ACTIVE LOAD-PULL MEASUREMENT SYSTEM



109035-1

BENEFITS OF REDUCED-PERIODICITY GaAs PBT



STANDARD-PERIODICITY PBT

REDUCED-PERIODICITY PBT

$$f_T = \frac{g_m}{2\pi(C_{BE} + C_{BC})} = \frac{\langle v \rangle}{2\pi L_{eff}}$$

$$f_{max}^2 = \frac{f_T}{2\sqrt{\frac{R_B + R_E}{R_O} + \frac{R_B g_m C_{BC}}{C_{BE} + C_{BC}}}}$$

PBT PERFORMANCE

- 7.5 dB GAIN AT 92 GHz IN A REGENERATIVELY TUNED AMPLIFIER
- 6 dB GAIN AT 93.5 GHz IN A NONREGENERATIVE AMPLIFIER
- 15 dB MAXIMUM STABLE GAIN AT 40 GHz FROM A PBT ON A SEMI-INSULATING SUBSTRATE
- 20.1 dB MAXIMUM STABLE GAIN AT 26.5 GHz
- EXTRAPOLATED f_{\max} OF 265 GHz
- EXTRAPOLATED f_T OF 40 GHz
- 5-GHz SIGNAL SAMPLED WITH PBT TRACK-AND-HOLD CIRCUIT

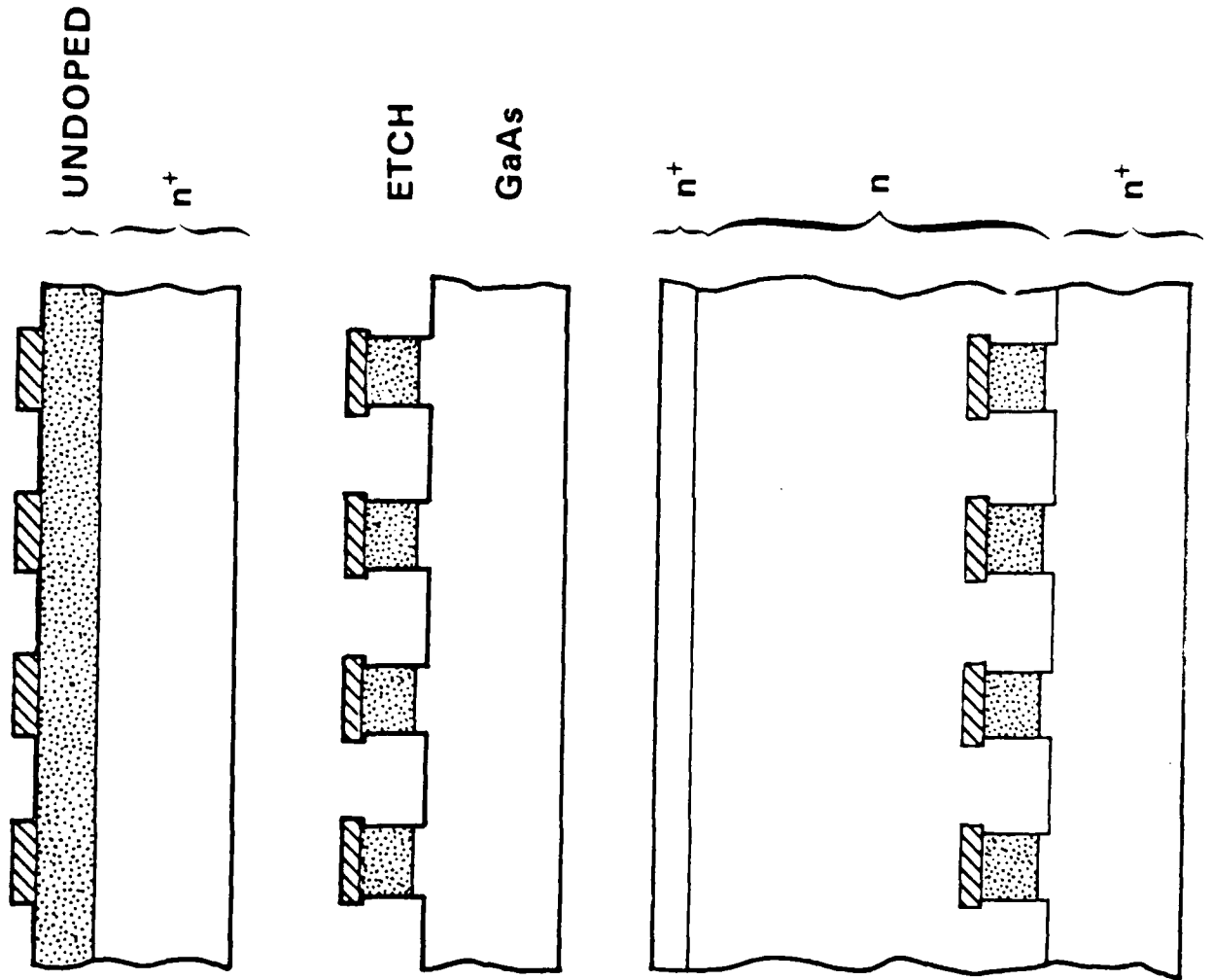
PBT POWER DATA

FREQUENCY (GHz)	<u>1.3</u>	<u>1.3</u>	<u>22</u>	<u>22</u>
POWER (mW)	100	1000	501	83
$\eta_{\text{POWER-ADDED}}$	66%	35%	30%	45%
GAIN (dB)	15	19	5.0	6.2
CLASS	AB	A	AB	AB

ADVANCED STRUCTURES

- PBTs HAVE DEMONSTRATED f_{\max}/f_T ratios of 7:1
 - LOW PARASITICS, HIGH OUTPUT IMPEDANCE
 - DOUBLING $f_T \Rightarrow f_{\max} \geq 500$ GHz
- STRUCTURES FOR ENHANCED f_T :
 - ETCHED-EMITTER PBT
 - REDUCED-PERIODICITY PBT
 - MODIFIED STRUCTURES AND DOPING PROFILES
 - REGROWTH FET

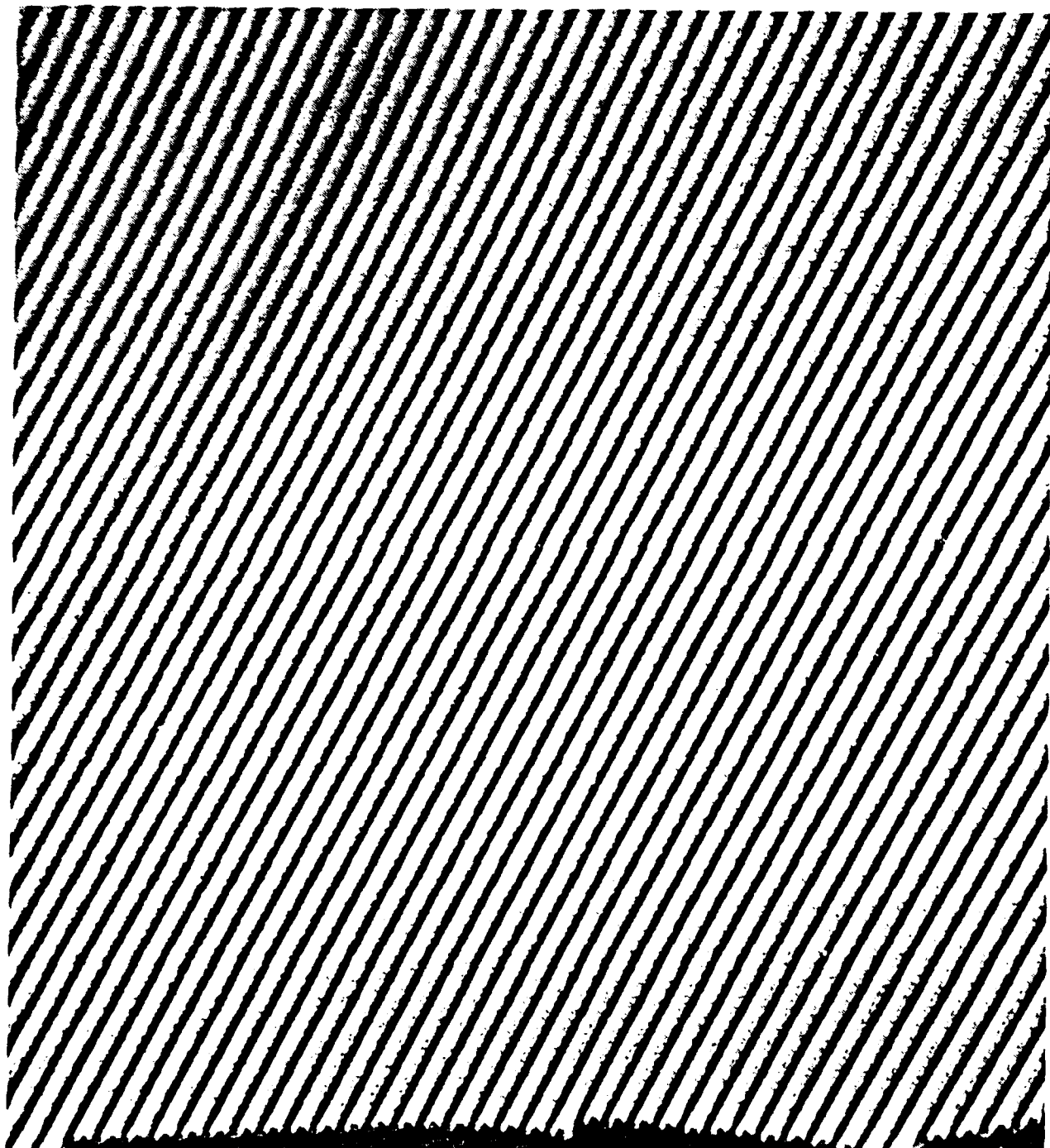
PBT WITH MODIFIED PROFILE



PBT DEVICE YIELD

<u>Wafer</u>	<u>YIELD (ALL BUT SHORTS & OPENS)</u>	<u>σ (I_{DSS})</u>	<u>σ (g_m)</u>
VC2	89 %	21 %	14.4 %
SP1	93 %	17.6 %	21 %

<u>Wafer</u>	<u>YIELD (ALL WITHIN 10 % OF $\overline{I_{DSS}}$, $\overline{g_m}$)</u>	<u>σ (I_{DSS})</u>	<u>σ (g_m)</u>
VC2	57 %	5.4 %	6 %
SP1	45.6 %	7.9 %	6.7 %

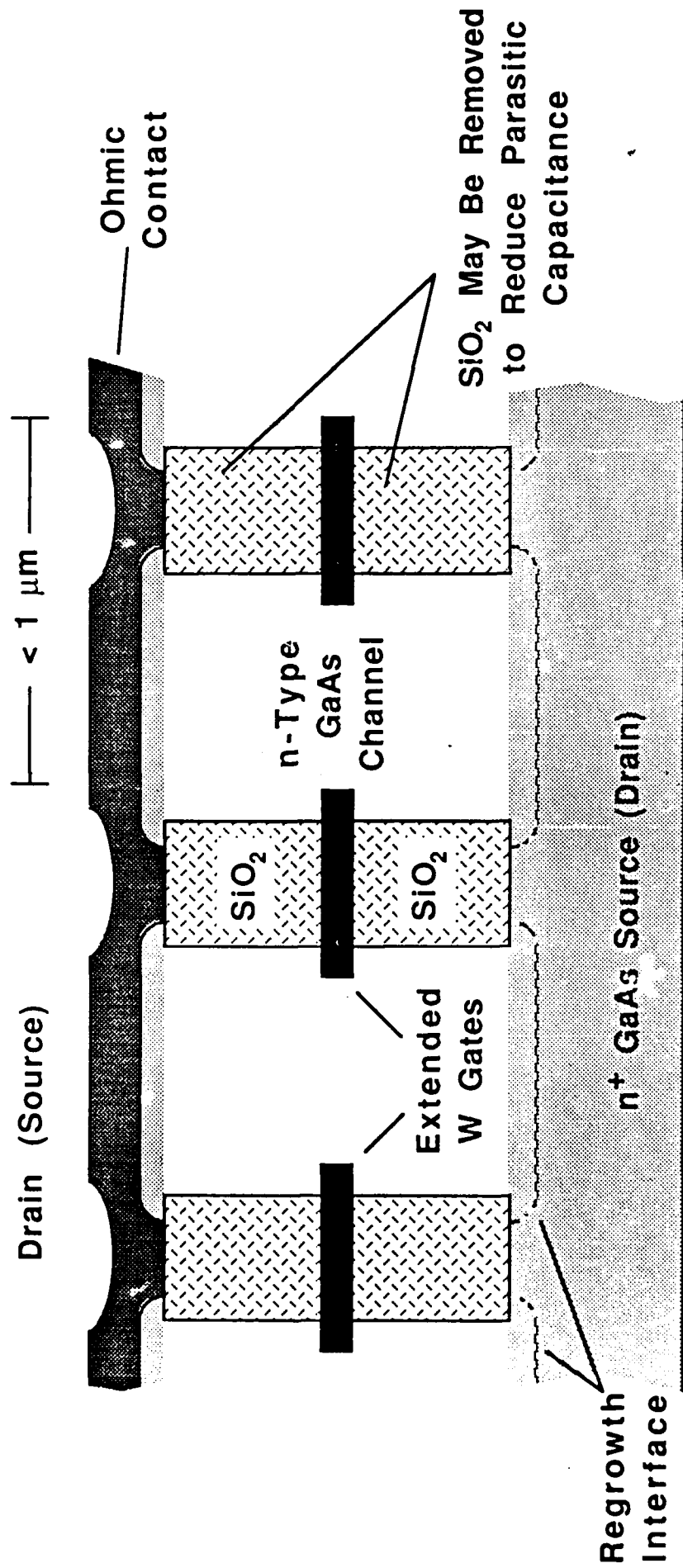


052414 25KV X7.00K 4.3um

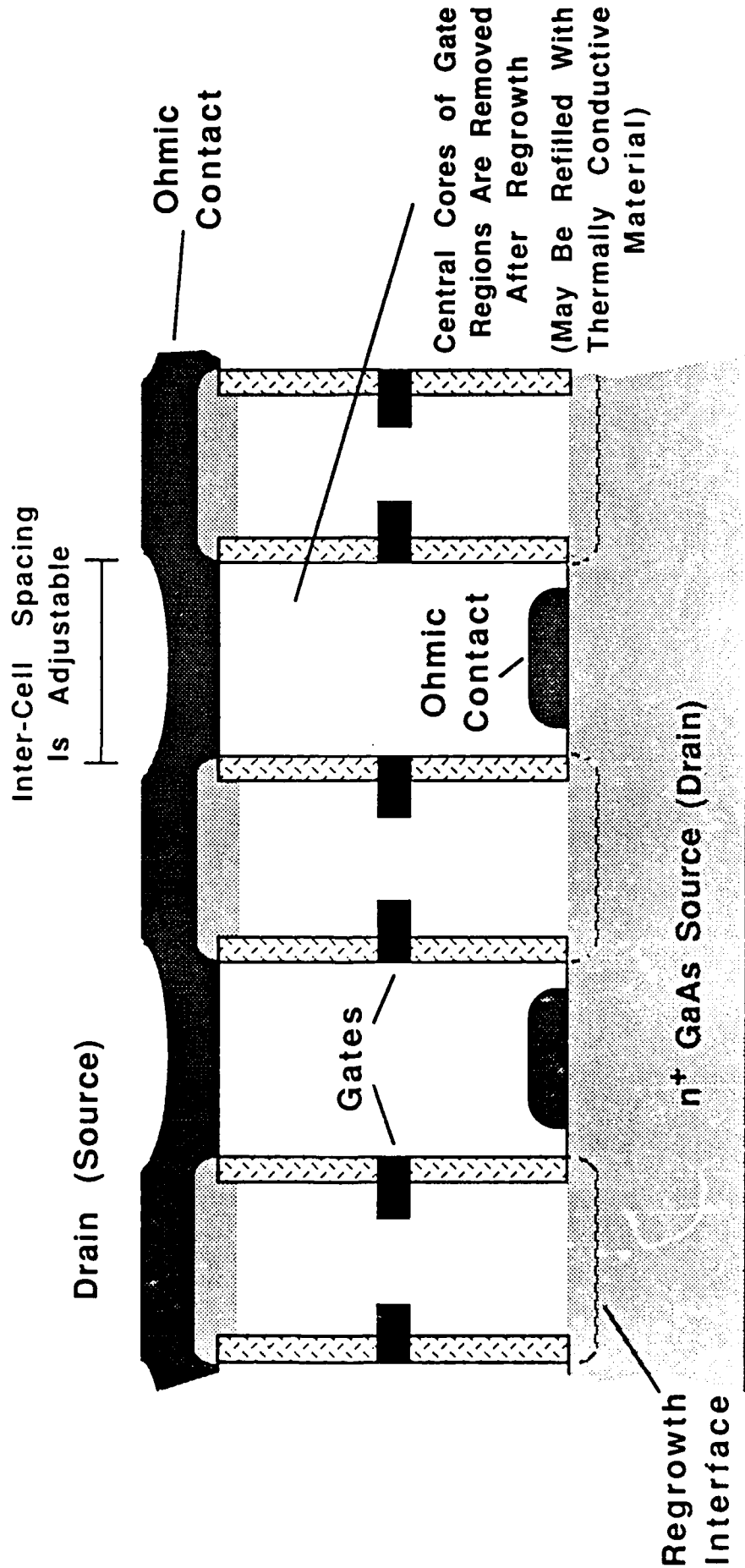
PBT SUMMARY

- **PBTs HAVE DEMONSTRATED HIGH PERFORMANCE AT EHF**
- **HIGH-PERFORMANCE PBTs HAVE BEEN FABRICATED ON SEMI-INSULATING GaAs SUBSTRATES**
- **PBTs CAN BE FABRICATED ACROSS A FULL GaAs WAFER BY A HIGH-YIELD MANUFACTURING PROCESS**
- **ONGOING CIRCUIT EFFORTS AT**
 - 22 GHz**
 - 40 GHz**
 - 94 GHz**
- **ADVANCED STRUCTURES**

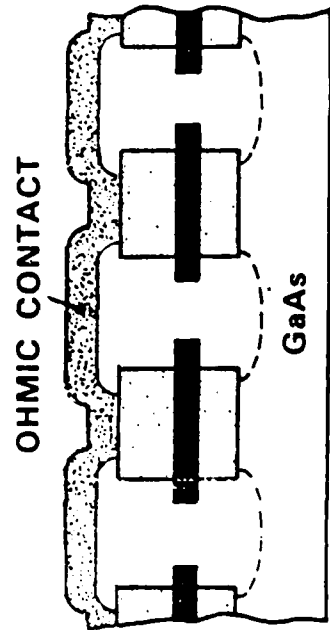
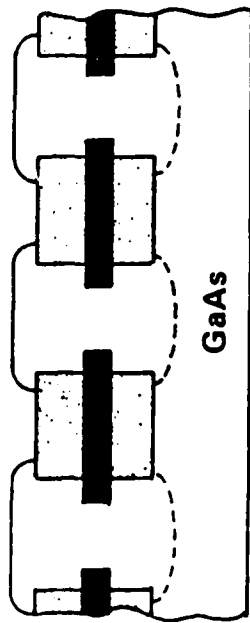
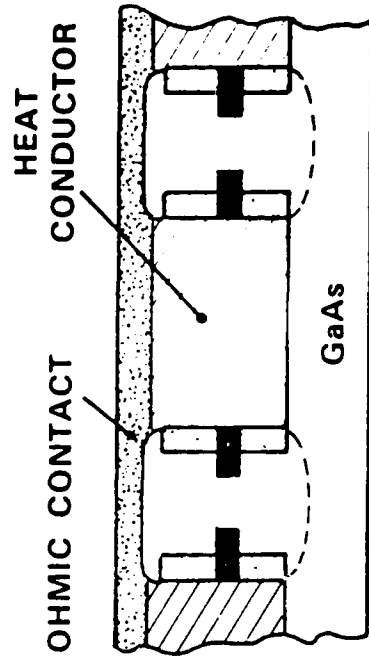
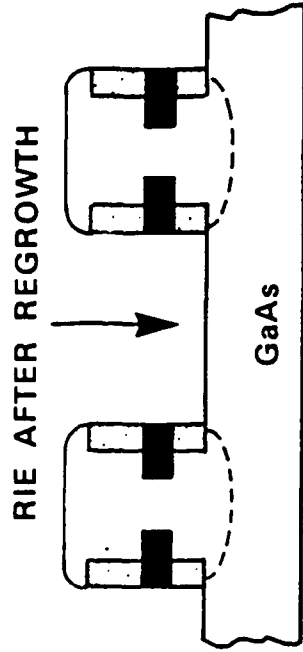
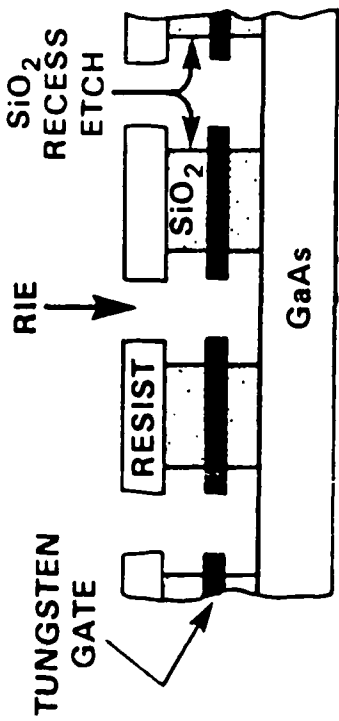
REGROWTH FET (STANDARD DESIGN)



REGROWTH FET (THERMAL DESIGN)

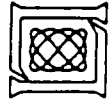


METHODS OF FABRICATING REGROWTH FET



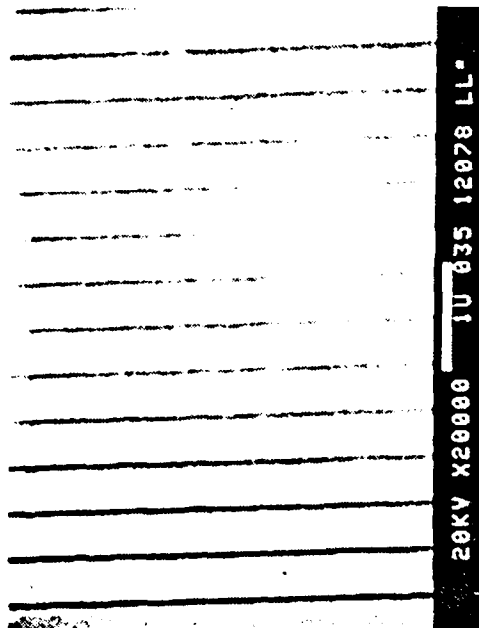
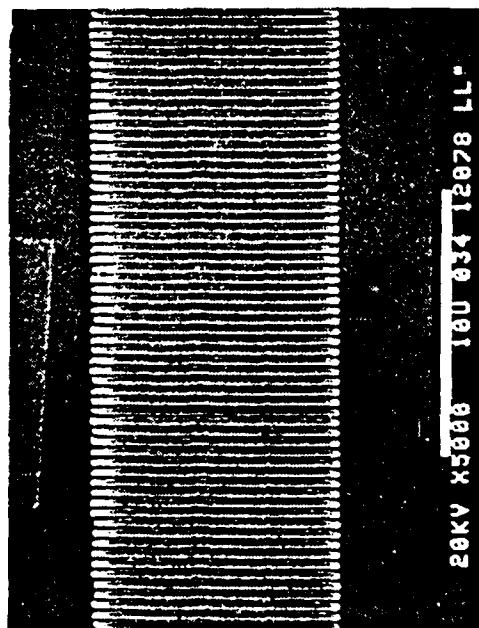
THERMAL DESIGN

STANDARD DESIGN

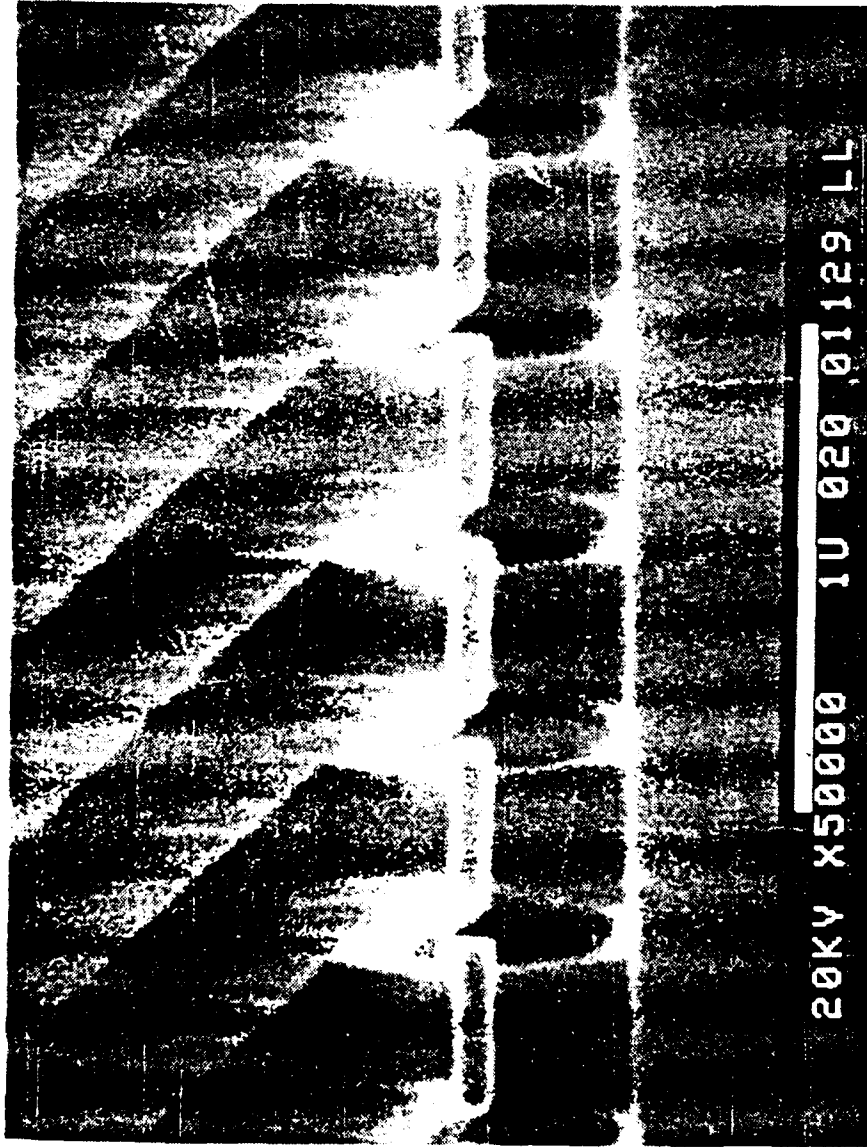


95947.1

RFET GRATINGS FABRICATED USING ELECTRON-BEAM LITHOGRAPHY



RFET AFTER SiO₂ RECESS ETCH



REGROWTH FET SUMMARY

- **REGROWTH FET ADVANTAGES:**
 - HIGH SPEED
 - DESIGN FLEXIBILITY
 - THERMAL MANAGEMENT \Rightarrow HIGH POWER
- **PROTRUDING-GATE PROCESS FULLY DEVELOPED**
- **VIABILITY OF ELECTRON-BEAM LITHOGRAPHY SHOWN**
- **STUDY OF GaAs CRYSTAL GROWTH AROUND PROTRUDING GATES UNDERWAY**
- **DEVICE WAFERS FABRICATED USING PBT CRYSTAL GROWTH PARAMETERS**

Transport Considerations for EHF Devices

H. L. Grubin

*Scientific Research Associates
Glastonbury, CT*

TRANSPORT CONSIDERATIONS FOR EHF DEVICES SCIENTIFIC RESEARCH ASSOCIATES

PROGRAM OBJECTIVE

- USE NUMERICAL SIMULATION TO ASSIST IN THE DESIGN OF HIGH FREQUENCY AND HIGH SPEED SEMICONDUCTOR DEVICES
- DETERMINE REALISTIC GOALS FOR HIGH SPEED APPLICATIONS

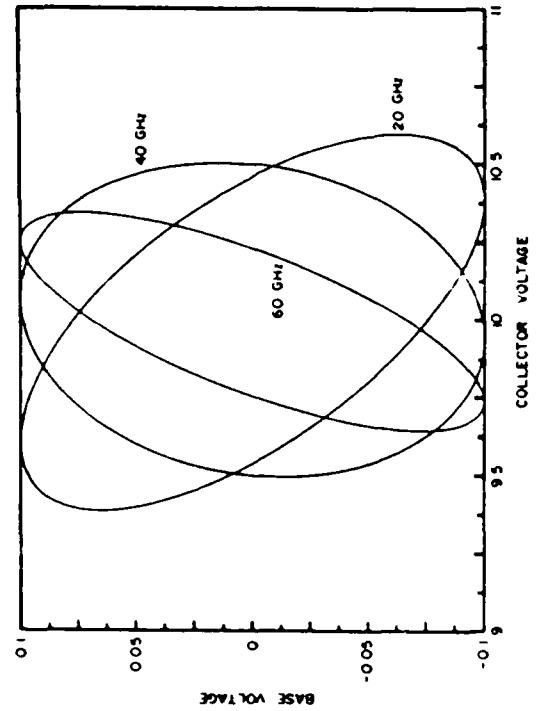
PROGRAM APPROACH

- NUMERICALLY SOLVE TRANSIENT SEMICONDUCTOR DRIFT AND DIFFUSION EQUATIONS
- NUMERICALLY SOLVE MOMENTS OF BOLTZMANN EQUATION FOR SUBMICRON DEVICES
- NUMERICALLY IMPLEMENT MONTE CARLO PROCEDURES FOR MATERIAL CHARACTERIZATION
- ONGOING INTERACTION WITH DEVICE DESIGNERS

PROGRAM STATUS

- ACHIEVED LARGE SIGNAL PBT GAIN IN EXCESS OF 7 db AT 40 GHz AND 11 db AT 20 GHz
- ACHIEVED INDIUM BASED HBT GAINS SIGNIFICANTLY LARGER THAN GALLIUM ARSENIDE BASED HBTs

BASE VS. COLLECTOR VOLTAGE LISSAJOUS



Scientific
Research
Associates

CONTRIBUTORS

GEORGE ANDREWS

JOHN KRESKOVSKY

RALPH LEVY

MEYYA MEYYAPPAN

BEVERLY MORRISON

MOHAMED OSMAN

HAROLD GRUBIN

*Scientific
Research
Associates*

- DESIGN OF GaAs PBT's
- DESIGN OF COMPOUND SEMICONDUCTOR HBT'S

Scientific
Research
Associates

PBT STUDIES

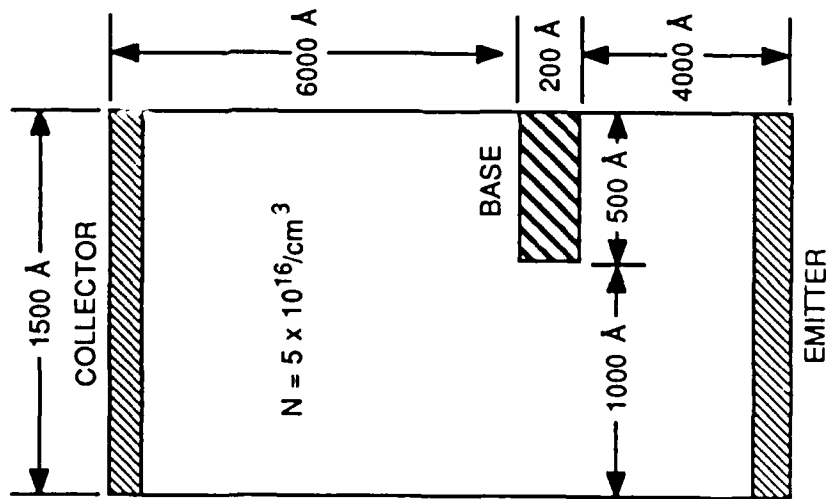
DESIGN PBT STRUCTURES FOR

- **HIGH POWER**
- **HIGH GAIN**
- **HIGH POWER ADDED EFFICIENCY**

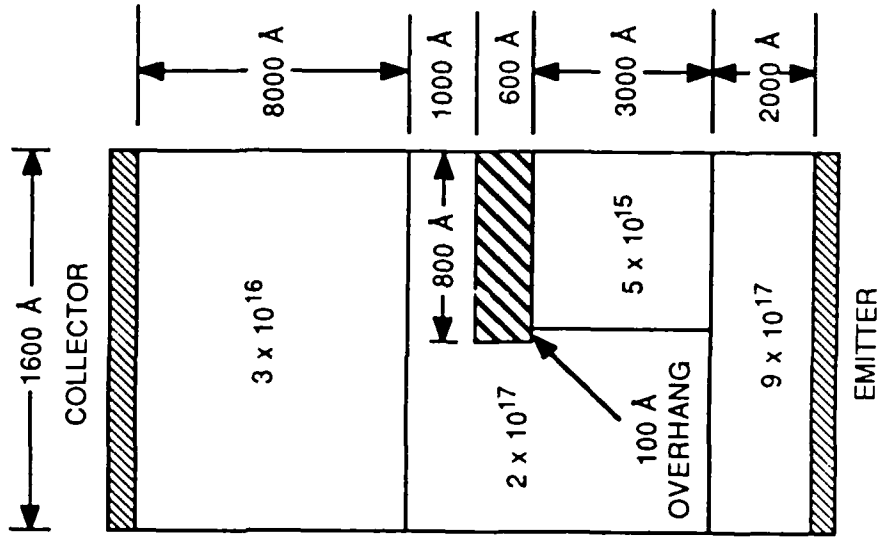
NEED LARGE SIGNAL CALCULATIONS

PBT STRUCTURES

UNIFORM DOPING



NONUNIFORM DOPING



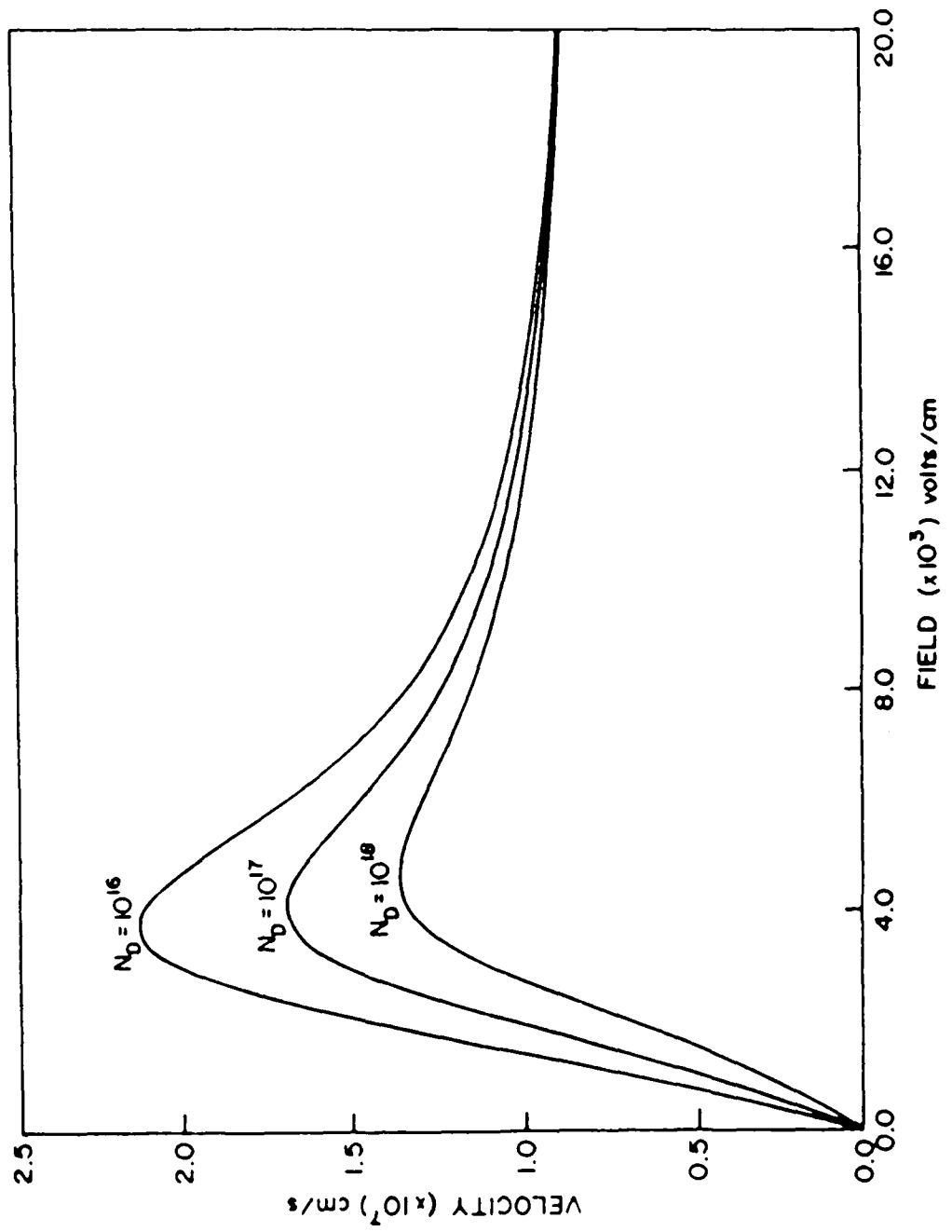
WHAT IS THE RELATIONSHIP BETWEEN LARGE AND SMALL SIGNAL CALCULATIONS AND BY SMALL SIGNAL WE MEAN THAT SUCH QUANTITIES AS THE CUT-OFF FREQUENCY AND f_{max} ARE RELEVANT.

- OUR LATEST CALCULATIONS INDICATE THAT ANY CONNECTION BETWEEN CUT-OFF FREQUENCY AND LARGE SIGNAL OPERATION MAY BE COINCIDENTAL.
- THIS IMPLIES THAT THE DESIGN OF A DEVICE FOR HIGH CUT-OFF FREQUENCY OPERATION WILL NOT NECESSARILY YIELD SATISFACTORY OR IMPROVED LARGE SIGNAL POWER OPERATION.
- RECALL THAT SMALL SIGNAL OPERATION IMPLIES SMALL PERTURBATIONS ABOUT A RECOGNIZABLE INPUT.

THE NEXT TWO VIEWGRAPHS ILLUSTRATE THE EXTENT TO WHICH THIS ASSUMPTION IS VALID.

- THE APPROACH TAKEN IS TO ASSUME THAT THE PBT IS CONNECTED TO A DC COLLECTOR POWER SUPPLY THROUGH THE EXTERNAL CIRCUIT.
 - THE CALCULATIONS ARE CONCERNED WITH DETERMINING THE POWER DELIVERED TO THIS EXTERNAL CIRCUIT.
 - THE EXTERNAL CIRCUIT, BY CONTROLLING THE RELATIVE PHASE OF THE BASE AND COLLECTOR VOLTAGE, EXERTS FIRST-ORDER EFFECTS ON THE OUTPUT OF THE DEVICE.
 - BASIC REQUIREMENT FOR POWER FETs AND PBTs IS THAT DECREASES IN BASE VOLTAGE SHOULD BE ACCOMPANIED BY LARGE INCREASES IN COLLECTOR VOLTAGE.
- THIS IS ALWAYS SATISFIED AT LOW FREQUENCY CONDITIONS BUT IS NOT SATISFIED, WITHOUT EXTERNAL ADJUSTMENTS AT HIGH FREQUENCIES.
- SUBSEQUENT CALCULATIONS REVEAL THESE FEATURES.

VELOCITY-FIELD CURVE FOR GaAs



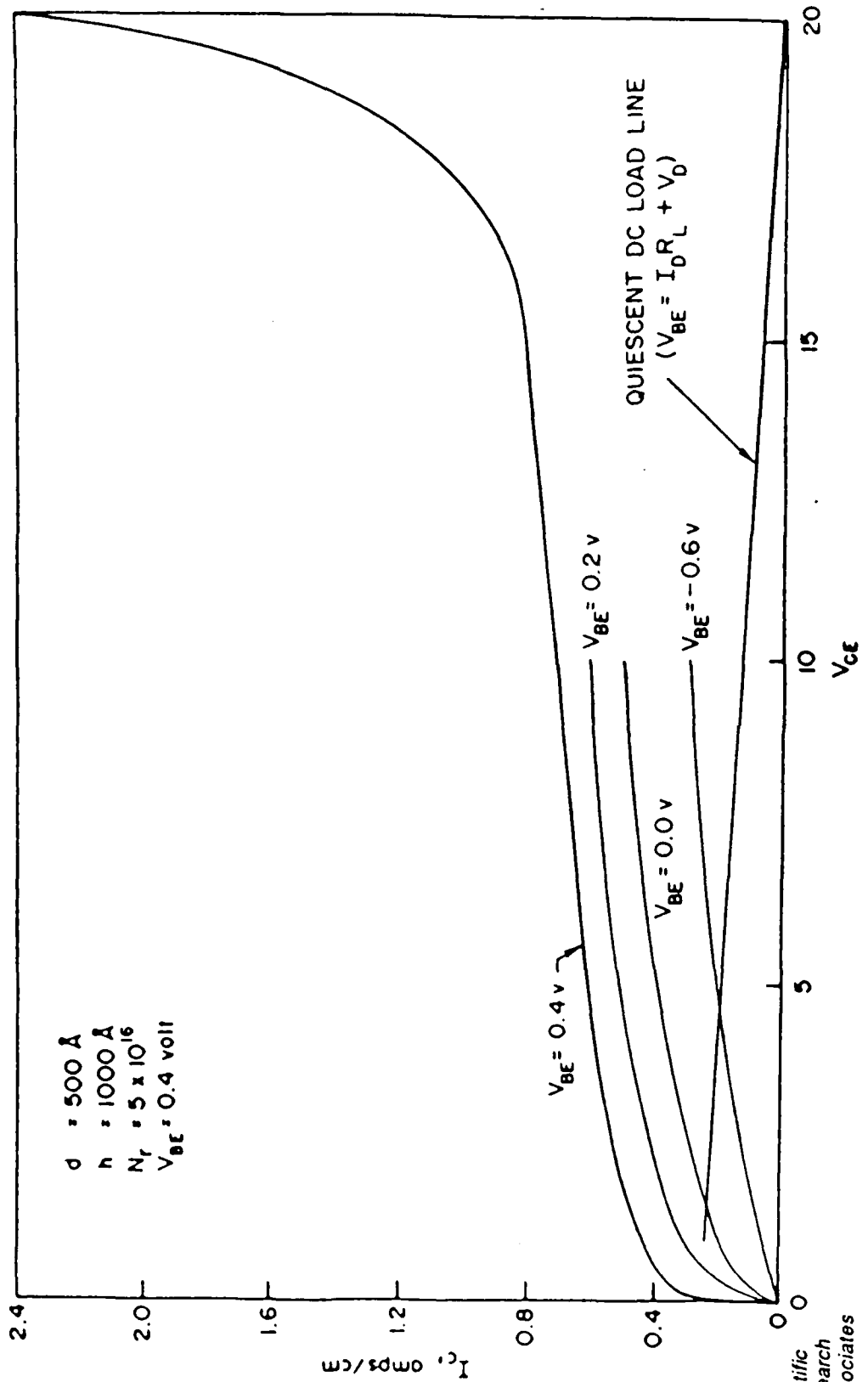
Scientific
Research
Associates

ORDER OF THE CALCULATIONS

- DC CALCULATIONS AND SMALL SIGNAL CHARACTERIZATION
- LARGE SIGNAL RESISTIVE CIRCUIT CALCULATIONS
- LARGE SIGNAL REACTIVE CIRCUIT CALCULATIONS WHERE THE CIRCUIT FREQUENCY IS BELOW AND ABOVE THE DRIVING FREQUENCY

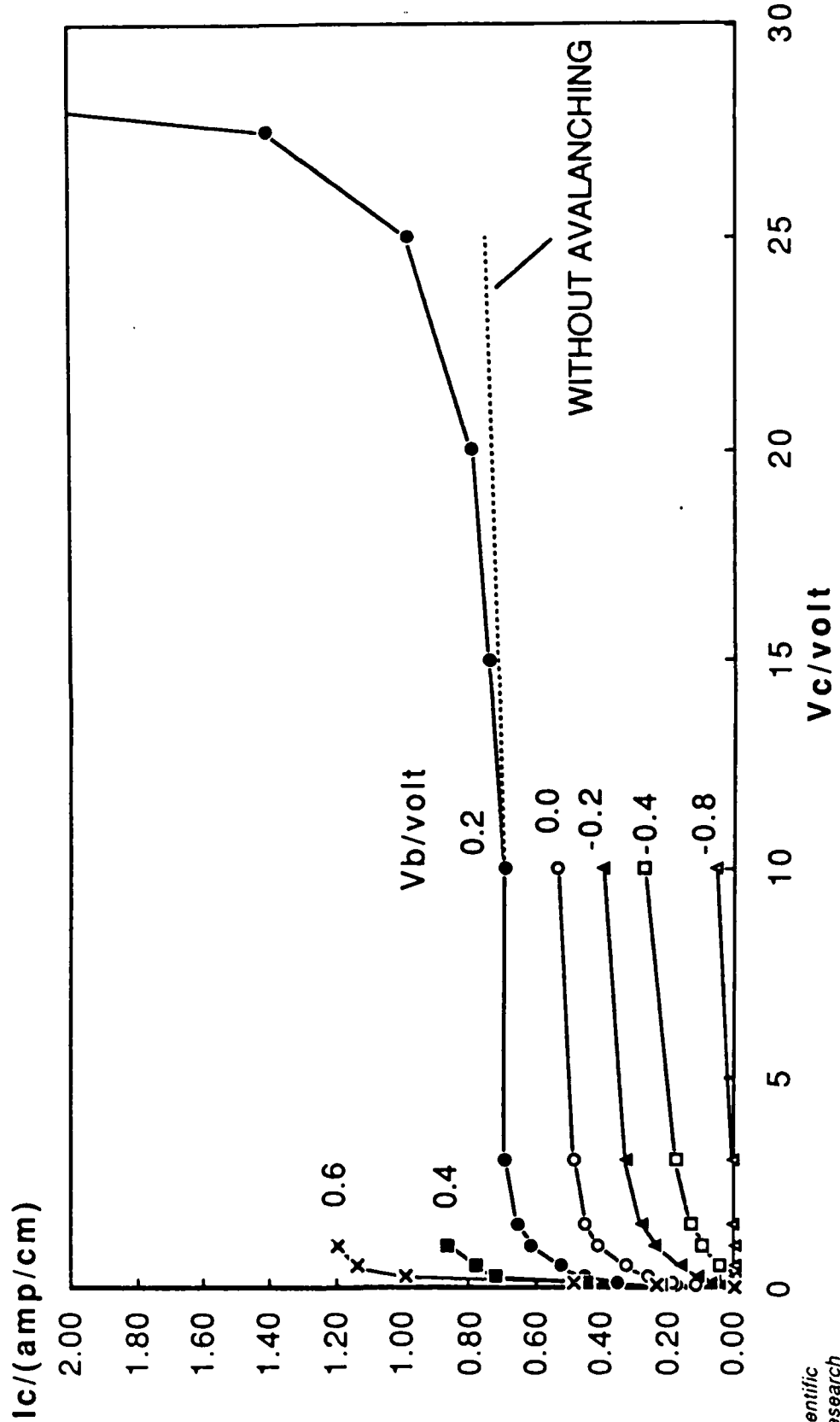
SELECT DC CHARACTERISTICS / BREAKDOWN CURVE

UNIFORMLY DOPED PBT



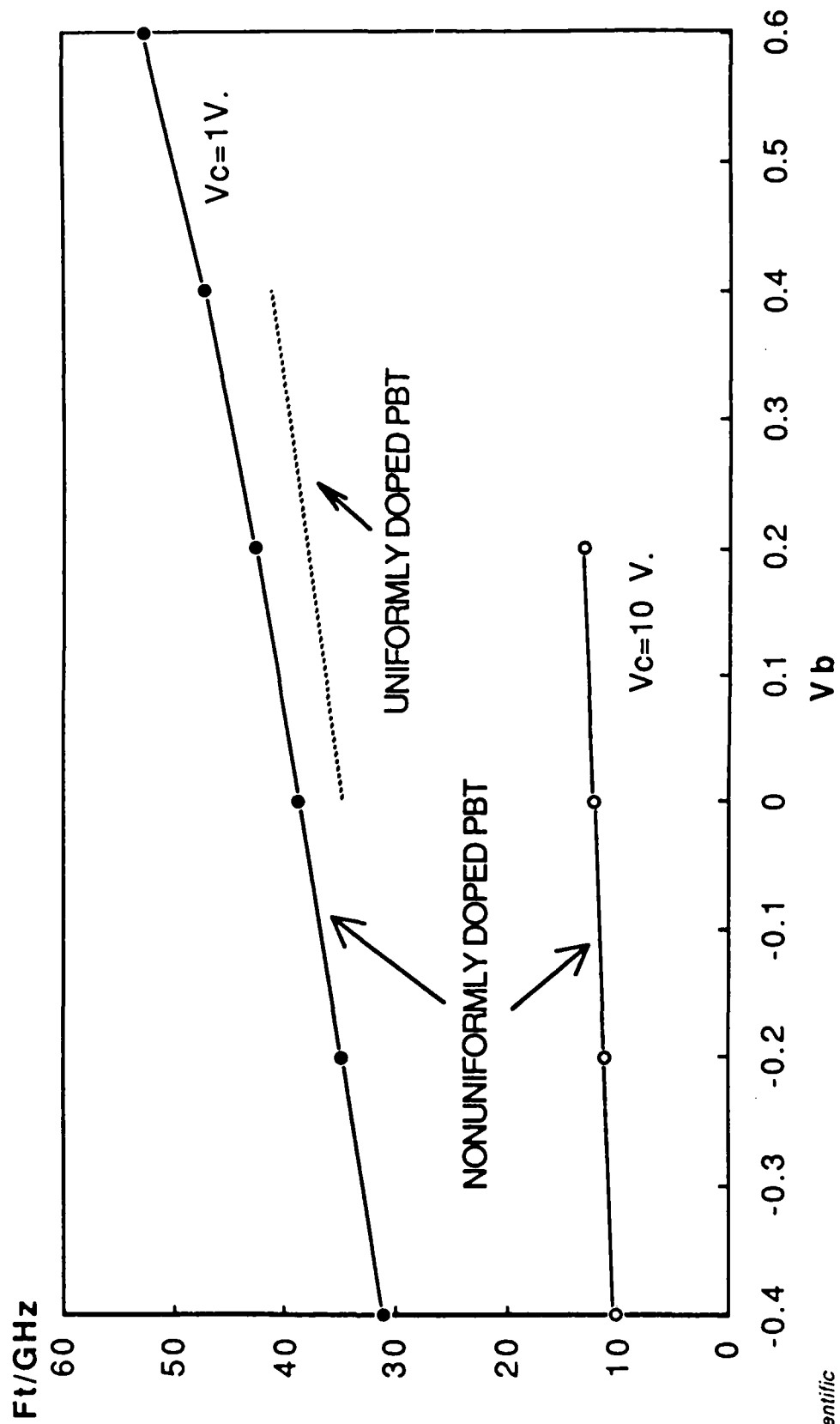
Scientific
Research
Associates

SELECT DC CHARACTERISTICS / BREAKDOWN CURVE NONUNIFORMLY DOPED PBT



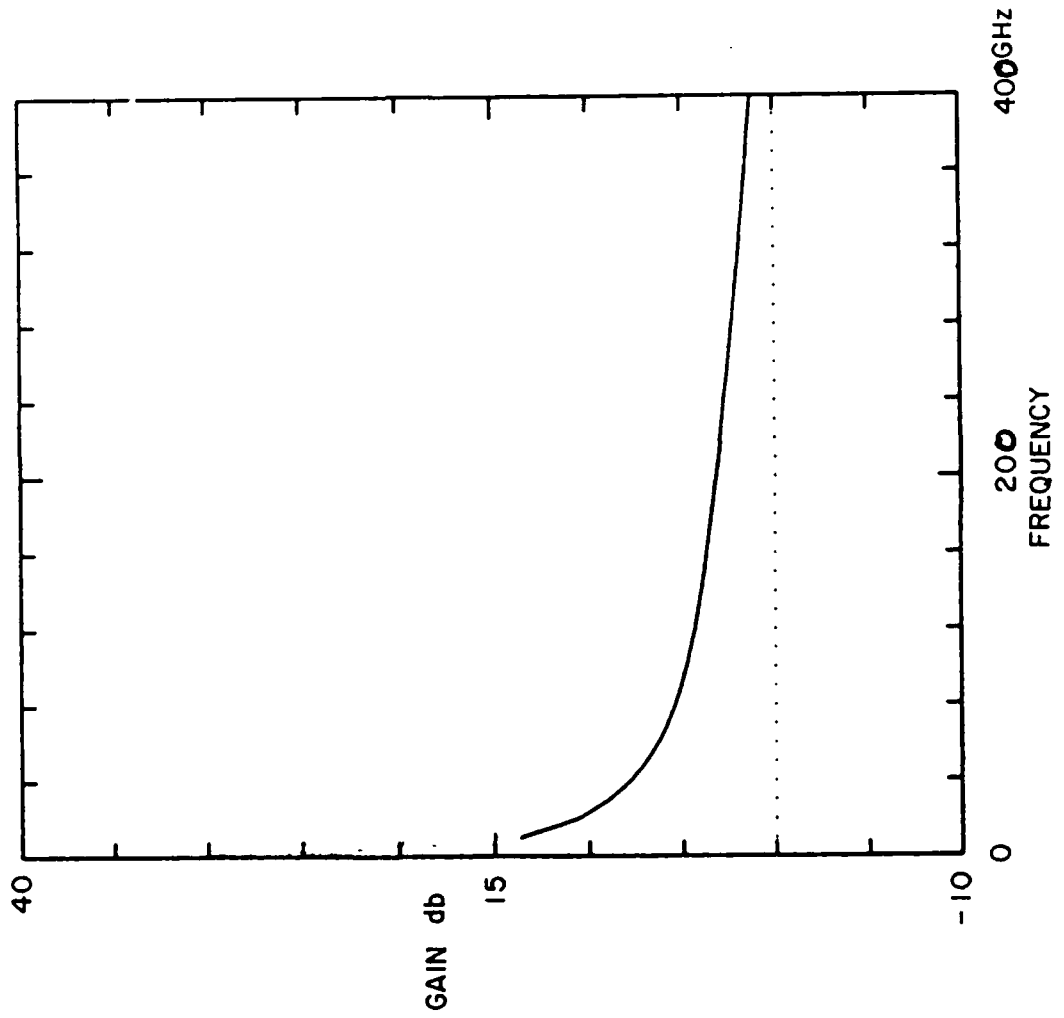
Scientific
Research
Associates

f_T DEPENDENCE ON BIAS



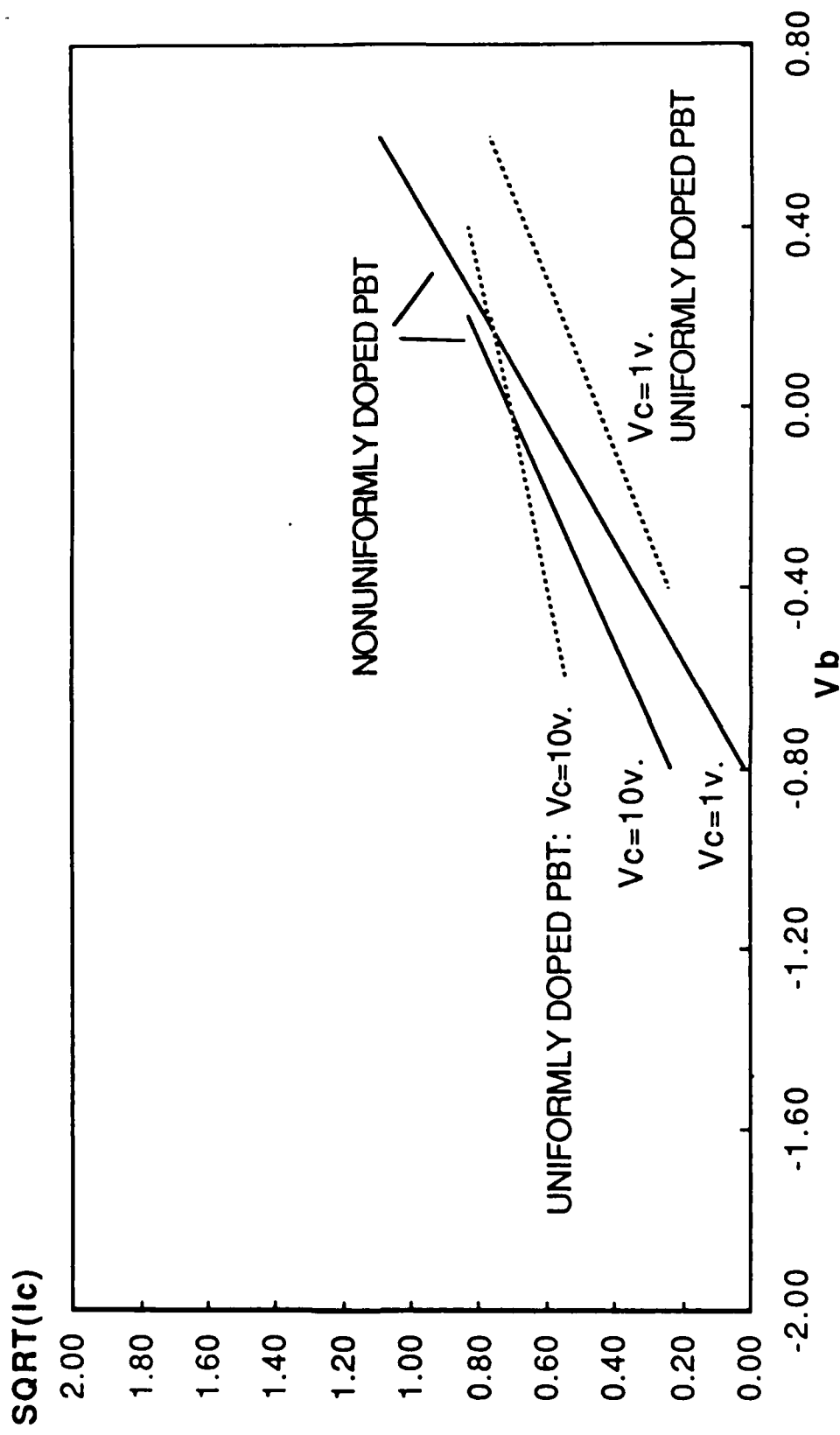
Scientific
Research
Associates

**MAXIMUM STABLE GAIN
NONUNIFORM PBT $V_C = 1.0, V_B = 0.2$**



Scientific
Research
Associates

THRESHOLD VOLTAGE DEPENDENCE ON BIAS

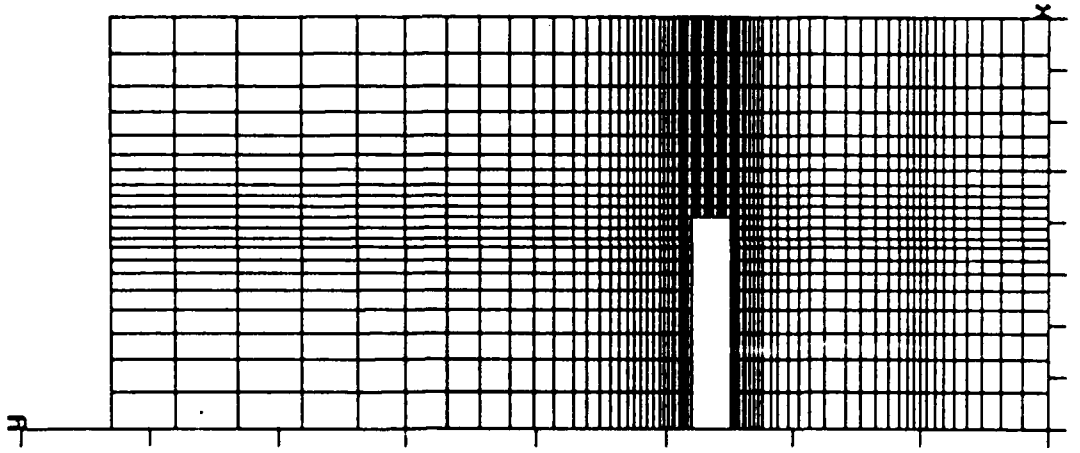


Scientific
Research
Associates

ACTUAL SHAPE
GRID 22 x 80



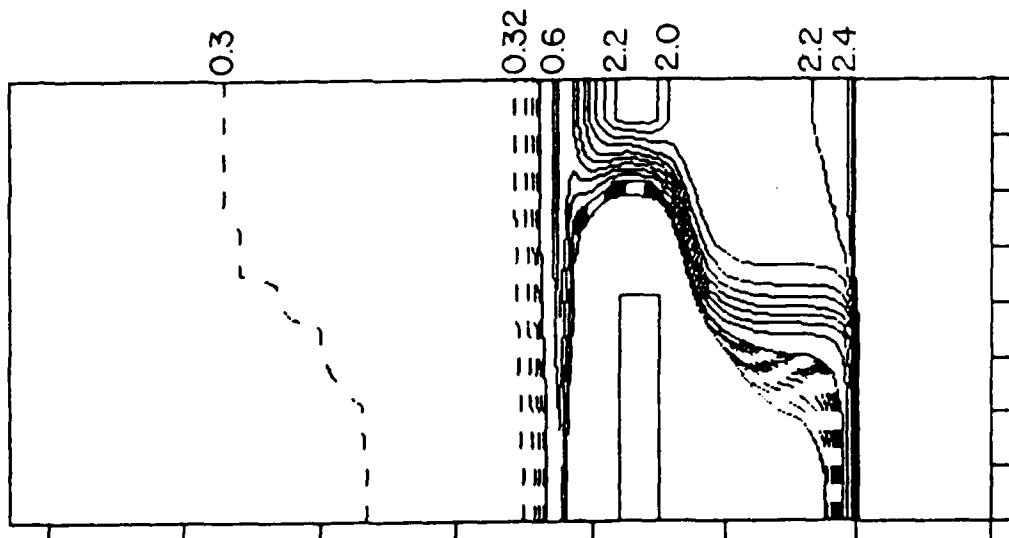
**SHAPE USED IN
CONTOUR PLOTS**



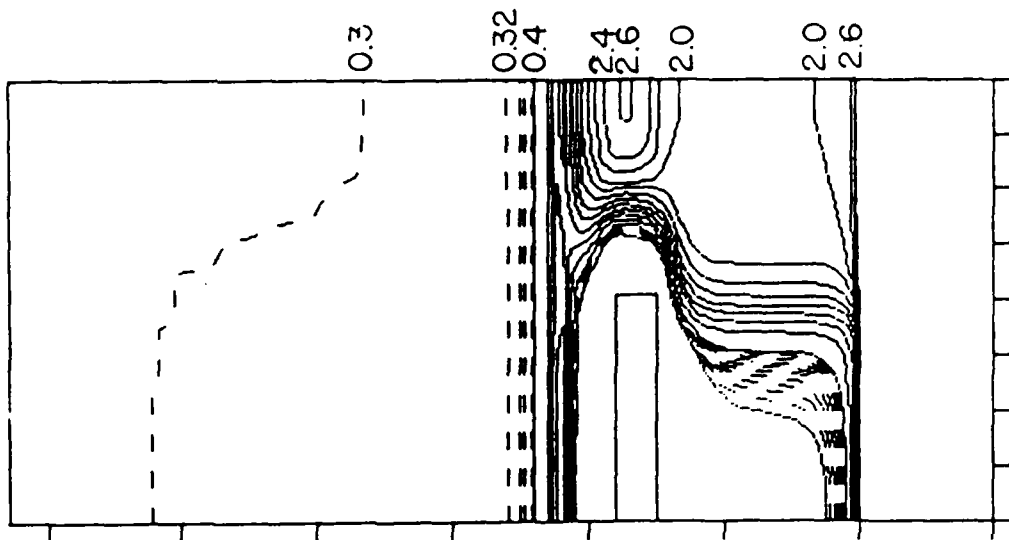
Scientific
Research
Associates

CARRIER DENSITY DISPLAYS (SMALL SIGNAL ?)

$V_c = 1.0, V_b = 0.2$

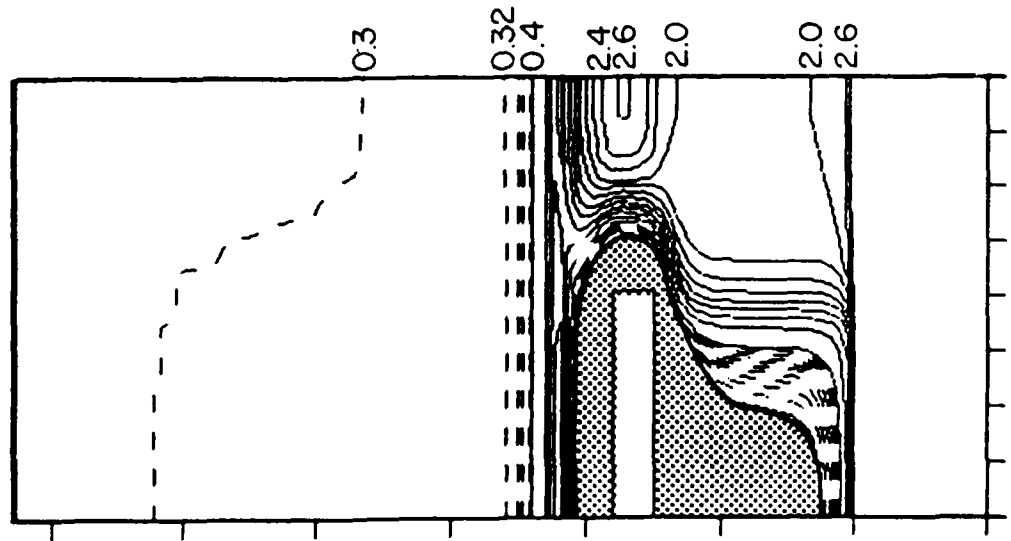


$V_c = 1.0, V_b = 0.6$

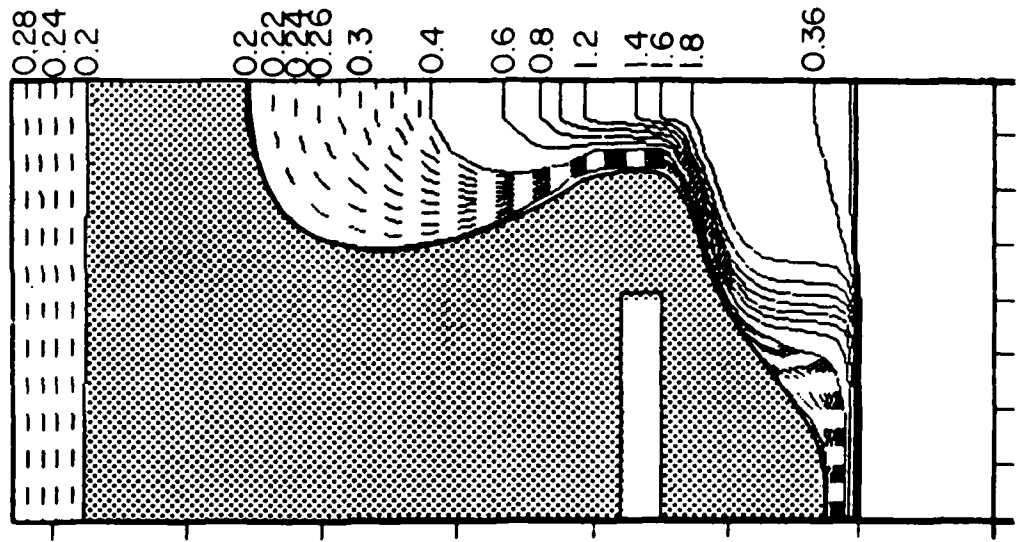


CARRIER DENSITY DISPLAYS (LARGE SIGNAL)

$V_c = 1.0, V_b = 0.6$



$V_c = 10.0, V_b = -0.4$

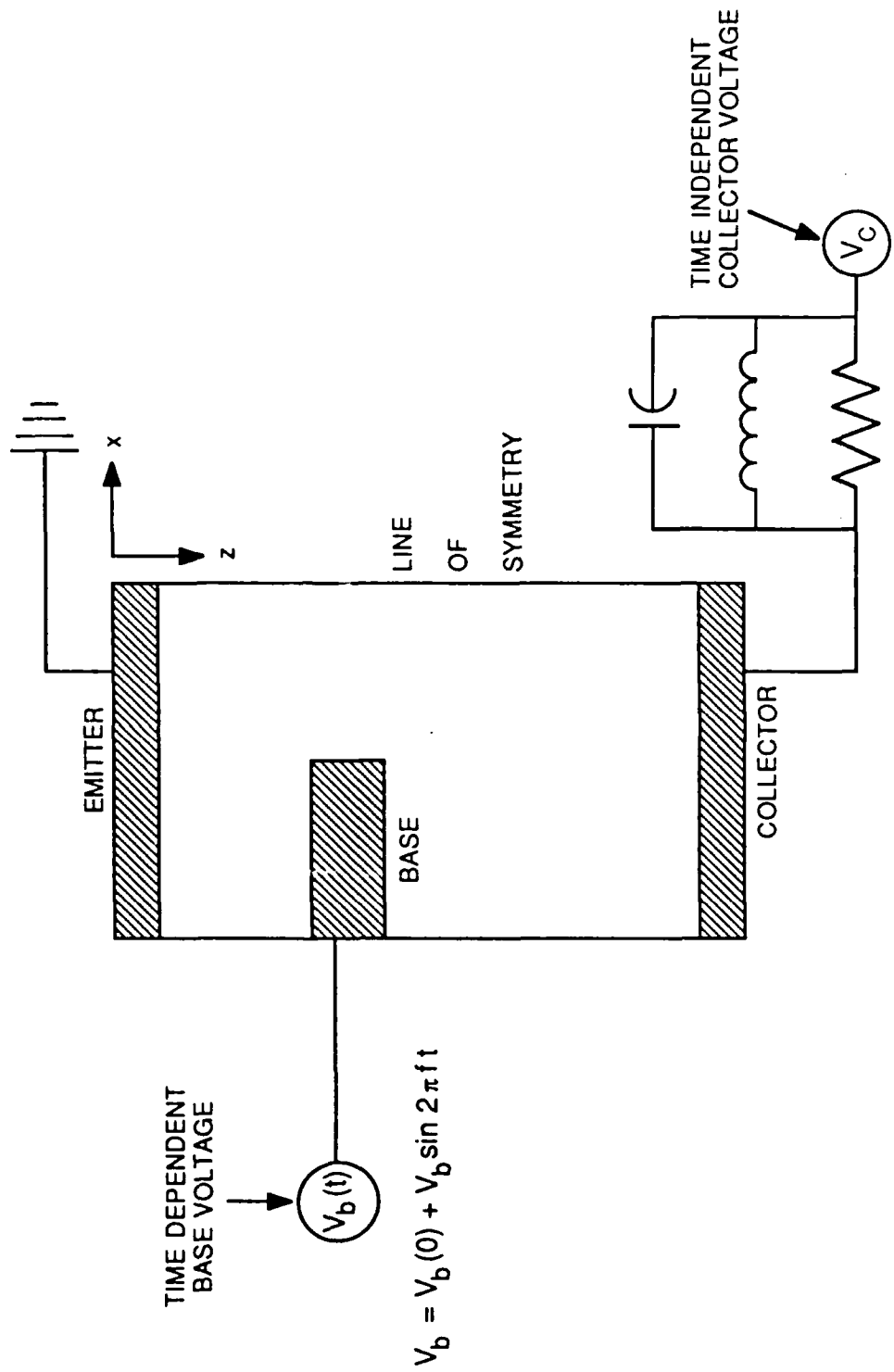


Scientific
Research
Associates

LARGE SIGNAL POWER CALCULATION

ASSUME 25 μm DEPTH AND 150 FINGERS (7mm)

LARGE SIGNAL PBT - CIRCUIT CONFIGURATION TIME DEPENDENT BASE AND COLLECTOR PERTURBATION

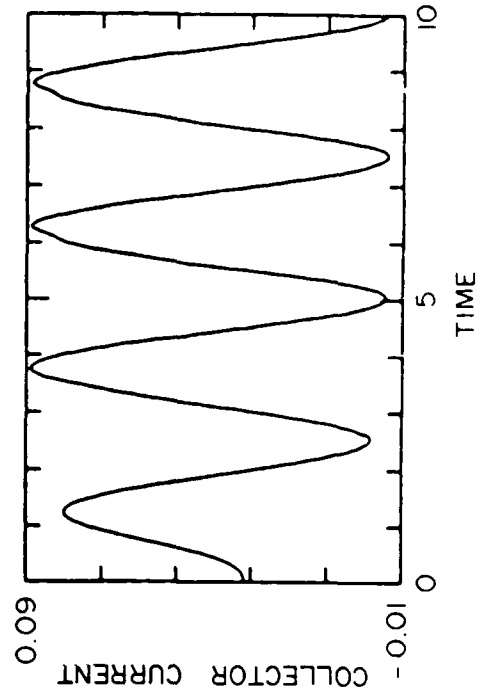
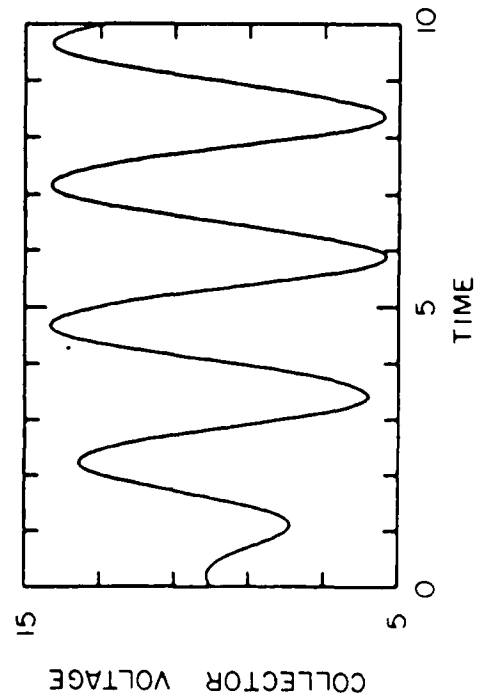
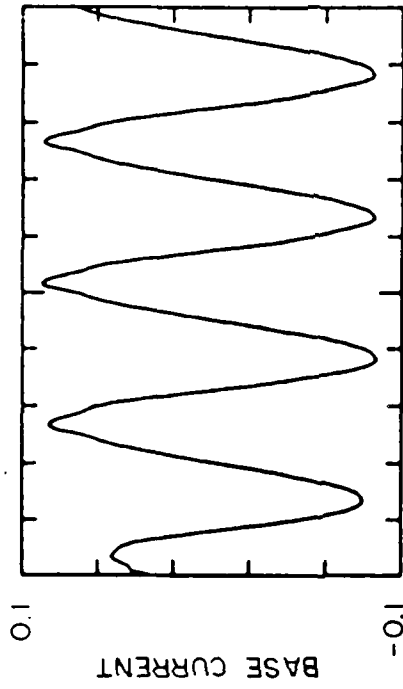
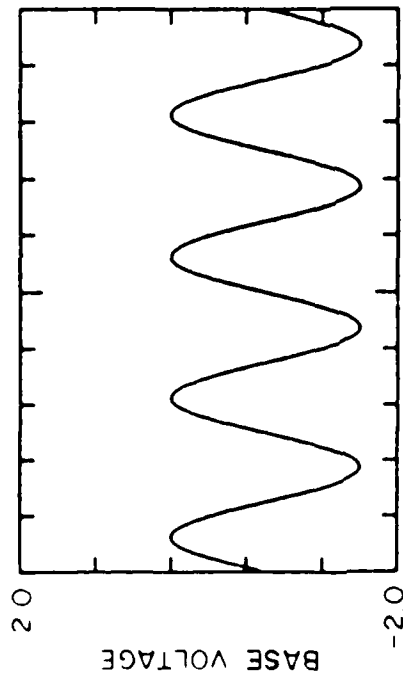


Scientific
Research
Associates

QUESTIONS

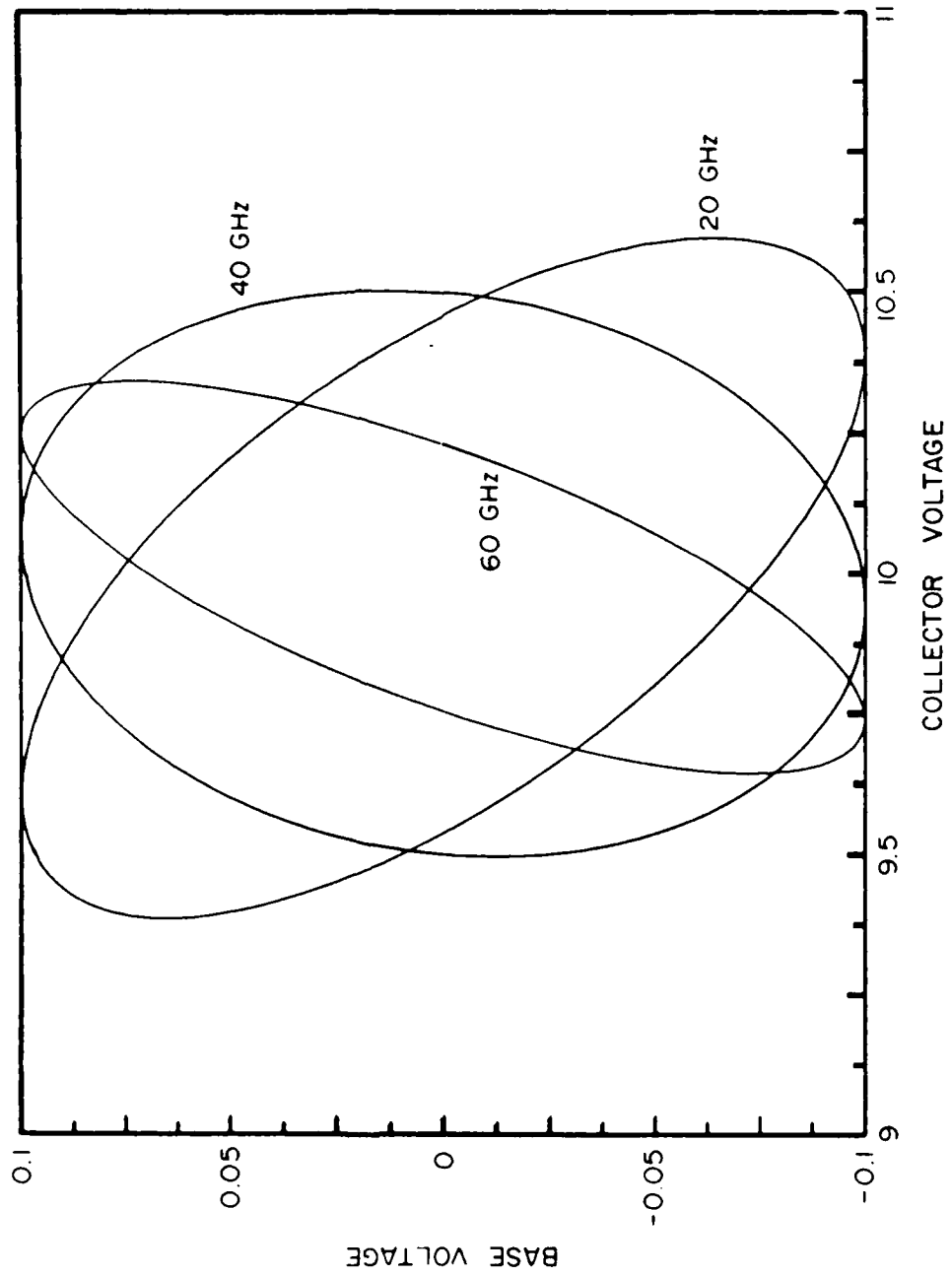
- HOW DO WE CHARACTERIZE THE LARGE SIGNAL BEHAVIOR OF THE PBT?

TIME DEPENDENT CURRENT AND VOLTAGE THROUGH BASE AND COLLECTOR



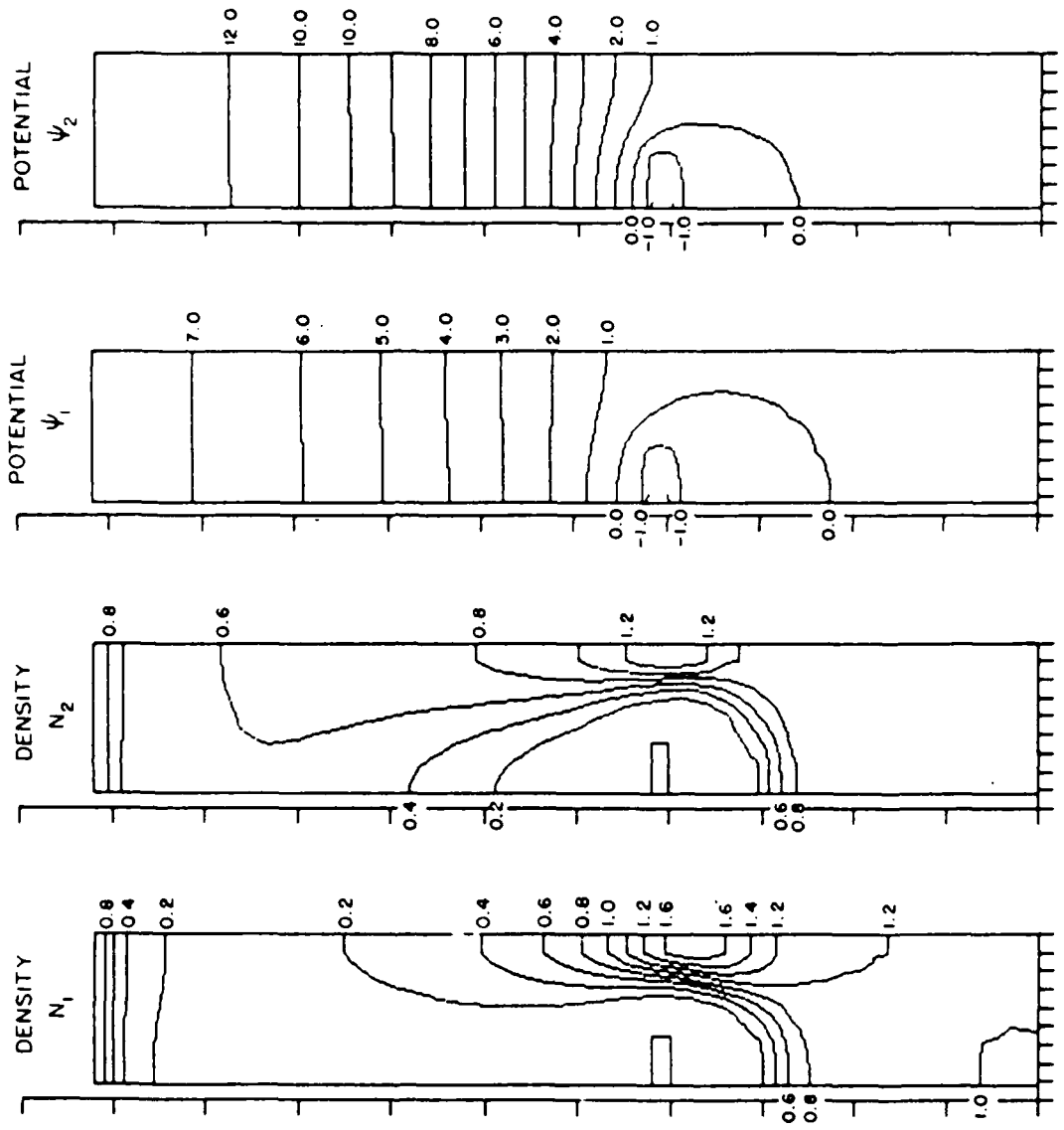
Scientific
Research
Associates

V_b vs. V_c LISSAJOUS

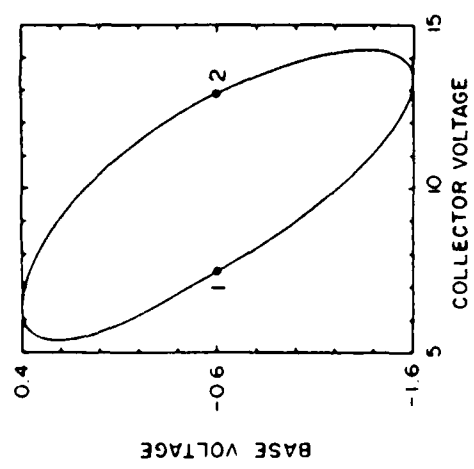


Scientific
Research
Associates

**DENSITY AND POTENTIAL CONTOURS FOR $V_b(0) = -0.6$, $V_b = 1.0$
CIRCUIT FREQUENCY = 60 GHz AND DRIVE FREQUENCY = 40 GHz**



$C = 5.10 \times 10^{-16}$ farad
 $L = 1.38 \times 10^{-6}$ henry

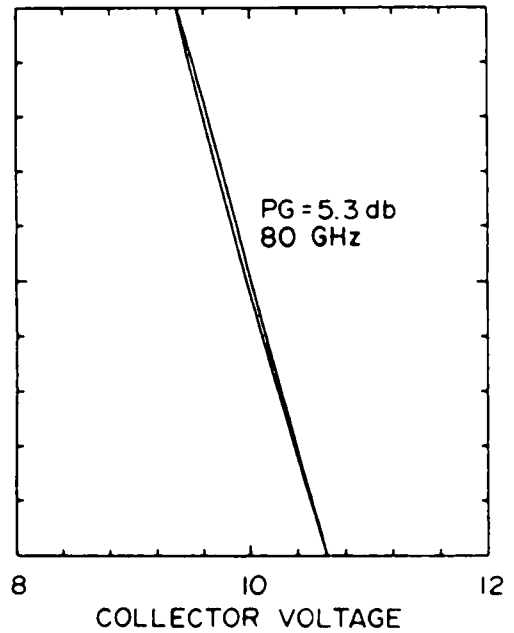
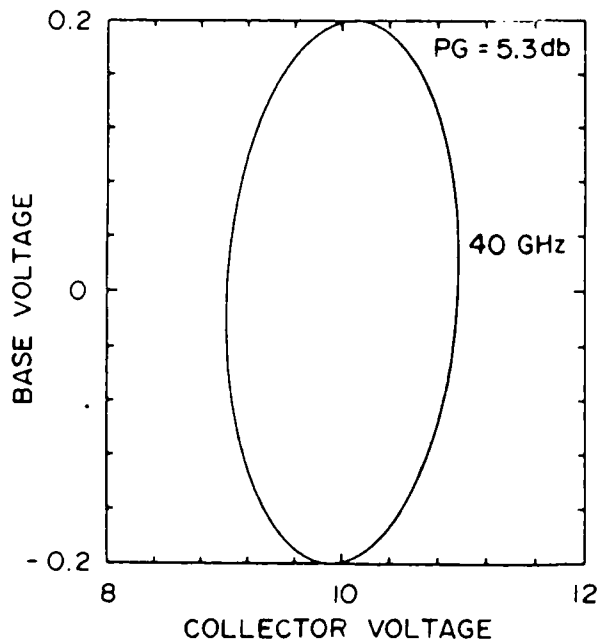
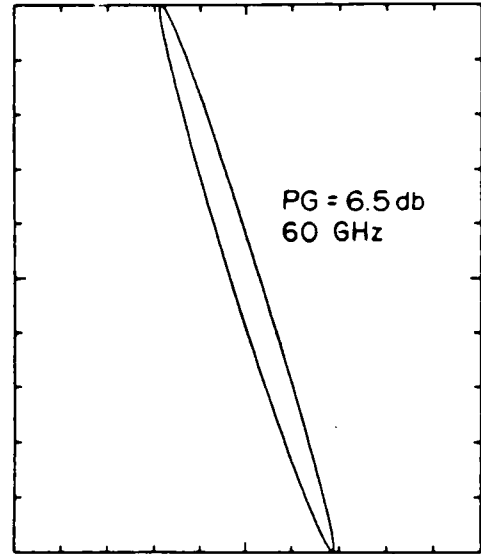
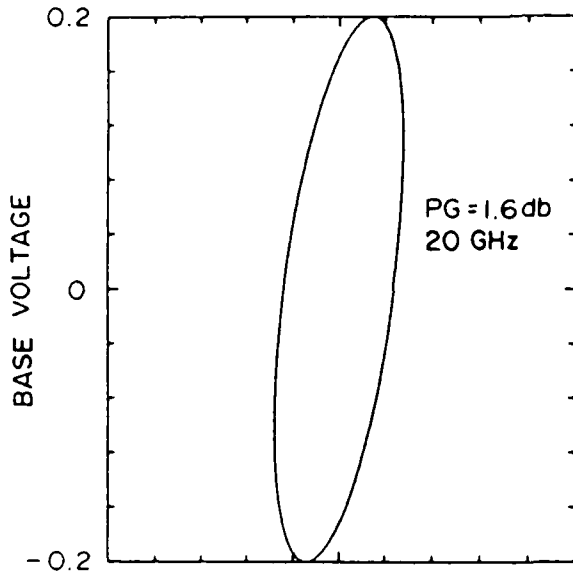


Scientific
Research
Associates

COMMENT ON THE RESISTIVE CIRCUIT CALCULATIONS

- AT THE LOWEST FREQUENCY OSCILLATION THE ELECTRONS HAVE AMPLE TIME TO RESPOND TO CHANGES IN THE BASE VOLTAGE.
DECREASES IN BASE VOLTAGE ARE ACCOMPANIED BY INCREASES IN COLLECTOR VOLTAGE.
 - AS THE FREQUENCY INCREASES ELECTRONS DO NOT HAVE SUFFICIENT TIME TO RESPOND TO THE CHANGE IN BASE VOLTAGE.
DECREASES IN BASE POTENTIAL ARE NOT NECESSARILY ACCOMPANIED BY INCREASES IN COLLECTIVE POTENTIAL.
- THIS IS AN UNSATISFACTORY SITUATION.

$V_B - V_C$ LISSAJOUS FOR $V_b(0) = 0.0, V_b = 0.2$
DRIVE FREQUENCY = 40 GHz, CIRCUIT FREQUENCY INDICATED



Scientific
 Research
 Associates

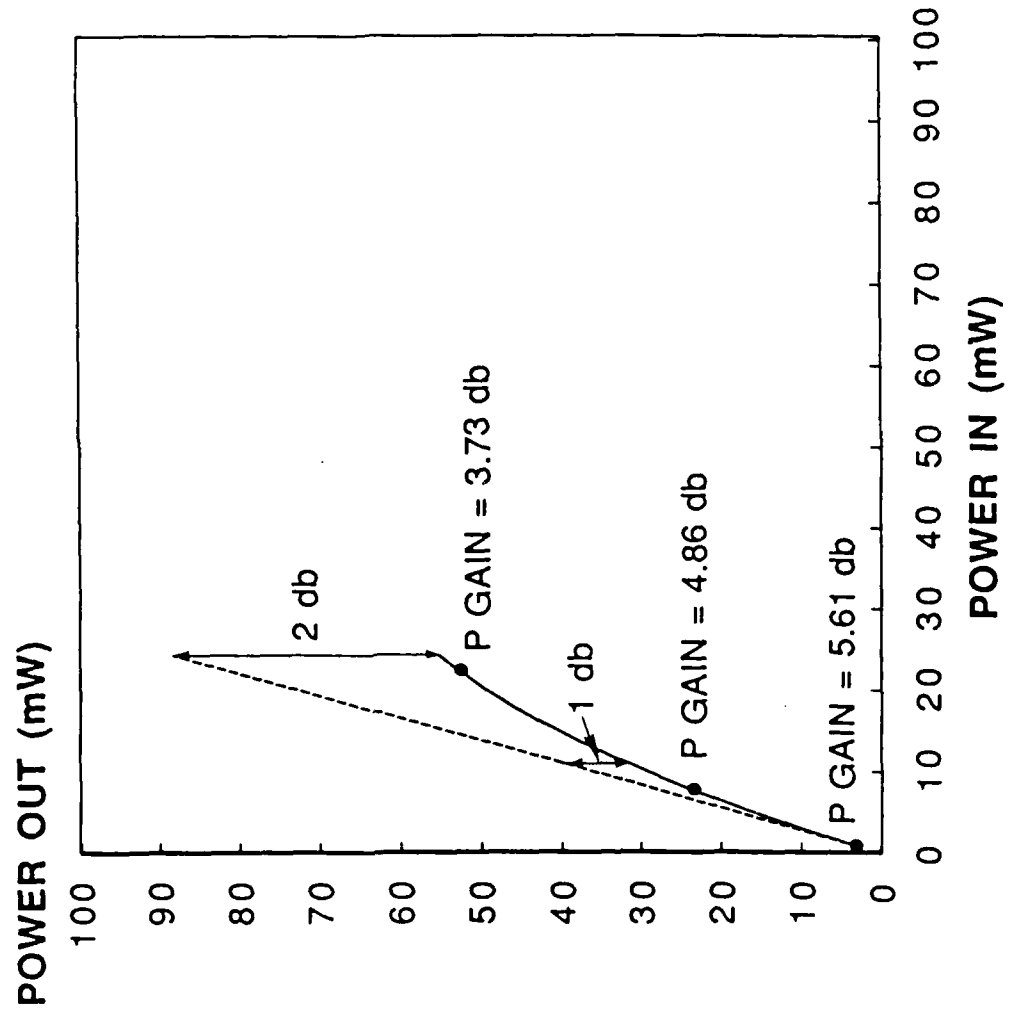
COMMENTS ON REACTIVE CIRCUIT CALCULATIONS

- THE CIRCUIT USED IS A SIMPLE REACTIVE ELEMENT CIRCUIT.

THE PHASE RELATIONSHIP BETWEEN THE REACTIVE CIRCUIT AND THE COLLECTOR CURRENT IS EASILY OBTAINED AND DEMONSTRATES THAT AT CIRCUIT FREQUENCIES ABOVE THE DRIVING FREQUENCY, IT IS POSSIBLE TO RESTORE A SUITABLE PHASE RELATIONSHIP SUCH THAT DECREASES IN BASE VOLTAGE ARE ACCOMPANIED BY INCREASES IN COLLECTOR VOLTAGE.

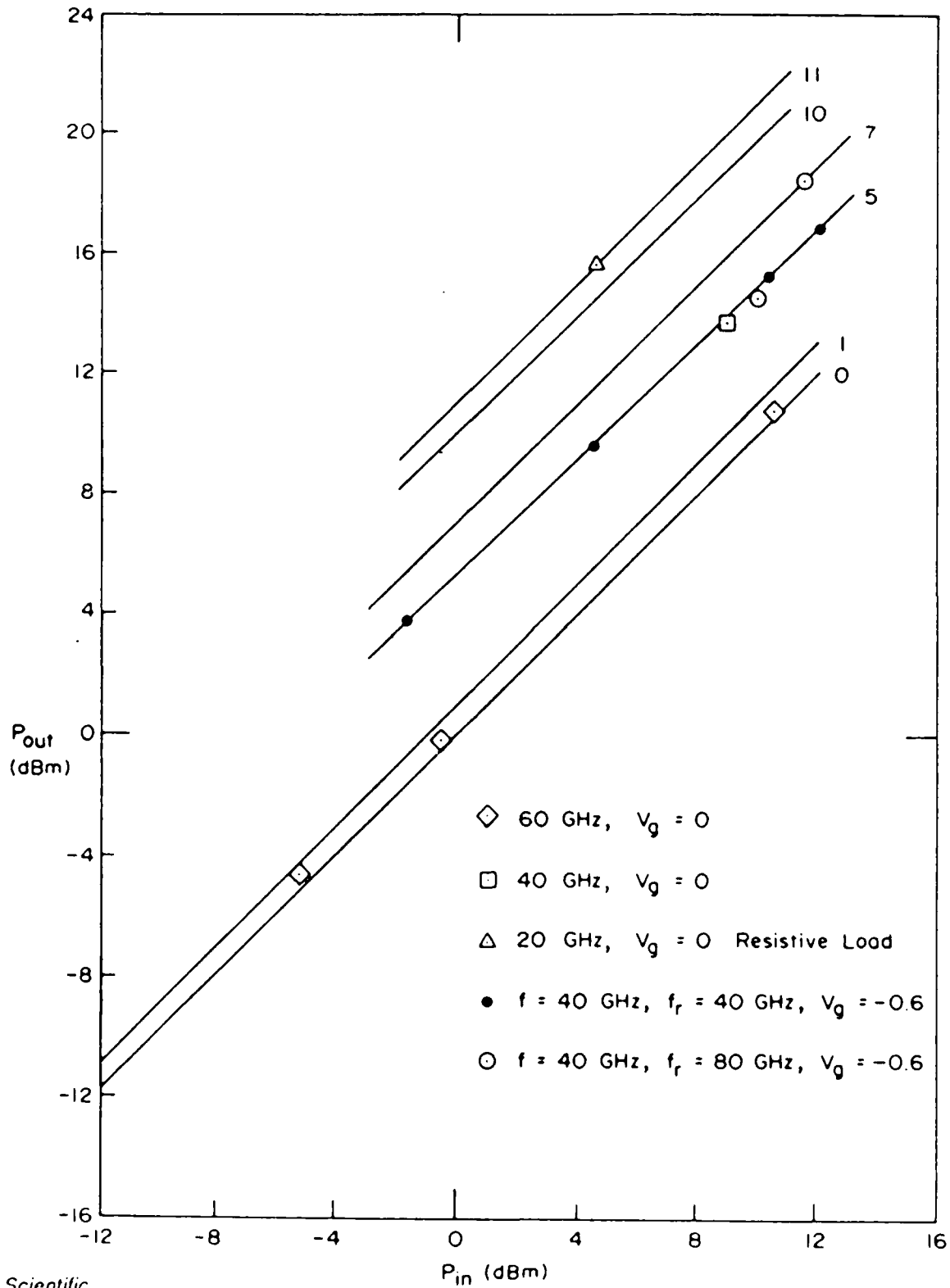
- SINCE CIRCUIT DESIGNERS CAN EXPERIMENTALLY OBTAIN LISSAJOUS FIGURES, THE LISSAJOUS IS AN IMPORTANT DESIGN PARAMETERS .

POWER (NEW DESIGN)



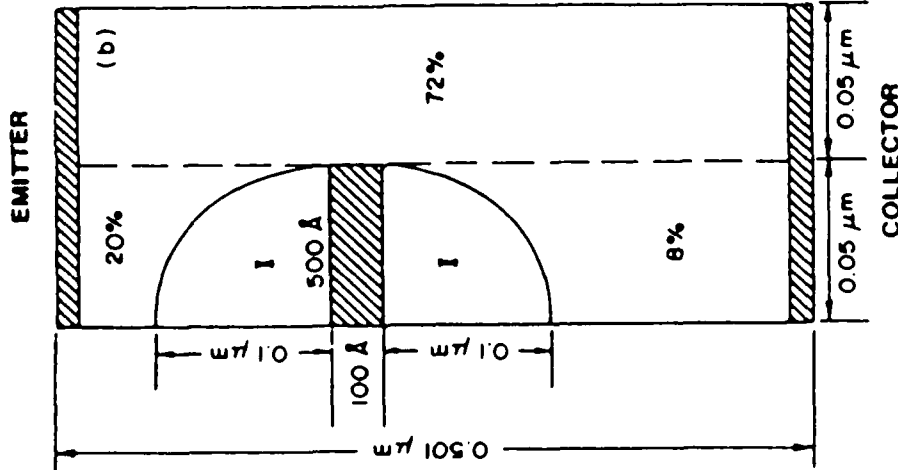
Scientific
Research
Associates

POWER (UNIFORM DOPING)



Scientific
Research
Associates

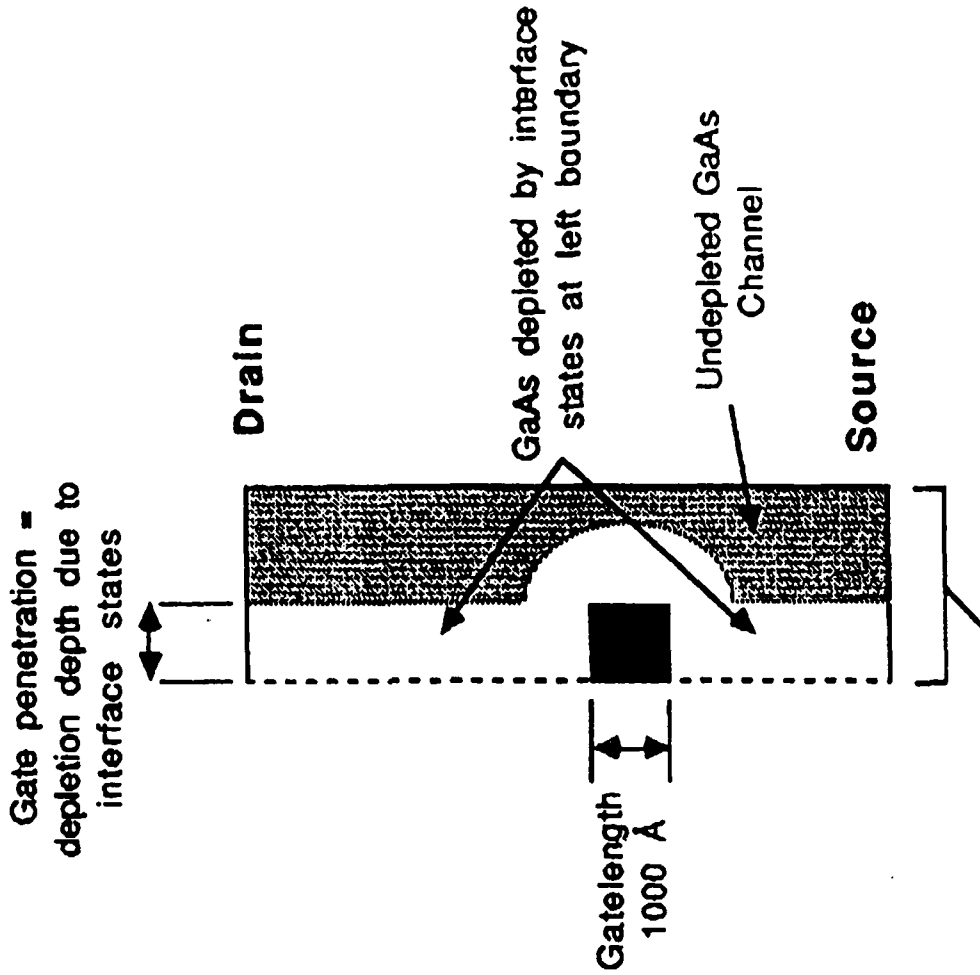
SRA



$N = 2.0 \times 10^{17}$
 $f_T = 80.5 \text{ GHz}$
 $I_D = 0.737 \text{ A/cm}$

LINCOLN LABS

REGROWTH FET WITH 1000 Å GATELENGTH



SRA STRUCTURE

- MEYYPAN et al., JOURNAL OF APPLIED PHYSICS
VOL. 64(9), p. 4733, NOVEMBER 1988
- MOTIVATION
 - CAPACITANCE SURROUNDING THE BASE IN
CONVENTIONAL PBT LARGELY PARASITIC
 - REGION OF SI GaAs PROVIDES A CONTOURED
BARRIER REDUCING UNWANTED STORED CHARGE
 - INCREASE IN f_T DEMONSTRATED

NEW WORK

- **CONTINUE POWER CHARACTERIZATION OF NONUNIFORMLY DOPED PBT**
- **STUDY NONUNIFORMLY DOPED PBT WITH REDUCED BASE PENETRATION**
- **STUDY PBT / REGROWTH FET**

*Scientific
Research
Associates*

PBT SUMMARY

- LARGE SIGNAL PBT DC CALCULATIONS DEMONSTRATE VERY HIGH BREAKDOWN VOLTAGES FOR DEVICES
- UNIFORM STRUCTURES AT $5 \times 10^{16} / \text{cm}^3$ OFFER OUTPUT POWERS AND LINEAR GAINS IN EXCESS OF 50 mW
- SCALING TO A DENSITY OF $2 \times 10^{17} / \text{cm}^3$ AND A FOURFOLD INCREASE IN CROSS-SECTIONAL AREA SUGGEST THE POSSIBILITY OF 3/4 WATT OF POWER AT 40 GHz

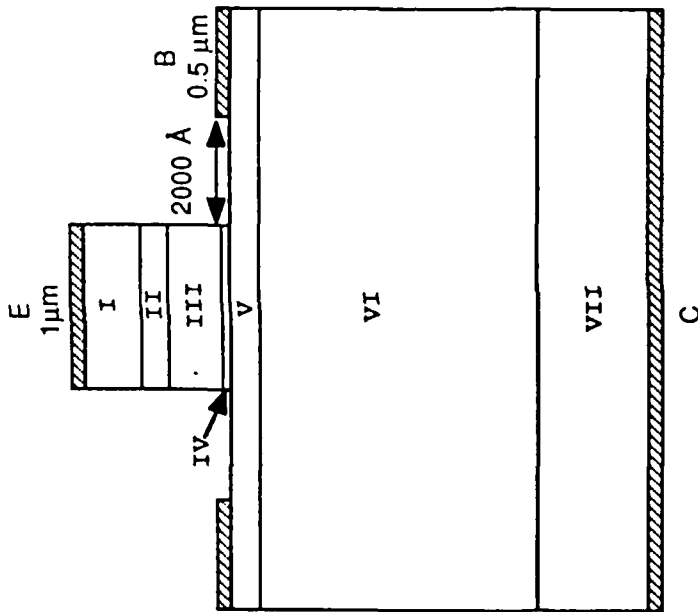
**InP/InGaAs HETEROSTRUCTURE
BIPOLAR TRANSISTORS**

**SCIENTIFIC RESEARCH ASSOCIATES, INC.
GLASTONBURY, CT**

*Scientific
Research
Associates*

InP / InGaAs HBT's ADVANTAGES

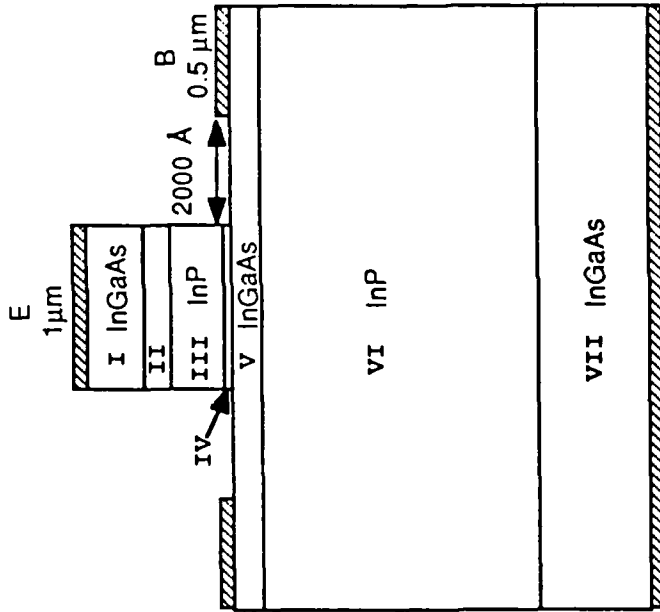
- BETTER ELECTRON INJECTION DUE TO SMALLER CONDUCTION BAND-SPIKE THAN AlGaAs/GaAs SYSTEM
- EFFECTIVE BLOCKING OF HOLES DUE TO HIGHER ΔE_v THAN AlGaAs/GaAs SYSTEM
- LOWER RECOMBINATION (100 ns InP/InGaAs, 1 ns AlGaAs/GaAs)
- SELECTIVE TRANSPORT PROPERTIES SUPERIOR TO GaAs
 - HIGHER DRIFT VELOCITY OF InP (COLLECTOR REGION)
 - HIGHER ELECTRON MOBILITY OF InGaAs (BASE REGION)
- COMPATIBILITY WITH OPTOELECTRONIC IC'S



I	EMITTER CAP	$\text{In}_{0.53}\text{Ga}_{0.47}\text{As}$	1000 Å	$5 \times 10^{18} \text{ N}^+$
II	GRADED LAYER	$\text{InGaAs} \rightarrow \text{InP}$	500 Å	$5 \times 10^{18} \text{ N}^+$
III	EMITTER	InP	1000 Å	$2 \times 10^{17} \text{ N}$
IV	GRADED LAYER	$\text{InP} \rightarrow \text{InGaAs}$	100 Å	$2 \times 10^{17} \text{ N}$
V	BASE	BANDGAP GRADING $\text{In}_{0.53}\text{Ga}_{0.47}\text{As}$	500 Å	$5 \times 10^{18} \text{ P}^+$
VI	COLLECTOR	InP	5000 Å	$1 \times 10^{17} \text{ N}$
VII	SUBCOLLECTOR	$\text{In}_{0.53}\text{Ga}_{0.47}\text{As}$	2000 Å	$5 \times 10^{18} \text{ N}^+$

Scientific
Research
Associates

DOUBLE HETEROSTRUCTURE, InP/InGaAs/InP



Layer	Material	Thickness	Doping
I	EMITTER CAP	1000 Å	$5 \times 10^{18} \text{ N}^+$
II	GRADED LAYER	500 Å	$5 \times 10^{18} \text{ N}^+$
III	EMITTER	1000 Å	$2 \times 10^{17} \text{ N}$
IV	GRADED LAYER	100 Å	$2 \times 10^{17} \text{ N}$
V	BASE	500 Å	$5 \times 10^{18} \text{ P}^+$
VI	COLLECTOR	5000 Å	$1 \times 10^{17} \text{ N}$
VII	SUBCOLLECTOR	2000 Å	$5 \times 10^{18} \text{ N}^+$

Scientific
Research
Associates

CRITICAL DEVICE FEATURES

- SELF-ALIGNED STRUCTURE
- 500 Å BASE, BAND-GAP GRADING EMPLOYED
- 5000 Å COLLECTOR DOPED, 10^{17} N
- 1 μm STRIPE-WIDTH FOR EMITTER

Scientific
Research
Associates

GOVERNING EQUATIONS

- POISSON'S EQUATION

$$\nabla \cdot (\epsilon \nabla \psi) = +e(n - p - C)$$

- DRIFT AND DIFFUSION EQUATIONS

$$\partial n / \partial t = \nabla \cdot J_n / e - R_n$$

$$\partial p / \partial t = \nabla \cdot J_p / e - R_p$$

$$J_n = e(n\mu_n F_n - n\mu_n \nabla \psi - D_n \nabla n)$$

$$J_p = -e(p\mu_p F_p + p\mu_p \nabla \psi + D_p \nabla p)$$

$$F_n = \nabla(\chi / e + (kT / e) \ln N_c)$$

$$F_p = \nabla(\chi / e + E_g / e - (kT / e) \ln N_v)$$

GOVERNING EQUATIONS (continued)

- RECOMBINATION

$$R_{SRH} = R_n = R_p + [pn - n_i^2] / [\tau_p(n + n_i) + \tau_n(p + p_i)]$$

$$R_{Aug} = r(n + p) (np - n_i^2)$$

- TRANSPORT PROPERTIES

$$\mu = \frac{V}{F}$$

WHERE $F = -\nabla\psi \cdot F_n$ FOR ELECTRONS

$F = -\nabla\psi \cdot F_p$ FOR HOLES

$$D = \frac{kT}{q} \mu \quad (\text{EINSTEIN RELATION})$$

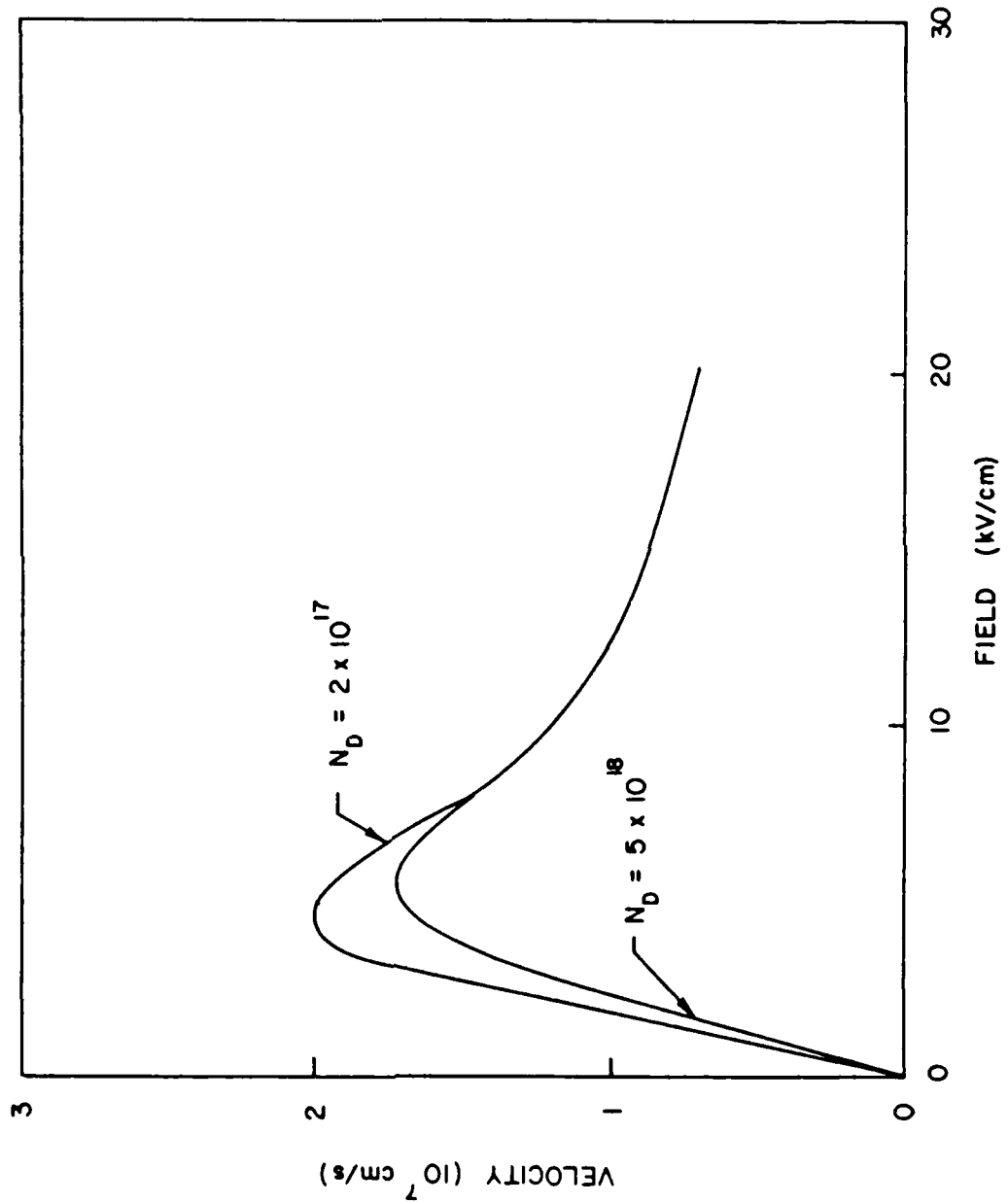
- BOUNDARY CONDITION AT THE OHMIC CONTACTS

$$\psi = \psi_{\text{applied}} - \frac{kT}{e} \ln \frac{N_c}{N_D} - \chi / e$$

TRANSPORT PROPERTIES

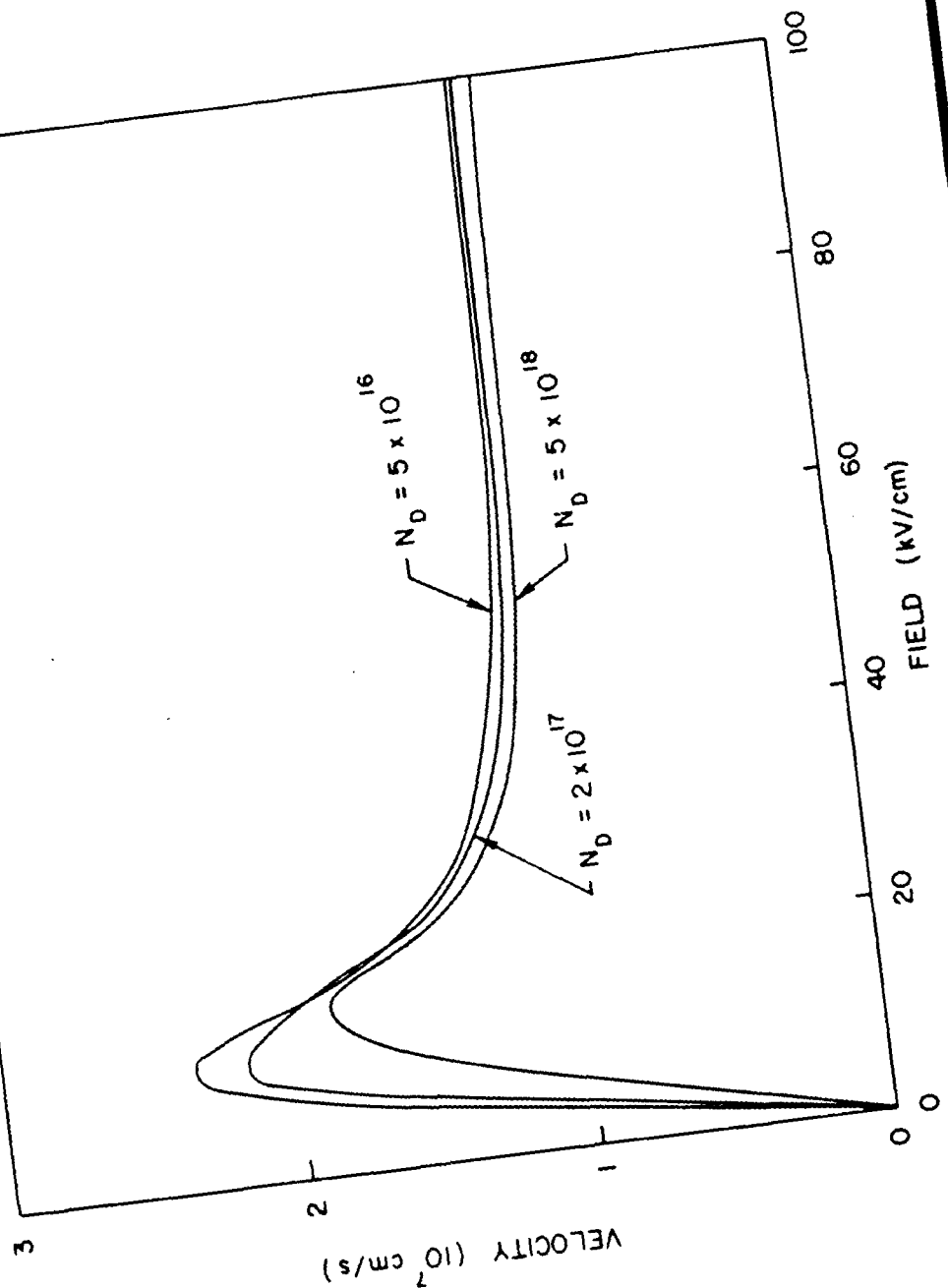
- VELOCITY-FIELD CHARACTERISTICS, LOW-FIELD MOBILITY
- EVALUATED FOR BOTH InP AND $\text{In}_{0.53}\text{Ga}_{0.47}\text{As}$ AT VARIOUS DOPING LEVELS USING A MONTE-CARLO PROCEDURE

VELOCITY-FIELD CHARACTERISTICS: $\text{In}_{0.53}\text{Ga}_{0.47}\text{As}$



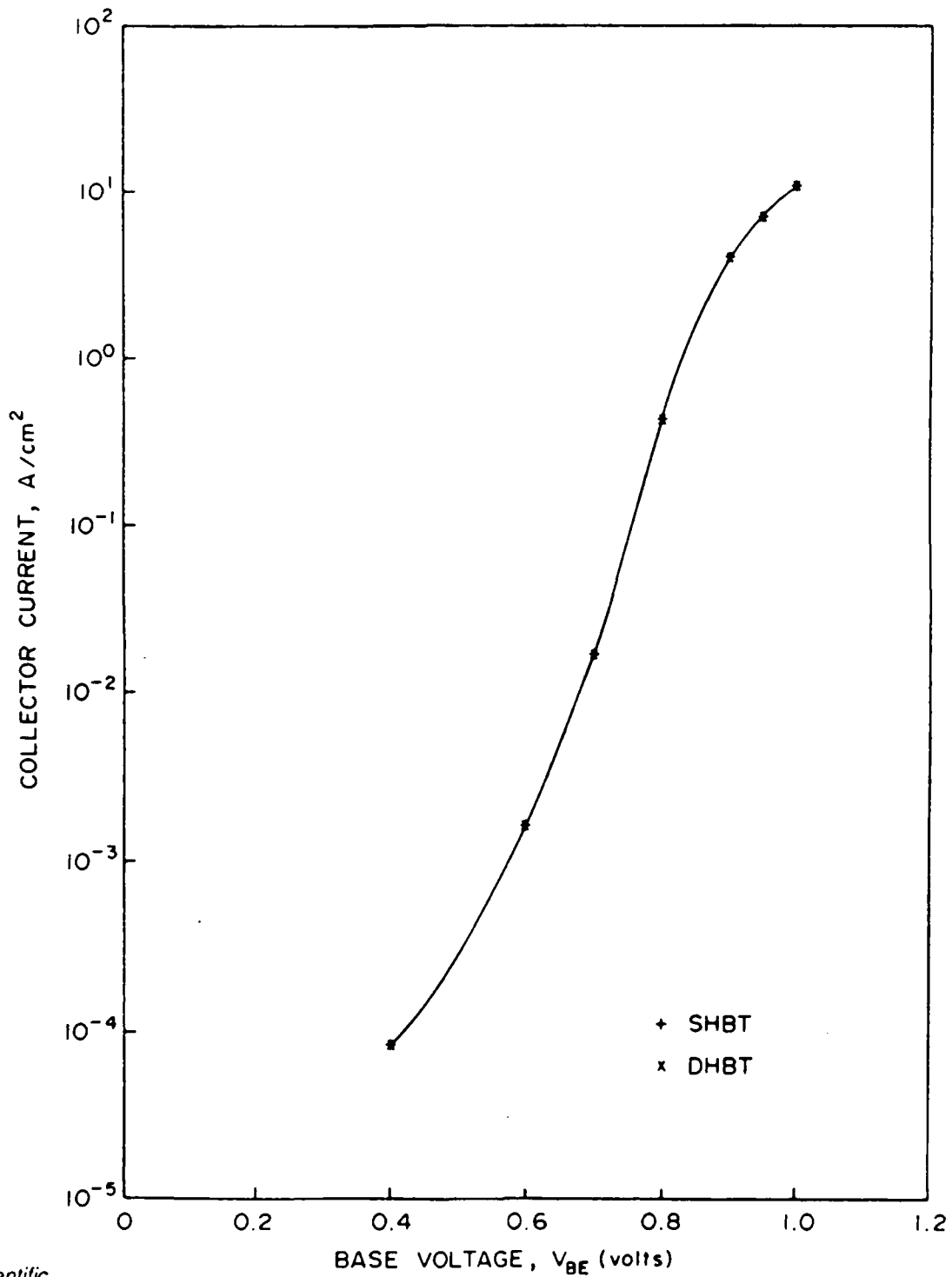
Scientific
Research
Associates

VELOCITY-FIELD CHARACTERISTICS: InP



Scientific
Research
Associates

COLLECTOR CURRENT vs. V_{BE} FOR InP/InGaAs DHBT AND SHBT



Scientific
Research
Associates

• VARIATION OF I_C WITH V_{BE} IDENTICAL FOR SHBT AND DHBT

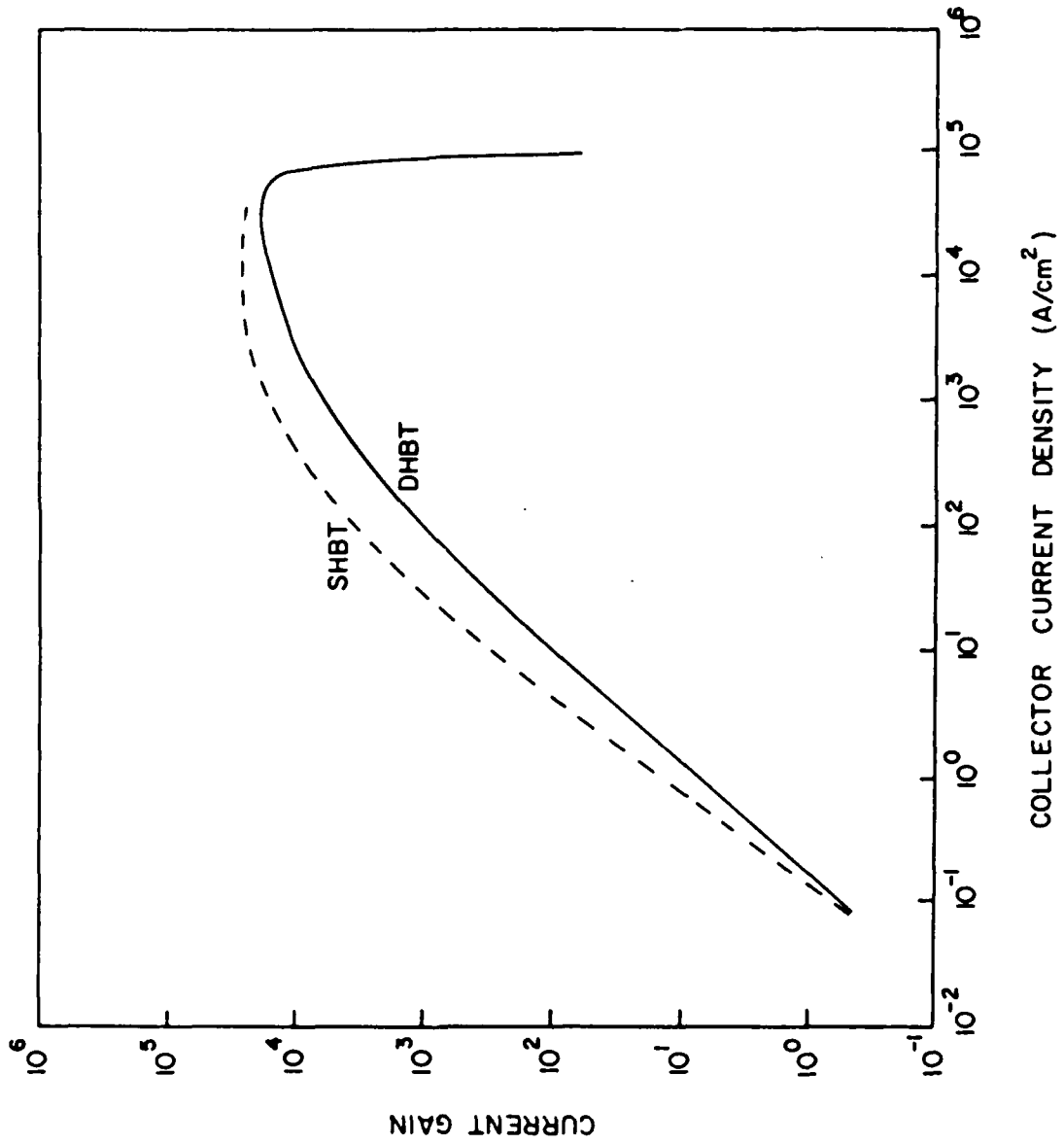
• CURRENT LIMITED BY EMITTER INJECTION:
EMITTER / BASE DESIGN SAME IN BOTH CASES

• COLLECTOR TRANSPORT DETERMINED BY
SATURATION VELOCITY

• $V_{sat, InP} / V_{sat, InGaAs} \approx 3$

• CARRIER DENSITY IN THE COLLECTOR
ADJUSTS $n_{InP} / n_{InGaAs} \sim 1/3$

CURRENT GAIN vs. COLLECTOR CURRENT



Scientific
Research
Associates

CONCLUSIONS

- HIGHER CUT-OFF FREQUENCY POSSIBLE WITH
InP/InGaAs THAN THE AlGaAs/GaAs SYSTEM
- HIGHER CURRENT GAIN POSSIBLE WITH
InP/InGaAs THAN THE AlGaAs/GaAs SYSTEM
- FURTHER CALCULATIONS NEEDED TO OPTIMIZE
InP/InGaAs/InP HBT

COMPARISON AGAINST EXPERIMENTAL RESULTS

• NOTTENBURG et al.: JANUARY 1989

STRUCTURE WITH 3000 Å COLLECTOR, $N_D = 2 \times 10^{16}$

650 Å BASE DOPED $N_A = 5 \times 10^{19}$

3000 Å EMITTER $N_D = 5 \times 10^{17}$

HIGHEST $f_T = 110$ GHz

$f_{max} = 58$ GHz

CURRENT GAIN = 11000

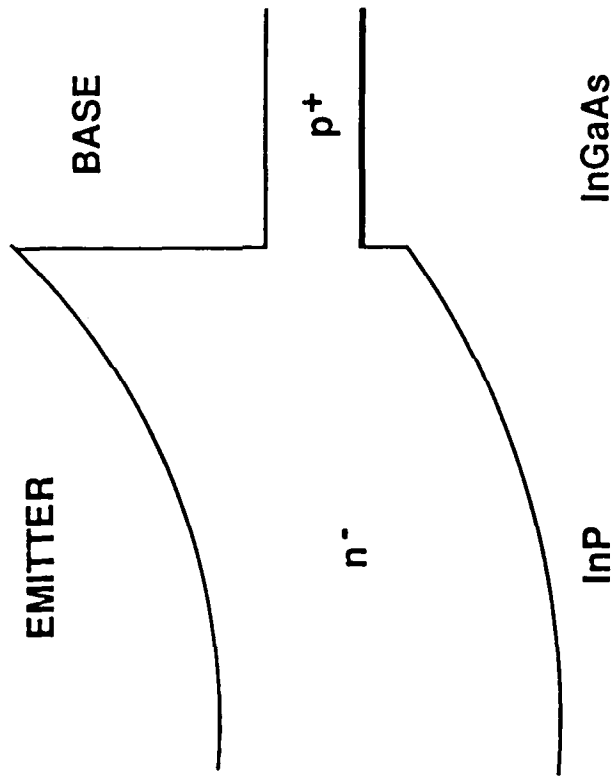
Scientific
Research
Associates

FIGURES-OF-MERIT

• CURRENT GAIN 2.63×10^4 FOR DHBT
vs. 2.55×10^4 FOR SHBT

• CUT-OFF FREQUENCY 78.6 GHz AT $I_c = 5.5 \times 10^4$ A/cm²
FOR DHBT vs. 46.9 GHz AT $I_c = 3.6 \times 10^4$ A/cm²

BAND DIAGRAM

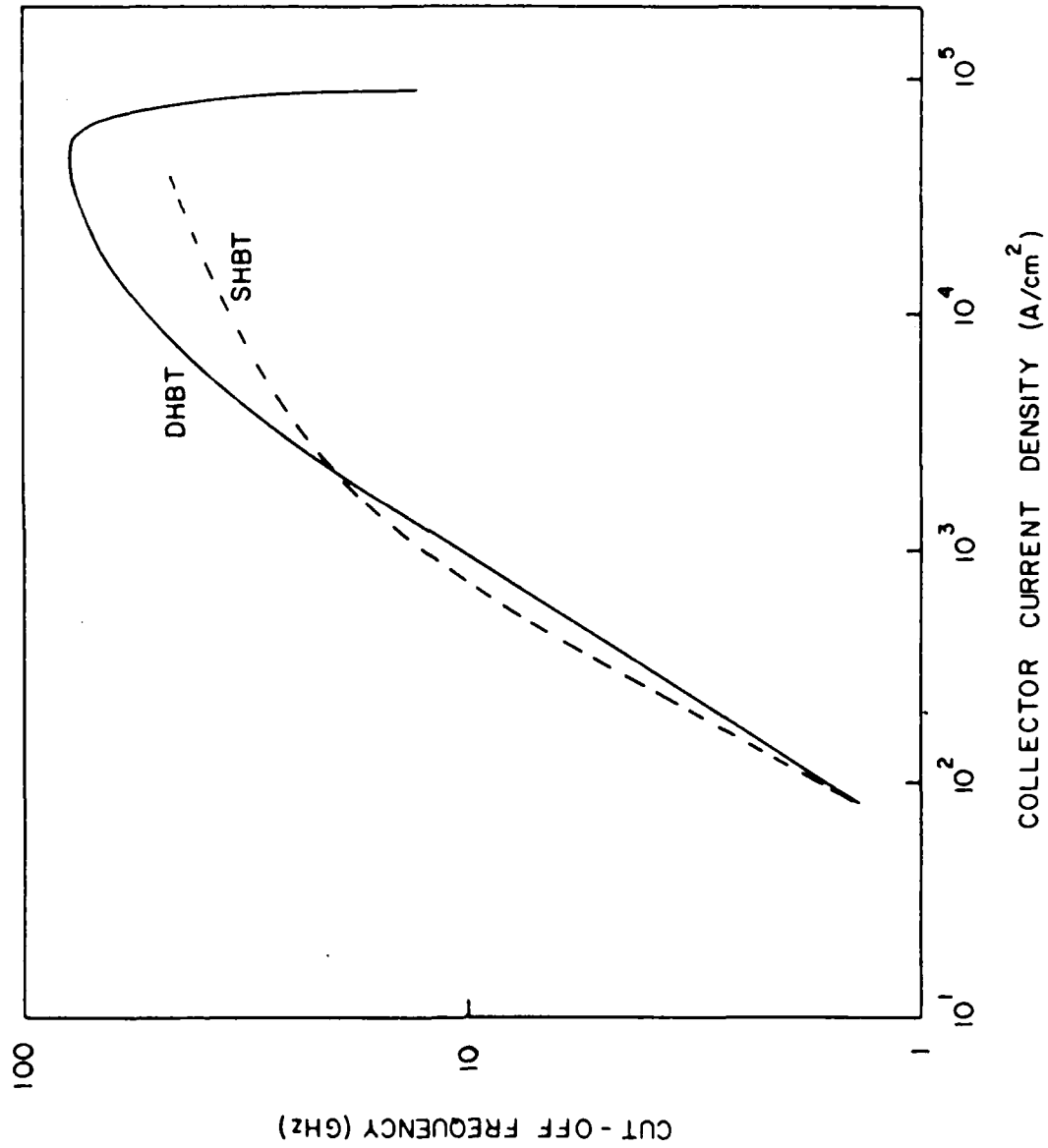


$$\Delta E_c = 0.22 \text{ eV}$$

$$\Delta E_v = 0.37 \text{ eV}$$

Scientific
Research
Associates

CUT-OFF FREQUENCY vs. COLLECTOR CURRENT



Scientific
Research
Associates

FUTURE WORK

- INCREASE BASE DOPING TO REDUCE SHEET RESISTANCE AND INCREASE f_{\max}
- REDUCE COLLECTOR WIDTH TO DECREASE COLLECTOR TRANSIT TIME
- OPTIMIZE EMITTER DIMENSIONS FOR POWER
- PERFORM TRANSIENT ACCURATE, SMALL SIGNAL CALCULATIONS
- PNP STRUCTURES FOR COMPLEMENTARY DEVICE CIRCUITS

FUTURE WORK (cont.)

LARGE SIGNAL SWITCHING:

- SWITCHING FROM "OFF" TO A HIGH CONDUCTION STATE BY IMPOSING A STEP CHANGE IN BASE VOLTAGE KEEPING COLLECTOR BIAS FIXED
- COMPUTING DEVICE RESPONSE TIME THROUGH TRANSIENT ACCURATE CALCULATIONS

SMALL SIGNAL AMPLIFICATION:

- IMPOSE A SINUSOIDAL SIGNAL ON THE BASE CONTACT, KEEPING COLLECTOR BIAS FIXED
- FOURIER ANALYZE THE RESULTS TO COMPUTE f_{\max} AND POWER

MATERIAL AND TRANSPORT PROPERTIES

E_g : $\text{Al}_{0.3}\text{GaAs}$ (1.8 ev) > GaAs (1.424 ev) > InP (1.34 ev) > $\text{In}_{0.53}\text{GaAs}$ (0.75 ev)

x: $\text{In}_{0.53}\text{GaAs}$ (4.6 ev) > InP (4.38 ev) > GaAs (4.07 ev) > $\text{Al}_{0.3}\text{GaAs}$ (3.752 ev)

V_{sat} : 10^7 cm/s FOR InP

7.5×10^6 cm/s FOR GaAs

5×10^6 cm/s FOR $\text{Al}_{0.3}\text{GaAs}$

3.5×10^6 cm/s FOR $\text{In}_{0.53}\text{GaAs}$

ΔE_c : 0.22 ev FOR InP/InGaAs vs. 0.318 ev FOR AlGaAs/GaAs

ΔE_v : 0.37 ev FOR InP/InGaAs vs. 0.057 ev FOR AlGaAs/GaAs

Scientific
Research
Associates

CURRENT GAIN

- TWO ORDERS OF MAGNITUDE HIGHER THAN AlGaAs/GaAs SYSTEM
- DUE TO LONGER CARRIER LIFE-TIME (100 ns vs. 1 ns)
- NEGLIGIBLE SURFACE RECOMBINATION
- LARGE VALENCE BAND DISCONTINUITY ($\Delta E_v = 0.37$ eV) TO PREVENT HOLE INJECTION INTO EMITTER (COMPARE 0.059 FOR AlGaAs/GaAs SYSTEM)
- CONDUCTION BAND DISCONTINUITY 0.22 V FOR ELECTRON INJECTION (COMPARE 0.318 FOR AlGaAs/GaAs SYSTEM)

GaAlAs/GaAs Heterojunction Bipolar Transistors for mm-Wave Applications

Peter Asbeck

*Rockwell International, Science Center
Thousand Oaks, CA*

**GaAlAs/GaAs HETEROJUNCTION BIPOLAR
TRANSISTORS FOR mm-WAVE APPLICATIONS**

**CONTRACT N00014-86-C-0078
MONITORED BY ONR**

**ROCKWELL INTERNATIONAL, SCIENCE CENTER
THOUSAND OAKS, CA**



GaAlAs/GaAs HETEROJUNCTION BIPOLAR TRANSISTOR DEVELOPMENT

ROCKWELL INTERNATIONAL

SC44039

OBJECTIVE

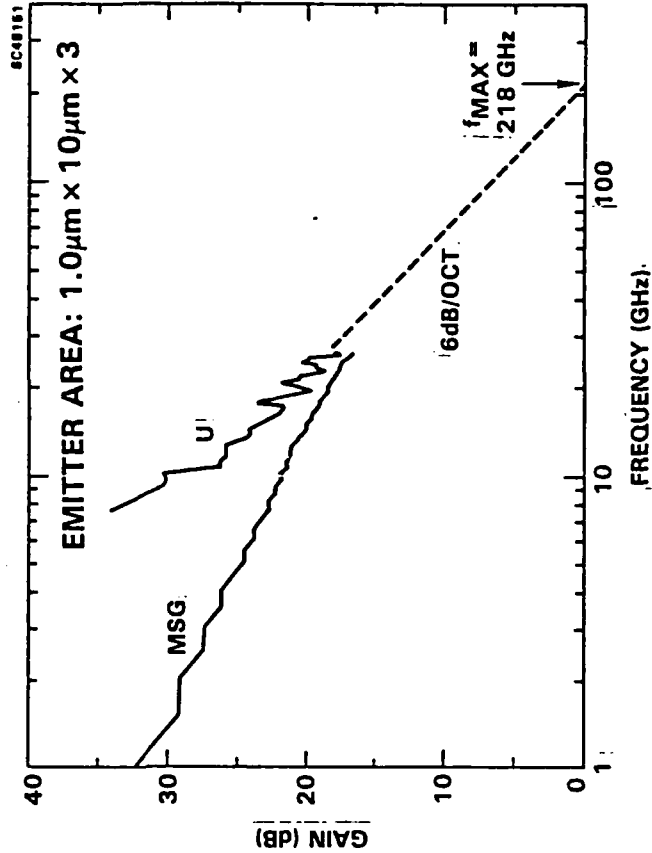
DEVELOP TRANSISTORS WITH
SUPERIOR GAIN AND POWER HANDLING
CAPABILITY AT 60 GHz AND 94 GHz

APPROACH

UTILIZE GaAlAs/GaAs MULTILAYER
STRUCTURES TO OPTIMIZE THE
PERFORMANCE OF BIPOLAR
TRANSISTORS

STATUS

- FIRST HIGH PERFORMANCE, MM-WAVE
COLLECTOR UP HBTs DEMONSTRATED-
FMAX = 100 GHz
- FMAX OF EMITTER-UP HBTs INCREASED
TO 215 GHz
- MMIC COMPATIBLE TECHNOLOGY
DEMONSTRATED
- AMPLIFIER BEHAVIOR AT 94 GHz
MODELED



Rockwell International
Science Center

MM-WAVE HBT TEAM

MBE

G. Sullivan
M. Szwed

PROCESS

F. Chang
W.J. Ho
R. Anderson
R. Pierson
K. Steckbauer

**CHARACTERIZATION
& MODELING**

N.H. Sheng
P. Asbeck
J.A. Higgins
E. Sovero
K.C. Wang
D. Deakin

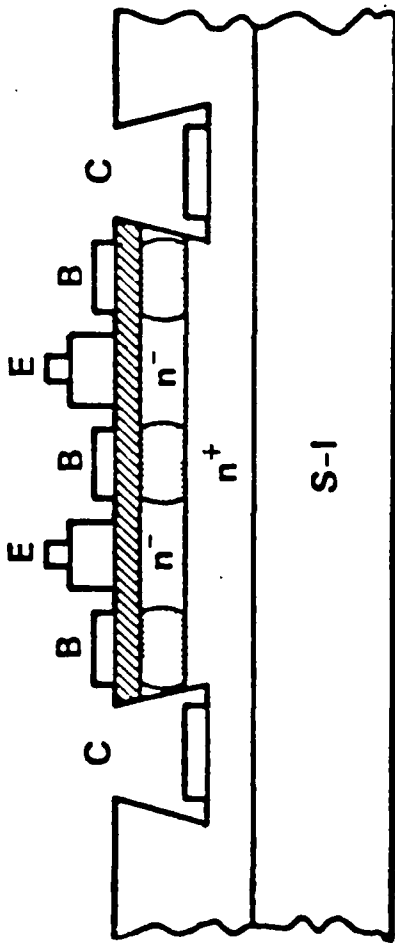
SPONSOR

J. MURPHY

WHY HBTs FOR mm-WAVE OPERATION?

- VERTICAL STRUCTURE
 - CONTROLLABLE SHORT DIMENSIONS
 - EASE OF VARYING COMPOSITION PROFILE
 - HIGH POWER DENSITY
 - NO SUBSTRATE LEAKAGE
- ROBUST FABRICATION WITH SIMPLE LITHOGRAPHY
- LOW OUTPUT CONDUCTANCE
- CONTROLLABLE BREAKDOWN VOLTAGE

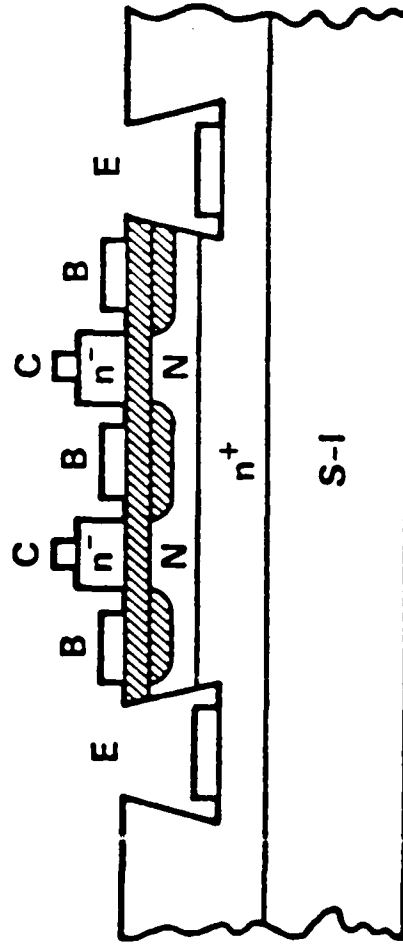
EMITTER-Up mm-WAVE HBT



- SIMPLER FABRICATION
- LOWER EMITTER RESISTANCE

$$f_{\max} = \sqrt{\frac{ft}{8 \pi R_B C_{BC}}}$$

COLLECTOR-Up mm-WAVE HBT



- LOWER BASE-COLLECTOR CAPACITANCE
- LOWER EMITTER INDUCTANCE



Rockwell International
Science Center

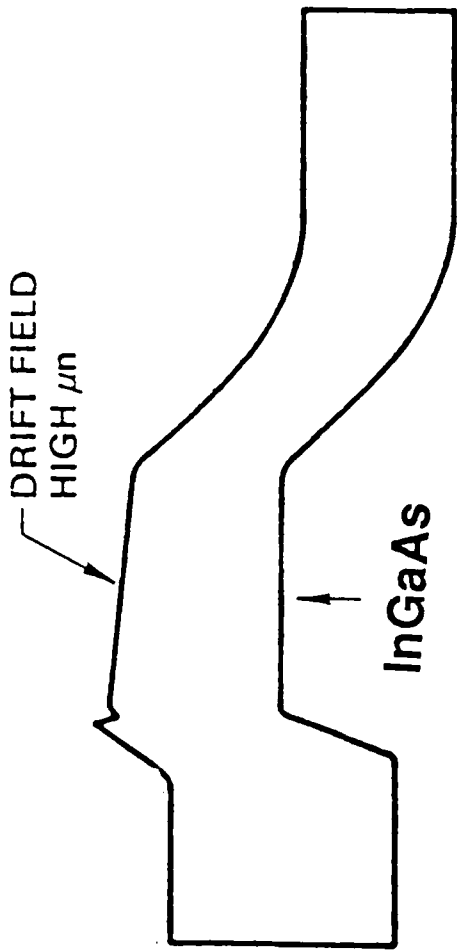


OUTLINE

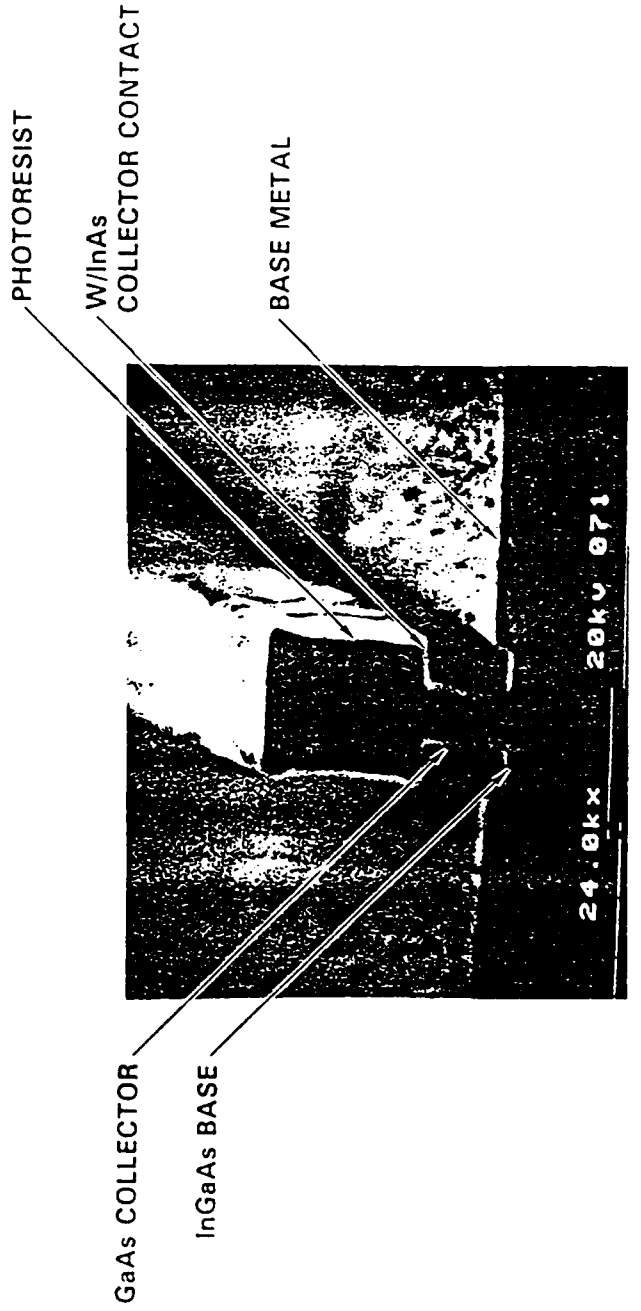
- COLLECTOR-UP FABRICATION AND RESULTS
- EMITTER-UP FABRICATION AND RESULTS
- DEVICE AND CIRCUIT MODELING
- HBT PROGRESS AT LOWER FREQUENCIES

APPROACH TO BASE ETCH

InGaAs IS ETCH STOP FOR RIE

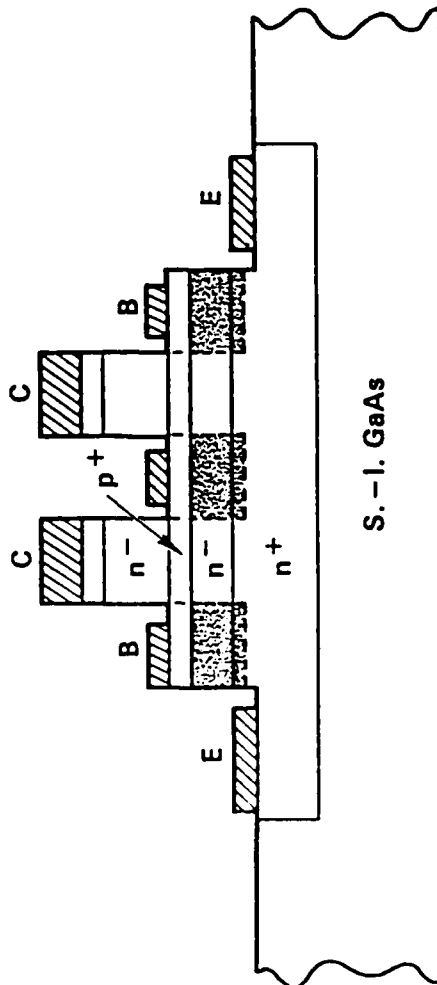
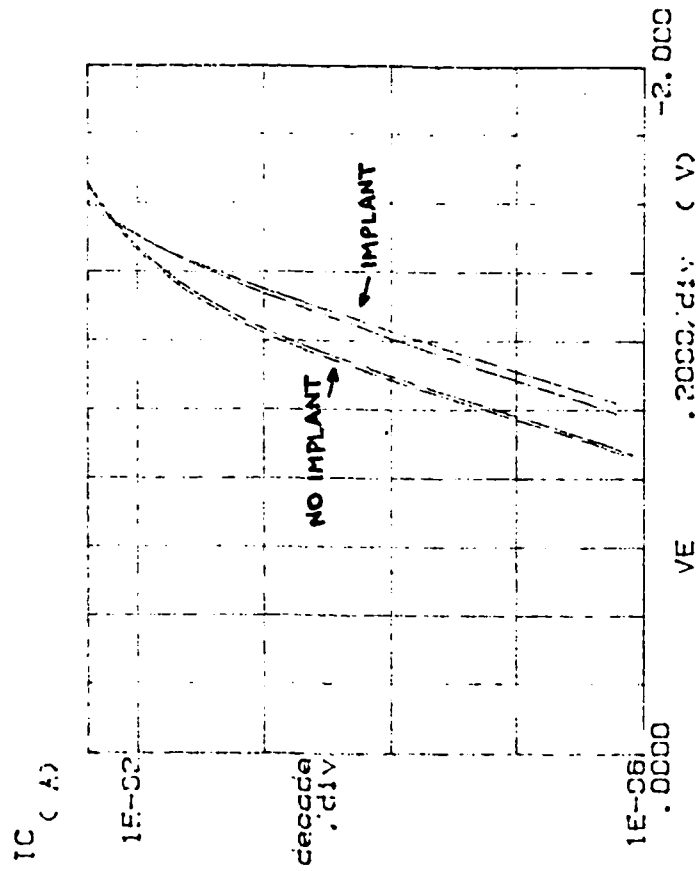


SC41684



APPROACH TO SUPPRESS INJECTION UNDER CONTACTS

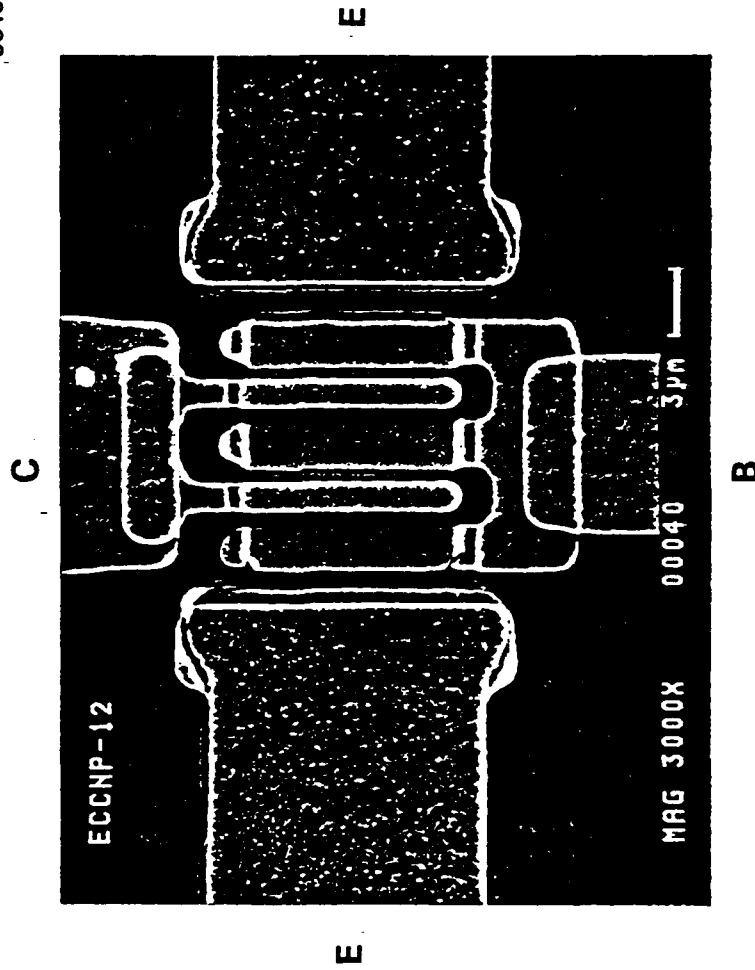
SELF-ALIGNED PROTON BOMBARDMENT REDUCES INJECTION BY X10



I-V Characteristics of Test B-E Diodes

COLLECTOR-UP HBT

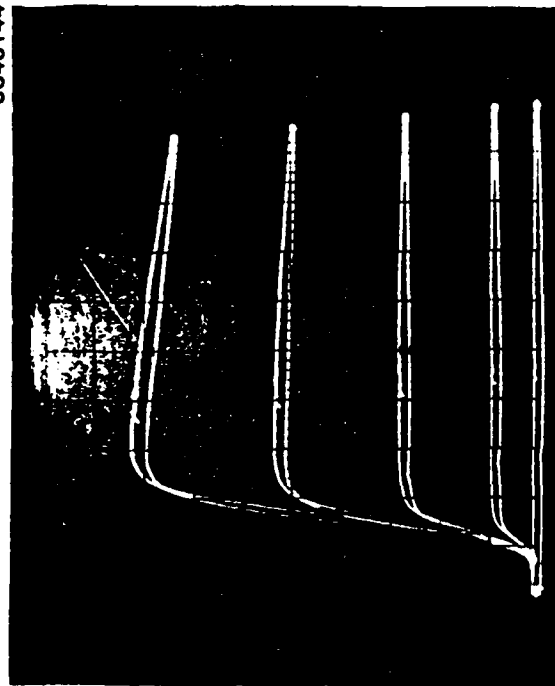
SC48142



COLLECTOR-UP HBT — I-V CHARACTERISTICS

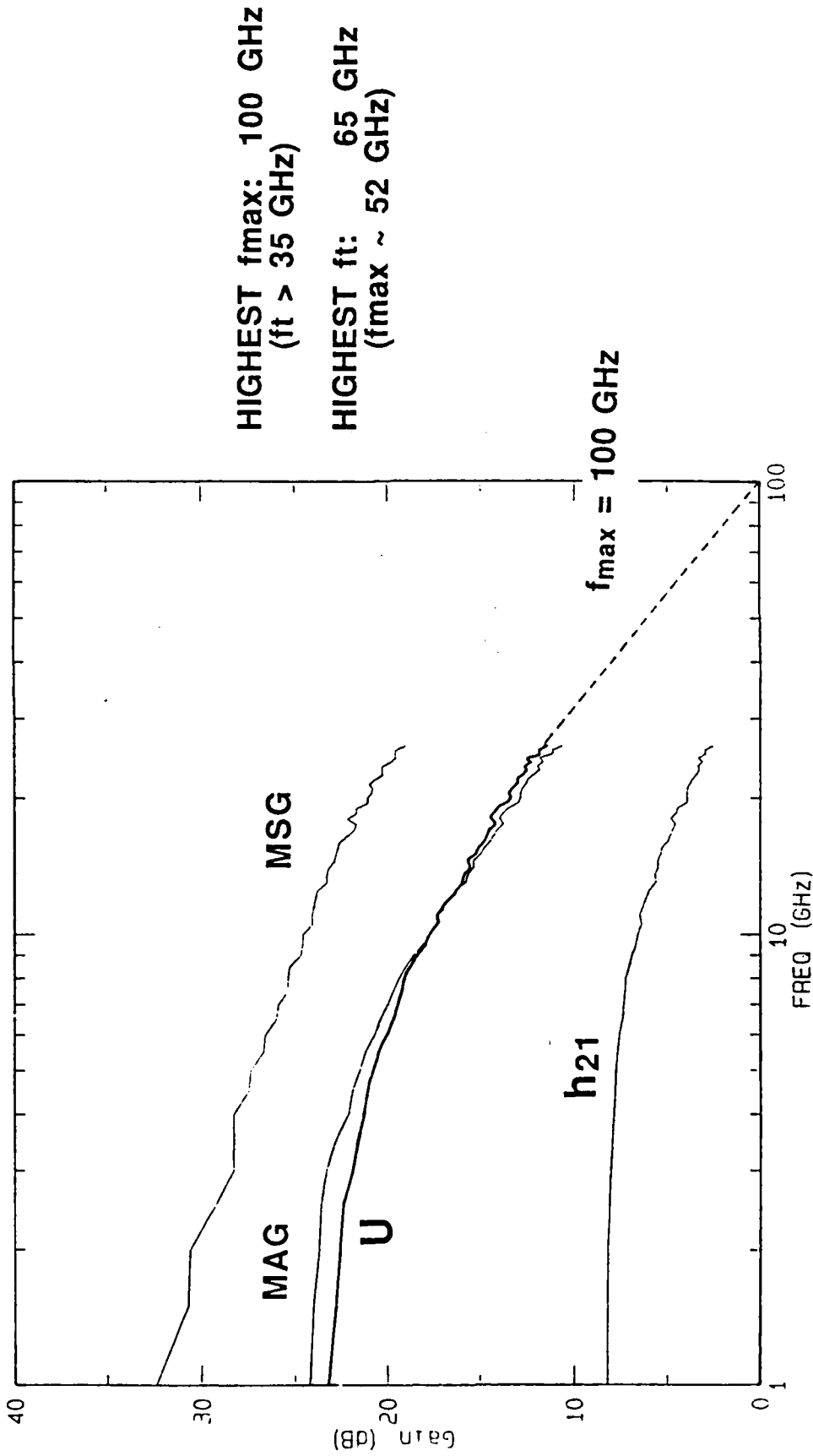
COLLECTOR AREA: $2\mu\text{m} \times 10\mu\text{m} \times 2$

SC48144

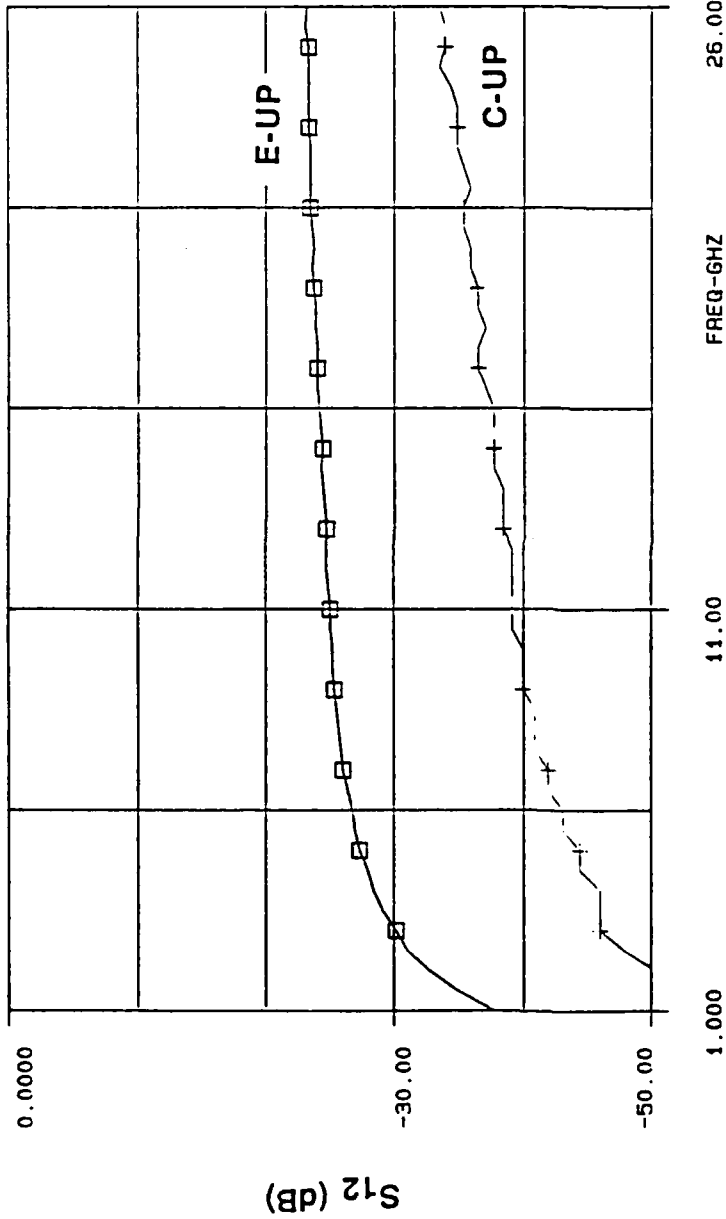


I_C : 2mA/DIV
 V_{CE} : 0.5 V/DIV
 I_B : 0.5 mA/STEP

COLLECTOR - UP HBT RF GAIN



COMPARISON OF S₁₂ IN C-UP AND E-UP HBTs



UNILATERAL FIGURE-OF-MERIT

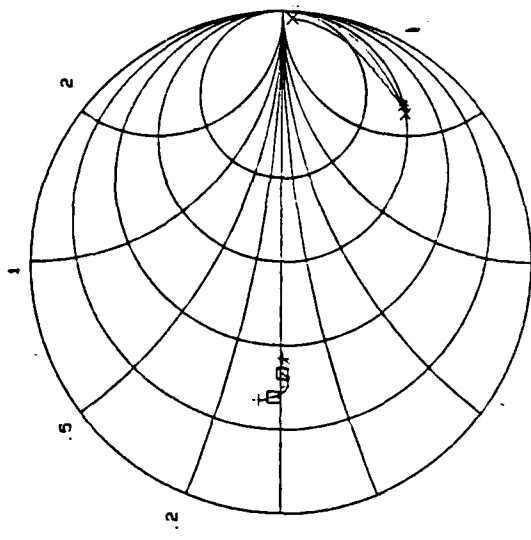
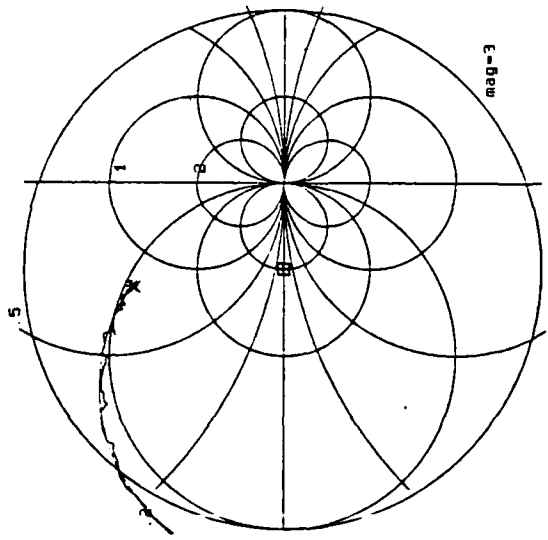
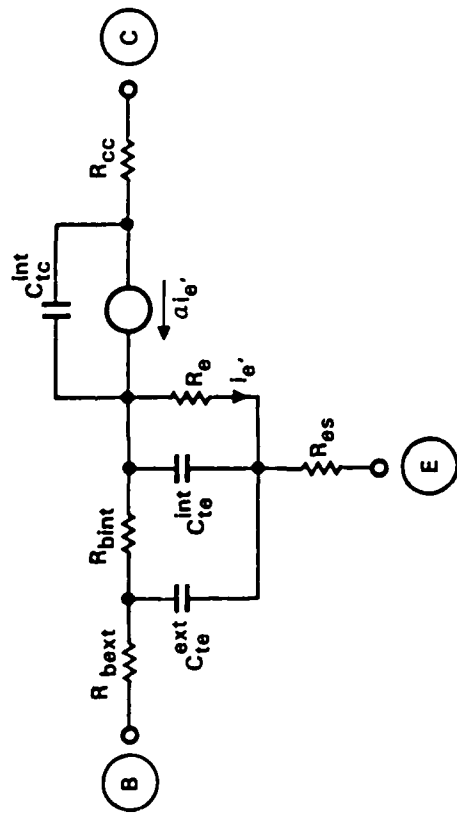
$$\mu = \frac{|S_{11} S_{12} S_{21} S_{22}|}{(1 - |S_{11}|^2)(1 - |S_{22}|^2)}$$

μ @ 20 GHz

HEMT	f _{max} = 100 GHz	0.46
E-UP	HBT	0.12
C-UP	HBT	0.06

(want small μ for best isolation)

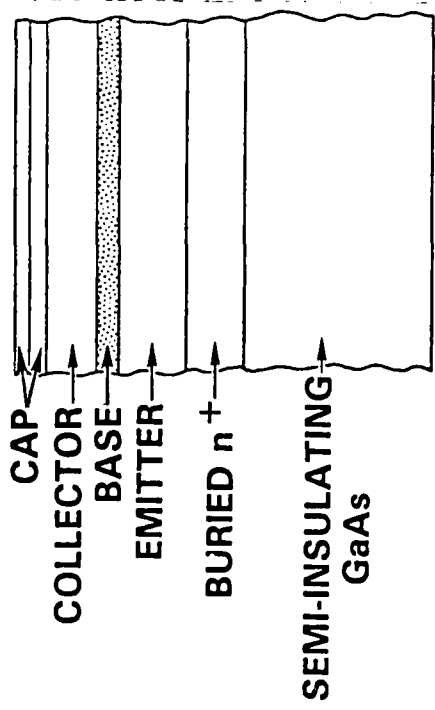
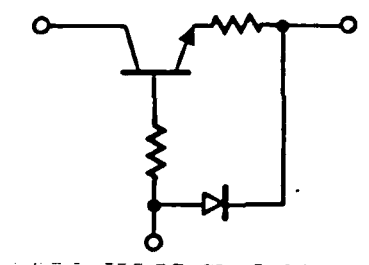
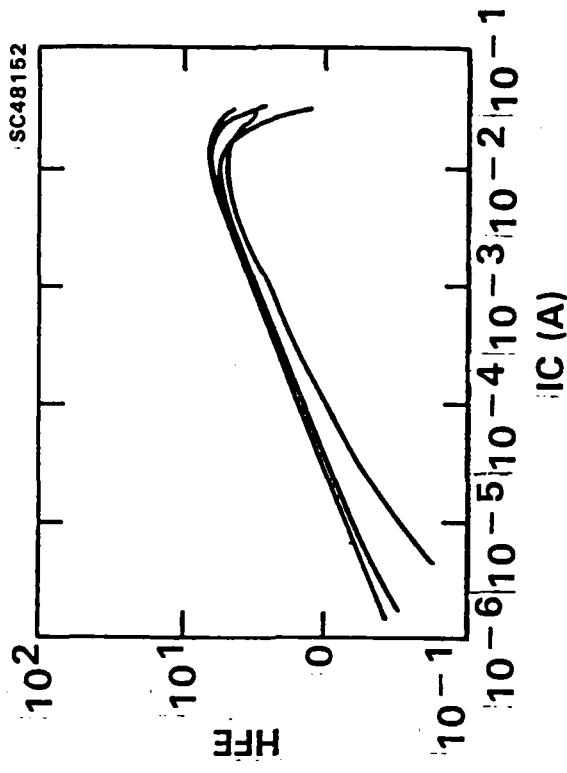
C-UP HBT MODEL



CTC	= 14 fF	α_0	= 0.7
CTEi	= 240 fF	T_B	= 1.8 pS
CTEe	= 22 fF	T_C	= 0.6 pS
R_{vext}	= 6.3	L_e	= 5 pH
R_{bint}	= 4.2	L_b	= 26 pH
R_{es}	= 1.2	L_c	= 20 pH
R_{cc}	= 4.5		

REMAINING ISSUE

EMITTER STRUCTURE DESIGN TO DECREASE RE



THE FUTURE OF C-UP HBT TECHNOLOGY

1. BASE DOPING CAN BE INCREASED SIGNIFICANTLY
(GROWTH ORDER FAVORS LOW T GROWTH)
2. EMITTER LAYER STRUCTURE CAN BE IMPROVED SIGNIFICANTLY
==> HIGHER H_{21} , lower R_E
3. SELF-ALIGNED COLLECTOR AND EMITTER CONTACTS CAN BE
IMPLEMENTED

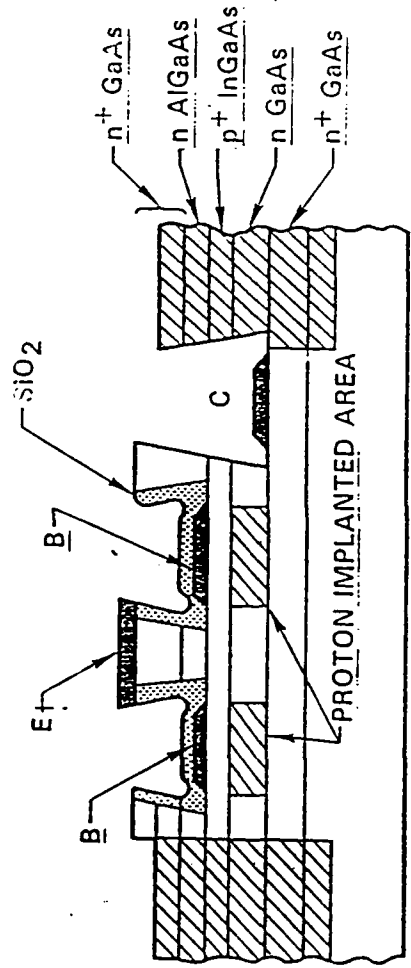
EXPECT $f_{\max} > 300$ GHz WITH 1 μm DIMENSIONS

E-UP FABRICATION CHALLENGES

- MINIMIZE BASE RESISTANCE
- MINIMIZE BASE-COLLECTOR CAPACITANCE

APPROACH

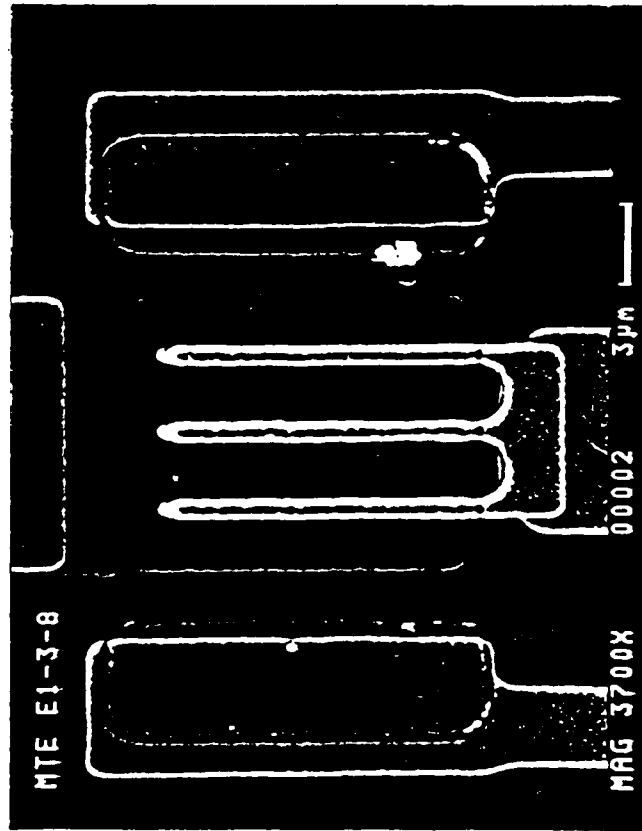
- ULTRAHIGH BASE DOPING ($1 \times 10^{20} \text{ CM}^{-3}$)
- FULLY SELF-ALIGNED PROCESS
- PROTON-IMPLANTS IN EXTRINSIC COLLECTOR



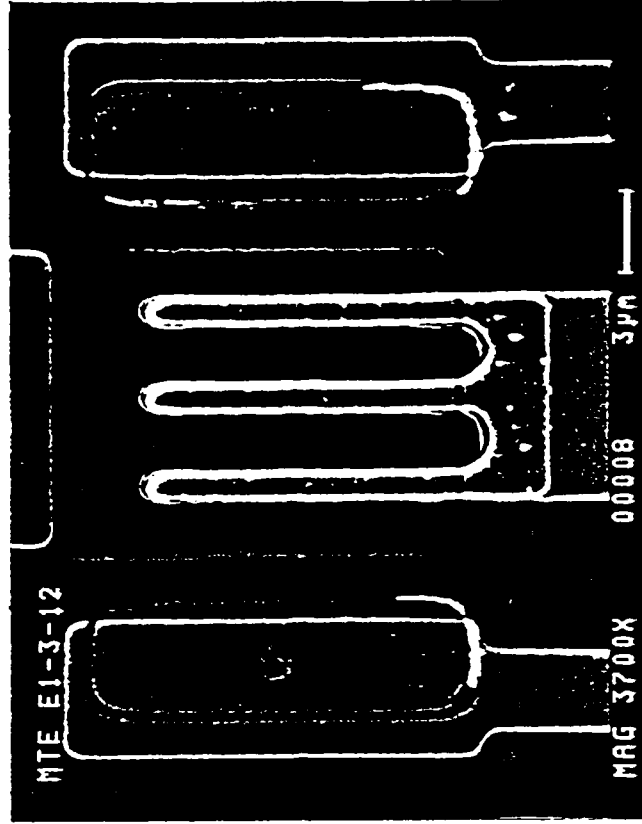
MASK SET MB1

PROJECTION OPTICAL LITHOGRAPHY

SC48146



$W_E = 0.8\mu\text{m}$

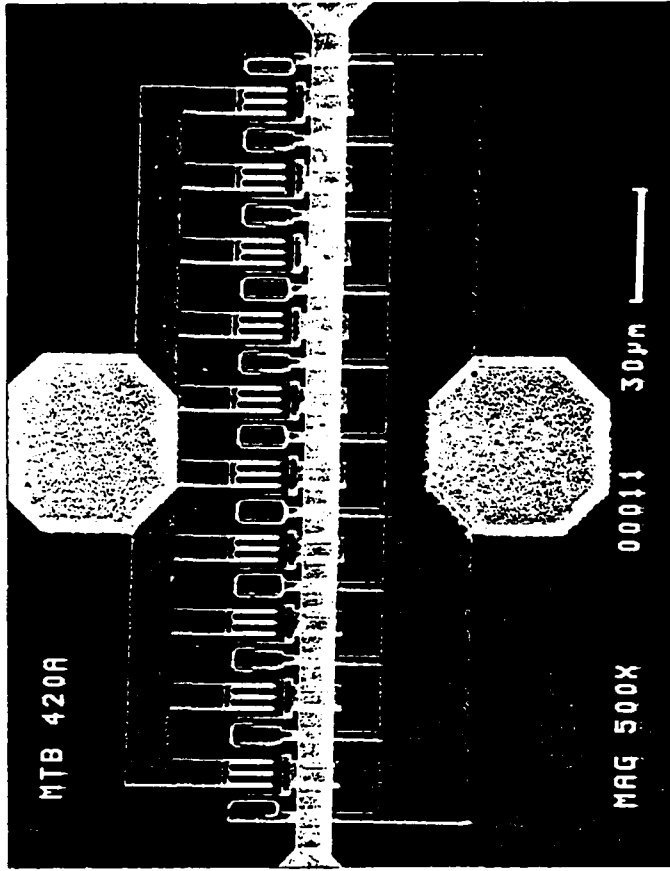
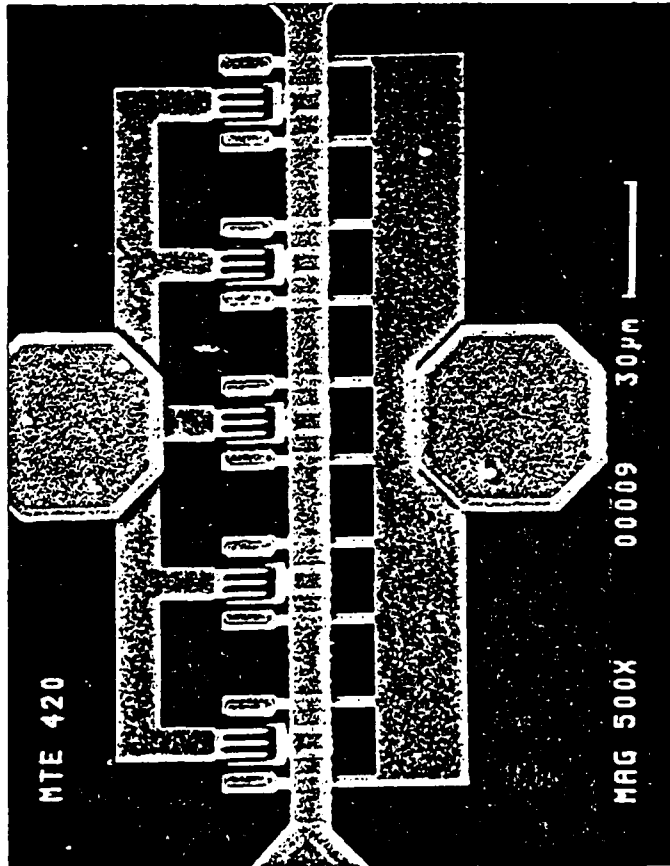


$W_E = 1.2\mu\text{m}$

EXPERIMENTAL VARIATIONS

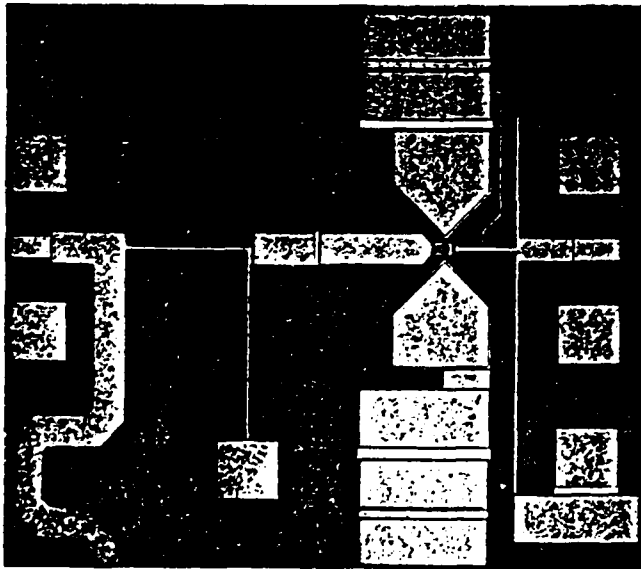
SC48145

COMMON EMITTER — COMMON BASE MULTIPLE CELLS VARIATIONS IN SPACING



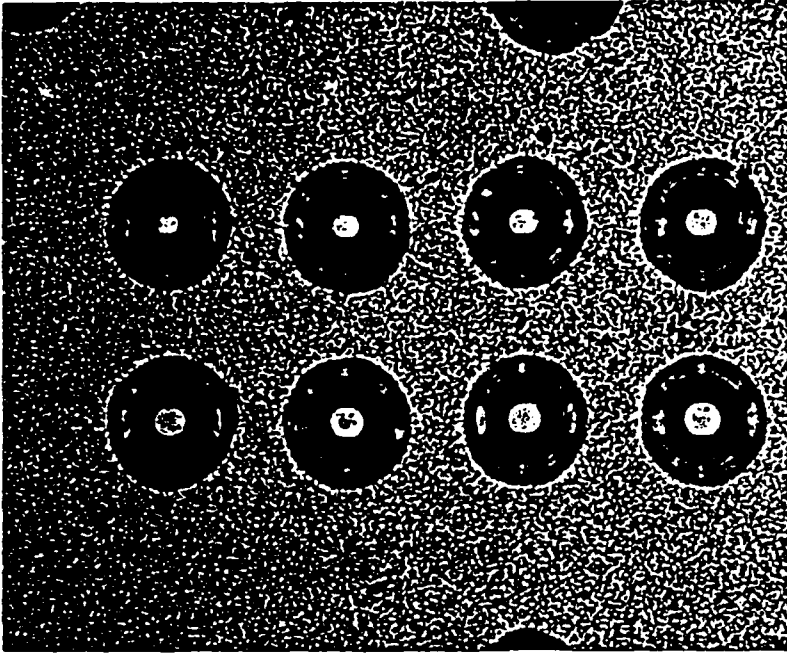
Rockwell International
Science Center

HBT MMIC TECHNOLOGY

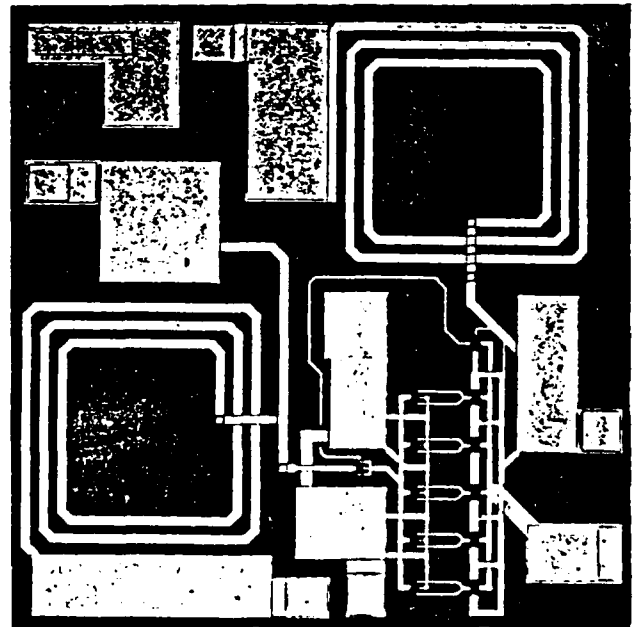


22 GHz
AMPLIFIER

ISC48143



THROUGH-SUBSTRATE
VIA HOLES



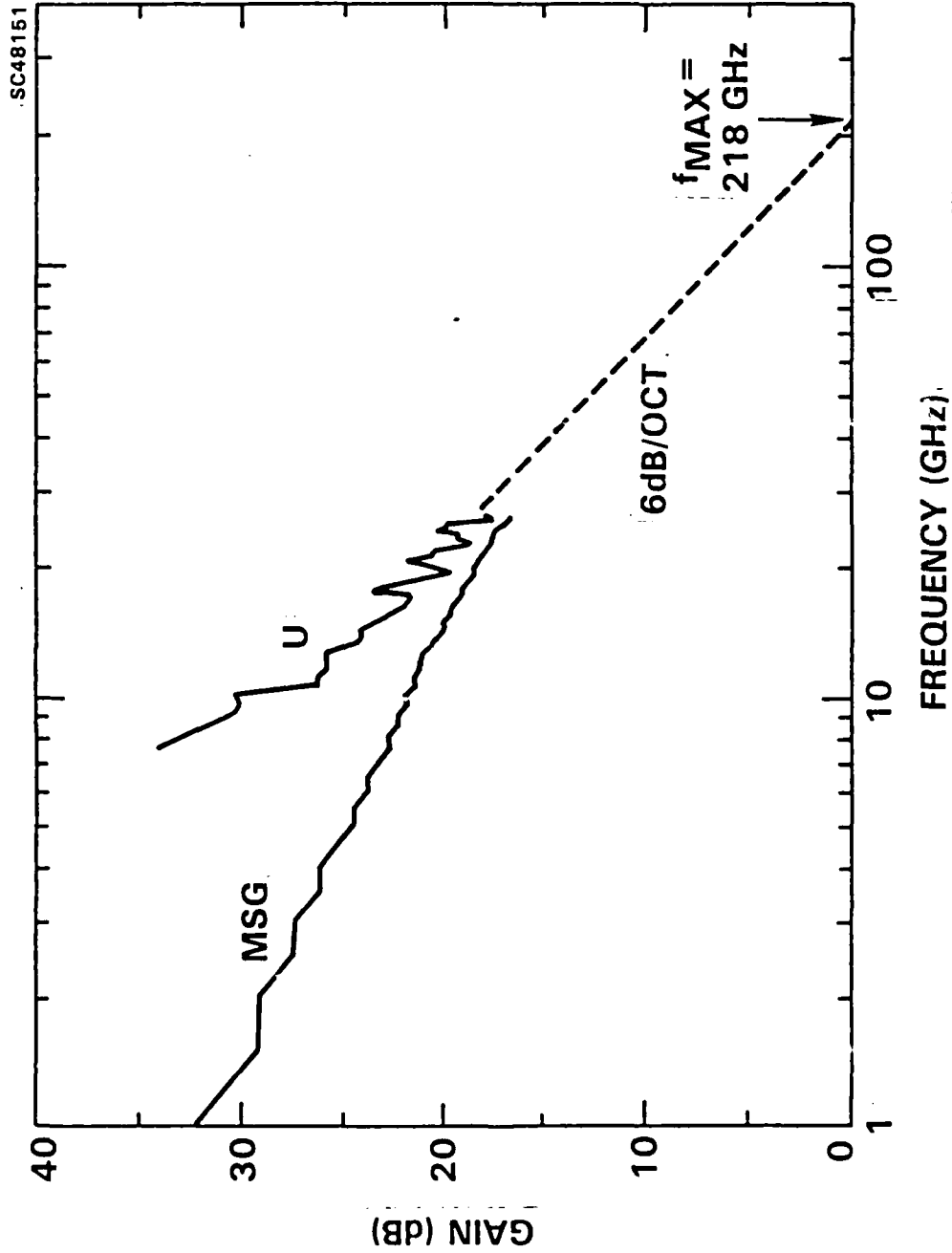
10 GHz
AMPLIFIER



Rockwell International
Science Center

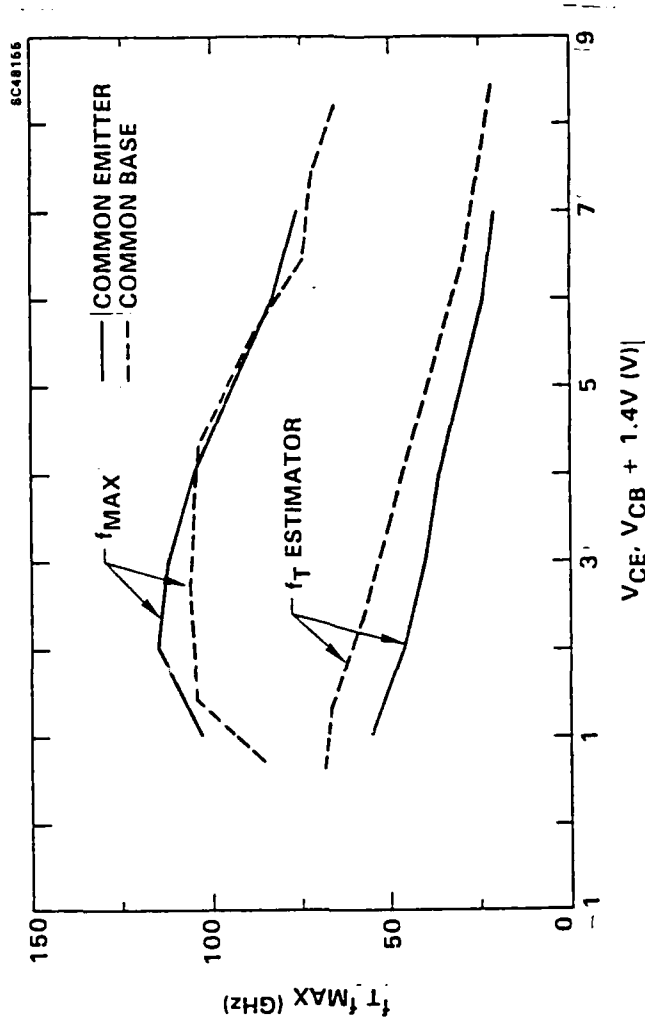
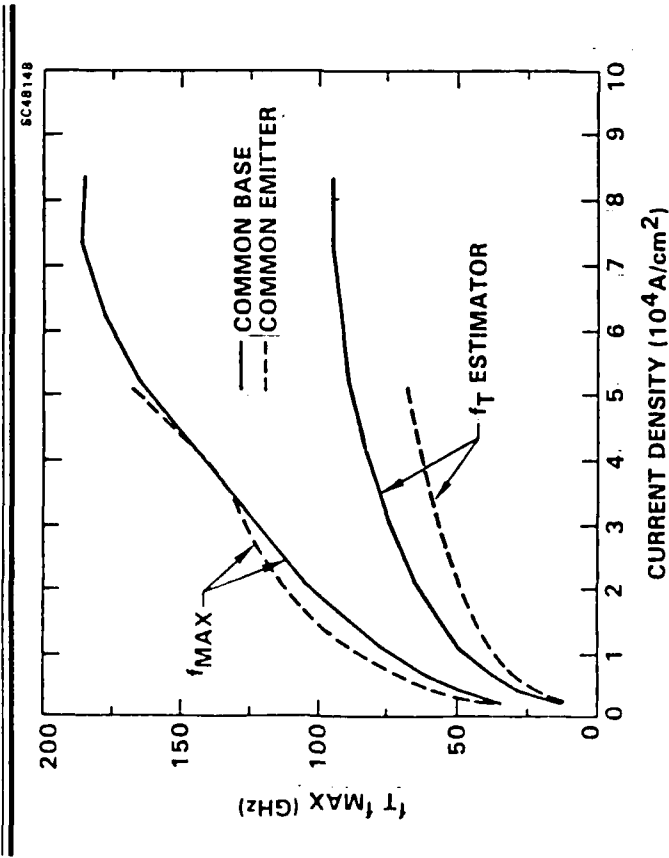
GAIN VS FREQUENCY — COMMON-BASE HBT

EMITTER AREA: $1.0\mu\text{m} \times 10\mu\text{m} \times 3$, $I_C = 20\text{mA}$, $V_{CB} = 0\text{V}$



Rockwell International
Science Center

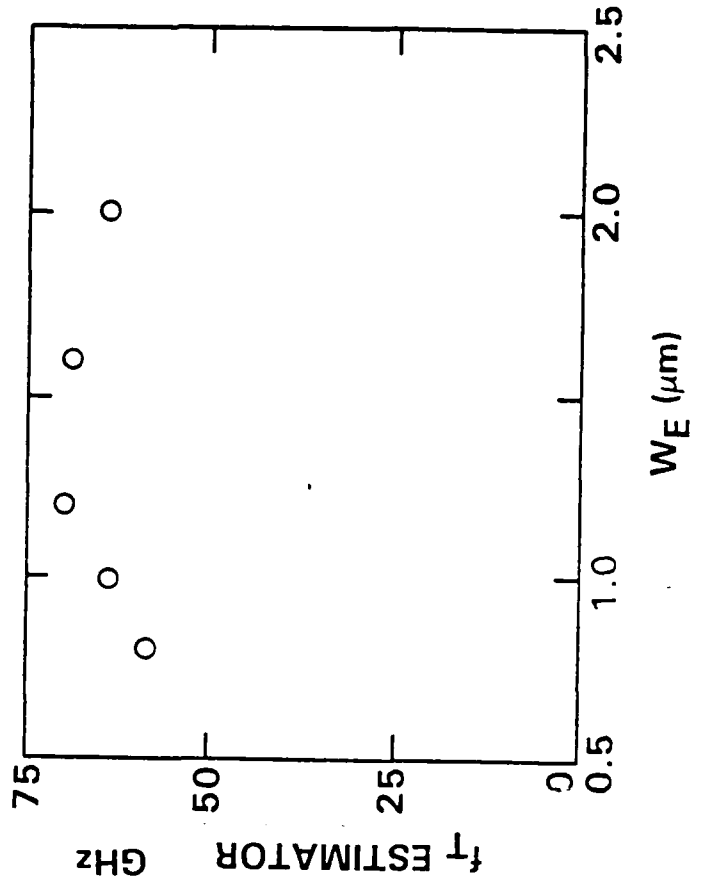
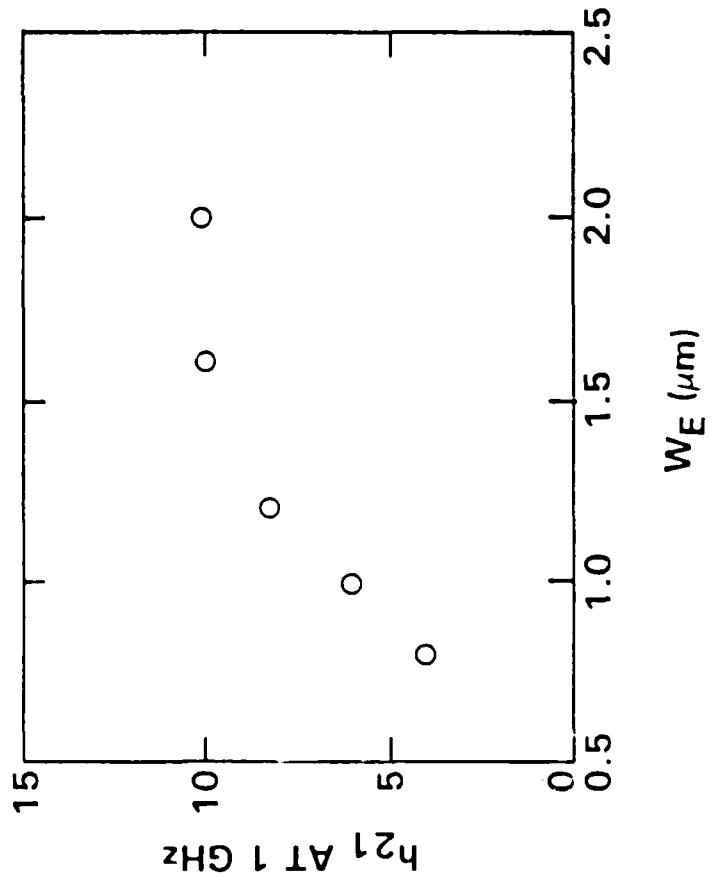
VARIATION OF GAIN WITH J_C



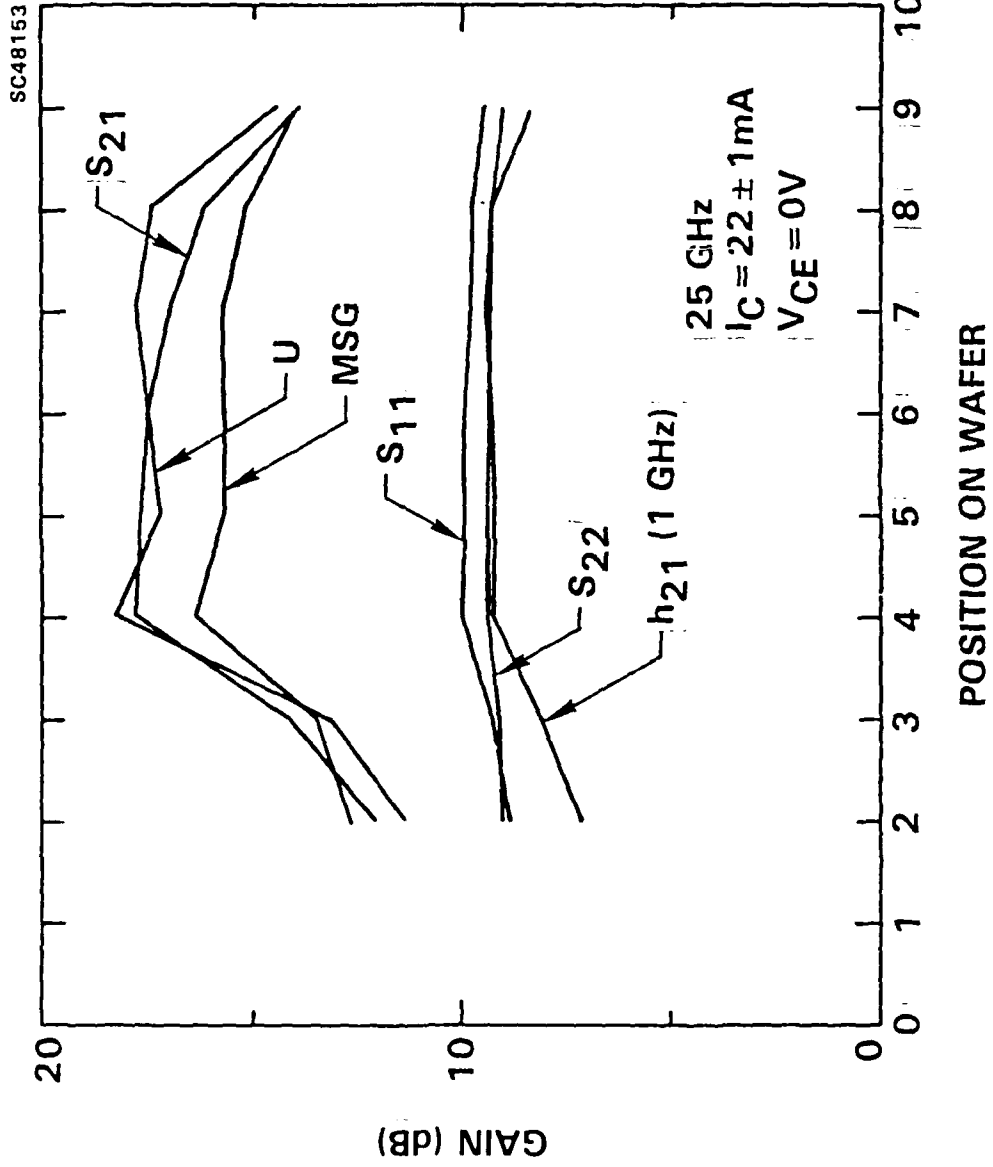
GAIN VS EMITTER WIDTH

SMALLER EMITTER WIDTH

- LOWERS R_b , INCREASES f_{max}
- DECREASES dc CURRENT GAIN (MAKING EXTRAPOLATION TO 26 GHz LESS RELIABLE)
- MAKES PAD CAPACITANCE PROPORTIONALLY MORE IMPORTANT
- (2 UNIT CELLS GIVE f_t , f_{max} HIGHER THAN ONE CELL)

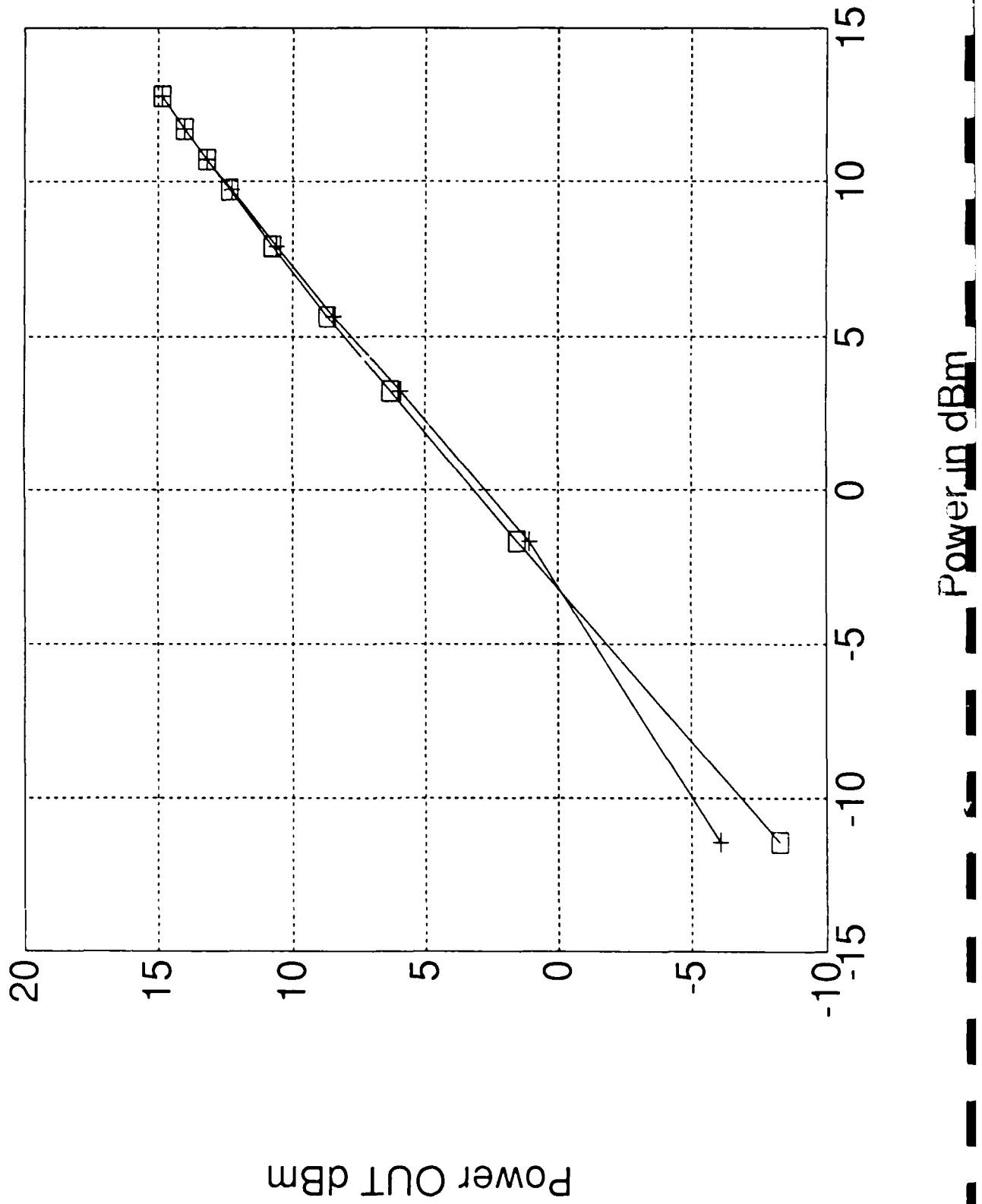


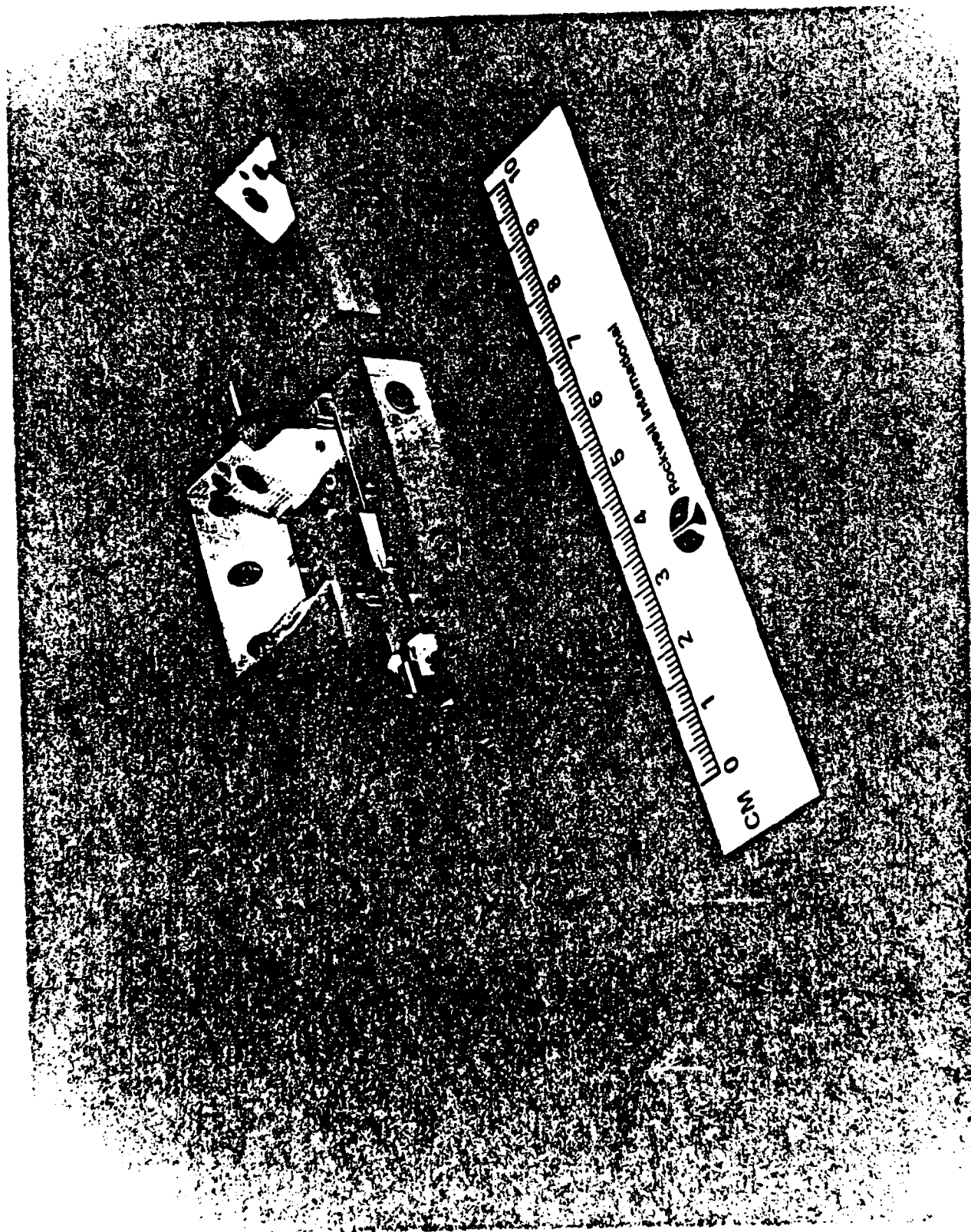
VARIATION OF GAIN ACROSS A WAFER



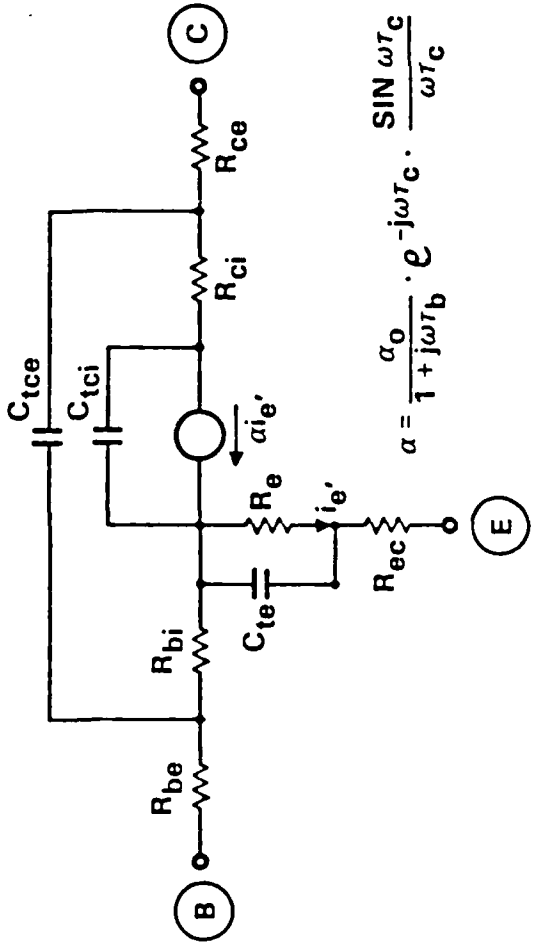
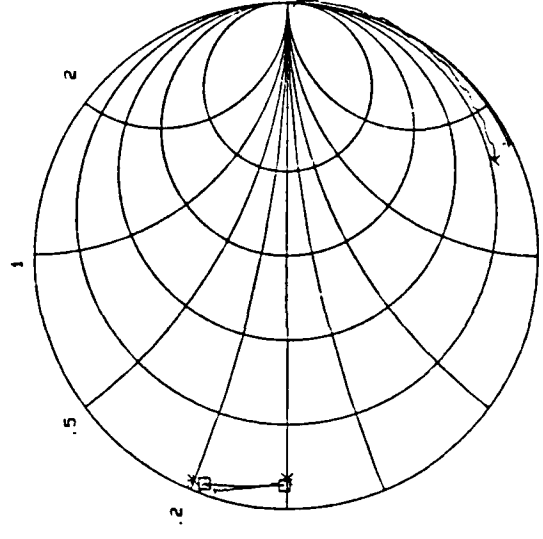
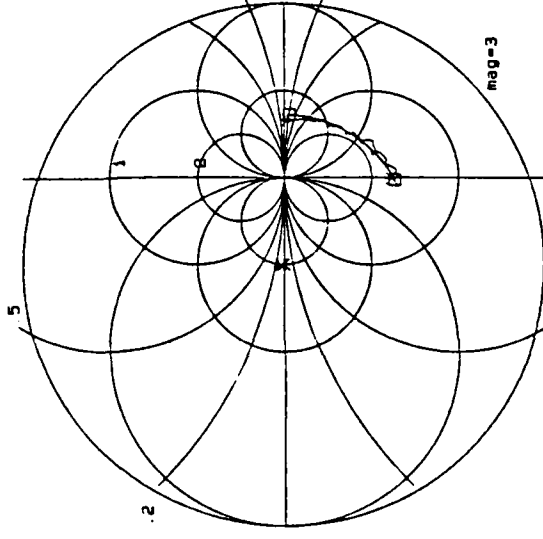
Rockwell International
Science Center

58.5 GHz HBT





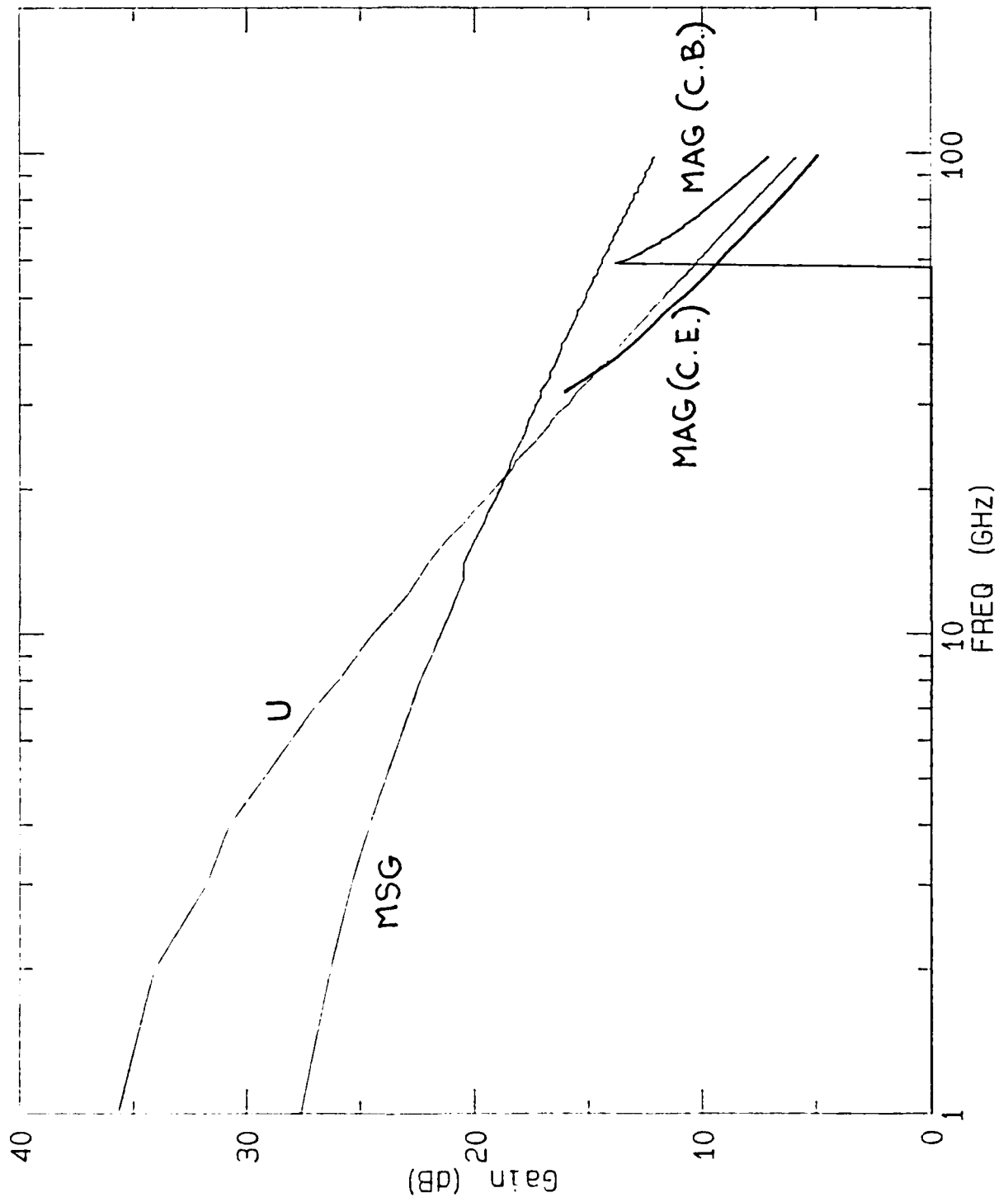
HBT MODEL



$$\alpha = \frac{\alpha_0}{1 + j\omega T_b} \cdot e^{-j\omega T_C} \cdot \frac{\text{SIN } \omega T_C}{\omega T_C}$$

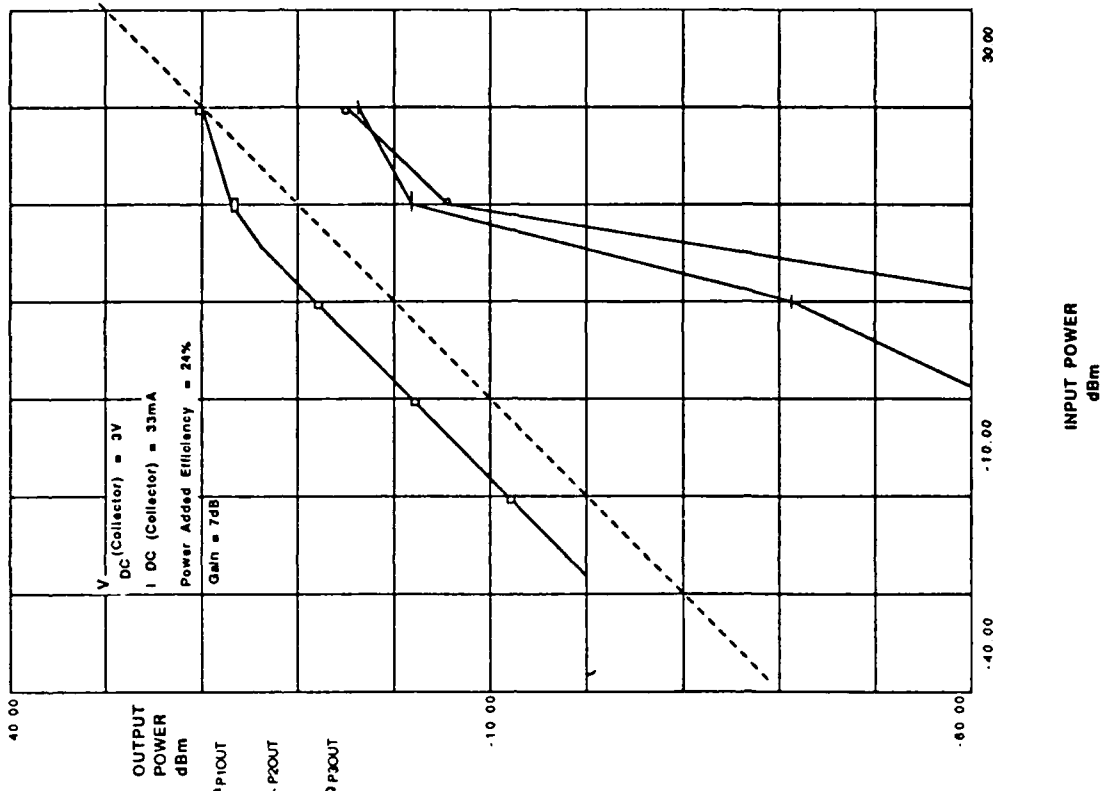
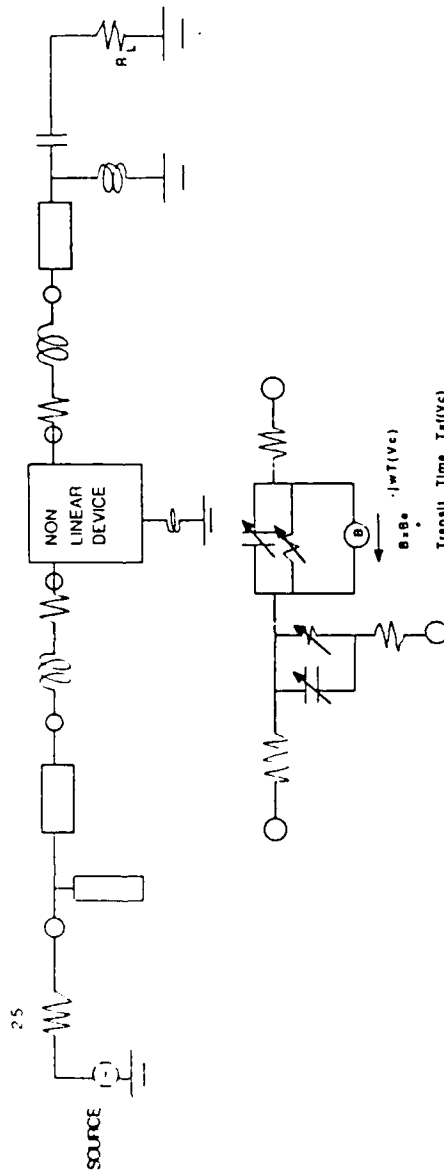
CTE	= 150 fF	α_0	= 0.9
CTCi	= 8 fF	Tb	= 0.4 pS
CTCe	= 29 fF	Tc	= 0.4 pS
Rbext	= 1.9	Res	= 0.8
Rbint	= 1.8	Rcc	= 12

HIGH FREQUENCY MODELING



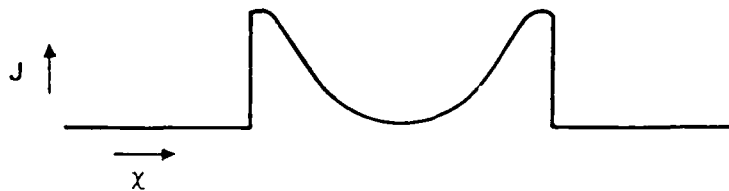
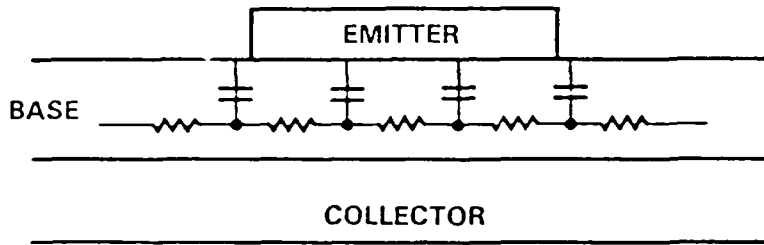
AMPLIFIER MODELLING

NONLINEAR HBT MODEL

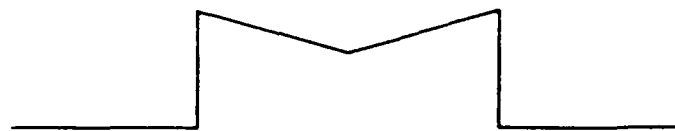


EMITTER UTILIZATION FACTORS

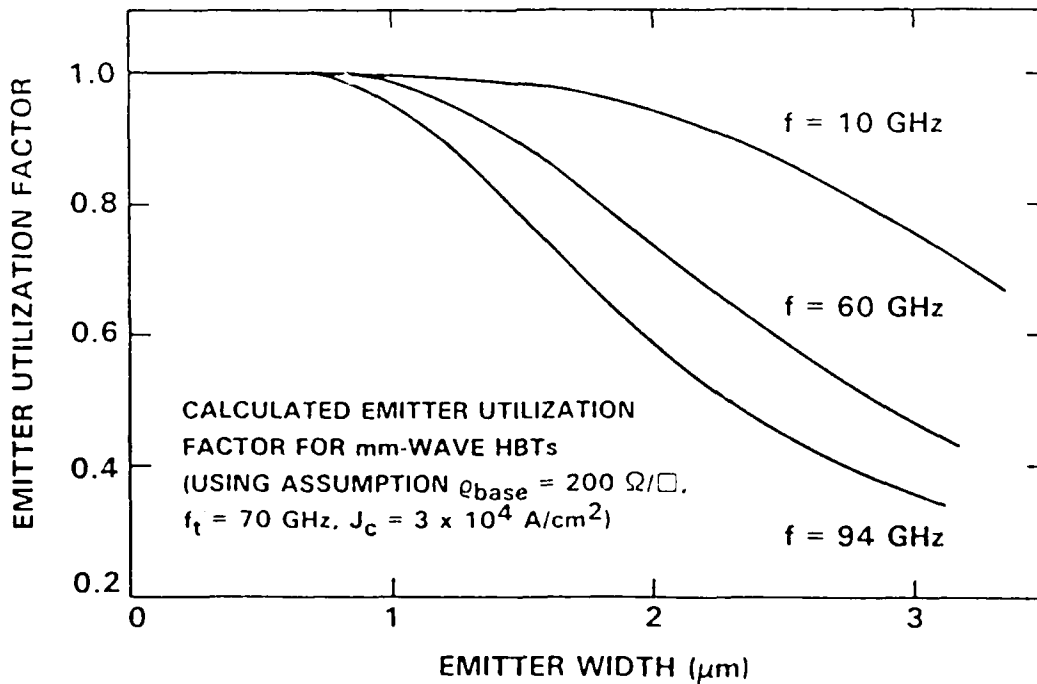
SC47338



Si BIPOLAR

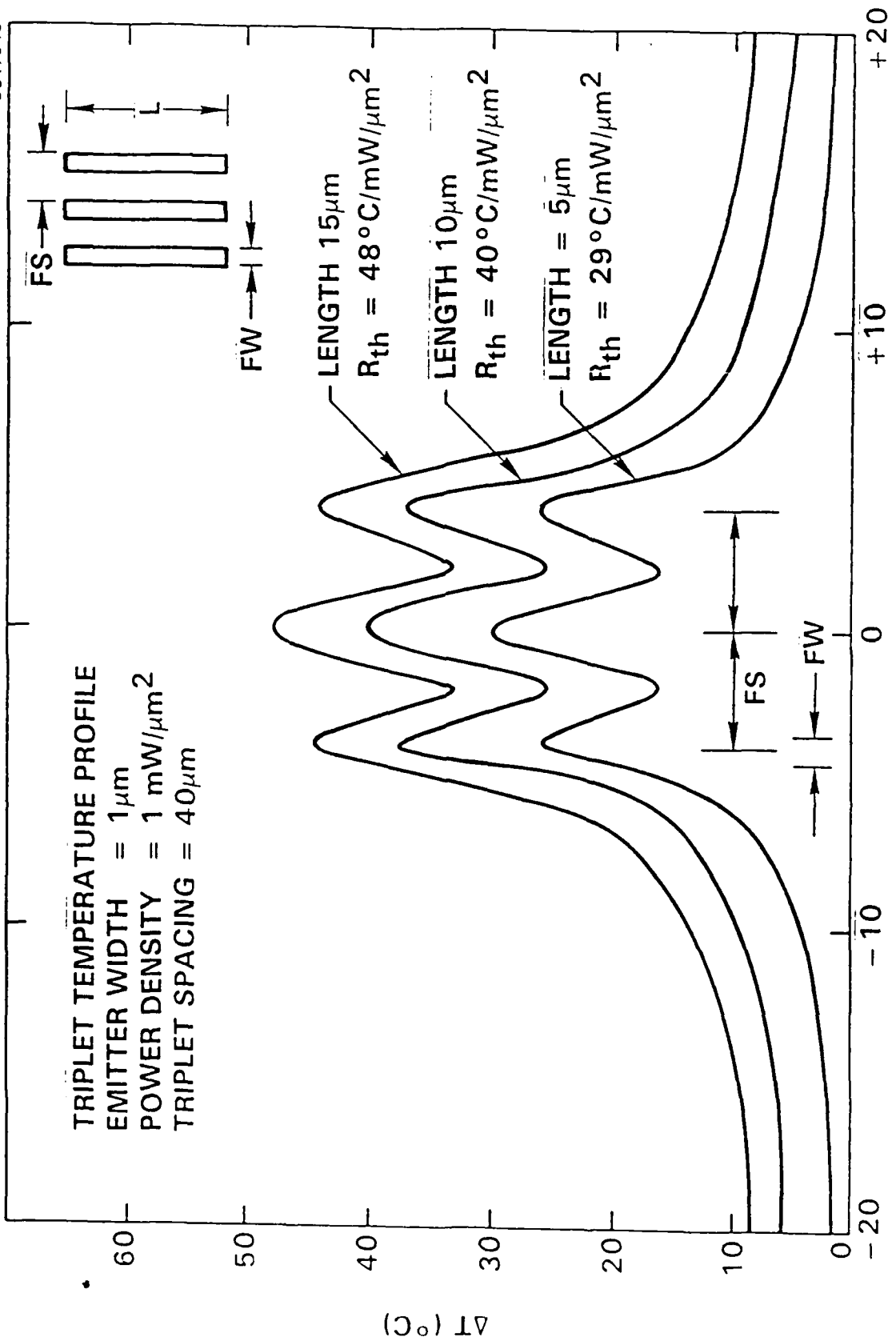


GaAs BIPOLAR

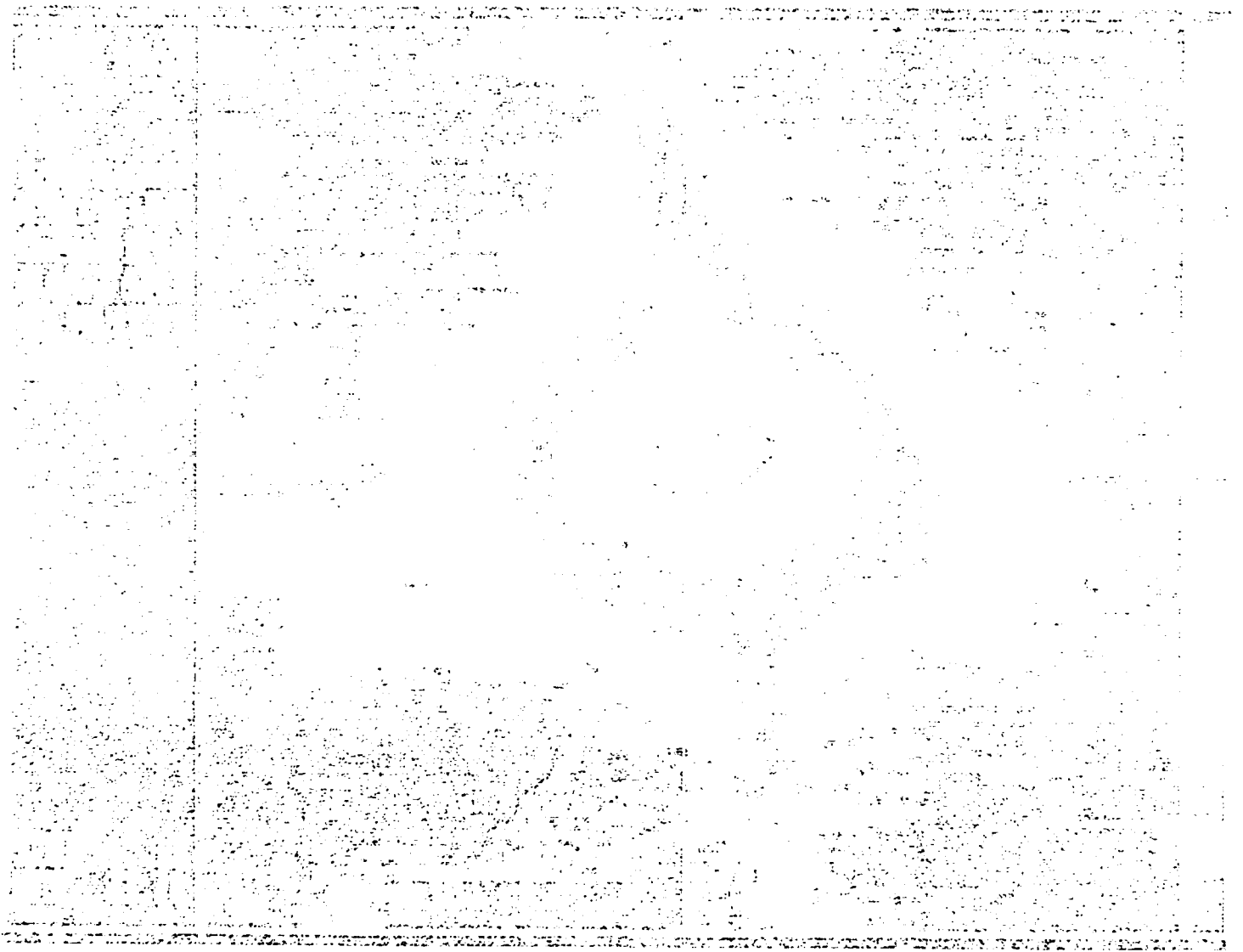


Rockwell International
Science Center

SC47943



THERMAL IMAGE PROFILE



SEELIN TECHNOLOGY

DEVICE: 17D/5 (Coated) 40x magn.

CONDITIONS:

Base Temperature: 83.6 °C

Power : 0.1 W

6106 Del Canto dr., SAN JOSE CA-95119

ANALYSIS

EXPERIMENT (THERMAL IMAGING): $31 \pm 5^{\circ}\text{C}$ $\mu\text{m}^2/\text{mW}$

SIMULATION (15 μm SPOT SIZED ASSUMED): 60°C $\mu\text{m}^2/\text{mW}$

DISCREPANCY MAY BE DUE TO SURFACE COOLING FROM METALLIZATIONS

PROJECTIONS FOR MM-WAVE OPERATION

FOR BIAS CONDITIONS: $V_{\text{CE}} = 4\text{V}$, $J_{\text{c}} = 5 \times 10^4 \text{ A/cm}^2$

$P_{\text{dc}} = 2 \text{ mW}/\mu\text{m}^2$, $P_{\text{diss}} = P_{\text{dc}} (1-\eta_{\text{add}})$

WORST-CASE PROJECTED: $\Delta T = 40^{\circ}\text{C}$ $\mu\text{m}^2/\text{mW} \times 2 \text{ mW}/\mu\text{m}^2 = 80^{\circ}\text{C}$

PROGRESS SUMMARY

- FIRST HIGH PERFORMANCE MM-WAVE COLLECTOR-UP HBTs DEMONSTRATED - $f_{\max} = 100$ GHz
- EMITTER-UP HBTs IMPROVED TO $f_{\max} = 218$ GHz
- MMIC-COMPATIBLE HBT TECHNOLOGY DEMONSTRATED
- PROJECTION OPTICAL LITHOGRAPHY USED
- HIGH FREQUENCY MODELING AND THERMAL MODELING DONE

PLANS

- **COLLECTOR-UP HBT IMPROVEMENT:**

 - HIGHER BASE DOPING

 - Expect

 - IMPROVED EMITTER DESIGN

 - ==> $f_{\max} > 300$ GHz

 - FULLY SELF-ALIGNED

- **EMITTER-UP HBT IMPROVEMENT:**

 - HIGHER BASE DOPING: C-SOURCE IN MBE, GROWTH VARIATIONS

 - GRADED COMPOSITION BASE

 - Expect

 - VELOCITY OVERSHOOT STRUCTURES

 - ==> $f_{\max} > 270$ GHz

- **CHARACTERIZATION:**

 - ADDITIONAL 60 AND 94 GHz RESULTS

 - TEST LARGER STRUCTURES

 - COLLABORATION WITH STANFORD UNIVERSITY

- **AMPLIFIER MODELING:**

 - REFINE NONLINEAR MODELS FOR HARMONIC BALANCE ANALYSIS

MMW HBT TECHNOLOGY

- EFFICIENT 3-TERMINAL SOLID STATE DEVICES
COMMUNICATION SYSTEMS/SEEKERS/PHASE ARRAYS
FLEXIBLE CONFIGURATION (E-UP, C-UP, CLASS A, AB, ETC.)
- MANUFACTURABLE, HIGH YIELD TECHNOLOGY
BIPOLAR TRANSISTOR TECHNOLOGY
STANDARD OPTICAL LITHOGRAPHY
COMPATIBILITY WITH GaAs PILOT LINE
- RAPID PROGRESS/CLEAR PATH FOR FUTURE
MBE TECHNOLOGY MATURING
 $f_{\max} = 215 \text{ GHz}$ WITH $1 \mu\text{m}$ LITHOGRAPHY, $f_{\max} > 300 \text{ GHz}$ EXPECTED

Heterojunction Power FET Technology

Buman Kim

*Texas Instruments
Dallas, TX*



HETEROJUNCTION POWER FET TECHNOLOGY

OBJECTIVE

DEVELOP A HIGH EFFICIENCY
HETEROSTRUCTURE POWER FETS
AND AMPLIFIERS FOR OPERATION
AT 60 AND 94 GHz

APPROACH

QUANTUM WELL FETS

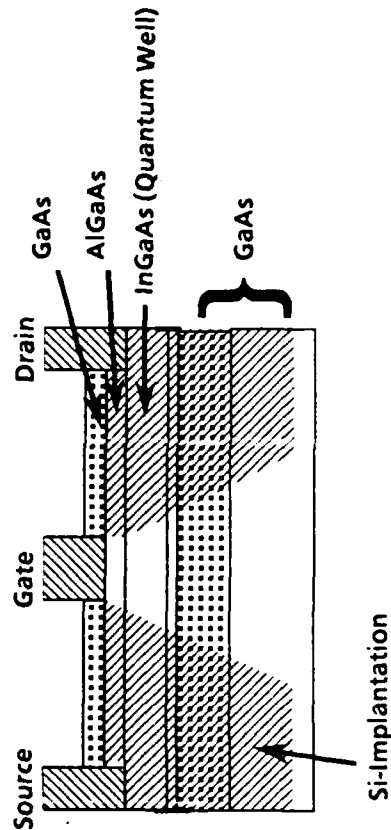
- QUANTUM WELL FOR GOOD CHARGE CONFINEMENT
- HIGH SHEET CARRIER DENSITY IN A THIN LAYER
- UNDOPED AlGaAs LAYER FOR HIGH BREAKDOWN VOLTAGE

STATUS

A 0.25 μm FET at 60 GHz

POWER DENSITY (W/mm)	EFFICIENCY (%)	GAIN (dB)	f_t (GHz)
1.0	27	3.2	120

QUANTUM WELL FET STRUCTURE





HETEROJUNCTION POWER FET TECHNOLOGY

OBJECTIVE

DEVELOP A HIGH EFFICIENCY
HETEROSTRUCTURE POWER FETs
AND AMPLIFIERS FOR OPERATION
AT 60 AND 94 GHz

APPROACH

QUANTUM WELL FETs

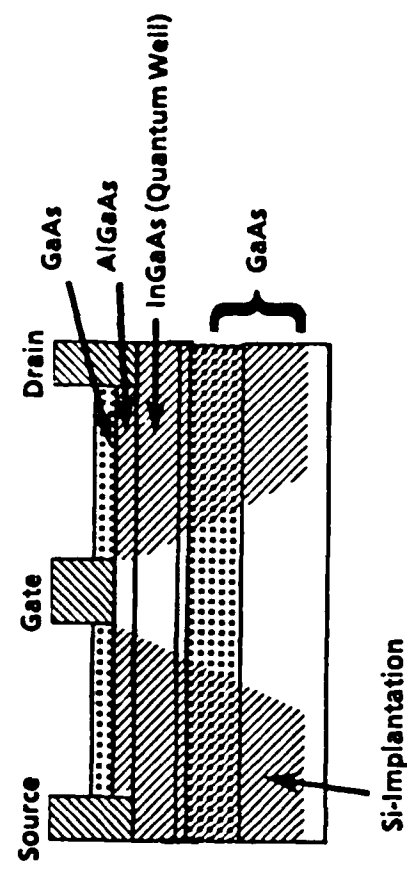
- QUANTUM WELL FOR GOOD CHARGE CONFINEMENT
- HIGH SHEET CARRIER DENSITY IN A THIN LAYER
- UNDOPED AlGaAs LAYER FOR HIGH BREAKDOWN VOLTAGE

STATUS

A 0.25 μm FET at 60 GHz

POWER DENSITY (W/mm)	EFFICIENCY (%)	GAIN (dB)	f _t (GHz)
1.0	27	3.2	120

QUANTUM WELL FET STRUCTURE





CENTRAL RESEARCH LABORATORIES

HETEROJUNCTION POWER FET TECHNOLOGY

**Texas Instruments
Dallas, Texas**

Contract No. N66001-86-C-0211

**Contract Monitors: Jim Zeidler (NOSC)
Jim Murphy (DARPA)**



CENTRAL RESEARCH LABORATORIES

AGENDA

- Introduction
- Device Design
- Device Performance
 - Undoped well
 - Doped well
- Summary



OBJECTIVE

- Develop heterojunction power FETs at 60 GHz and 94 GHz
- Develop amplifiers at 60 GHz and 94 GHz

Frequency (GHz)	60	94	94
Output power (mW)	200	30	100
Efficiency (%)	20	30	20



ISSUES

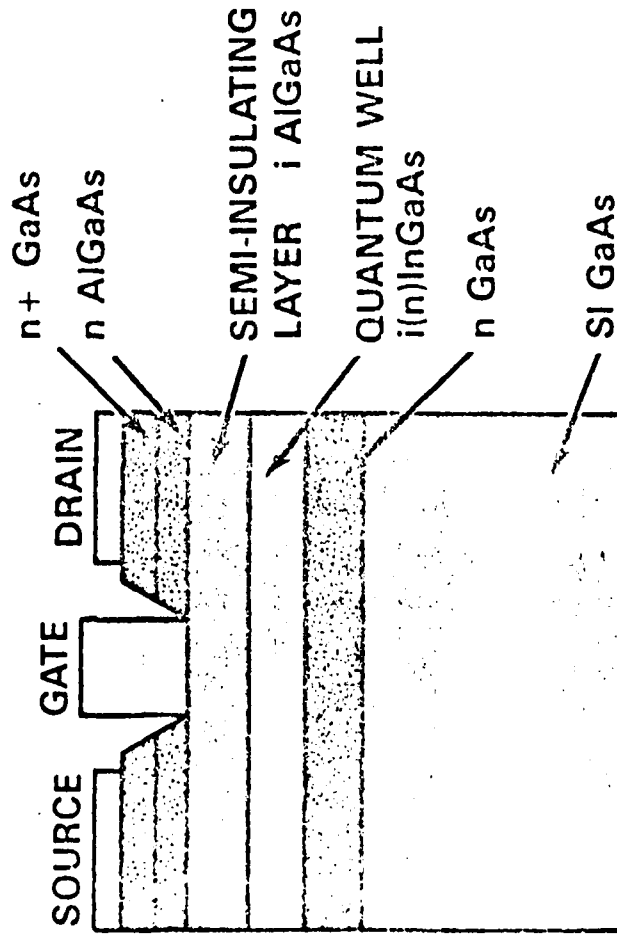
- CARRIER TRANSIT TIME
 - QUARTER μm OR SUB-QUARTER μm GATES
 - REDUCE PARASITICS
 - BETTER MATERIAL (InGaAs CHANNEL) ↔

- SHORT CHANNEL EFFECTS
 - THIN ACTIVE LAYER (UNDER 500 Å)
 - CHARGE CONFINEMENT USING POTENTIAL WELL ↔
(HETEROINTERFACE)

- POWER DENSITY
 - HIGH SHEET CARRIER DENSITY ↔
 - HIGH BREAKDOWN VOLTAGE (MISFET) ↔



MILLIMETER-WAVE QUANTUM-WELL MISFET



ADVANTAGE

- HIGH BREAKDOWN VOLTAGE
- CHARGE ACCUMULATION
- EXCELLENT CHARGE MODULATION
- SELF-ALIGNED GATE
- SELECTIVE ETCH FOR GATE RECESS

(a) Material Structure

Thickness	Composition	Doping	Electron Density
20 nm	$\text{Al}_{0.40}\text{Ga}_{0.60}\text{As}$	$1.0 \times 10^{10} \text{ cm}^{-3}$	$3.11 \times 10^4 \text{ cm}^{-2}$
15 nm	$\text{In}_{0.15}\text{Ga}_{0.85}\text{As}$	$1.0 \times 10^{10} \text{ cm}^{-3}$	$2.18 \times 10^{12} \text{ cm}^{-2}$
2 nm	GaAs	$1.0 \times 10^{10} \text{ cm}^{-3}$	$2.05 \times 10^{10} \text{ cm}^{-2}$
5 nm	GaAs	$3.0 \times 10^{18} \text{ cm}^{-3}$	$1.53 \times 10^{11} \text{ cm}^{-2}$
100 nm	GaAs	$1.0 \times 10^{13} \text{ cm}^{-3}$	$3.31 \times 10^{11} \text{ cm}^{-2}$

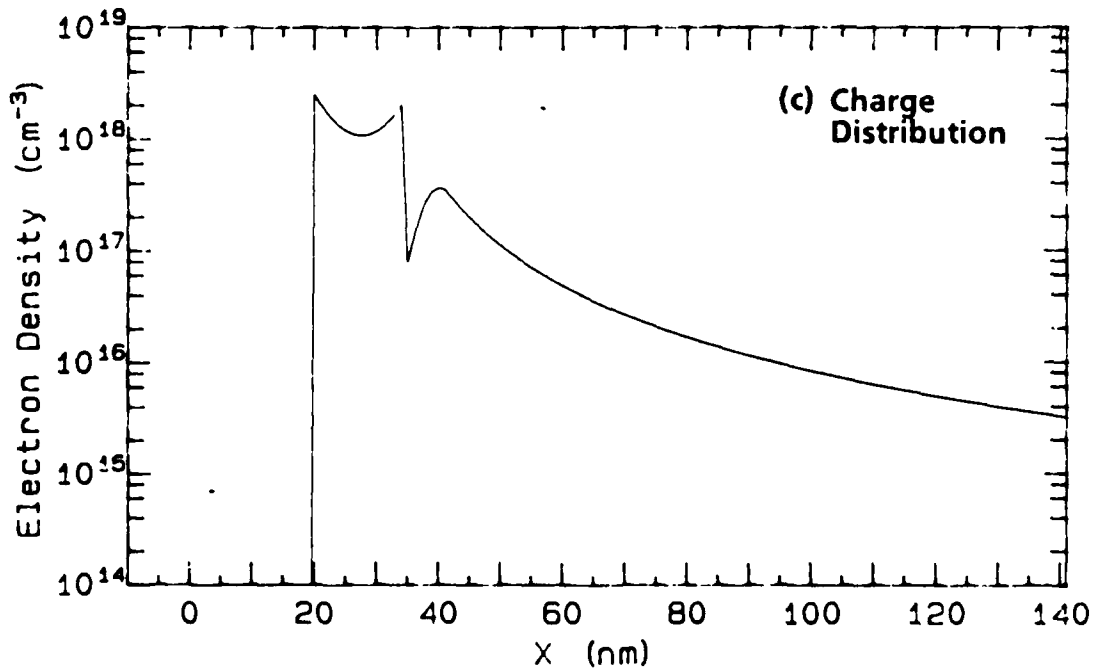
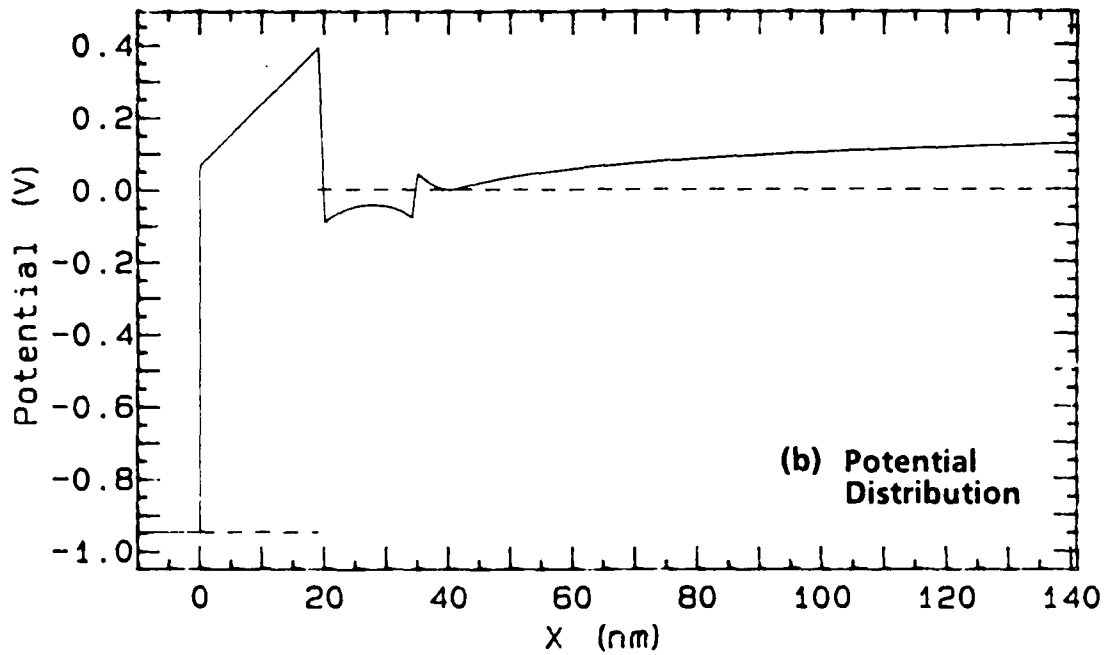
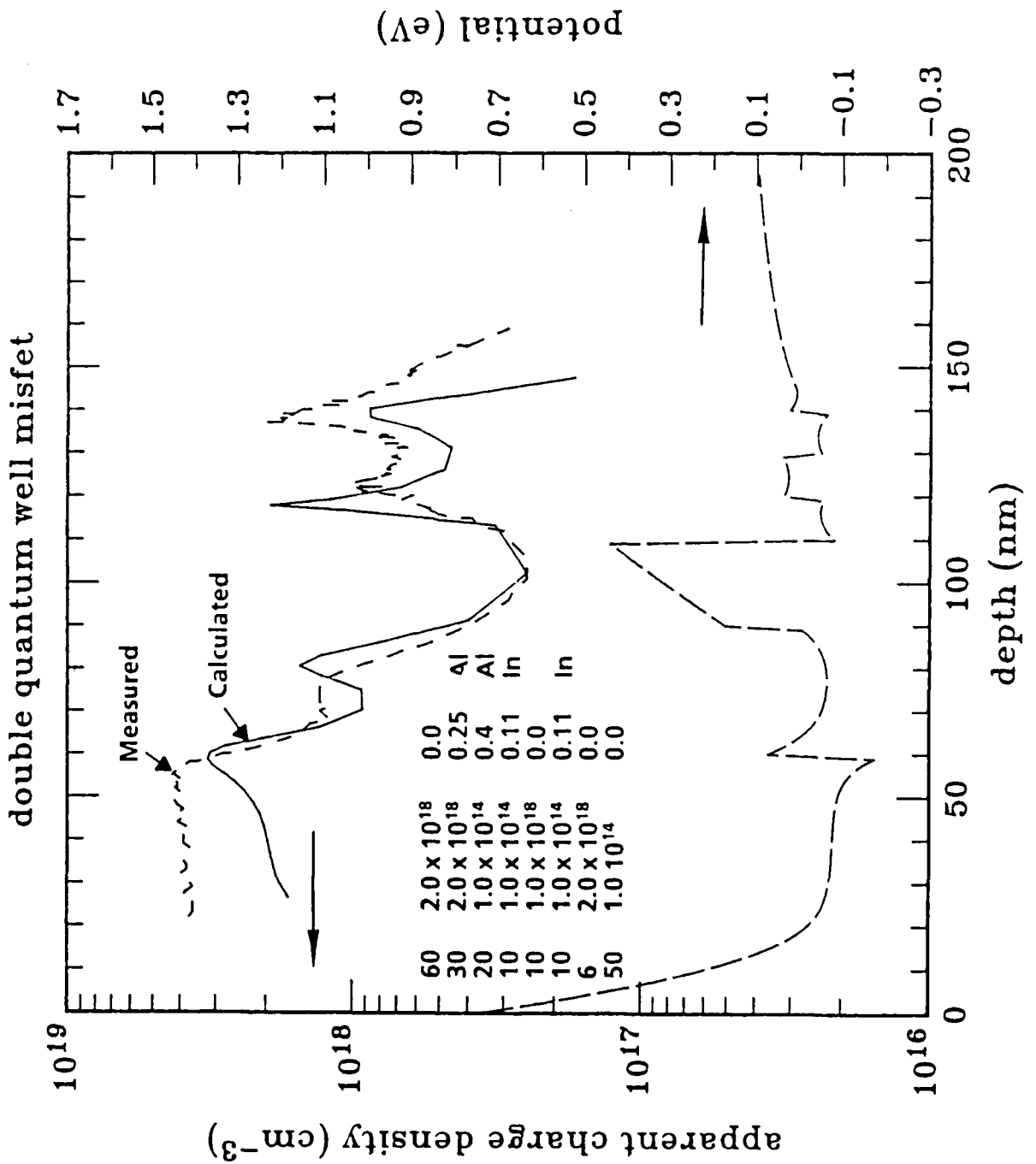


Figure 1. Quantum well MISFET with normal structure. (a) Material structure; (b) potential distribution; (c) charge distribution.



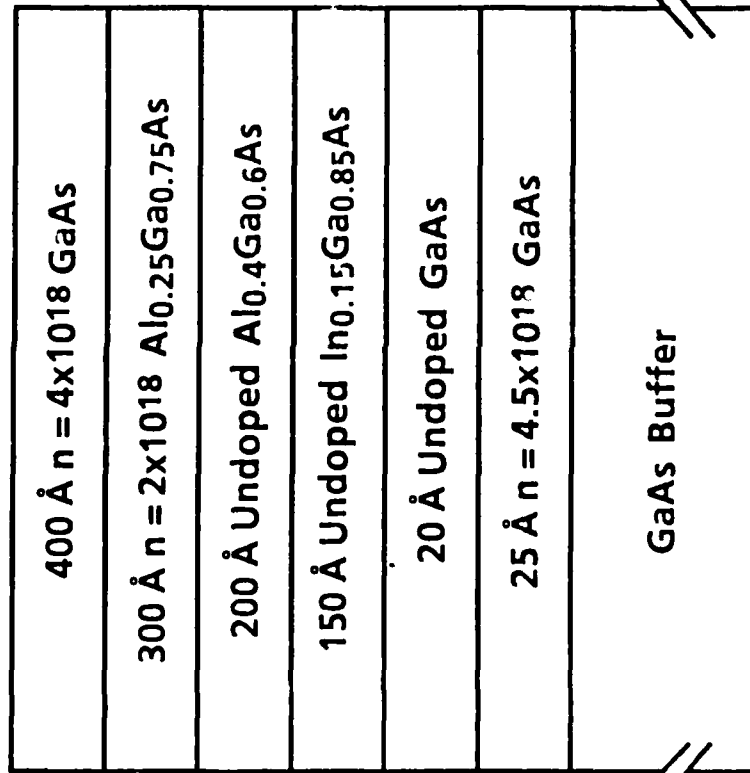


TEXAS
INSTRUMENTS

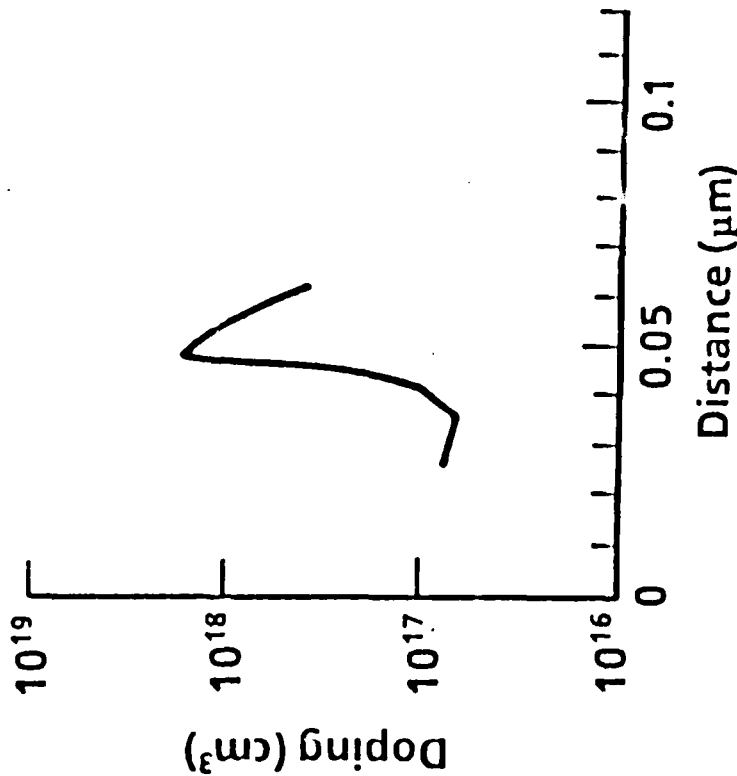
BK
008:0260
11/88

CENTRAL RESEARCH LABORATORIES

Quantum Well MISFET with Undoped Channel



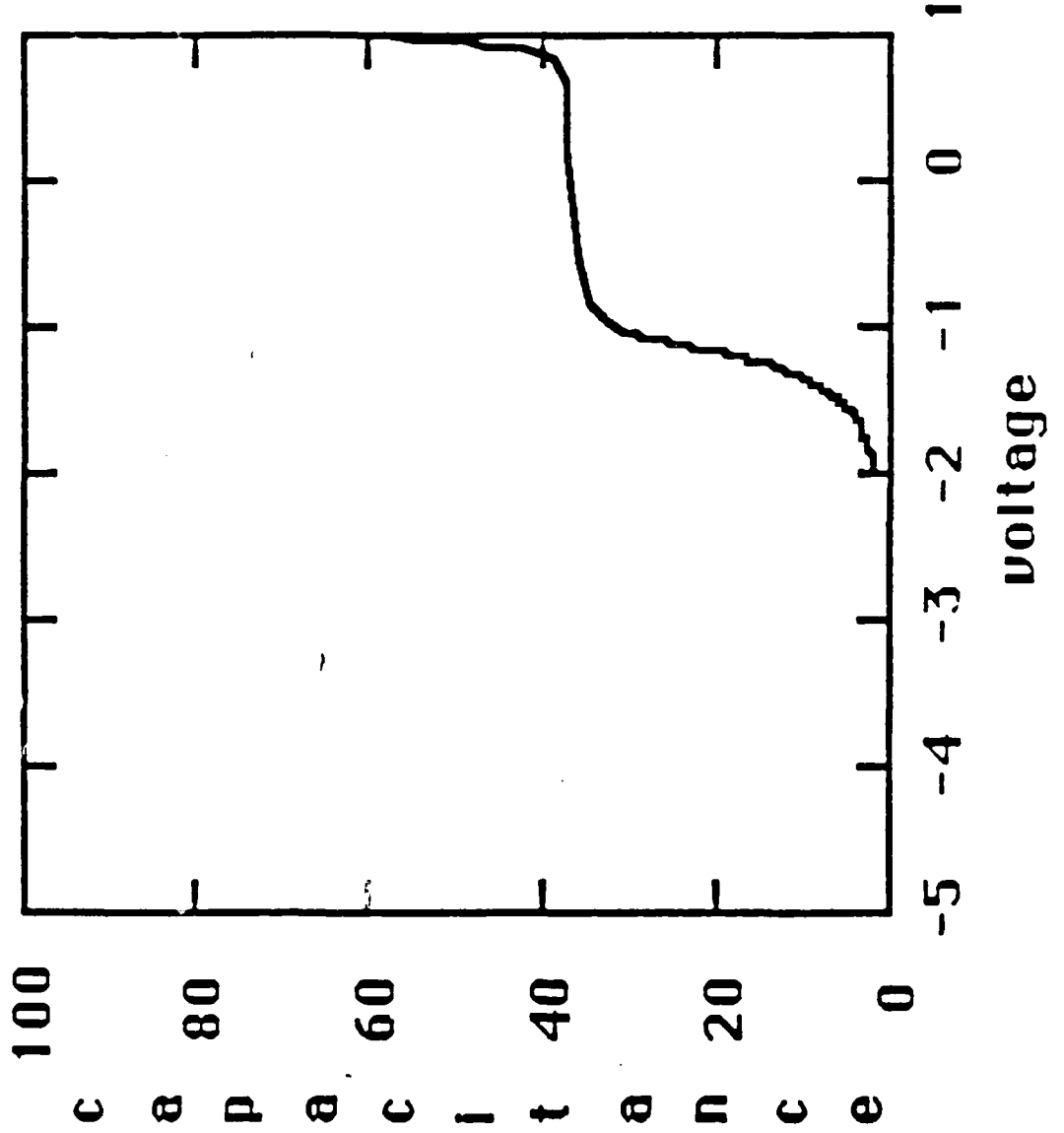
Material Structure

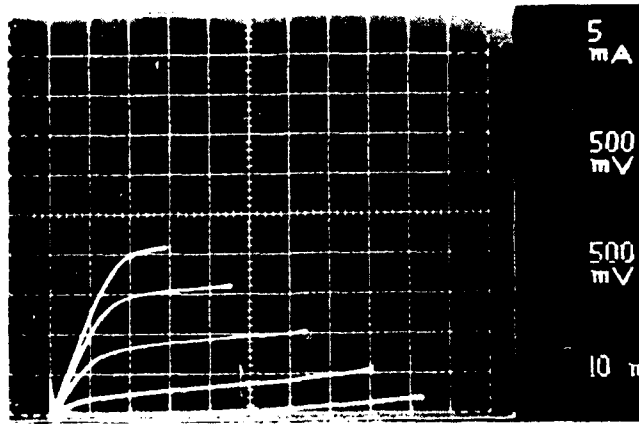


Charge Carrier Profile

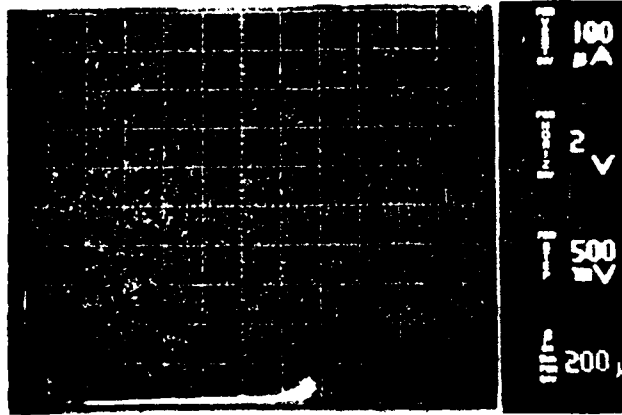


GATE CAPACITANCE VS GATE VOLTAGE OF A QUANTUM WELL MISFET

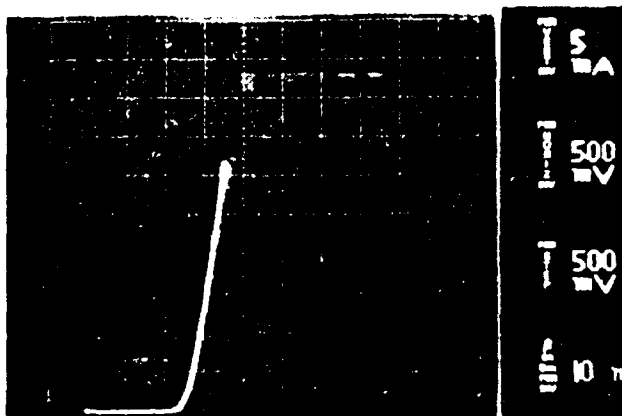




(a) I-V Curve



(b) Gate-Drain Breakdown Curve



(c) Gate Forward Characteristic

Figure 22. Dc characteristics of quantum well MISFETS. (a) I-V curve; (b) gate-drain breakdown curve; (c) gate forward characteristic.



TEXAS
INSTRUMENTS

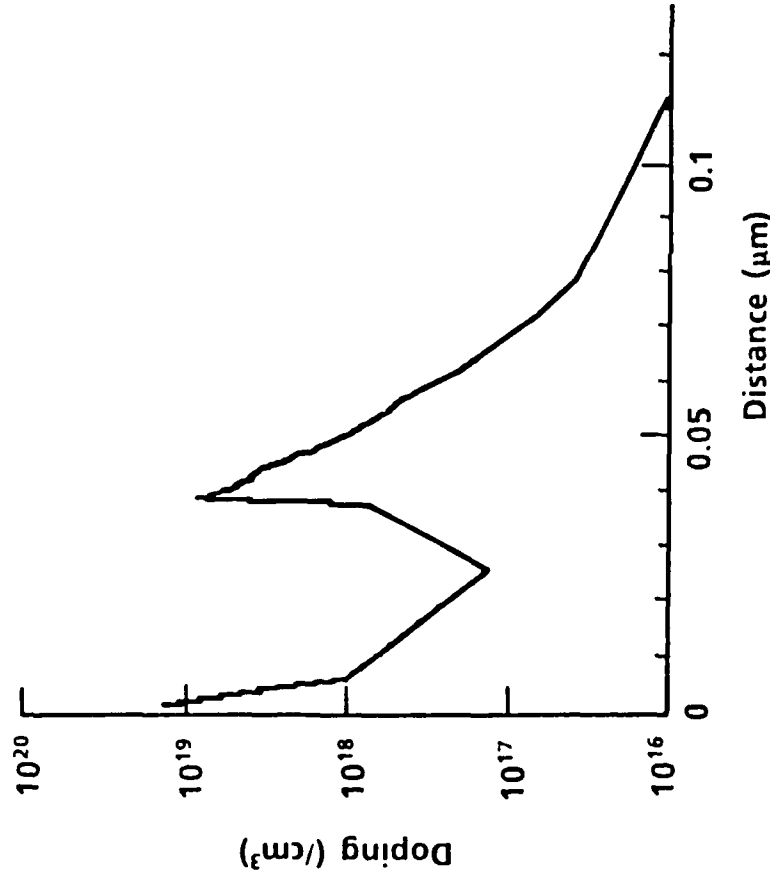
BK
008:0250
11/88

CENTRAL RESEARCH LABORATORIES

Quantum-Well MISFET with Doped Well

GaAs	400 Å	$n = 4 \times 10^{18}$
$\text{Al}_{0.2}\text{Ga}_{0.8}\text{As}$	300 Å	$n = 2 \times 10^{18}$
$\text{Al}_{0.34}\text{Ga}_{0.66}\text{As}$	200 Å	Undoped
$\text{In}_{0.15}\text{Ga}_{0.85}\text{As}$	120 Å	$n = 3 \times 10^{18}$
GaAs	80 Å	$n = 2 \times 10^{18}$

Material Structure



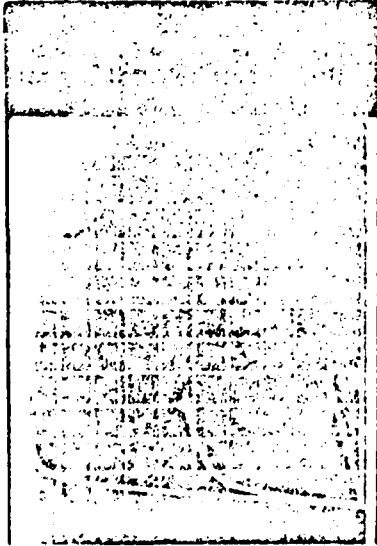
Charge Density Profile



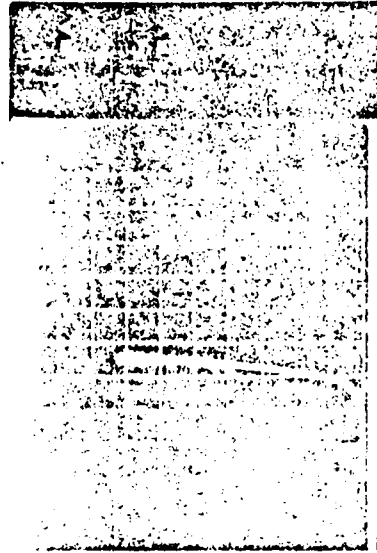
TEXAS
INSTRUMENTS

CENTRAL RESEARCH LABORATORIES

CHARACTERISTICS OF QUANTUM WELL MISFET WITH DOPED CHANNEL ($0.25\mu\text{m} \times 50\mu\text{m}$)



I-V CURVE



SCHOTTKY PROPERTIES

DC
• TRANSCONDUCTANCE

500 mS/mm

• I_{max} 1000 mA/mm

• SCHOTTKY BARRIER 1.4 V

RF

60 GHz

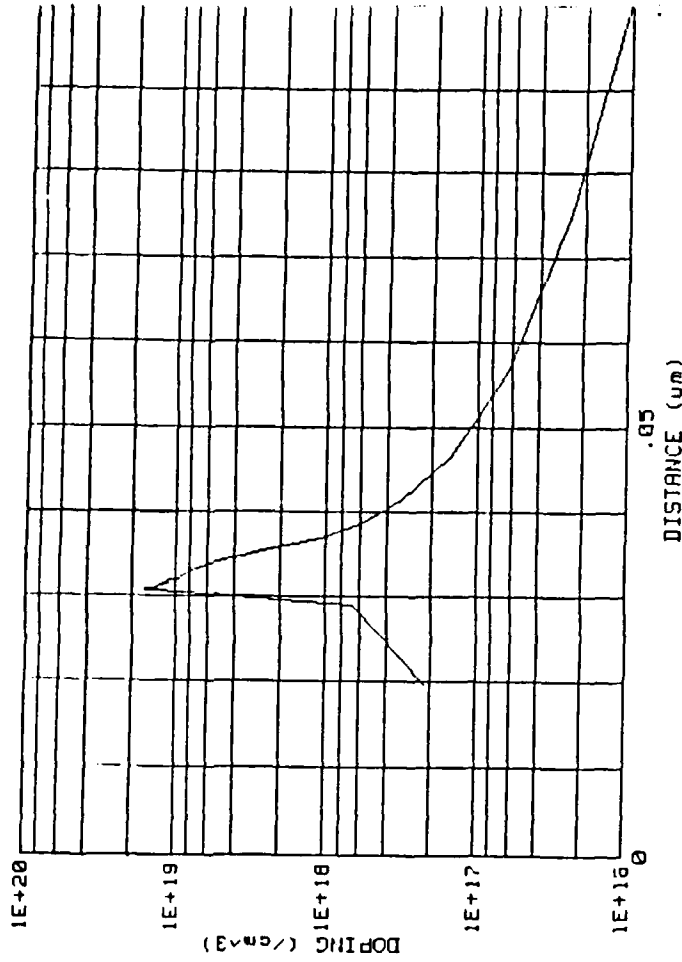
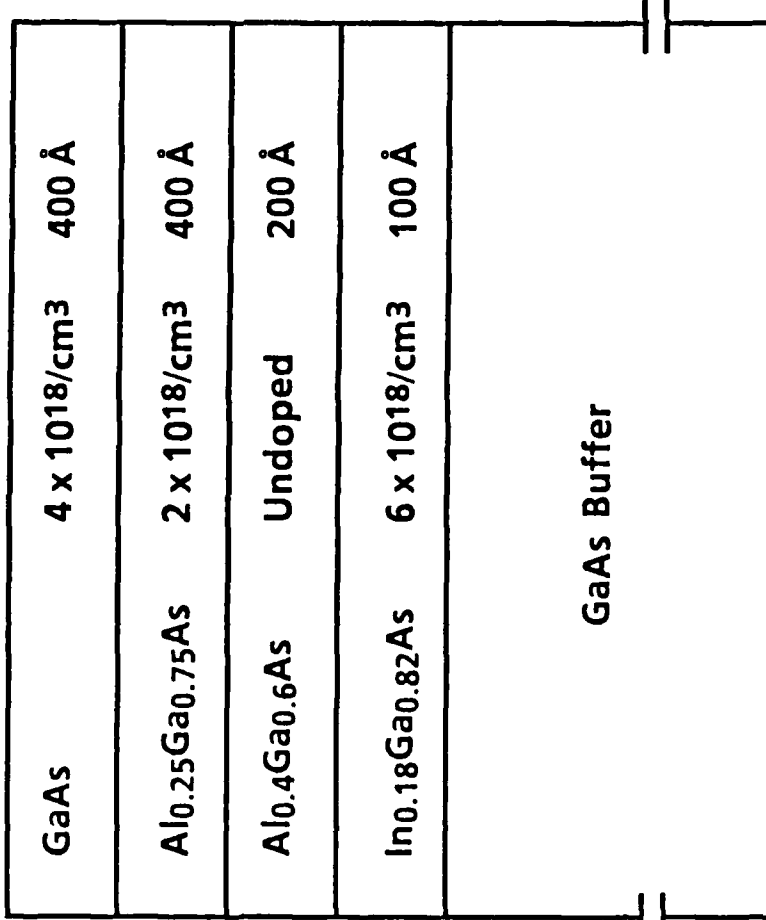
0.95 W/mm, 24% EFFICIENCY

3dB GAIN

GATE-DRAIN BREAKDOWN



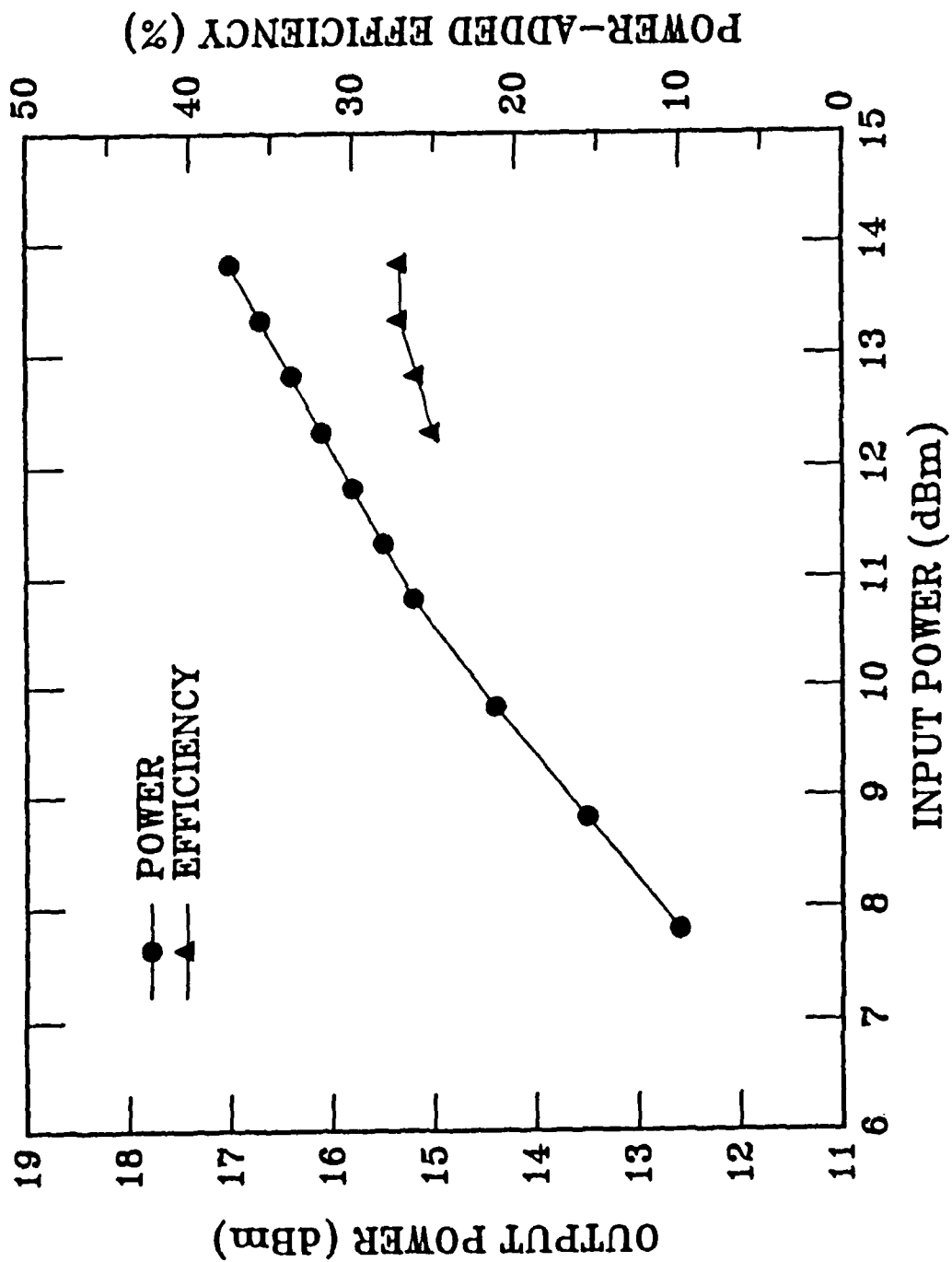
Quantum well MISFET



Material Structure

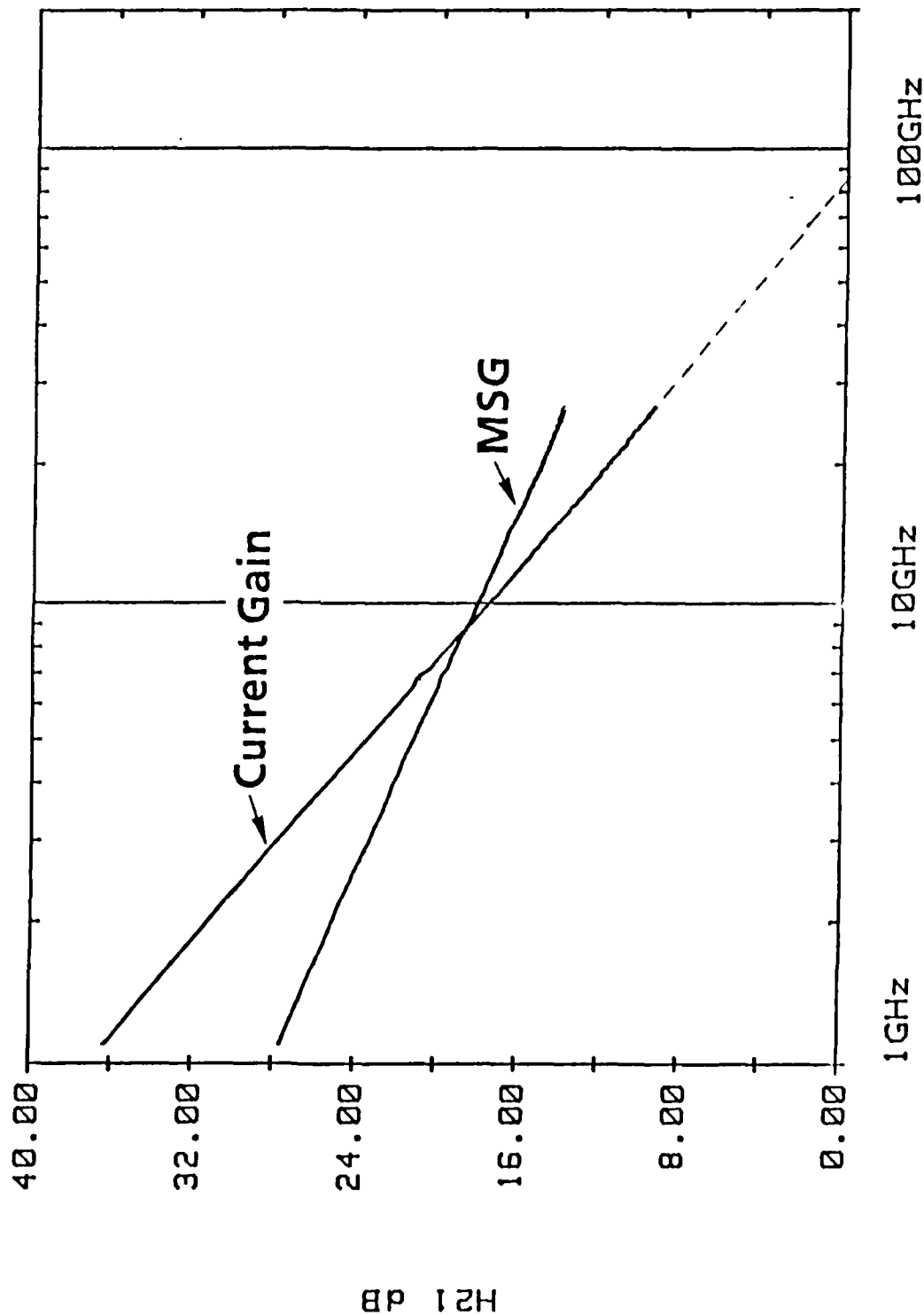
Charge Carrier Profile

PERFORMANCE OF 50 μm x 0.25 μm MISFET AT 60 GHz



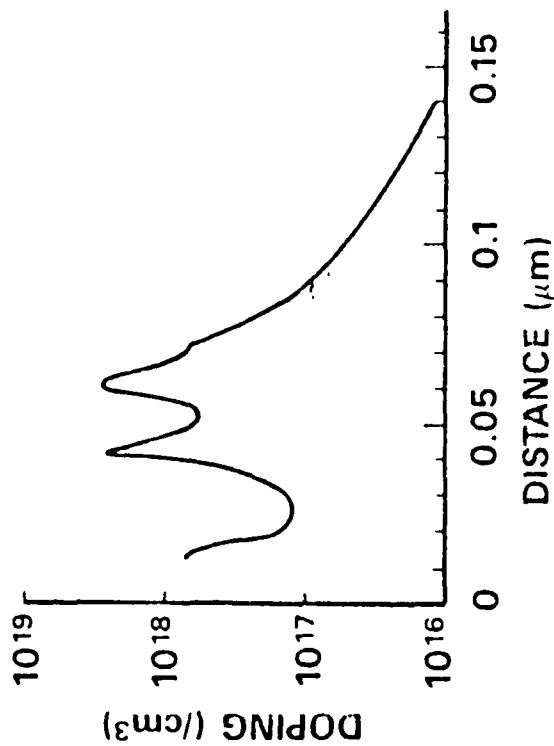


Current Gain and Maximum Stable Gain of QW MISFET



DOUBLE QUANTUM WELL MISFET

$n = 4 \times 10^{18}$	GaAs	500 Å
$n = 2 \times 10^{18}$	$\text{Al}_{0.25}\text{Ga}_{0.75}\text{As}$	300 Å
UNDOPED	$\text{Al}_{0.4}\text{Ga}_{0.6}\text{As}$	200 Å
$n = 1 \times 10^{18}$	$\text{In}_{0.15}\text{Ga}_{0.85}\text{As}$	120 Å
$n = 1.5 \times 10^{18}$	GaAs	100 Å
$n = 1 \times 10^{18}$	$\text{In}_{0.15}\text{Ga}_{0.85}\text{As}$	120 Å
$n = 2 \times 10^{18}$	GaAs	80 Å
GaAs BUFFER (1 μm)		



MATERIAL STRUCTURE

CHARGE DENSITY PROFILE



**TEXAS
INSTRUMENTS**

BK
008:0260

CENTRAL RESEARCH LABORATORIES

Performance of a 0.25 x 50 μm Double Quantum Well MISFET

FREQUENCY (GHZ)	POWER DENSITY (W/mm)	GAIN (DB)	EFFICIENCY (%)
55	0.68	4.0	31
55	0.89	3.7	26
55	0.96	3.0	24
60	0.6	3.4	20

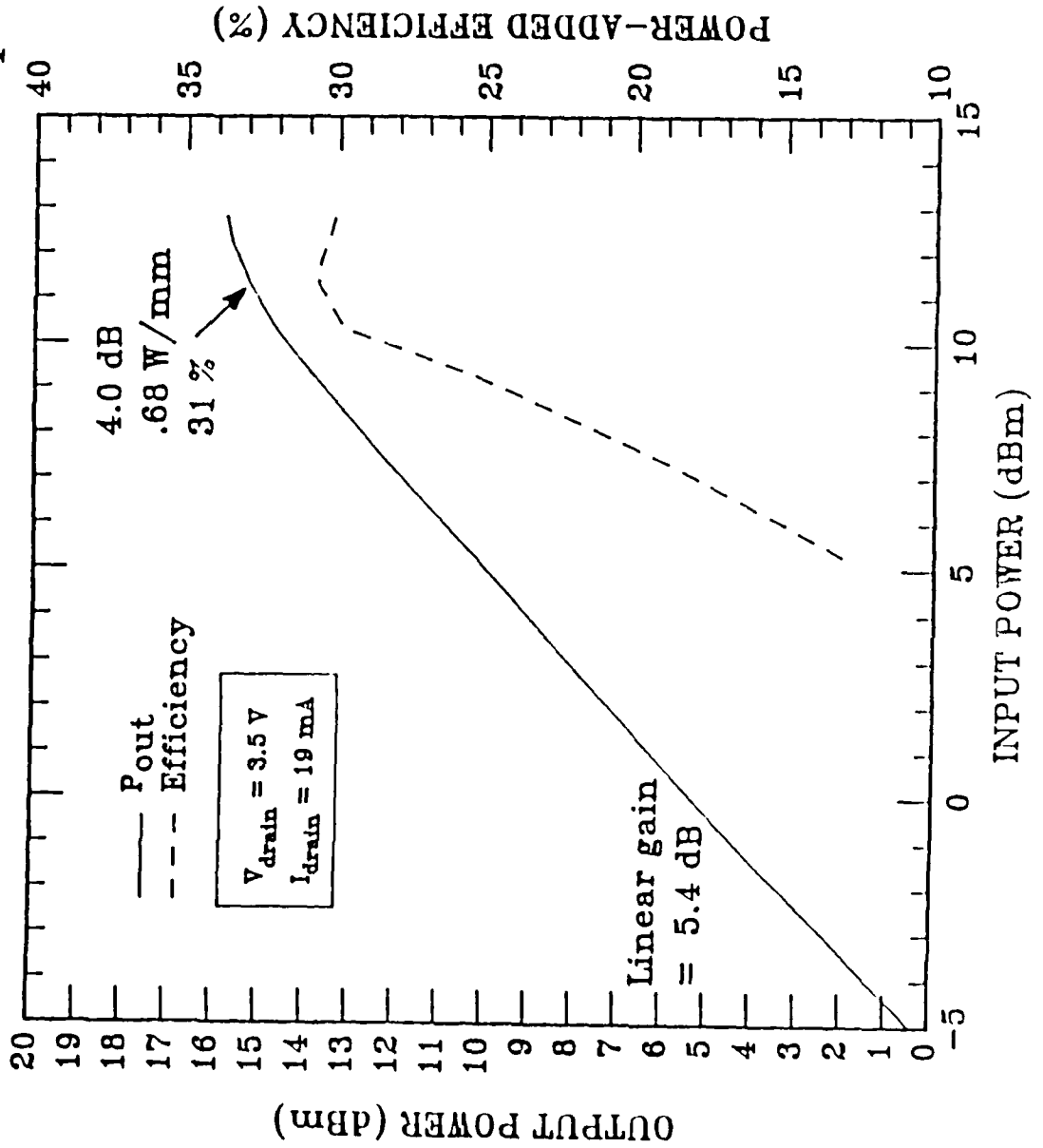


TEXAS
INSTRUMENTS

BK
008:0260
11/88

CENTRAL RESEARCH LABORATORIES

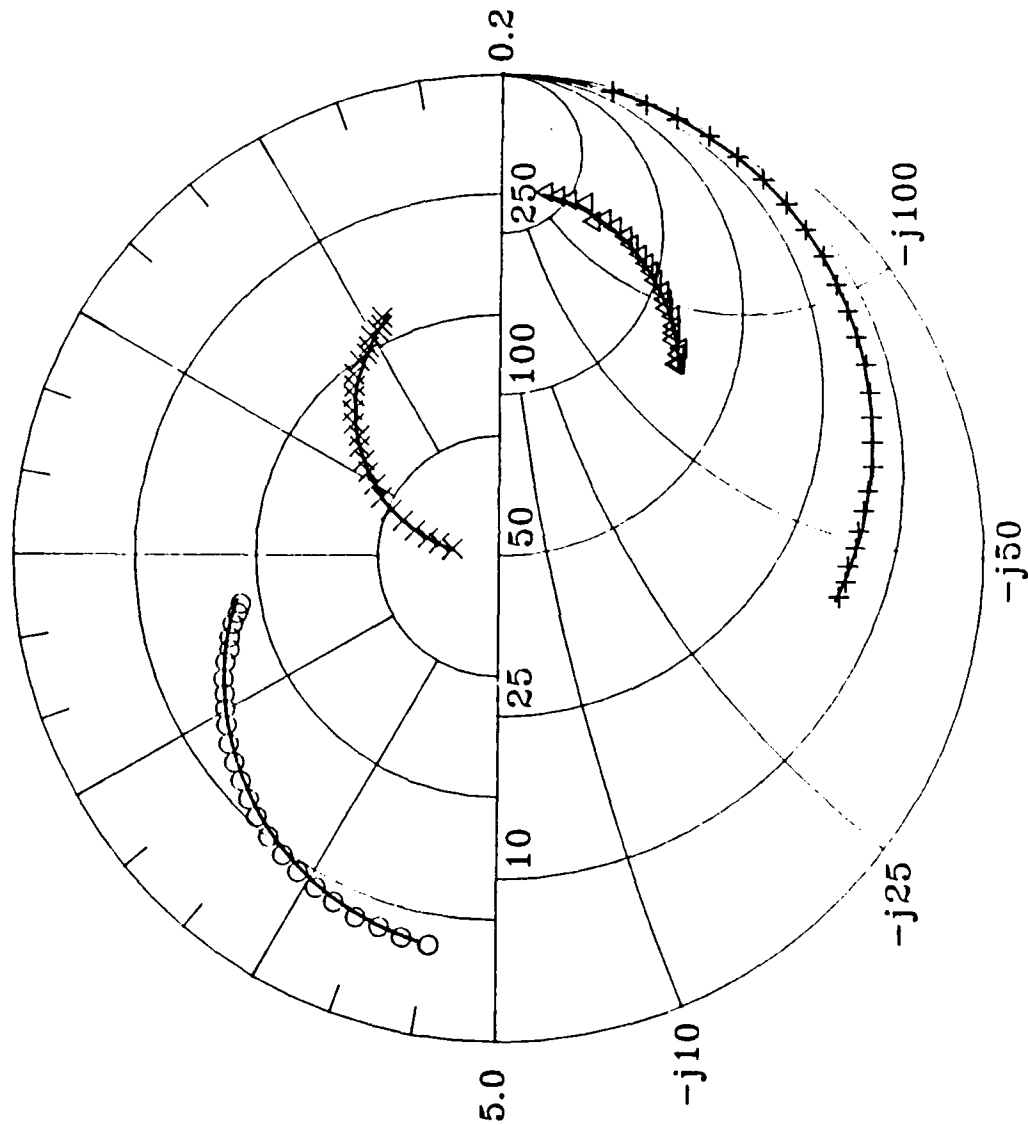
Performance of a Double Quantum Well MISFET at 55 GHz ($0.25 \times 50 \mu\text{m}$)





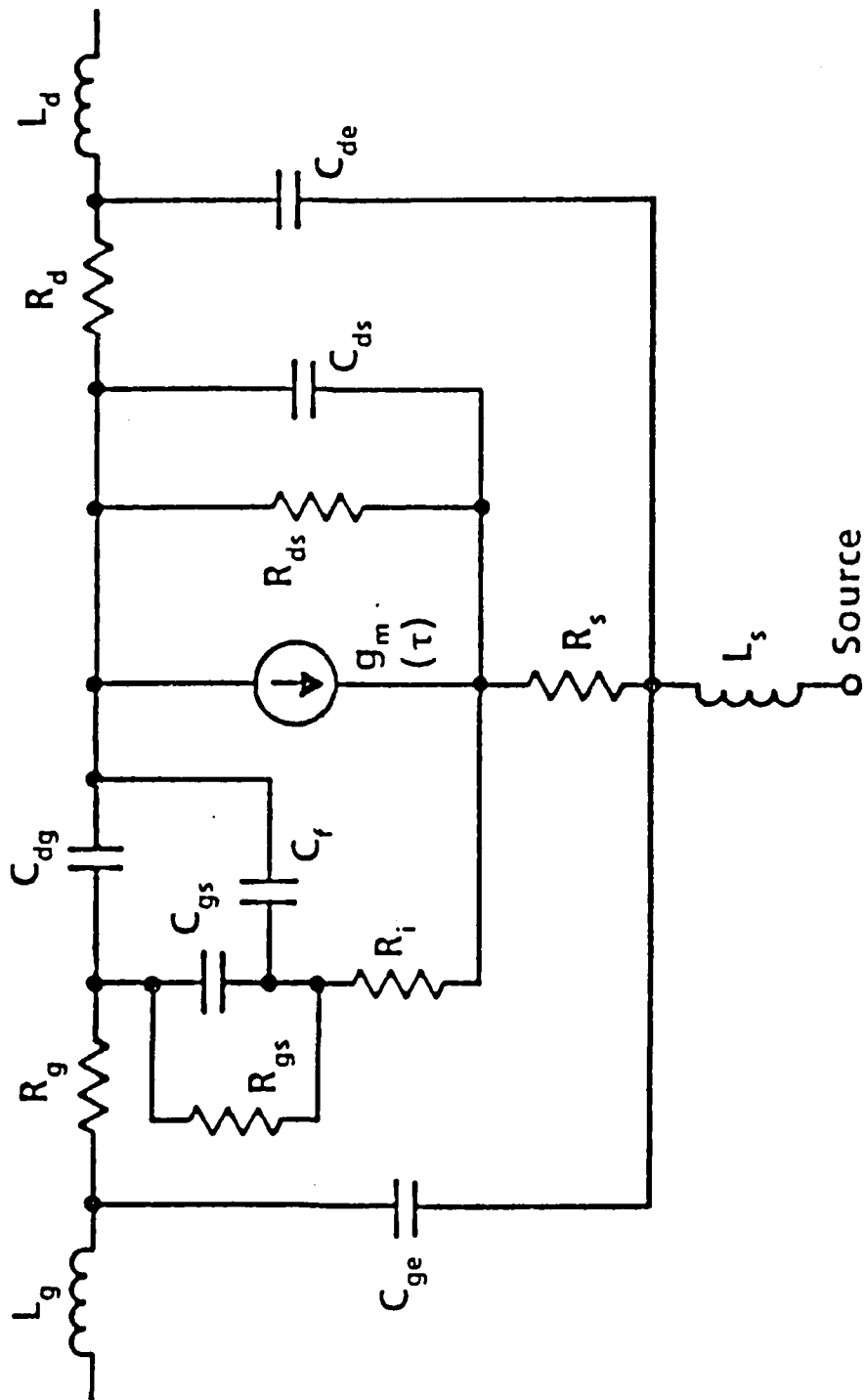
QW MISFET

- + S11
- Δ S22
- S21
- × S12
- MODEL





EQUIVALENT CIRCUIT MODEL OF FET





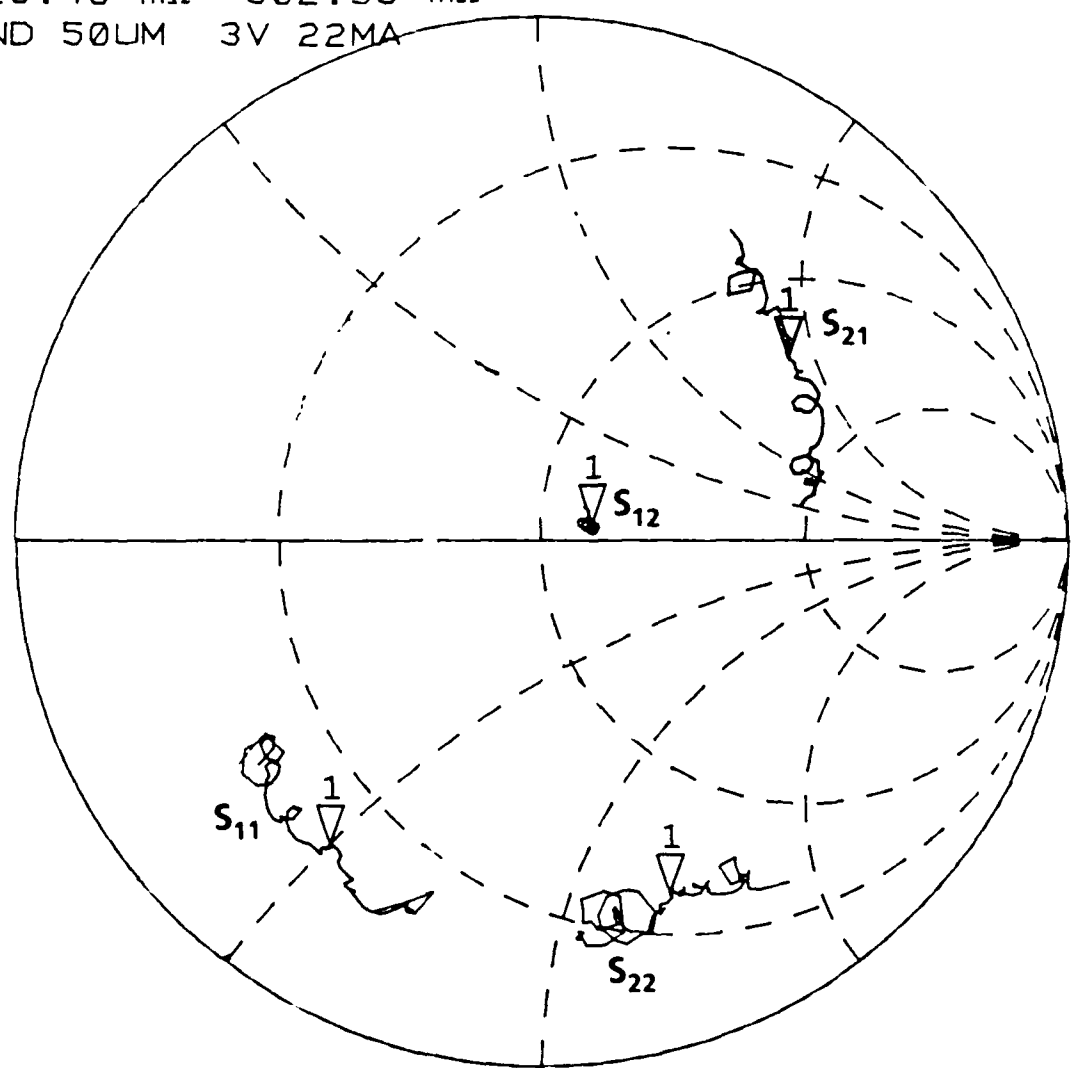
CENTRAL RESEARCH LABORATORIES

Equivalent Circuit Parameters of 0.25 x 50 μm Quantum Well MISFETs

Parameter	Undoped-Well	Doped-Well	Double-Wells
C_{gs} (pF)	0.074	0.04	0.05
g_m (mS)	20.5	37.5	26.6
C_{dg} (pF)	0.008	0.008	0.008
R_{ds} (Ω)	980	504	622
f_t (GHz)	40	120	72

Z
 REF 1.0 Units
 1 200.0 mUnits/
 ▽ 220.46 mΩ -502.59 mΩ
 V-BAND 50UM 3V 22MA

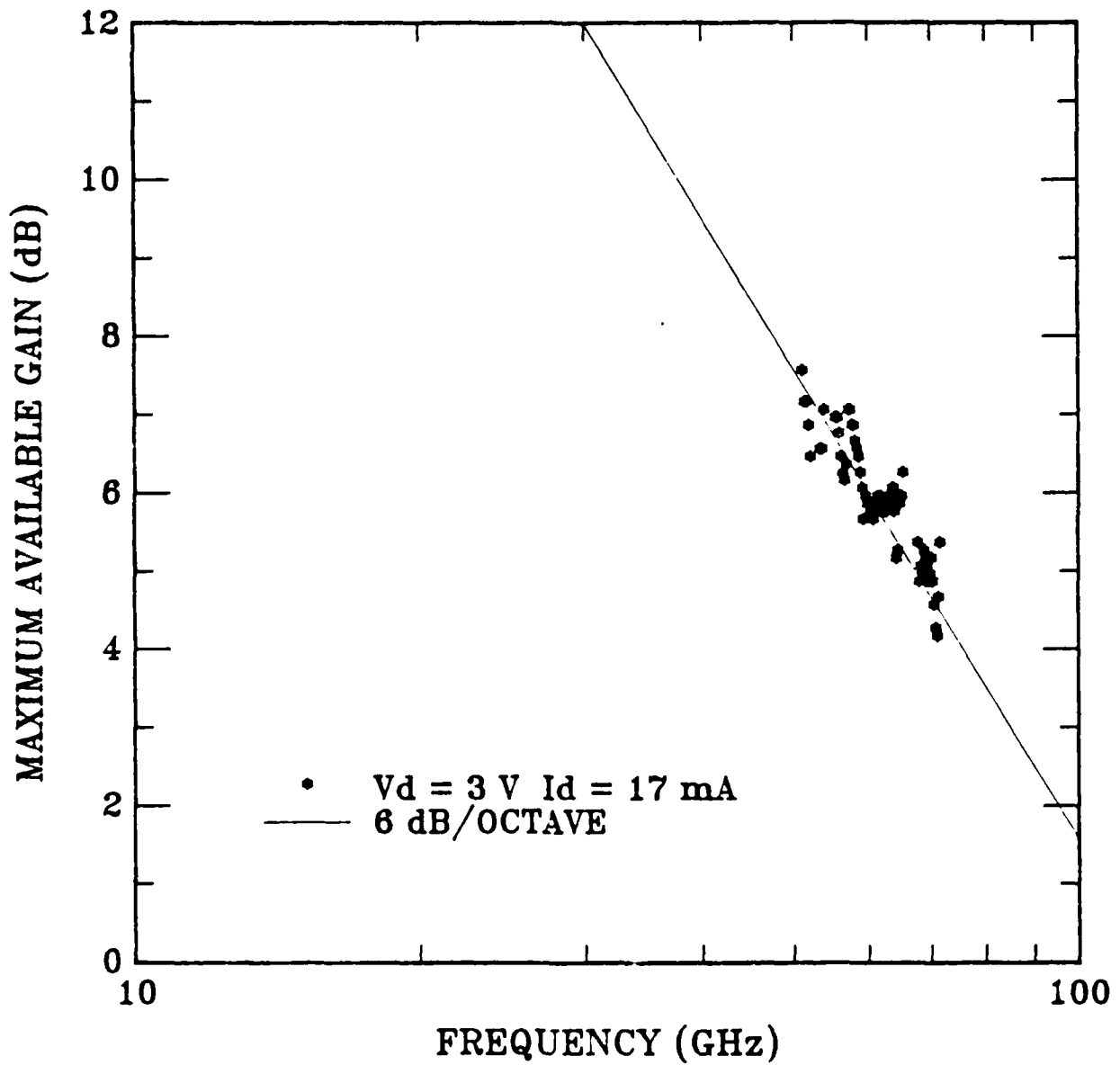
*
 C
 A
 I
 D



START 49.999999920 GHz
 STOP 74.999983920 GHz

S-Parameters at V-band (50-75 GHz)

MAXIMUM AVAILABLE GAIN OF V-BAND FET



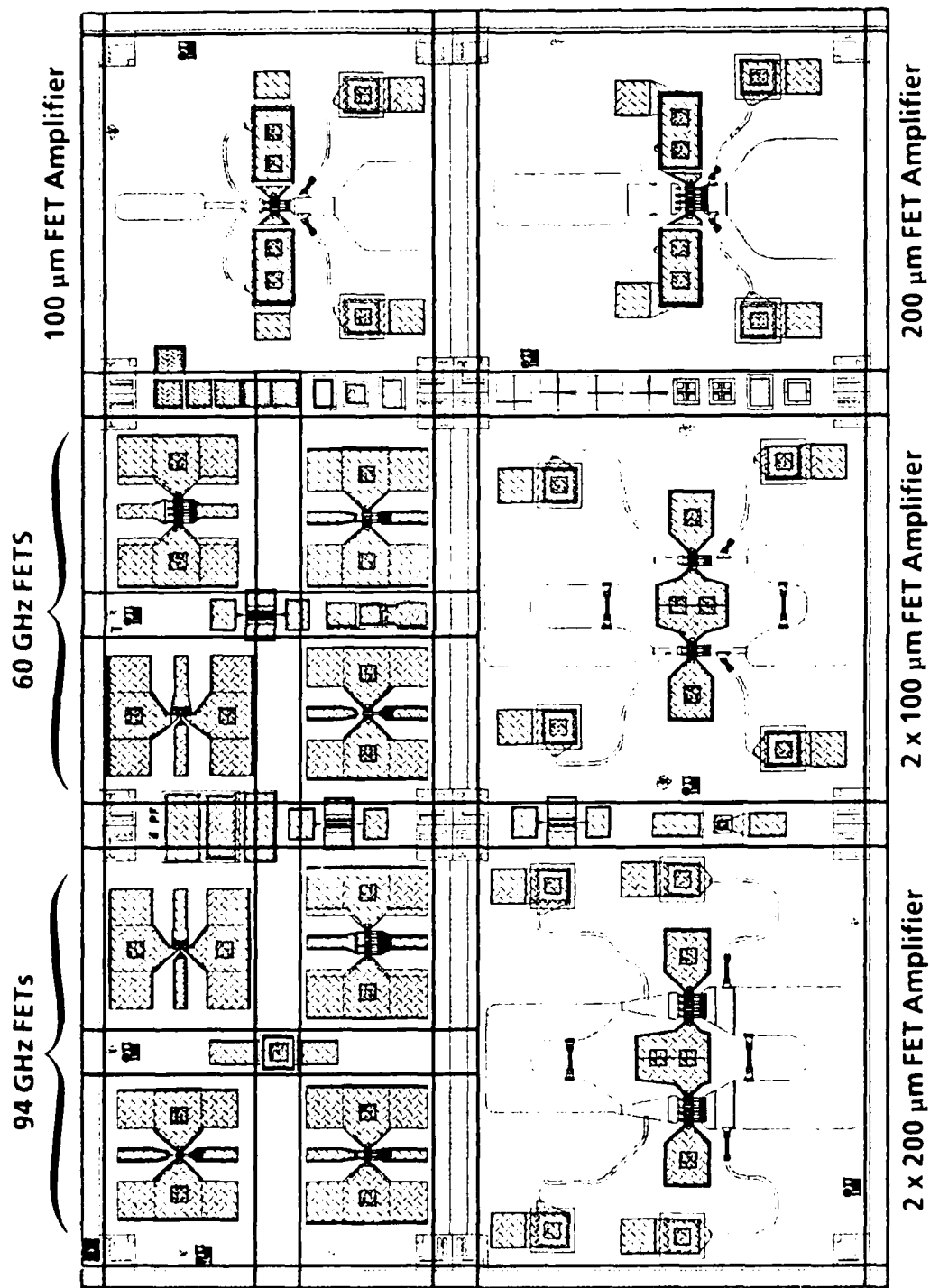
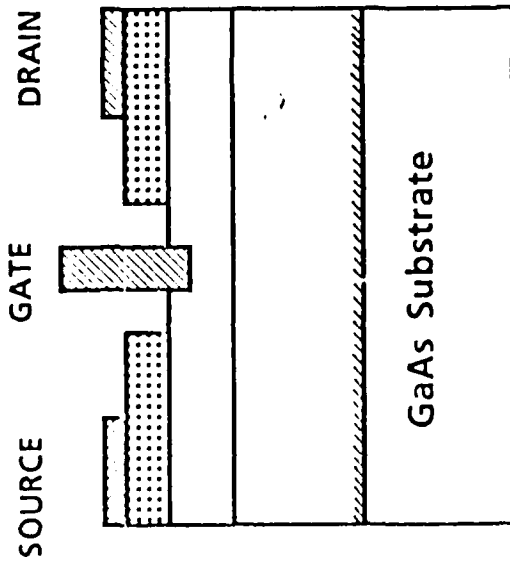


Figure 32. Mask layout.



InGaAs MESFET



- Good Transport Properties of InGaAs
- Heteroepitaxy Growth
- mm-Wave MISFET

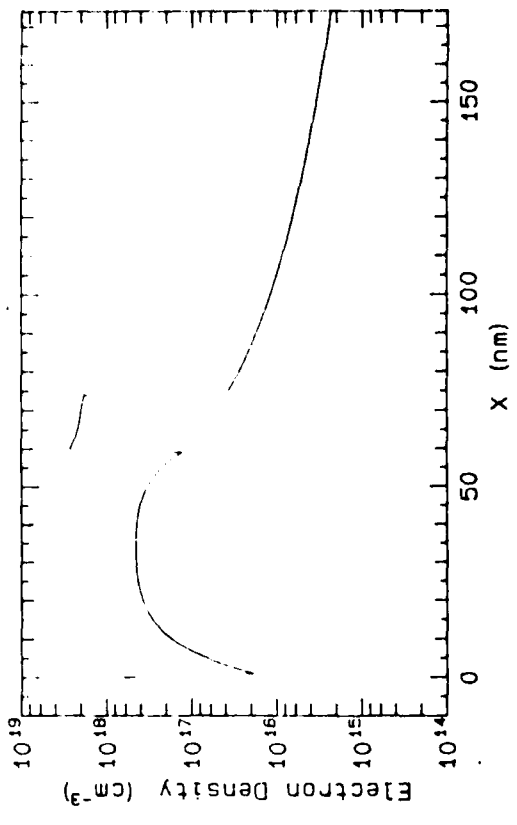
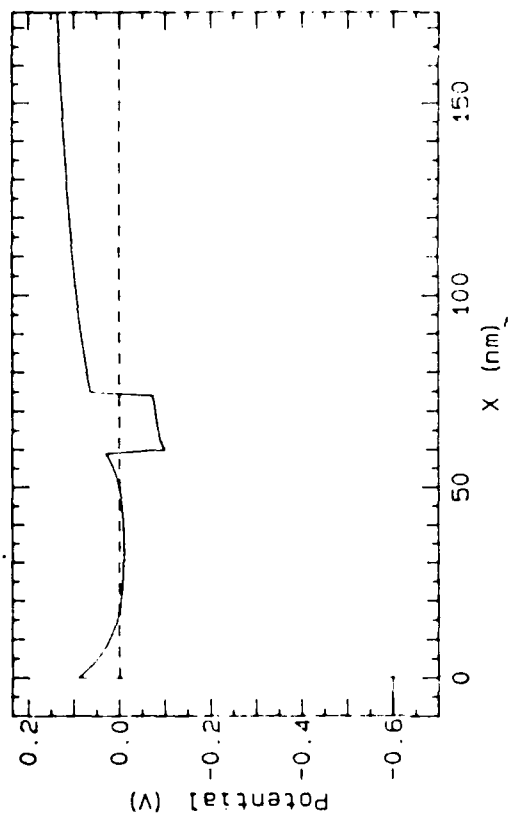
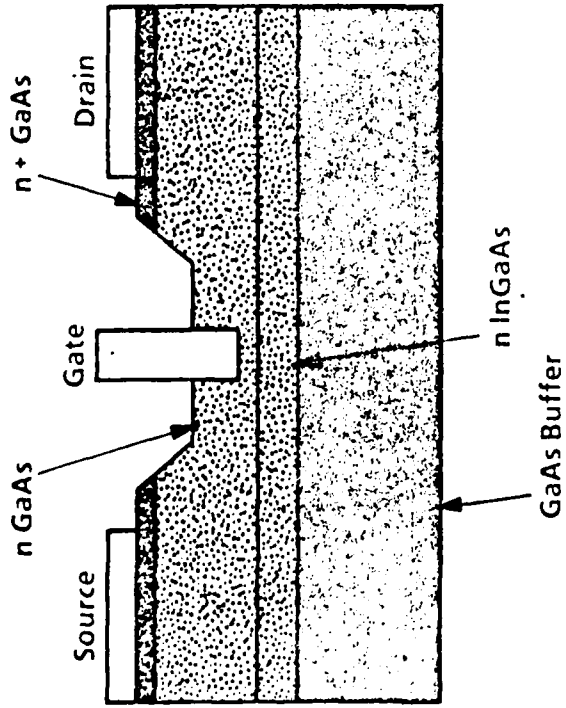
Device Performance

At 60 GHz

Power Density = 0.5 w/mm with 4dB gain and 20% Efficiency

$f_t = 65$ GHz for 0.25 μ m gate

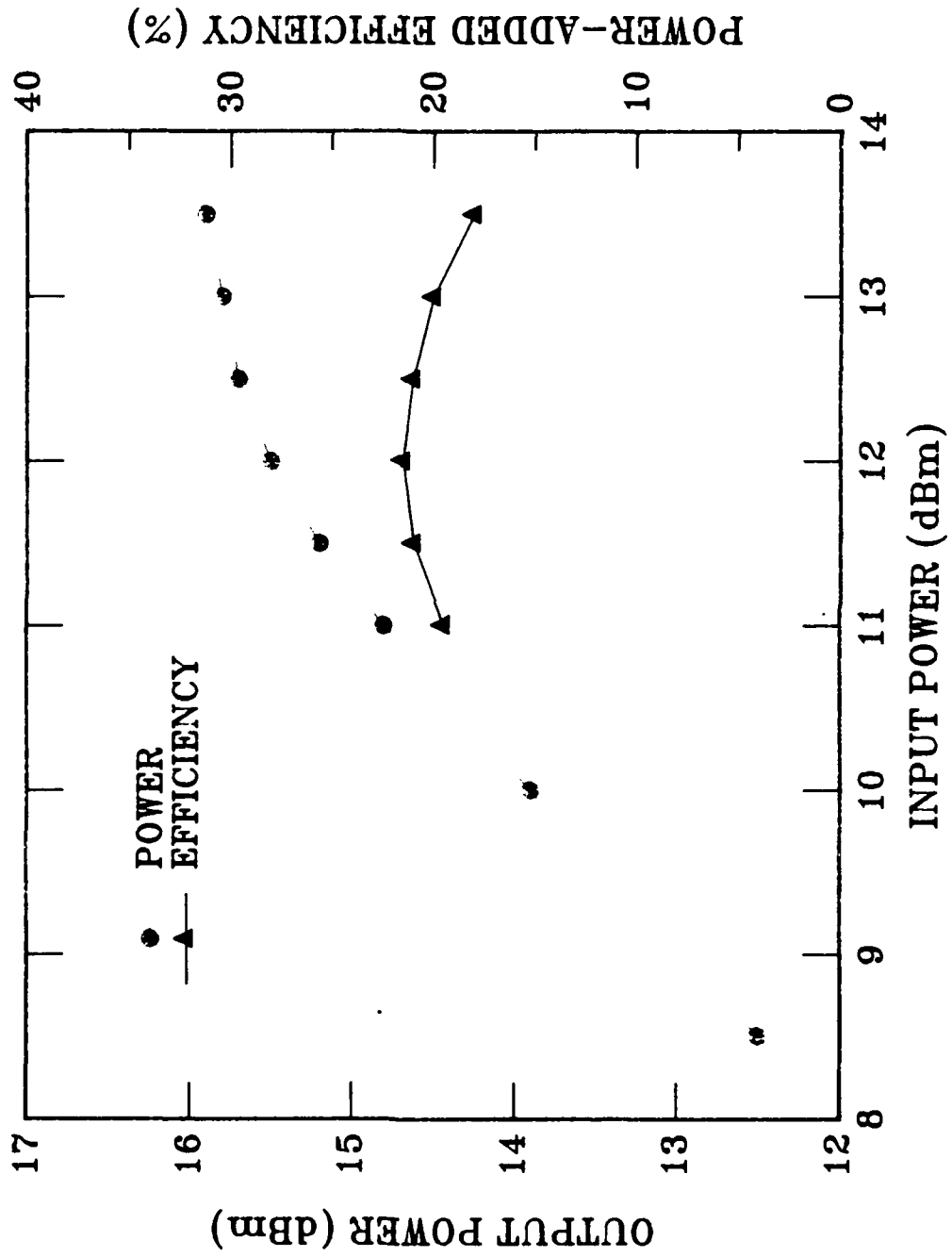
InGaAs PULSE-DOPED MESFET



Advantages

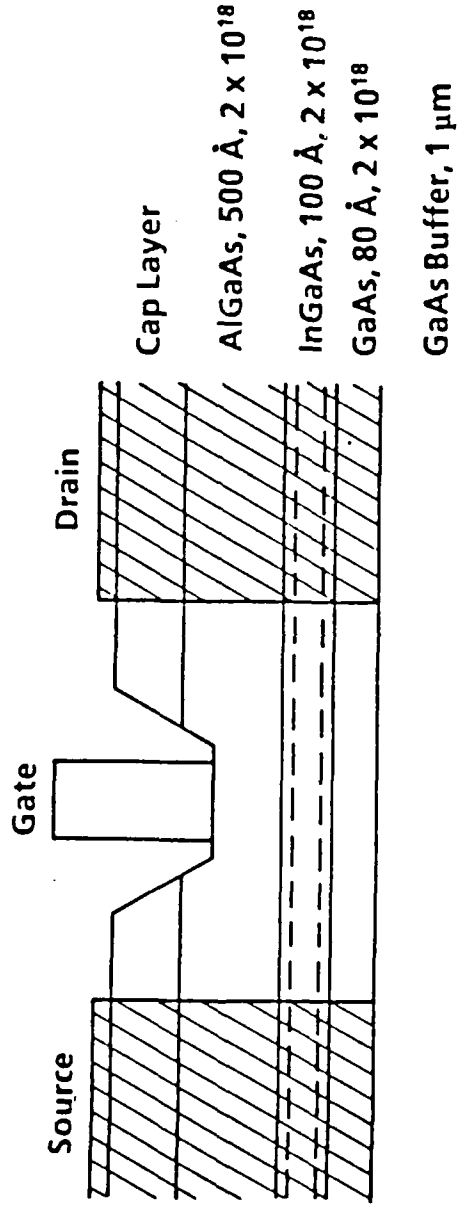
- Better Transport Properties
- High Carrier Density
- Tight Electron Confinement
- Easy of Manufacturing

PERFORMANCE OF 0.25 μ m InGaAs PULSE-DOPED FET AT 60 GHz



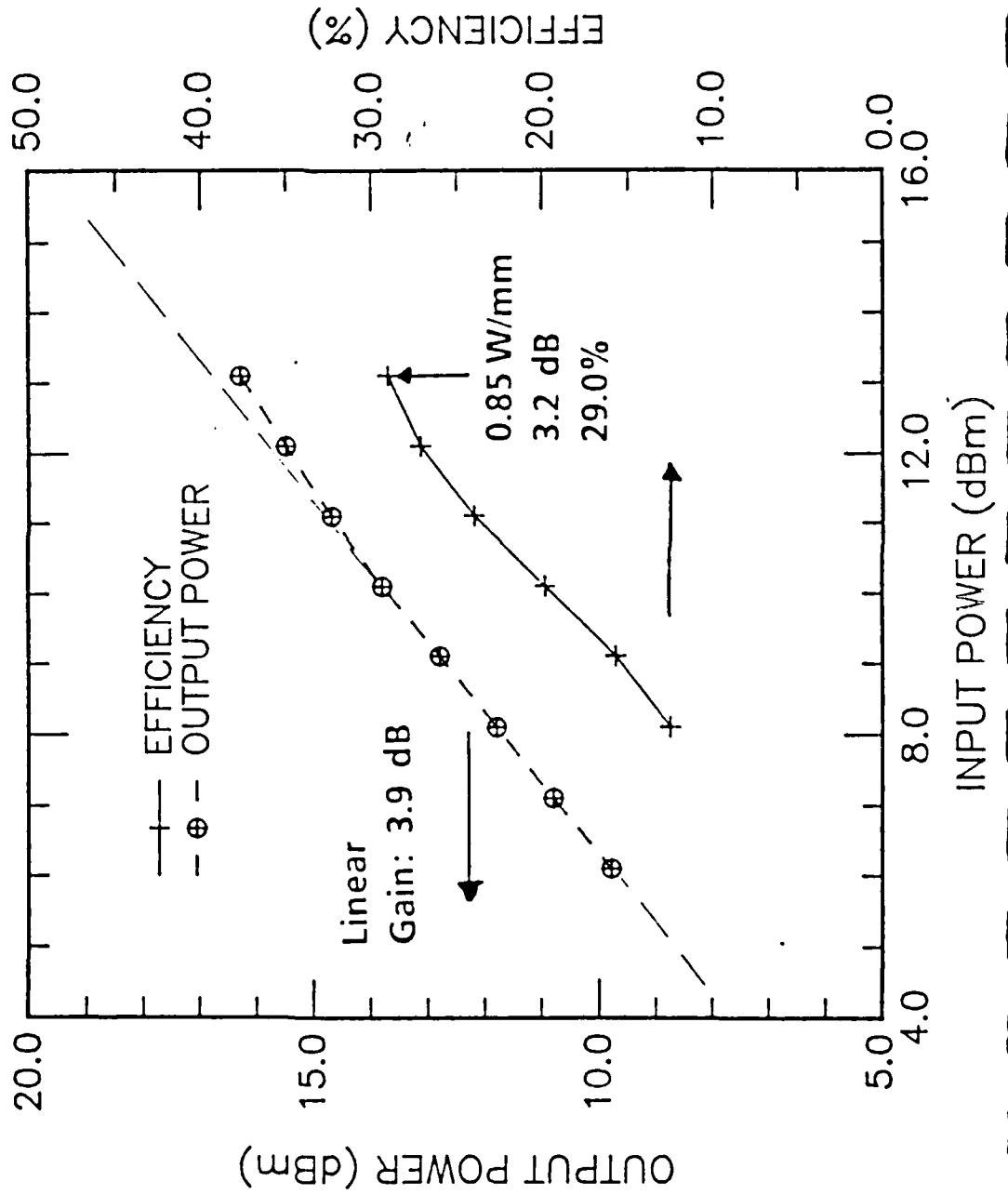


MATERIAL STRUCTURE OF DOUBLE CHANNEL PSEUDOMORPHIC HEMTs

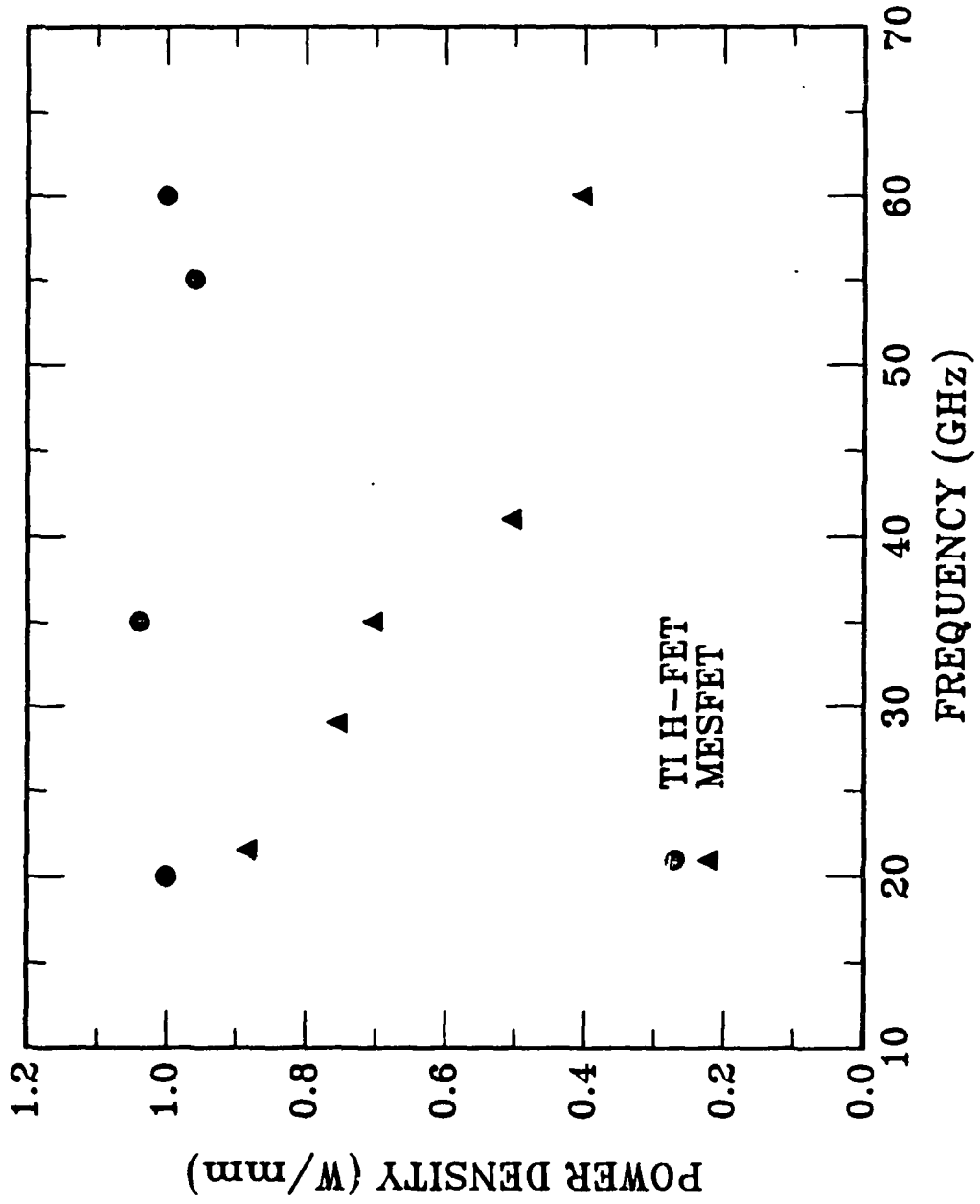




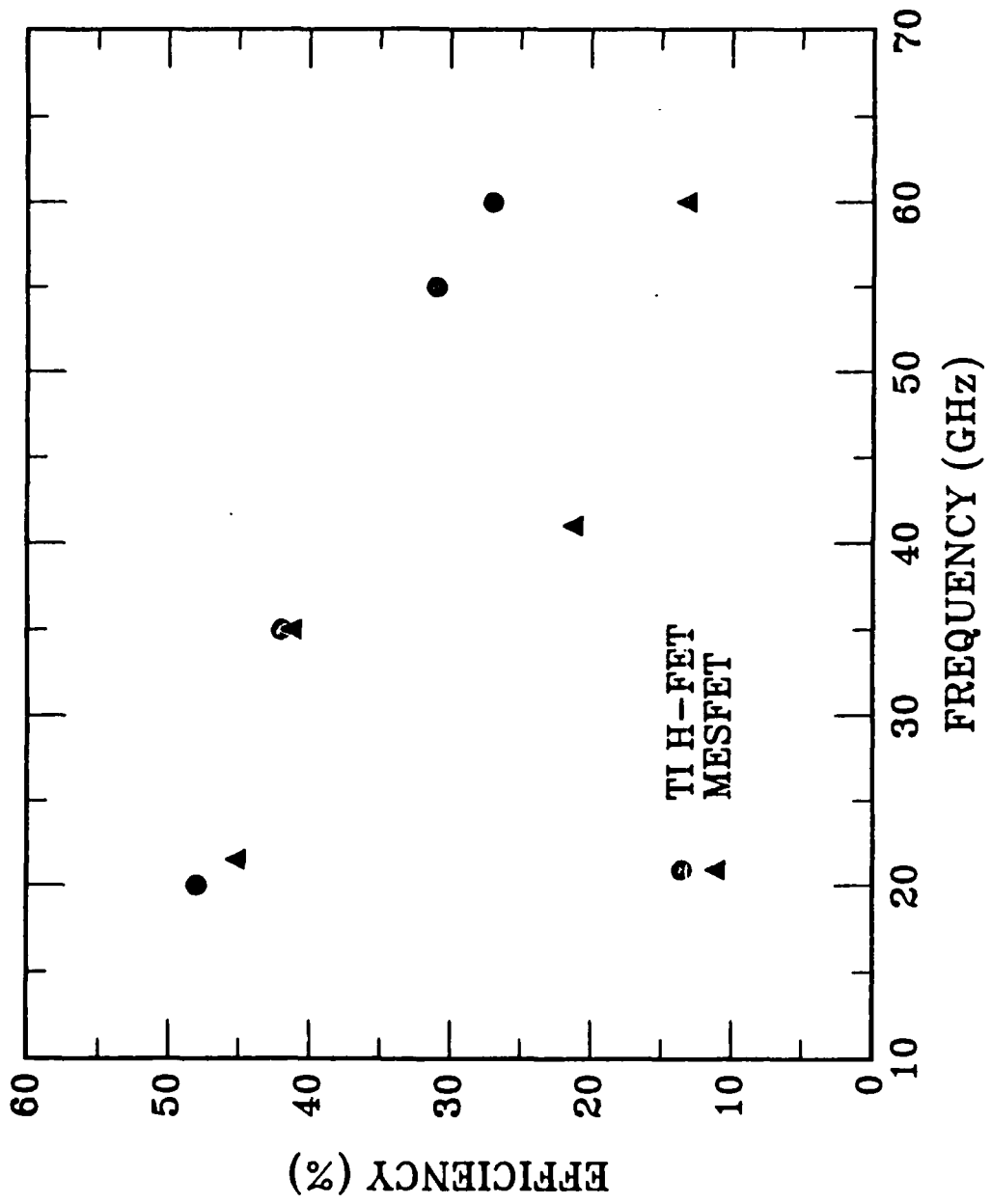
POWER PERFORMANCE OF DOUBLE CHANNEL PSEUDOMORPHIC HEMTs



POWER DENSITY OF 0.25 μm FET'S



EFFICIENCY OF 0.25 μm FET'S





SUMMARY

- Developed quantum well power MISFET at mm-wave frequencies
- Improved device performance by doping the well
- Achieved 1 W/mm with 3.2 dB gain and 27% efficiency at 60 GHz
- Designed monolithic power amplifiers

Molecular Beam Epitaxy and Resonant Tunneling Devices

J. S. Harris

*Stanford University
Stanford, CA*

**MOLECULAR BEAM EPITAXY
AND
RESONANT TUNNELING DEVICES**

**J. S. Harris
Solid State Electronics Laboratory
Stanford University
(415)723-9775**

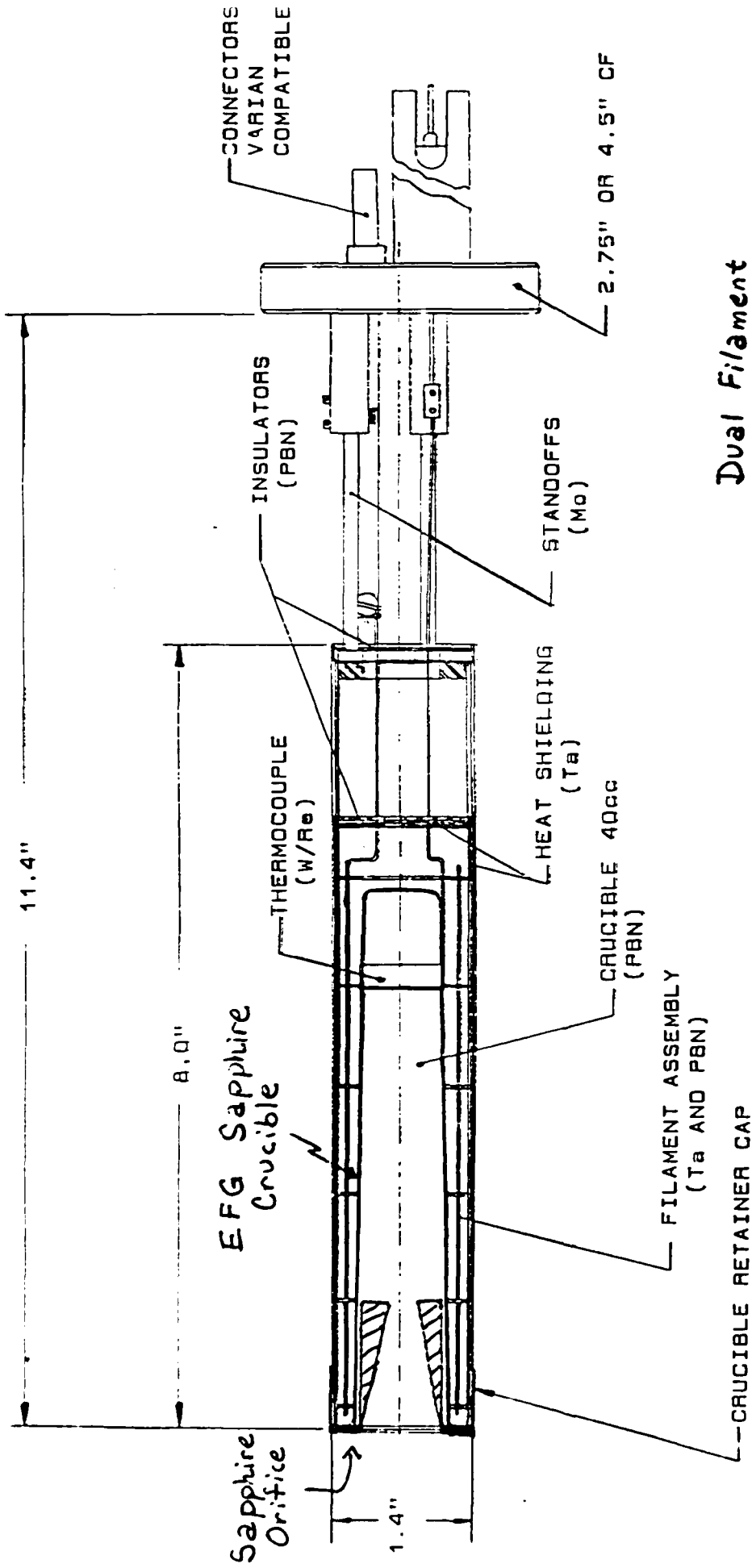
**DARPA EHF Monolithic Materials
Devices and Arrays Review
January 24-25, 1989
San Diego, CA**

OUTLINE

- **Oval Defects in MBE**
- **Resonant Tunneling Studles**
 - **Modeling**
 - **Double Barrier Structures**
 - **Lateral Barrier Structures**

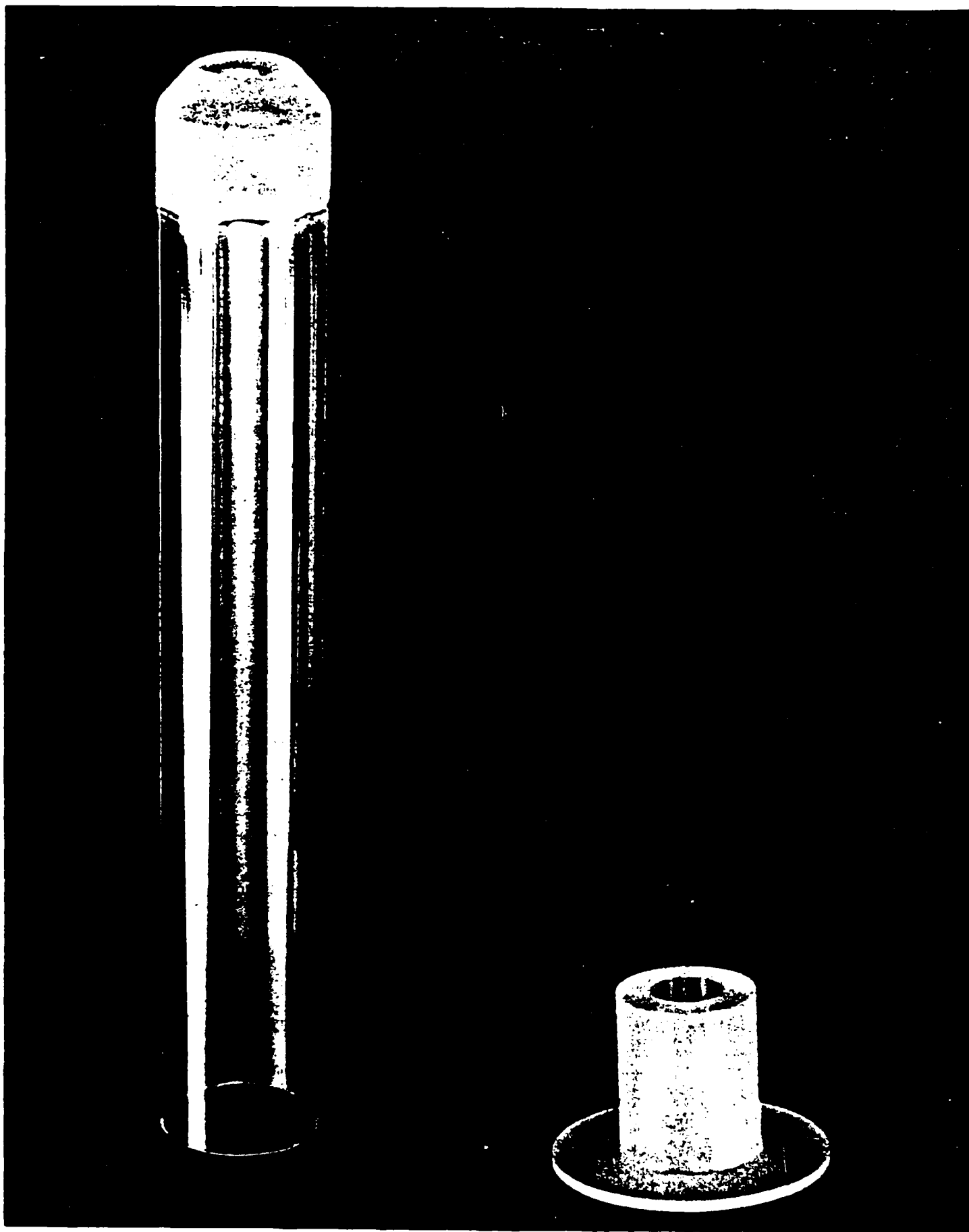
MOTIVATION

- (CBE & GSMBE too)
- * MOMBE \wedge has no gallium-related oval defects
 - * Overheating gallium cell increases gallium-related oval defects
 - * Aluminum addition (add ~.1% after system bakeout) helps (Woodall), but we still see gallium-related oval defects.
 - * Gallium "spitting" / Ga_2O_3 oval defect cause not resolved (maybe both at work)



Dual Filament

EPI Systems
 Model VA-40
 Effusion Cell
 June 1987



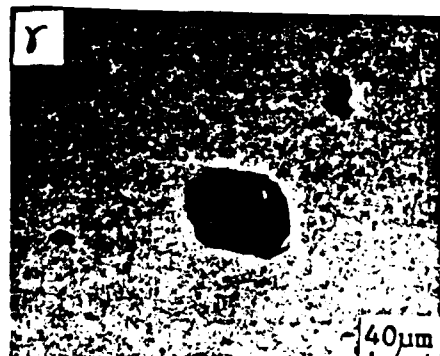
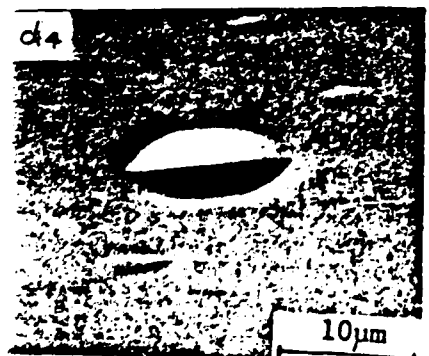
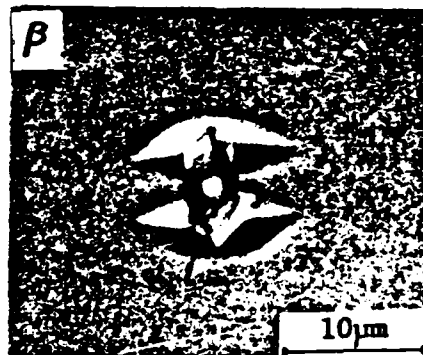
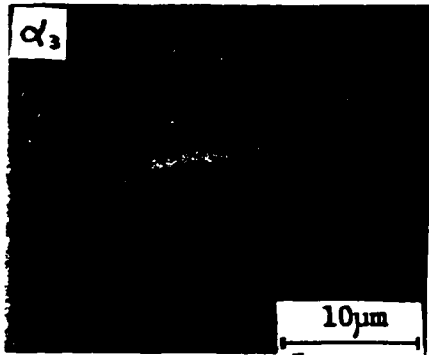
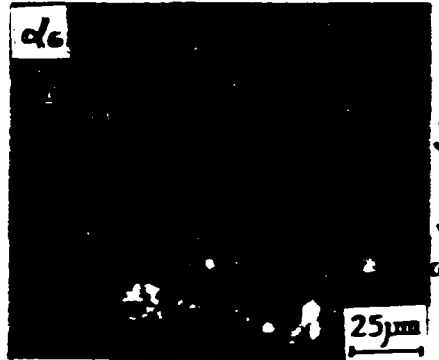
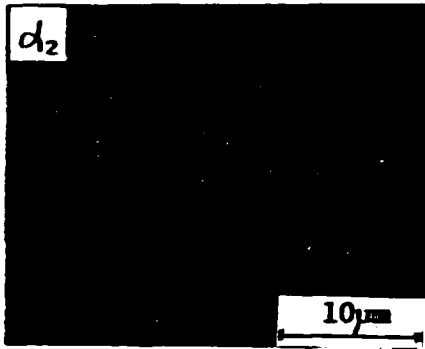
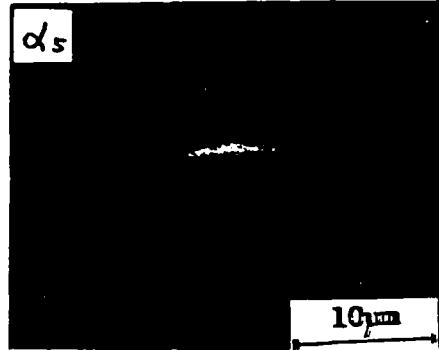
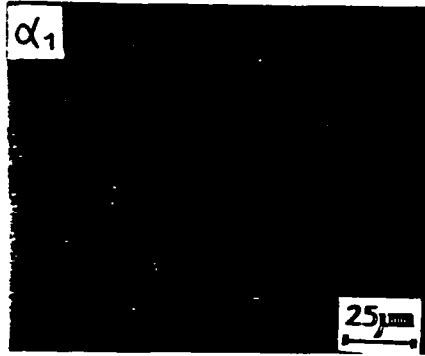
THE MANY "OVAL DEFECTS"

From: K. Fujiwara, K. Kanamoto, Y. N. Ohta, Y. Tokuda, & T. Nakayama
(Mitsubishi)

K. Fujiwara et al. / GaAs oval defects grown by MBE

Cause: As_2O_3 Octahedra? (Ploog)

Carbon? (Mitsubishi)



Sulfur on Substrate

Sulfur on Substrate
"Pair Defect" (Varian)

Flat Facet along Center

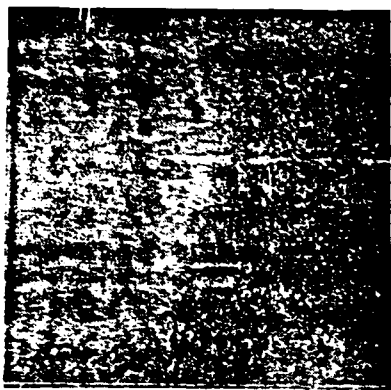
Gallium Source Related

Ga Rich? (Fujitsu)

Insufficient Outgassing of Furnace or Shutters

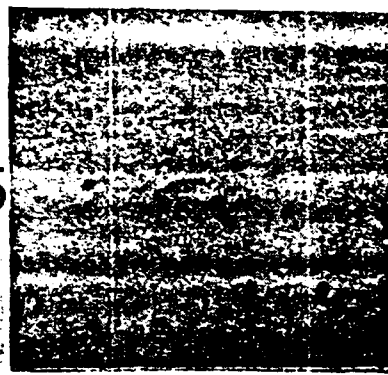
Fig. 1. Nomarski phase-contrast micrographs of seven types of GaAs oval defects and an irregular surface defect.

α_1
&
 α_5



#1041

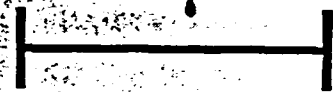
α_5



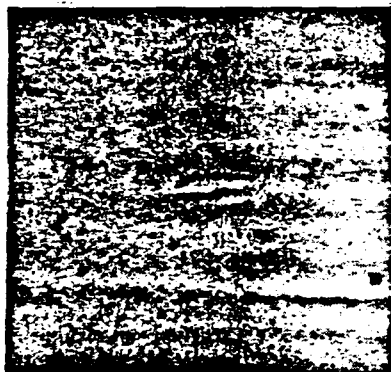
#1041

$[1\bar{1}0]$ →

50 μm

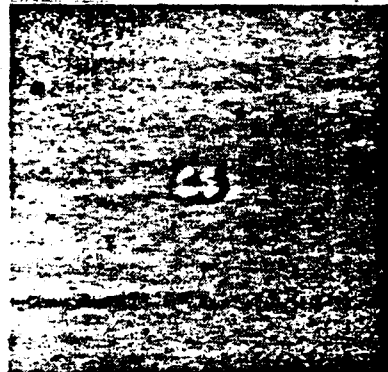


α_2



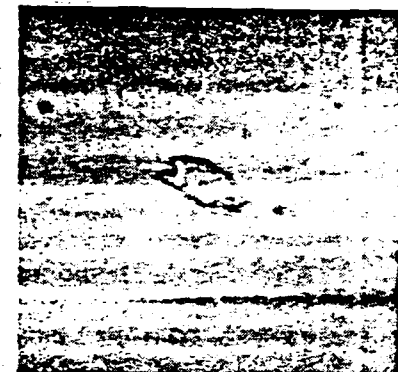
#1042

β



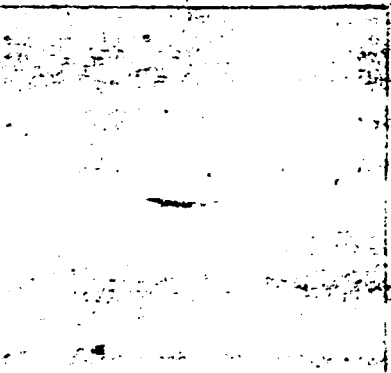
#1042

γ

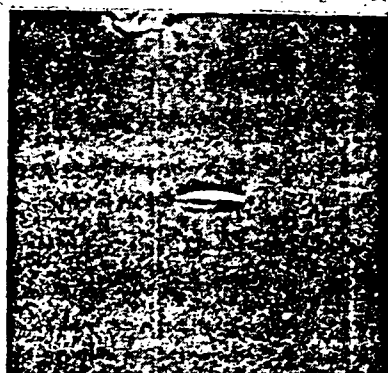


#1042

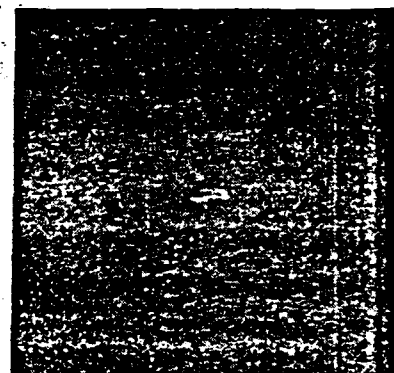
α_3



#1041



#1041



#1051

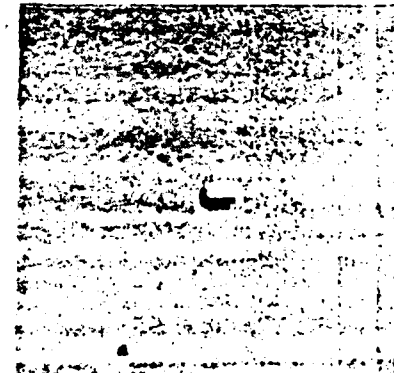
α_4



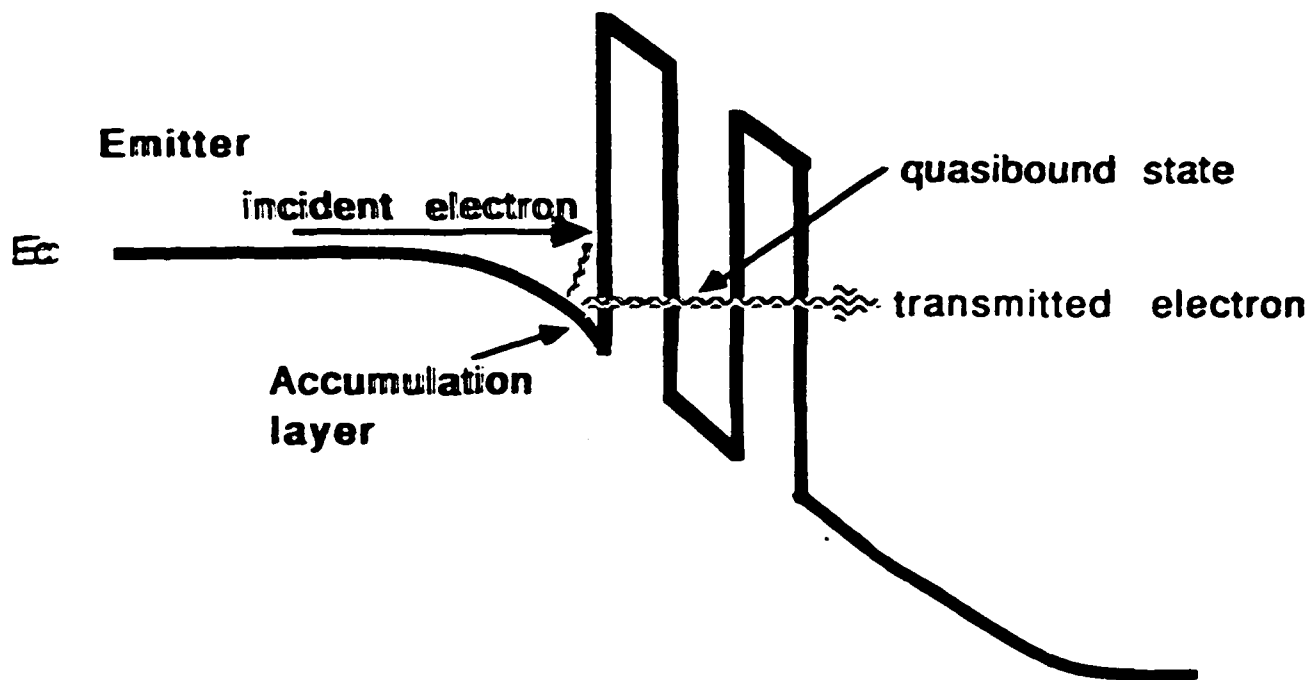
#1041



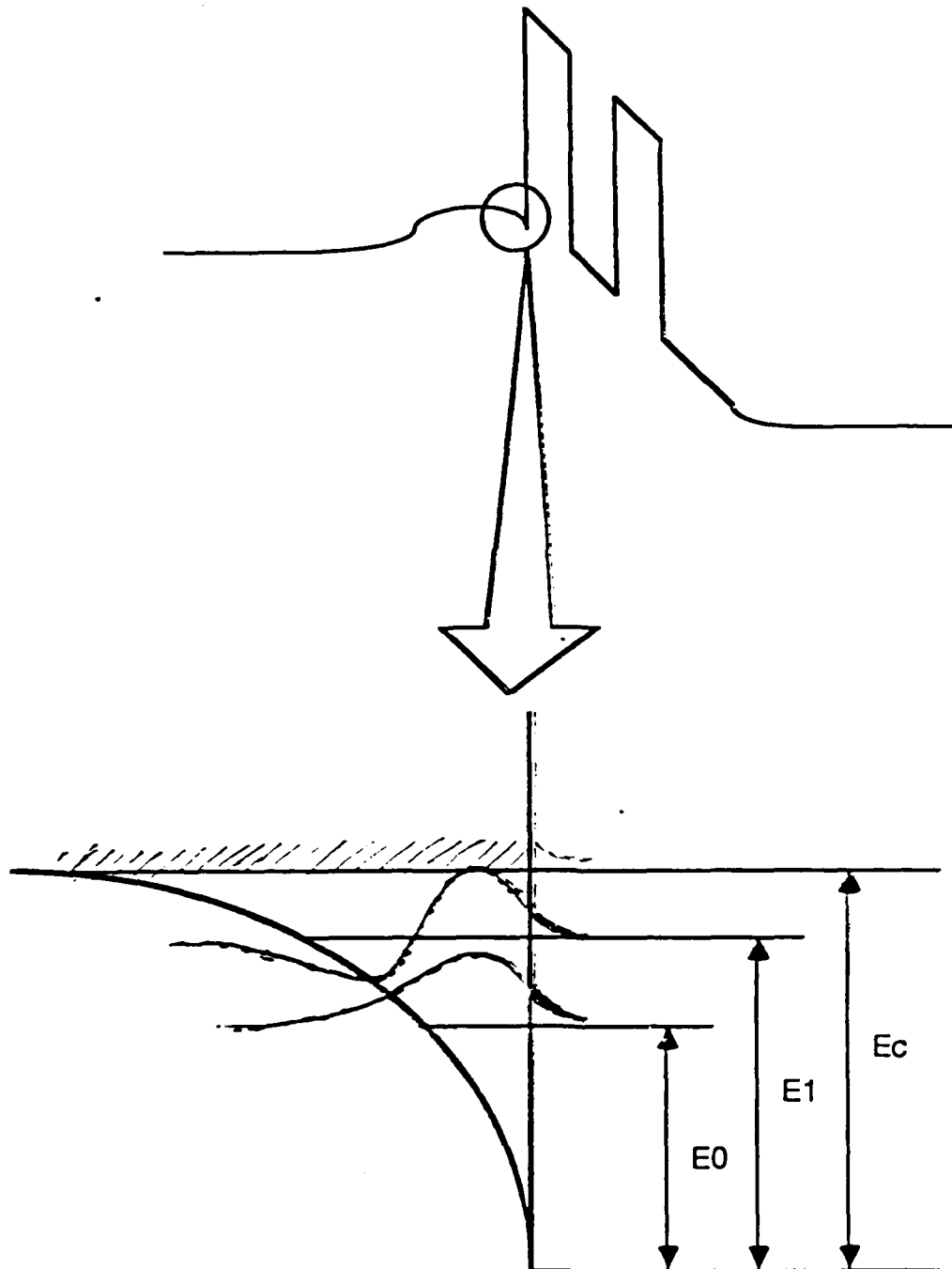
#1041



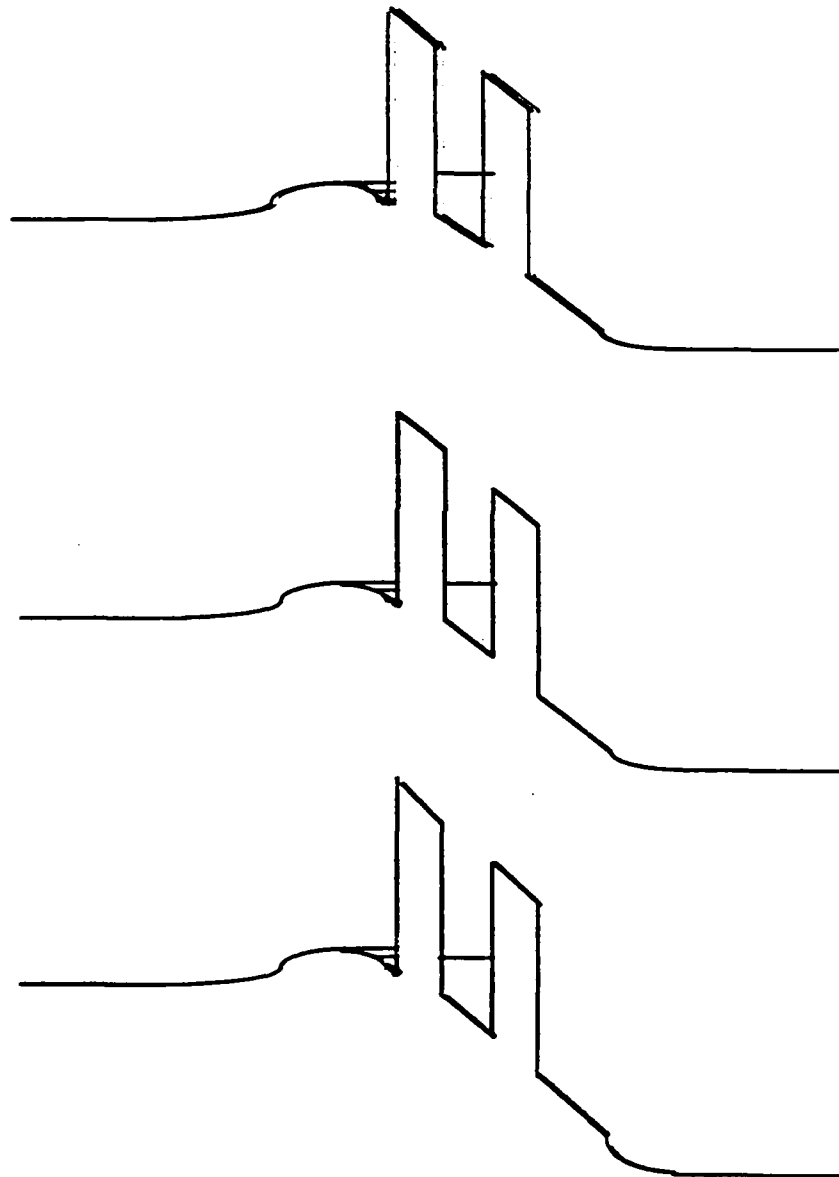
#1051

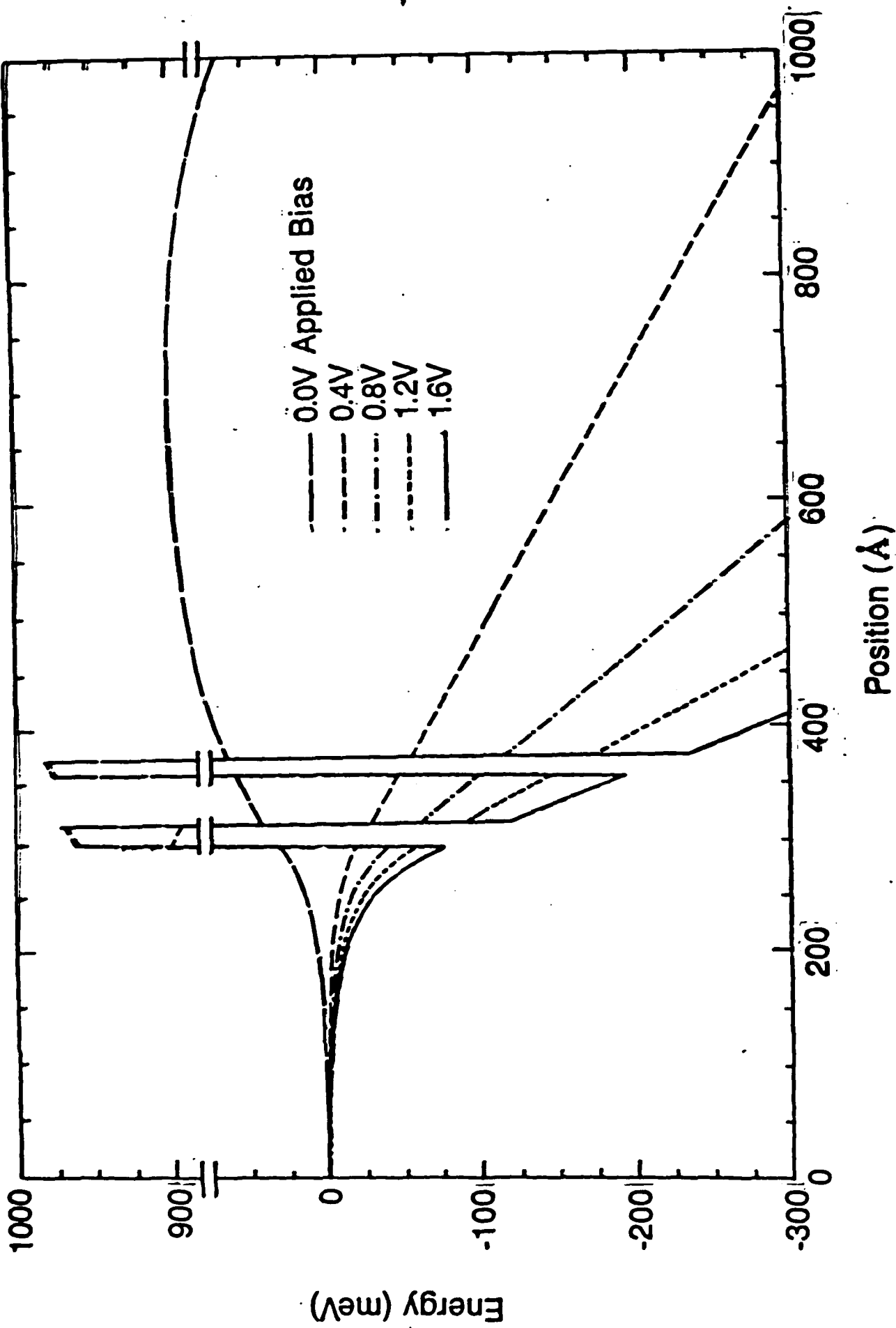


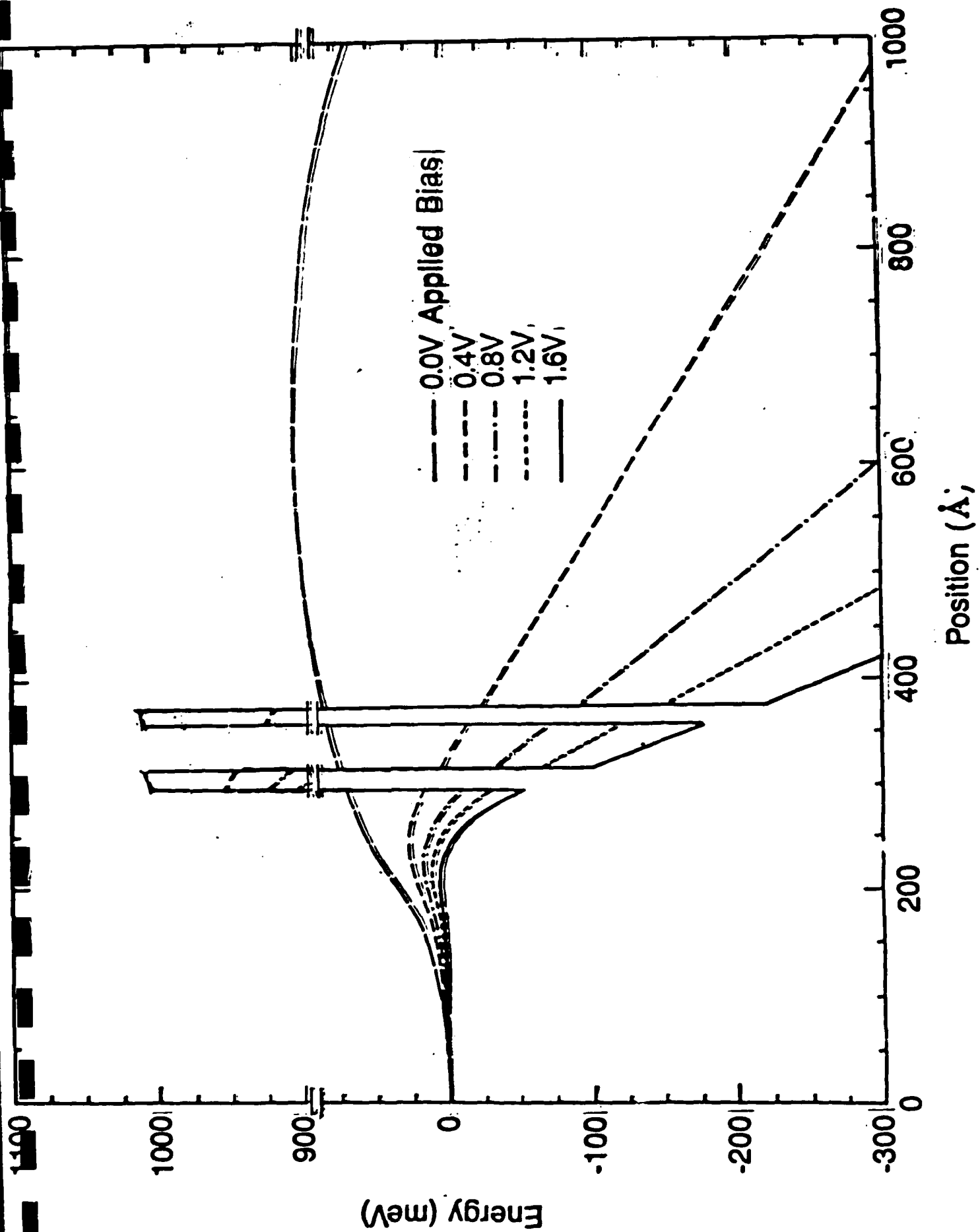
Quasi-Bound States in the Accumulation Layer



Finding the Bias Voltage for the Peak Current







RESONANT TUNNELING DIODE DESIGN TRADEOFFS

High Current Density

- Transparent Barriers

- High Contact Doping

- Large difference in electron occupation at resonance.

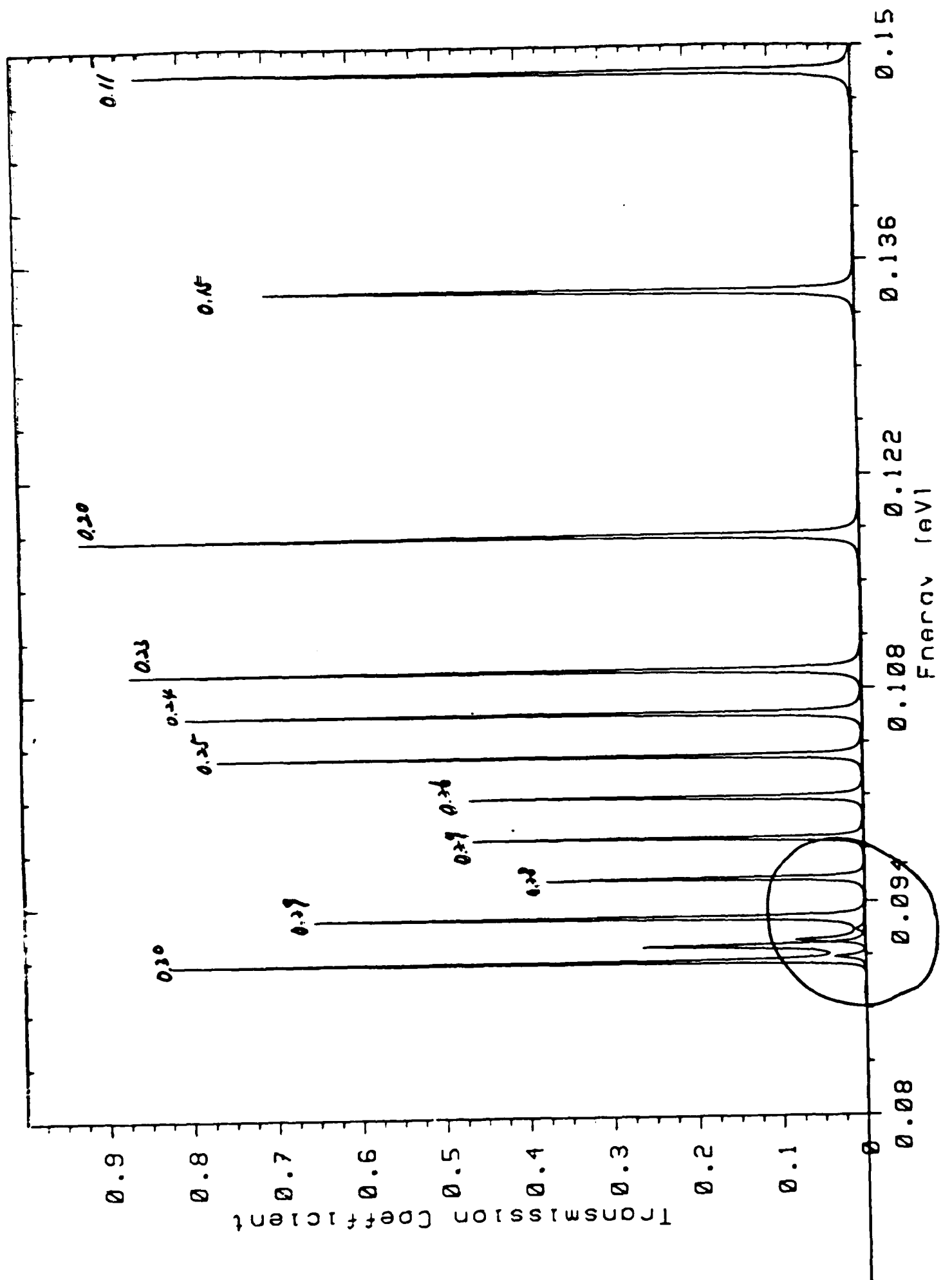
**High Peak to Valley
Ratio**

- Less transparent barriers

- Lower contact doping.

- Undoped spacer layers.

- Good interfaces and crystal quality.



Structure 1
with positive voltage
on ohmic

peak current during
 $\sim 15 \text{ mV} (\Delta V)$

6 —
5 —
4 —
3 —
2 —
1 —

dI/dV

dI/dV

I [mA]

30

25

10

5.246

5

0.1

0.2

0.3

0.4

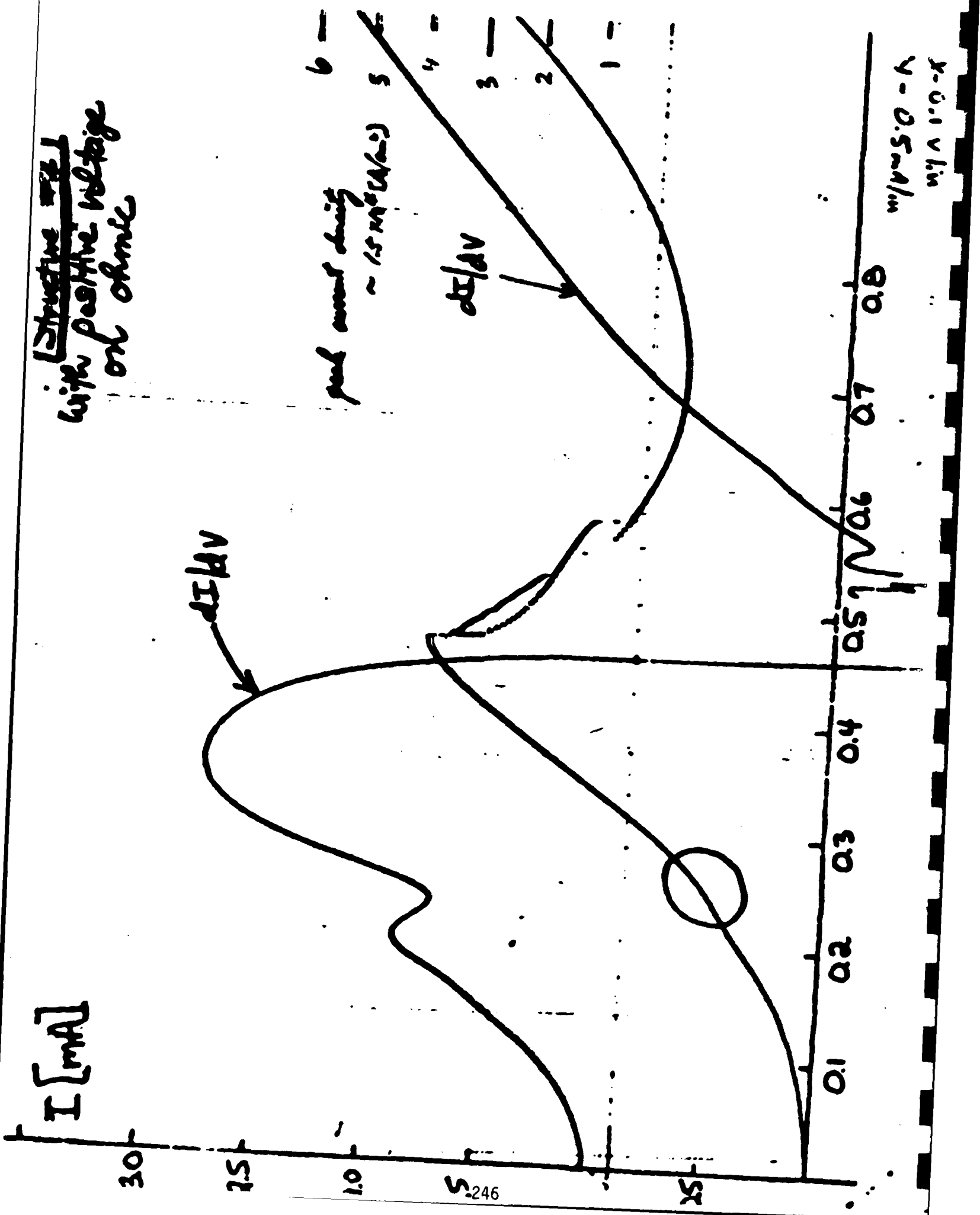
0.5

0.6

0.7

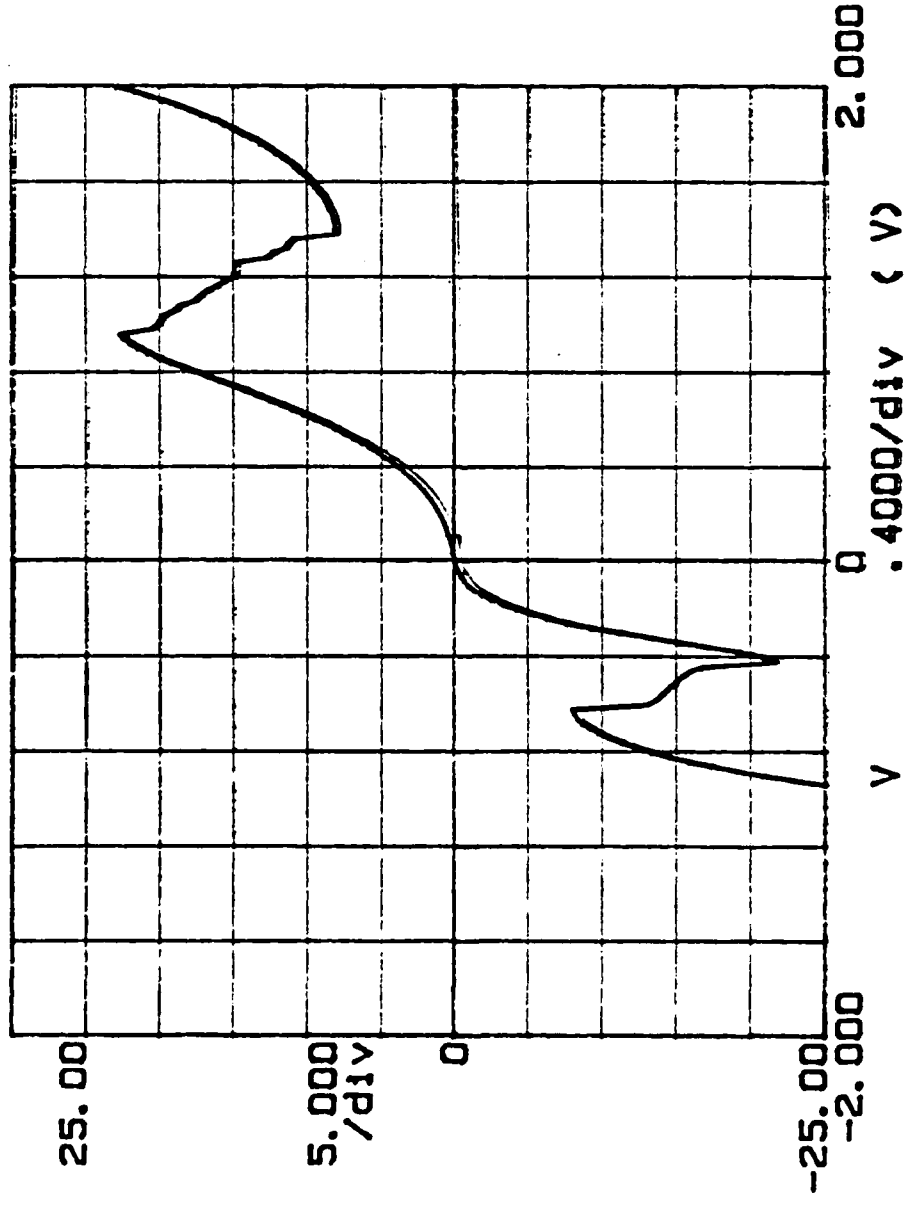
0.8

$v = 0.1 \text{ V/min}$
 $v = 0.5 \text{ mV/min}$



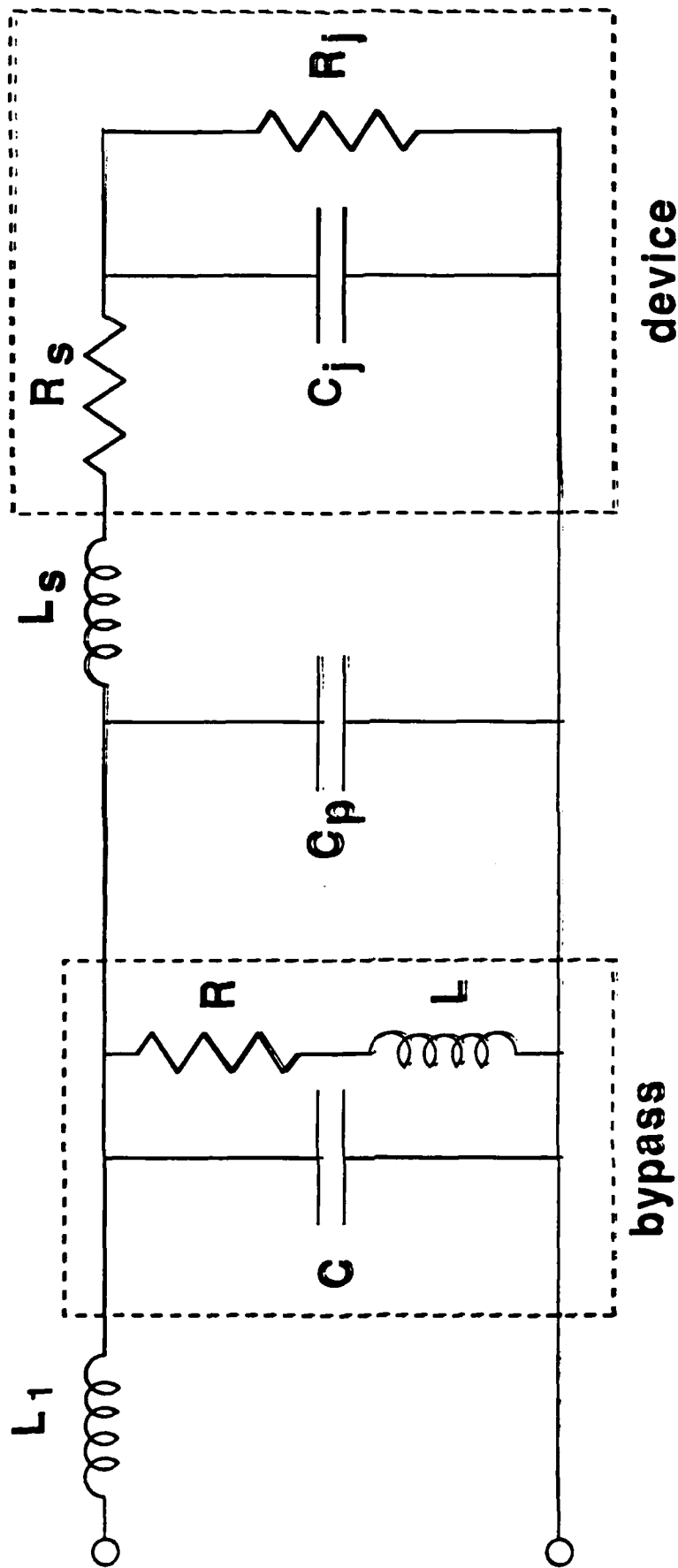
***** GRAPHICS PLOT *****
 1071A-E3(P) 14um DIA 300K

I (mA)

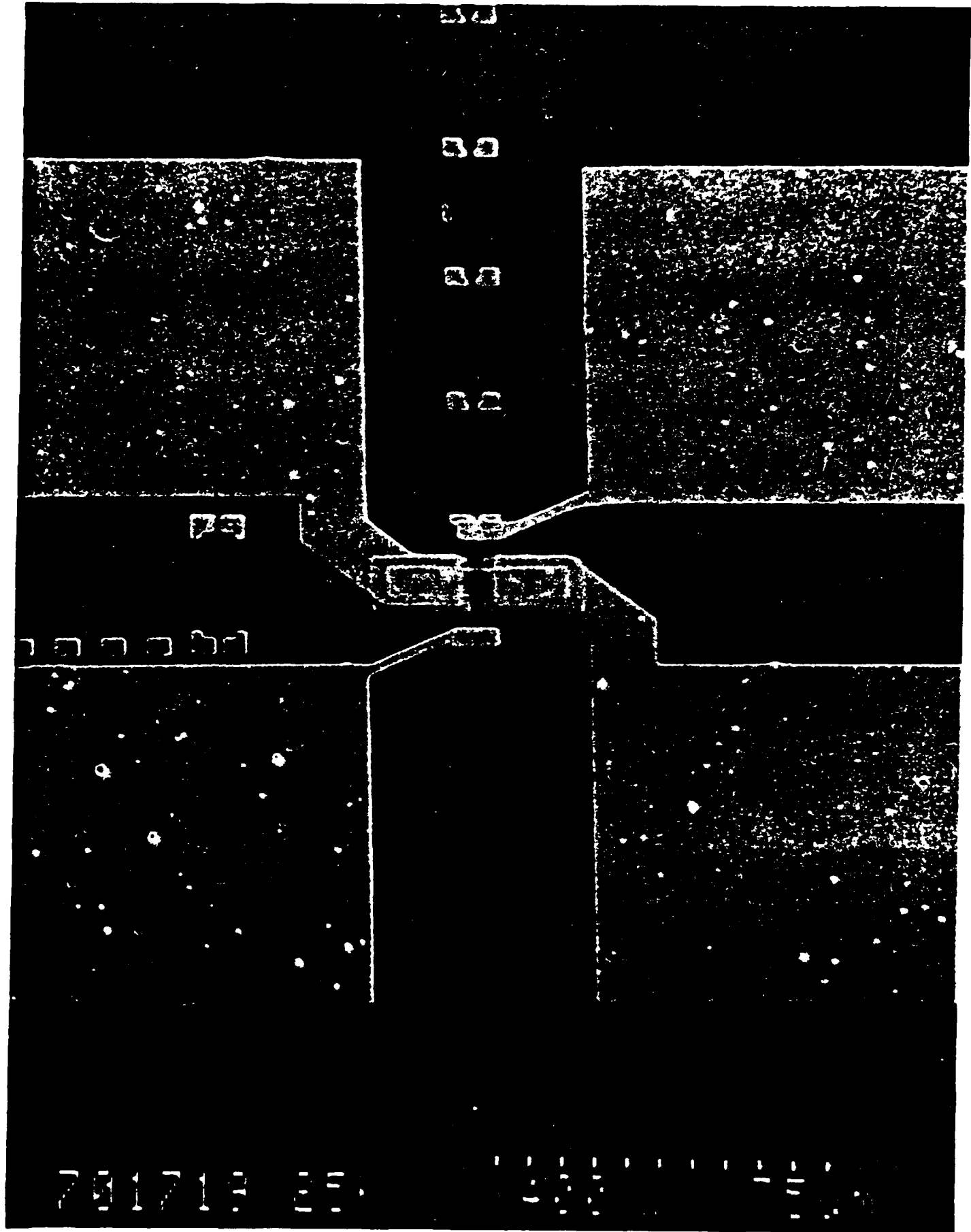


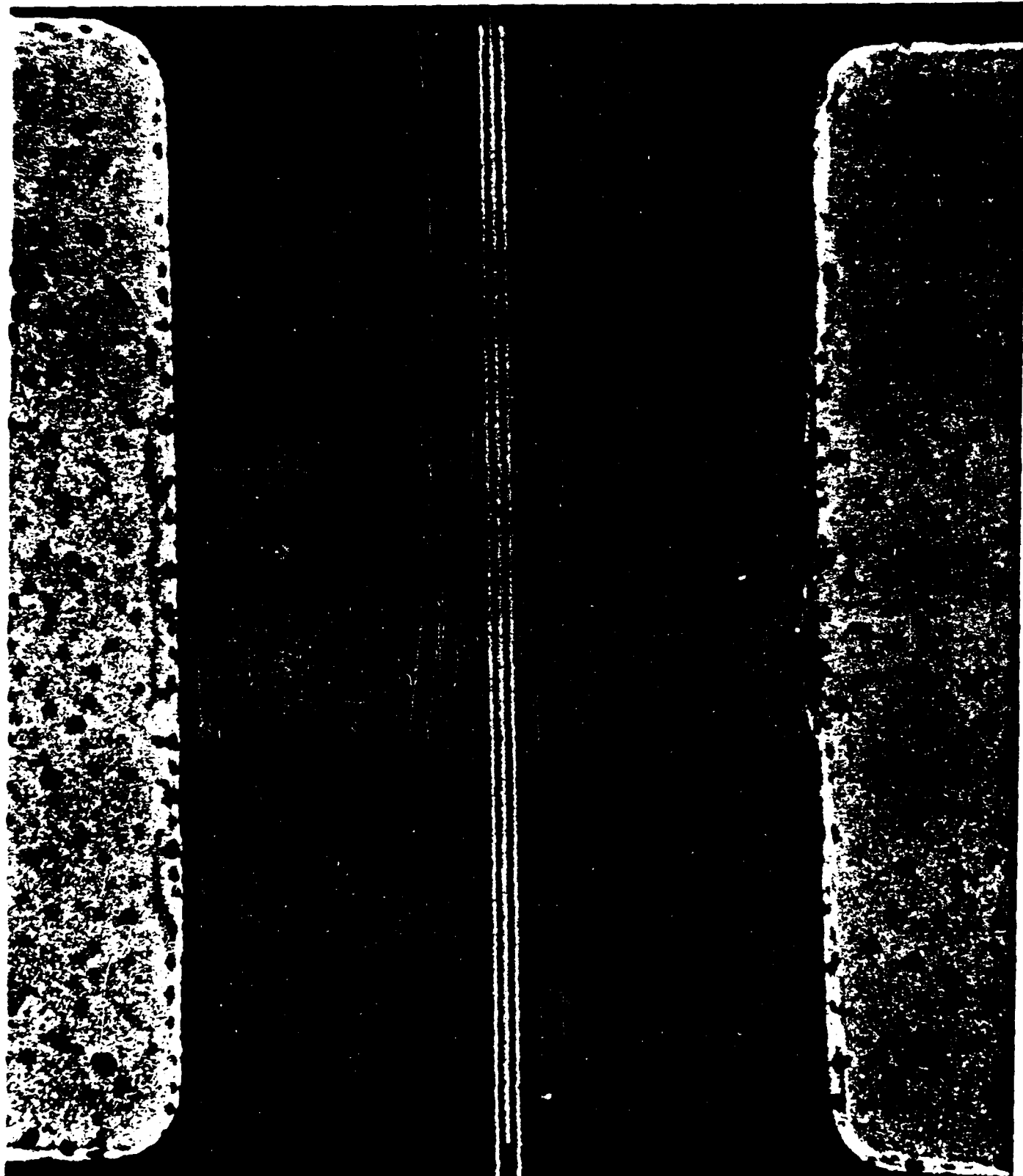
S (S) = $\Delta I / \Delta V$
 R (R) = V / I

Equivalent Circuit for RTD and test fixture

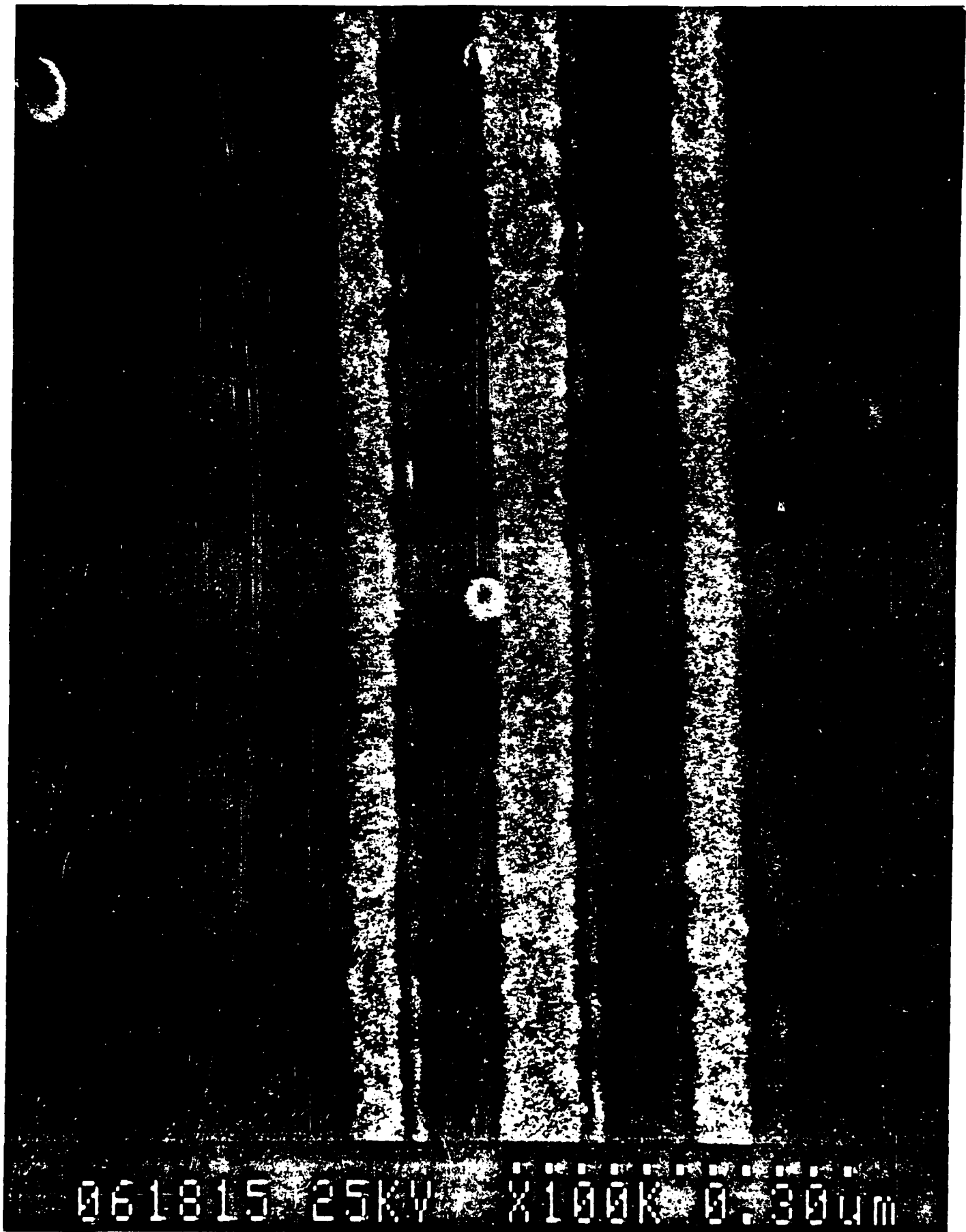


$L_1 = .65\text{nH}$, $L = .6\text{nH}$, $C = .2\text{pF}$, $R = 10\Omega$, $C_p = .28\text{pF}$, $L_s = .5\text{nH}$, $R_s = 10\Omega$,
 $C_j = .68\text{pF}$, $R_j = 200\Omega$ ($V = 0\text{V}$.) or $C_j = .75\text{pF}$, $R_j = 140\Omega$ ($V = 1\text{V}$.)



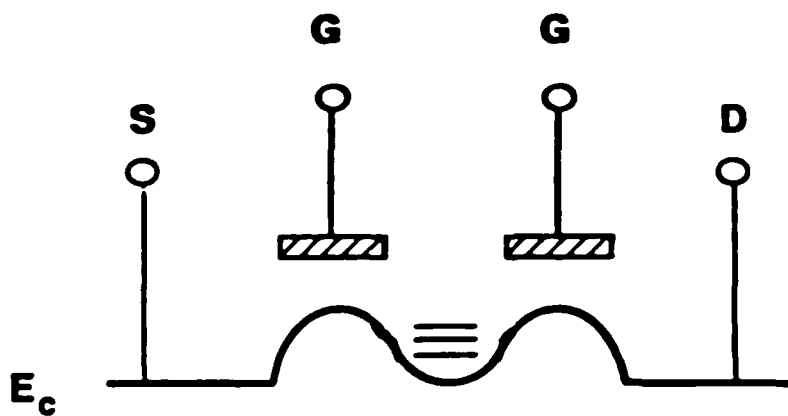
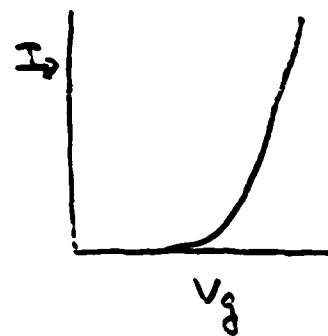
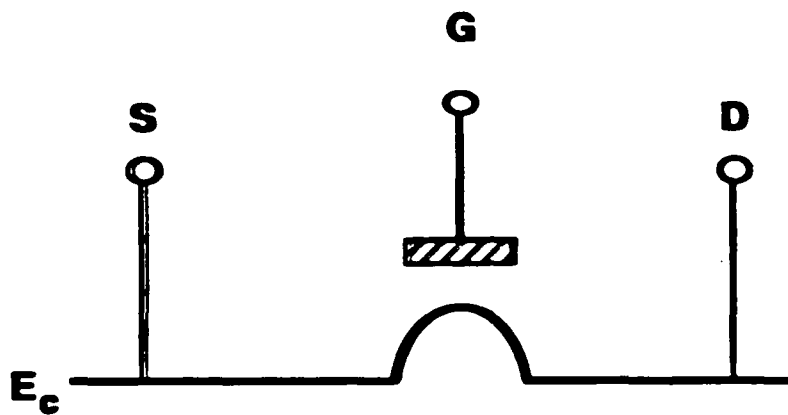


061820 25KV X6.00K 5.0um

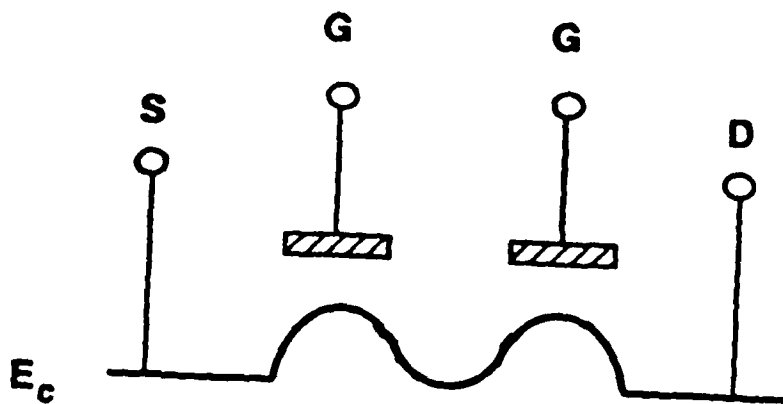
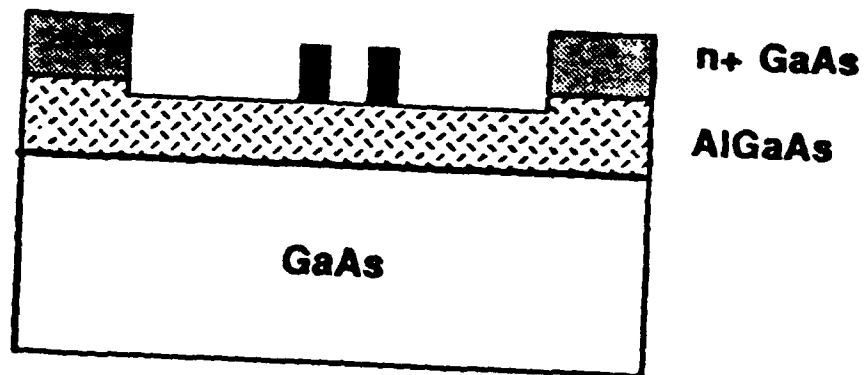


Operation Mode 1:

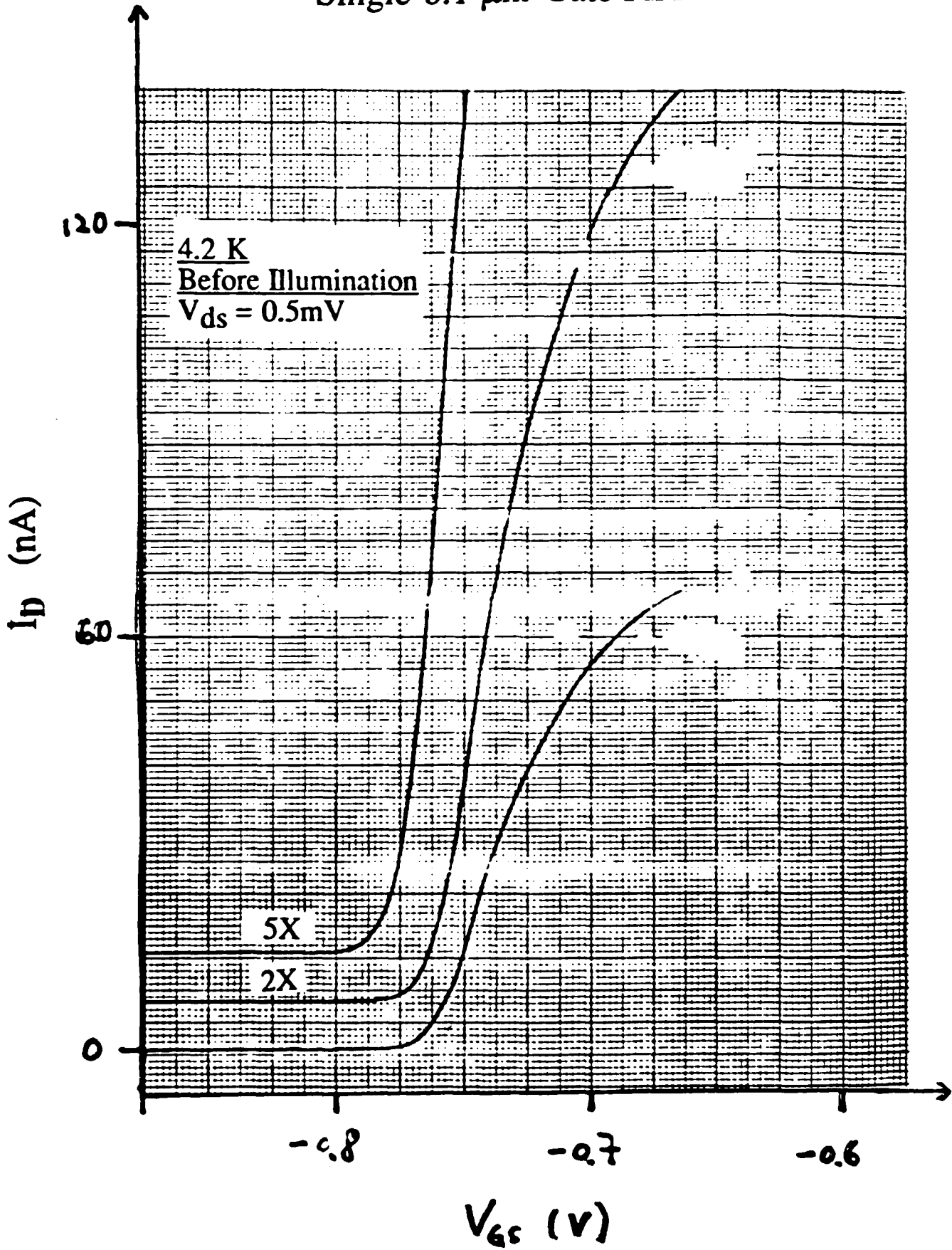
Fix V_{ds} , Vary V_g .



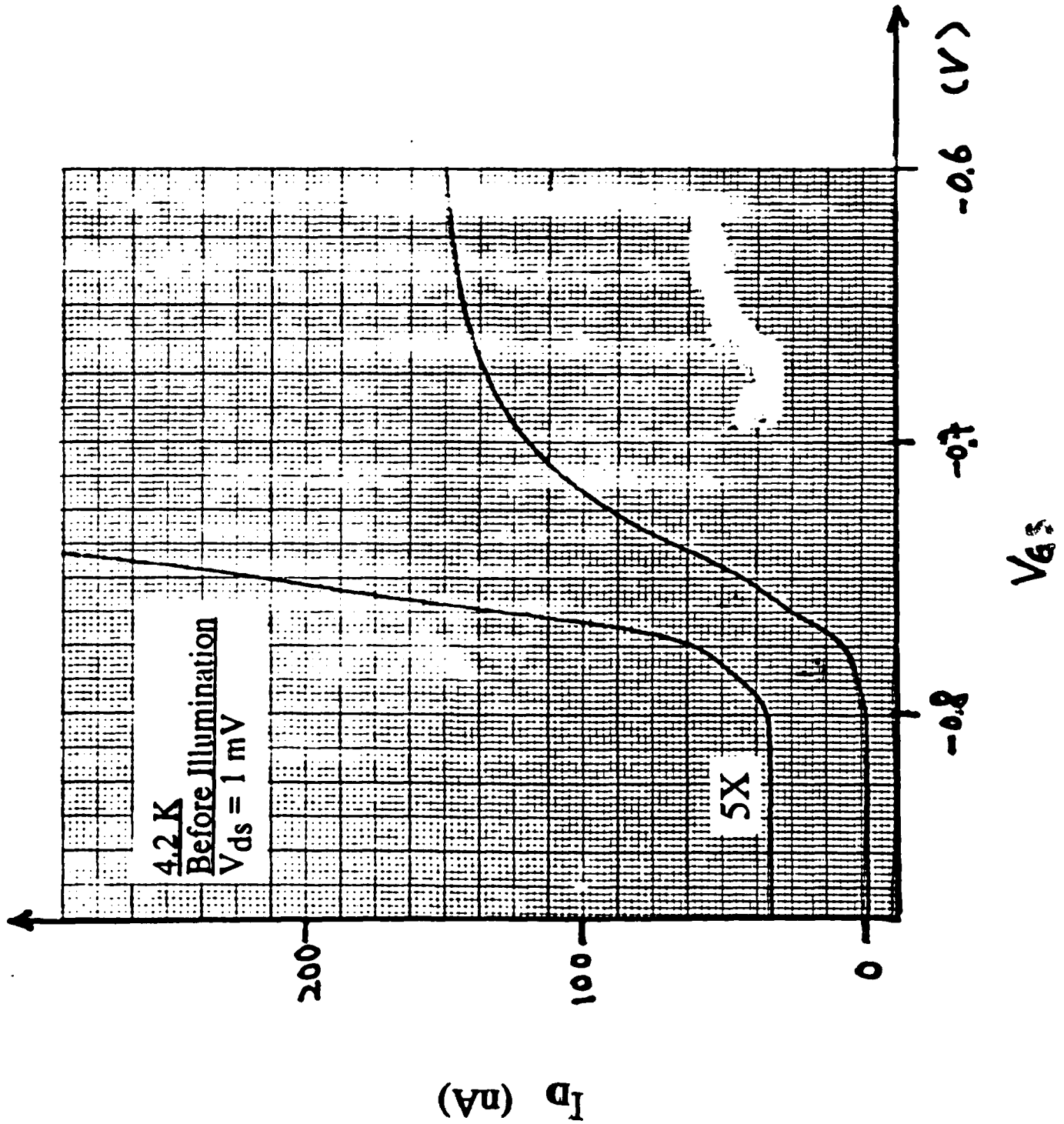
Dual-Gate LRTFET



Single-0.1 μm -Gate FET D2A1

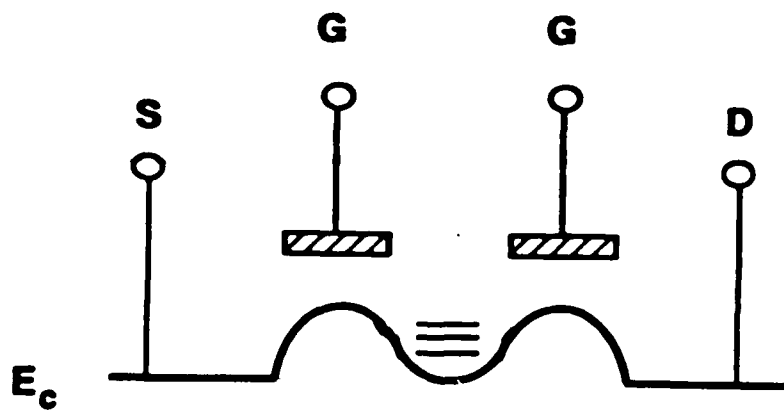
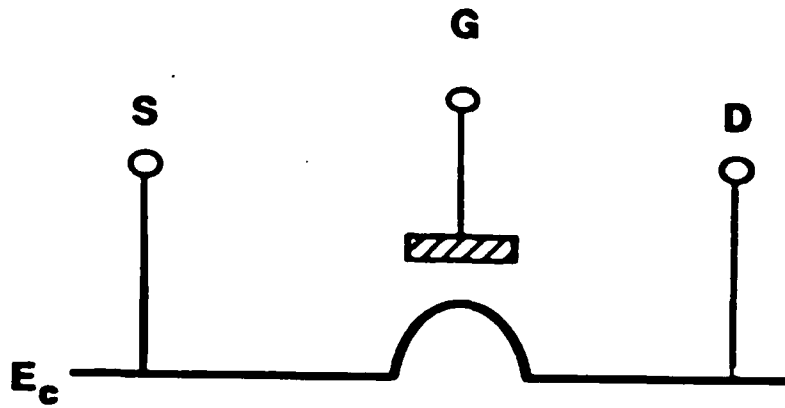


Dual-0.1 μm -Gates FET (Gate Spacing 0.1 μm) D2A2



Operation Mode 2:

Fix V_g , Vary V_{ds} .



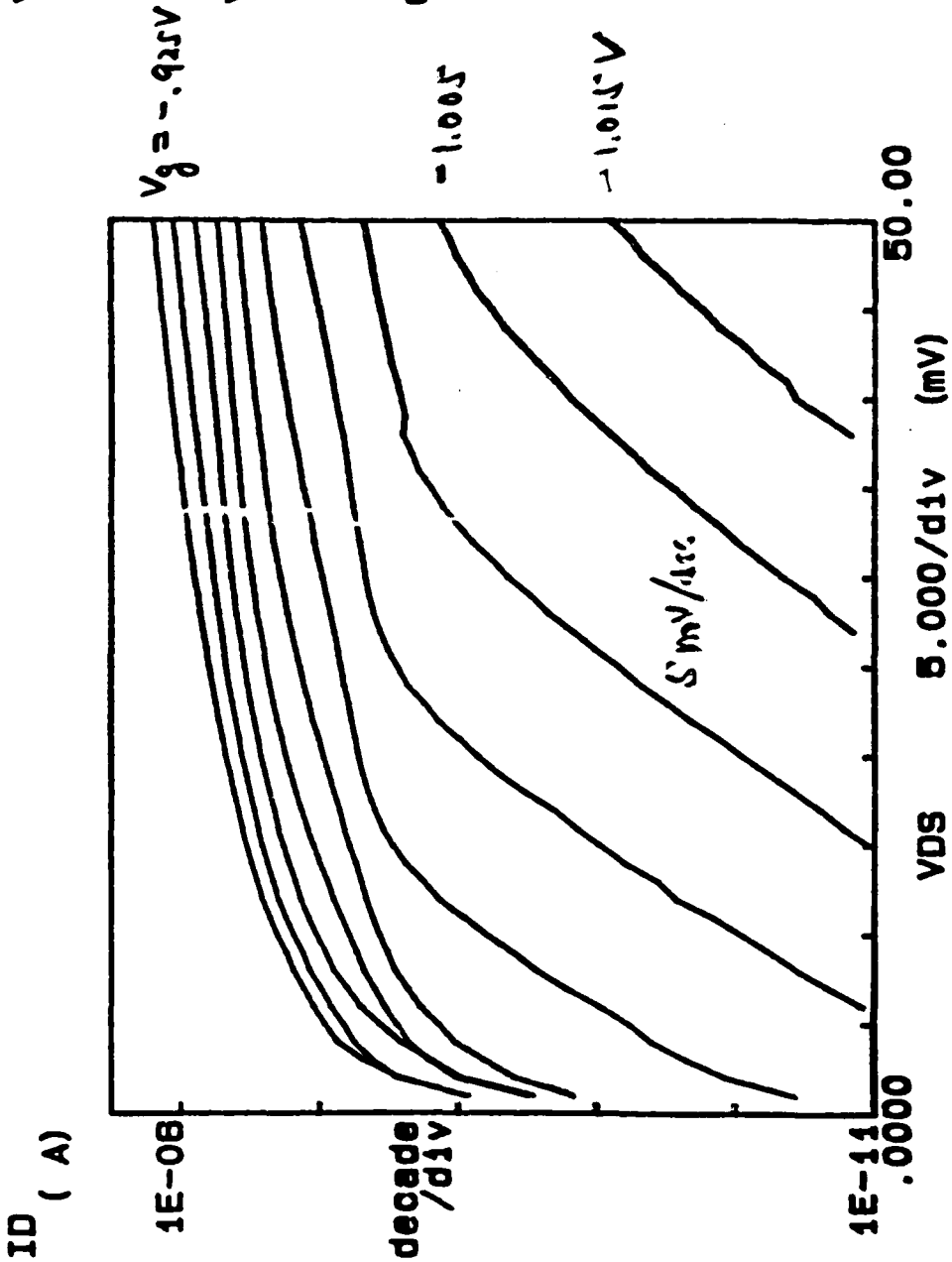
Single 0.1 μ m gate F&T.

***** GRAPHICS PLOT *****
 N7NAN2

Variable1:
 VD8 -Ch1
 Linear sweep
 Start .0000V
 Stop .0500V
 Step .0010V

Variable2:
 VS -Ch2
 Start -.8250V
 Stop -1.0150V
 Step -.0100V

Constants:
 VS -Ch3 .0000V



Dual 0.1 μm -gate LRTFET

+

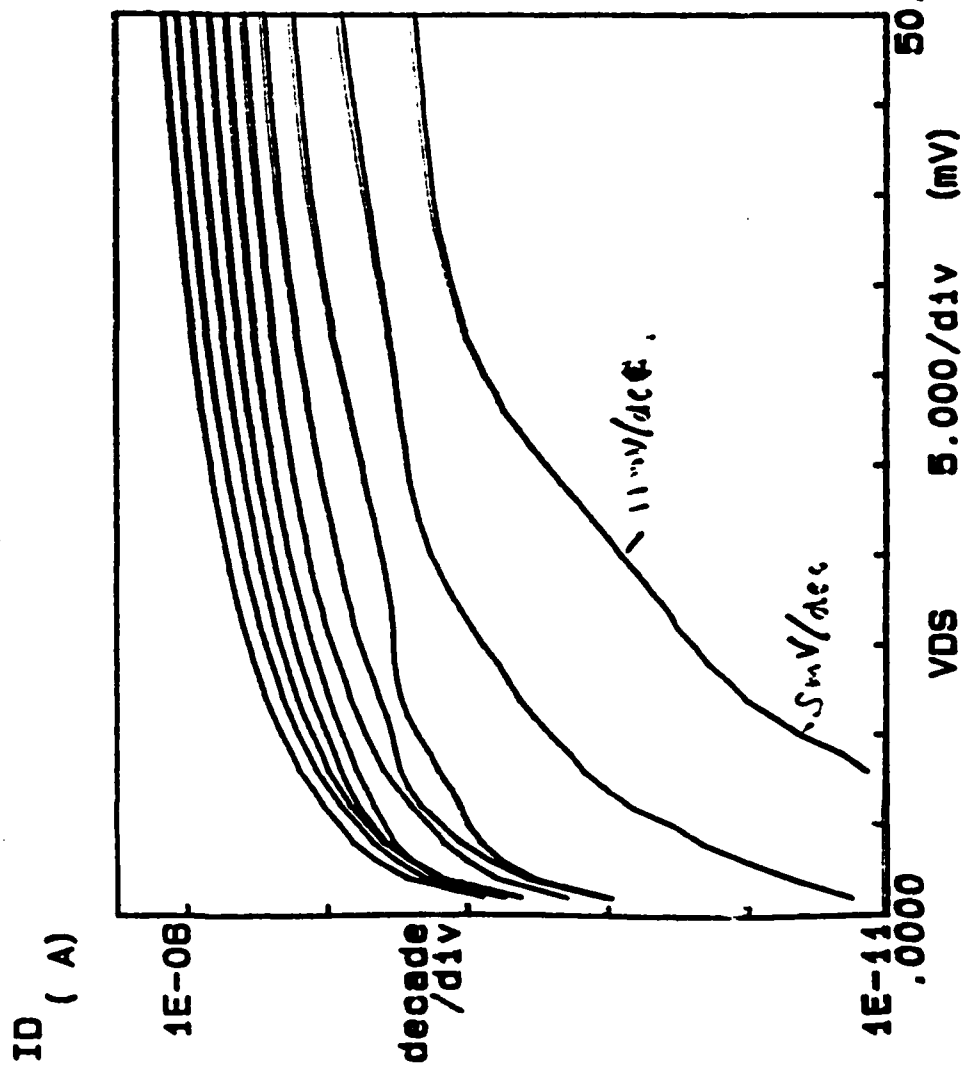
***** GRAPHICS PLOT *****
N7DUA2

Variables:
VDS -Ch1
Linear sweep
Start .0000V
Stop .0500V
Step .0010V

$V_g = -1.925V$

Variables:
Vg -Ch2
Start -.8250V
Stop -1.0150V
Step -.0100V

Constants:
Vg -Ch3 .0000V



+

ID (A)

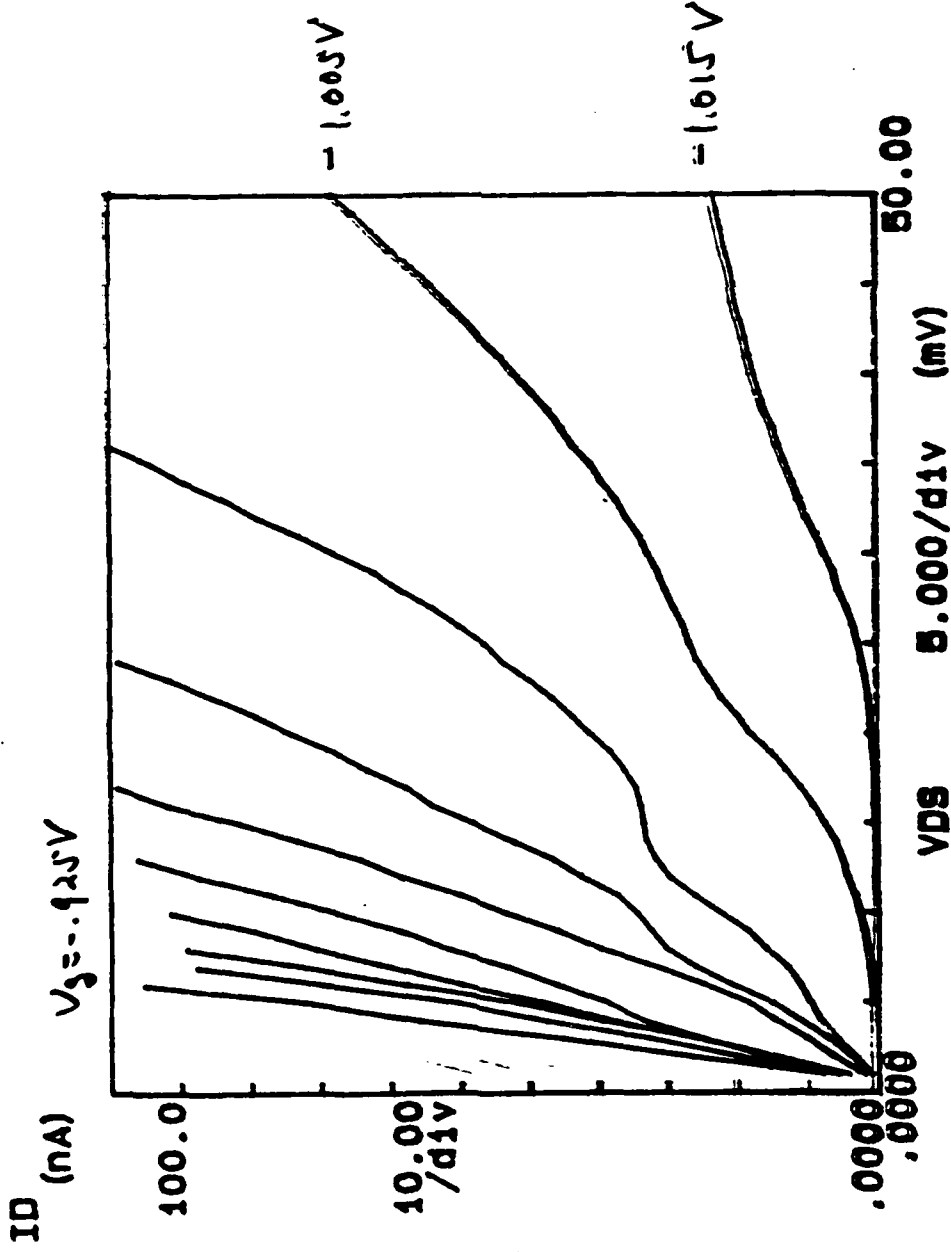
Dual 0.1mm-gate LRTFET.

***** GRAPHICS PLOT *****
N70UA2

Variable1:
VDS -Ch1
Linear sweep
Start .0000V
Stop .0000V
Step .0010V

Variable2:
Vg -Ch2
Start -.9250V
Stop -1.0150V
Step -.0100V

Constant1:
Vg -Ch3
Start .0000V



Array Applications

Phillip M. Smith

*General Electronics
Syracuse, NY*

ARRAY APPLICATIONS

Phillip Smith
GE Electronics Laboratory
Syracuse, NY



Collaborators: P.C. Chao, J.M. Ballingall, K.H. Duh, L.F. Lester, P. Ho,
B. Lee, R.P. Smith, D.W. Ferguson, A.A. Jabra, W. Kopp,
A. Tessmer, M. Kao, D.A. Bates

■ Phased Arrays

- MMW Applications
- GE V-Band Array Development

■ Device Technology for MMW Phased Arrays

- InGaAs Pseudomorphic Power HEMT
- Low Noise HEMT
- 0.1 μ m Pseudomorphic HEMT
- InP-Based HEMT

Millimeter-Wave Applications

GE Aerospace

(From R. Sudbury)

FREQUENCY	APPLICATION
20 GHz	Communications
30 GHz	* Communications
32 GHz	* Deep Space Communications
35 GHz	Seekers Guidance Communications
44 GHz	* Communications
60 GHz	* Inter Satellite Communication Short Range Covert Communication * Space Based Radar
94 GHz	Fuze Projectiles Radar Smart Munitions

* Contracts using GE HEMTs

Why Solid State Phased Array?

GE Aerospace

- Agile Beam
- Efficient Power Combining in Space
- Solid-State Reliability
- Graceful Degradation

ISSUES FOR MMW PHASED ARRAYS	SOLUTION
Cost of Large Number of Elements	MMICs
Generation of Sufficient Power Per Element	Pseudomorphic HEMTs
Power Consumption/Thermal Loading	High Efficiency

60 GHz Communication Arrays

GE Aerospace

Satellite Crosslink Application

Principal Advantages

- Small Size Circuitry
- Light Weight
- Resistance to Ground Based Jamming
- High Agility/Reconfigurable

Module Technology Status

- Pseudomorphic HEMT (High Power, Low Noise, and Phase Shifter)
 - 7 dB Gain, 1.8 dB NF
 - 100 mW Power, 22% Efficiency
 - (DSCS HESSA Amp is Approximately 25%)
 - AFWAL 60 GHz LNA Contract Shutting Down
 - 60 GHz LNA Being Process on AFWAL LNA Contracts (AFWAL Shutting Down)

Resulting Hardware Capability

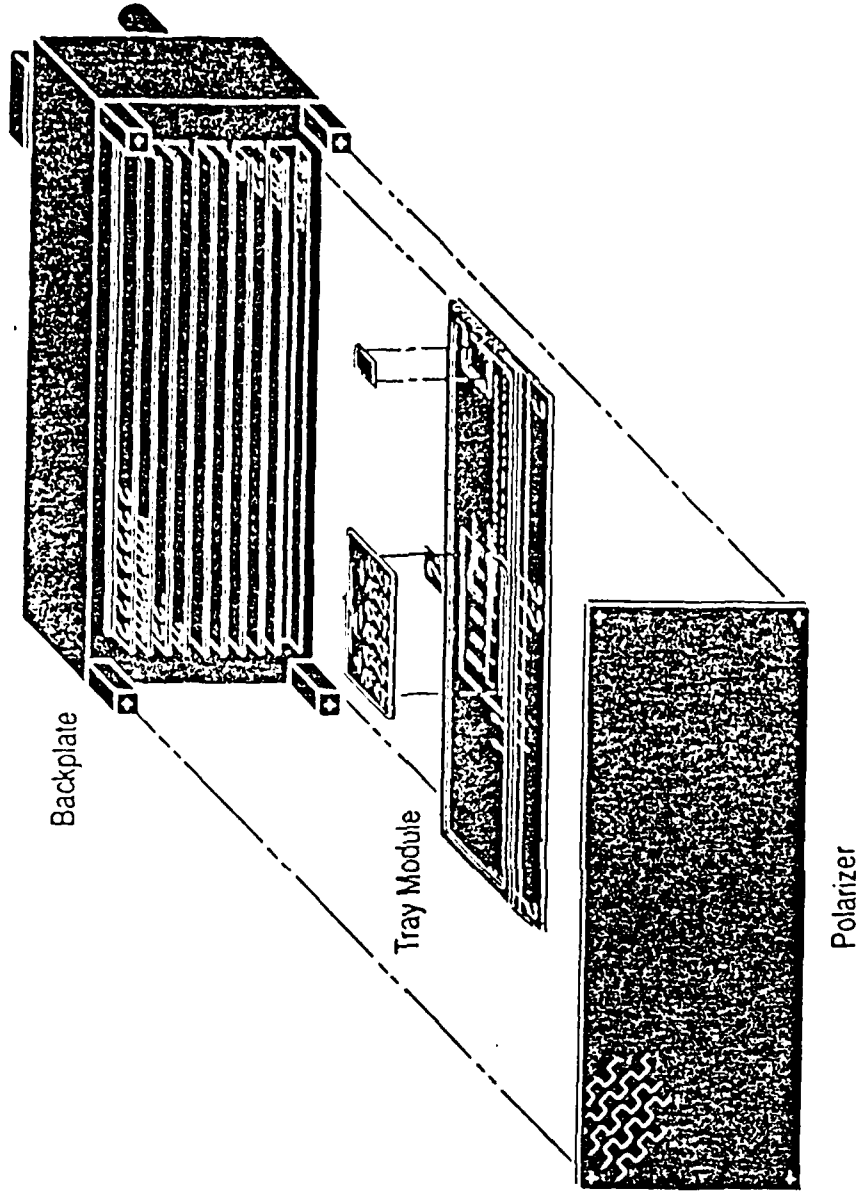
- Tx Array - EIRP 50 dBW, Approximately 4" x 4", 3 lbs (100 WRF)
- Rx Array - Gain 30dB, 4dB NF, 4" x 4", 3 lbs (5 dB/Degree K)

Communication Array Technology

GE Aerospace Laboratories

Key Technologies

- Array Construct
- HEMT MMICs
- Low Cost Tray Module
- Backplate Construction
- Circular Polarizer



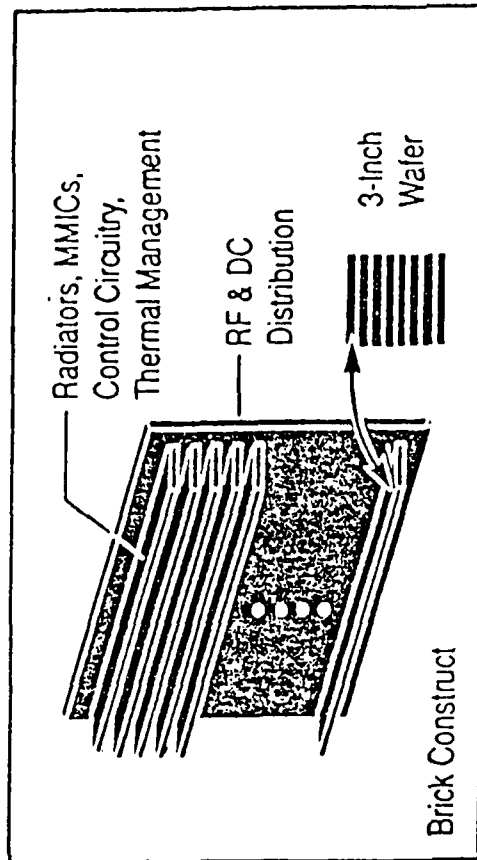
V-Band Phased Array Antenna Technology

GE Aerospace Laboratories

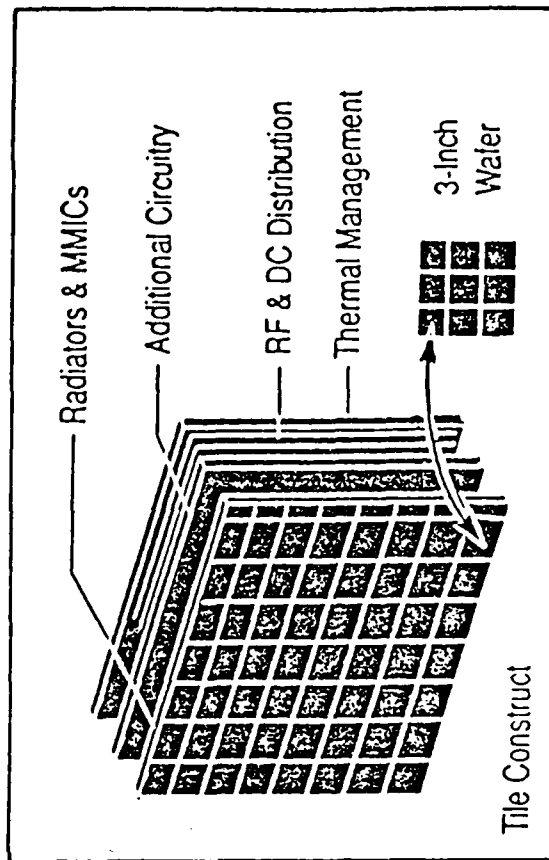
Brick Construct Advantages

- Modular Design With Tray Module.
- Depth Dimension Relaxes Size Restriction on MMICs Imposed by Element Pitch.
- Replaceable Tray Modules for Repairability/Maintainability.
- Array Design Not Constrained by MMIC Processing Yield.
- Accommodates Interleaved Thermal Cooling Channel and Tray Modules.
- Allows Hermetic Sealing and Shielding of Critical Circuitry.
- Applies to Both Transmit and Receive Arrays.

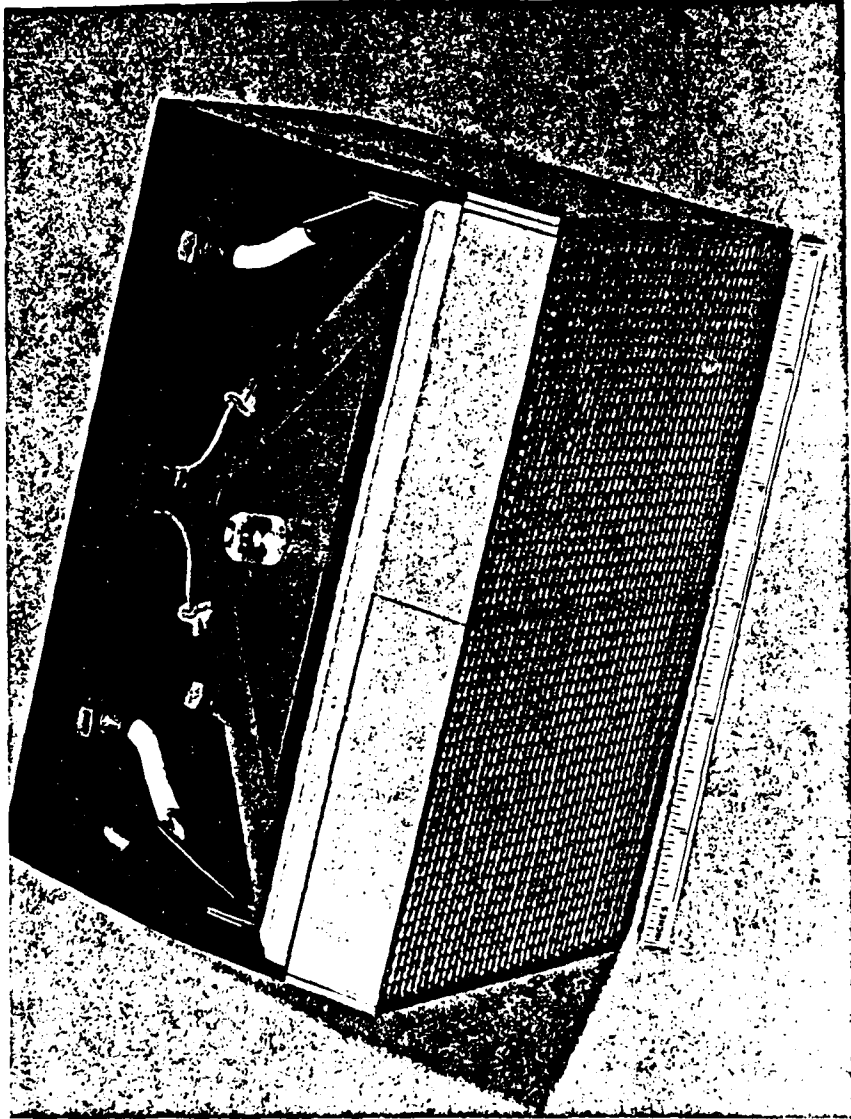
GE Approach



"Conventional" Approach

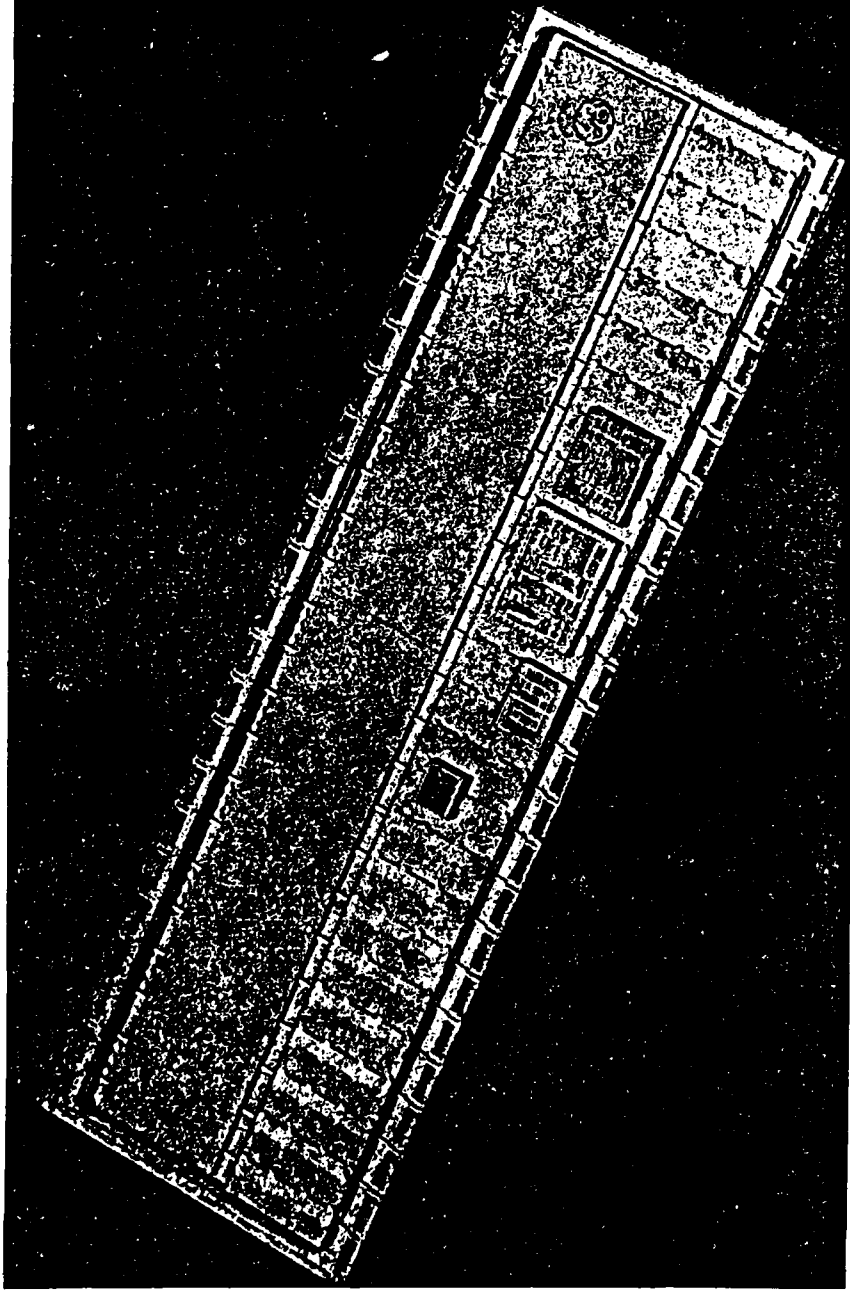


Model of 60 GHz Phased Array



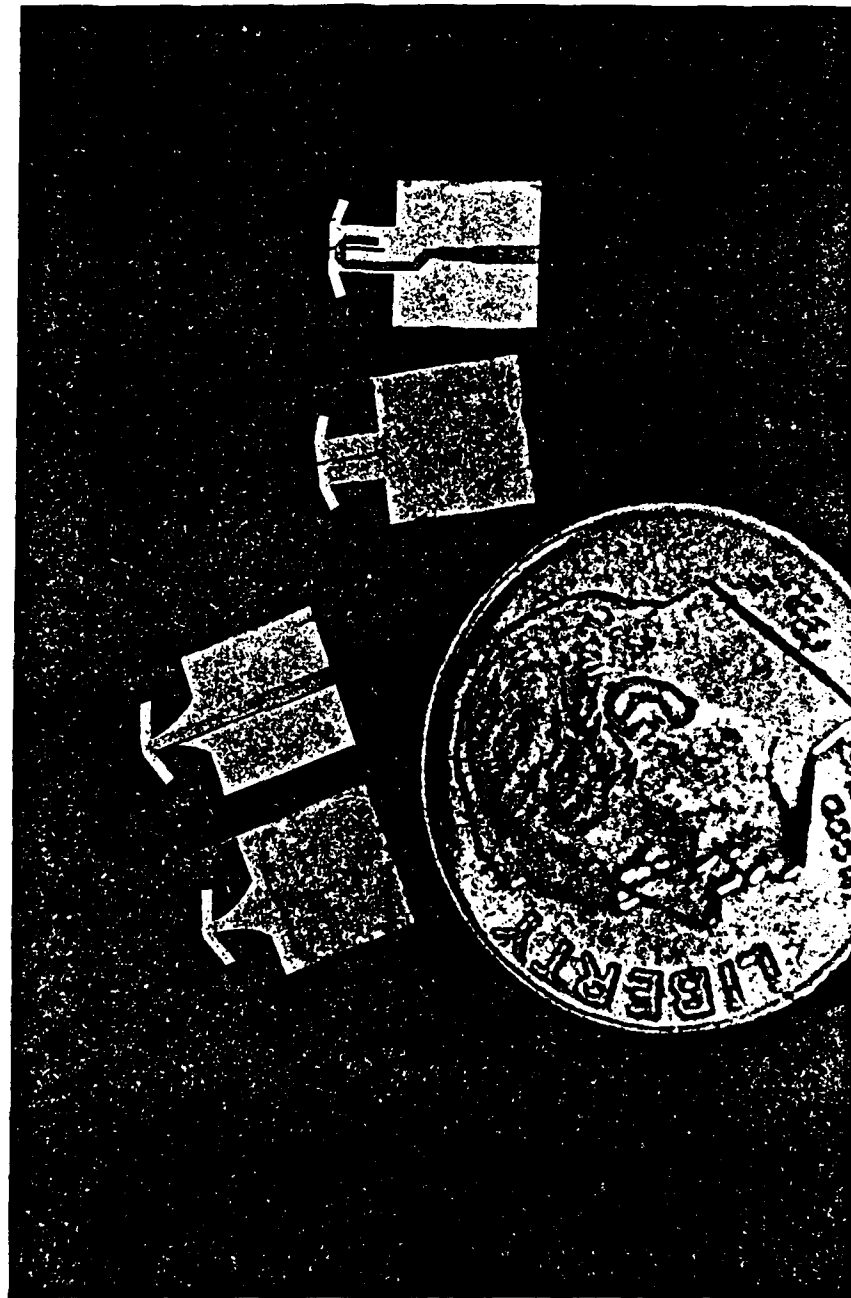
24 Element Tray Assembly - 60 GHz Phased Array

GE Aerospace



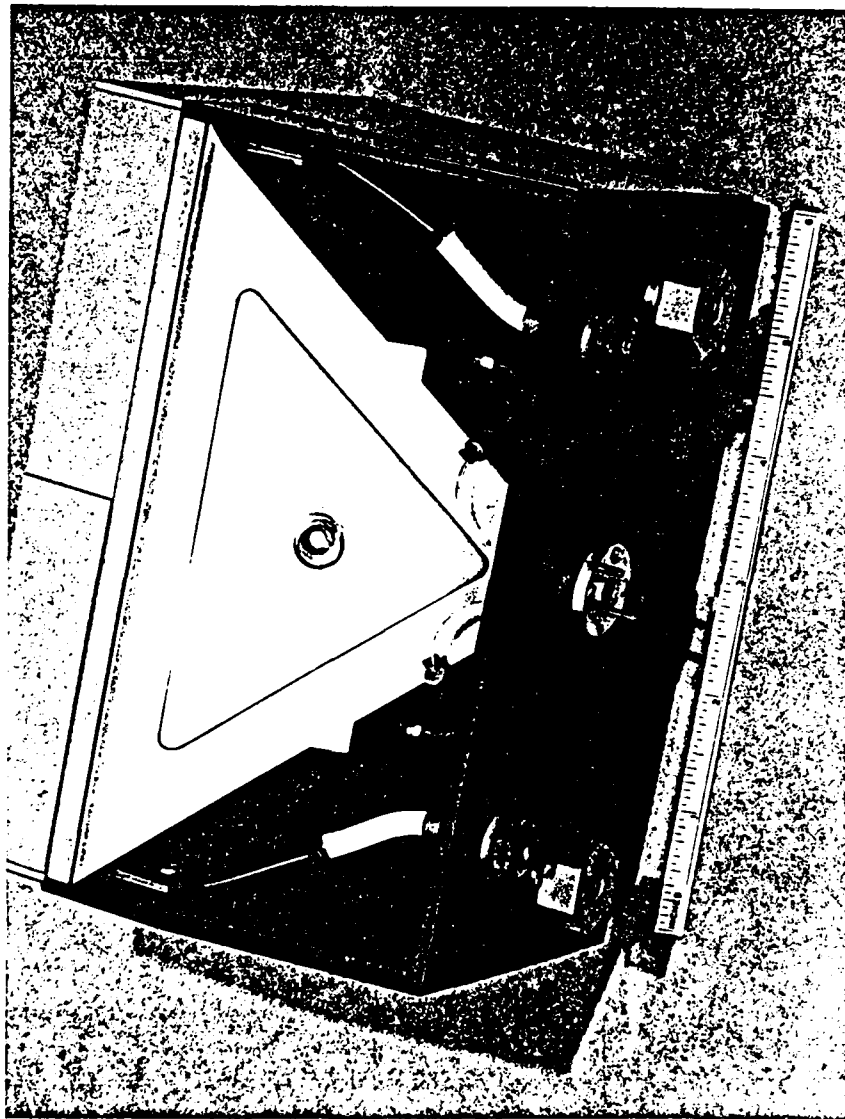
60 GHz Dipole Radiating Elements

GE Aerospace



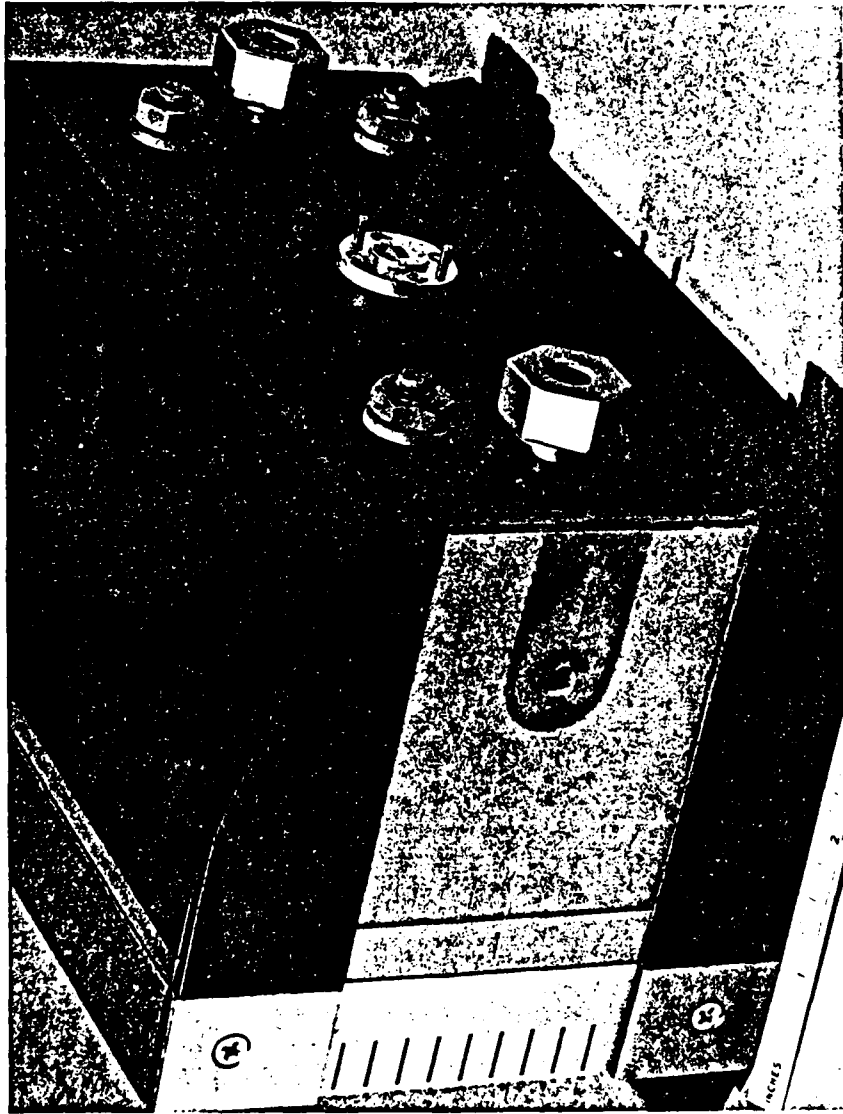
60 GHz Phased Array - Rear View

GE Aerospace



60 GHz Phased Array - Side View

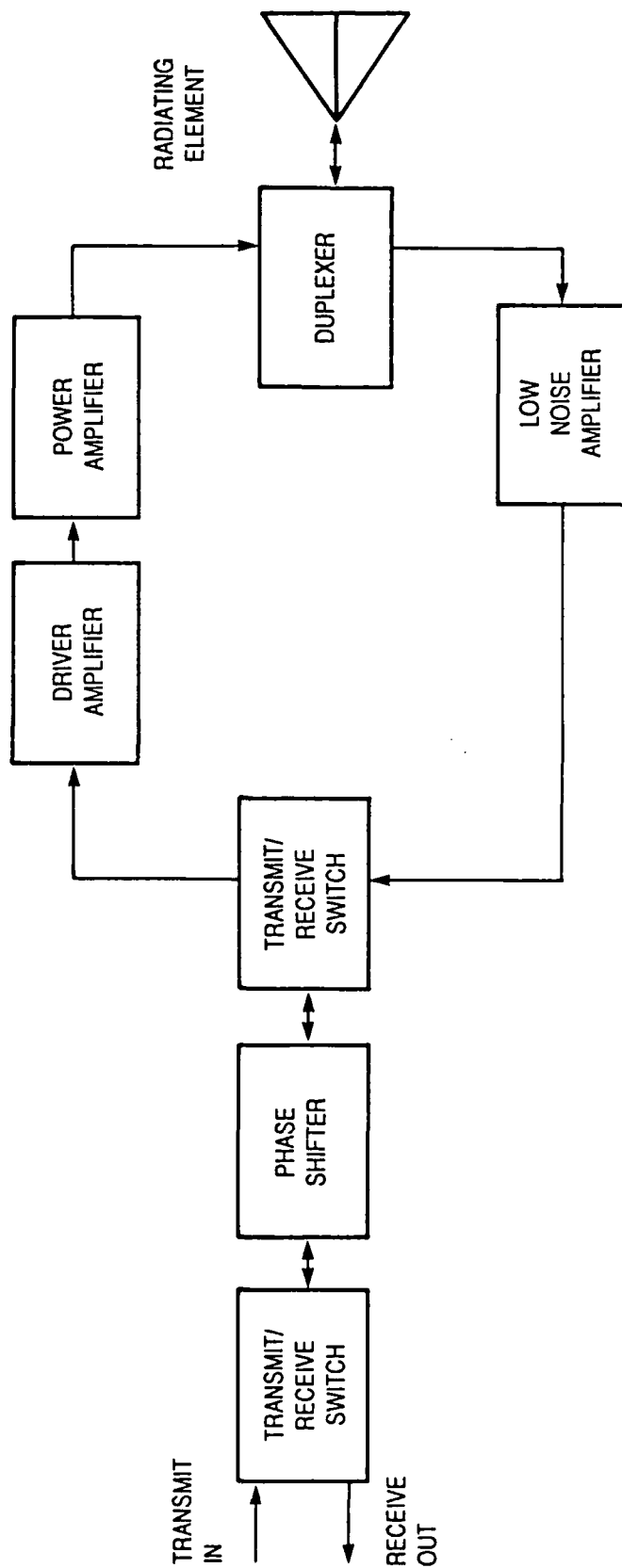
GE Aerospace



Transmit/Receive Module

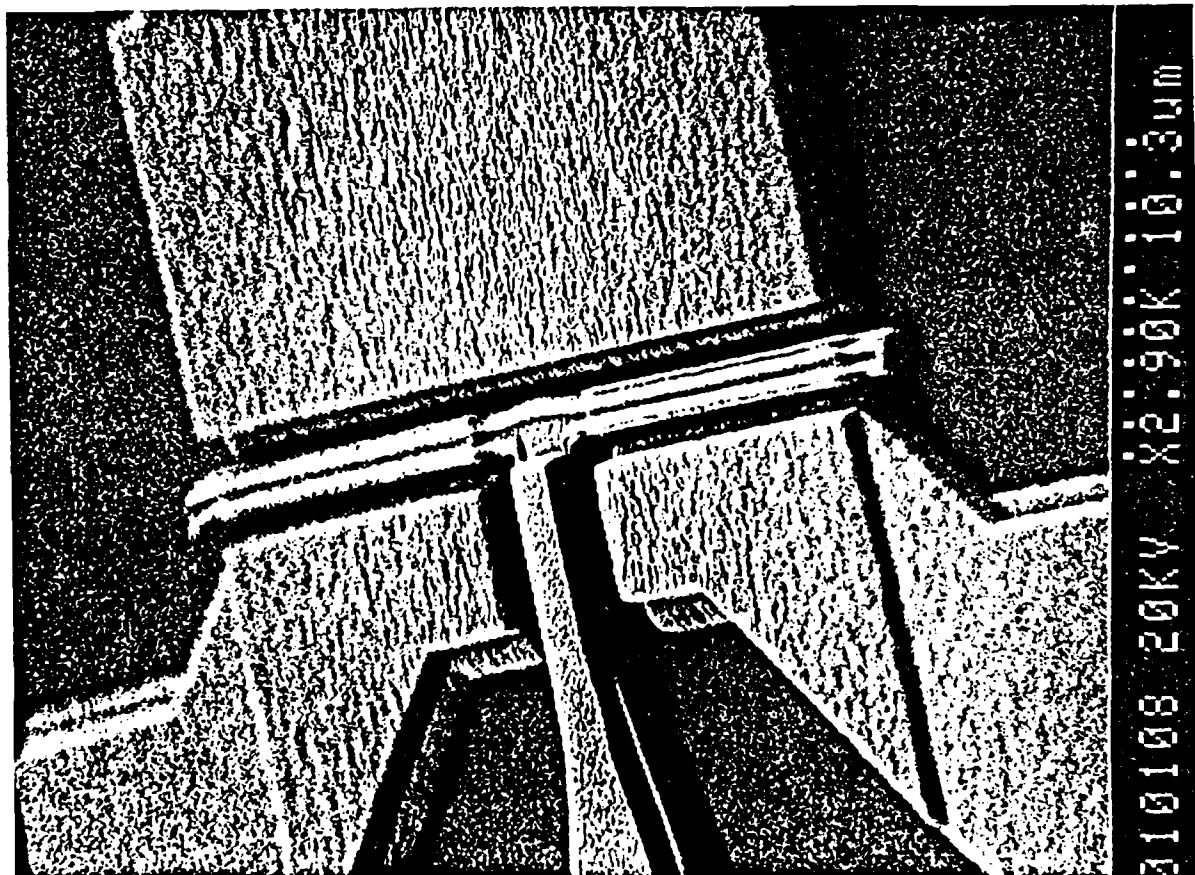
GE Aerospace

(From R. Sudbury)



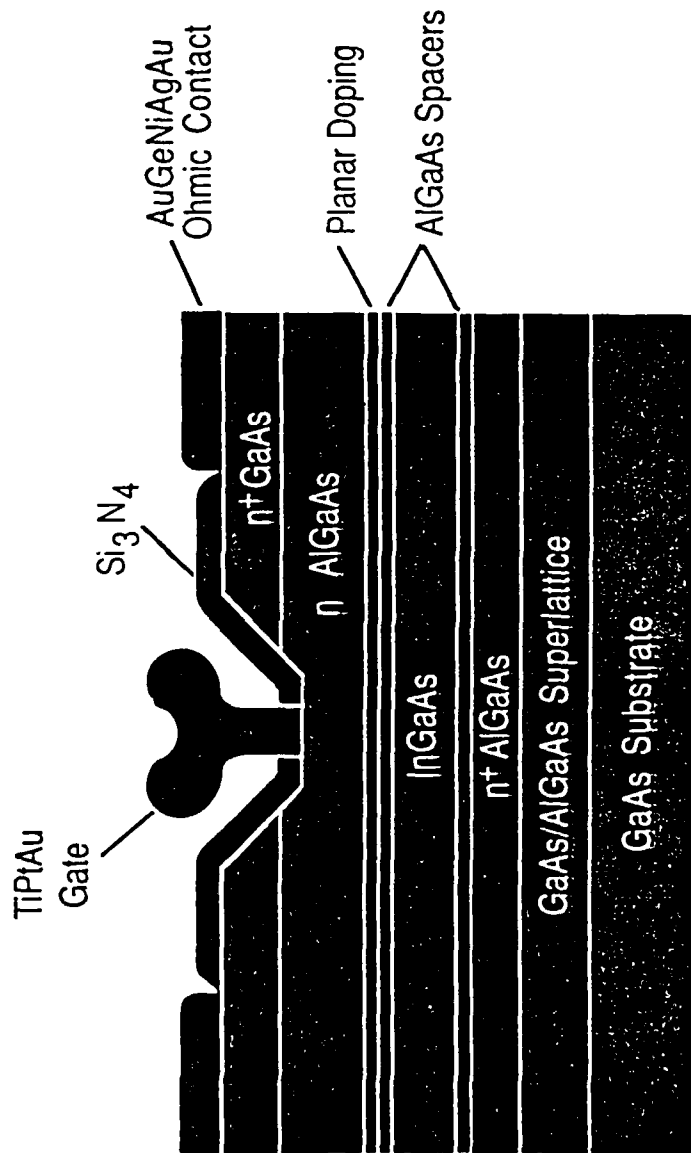
HEMT With 0.25 μ m T-Shaped Gate

GE Aerospace



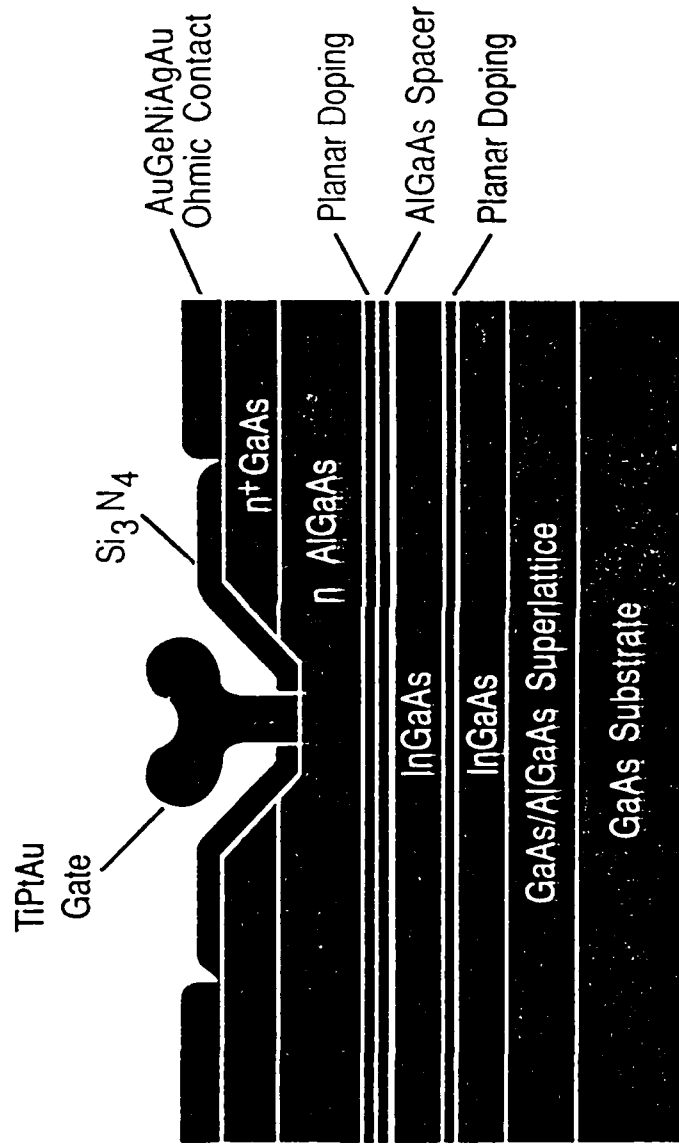
Double Heterojunction Pseudomorphic HEMT

GE Aerospace



Doped Channel Pseudomorphic HFET

GE Aerospace



Comparison of Pseudomorphic Device Structures

GE Aerospace

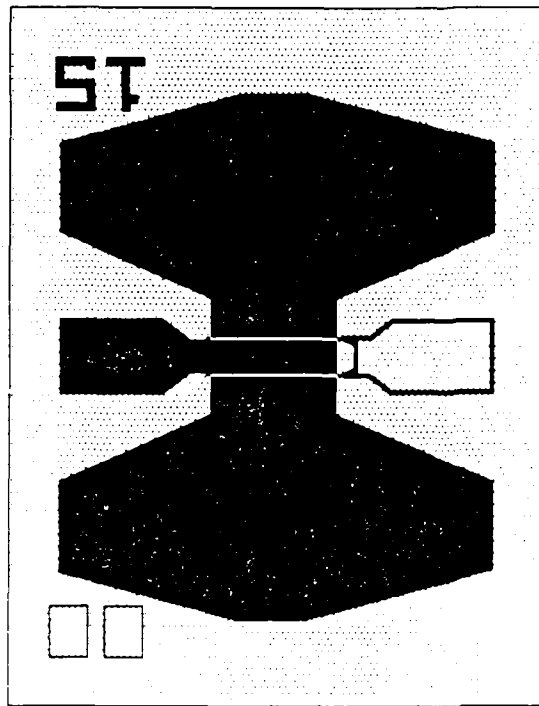
	DOUBLE HETEROJUNCTION	DOPED CHANNEL
μ_{77K} (cm ² /V-sec)	20,000	5,000
n_{s77K} (cm ⁻²)	3.6×10^{12}	3.6×10^{12}
g_m (mS/mm)	600	600
I_f (mA/mm)	600	600
V_{gdb} (V)	8	8
$L_g = 0.25\mu m$		
g_m (mS/mm)	700	700
I_f (mA/mm)	750	720
V_{gdb} (V)	5	5
$L_g = 0.1 - 0.15\mu m$		

Effect of Source Inductance

GE Aerospace



0.25 x 150µm HEMT



0.25 x 150µm HEMT with
Via-Hole Source Grounding

35GHz Performance

VIAS	V_{ds} (V)	I_{ds} (mA)	OUTPUT POWER (mW)	POWER DENSITY (W/mm)	POWER-ADDED EFFICIENCY (%)	GAIN (dB)
No	4.3	37	93	0.62	43	6.0
Yes	4.3	38	92	0.61	48	7.9

- 0.25 x 150µm Double Heterojunction Pseudomorphic HEMT
- Via Holes Increase Gain at Maximum Efficiency by ~2dB

35 and 44 GHz Pseudomorphic Device Power Results

GE Aerospace

— 0.25 x 150 μ m Double Heterojunction HEMTs

FREQUENCY (GHz)	SOURCE VIAS	POWER DENSITY (W/mm)	POWER-ADDED EFFICIENCY (%)	GAIN (dB)
35	YES	0.44	50*	8.6
	NO	0.97*	35	5.0
44	YES	0.63	48*	6.6
	NO	1.01*	32	4.1

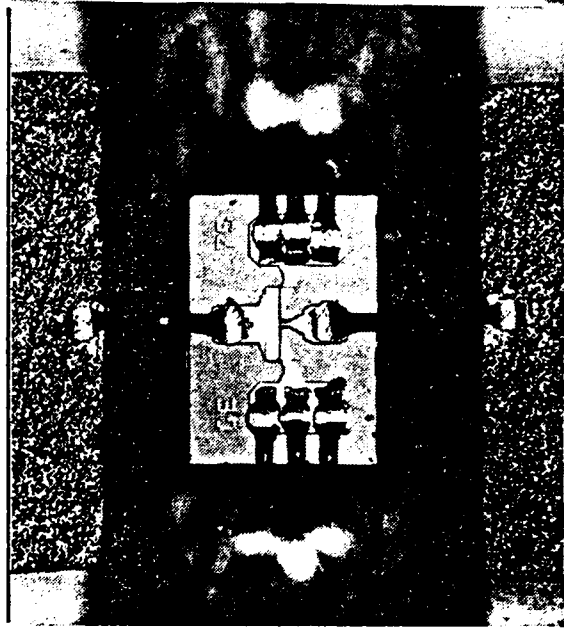
*maximum

~ 1 W/mm Power Density and ~50% Power-Added Efficiency
Demonstrated at 35 and 44 GHz

0.25 μ m Doped Channel Pseudomorphic HFET – 60 GHz Power Performance

GE Aerospace

OUTPUT POWER (mW)	POWER DENSITY (W/mm)	POWER-ADDED EFFICIENCY (%)	GAIN (dB)
52	0.69	40	5.8
68	0.91	38	6.0
75	1.00	36	4.4

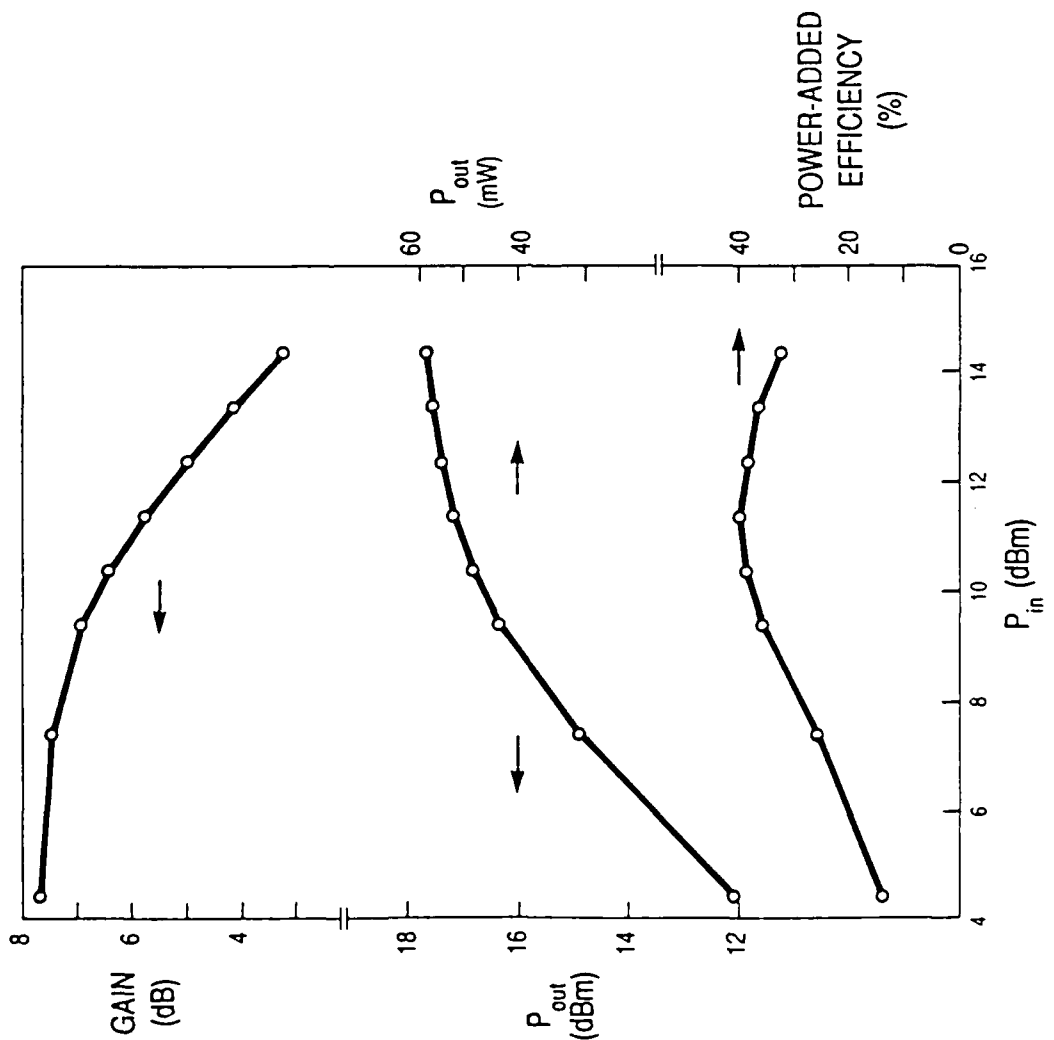


75 μ m Gate Width Device

60 GHz Power Data – Doped Channel Pseudomorphic HFET

GE Aerospace

• 0.25 x 75μm Device

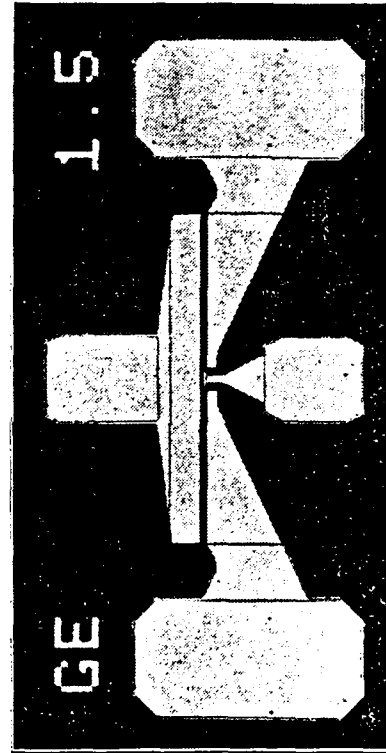


GAIN (dB)	POWER (mW)	EFFICIENCY (%)
5.8	52	40
6.4	48	39
7.0	43	36
7.5	31	26

0.15 μ m Double Heterojunction Pseudomorphic HEMT – 60 GHz Power Performance

GE Aerospace

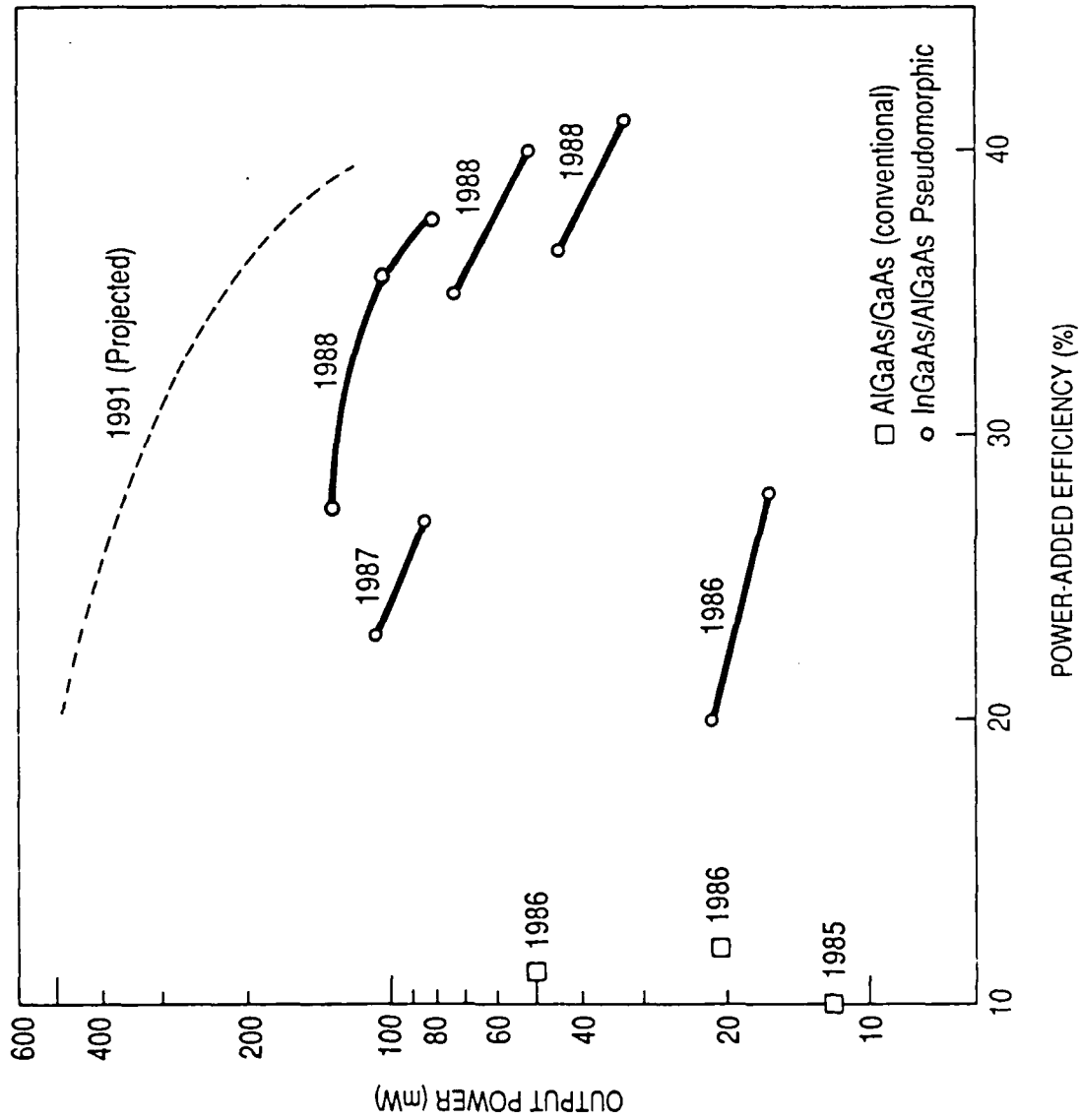
GATE WIDTH (μ m)	OUTPUT POWER (mW)		POWER DENSITY (W/mm)	POWER-ADDED EFFICIENCY (%)	GAIN (dB)
	33	42			
50	0.66	0.84	41	5.8	
	0.84	0.94	37	5.9	
	0.94		30	3.3	
150	0.55	0.83	38	4.7	
	0.83	0.93	32	4.5	
	0.93		28	3.0	



150 μ m Gate Width HEMT

60 GHz Performance of GE Power HEMTs

GE Aerospace



94 GHz Pseudomorphic HEMT Power Performance

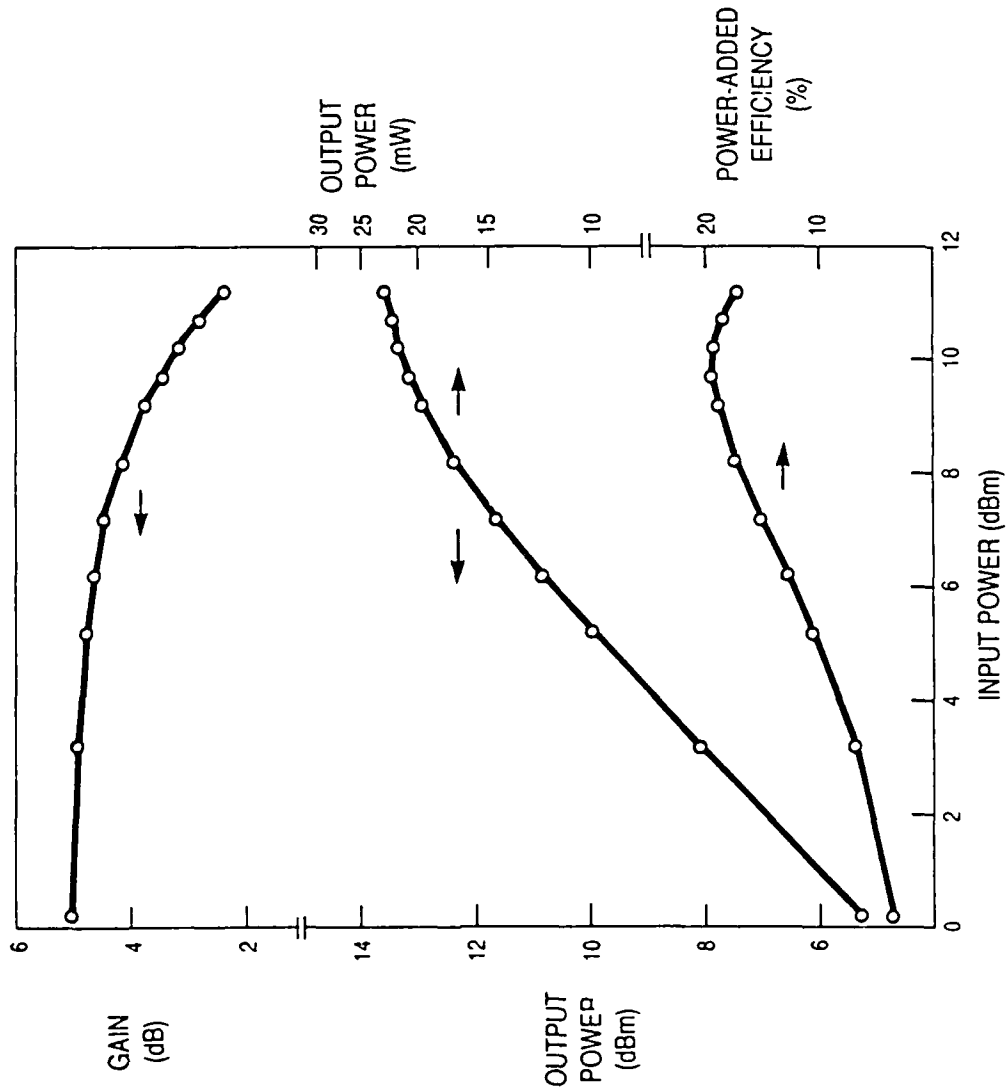
GE Aerospace

- 0.15 x 50 μ m Gate Dimensions
- Double Heterojunction Pseudomorphic HEMT

OUTPUT POWER (mW)	POWER DENSITY (W/mm)	POWER-ADDED EFFICIENCY (%)	GAIN (dB)
18	0.36	23	3.3
22	0.43	19	3.2

94 GHz Power Data – 0.15 μ m Pseudomorphic HEMT

GE Aerospace



GAIN (dB)	POWER (mW)	EFFICIENCY (%)
3.2	22	19
3.7	20	19
4.2	17	18
4.5	15	15
4.8	10	11

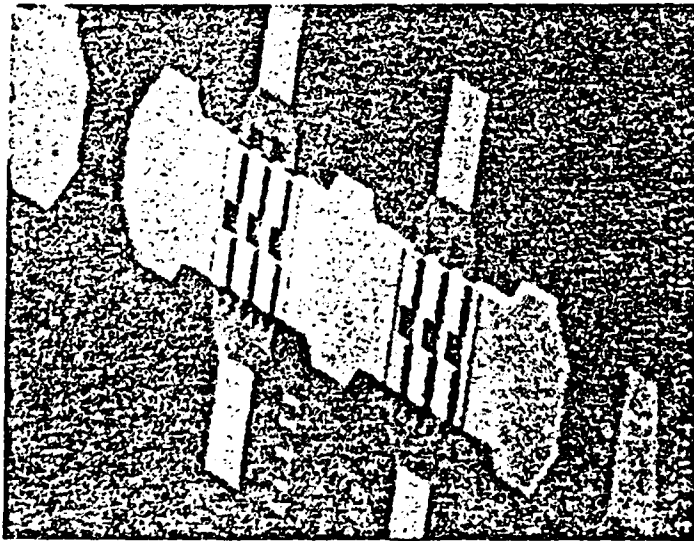
Editorial Comment/Observations

GE Aerospace

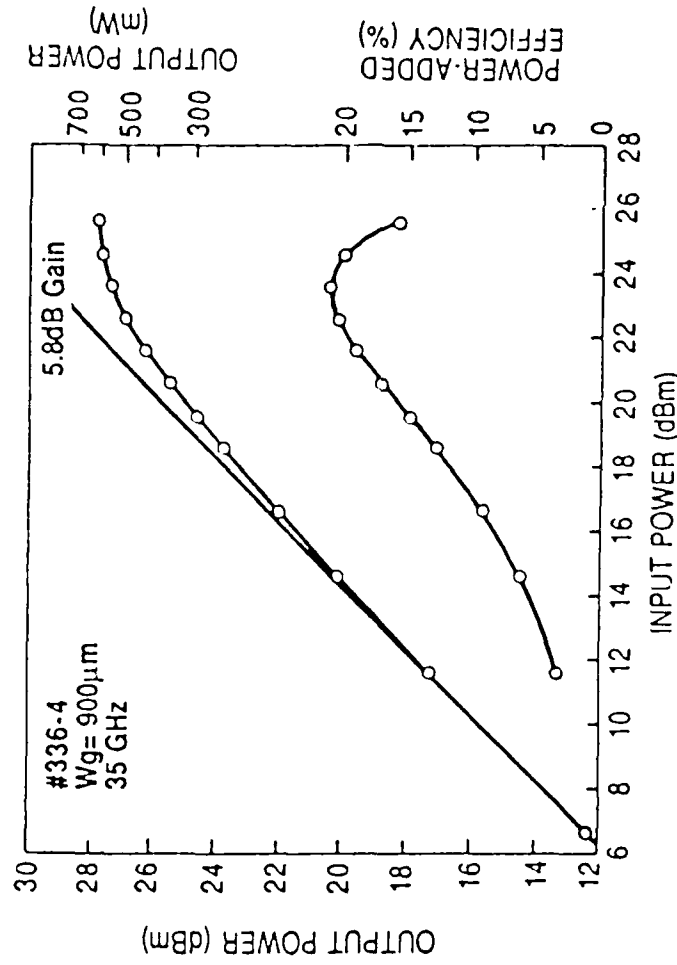
- **Not Valid to Compare Power Density for Different Device Types**
- **Universal Figures of Merit for Power Device are Output Power and Efficiency**
- **Compact Size is not an Advantage for Power Device – High Dissipated Power/Area → High Junction Temperature → Poor Reliability/RF Performance Degradation**
- **Power Density of HEMTs at 60 GHz is High Enough: 1 W/mm**
 - For High Efficiency/High Reliability, GaAs FETs Normally Operated at 0.3-0.5 W/mm
 - Higher Power Density Only Acceptable With Improved Thermal Resistance – Geometry, Substrate Thickness, Substrate Thermal Conductivity (InP)
- **Power HEMT Performance Degrades with Increasing Gate Width**
 - Source Inductance
 - Gate Resistance/Gate Line Attenuation
- **Need to Increase Output Power by Increasing Gate Width Without Sacrificing Too Much Gain and Efficiency**
 - Interdigitated Geometries
 - Low Resistance T-Gates
 - Via Holes

High Power Pseudomorphic HEMT

GE Aerospace Laboratories



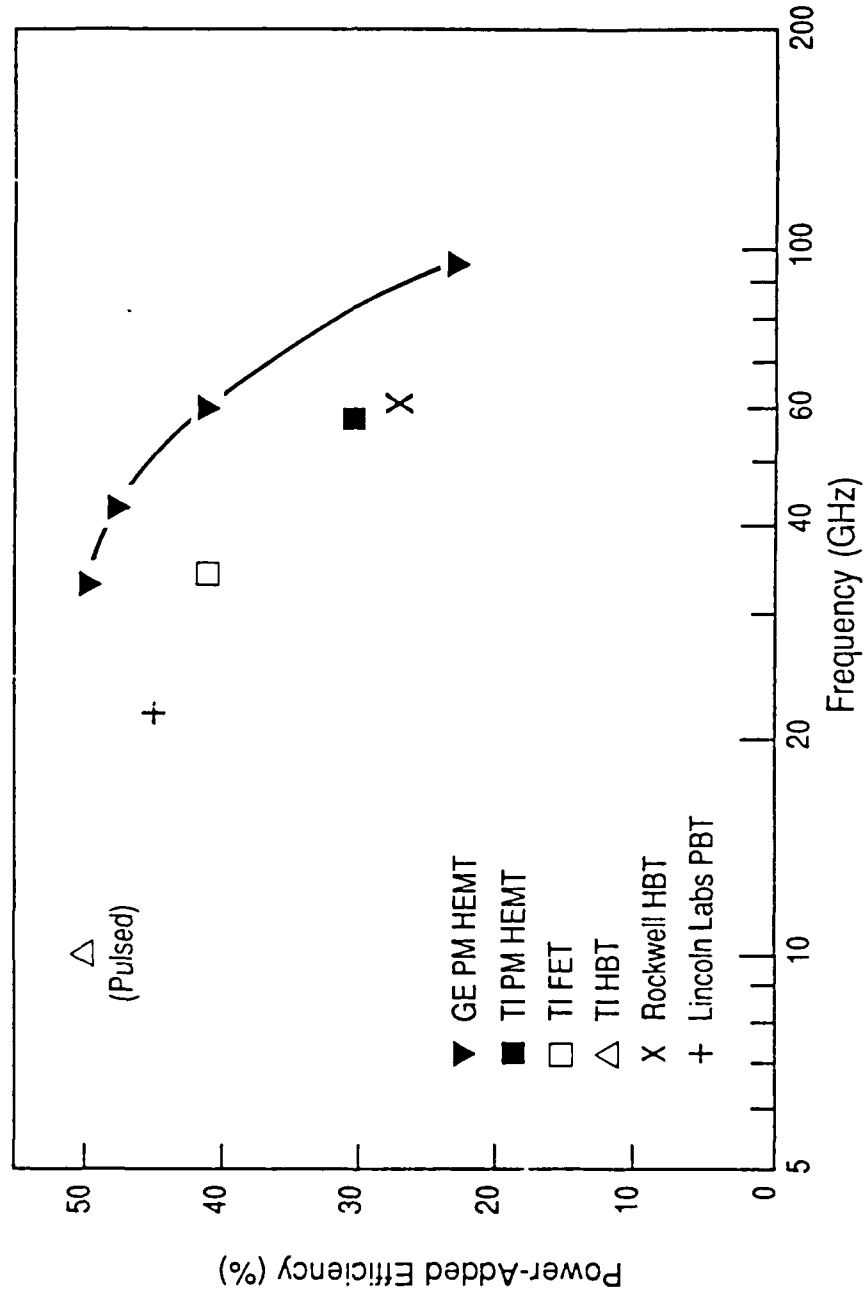
0.25 μ m Gate Length
 900 μ m Gate Width
 2 Cells



35GHz: 550mW Output Power With 3.8dB Gain, 21% Power-Added Efficiency

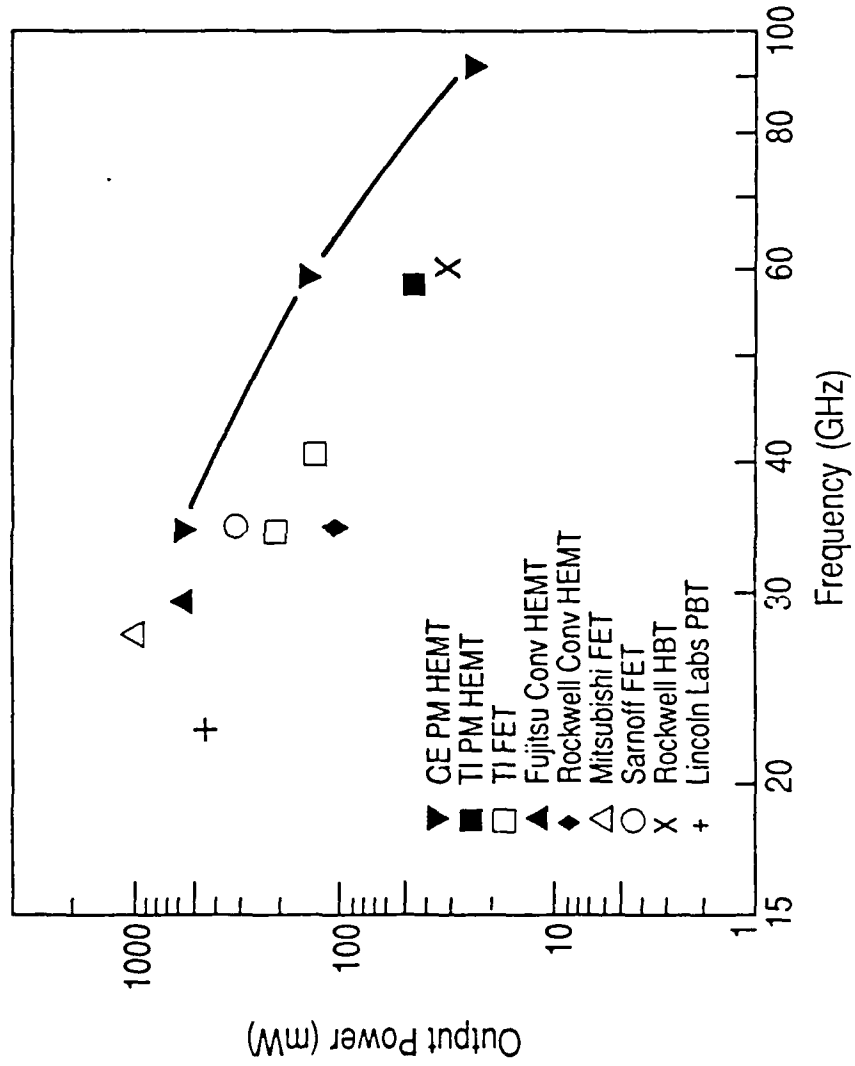
State-of-the-Art: Efficiency

GE Aerospace



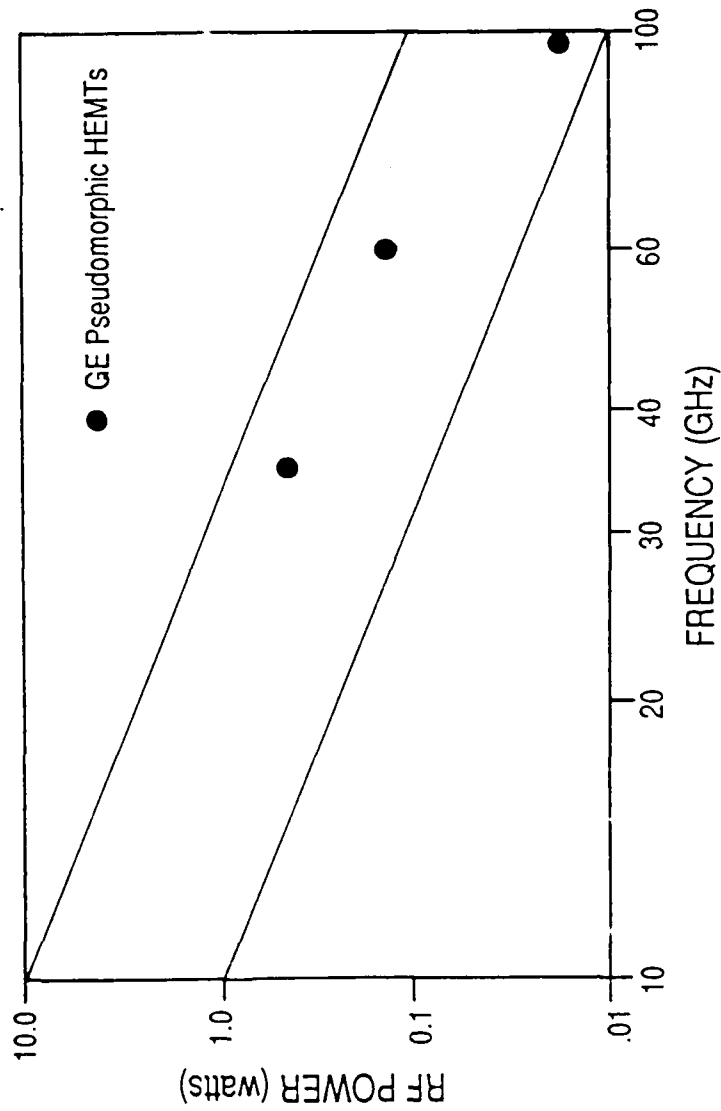
State-of-the-Art: Output Power

GE Aerospace



Typical Radiated Power/Element Requirements for Solid State Arrays

GE Aerospace



OUTPUT POWERS OF CURRENT TRANSISTORS ADEQUATE FOR SOME MMW PHASED ARRAYS

0.15 μ m Double Heterojunction Pseudomorphic HEMT

GE Aerospace

Excellent Power Performance

60 GHz: 41% Maximum Efficiency with 5.8 dB Gain, 0.66 W/mm Power Density

Excellent Noise Performance

18 GHz: 0.6dB NF with 14.5 dB Ga

60 GHz (Projected): 1.7 dB NF with 7 dB Ga

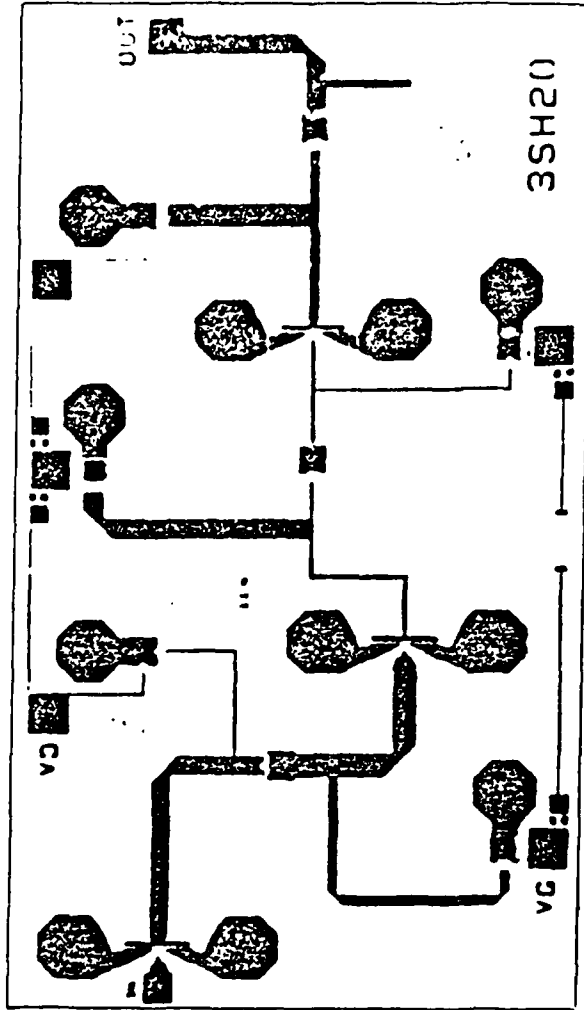
Same Device Structure Suitable for Both Low Noise and Power Amplification



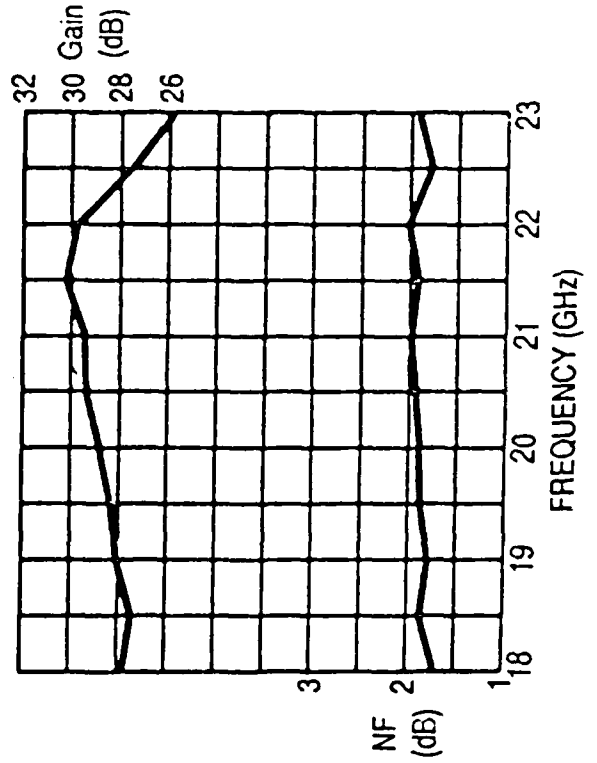
- Possible to Integrate LNA and Power Amplifier on Same GaAs Chip (Single-Chip T/R Module)
- OR
- Possible to Develop Generic Amplifier MMIC that can Serve as LNA or Power Amplifier

20 GHz 3-Stage HEMT MMIC LNA

GE Aerospace Laboratories



- 0.25 μ M HEMTs
- Input Match: Off-Chip for Lowest Noise Figure
- 20.2-21.2 GHz Design Band

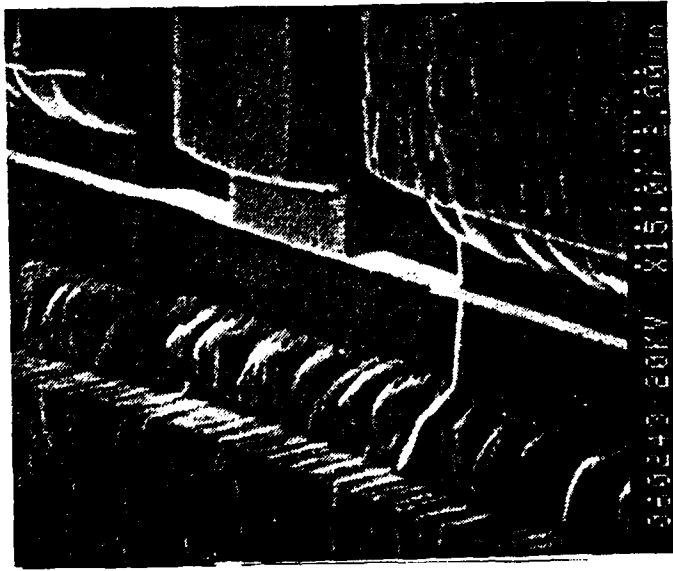


Performance: 20.2-21.2 GHz

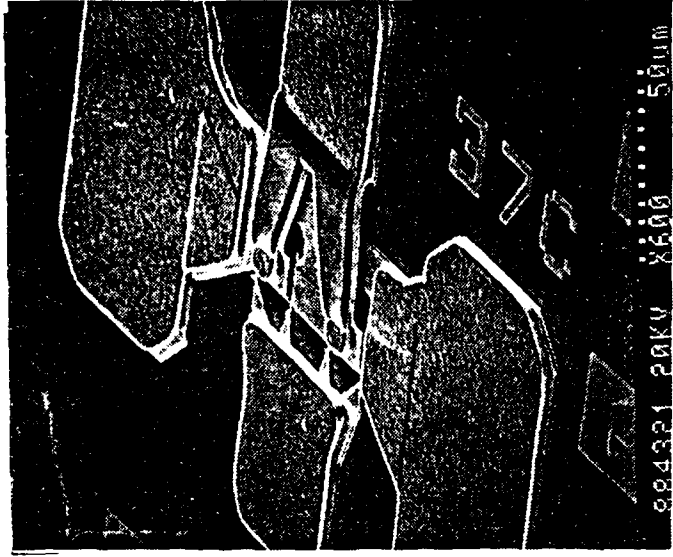
- Gain = 29.4 \pm 0.4 dB
- NF \leq 2.0 dB

0.1 μ m Pseudomorphic HEMT

GE Aerospace



Channel Region



50 μ m Gate Width Device Geometry

- Planar-Doped Pseudomorphic Structure for High Aspect Ratio
- 4-Finger Air-Bridged Geometry to Reduce R_g
- DC $g_m = 930$ mS/mm
- Excellent Noise Figure, High Gain Despite High R_g :

FREQUENCY (GHz)	NOISE FIGURE (dB)	GAIN (dB)
60	1.9	9.2
94	3.0	5.1

0.25μm InAlAs/InGaAs/InP HEMT

GE Aerospace

Noise

FREQUENCY (GHz)	NOISE FIGURE (dB)	GAIN (dB)
18	0.5	15.2
60	1.2	8.5
94	2.1	6.4

Power

- 150μm Gate Width HEMT Tested at 35 GHz
- At $V_{ds} = 3.6$ V, Output Power = 66mW
Power Density = 0.44 W/mm
Power-Added Efficiency = 38%
Gain = 6.5 dB

Gain

- Maximum Small-Signal Gain:

FREQUENCY (GHz)	GAIN (dB)
63	15.5
95	12.0

- Extrapolated $f_{max} = 380$ GHz

Summary

GE Aerospace

- **Potential Array Applications at 35, 44, 60 and 94 GHz Demand High Performance Devices and Circuits**
- **Current HEMTs Offer Useable Device Performance for Arrays up to 60 GHz**
 - V-Band Subarray Demonstration Contract Using Present 0.25 μ m HEMT Technology
- **HEMTs Exhibit Excellent Noise Performance to 94GHz (1-2 db NF @ 60 GHz, 2-3 dB NF @ 94 GHz)**
- **Significant Progress was made in 60 and 94 GHz Pseudomorphic Power HEMTs with Double Heterojunction and Doped Channel Devices:**
 - 60 GHz
 - Power Gain of 6-7 dB with 40% Efficiency, 0.6-0.7 W/mm Power Density for Small Devices (50, 75 μ m Gate Width)
 - Output Power of 125 mW with 32% Efficiency, 4.5 dB Gain.
 - Gain, Efficiency of 150 μ m Device will be Improved with Vias
 - Power Density of 1 W/mm is High Enough
 - Output Power can be Increased to 0.5 Watt
 - 94 GHz
 - 22mW Output Power, 23% Peak Efficiency, ~3 dB Power Gain
 - Higher Gain, Power Desirable for Applications
- **Low Noise and Power Pseudomorphic HEMTs Easily Integrate into GaAs MMICs**
- **New Devices for Improved Performance – 0.1 μ m Pseudomorphic HEMT, InP-Based HEMT**

mm-Wave Phased-Array Antenna Concepts

Charles A. Liechti

*Rockwell International, Science Center
Thousand Oaks, CA*

**MM-WAVE PHASED-ARRAY
ANTENNA CONCEPTS**

Charles A. Liechti

**ROCKWELL INTERNATIONAL
SCIENCE CENTER**

OUTLINE

1. TECHNICAL GOALS AND DESIGN PARAMETERS
2. ARRAY CONSTRUCTION
3. PRINTED MICROSTRIP MM-WAVE RADIATORS
4. PROPOSED SPACE-FED SUB-ARRAY DESIGN
5. GaAs IC BLOCK DIAGRAM
6. CONCLUSIONS



PHASED-ARRAY TRANSMIT ANTENNA
FOR TELECOMMUNICATION

TECHNICAL GOALS

TRANSMIT ARRAY:

* FREQUENCY	60 GHz	94 GHz
* BANDWIDTH	2 GHz	3 GHz
* SCAN ANGLE	60°	60°
* POLARIZATION	CIRCULAR	CIRCULAR
* POINTING ACCURACY	1/10 BEAMWIDTH	1/10 BEAMWIDTH
* GAIN X POWER (EIRP)	50 dBW	50 dBW
* BEAM SWITCHING TIME	<20 ns	<20 ns

PHASED-ARRAY TRANSMIT ANTENNA
FOR TELECOMMUNICATION

DESIGN PARAMETERS
ANTENNA

* FREQUENCY	60 GHz	94 GHz
* ELEMENT SPACING	2.5 mm	1.6 mm
* NUMBER OF MODULES	1000	1500
* TOTAL RF POWER OUTPUT	200 W	150 W
* ANTENNA GAIN	31 dB	32 dB
* BEAM WIDTH	3.4°	2.7°



DESIGN PARAMETERS GaAs CHIPS

PHASED-ARRAY TRANSMIT ANTENNA
FOR TELECOMMUNICATION

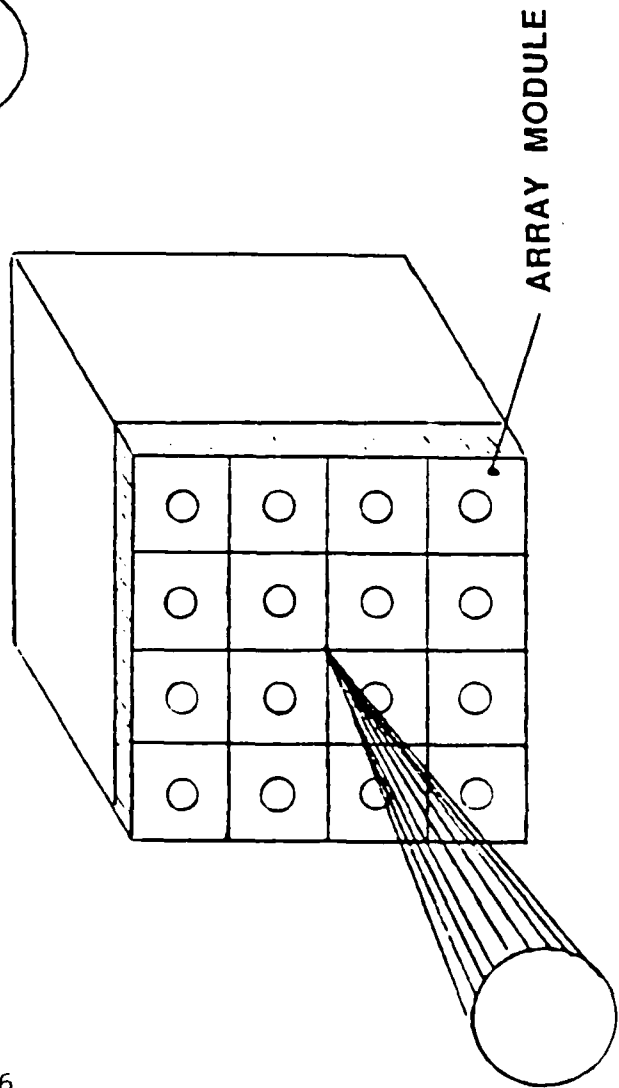
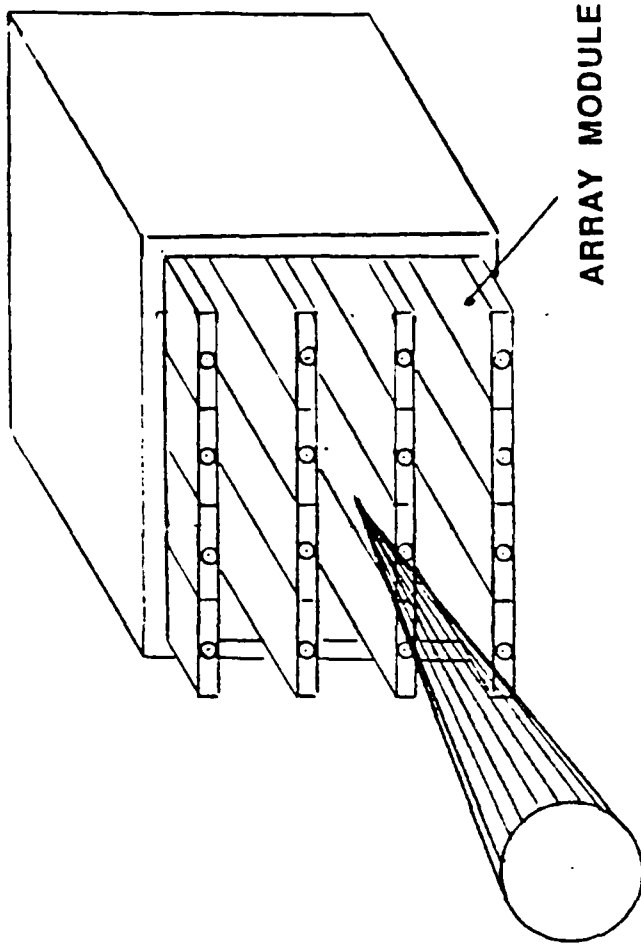
* FREQUENCY	60 GHz	94 GHz
* CW OUTPUT POWER PER MODULE	200 mW	100 mW
* MODULE GAIN	20 dB	16 dB
* INCREMENTAL PHASE SHIFT	45°	45°
* MODULE SIZE ON GaAs Chip	2.5 x 6.7 mm	1.6 x 4.3 mm
* NUMBER OF MODULES PER SUB-ARRAY	4 x 4	4 x 4
(For demonstration of concept)		
* NUMBER OF CHIPS PER SUB-ARRAY	4	4
* CHIP SIZE	10 x 6 mm	6.4 x 6 mm
* POWER DISSIPATION PER CHIP	5 W	5 W



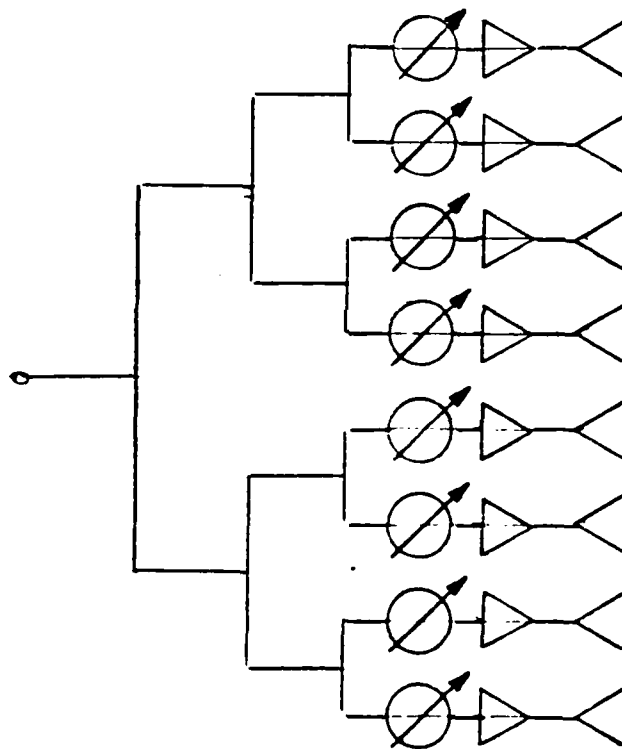
Rockwell International
Science Center

ARRAY CONSTRUCTION

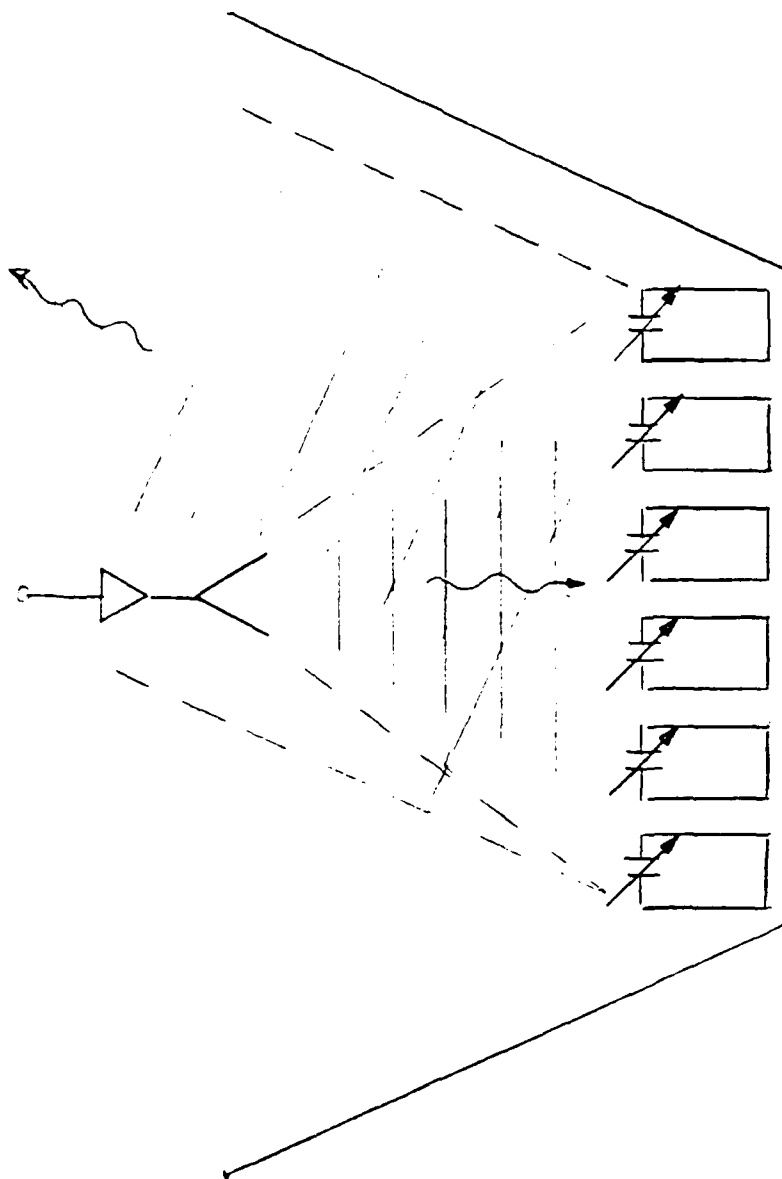
ARRAY CONSTRUCTION ALTERNATIVES



CORPORATE-FED ARRAY

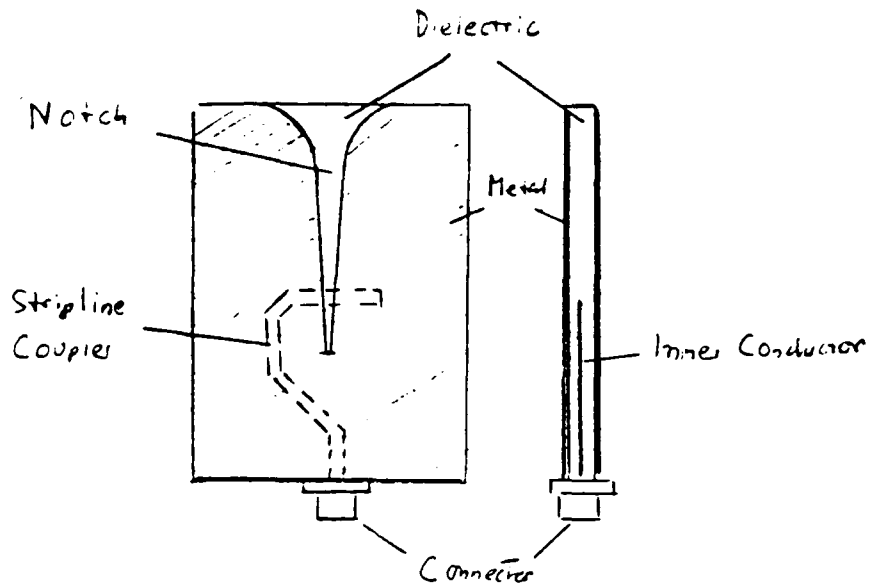


SPACE-FED REFLECTIVE ARRAYS

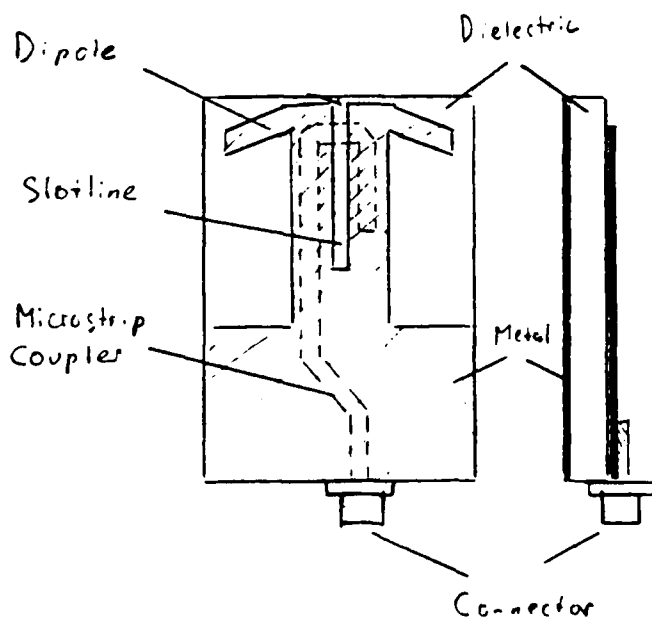


**PRINTED MICROSTRIP
MM-WAVE RADIATORS**

PRINTED MM-WAVE "END-FIRE" RADIATORS

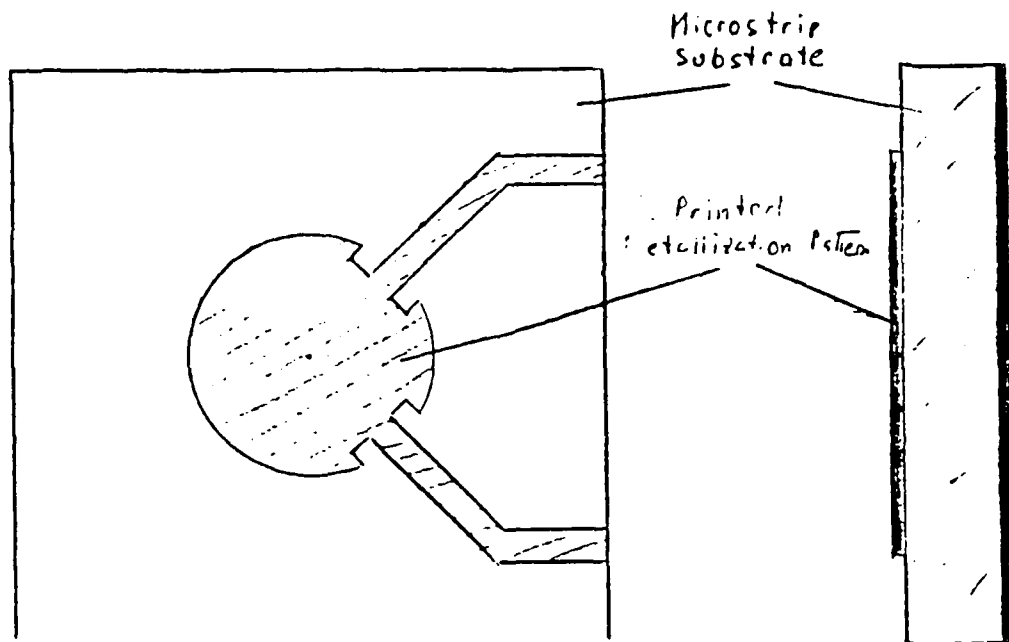


TAPERED-NOTCH RADIATING ELEMENT

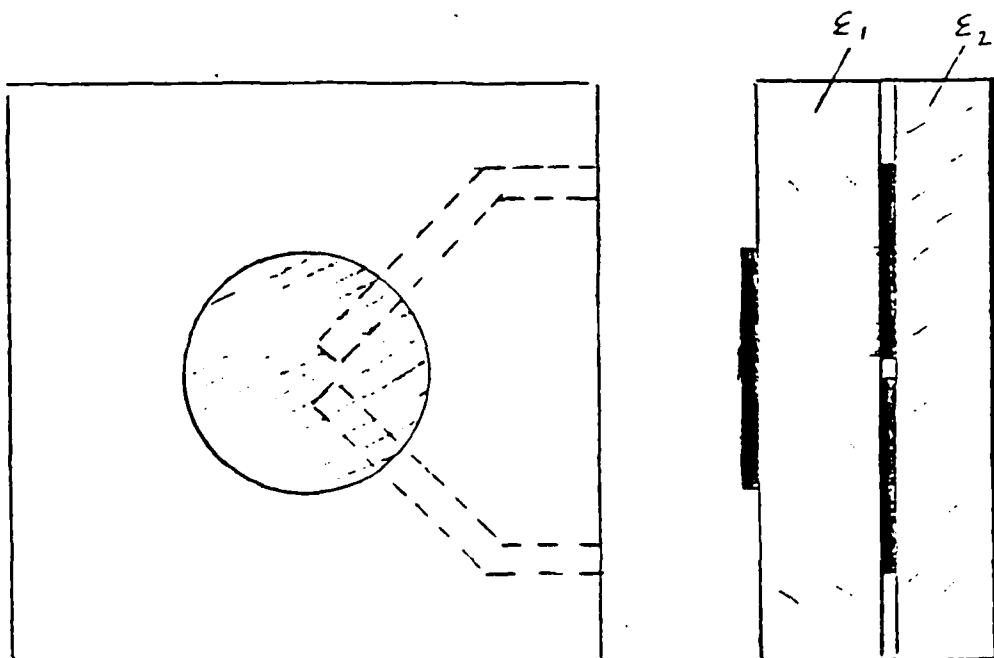


PRINTED DIPOLE RADIATING ELEMENT

PRINTED MM-WAVE "BROADSIDE-FIRED" RADIATORS

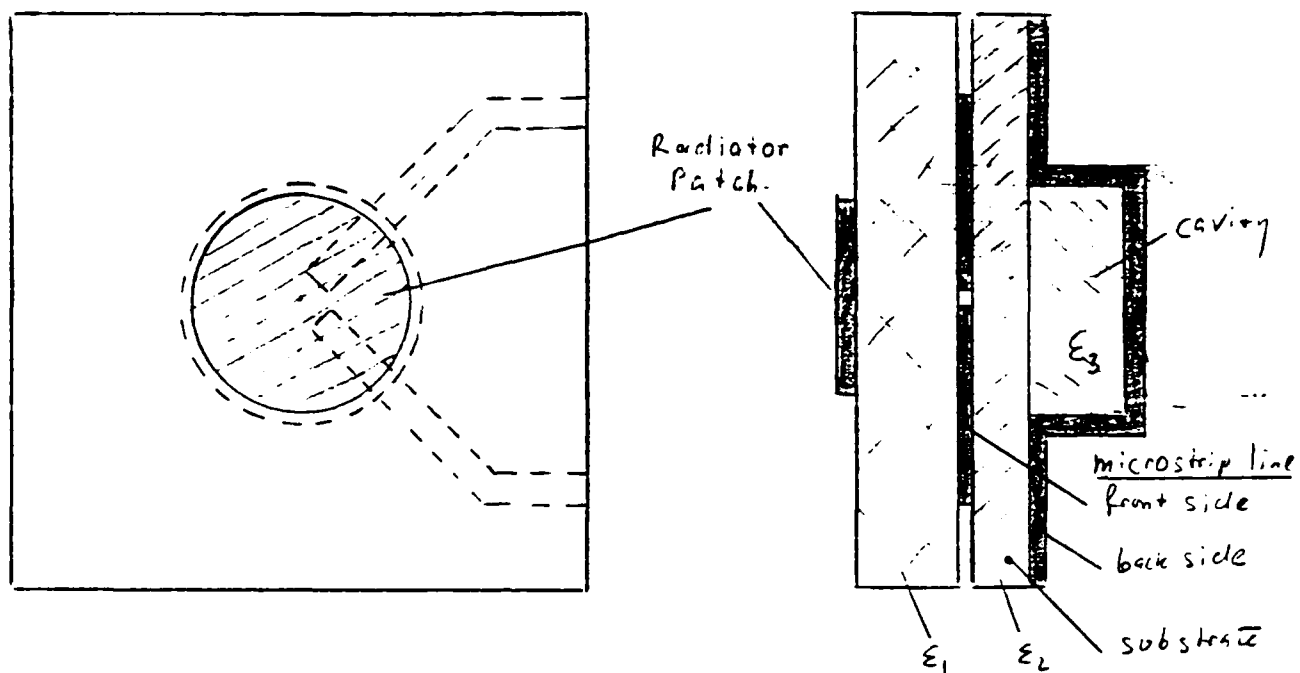


MICROSTRIP PATCH RADIATOR

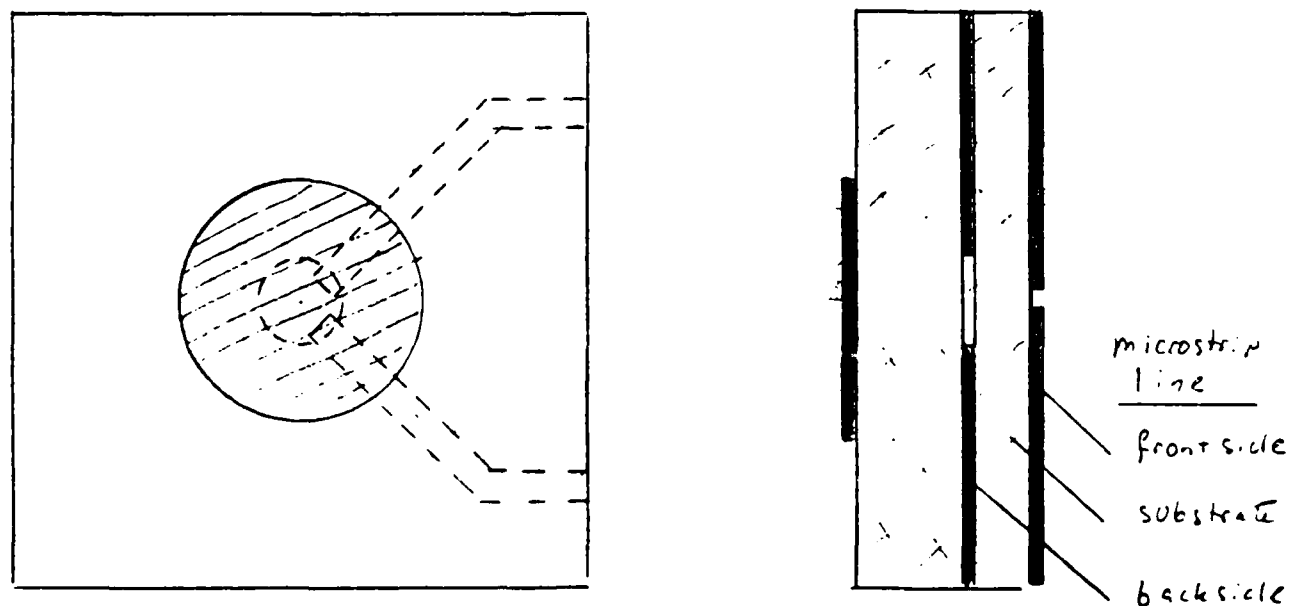


CAPACITIVELY-COUPLED MICROSTRIP RADIATOR

PRINTED MM-WAVE "BROADSIDE-FIRED" RADIATORS



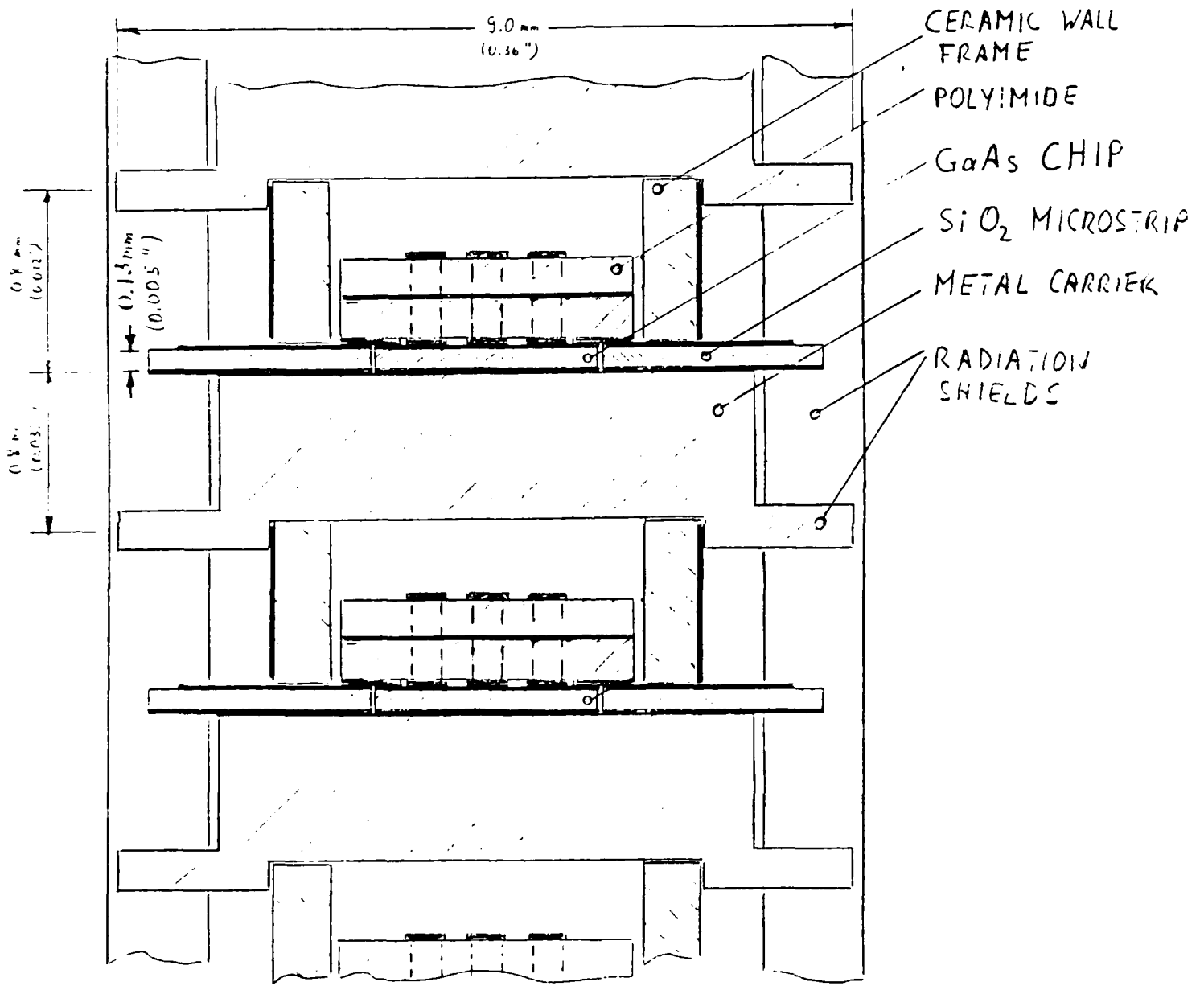
CAPACITIVELY-COUPLED MICROSTRIP RADIATOR, CAVITY-BACKED



CAPACITIVELY-COUPLED MICROSTRIP RADIATOR, COUPLED THROUGH OPENING IN BACKSIDE METALLIZATION OF MICROSTRIP LINE

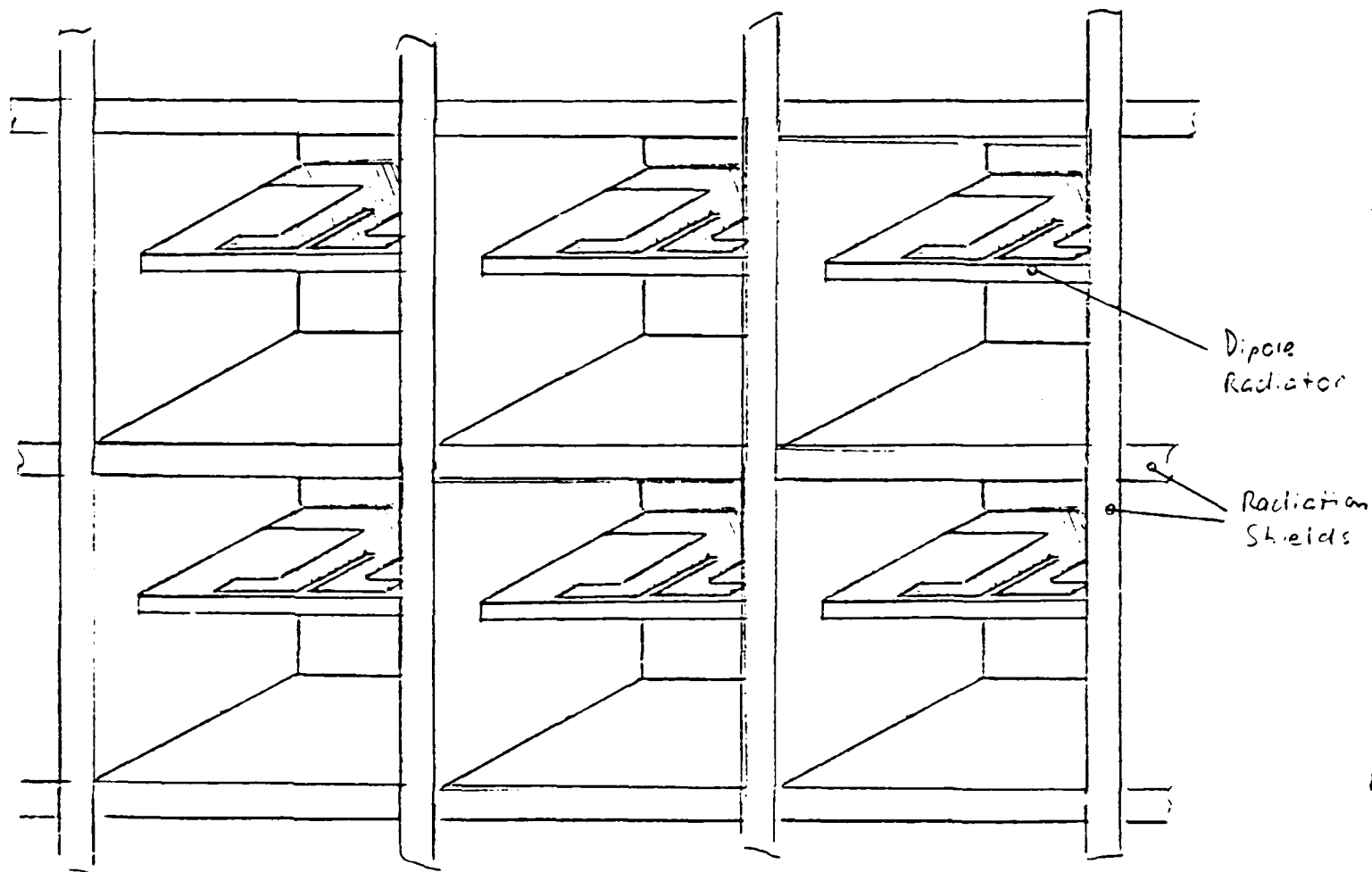
**PROPOSED
SPACE-FED
SUBARRAY DESIGN**

94 GHz PHASED ANTENNA SUBARRAY CROSS SECTION



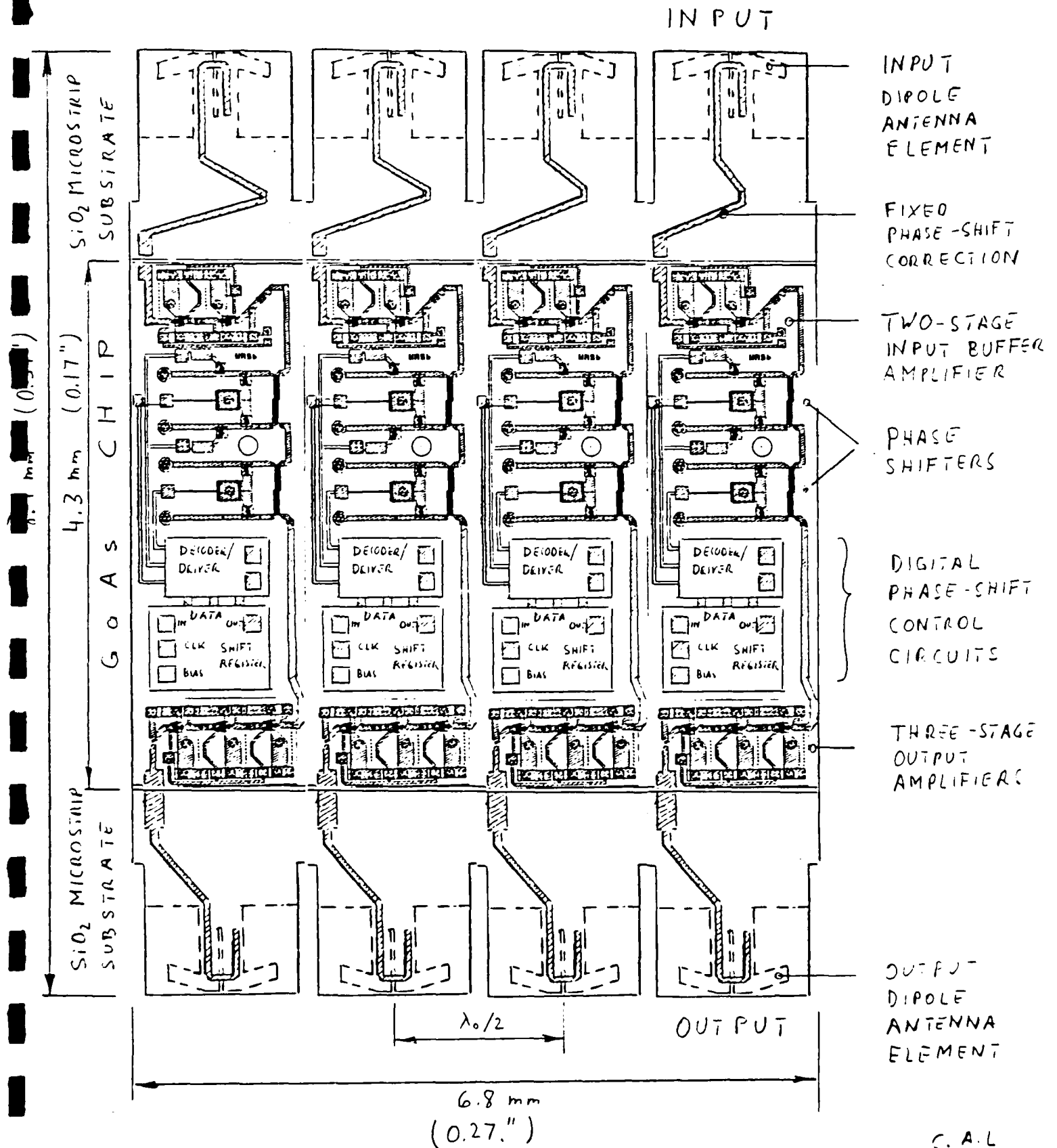
C.A.L
APRIL 1988

PHASED ANTENNA SUBARRAY VIEW OF ANTENNA FACE



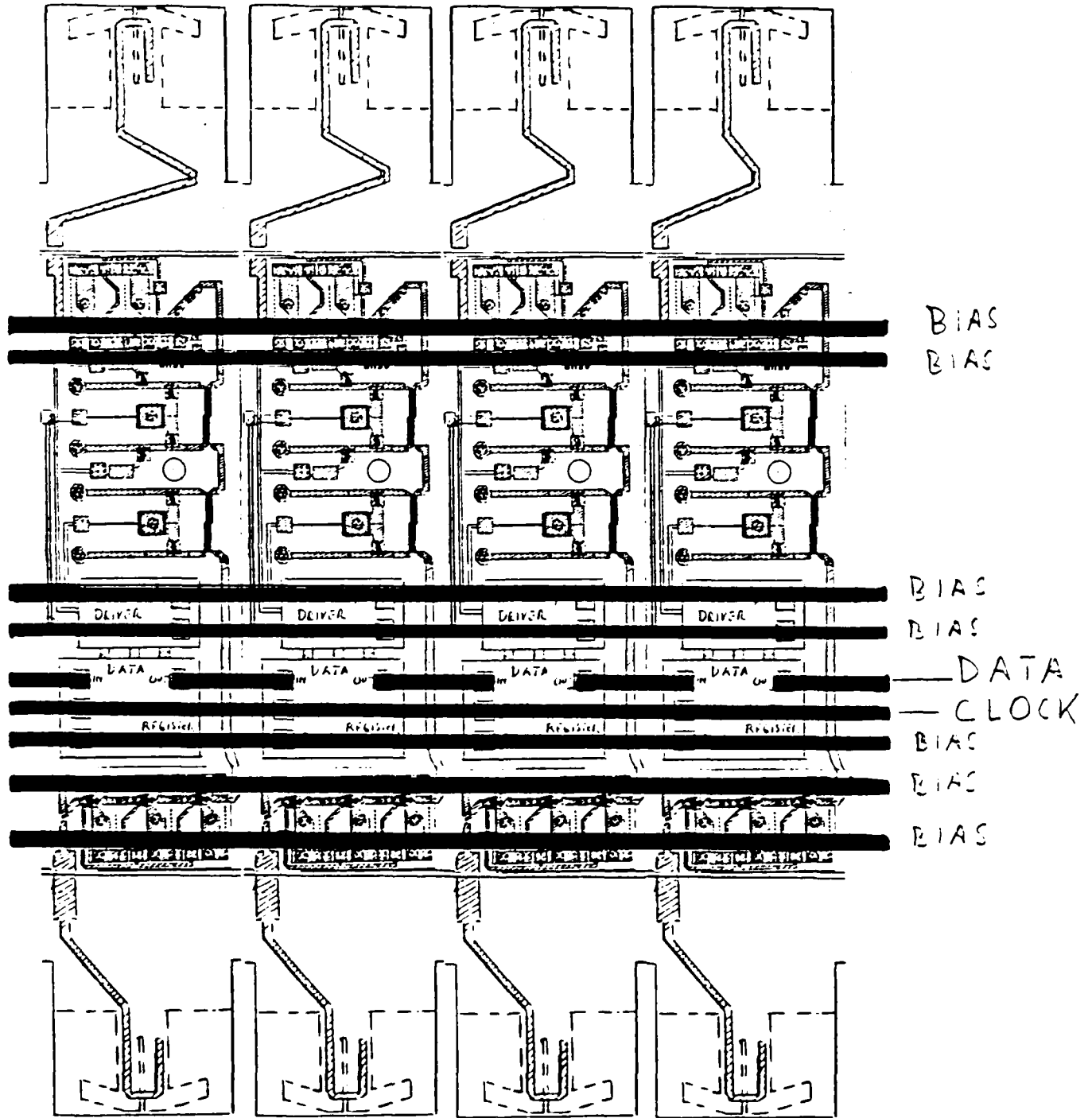
CAL
April 1966

94 GHz PHASED ANTENNA SUBARRAY



C. A. L
APRIL 1987

DC BIAS SUPPLY AND PHASE-SHIFT CONTROL INTERCONNECT LINES



C.A.L
APRIL 1972

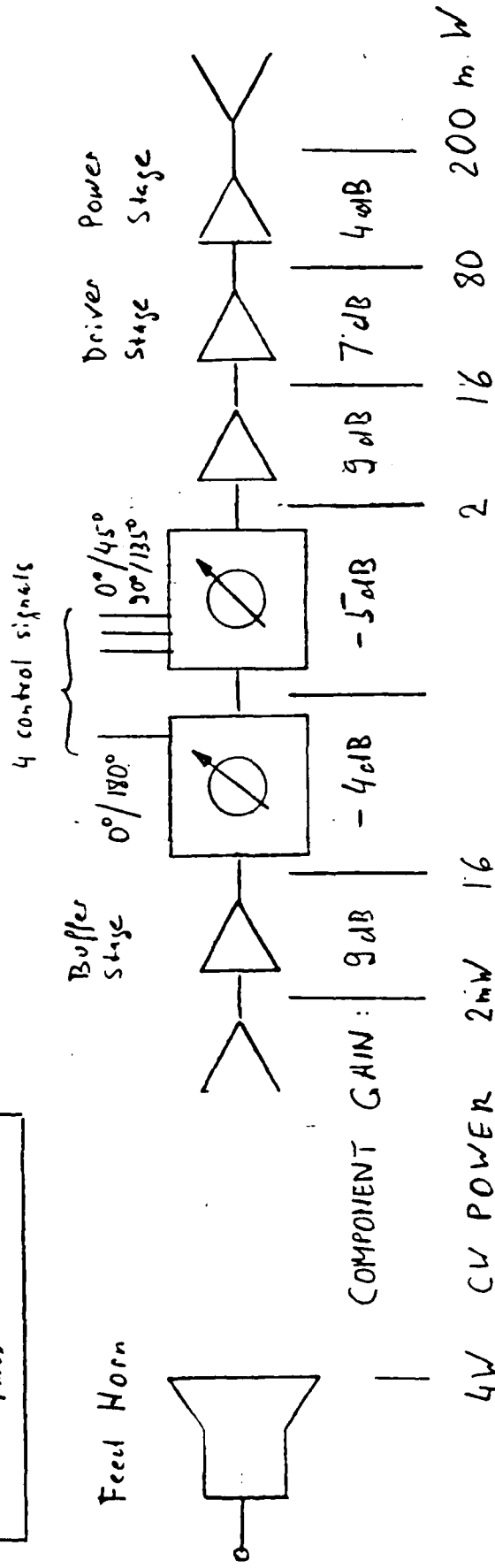
GaAs IC

BLOCK DIAGRAM

TRANSMIT MODULE BLOCK DIAGRAM

60 GHz PHASED-ARRAY TRANSMIT ANTENNA

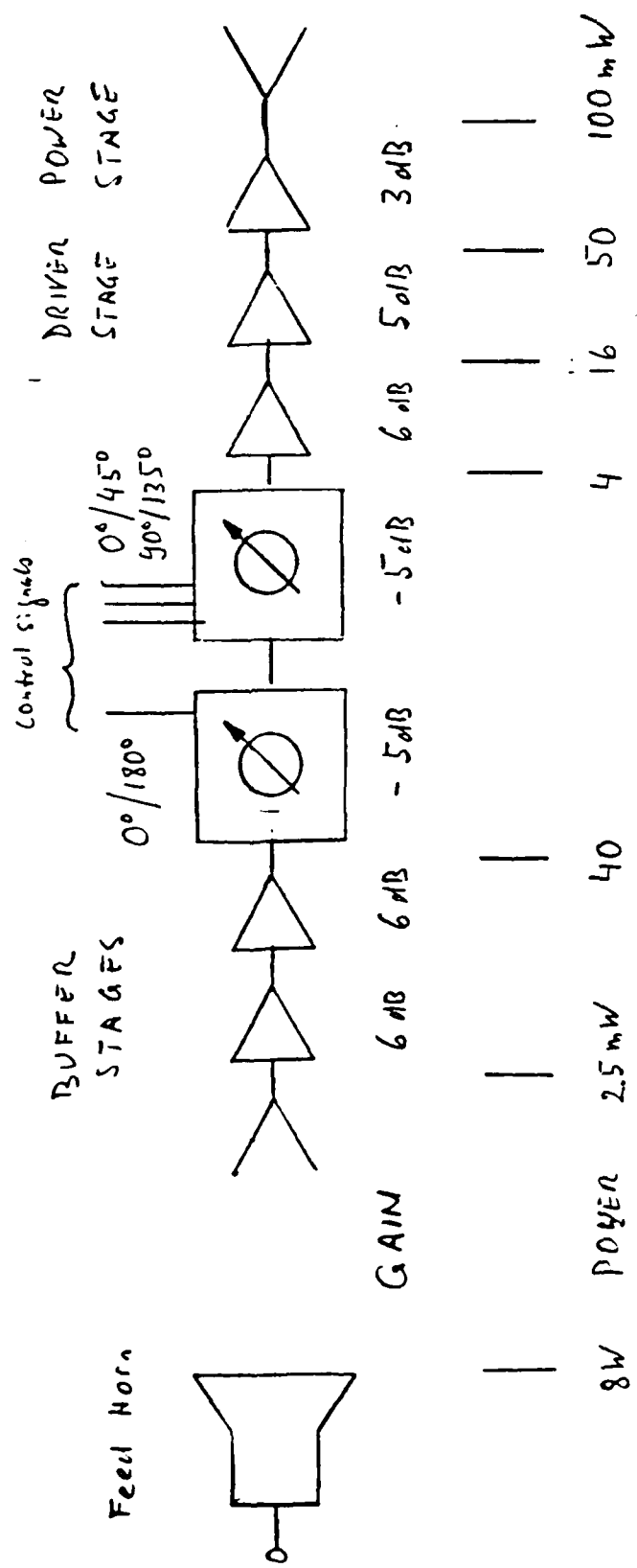
HBT $P_{max} = 240 \text{ GHz}$



94 GHz PHASED-ARRAY TRANSMIT ANTENNA

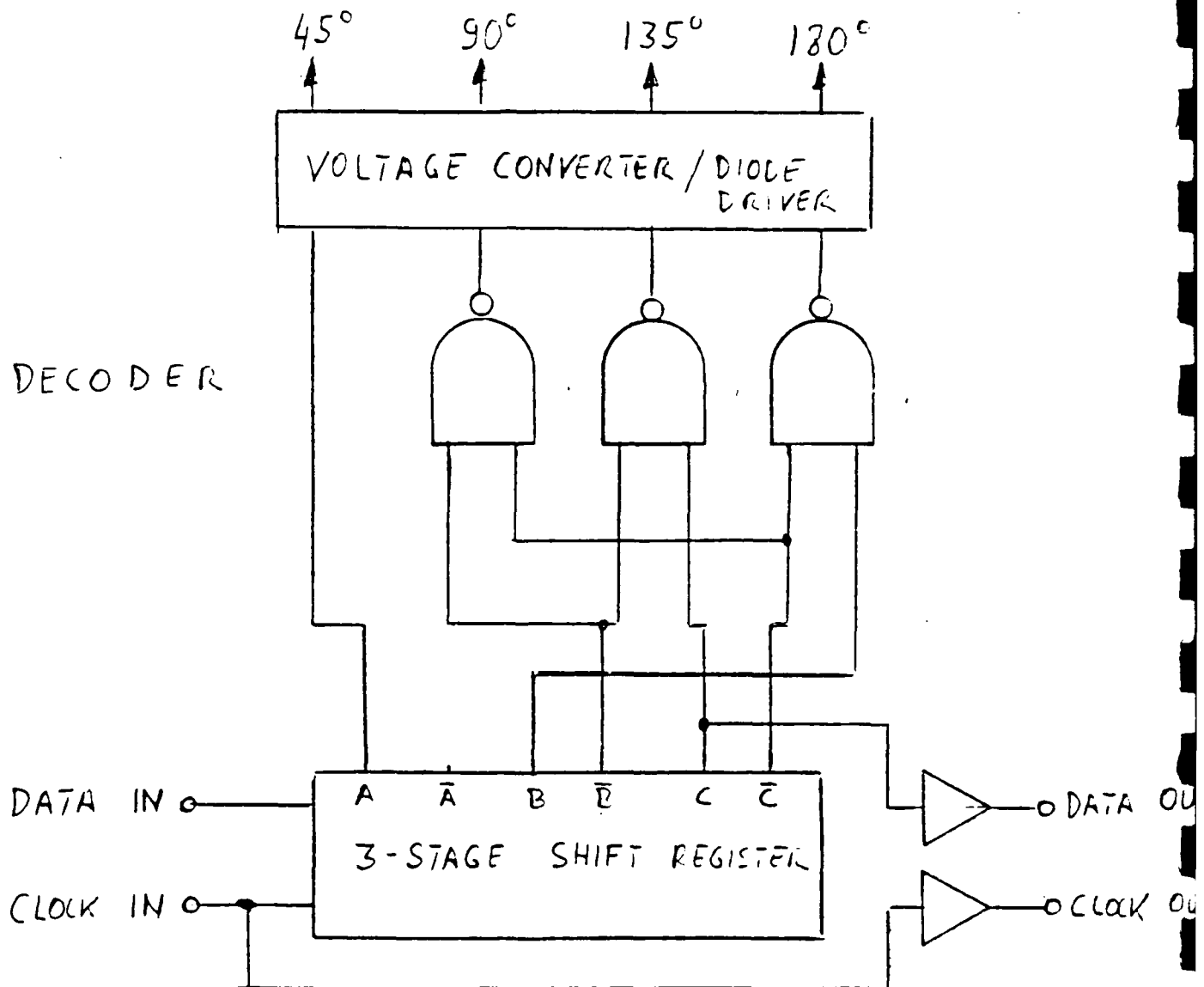
TRANSMIT MODULE BLOCK DIAGRAM

HBT $f_{max} = 240 \text{ GHz}$



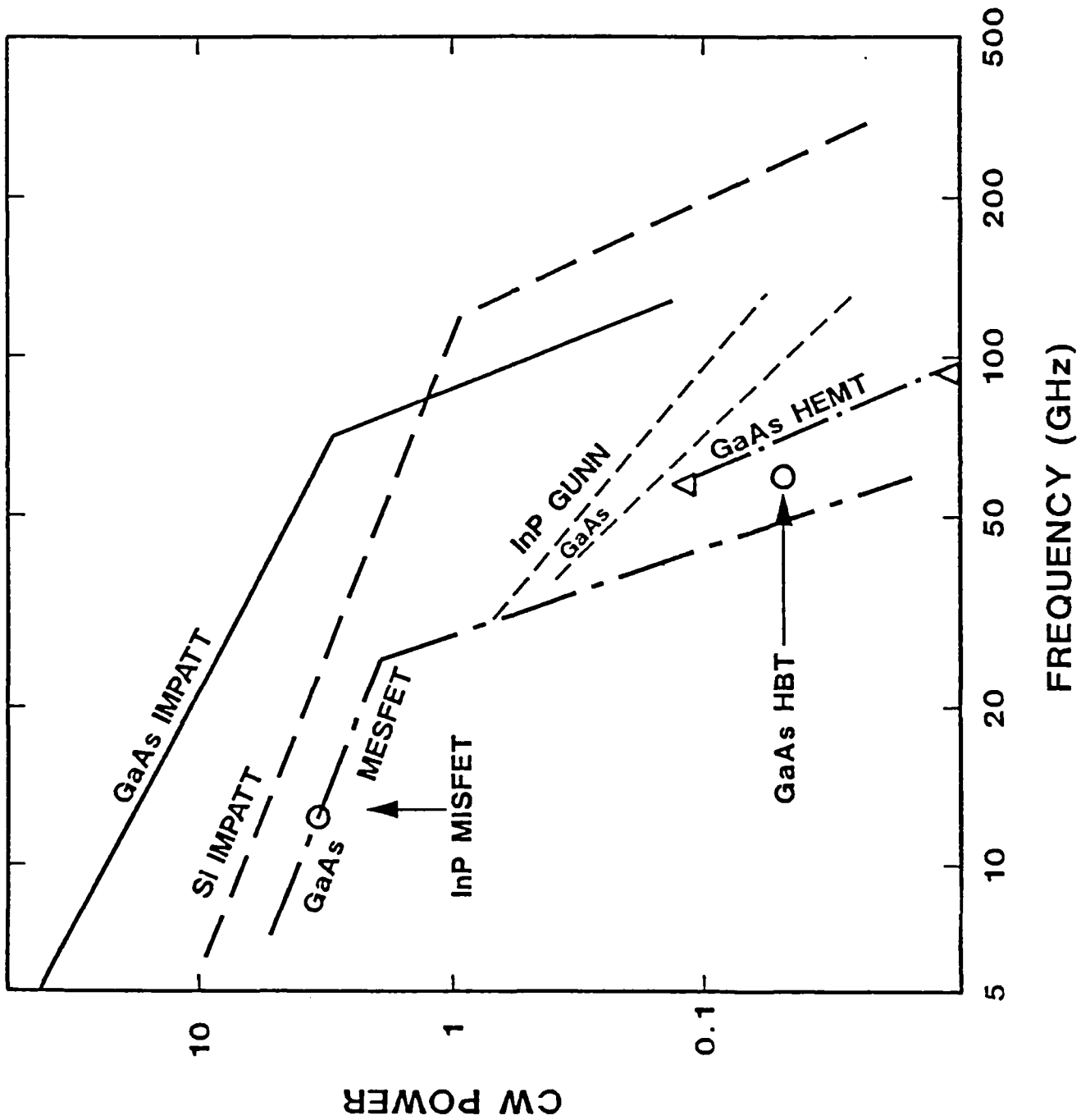
PHASED-ARRAY TRANSMIT ANTENNA

PHASE-SHIFT CONTROL UNIT



MICROWAVE AND MM-WAVE SOLID-STATE POWER AMPLIFIERS

SC-C0020



CONCLUSIONS

CONCLUSIONS

- * 94 GHz PHASED-ARRAY TRANSMIT ANTENNA (WITH EIRP OF 50 dBW AND 1500 MODULES) MIGHT BE FEASIBLE, PROVIDING THAT HBTs WITH f_{max} OF 240 GHz AND POWER-ADDED EFFICIENCY IN EXCESS OF 30% (AT 94 GHz) BECOME AVAILABLE
- * AS A FIRST STEPPING STONE, A 60 GHz 4 X 4 ELEMENT SUBARRAY WITH "END FIRE" RADIATORS IS A SENSIBLE DEMONSTRATION VEHICLE

CONCLUSIONS (Cont.)

* FOR THE SUBARRAY, THE FOLLOWING KEY ISSUES MUST BE ADDRESSED:

- POWER DISSIPATION
- CHIP SIZE, COMPONENT PARAMETER UNIFORMITY, AND PROCESSING YIELD
- SUBARRAY INTEGRATION
- SURFACE WAVES, BLIND ANGLES AND CROSS-COUPLING WITHIN CIRCUITS AND BETWEEN RADIATORS
- GENERATION OF HIGH QUALITY CIRCULAR POLARIZATION

Materials Choice for Ballistic and Drift Transport Devices

S. Krisnamurphy

*SRI International
Menlo Park, CA*

MATERIALS CHOICE FOR BALLISTIC AND DRIFT TRANSPORT DEVICES

S. KRISNAMURTHY, A. SHER AND A.-B. CHEN
SRI INTERNATIONAL AUBURN UNIVERSITY
MENLO PARK, CA AUBURN, AL

TOPICS:

- FACTORS THAT INFLUENCE MAT. SELECTION

- QUANTITATIVE ESTIMATION

- RELATIVE EVALUATION OF VARIOUS
SEMICONDUCTORS COMPOUNDS & ALLOYS

- COMPARISON WITH EXPERIMENT

- FUTURE WORK

SEMICONDUCTOR ALLOY ENGINEERING FOR HIGH-SPEED DEVICES

PROJECT F49620-85-C-0103 SRI INTERNATIONAL

Objective

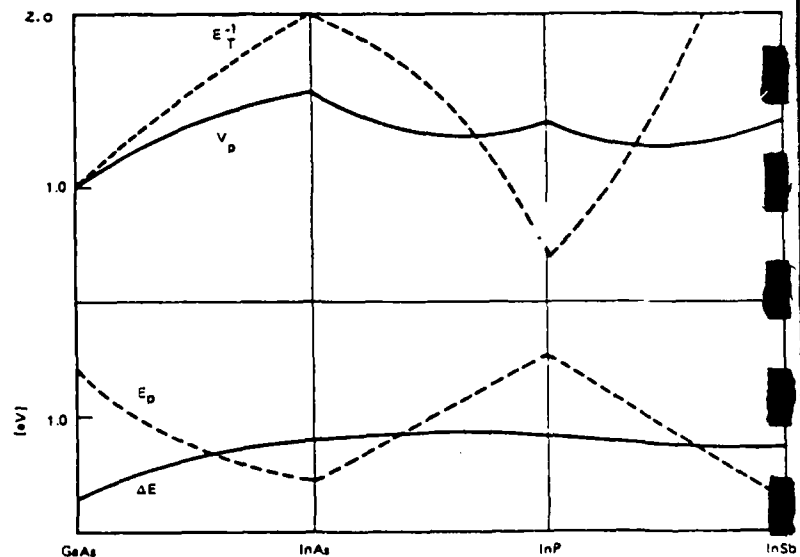
To develop a comprehensive theory of electronic transport properties of semiconductor materials with emphasis on optimal materials for High-speed devices

APPROACH

- Calculate computed band structure and scattering rate in the semiconductor alloys incorporating diagonal and off-diagonal disorder in the coherent potential approximation (CPA)
- Using simple models, calculate peak velocity and threshold field to study trends
- Once candidates for high-speed devices are chosen, carry out detailed quantum transport calculations

STATUS

- Full band structure
- Free of transport related parameters
- Quantitative understand of various mechanisms
- Faster solution to Boltzmann Equation
- Optimum base materials for draft and quasi-ballistic transport



FACTORS

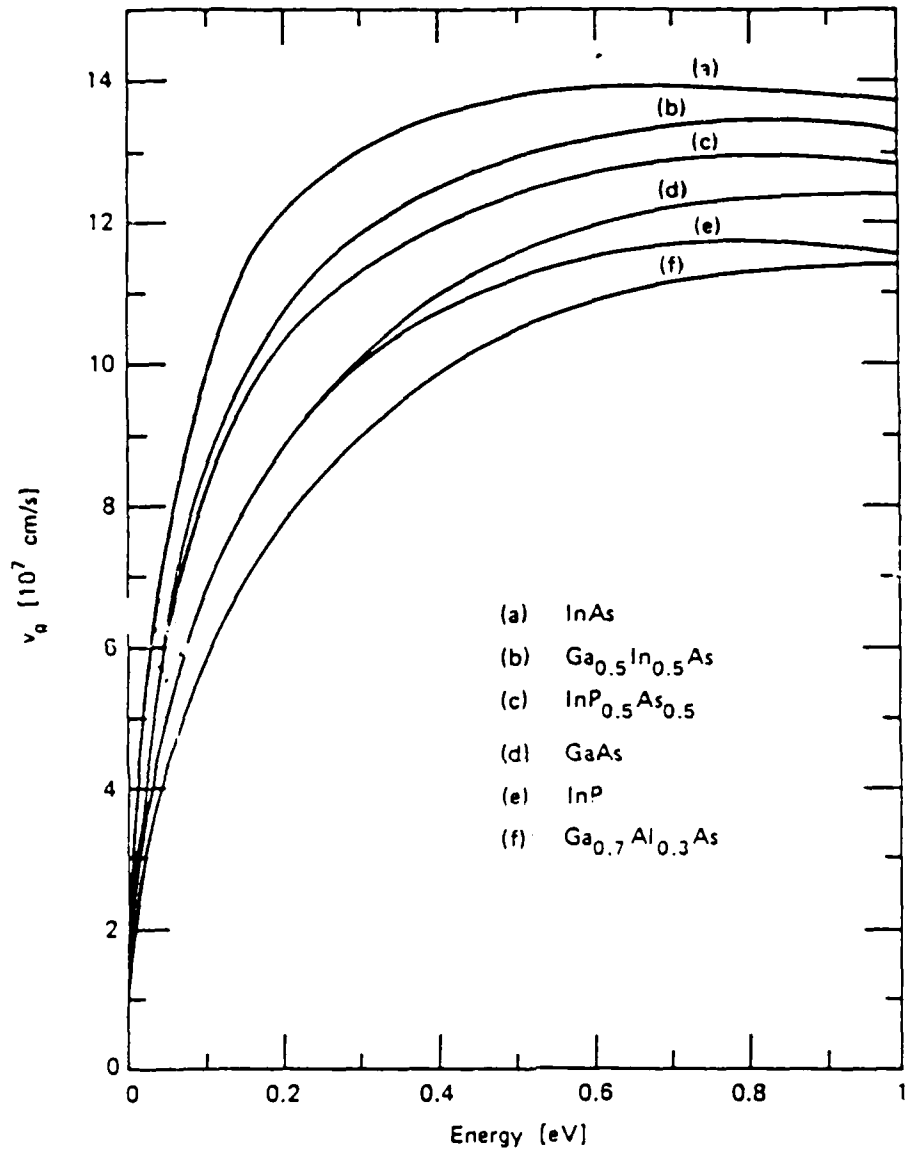
BALLISTIC MODE DRIFT MODE

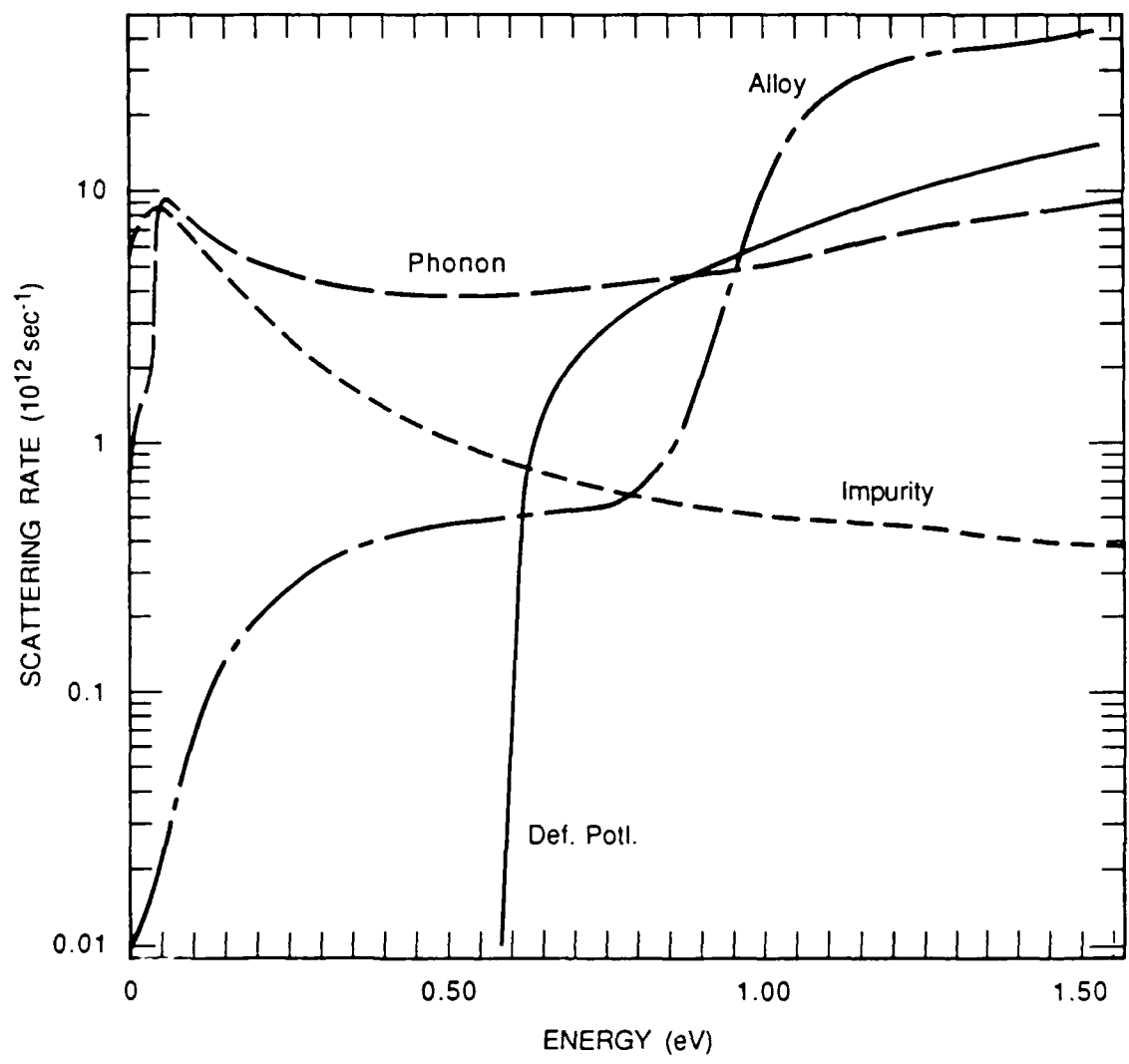
- BANDSTRUCTURE

- | | |
|---------------------------|---------------------------------|
| - GROUP VELOCITY | - PEAK DRIFT VELOCITY |
| - SCATTERING MECHANISMS | - THRESHOLD ELECTRIC FIELD |
| - INJECTION ENERGY | - SATURATED DRIFT VELOCITY |
| - INJECTION DIRECTION | - Γ -L ENERGY SEPARATION |
| - ELECTRIC FIELD | - ENERGY GAP |
| - VELOCITY MEAN FREE PATH | - SCATTERING MECHANISMS |
| | - v-E CURVES |

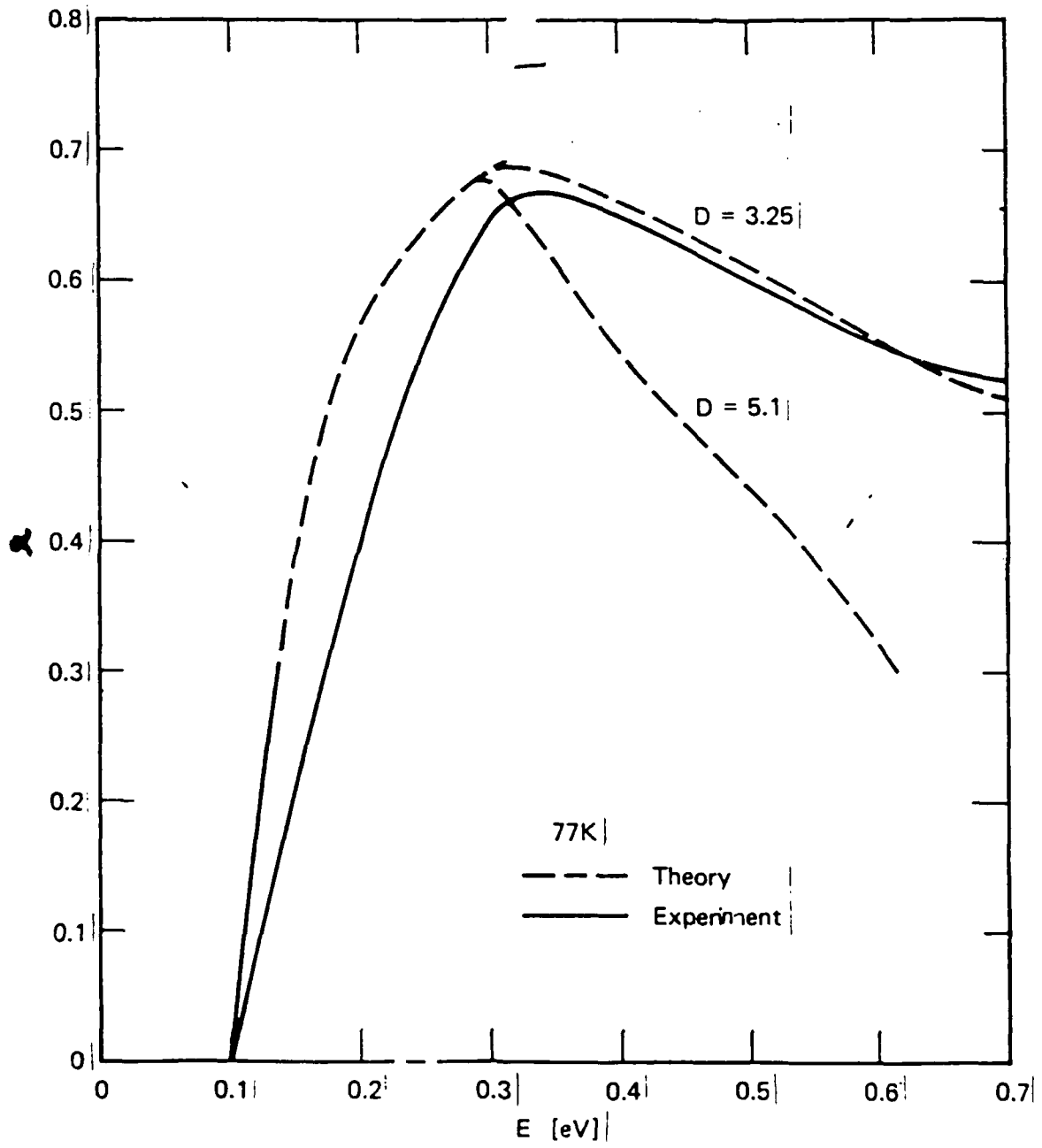
INTRA-and INTER-VALLEY SCATTERING MECHANISMS

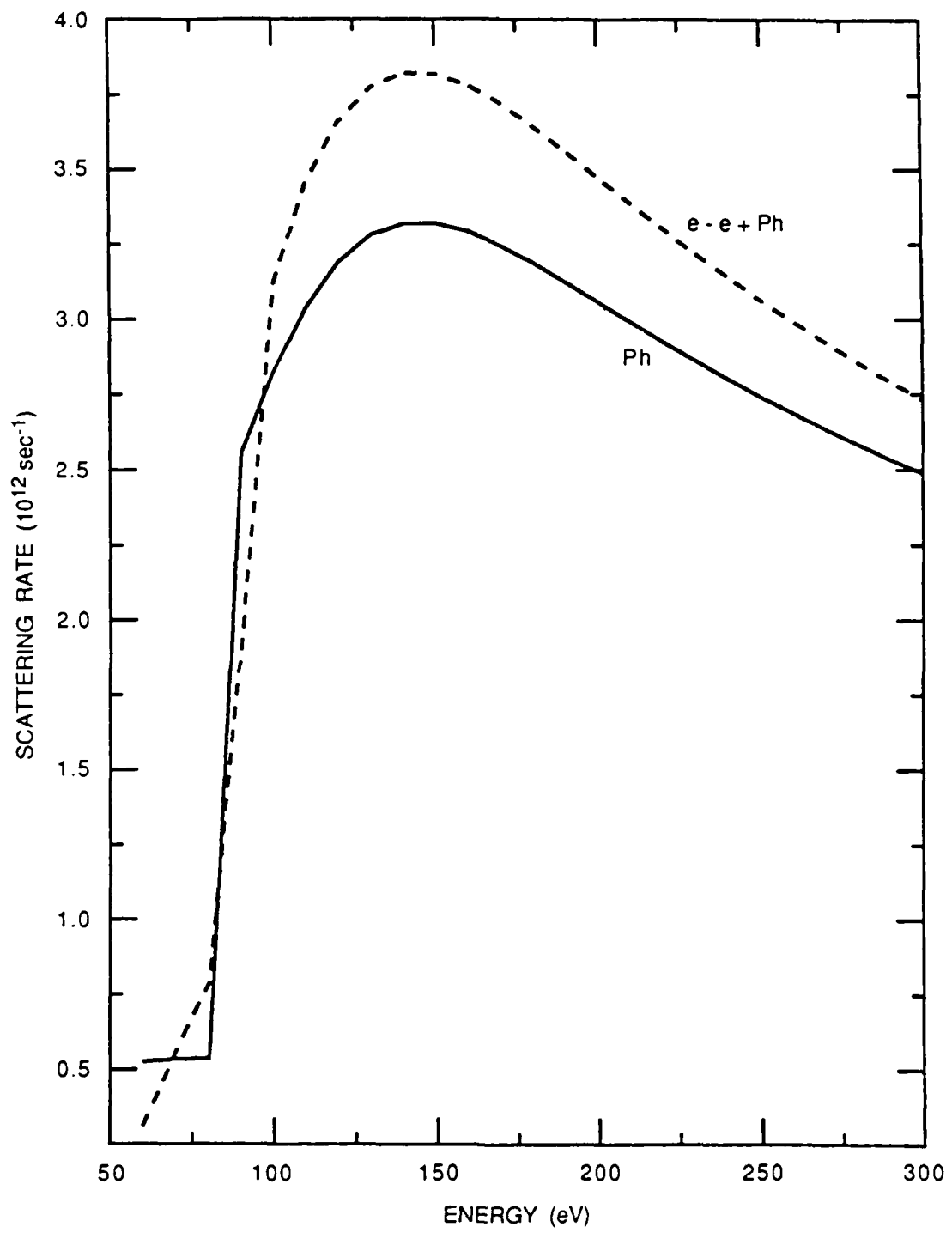
- IONIZED IMPURITIES
- PHONONS IN COMPOUNDS AND ALLOYS
 - TYPES
 - ACOUSTIC
 - OPTIC
 - COUPLING CONSTANTS
 - DEFORMATION POTENTIAL
 - POLAR
- ELECTRON-ELECTRON
- ALLOY DISORDER
- IMPACT IONIZATION



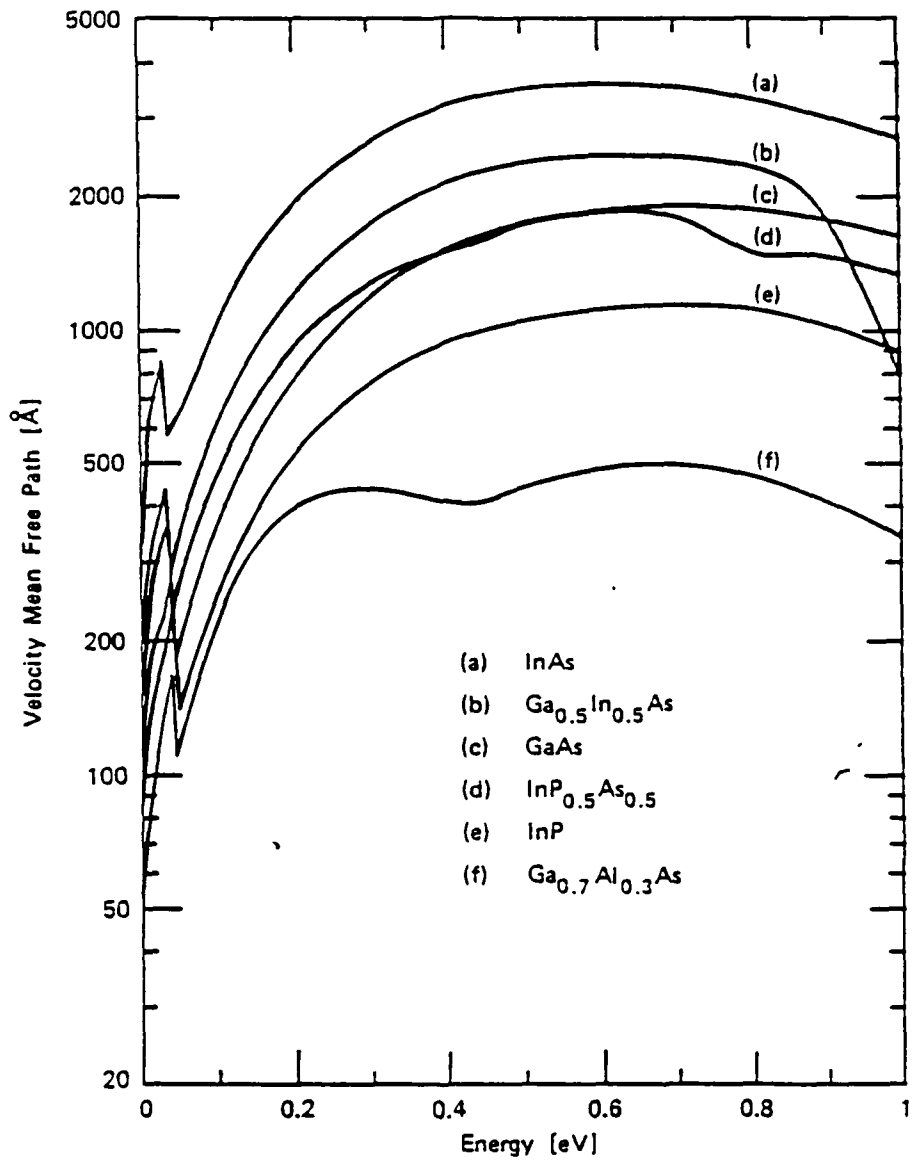


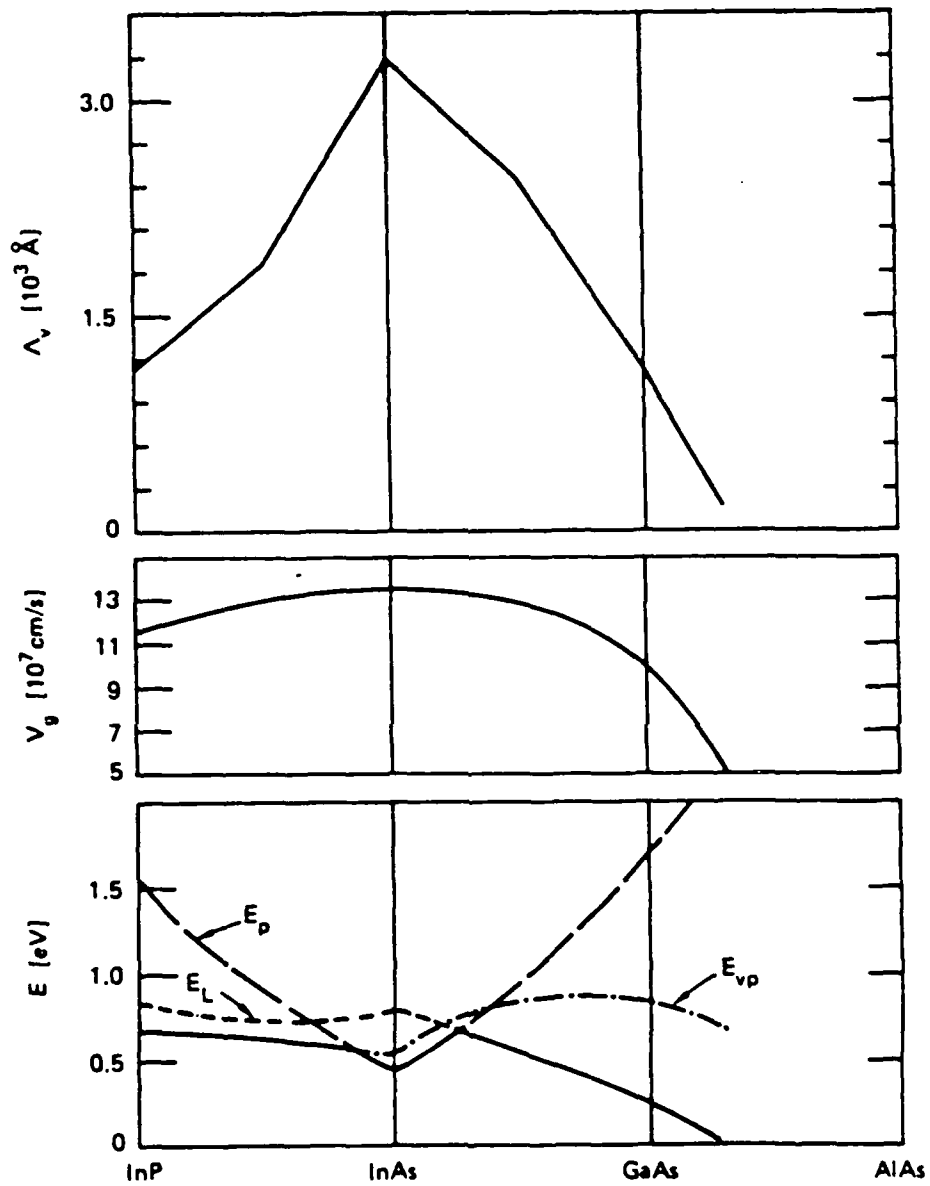
GaAs





GaAs





DRIFT TRANSPORT

- Solution to Boltzmann equation by eigen value method.

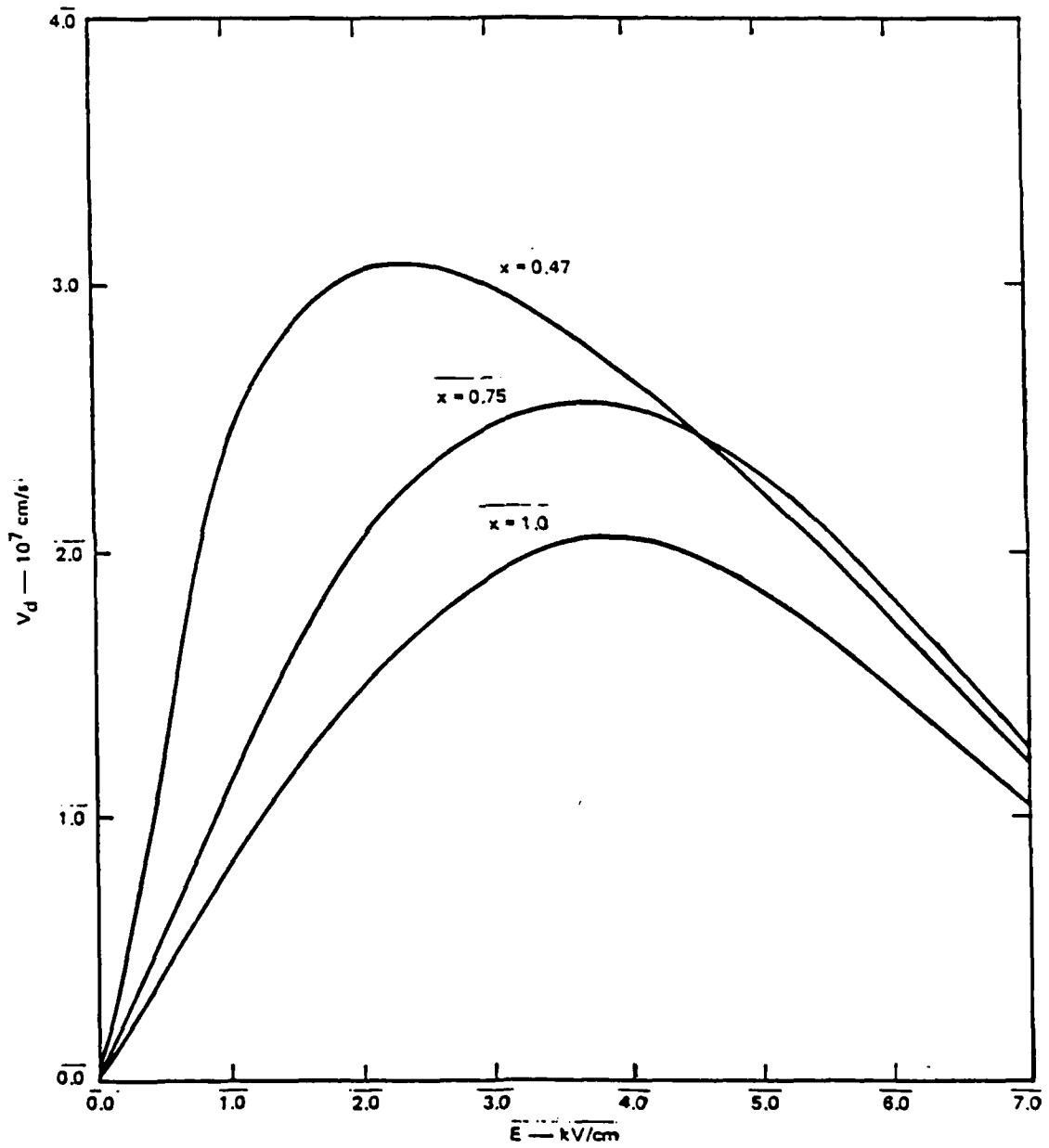
$$\frac{eE}{h} \frac{\partial}{\partial k_x} f(\vec{k}) - \sum_{k'} S(k, k') f(k') + \sum_k S(k', k) f(k) = 0$$

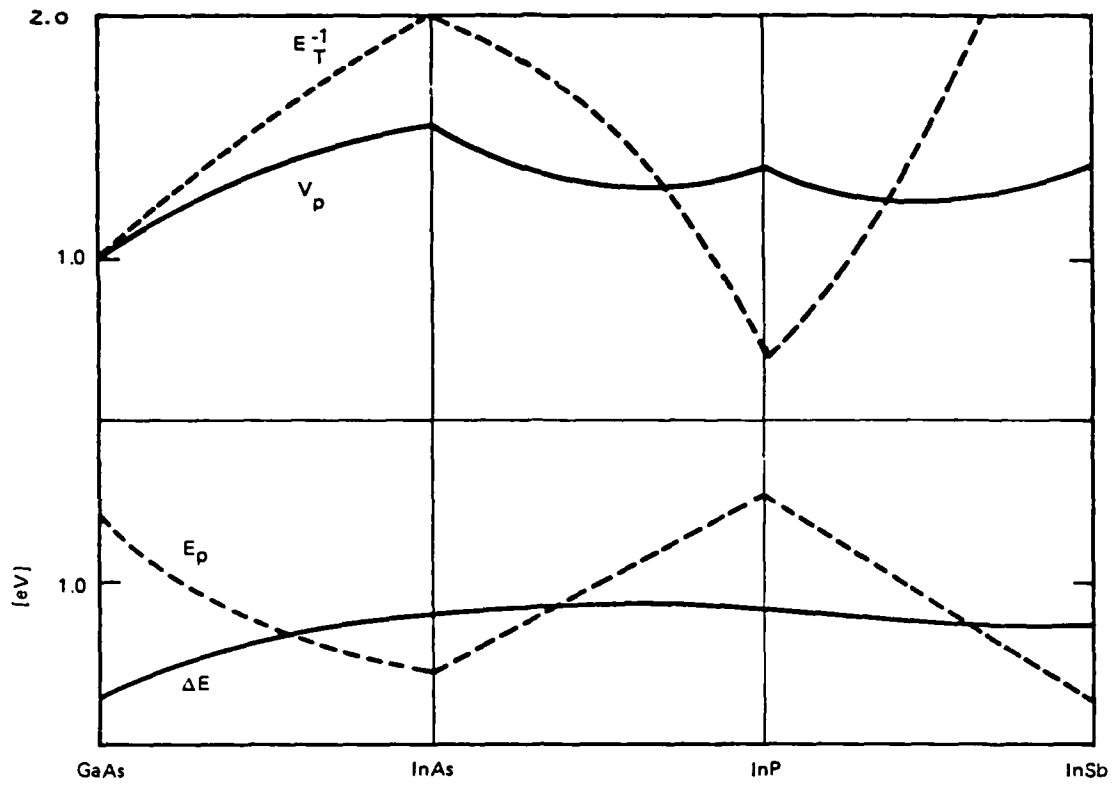
$$f(k) = \sum_n C_n \phi_n(k)$$

$$\Rightarrow \underline{M}C = 0$$

Eigen vector corresponding to zero eigen value gives the expansion coefficients C_n .

$G\alpha_x I_{n_{1-x}} A_s.$





STATUS

- FULL BAND STRUCTURE
- FREE OF TRANSPORT RELATED PARAMETERS
- QUANTITATIVE UNDERSTANDING OF VARIOUS MECHANISMS
- FASTER SOLUTION TO BOLTZMANN EQUATION
- OPTIMUM BASE MATERIALS FOR DRAFT AND QUASI-BALLISTIC TRANSPORT

FUTURE WORK FOR DEVICE DESIGN

- EMITTER SIDE
 - INJECTION "BALLISTIC" DEVICES
 - INJECTION DRIFT DEVICES
 - INTERFACE

- COLLECTOR SIDE
 - REDUCE SCATTERING
 - INTERFACE

- LARGE CURRENTS
 - SPACE CHARGE
 - POTENTIAL VARIATION IN THE BASE
 - SELF CONSISTENT SOLUTION TO POISSON AND BOLTZMANN EQUATIONS

FUTURE WORK (contd.)

- 2D NATURE
 - ALLOY SEGREGATION
 - COMPOSITION DEPENDS ON LOCATION OF THE LAYER
 - ORDER/DISORDER TRANSITION
 - ELECTRONIC STRUCTURE AND TRANSPORT

 - EFFECTIVE MASS APPROXIMATION NOT VALID
 - QUANTUM TRANSPORT
 - MATCHING 2D BLOCK STATES
 - GREENS FUNCTION APPROACH
 - SCATTERING MECHANISM
 - WIGNER FUNCTIONS

- DEVICE CHARACTERISTICS
 - TRANSANDUCTANCE

 - CUT OFF FREQUENCY

 - FREQUENCY DEPENDENT CURRENT GAIN

 - POWER OUTPUT

 - SELECT MATERIALS AND GEOMETRIES TO OPTIMIZE DEVICE CHARACTERISTICS

*AllnAs-GalnAs HEMTs
FOR HIGH SPEED APPLICATIONS*

U. K. Mishra

*North Carolina State University
Raleigh, NC*

AlInAs-GaInAs HEMTs

FOR HIGH SPEED APPLICATIONS

U.K. Mishra*, A.S. Brown, and J.F. Jensen**

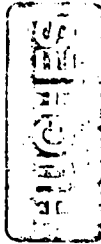
* Now at N.C. State University, Raleigh, NC

** Now at Army Research Office, Durham, NC



RESEARCH LABORATORIES

ACKNOWLEDGEMENTS



RESEARCH LABORATORIES

L. Jelloian
M. Melendes
C. Hooper
M. Pierce
D. Pierson
M. Thompson
L. McCray

S. Rosenbaum
S. Vaughn
L. Larson

MANAGERMENT SUPPORT: M.J. Delaney, P.T. Greiling, C.F. Krumm

OUTLINE



RESEARCH LABORATORIES

- ADVANTAGES AND DISADVANTAGES OF AlInAs-GaInAs HEMTs AND HBTs.
- AlInAs-GaInAs HEMTs (RELATIVE TO GaAs BASED HEMTs)
 - DEVICE RESULTS
 - CIRCUIT RESULTS
- CONCLUSIONS

AlInAs-GaNAs HBTs



RESEARCH LABORATORIES

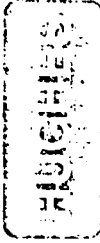
ADVANTAGES

- EXCELLENT THRESHOLD CONTROL
- COMPATIBLE WITH OTHER OPTO-ELECTRONIC ELEMENTS
- EXCELLENT DRIVE CAPABILITY
⇒ LOW FAN-OUT SENSITIVITY

DISADVANTAGES

- LOW COLLECTOR BREAKDOWN
- DIFFICULTY IN GROWING AlInAs
- LARGE NUMBER OF PROCESSING STEPS
- VERTICAL DEVICES ⇒ HIGH PARASITICS

AlInAs-GaInAs HEMT's



RESEARCH LABORATORIES

ADVANTAGES

- EXCELLENT LOW NOISE DEVICE
- SURFACE ORIENTED DEVICE
 - ⇒ Low Parasitics
- EXCELLENT DRIVE CAPABILITY
 - ⇒ Low Fan-Out Sensitivity in Circuits
- EXCELLENT HIGH FREQUENCY CHARACTERISTICS
- FEW MASK LEVELS

DISADVANTAGES

- LOW GATE BREAKDOWN
- POOR THRESHOLD CONTROL
- DIFFICULTY IN GROWING AlInAs

ADVANTAGES OF Ga_{0.47}In_{0.53}As THIN FILMS

18436-2

HIGH ELECTRON MOBILITY

*H₂, Pd

$$\left[\begin{array}{l} \mu(\text{Ga}_{0.47}\text{In}_{0.53}\text{As}) = 13,000 \text{ cm}^2\text{V}^{-1}\text{s}^{-1} \\ \mu(\text{GaAs}) = 8,000 \text{ cm}^2\text{V}^{-1}\text{s}^{-1} \end{array} \right]$$

LARGE Γ -L VALLEY SEPARATION

$$\left[\begin{array}{l} \Delta\Gamma\text{-L}(\text{Ga}_{0.47}\text{In}_{0.53}\text{As}) = 0.55\text{eV} \\ \Delta\Gamma\text{-L}(\text{GaAs}) = 0.31\text{eV} \end{array} \right]$$

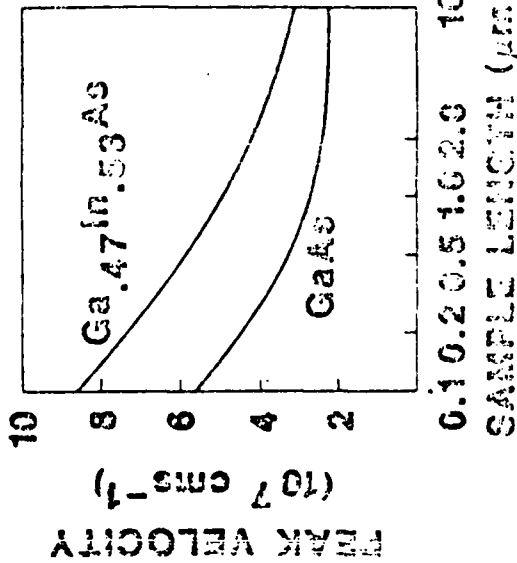
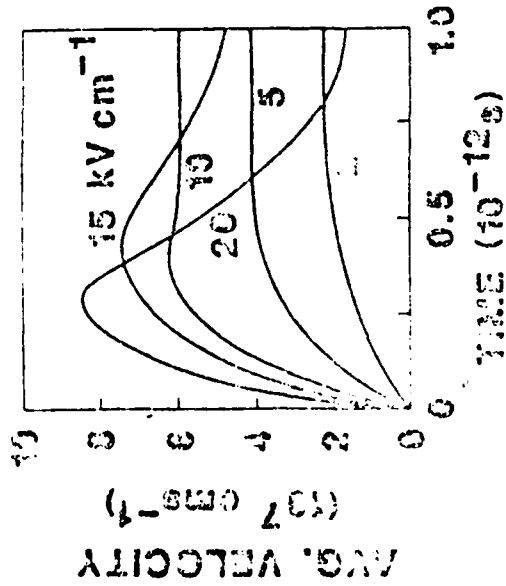
HIGH PEAK VELOCITY

*Ga⁺, In⁺

$$\left[\begin{array}{l} V_p(\text{Ga}_{0.47}\text{In}_{0.53}\text{As}) = 2.7 \times 10^7 \text{ cm s}^{-1} \\ V_p(\text{GaAs}) = 2 \times 10^7 \text{ cm s}^{-1} \end{array} \right]$$

STRONGER VELOCITY OVERSHOOT

*Ga⁺, In⁺



(NAG, et., al.)

AUGUST 1968

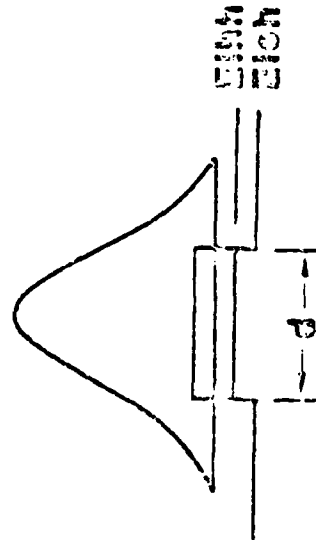
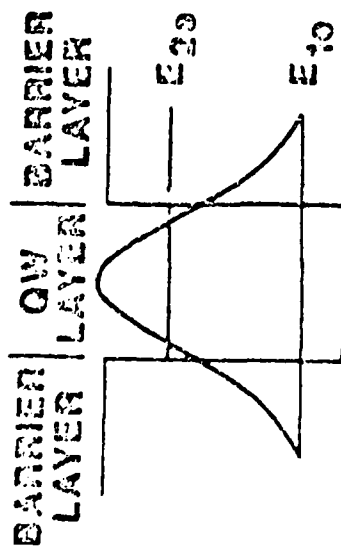
DIFFICULTIES IN GROWING AlInAs

HUGHES

- Al-Al and In-In bonds have widely different bond strengths
- High As₄ overpressure is needed to prevent In desorption
(reduces cation mobility)
- Low growth temperature to prevent In desorption
(reduces cation mobility)
- Alloy tends to cluster into component binaries

PHOTOLUMINESCENCE CHARACTERIZATION OF QUANTUM WELLS

FIGURE 1



RECOMBINATION EMISSION ENERGY
DETERMINED BY ΔE_{20} AND d

FULL WIDTH HALF MAXIMUM (FWHM)
DETERMINES:

- QUALITY OF WELL ($d > 100 \text{ \AA}$)
- QUALITY OF INTERFACE
($20 < d < 100 \text{ \AA}$)
- QUALITY OF CARRIER ($d < 20 \text{ \AA}$)
- ASSUMING THE EXCITON RADIUS
($\sim 200 \text{ \AA}$) IS $\leq d$ (THE ISLAND SIZE)

MATERIAL QUALITY

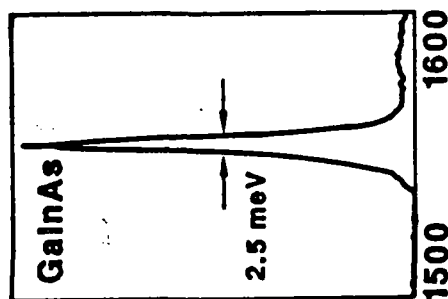
18430-10

GaInAs

11 K PL LINEWIDTH OF 2.5 meV

$$N_d - N_a = 2 \times 10^{15} \text{ cm}^{-3}$$

$$\mu(300 \text{ K}) = 8000 - 10000 \text{ cm}^2/\text{V}\cdot\text{s}$$

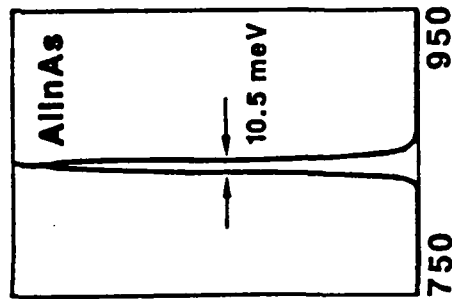


AlInAs

11 K PL LINEWIDTH OF 10.5 meV

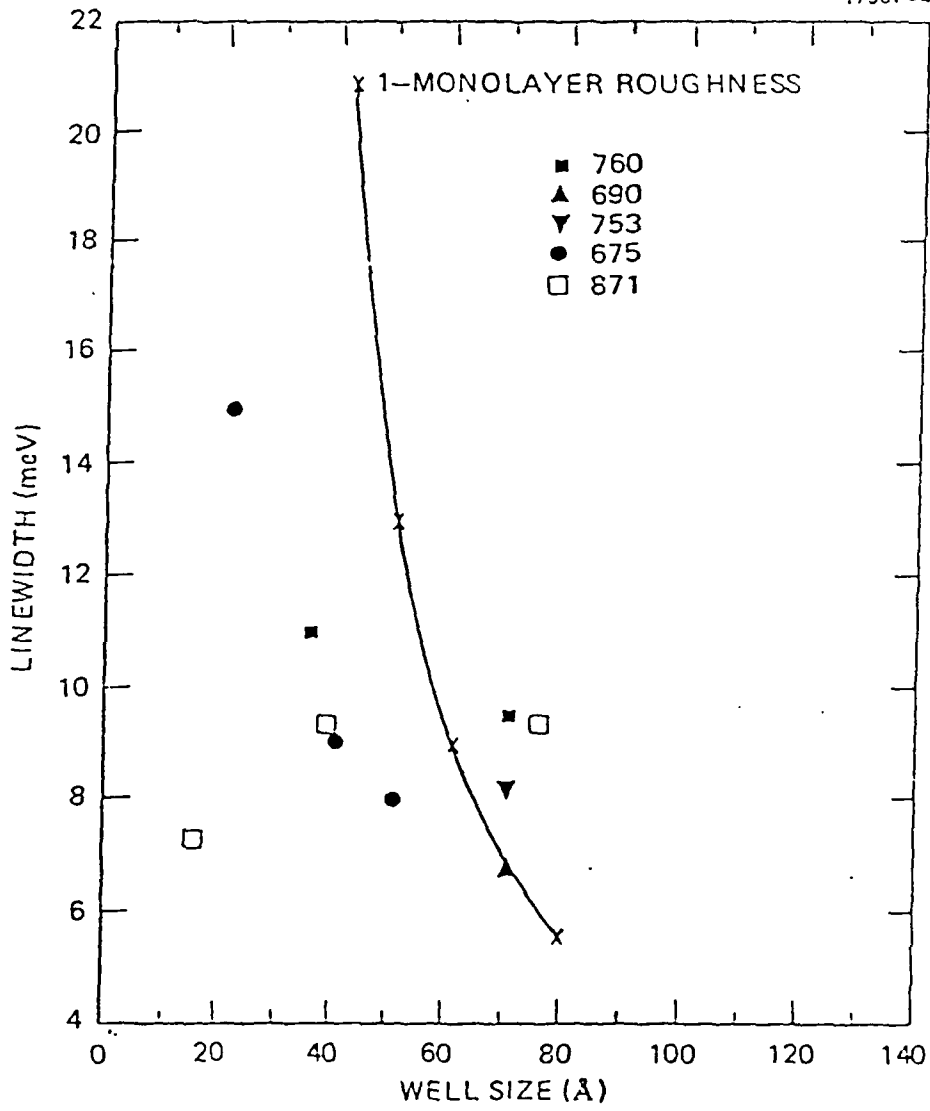
$$N_d - N_a = 1 \times 10^{15} \text{ cm}^{-3}$$

$$\mu(300 \text{ K}) = 1600 \text{ cm}^2/\text{V}\cdot\text{s}$$



WAVELENGTH (nm)

AUGUST 1988

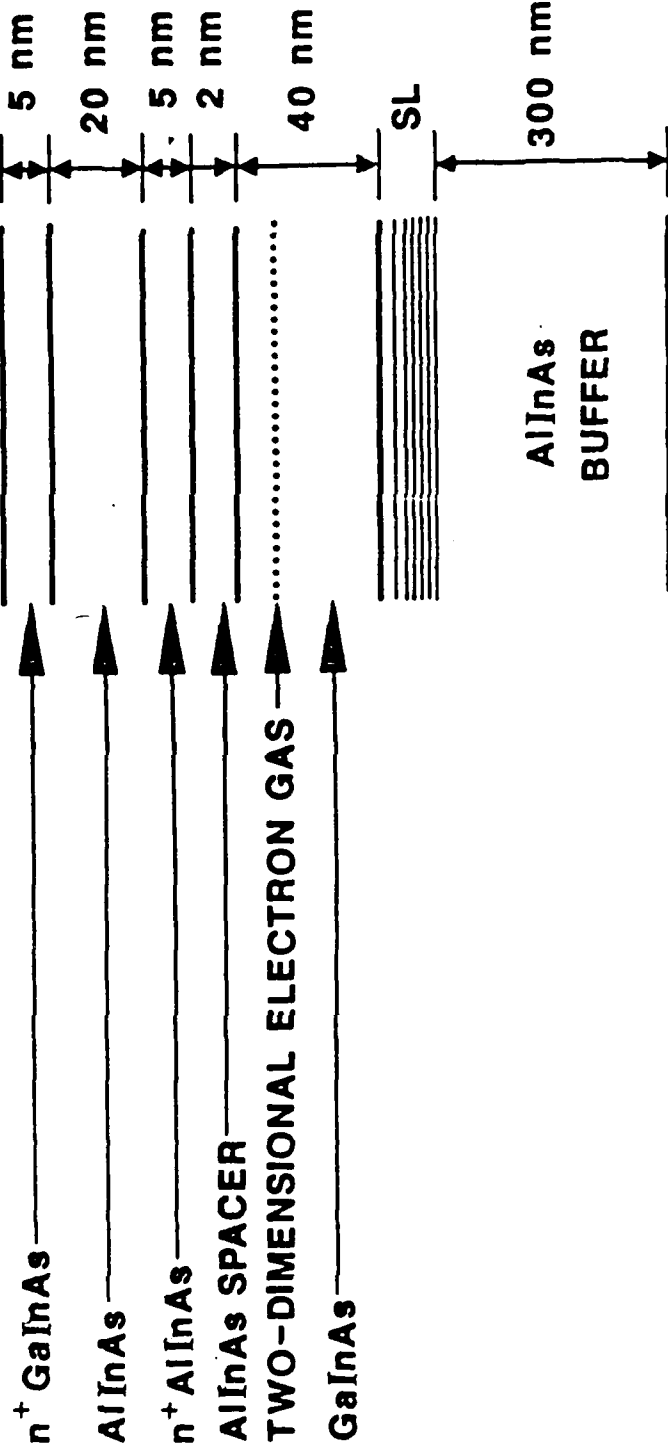




GaInAs/AlInAs HEMT LAYERED STRUCTURE

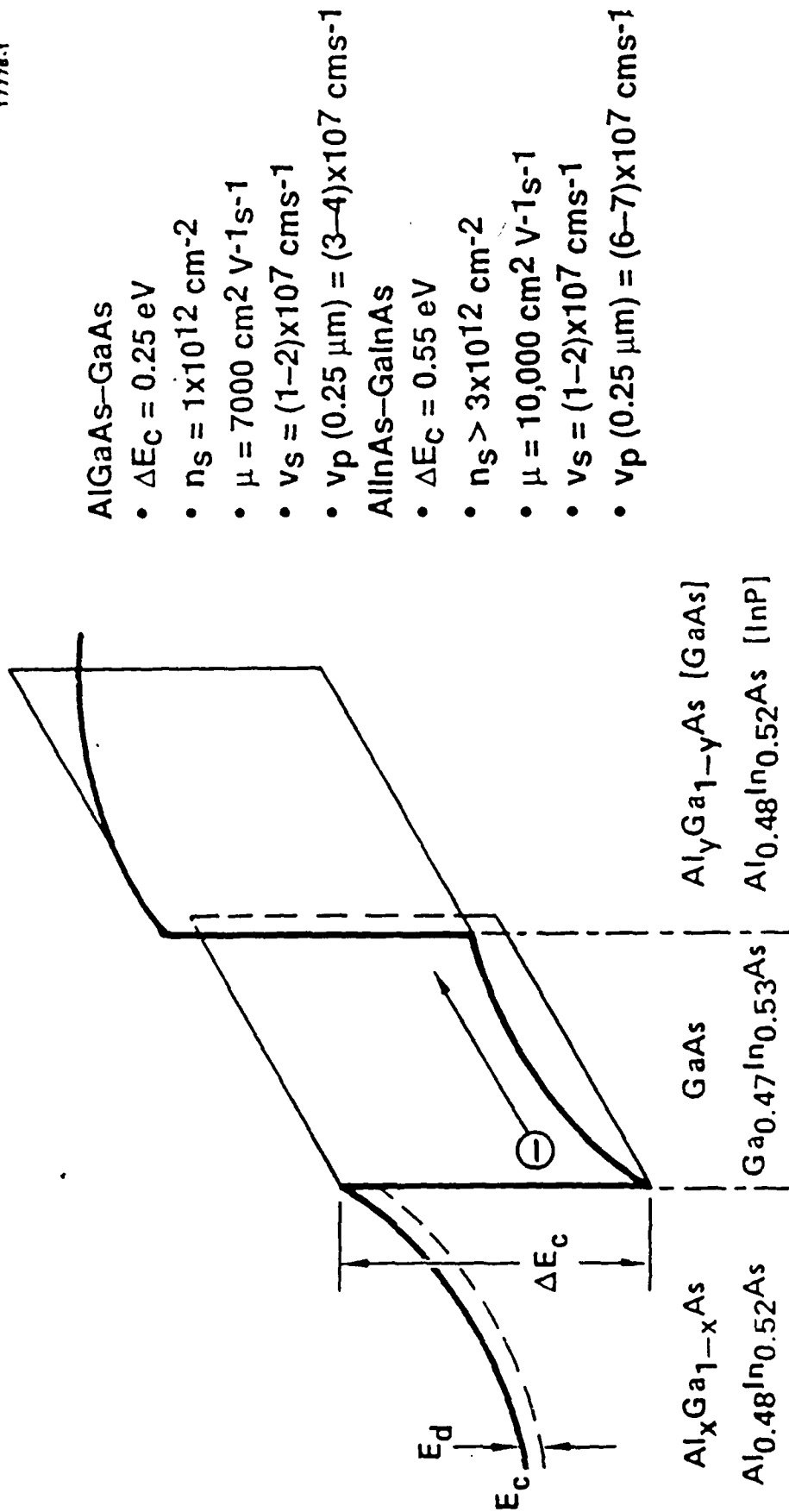
PROJECT 59

18430-33



COMPARISON OF AlGaAs-GaAs AND AlInAs-GaInAs HETEROSTRUCTURES

17778-1



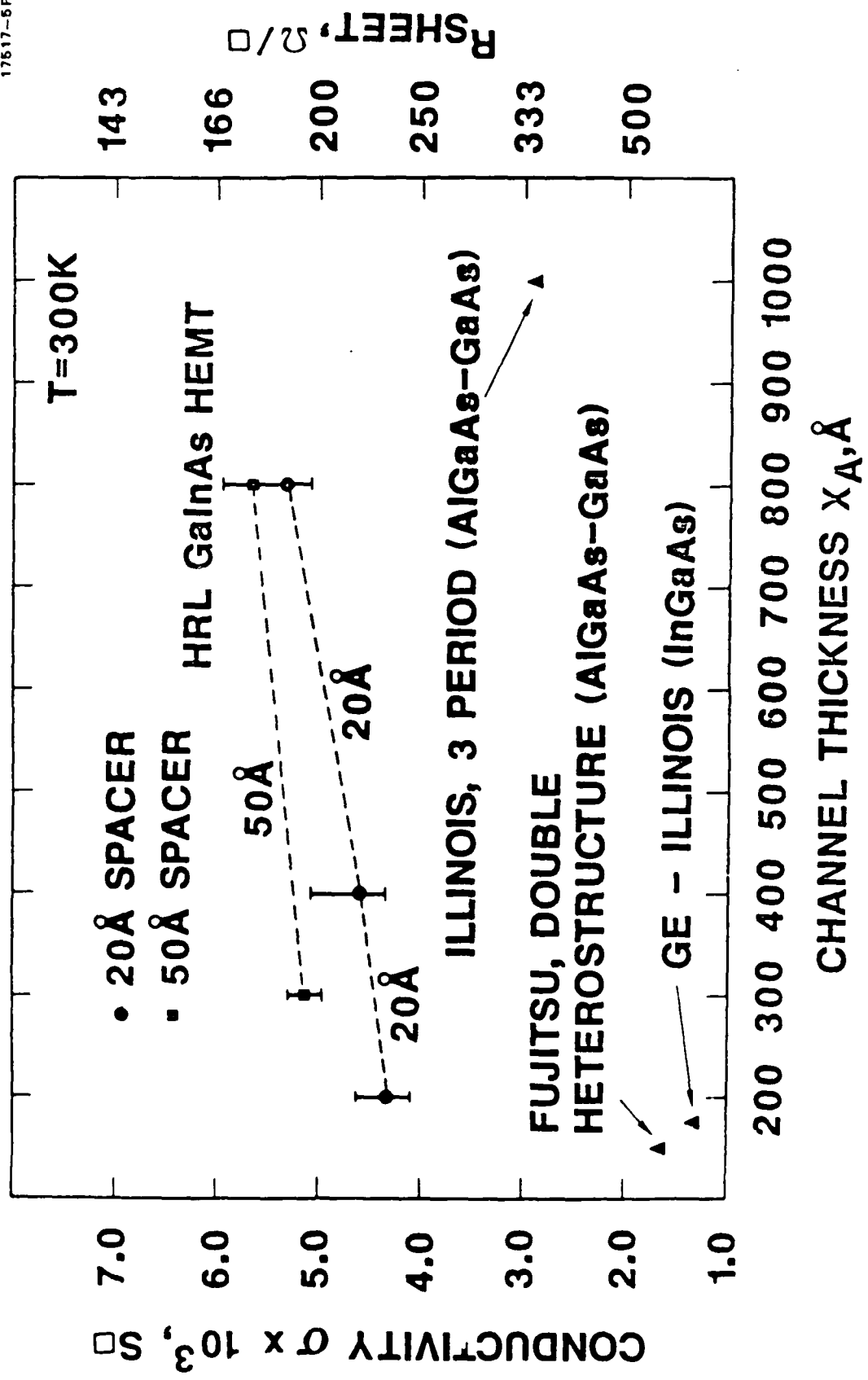
AUGUST 1988

CONDUCTIVITY VS. CHANNEL THICKNESS



PROJECT 59

17517-5R1



STRAINED GaInAs HEMT



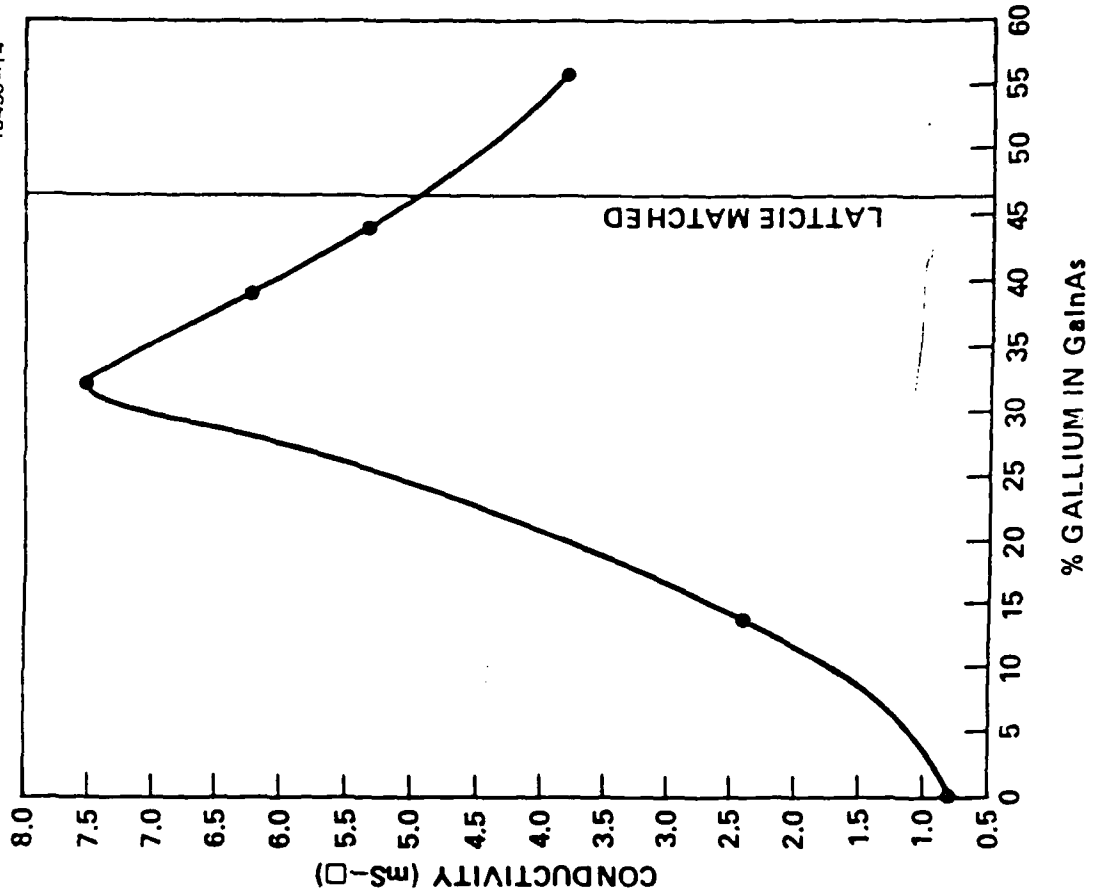
PROJECT 59

18430-14

STRAINED GaInAs-AlInAs HEMT

Ge .47-y In .53-y As CONTACT	$n = 2 \times 10^{18}$	100A
Al .48+u In .52-u As SCHOTTKY		200A
Al .48+u In .52-u As DONOR	$n = 4 \times 10^{18}$	125A
Al .48+u In .52-u As SPACER		20A
Ge .47-y In .53-y As CHANNEL		400A
Al .48 In .52 As BUFFER		2500A

InP SEMI-INSULATING SUBSTRATE



AUG 1988

WHY THE AlInAs-GaInAs HEMT FOR mm-WAVE LOW NOISE APPLICATIONS

C16305-2R1

- $F_{\min} = 1 + K_f \frac{f}{f_T} \sqrt{g_m(R_g + R_s)}$
- LARGE $\Gamma - L$ SEPARATION IN Ga_{.47}In_{.53}As ($\Delta\Gamma - L = 0.55$ eV)
LEADS TO LOW INTERVALLEY NOISE ($K_F \downarrow$)
- LOW SHEET RESISTANCE OF THE TWO DIMENSIONAL
ELECTRON GAS ($\rho \approx 150 \Omega/\square$) REDUCES THERMAL NOISE
- HIGH ELECTRON VELOCITY IN SHORT CHANNELS GaInAs
($V_p \sim 6.7 \times 10^7$ cm-s⁻¹) ($f_T \uparrow, g_m \uparrow$)

EPITAXIAL LAYER DESIGN OF $\text{Al}_{.48}\text{In}_{.52}\text{As} / \text{Ga}_{.47}\text{In}_{.53}\text{As}$ AND $\text{Al}_{.48}\text{In}_{.52}\text{As} / \text{Ga}_{.38}\text{In}_{.62}\text{As}$ HEMTs

$\text{Ga}_{.47}\text{In}_{.53}\text{As}$	CONTACT	$(n = 5 \times 10^{18})$	70Å
$\text{Al}_{.48}\text{In}_{.52}\text{As}$	SCHOTTKY		315Å
$\text{Al}_{.48}\text{In}_{.52}\text{As}$	DONOR	$(n = 5 \times 10^{18})$	80Å
$\text{Al}_{.48}\text{In}_{.52}\text{As}$	SPACER		15Å
$\text{Ga}_{.47}\text{In}_{.53}\text{As}$	CHANNEL		360Å
	SUPERLATTICE		360Å
AlInAs	BUFFER		2250Å
	InP:Fe		

μ (300K) = 9300 $\text{cm}^2\text{V}^{-1}\text{S}^{-1}$
 $n_s \geq 3 \times 10^{12} \text{ cm}^{-2}$

$\text{Ga}_{.47}\text{In}_{.53}\text{As}$	CONTACT	$(n = 5 \times 10^{18})$	cm^{-3}	70Å
$\text{Al}_{.48}\text{In}_{.52}\text{As}$	SCHOTTKY			200Å
$\text{Al}_{.48}\text{In}_{.52}\text{As}$	DONOR	$(n = 5 \times 10^{18})$	cm^{-3}	75Å
$\text{Al}_{.48}\text{In}_{.52}\text{As}$	SPACER			15Å
$\text{Ga}_{.38}\text{In}_{.62}\text{As}$	CHANNEL			270Å
	SUPERLATTICE			360Å
$\text{Al}_{.48}\text{In}_{.52}\text{As}$	BUFFER			2250Å
InP	SEMI-INSULATING SUBSTRATE			

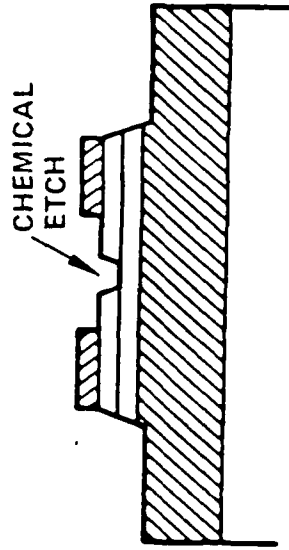
μ (300K) = 10,000 $\text{cm}^2\text{V}^{-1}\text{S}^{-1}$
 $n_s \geq 4 \times 10^{12} \text{ cm}^{-2}$

SUPERFET: PROCESS OUTLINE

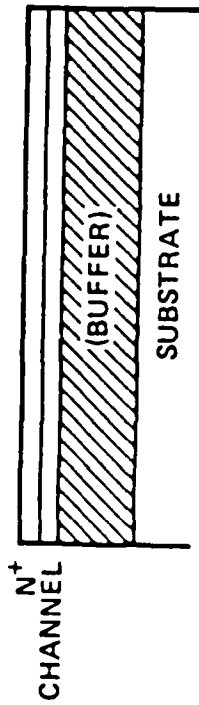


14754-3

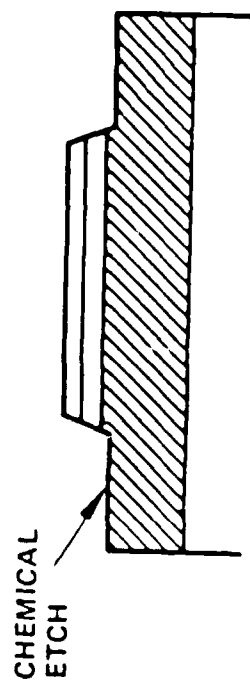
4. E-BEAM GATE RECESS - ESTABLISHES V_{PO}



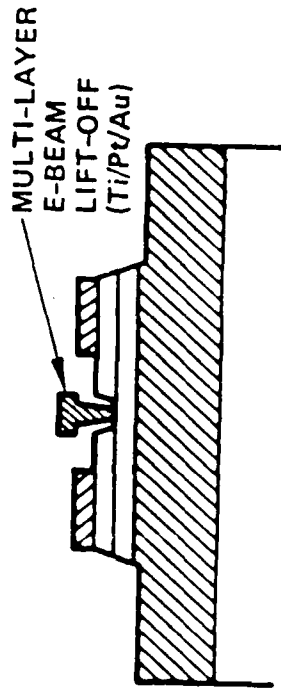
1. MBE LAYER GROWTHS - MULTI-EPI OR HEMT



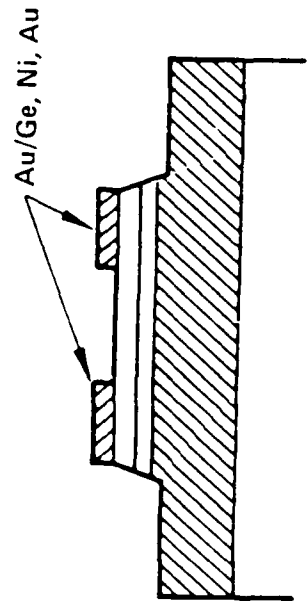
2. MESA ISOLATION



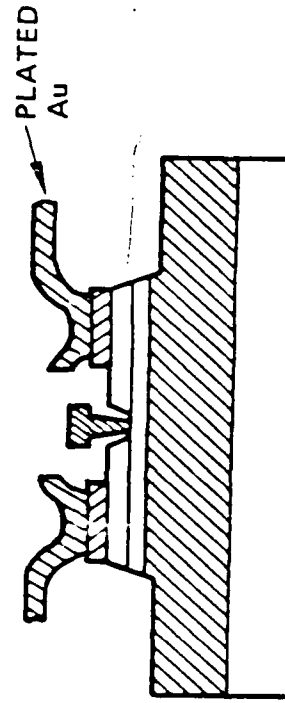
5. E-BEAM T-GATE FABRICATION



3. OHMIC CONTACTS



6. AIRBRIDGE FABRICATION



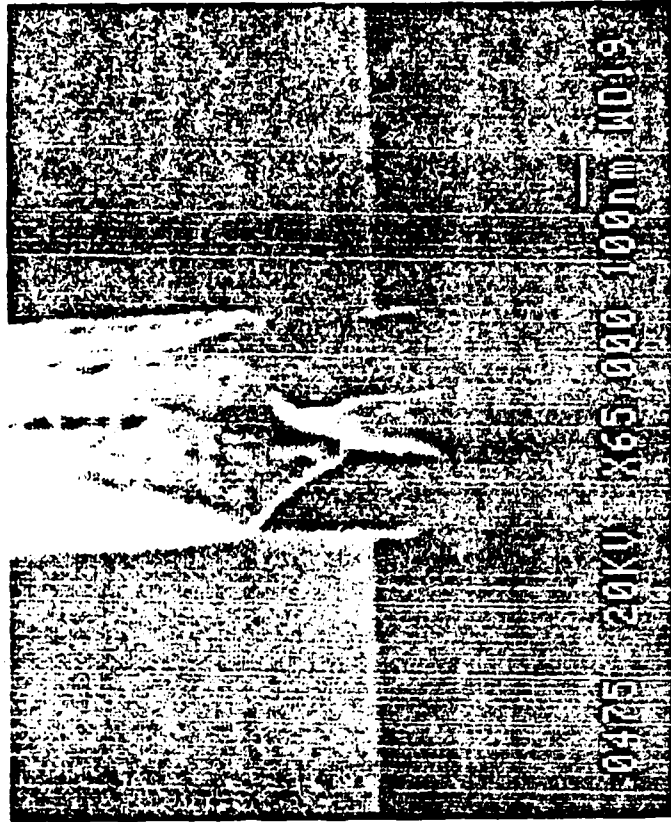
JANUARY 1985

0.1 μm T-GATE PROCESS



17564-11R1

- 4570 Å Ti-Pt-Au METALIZATION
- 0.1 μm T-GATE
- 7.5 INCREASE IN GATE CROSS-SECTIONAL AREA



OCTOBER 1987

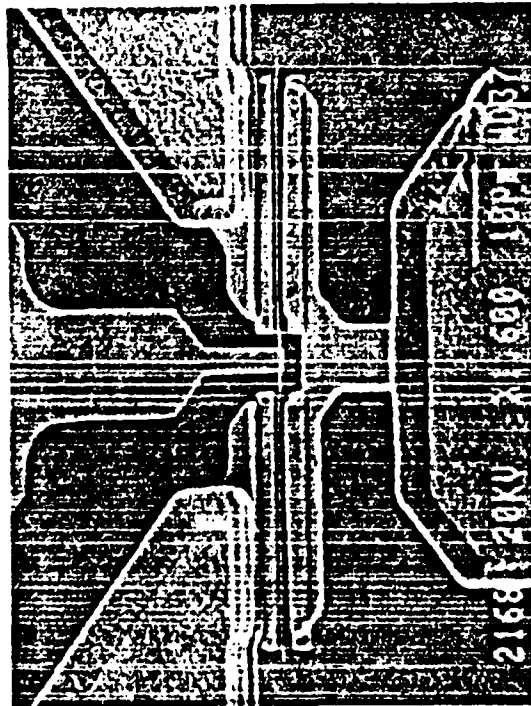
CLASSIFICATION

GainAs HEMT V-BAND DEVICE DESIGN

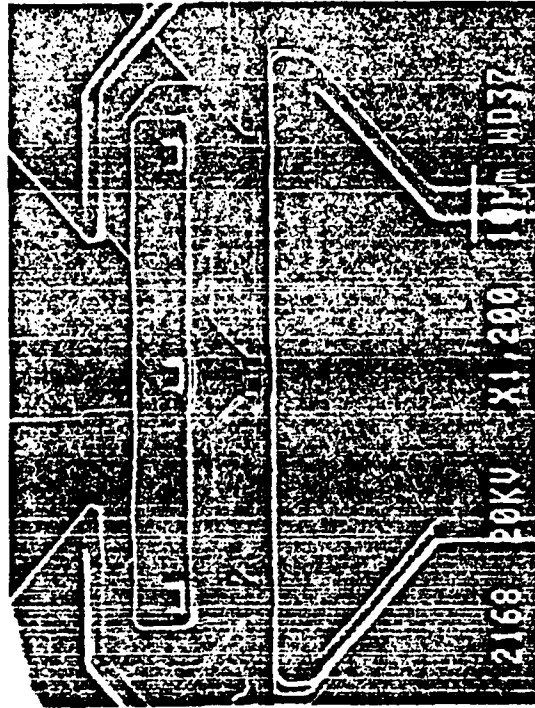
PROJECT 59



18430-18



50 μm WIDE DEVICE
T GATE FEED

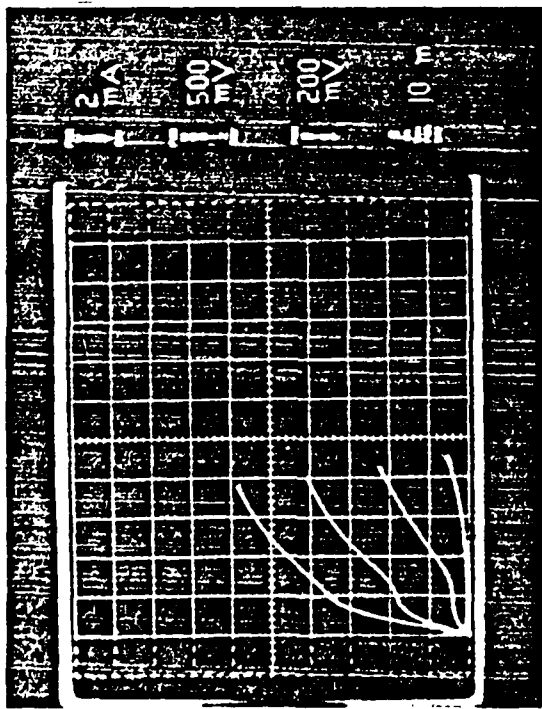


75 μm WIDE DEVICE
 π GATE FEED

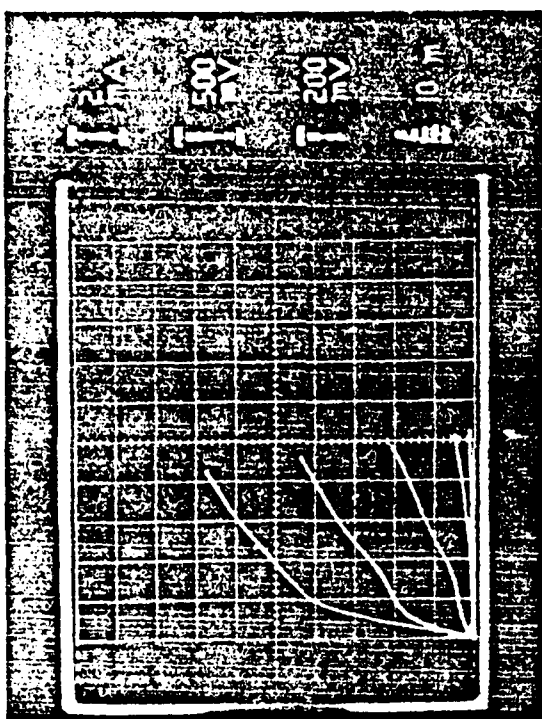
AUG 1988

DC I-V CHARACTERISTICS OF 0.2 μm AND 0.1 μm GATE LENGTH HEMT'S

18309-7R1



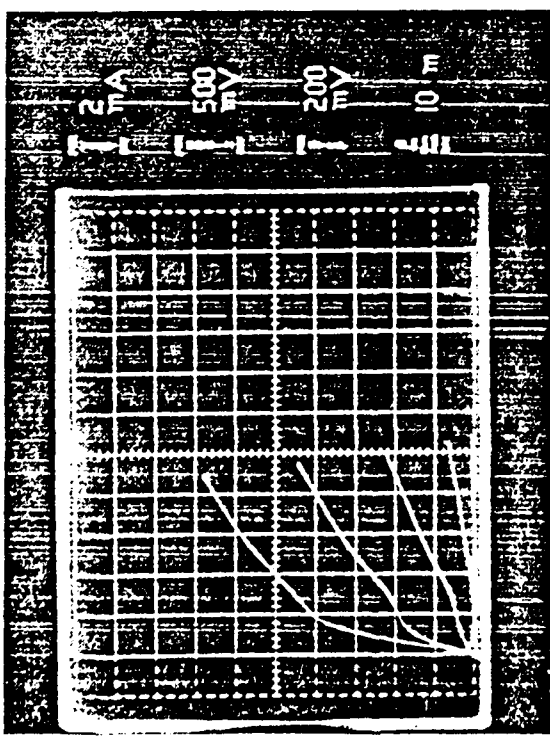
$g_m = 800 \text{ mS/mm}$
 $W = 25 \mu\text{m}$



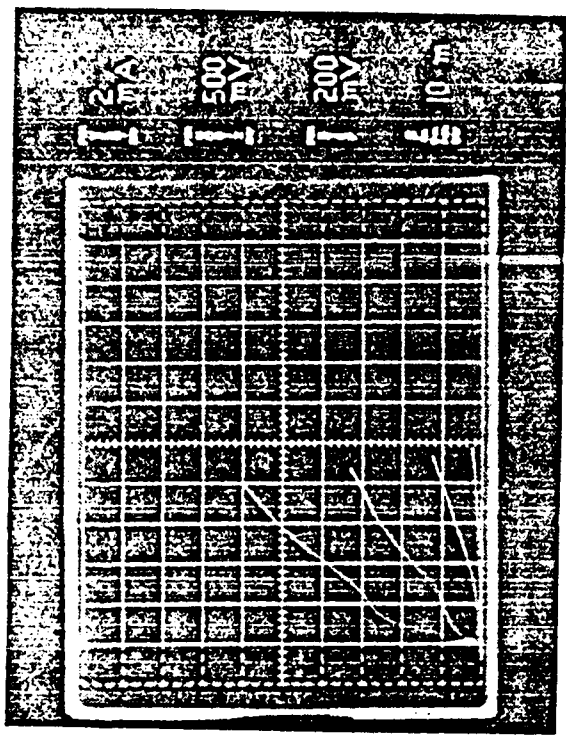
$g_m = 1080 \text{ mS/mm}$
 $W = 25 \mu\text{m}$

AUGUST 1988

DC I-V CHARACTERISTICS OF 0.1 μm GATE LENGTH
 $\text{Al}_{.48}\text{In}_{.52}\text{As} / \text{Ga}_{.47}\text{In}_{.53}\text{As} \text{ \& \ } \text{Al}_{.48}\text{In}_{.52}\text{As} / \text{Ga}_{.38}\text{In}_{.62}\text{As}$ HEMTs



$g_m = 1000 \text{ mS}/\mu\text{m}$
 $V_{FB} = 0.4 \text{ V}$
 $W = 25 \mu\text{m}$

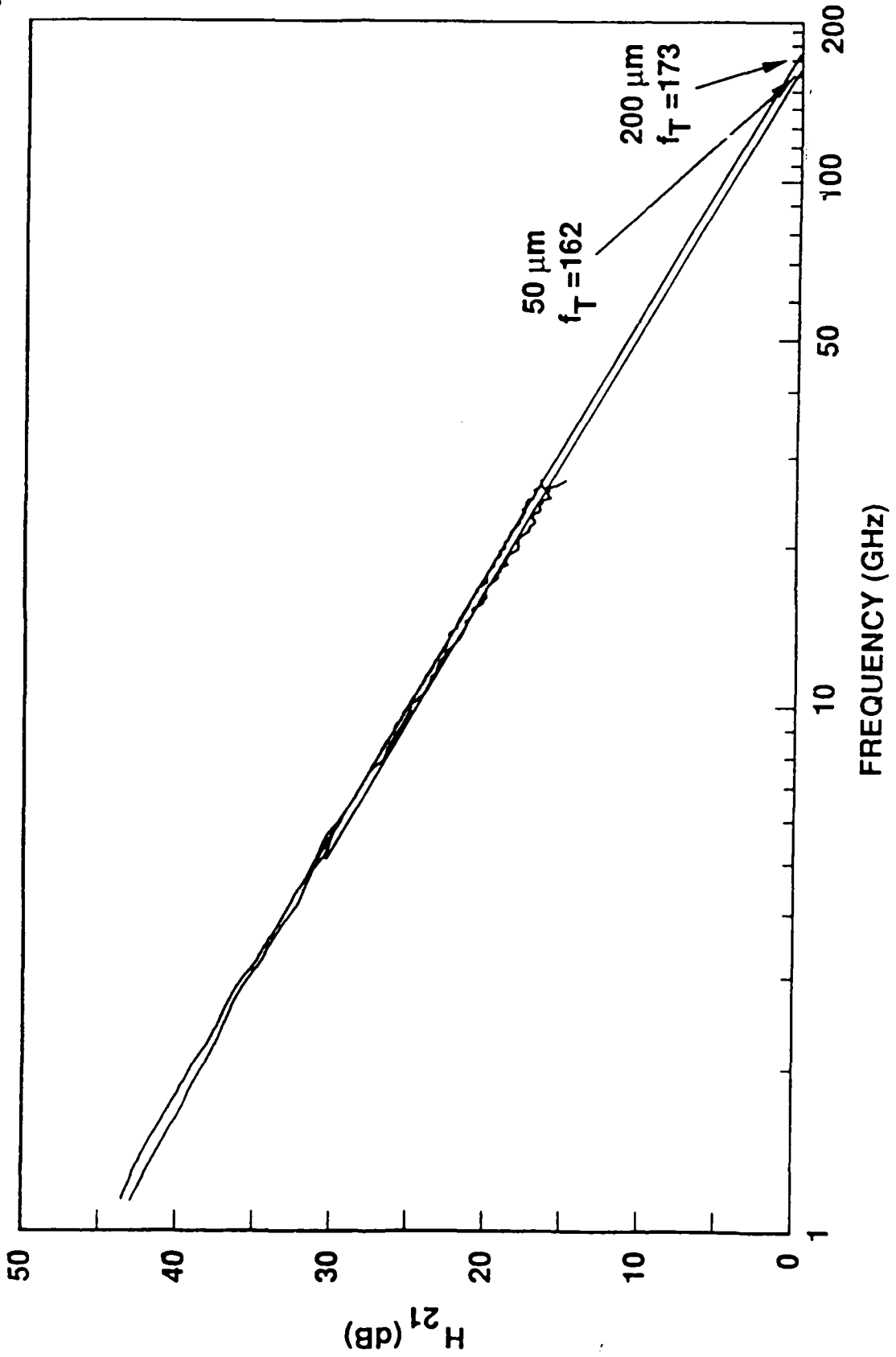


$g_m = 1160 \text{ mS}/\mu\text{m}$
 $V_{FB} = 0.28 \text{ V}$
 $W = 25 \mu\text{m}$

0.1 μm LATTICE MATCHED HEMT
 $\text{Al}_{.48}\text{In}_{.52}\text{As}/\text{Ga}_{.47}\text{In}_{.53}\text{As}$



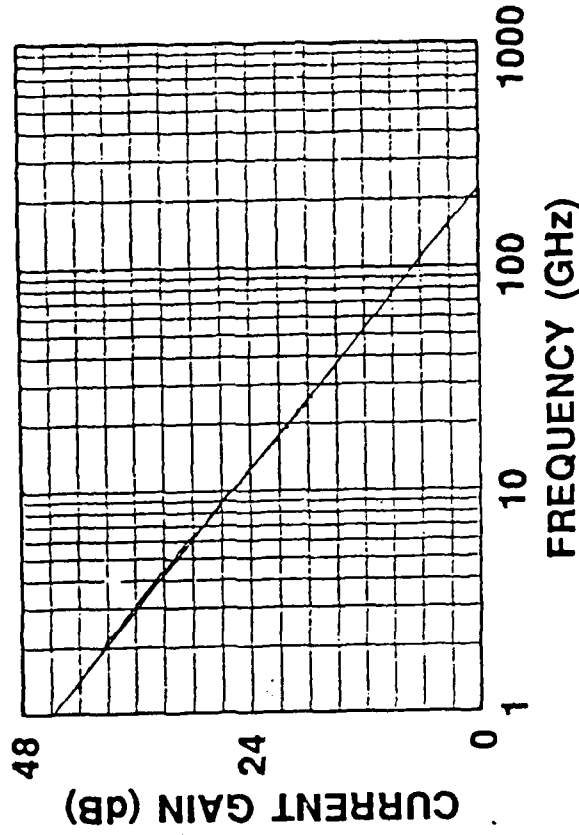
C8852-05-02





GainAs HEMT 0.1 μm T-GATE

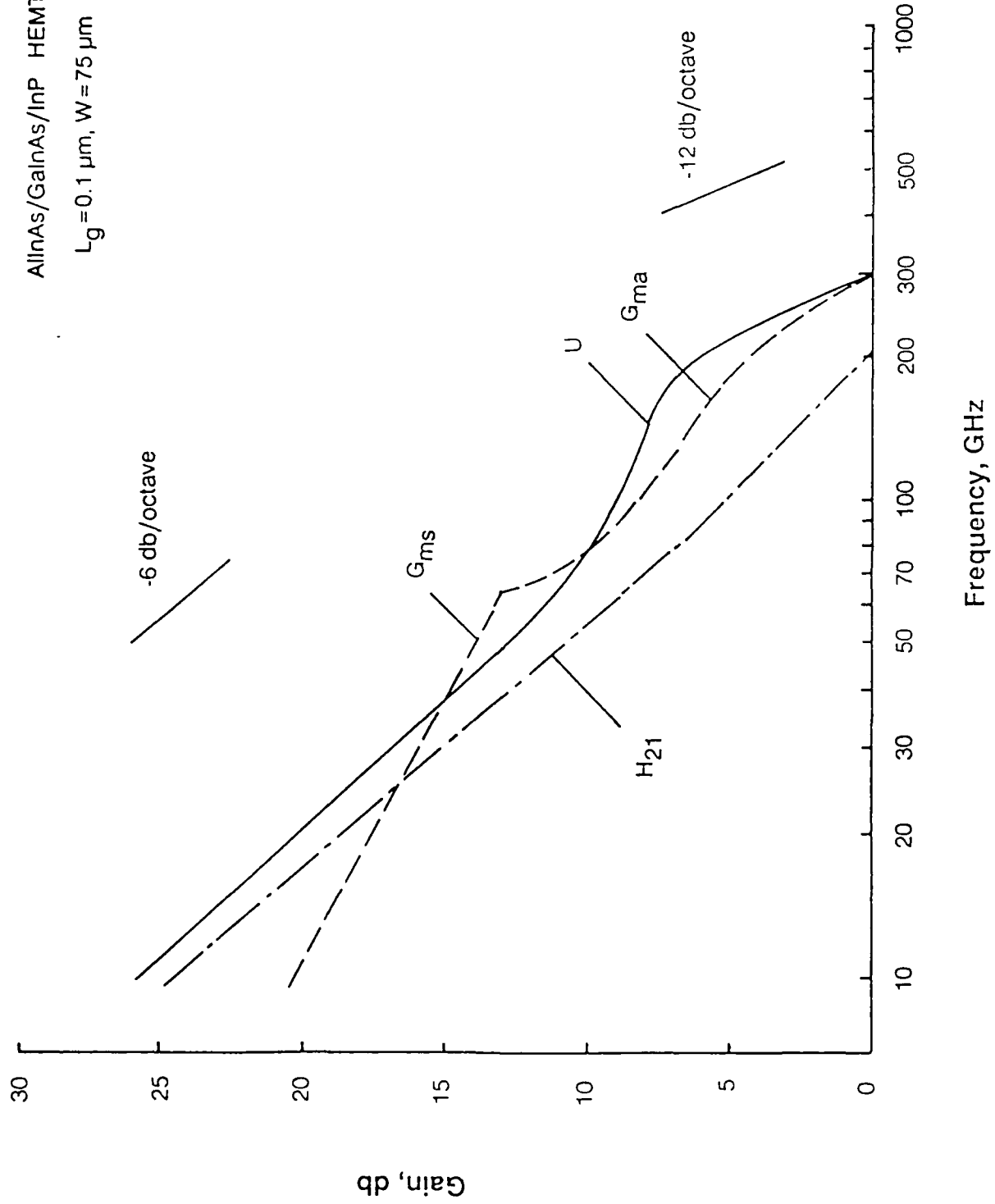
18335-1



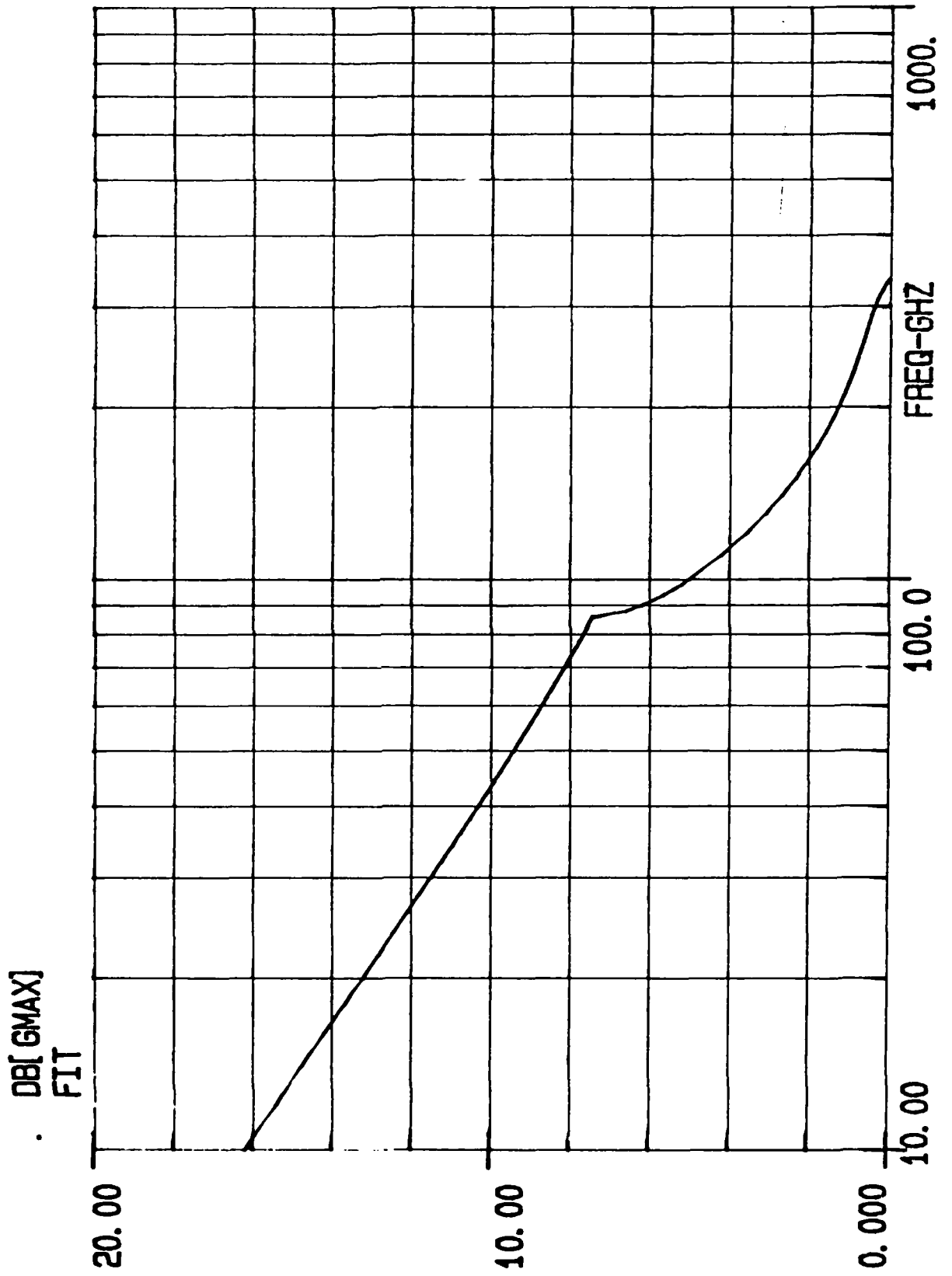
$$g_m = 1160 \text{ mS/mm}$$

$$f_t = 210 \text{ GHz}$$

AlInAs/GaInAs/InP HEMT
 $L_g = 0.1 \mu\text{m}$, $W = 75 \mu\text{m}$



EEsof - Touchstone - Thu Jun 16 16:38:20 1988 - 70051B

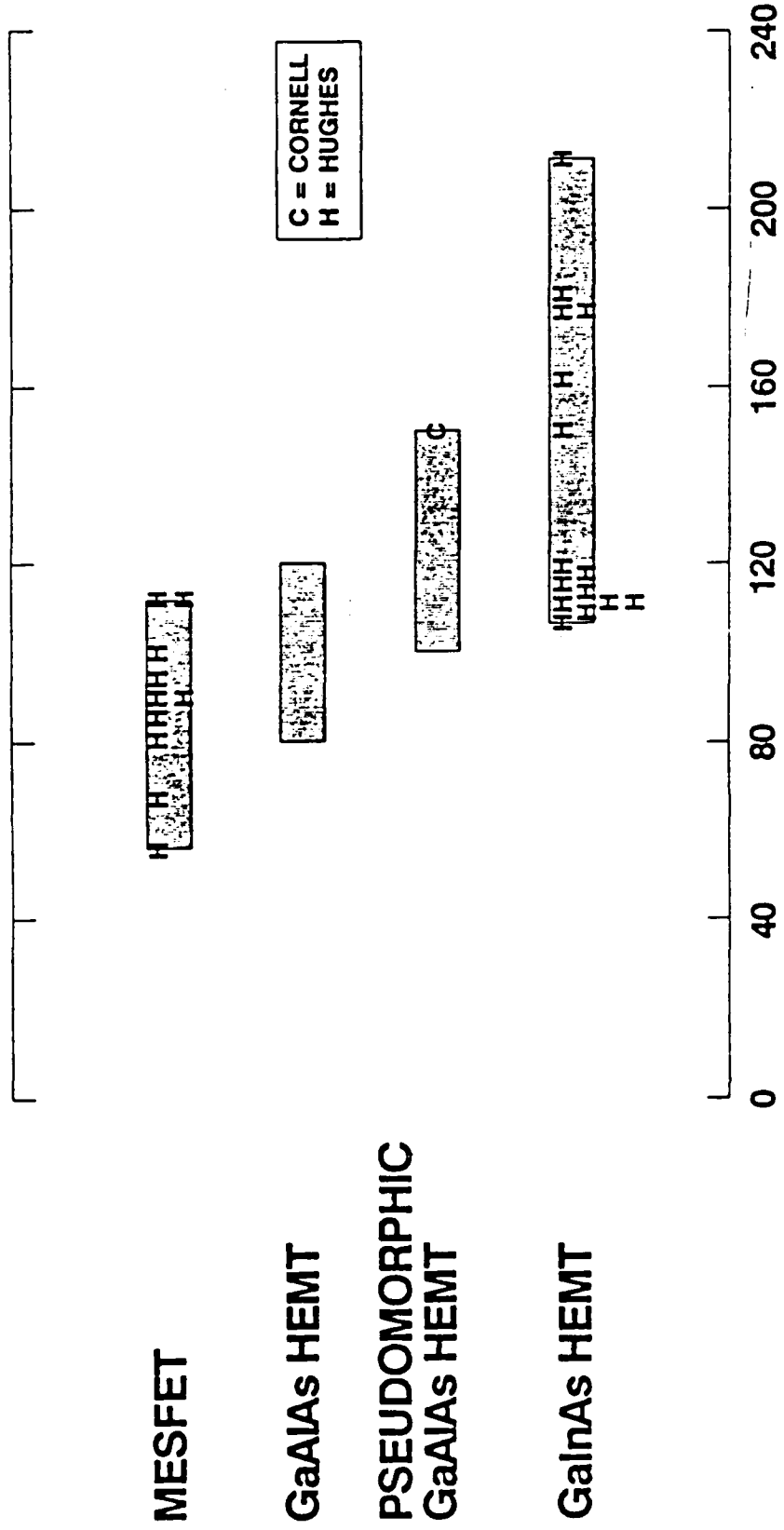


EXPERIMENTALLY MEASURED GAIN-BANDWIDTH PRODUCTS, Ft



C8852-02-02

0.1 - 0.2 MICROMETER GATELENGTH



MESFET

GaAlAs HEMT

PSEUDOMORPHIC
GaAlAs HEMT

GaInAs HEMT

C = CORNELL
H = HUGHES

FREQUENCY, GHz

OCTOBER 1988

V-BAND AlInAs-GaNAs HEMT AMPLIFIER NOISE AND GAIN PERFORMANCE

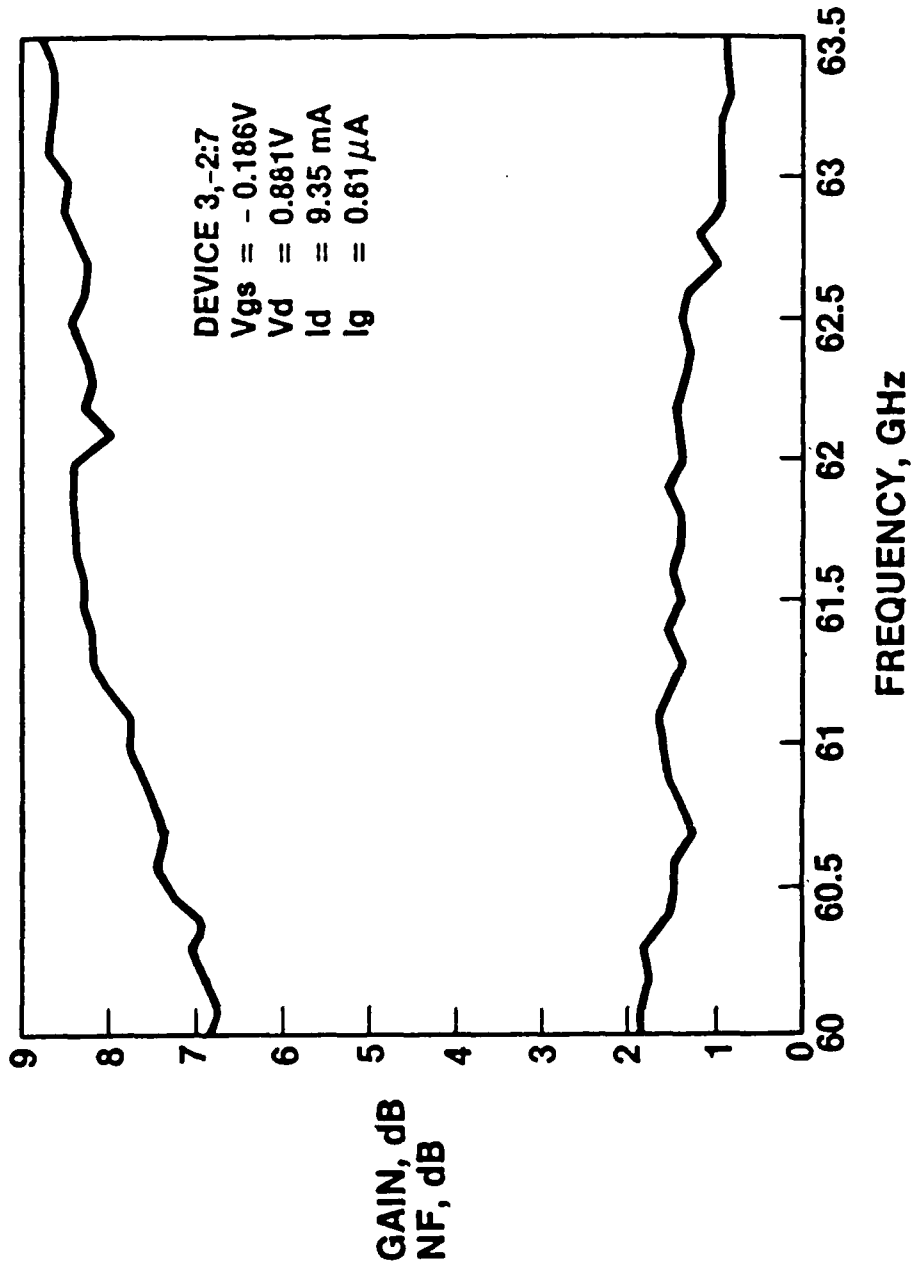
18309-6R1

$L_g = 0.2 \mu\text{m}$

$g_m = 800 \text{ mS/mm}$

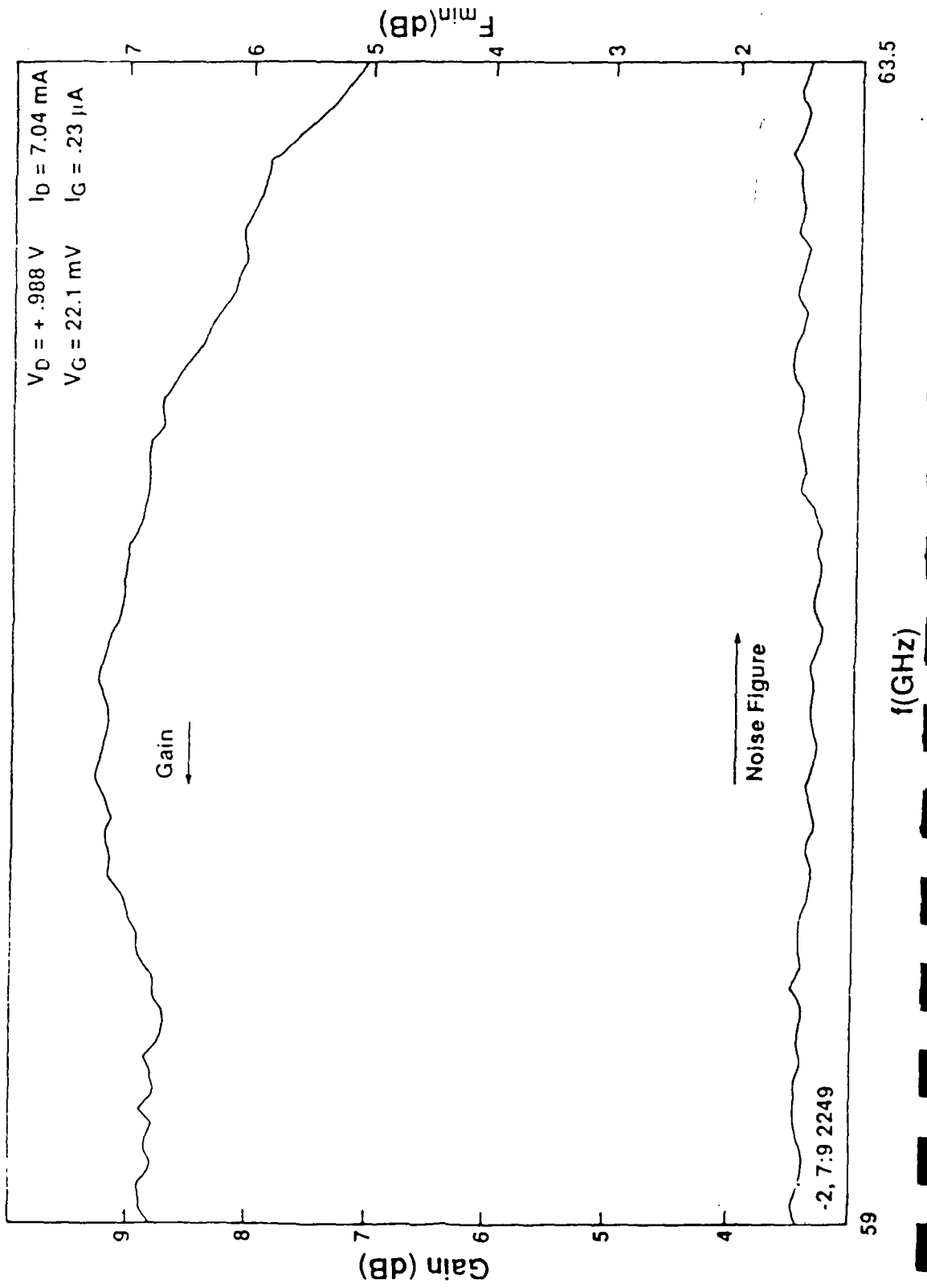
$f_T = 130 \text{ GHz}$

$W = 50 \mu\text{m}$

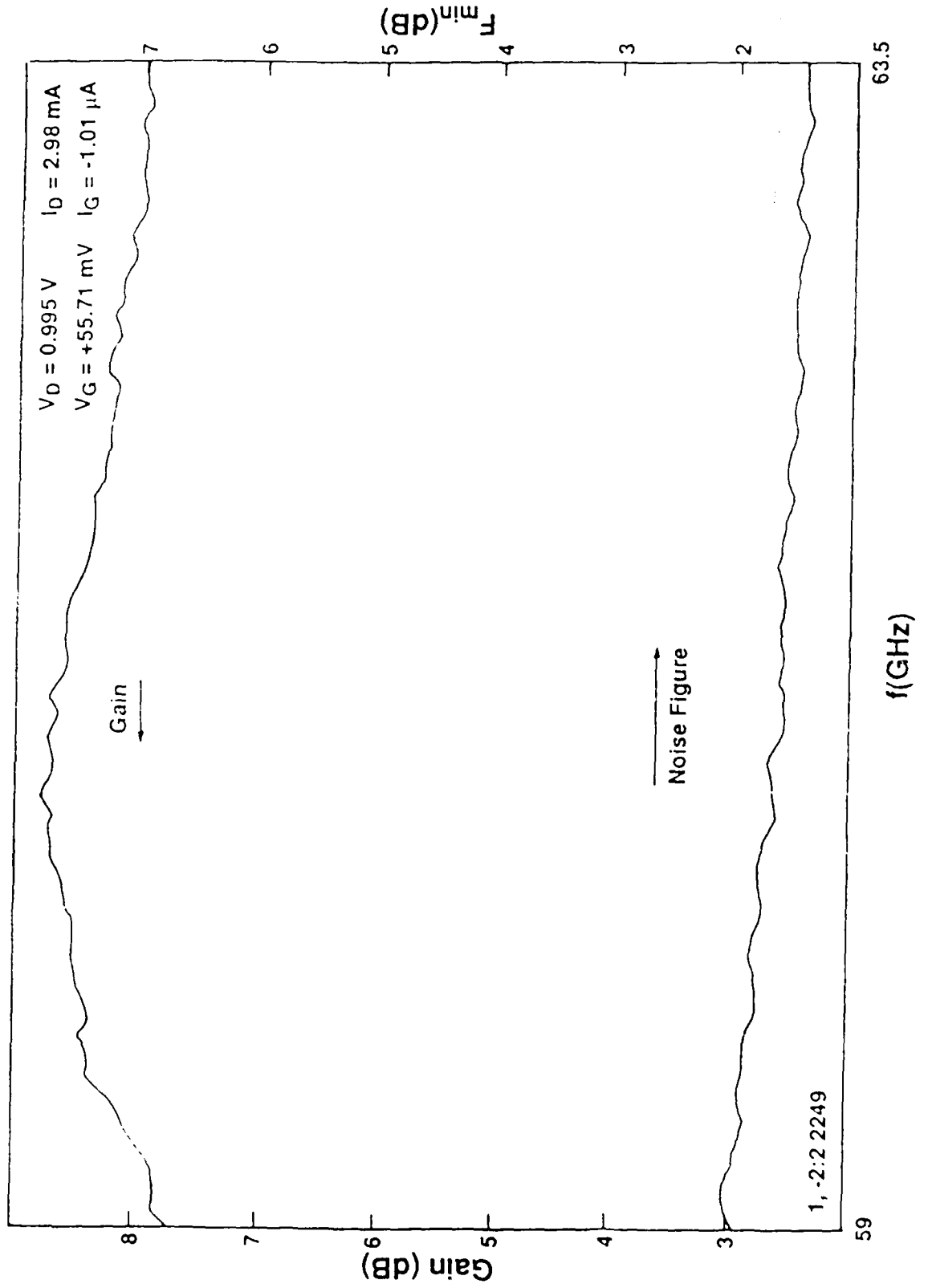


AUGUST 1988

V-BAND NOISE PERFORMANCE OF LATTICE MATCHED $\text{Al}_{.48}\text{In}_{.52}\text{As} / \text{Ga}_{.47}\text{In}_{.53}\text{As}$ HEMT AMPLIFIER



V-BAND NOISE PERFORMANCE OF PSEUDOMORPHIC Al_{0.48}In_{0.52}As / Ga_{0.38}In_{0.62}As HEMT AMPLIFIER



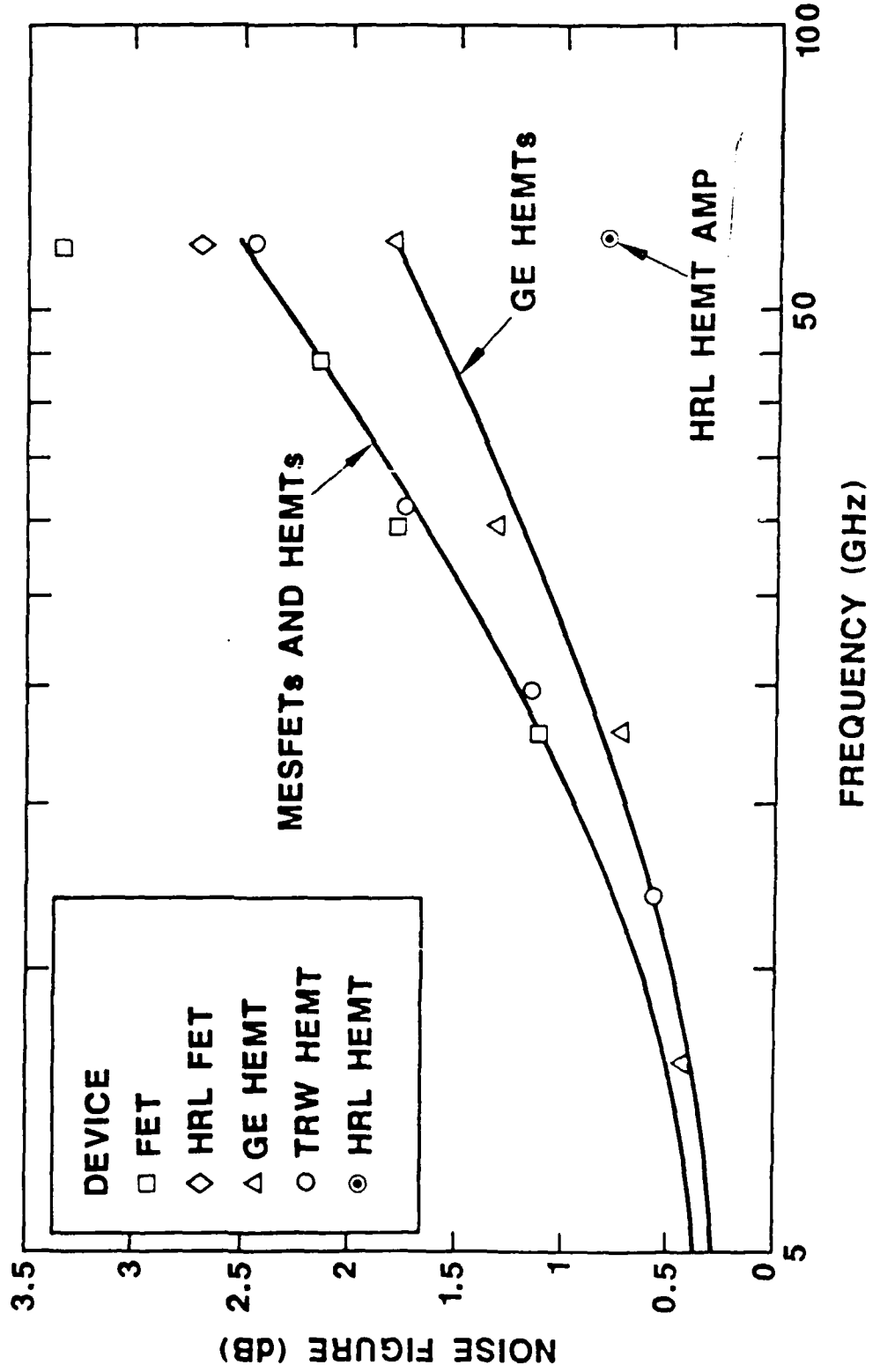
GainAs HEMT LOW NOISE AMPLIFIER



PROJECT 59

COMPARISON TO COMPETITION-1988

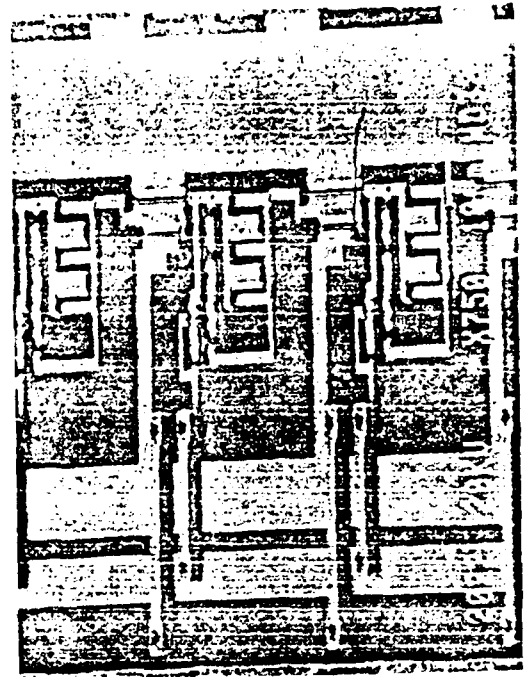
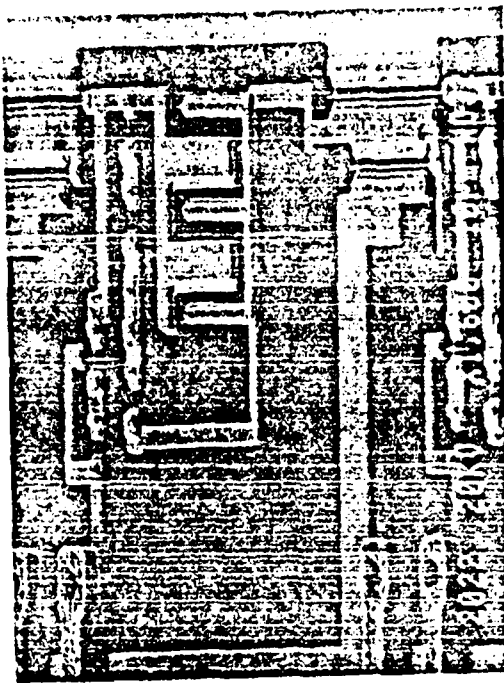
18430-46





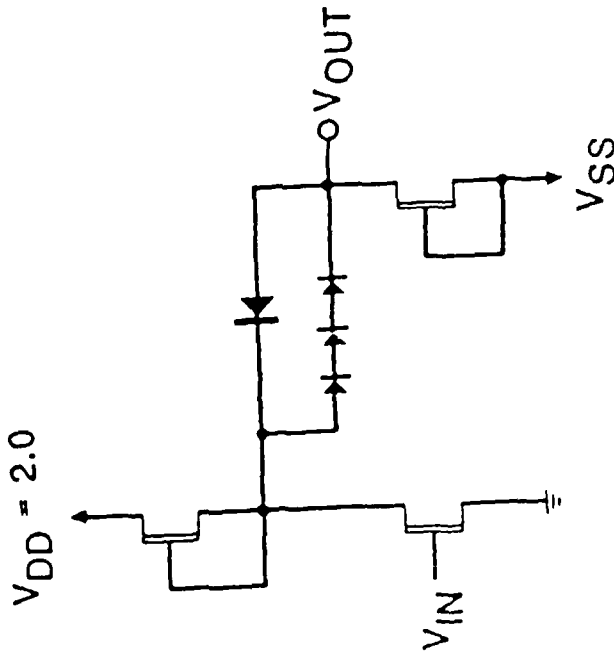
CAPACITIVELY ENHANCED LOGIC INVERTER AND RING OSCILLATOR

17772-3

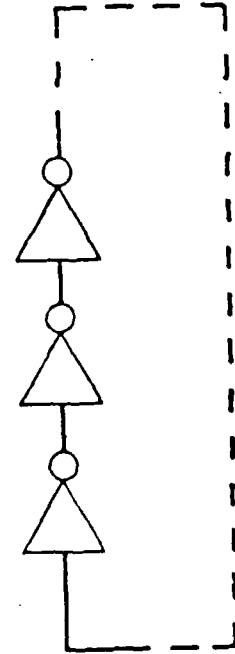


DECEMBER 1987

15392 2R58



CEL INVERTER



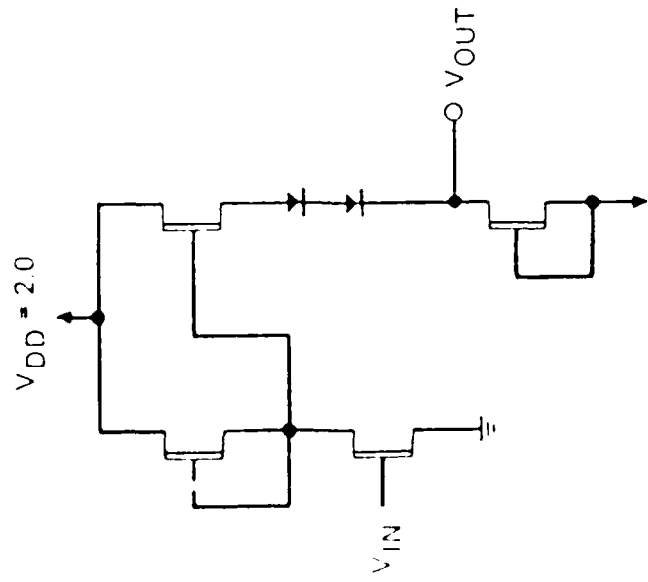
RING OSCILLATOR

BUFFERED FET LOGIC INVERTER AND RING OSCILLATOR

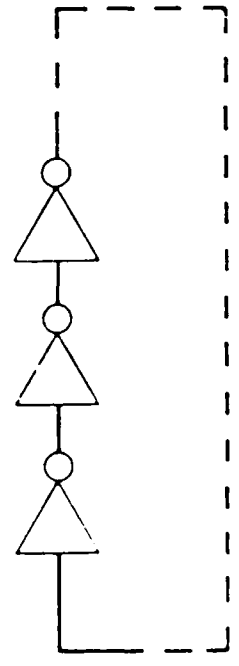


15392 2R6A

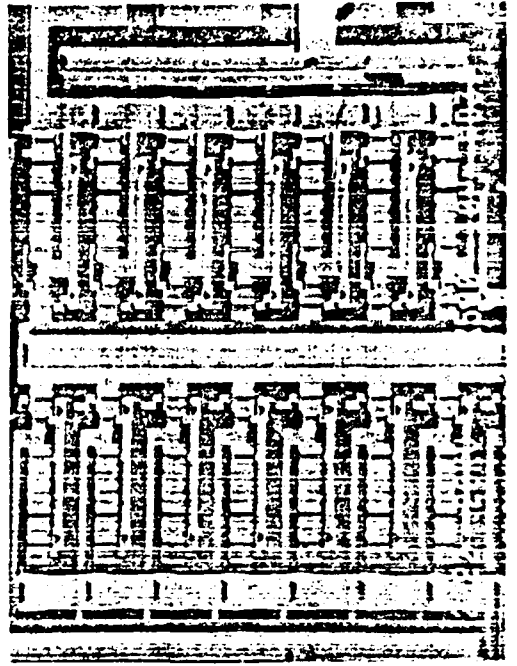
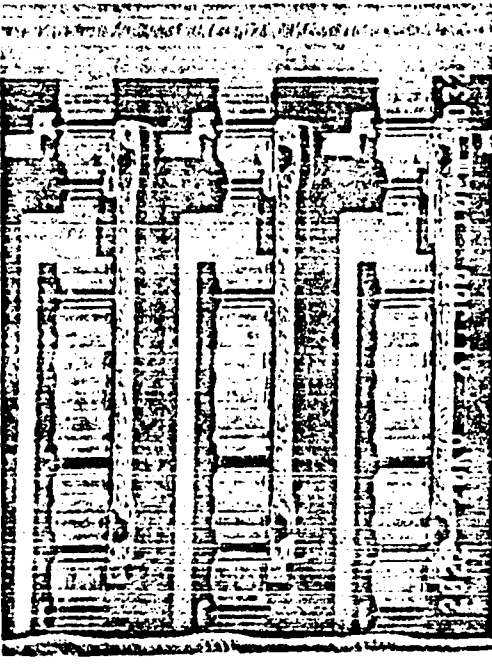
17772-2



BFL INVERTER



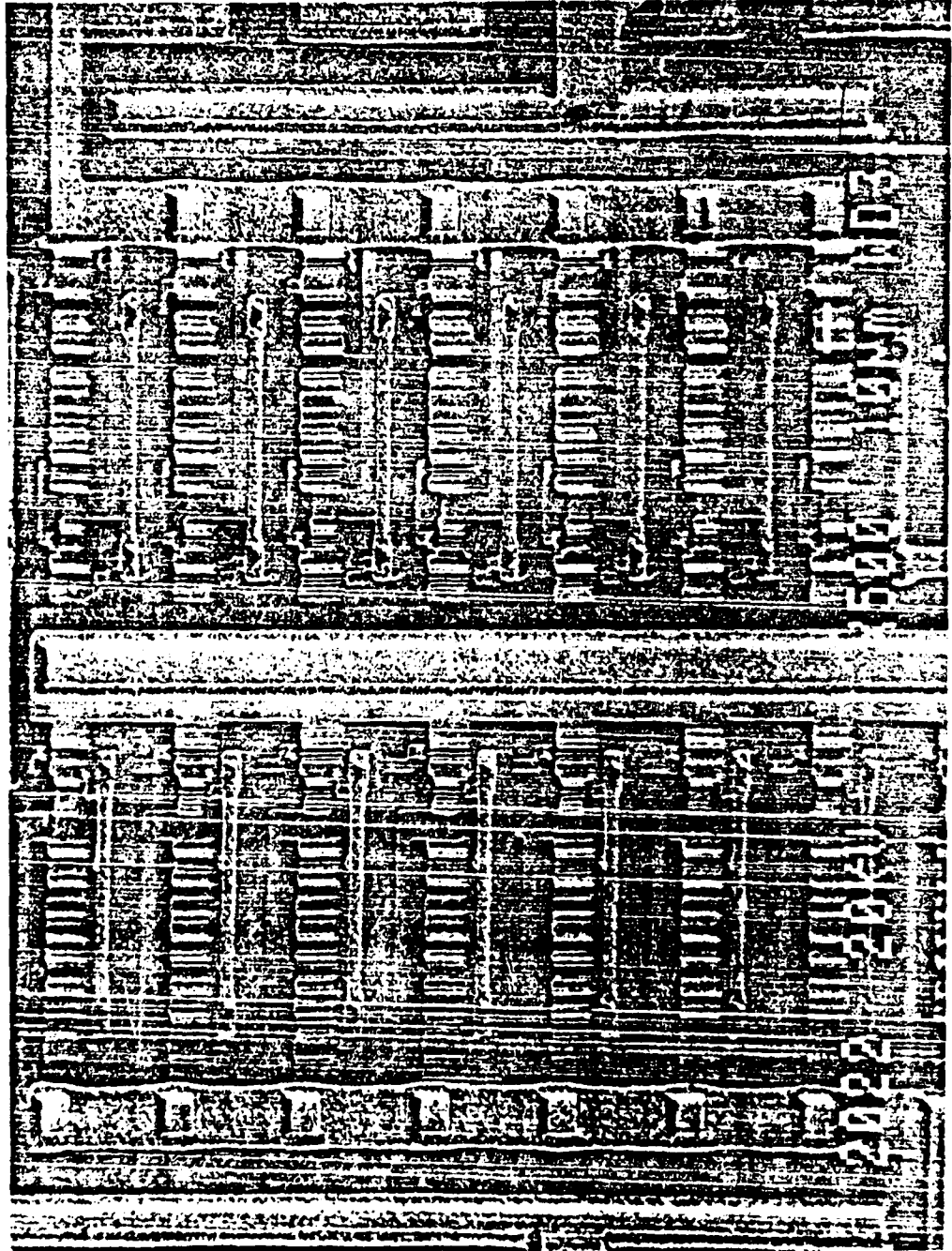
RING OSCILLATOR





15 STAGE BFL RING OSCILLATOR
IN 0.2 μm AlInAs-GaInAs HEMT TECHNOLOGY

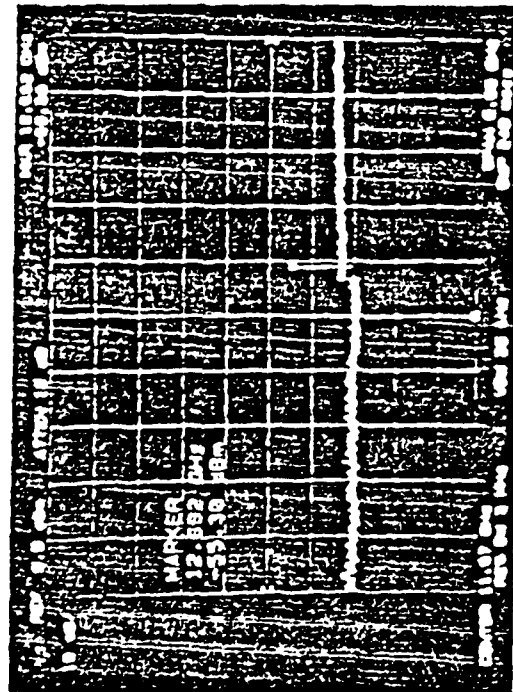
17772-1



DECEMBER 1987

AlInAs-GaInAs HEMT IC PERFORMANCE

25.4 GHz OPERATION

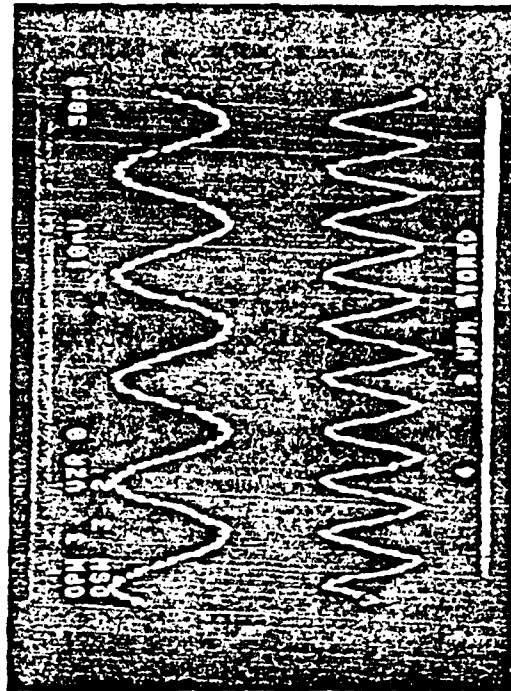


$f_{ck/2} = 12.69$ GHz

CEL DIVIDER

$F_{max} = 25.4$ GHz
 $P_D = 63.8$ mW

20 GHz OPERATION



BFL DIVIDER

$F_{max} = 25.2$ GHz
 $P_D = 450$ mW

RING OSCILLATOR RESULTS*

BFL $\tau_g = 9.26$ ps @ 66.7 mW/GATE

CEL $\tau_g = 7.21$ ps @ 24.5 mW/GATE

*REPORTED AT IEDM 1987

FAN-OUT SENSITIVITY 1.4 ps/gate [BFL]
 2.5 ps/gate [CEL]

FEBRUARY 1988

C17902-9

CONCLUSIONS

- Pseudomorphic $\text{Al}_{.48}\text{In}_{.52}\text{As-Ga}_{.38}\text{In}_{.62}\text{As}$ HEMTs have demonstrated an extrinsic f_T of > 200 GHz.
- Lattice matched and pseudomorphic HEMTs have comparable noise performance.
- With optimized epitaxial layer design an f_T of > 250 GHz is expected.
- f_{max} is limited by device output conductance.

Measurement of Response of High Speed Tunneling Devices

T. C. McGill

*California Institute of Technology
Pasadena, CA*



MEASUREMENT OF RESPONSE OF HIGH SPEED TUNNELING DEVICES

Principal Investigator: T. C. McGill, California Institute of Technology

DARPA ORDER 4833 ONR CONTRACT NO. N00014-84-C-0083

OBJECTIVE

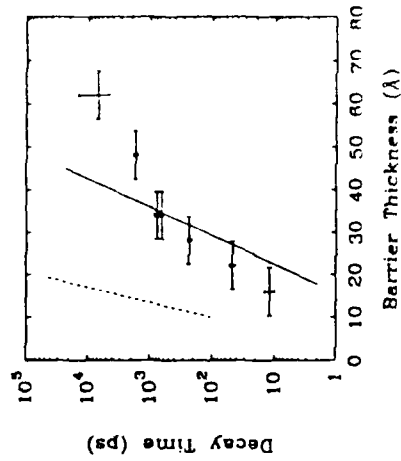
- Develop new and novel electronic devices
- Make appropriate measurements to characterize the high-speed device response

STATUS

- Fabricating tunnel device structures to order in MBE machine
- Perfected correlation technique for measuring decay of photoluminescence from quantum well
- Measured the response of photon-controlled electronic switches (PCE)
- Measured and reported the response of double barrier tunnel structures at speeds to 10ps
- Making measurements of bias dependence of decay of photoluminescence from quantum well
- Simulating the processes of making measurements

APPROACH

- Explore new phenomena potentially useful for making new devices
- Fabricate new device structures in MBE machine
- Develop and monitor techniques for measuring high speed devices
- Measure high-speed response using CPM laser with pulse width less than 300fs
- Simulate the measurement process



Decay times of the photoluminescence from a quantum well as a function of barrier thickness in double-barrier GaAs/AlAs tunnel structures. The solid line and dashed line are the theoretical values for the tunneling of electrons and heavy holes, respectively.

MEASUREMENTS OF RESPONSE
OF
HIGH SPEED TUNNELING DEVICES

by
T. C. McGill
California Institute of Technology
Pasadena, California 91125
(818)356-4849

COLLABORATORS

Matthew B. Johnson (*IBM T. J. Watson Research Center*)

Michael K. Jackson (*Caltech*)

David H. Chow (*Caltech*)

David Z. Ting (*Caltech*)

E. T. Yu (*Caltech*)

A. T. Hunter (*Hughes Research Laboratories*)

R. B. Hammond (*Los Alamos National Laboratories*)

N. Politer (*Los Alamos National Laboratories*)

OUTLINE

- I. WHAT AND WHY TUNNEL DEVICES?
 - A. TWO-TERMINAL
 - B. THREE-TERMINAL
- II. SPEED OF TUNNEL DEVICES
- III. PREVIOUS MEASUREMENTS
- IV. OUR MEASUREMENTS
- V. FUTURE PLANS

WHAT
AND
WHY
TUNNEL STRUCTURES

WHY TUNNEL DEVICES

A. HETEROJUNCTIONS VERSUS DOPING

- CHARACTERISTIC DIMENSIONS FOR DOPING CONTROL IS
1000Å
- HETEROJUNCTIONS GIVE SMALLER CHARACTERISTIC
DIMENSIONS 10Å

B. POTENTIAL FOR VERY HIGH DENSITY WITH REASONABLE BIASES ETC.

C. SMALL CHARACTERISTIC DIMENSIONS OF TUNNEL DEVICES GIVE POTENTIAL FOR VERY HIGH SPEED

TWO-TERMINAL TUNNEL DEVICES

Negative Resistance in Double Barriers

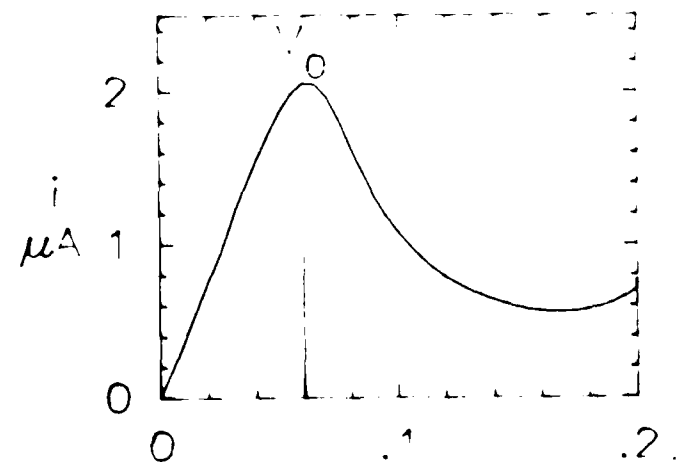
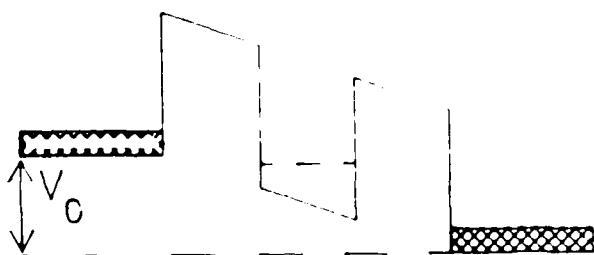
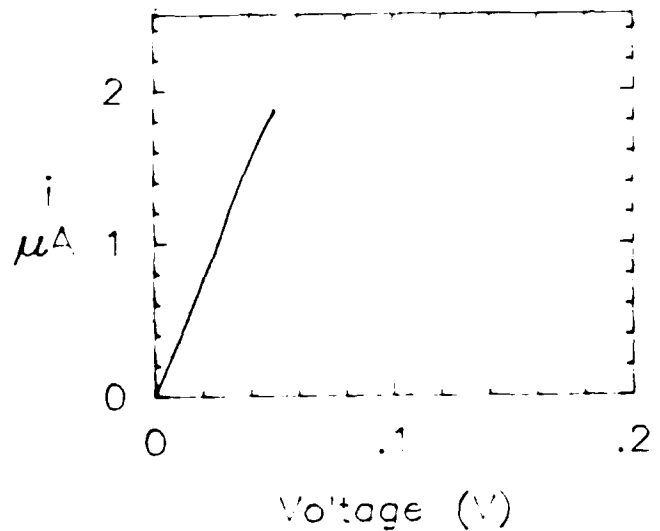
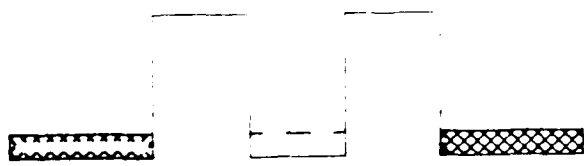
I. First approximation:

A. Energy conservation:

$$E = \hbar^2 k^2 / 2m$$

B. Parallel momentum (k_{\parallel}) conservation:

$$k = k_{\parallel} + k_{\perp}$$



THREE-TERMINAL DEVICES

Inverted base-collector tunnel transistors

A. R. Bonnefoi, D. H. Chow, and T. C. McGill
 T. J. Watson, Sr., *Laboratory of Applied Physics, California Institute of Technology, Pasadena, California*
 91125

(Received 1 July 1985; accepted for publication 7 August 1985)

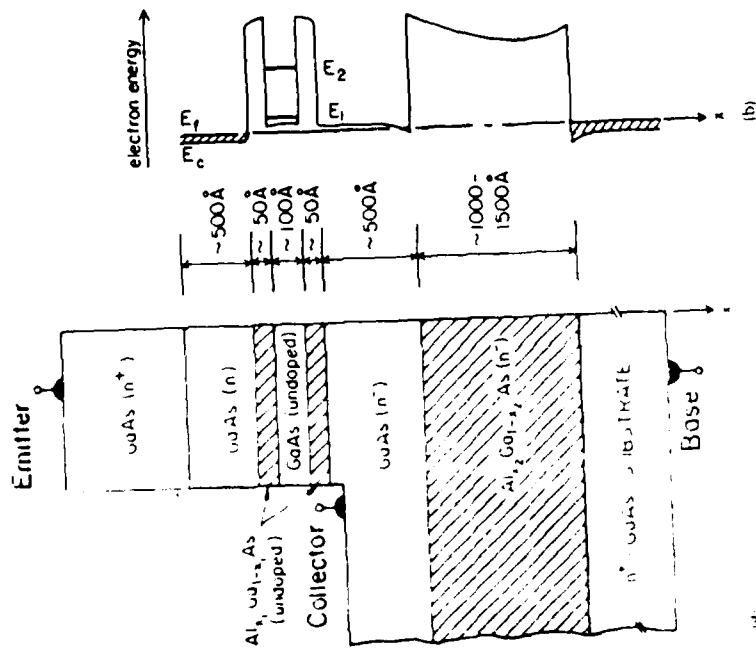


FIG. 3. Schematic diagrams (not to scale) of (a) a cross section of the proposed negative resistance Stark effect transistor (NERSET); (b) the conduction-band edge at equilibrium as a function of position in the x direction (perpendicular to the layers)

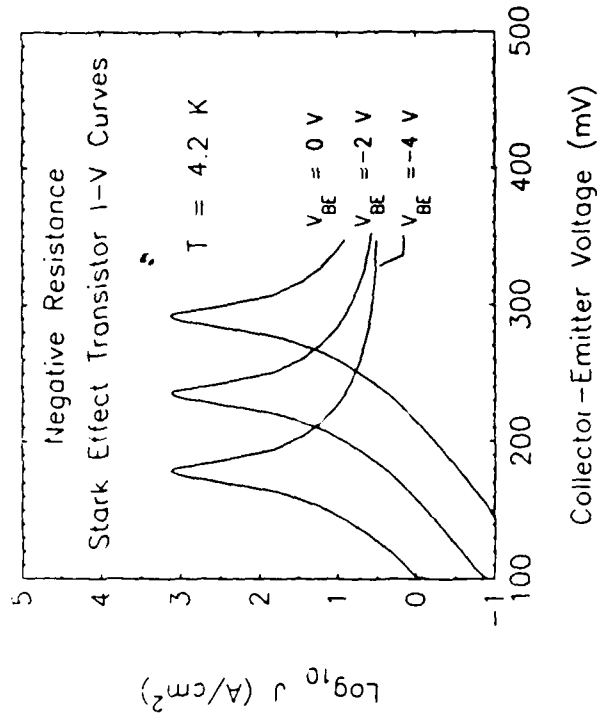


FIG. 4. Calculated current-voltage characteristics for the negative resistance Stark effect transistor (NERSET). The tunnel barriers are 20-Å-thick $\text{Al}_{0.5}\text{Ga}_{0.5}\text{As}$ layers and the well is 50-Å-thick GaAs layer. The conduction-band offset is taken to be 0.5 eV.

Inverted base-collector tunnel transistors

A. R. Bonnefoi, D. H. Chow, and T. C. McGill

T. J. Watson, Sr., Laboratory of Applied Physics, California Institute of Technology, Pasadena, California 91125

(Received 1 July 1985; accepted for publication 7 August 1985)

888

Appl. Phys. Lett. 47 (8), 15 October 1985

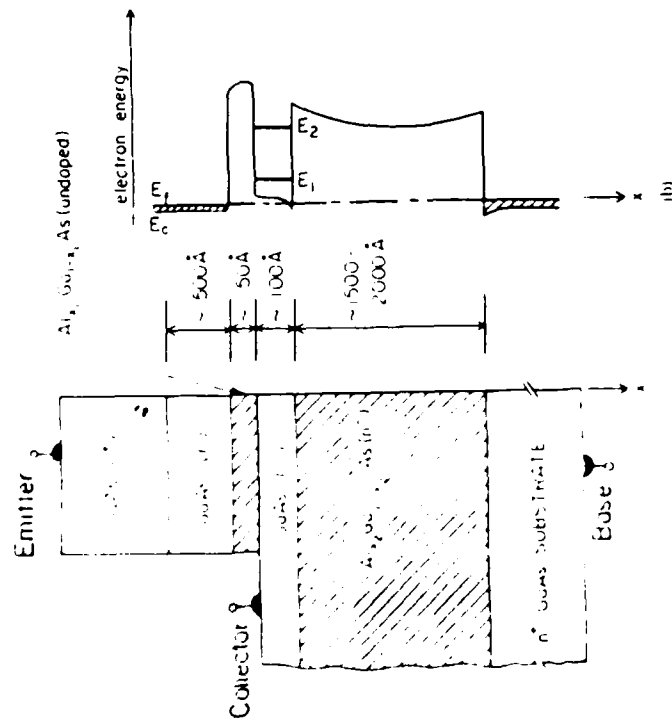


FIG. 1 Schematic diagrams (not to scale) of (a) a cross section of the proposed Stark effect transistor (SE-T); (b) the conduction-band edge at equilibrium as a function of position in the x direction (perpendicular to the layers).

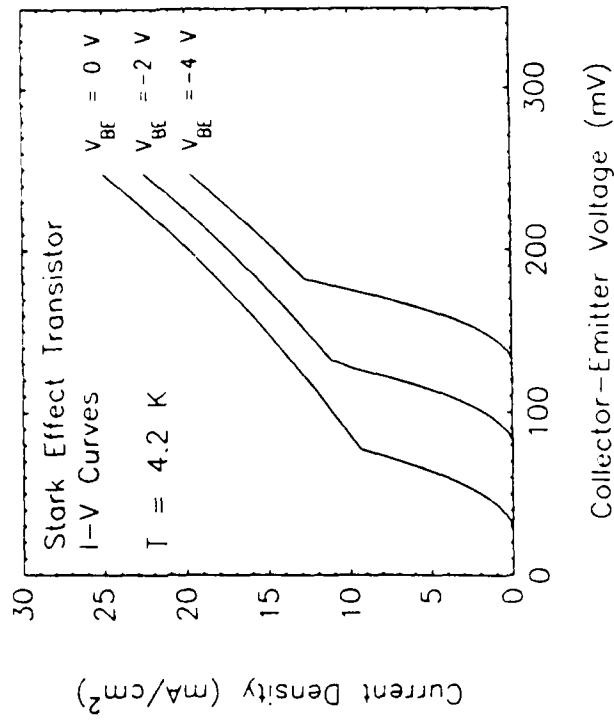


FIG. 2 Calculated current-voltage characteristics for the Stark effect transistor (SET). The barriers are pure AlAs, 50 and 1000 Å thick, respectively. The well is a 50-Å-thick GaAs layer. The conduction-band offset is taken to be 0.96 eV.

Negative transconductance via gating of the quantum well subbands in a resonant tunneling transistor

Fabio Beltram, Federico Capasso, Serge Luryi, Sung-Nee G. Chu, Alfred Y. Cho, and Deborah L. Sivco
 AT&T Bell Laboratories, Murray Hill, New Jersey 07974

(Received 25 February 1988; accepted for publication 9 May 1988)

219 Appl. Phys. Lett. 53 (3), 18 July 1988

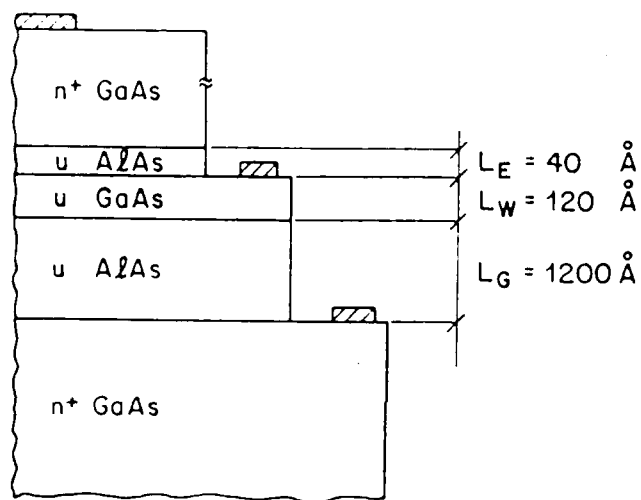


FIG 1 Schematic cross section of the resonant tunneling transistor.

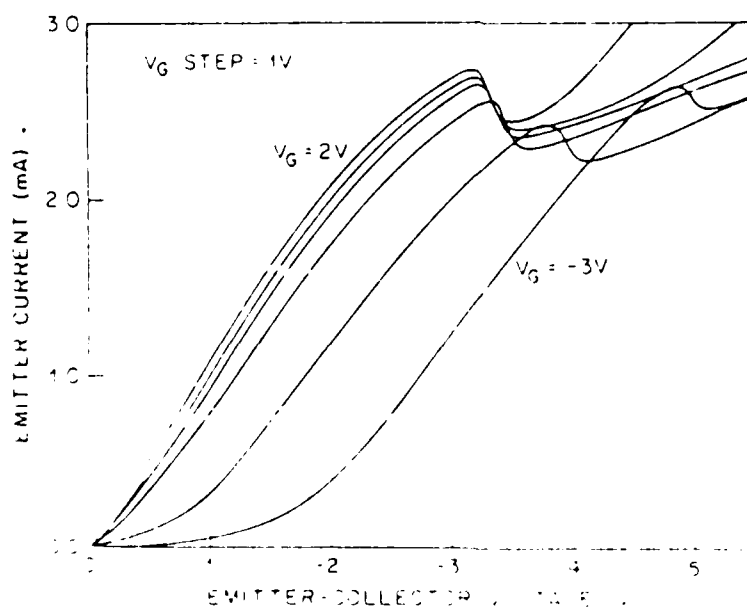
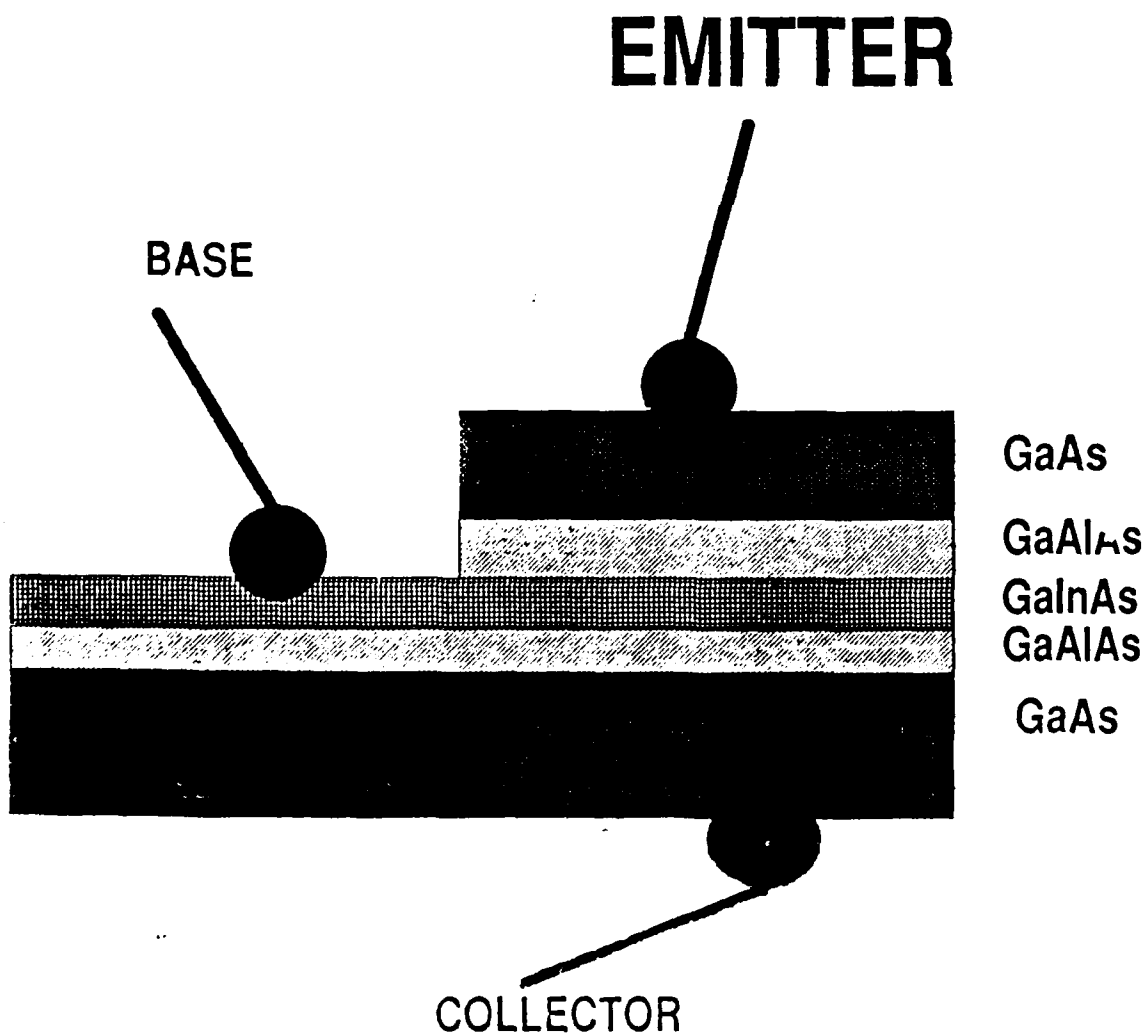


FIG 3 Collector characteristics of the resonant tunneling transistor at various V_G : (1) 2 V, (2) 0 V, (3) -3 V. Measurements were performed at 4 K.

TEXAS INSTRUMENTS THREE-TERMINAL DEVICE



RESONANT TUNNELING TRANSISTORS (RTT)

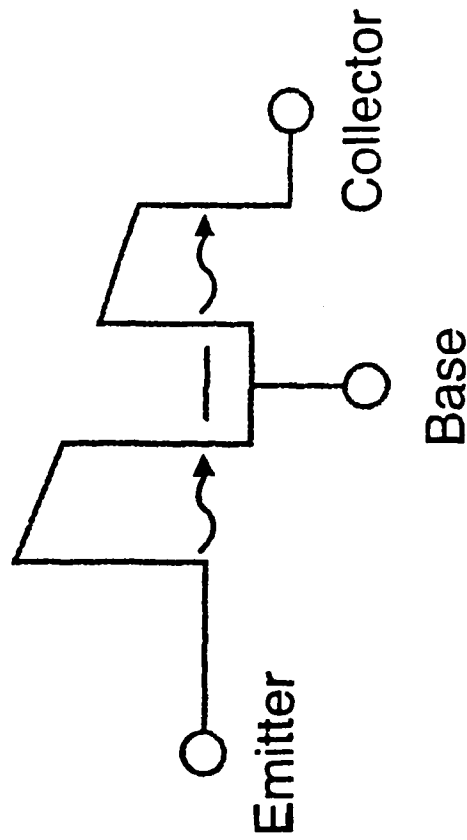
Pseudo RTT

- Resonant tunneling diode structures
- Inserted in bipolar or FET devices
- Series combination
- Developed by others

True RTT

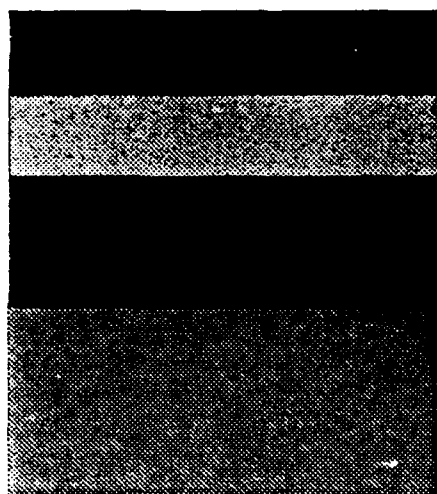
- Double barrier single well
- Direct contact to well for base
- Modulate resonance condition
- In development at TI
- Unipolar version needs no depletion layers
- Scalable well below $0.25\mu\text{m}$ geometries

True RTT



Si-Ge HETEROJUNCTION BIPOLAR TRANSISTOR

n-Si emitter
p-Si_{0.85}Ge_{0.15} base
n-Si collector
Si Substrate



- Wide-bandgap emitter suppresses hole current
- Strain splitting of conduction bands in SiGe improves electron transport in base

HJBT
Beta= 400
 $F_T = 100\text{GHz}$

Standard Si
Beta=100
 $F_T = 20\text{GHz}$

SPEED OF TUNNELING DEVICES

- A. TUNNELING DEVICES ARE VERY FAST-CHARACTERISTIC TIMES IN THE 100×10^{-15} SECOND RANGE

- B. TUNNELING DEVICES ARE SLOWER WITH CHARACTERISTIC TIMES IN THE 10^{-12} SECOND RANGE

- C. TUNNEL TIME OF ELECTRONS

TUNNELING TIMES

ON THE BASIS OF TWO OUT OF THREE "VOTES" IN FAVOR OF YOUR MANUSCRIPT, I AM INCLINED TO ACCEPT IT FOR PUBLICATION. BEFORE I DO SO, I WOULD LIKE TO HAVE YOUR ASSURANCE THAT YOU AND YOUR CO-AUTHORS HAVE CONSIDERED THE CRITICISMS CAREFULLY AND ARE SATISFIED THAT THEY ARE NOT VALID. I AWAIT YOUR REPLY WITH INTEREST.

F. E. Myers, Editor JAP December 8, 1966

K. K. Thornber, T. C. McGill, and C. A. Mead, J. Appl. Phys. **38**, 2384 (1967).

TUNNELING TIMES

τ_T

J. R. Barker's CLASSIFICATION

A. SCATTERING TIME GROUP

- DECAY OF METASTABLE STATES TIME INDEPENDENT
PERTURBATION THEORY
- TUNNELING TIME VARIES INVERSELY AS TRANSITION MATRIX
ELEMENT

$$\tau_T \sim \frac{1}{\textit{Transition Matrix Element}}$$

- EQUIVALENT TO RC TIME CONSTANT

B. DWELL TIME GROUP

- PROBABILITY DENSITY IN TUNNELING REGION
- INCIDENT CURRENT FLUX
- TUNNELING TIME IS RATIO

$$\tau_T \sim \frac{\textit{PROBABILITY DENSITY}}{\textit{INCIDENT CURRENT}}$$

TUNNELING TIMES

(CONTINUED)

C. SEMI-CLASSICAL TIME GROUP

- PARTICLE IN BARRIER DESCRIBED BY AN IMAGINARY WAVE VECTOR

$$k_{IMAGINARY} = \sqrt{\frac{2m^* \Delta E}{\hbar^2}}$$

- TUNNELING TIME IS THE ASSOCIATED VELOCITY DIVIDED INTO BARRIER THICKNESS (D)

$$\tau_T = \frac{m^* D}{\hbar k_{IMAGINARY}}$$

D. PHASE TIME GROUP

- CONSIDER THE ENERGY DEPENDENCE OF PHASE SHIFT OF THE TRANSMISSION COEFFICIENT $\eta(E)$
- TUNNELING TIME IS DERIVATIVE OF THIS PHASE SHIFT WITH ENERGY

$$\tau_T = \hbar \frac{d\eta}{dE}$$

TUNNELING TIMES

J. R. Barker's CLASSIFICATION

- A. SCATTERING TIME GROUP
- B. DWELL TIME GROUP
- C. SEMI-CLASSICAL TIME GROUP
- D. PHASE TIME GROUP

PREVIOUS WORK

MEASUREMENTS OF TUNNEL RESPONSE ON TWO-TERMINAL DEVICES

- A. MIXING EXPERIMENTS 2.5THz (SOLLNER)
- B. PL DECAY EXPERIMENTS (SAKAKI AND CO-WORKERS)
- C. ELECTRO-OPTIC TECHNIQUE (MOUROU AND CO-WORKERS)

Tunneling Escape Rate of Electrons From Quantum Well in Double-Barrier Heterostructures

M. Tsuchiya, T. Matsusue, and H. Sakaki

Institute of Industrial Science, University of Tokyo, Minato-ku, Tokyo 106, Japan

(Received 30 June 1987)

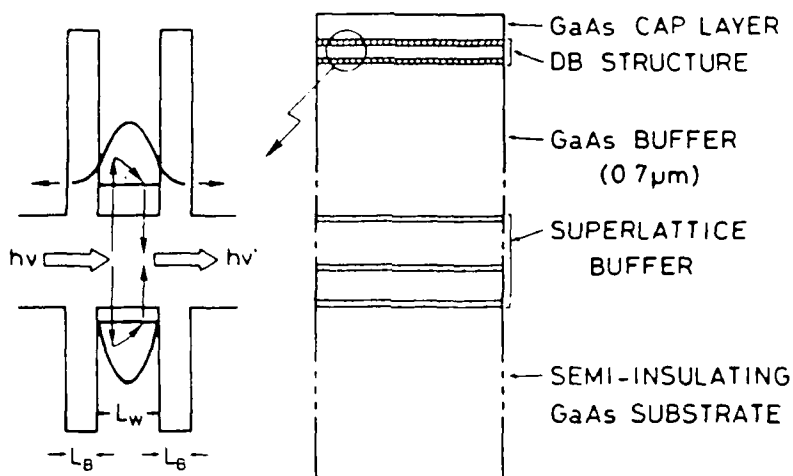


FIG. 1. Schematic structure of AlAs-GaAs-AlAs double-barrier samples used for the present study.

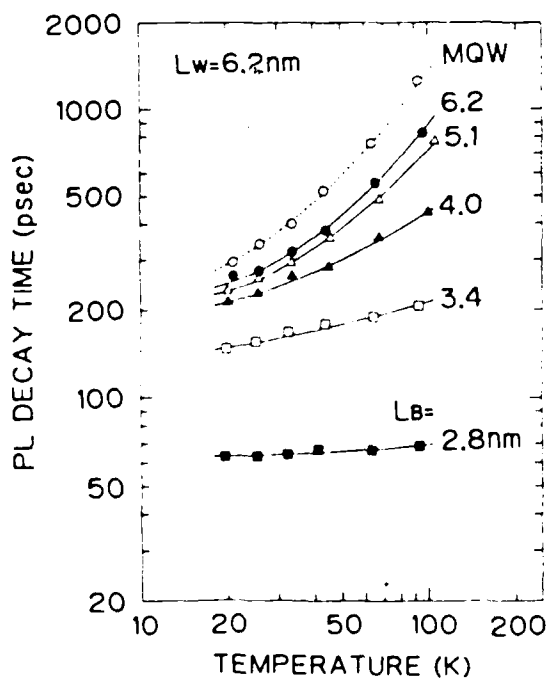


FIG. 4. The temperature dependence of PL decay time with barrier thickness as a parameter.

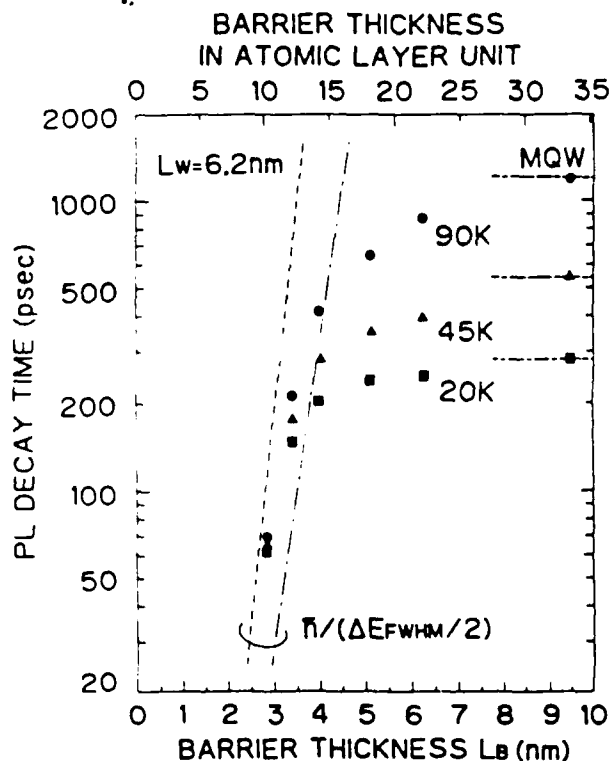


FIG. 5. PL decay times plotted as functions of barrier thickness L_B . When $L_B < 4$ nm, the tunneling escape process is dominant. Broken line and dot-dashed line are theoretical lifetimes calculated by $\hbar/(\Delta E_{FWHM}/2)$, with the assumption that the barrier heights are 1.36 and 0.96 eV, respectively.

PL DECAY EXPERIMENTS

- A. TIME LIMITED TO 60ps IN THE SAKAKI EXPERIMENTS

- B. MAJOR ERROR IN THE THEORETICAL EXPRESSION CLAIMED TO AGREE

- C. DIFFICULTY IN INTERPRETING EXPERIMENT
 - EXCITING LASER PRODUCES ELECTRONS AND HOLES
 - ELECTRONS AND HOLES DECAY WITH VERY DIFFERENT TIMES
 - CHARGING OF WELL DUE TO TUNNELING OF ELECTRON LEAVING HOLE BEHIND

Picosecond switching time measurement of a resonant tunneling diode

J. F. Whitaker and G. A. Mourou

Laboratory for Laser Energetics and Department of Electrical Engineering, University of Rochester, 250 East River Road, Rochester, New York 14623-1299

T. C. L. G. Sollner and W. D. Goodhue

Lincoln Laboratory, Massachusetts Institute of Technology, Lexington, Massachusetts 02173

(Received 7 March 1988; accepted for publication 1 June 1988)

385 Appl. Phys. Lett. 53 (5), 1 August 1988

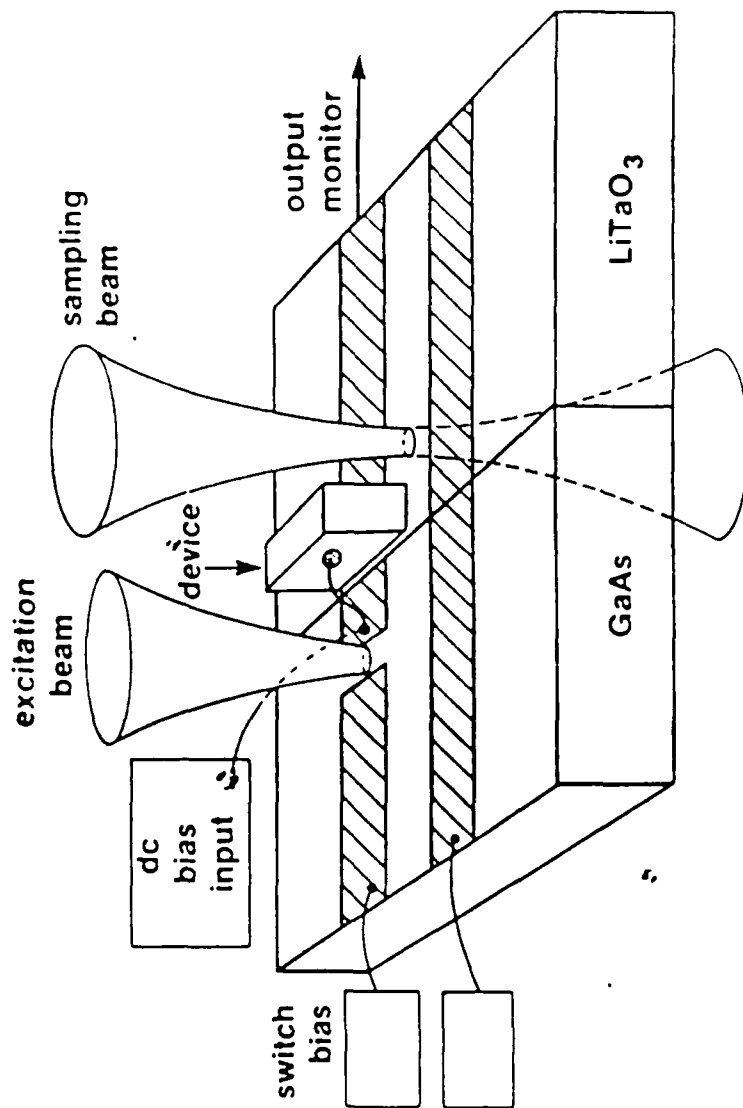


FIG. 1. Experimental configuration for electro-optic sampling of resonant-tunneling diode. A 12- μm -diam wire with a 1 μm tip contacts a mesa on the resonant-tunneling diode chip.

Picosecond switching time measurement of a resonant tunneling diode

J. F. Whitaker and G. A. Mourou

Laboratory for Laser Energetics and Department of Electrical Engineering, University of Rochester, 250 East River Road, Rochester, New York 14623-1299

T. G. L. G. Sollner and W. D. Goodhue

Lincoln Laboratory, Massachusetts Institute of Technology, Lexington, Massachusetts 02173

(Received 7 March 1988; accepted for publication 1 June 1988)

385

Appl. Phys. Lett. 53 (5), 1 August 1988

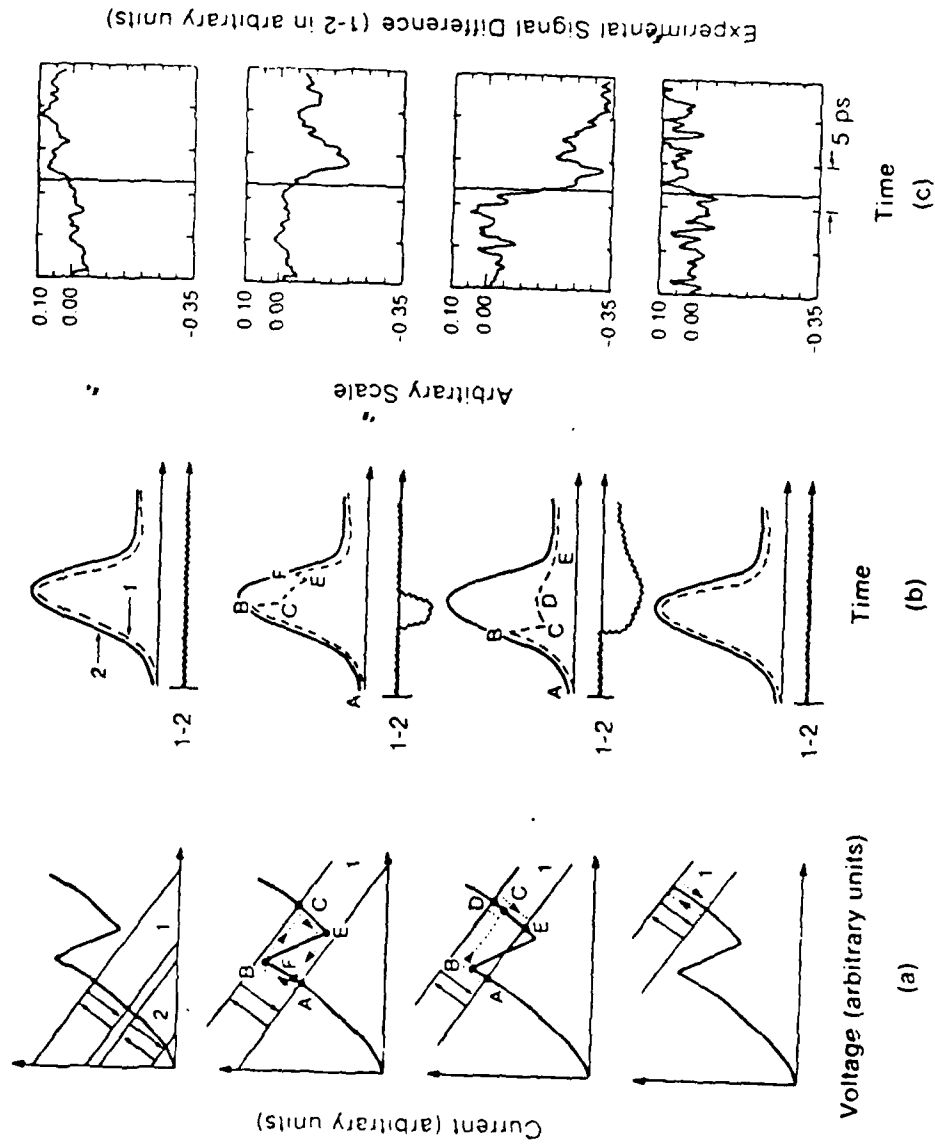


FIG. 3. Resonant-tunneling diode switching as a function of bias: (a) I - V curve with load lines, (b) analytic representation of waveforms resulting from movement of load lines in (a) and the difference of these waveforms, and (c) experimental signal difference.

ELECTRO-OPTIC TECHNIQUE

A. DIFFICULTY OF INTERPRETING DATA

B. NOISY SIGNAL

C. RESULTS IN DISAGREEMENT WITH SAKAKI

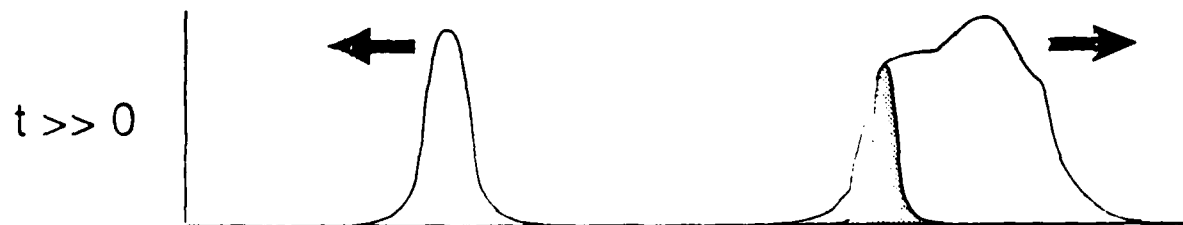
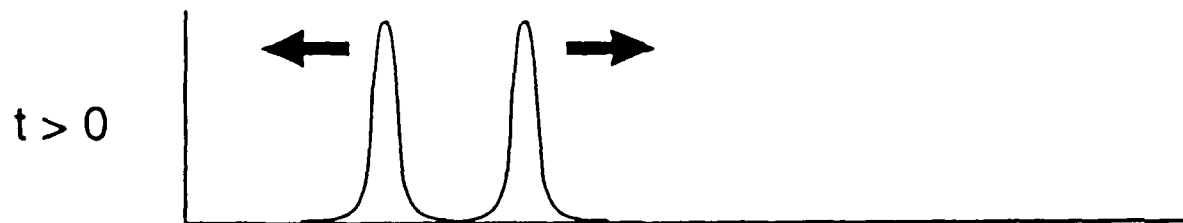
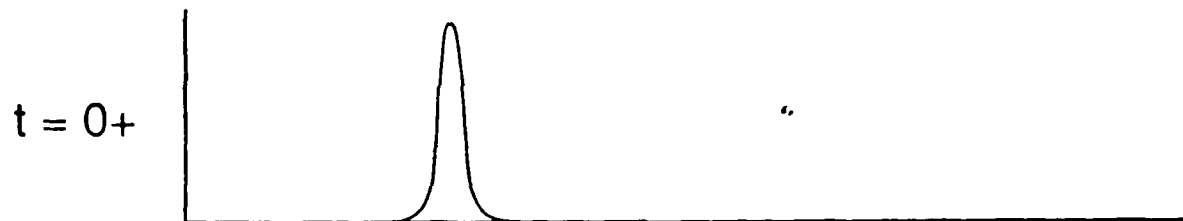
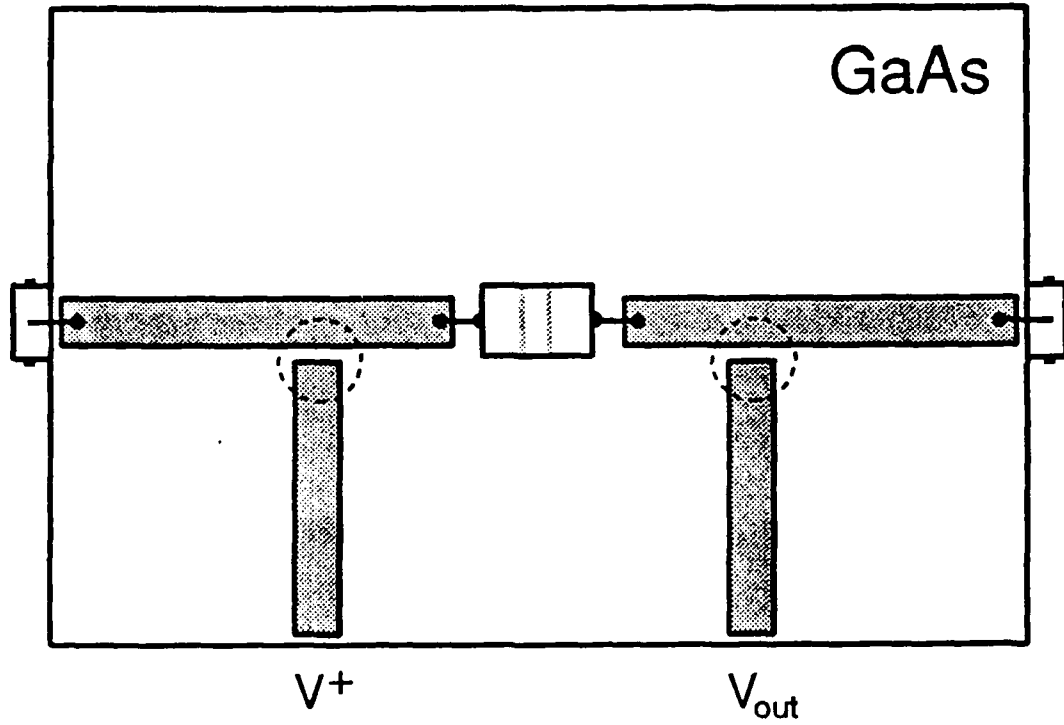
- SWITCHING TIME MEASURED 2ps
- SAKAKI DATA GIVES 8ps FOR THIS STRUCTURE

OUR WORK

A. USE OF PCE'S FOR MEASUREMENTS

B. USE OF CORRELATION TECHNIQUE FOR MEASURING PL DECAY

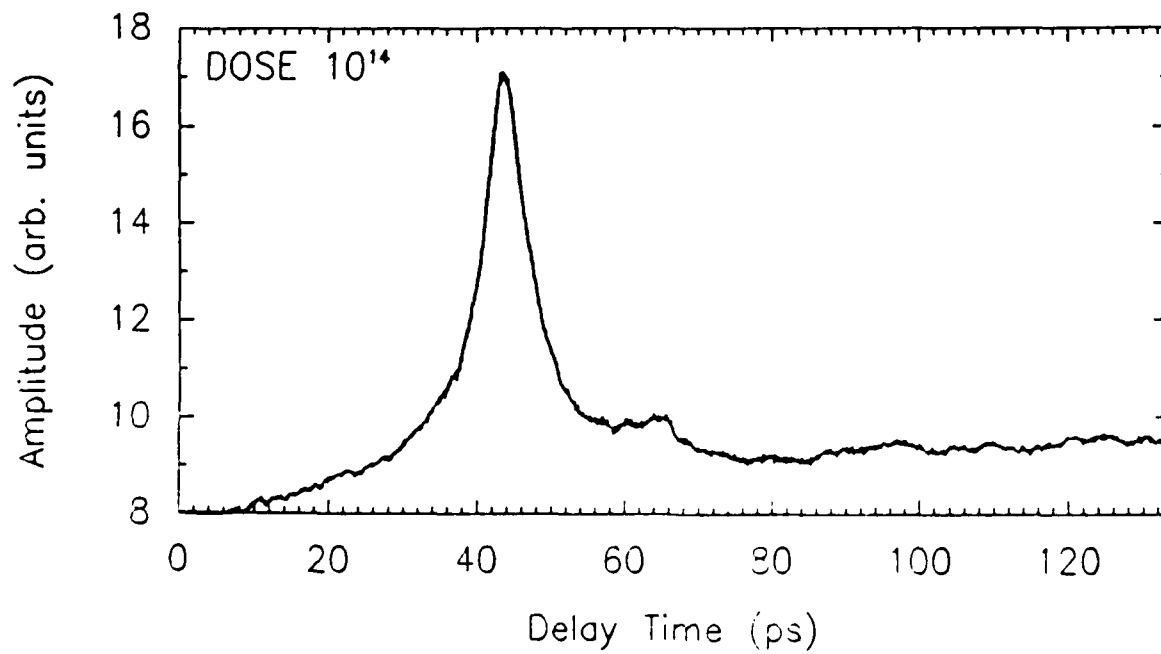
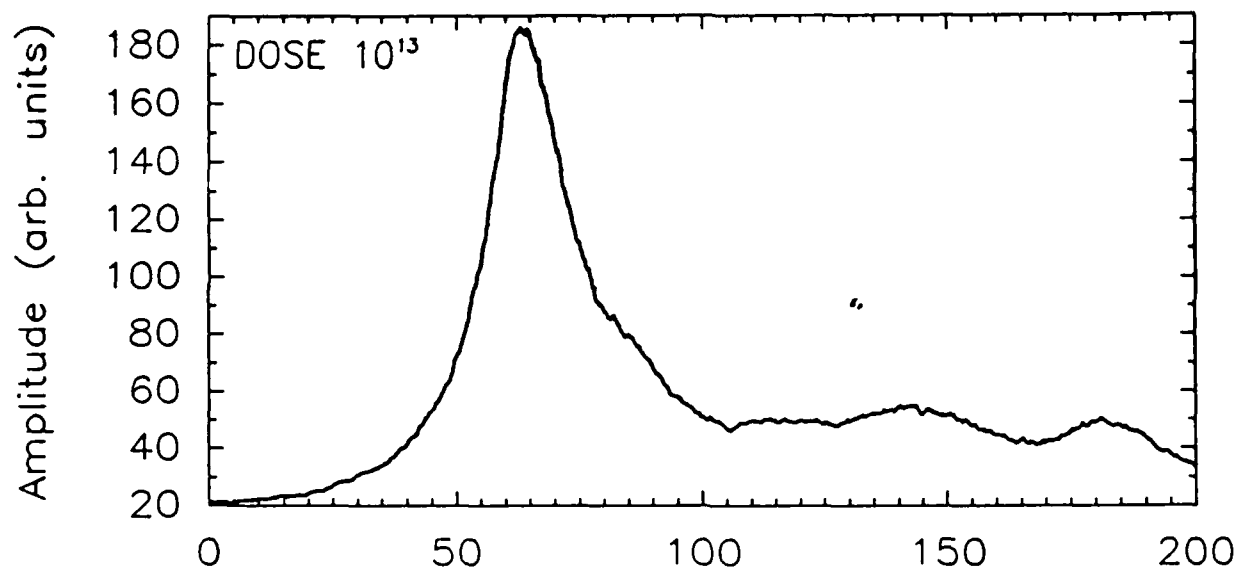
- LIMITED BY LASER SPEED
- TIMES SUBSTANTIALLY BELOW 10ps

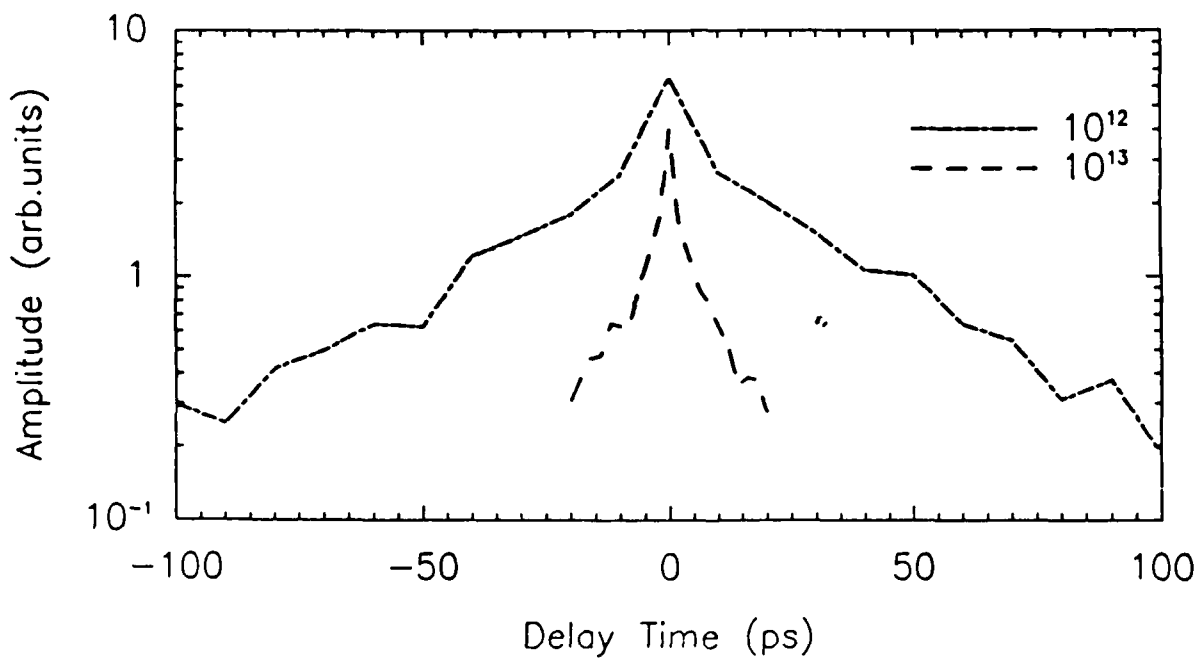
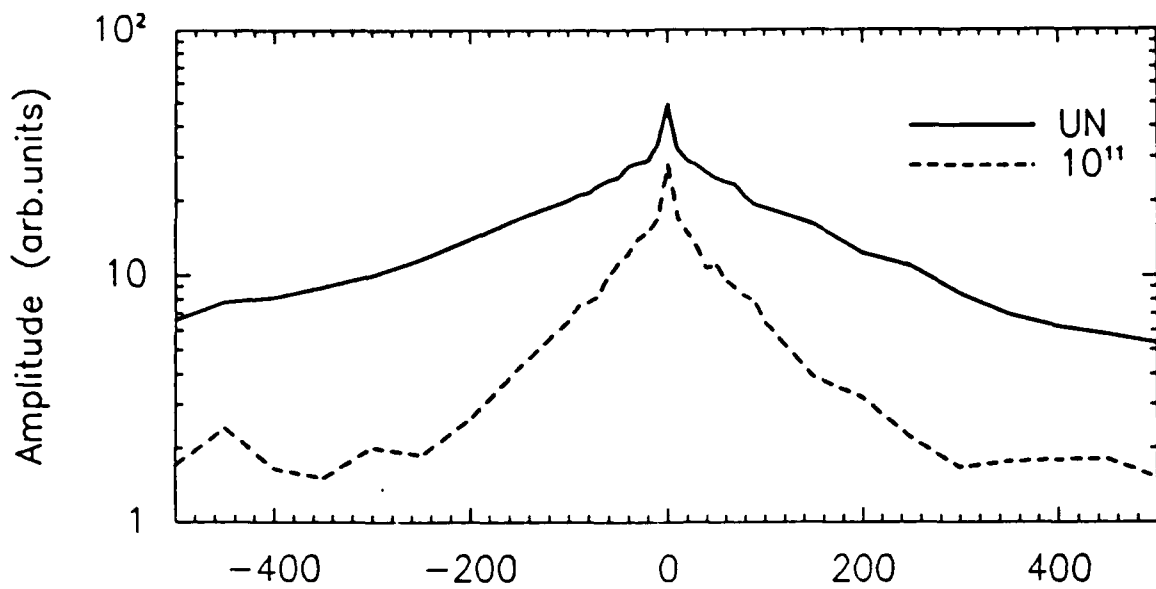


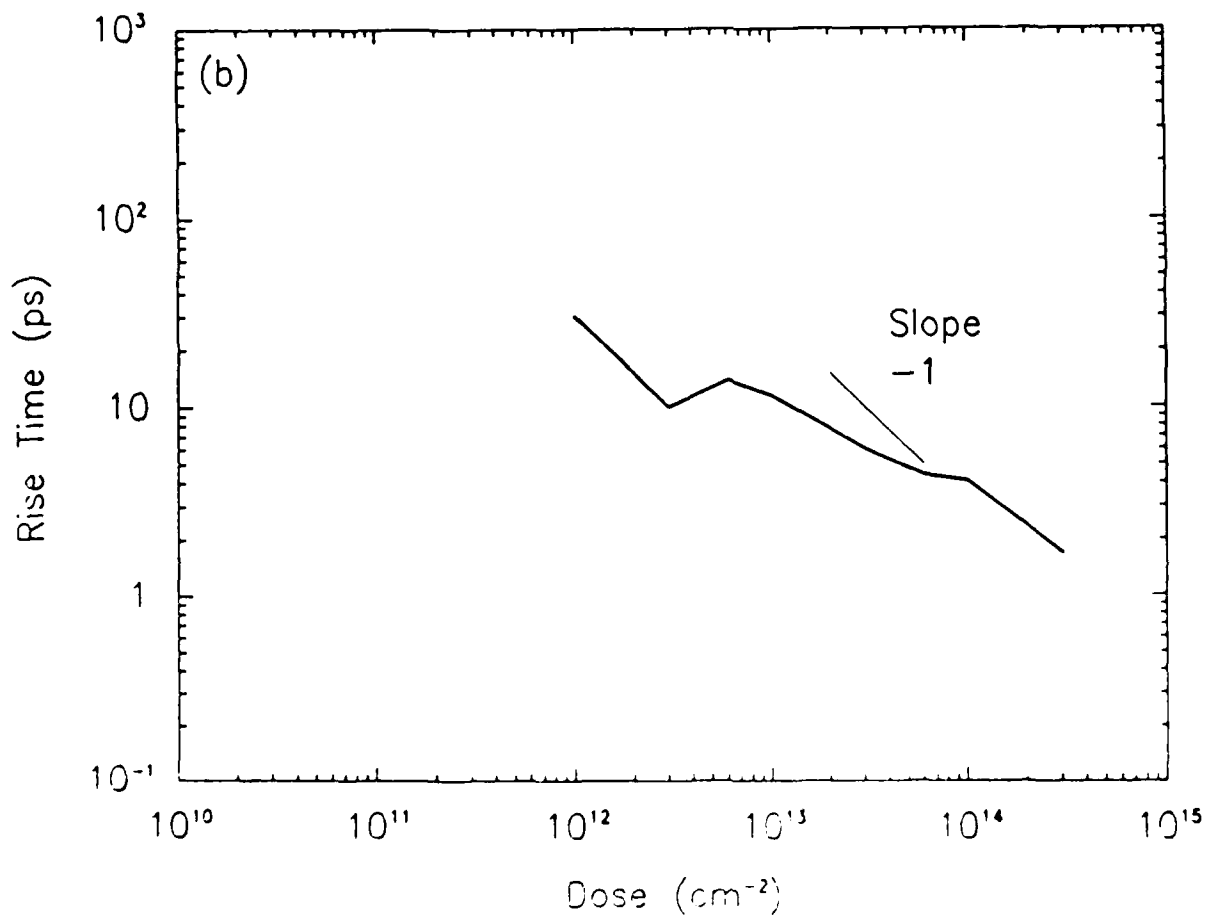
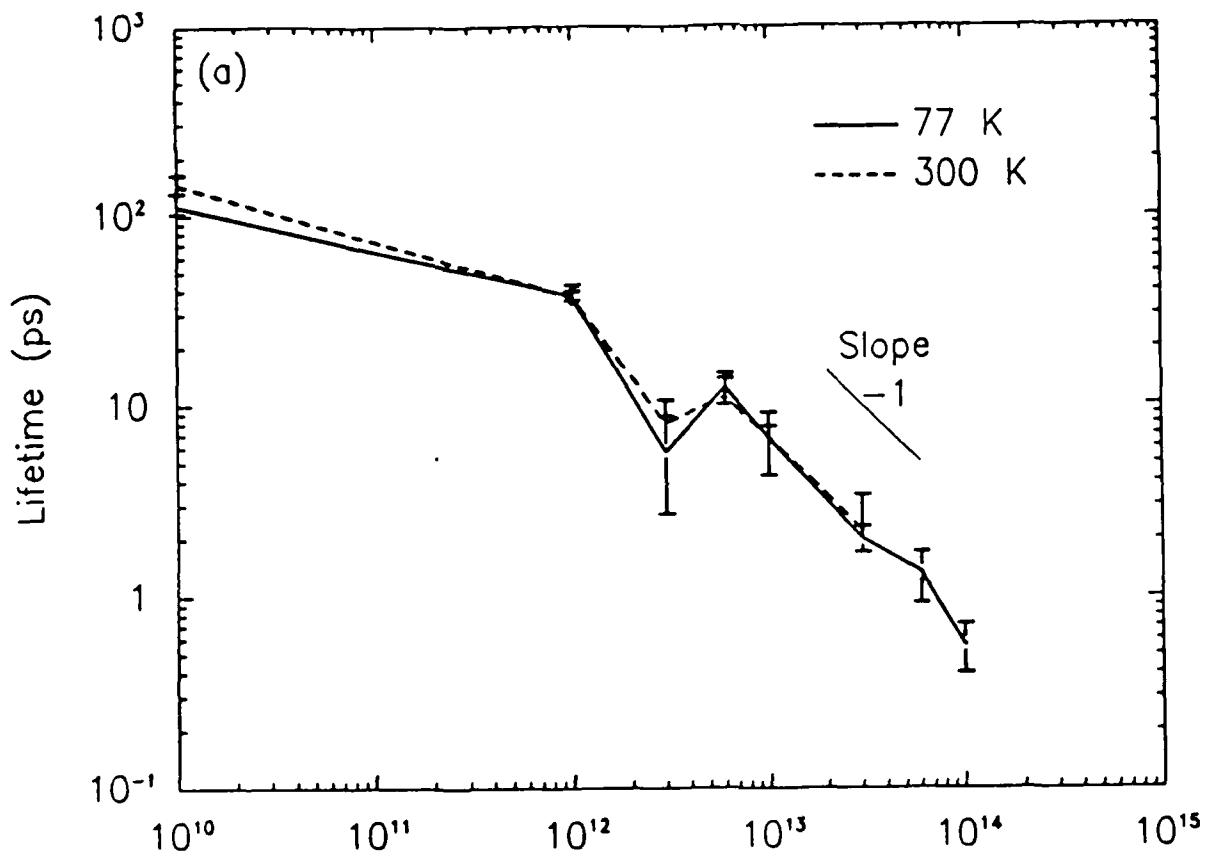
PCE MEASUREMENTS

- A. DESIGNED STRUCTURES AND SIMULATED PROPAGATION OF HIGH-SPEED PULSE ON STRIP-LINES

- B. CHARACTERIZED PCE MATERIAL



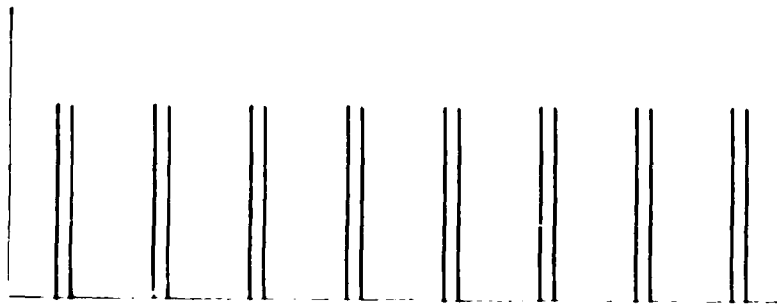
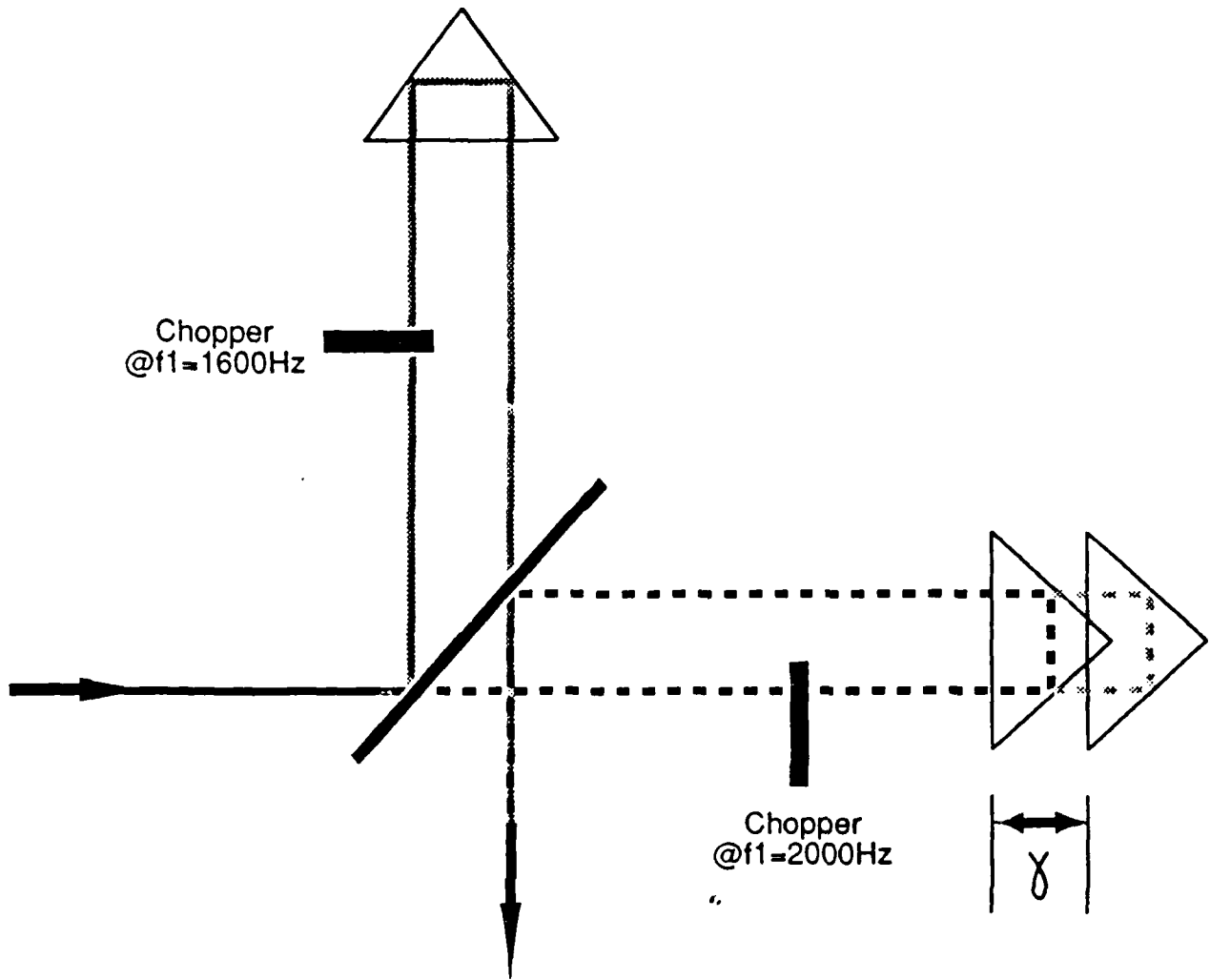




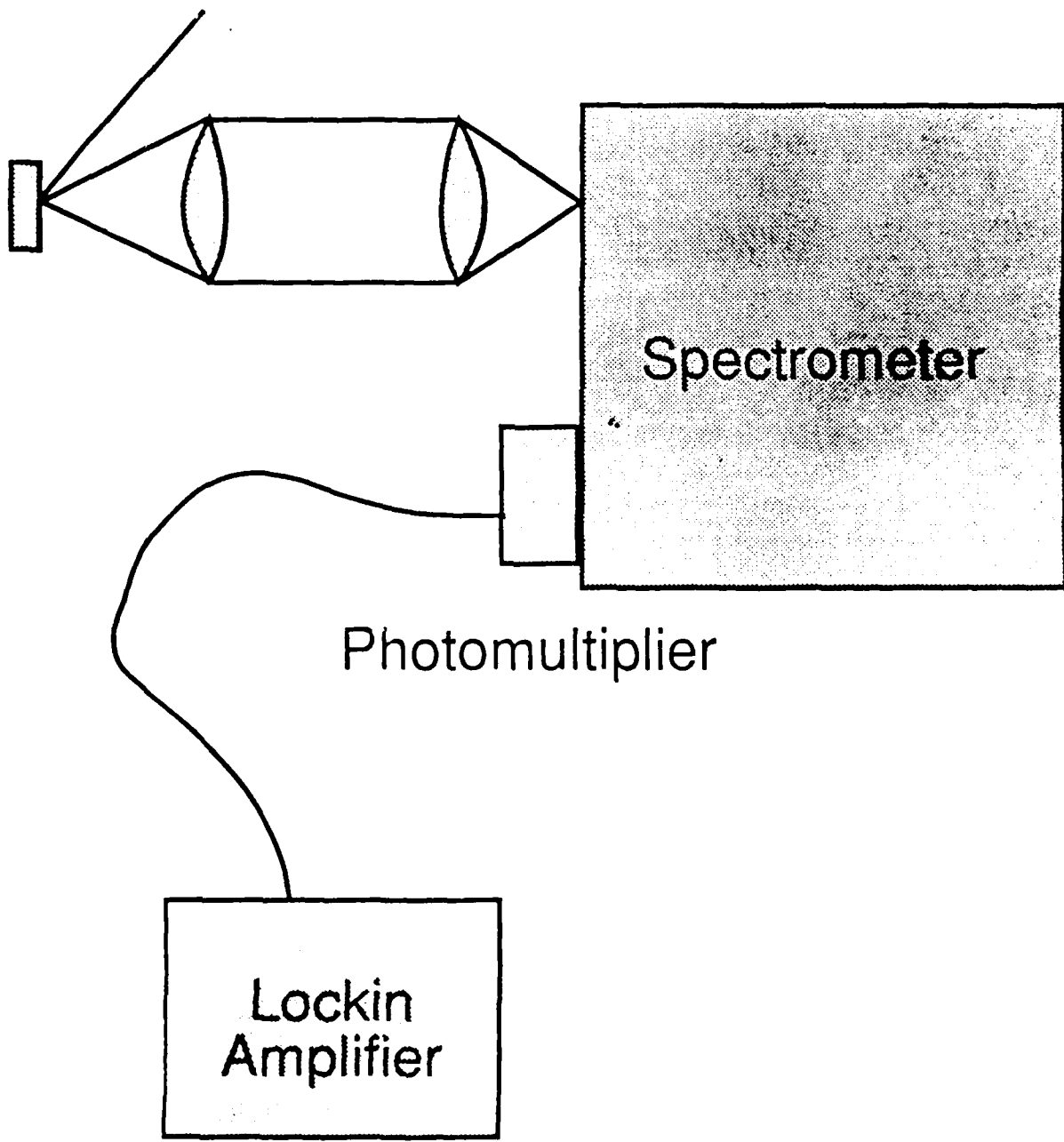
PL DECAY USING CORRELATION METHOD

A. THE METHOD

B. THE RESULTS



Time

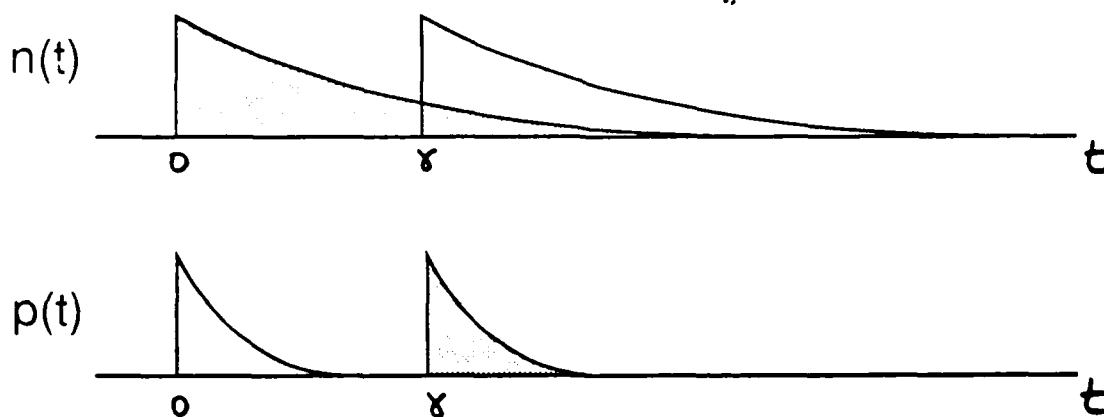


Photoluminescence Excitation Correlation Spectroscopy

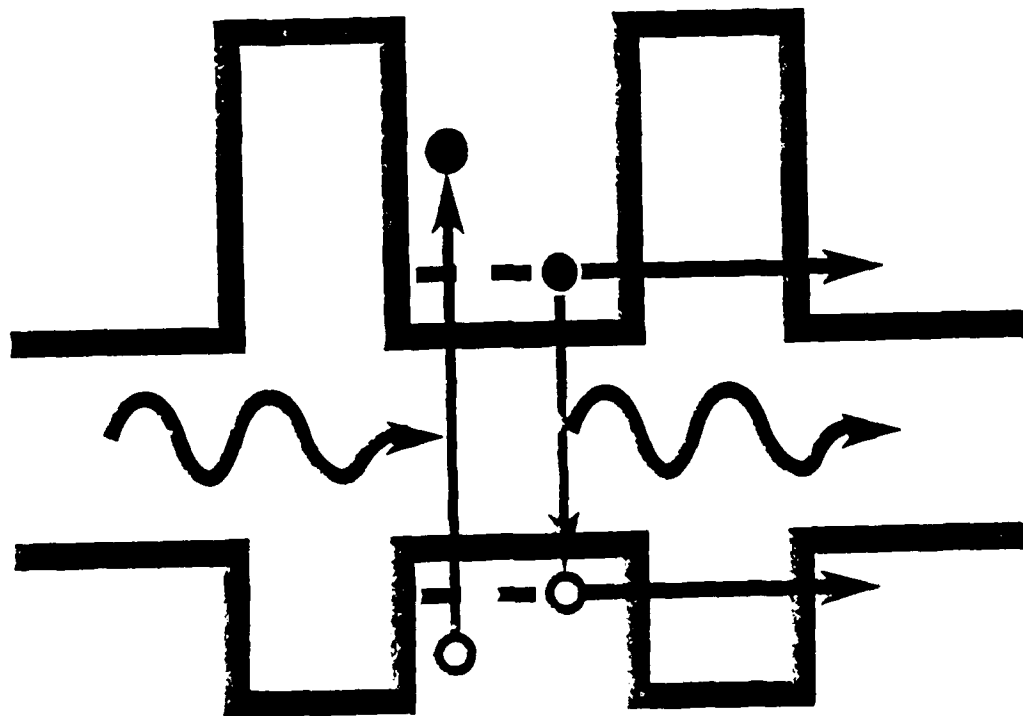
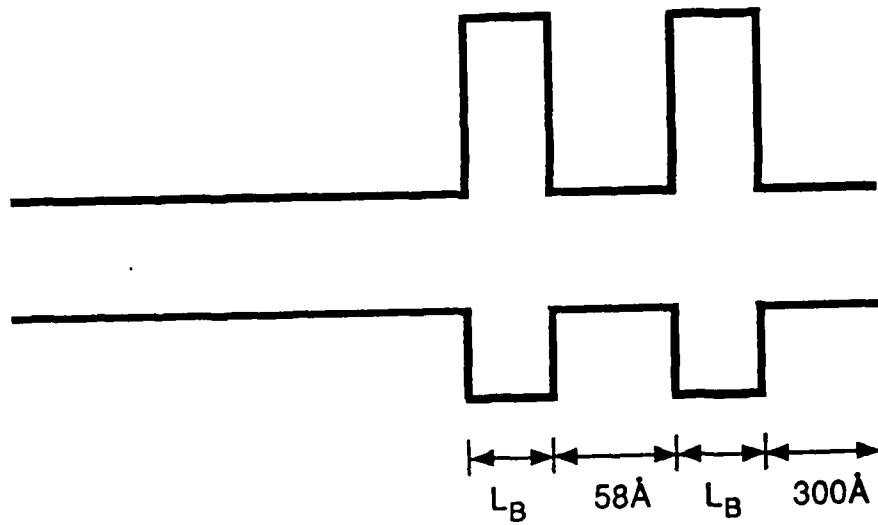
Detect at sum frequency

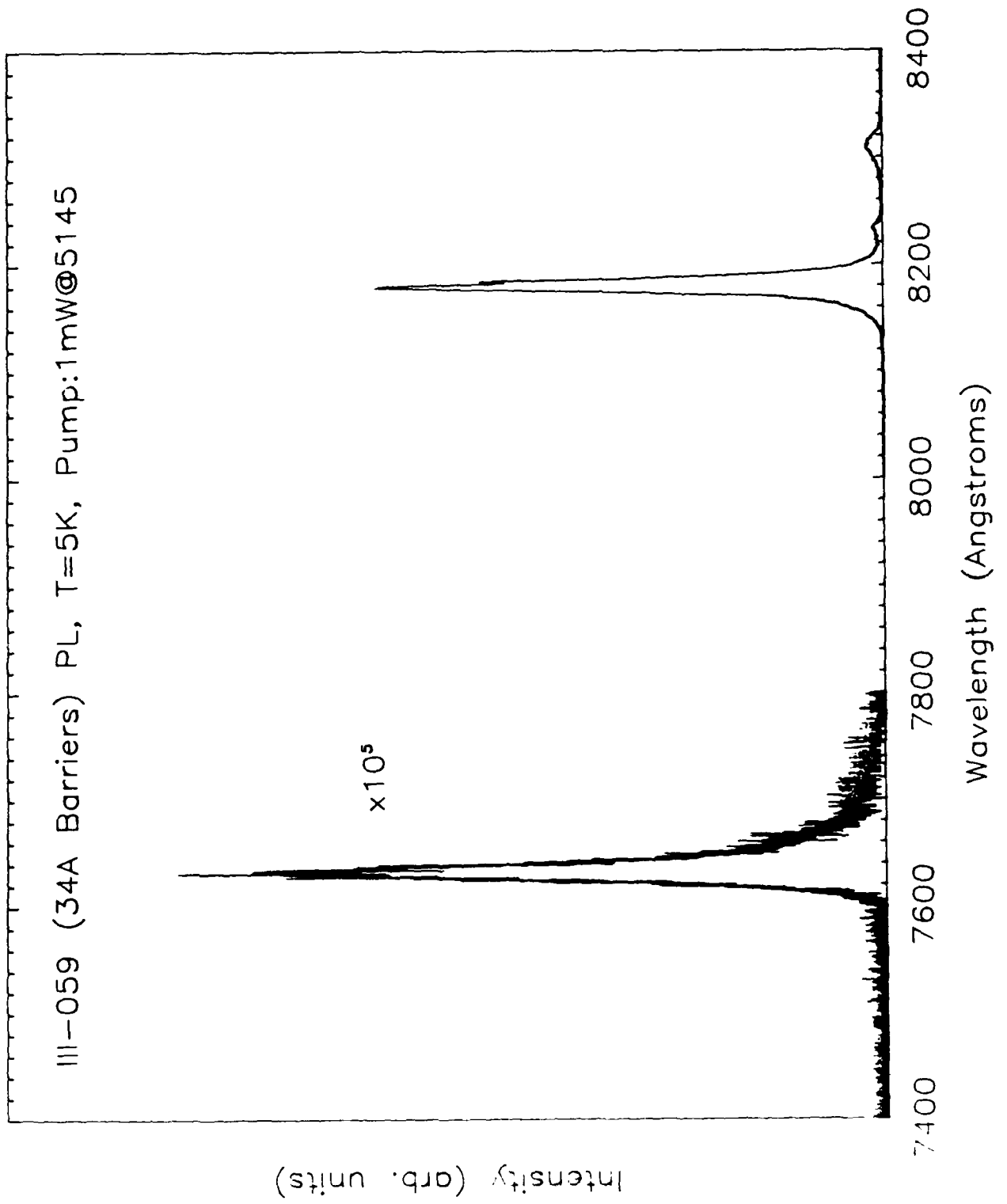
Cross correlation

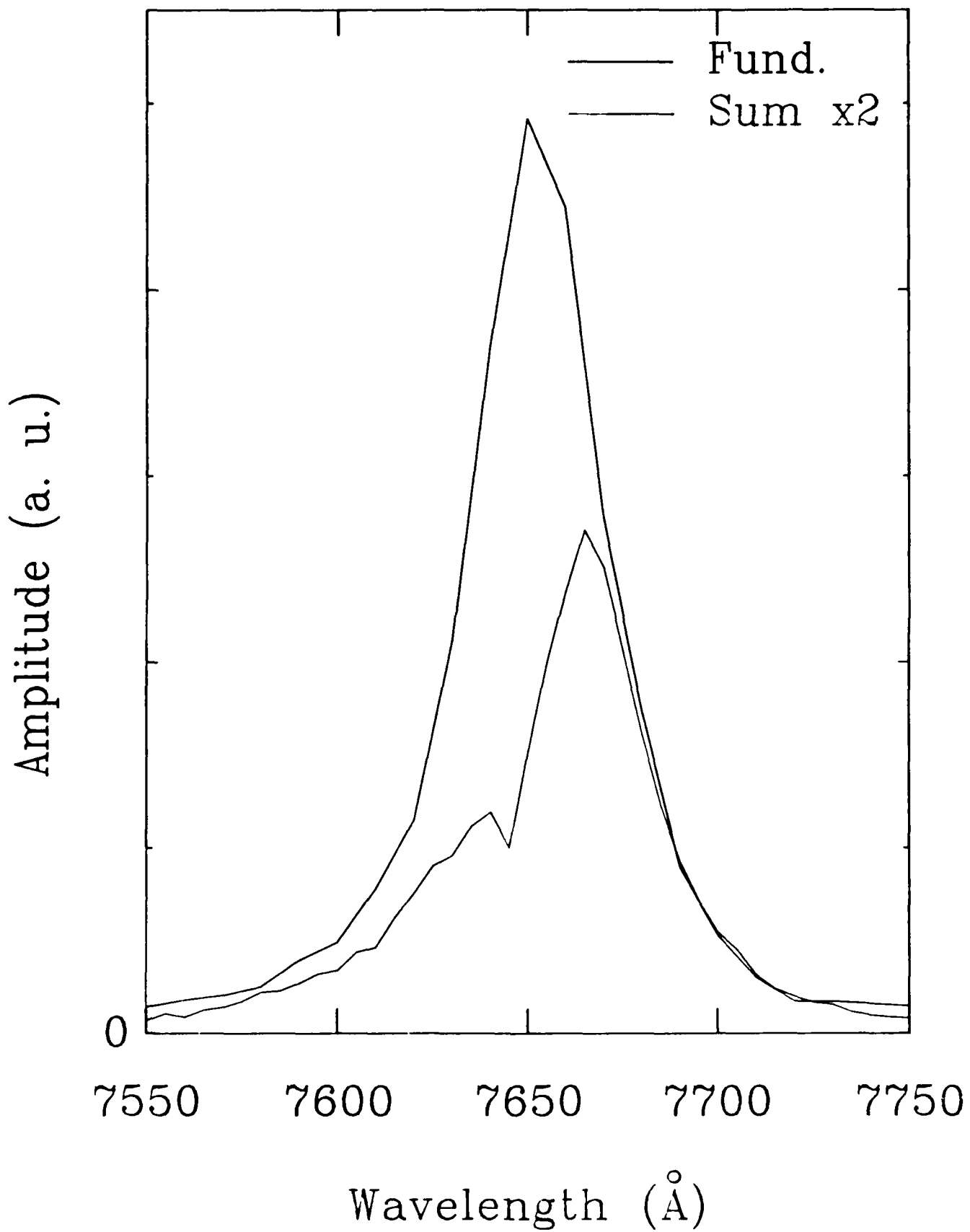
$$I_{\text{sum}}(\delta) \propto \int [n(t)p(t-\delta) + n(t-\delta)p(t)] dt$$

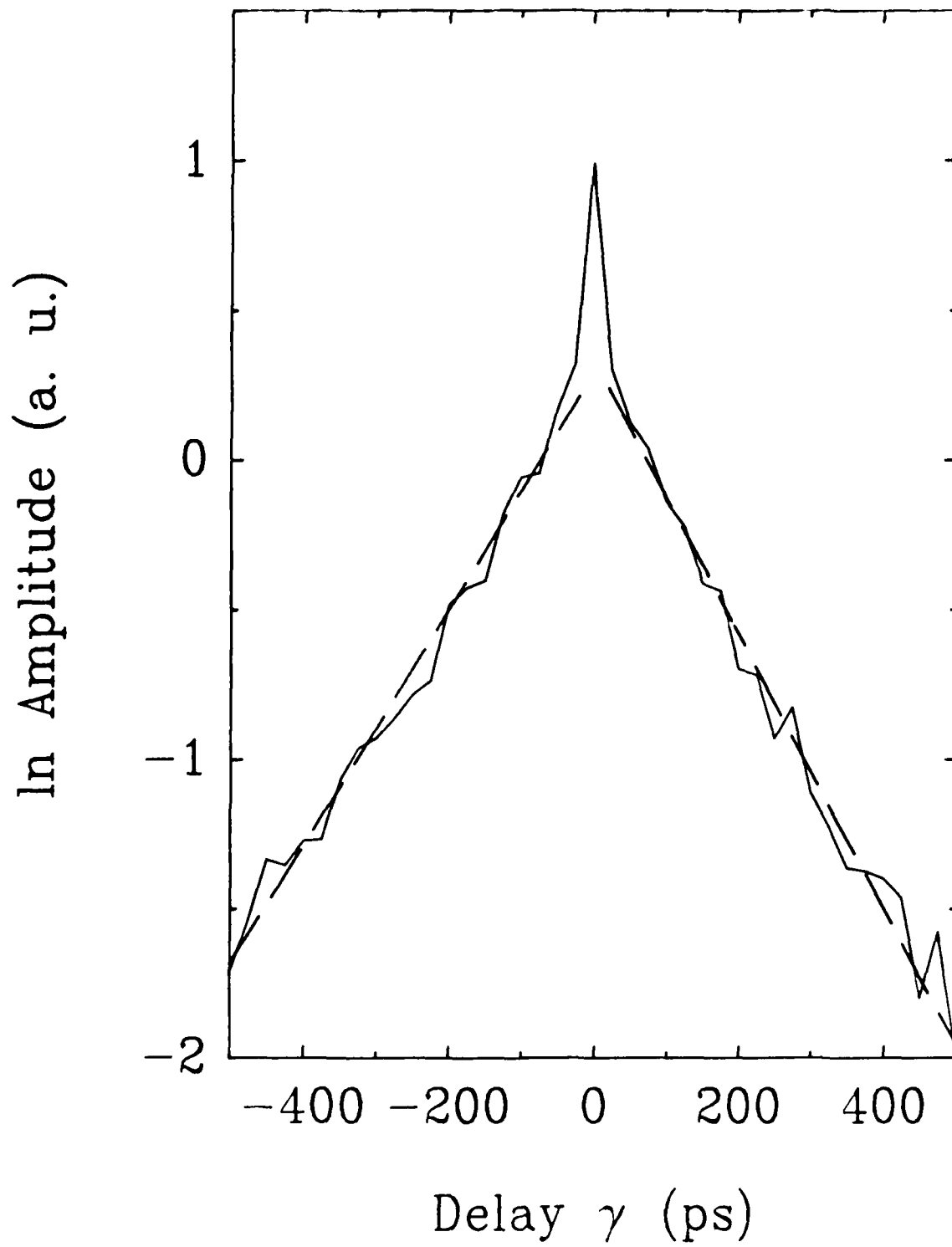


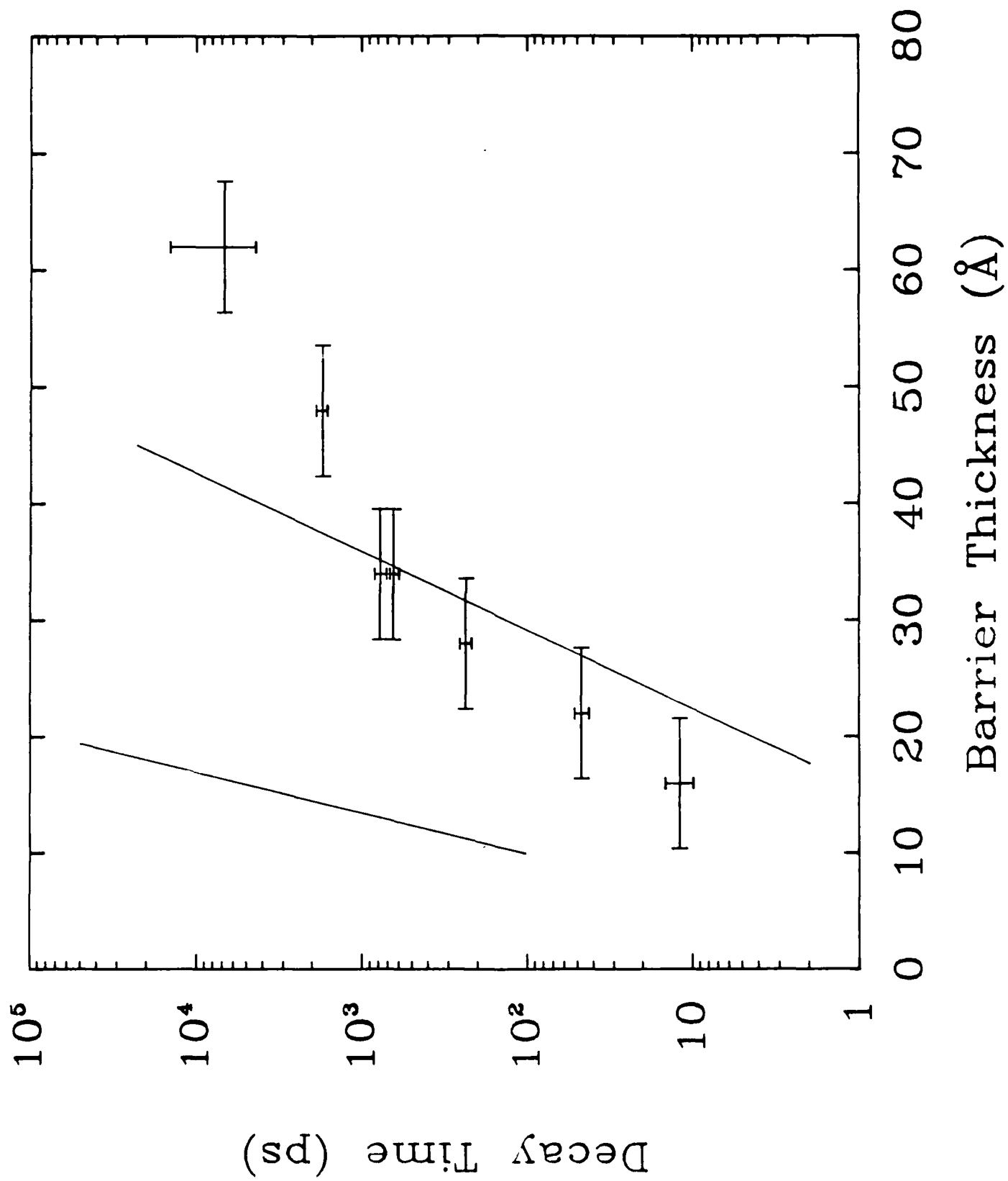
$$I_{\text{sum}}(\delta) \propto \left[e^{-|\delta|/\tau_1} + e^{-|\delta|/\tau_2} \right]$$



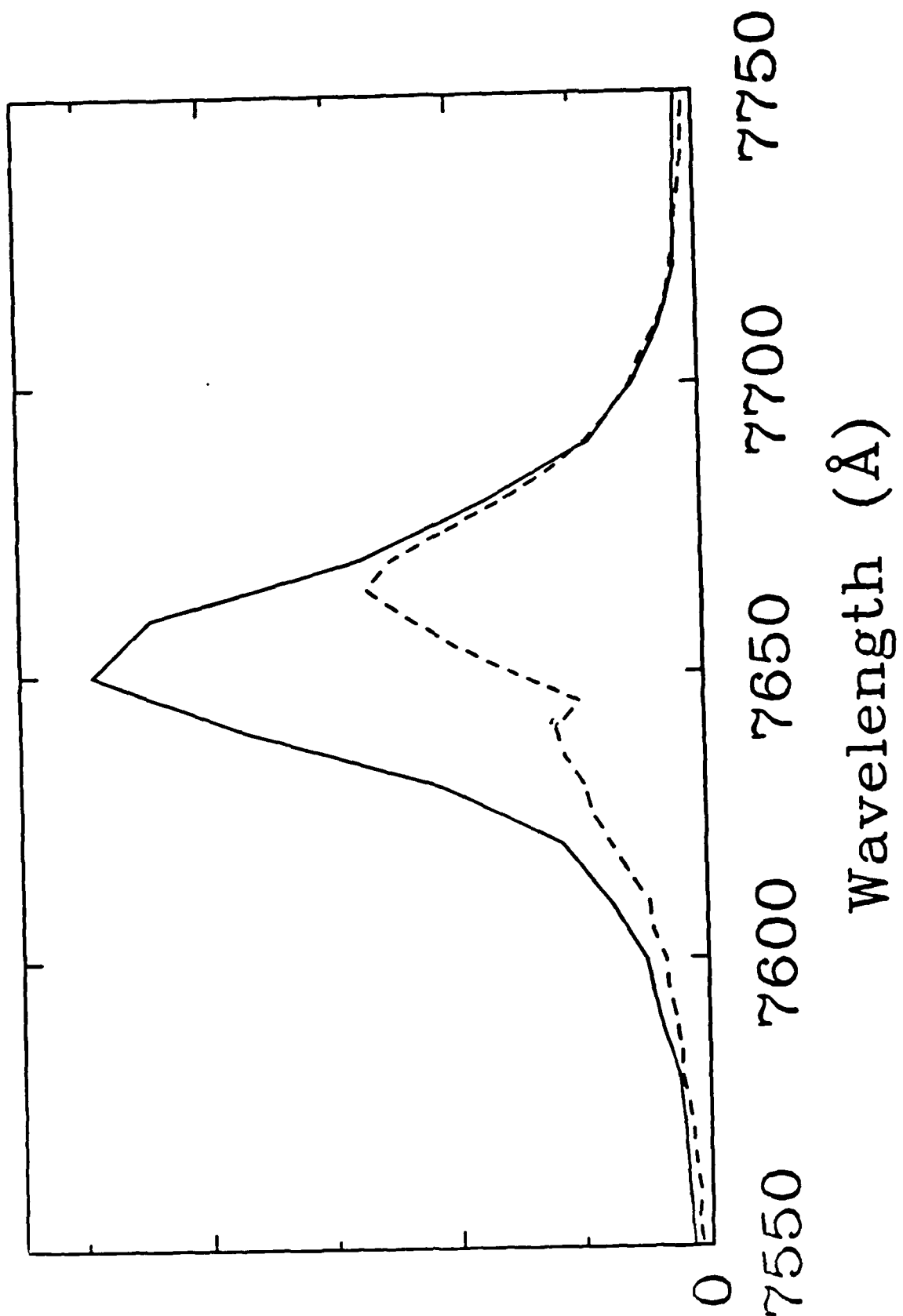


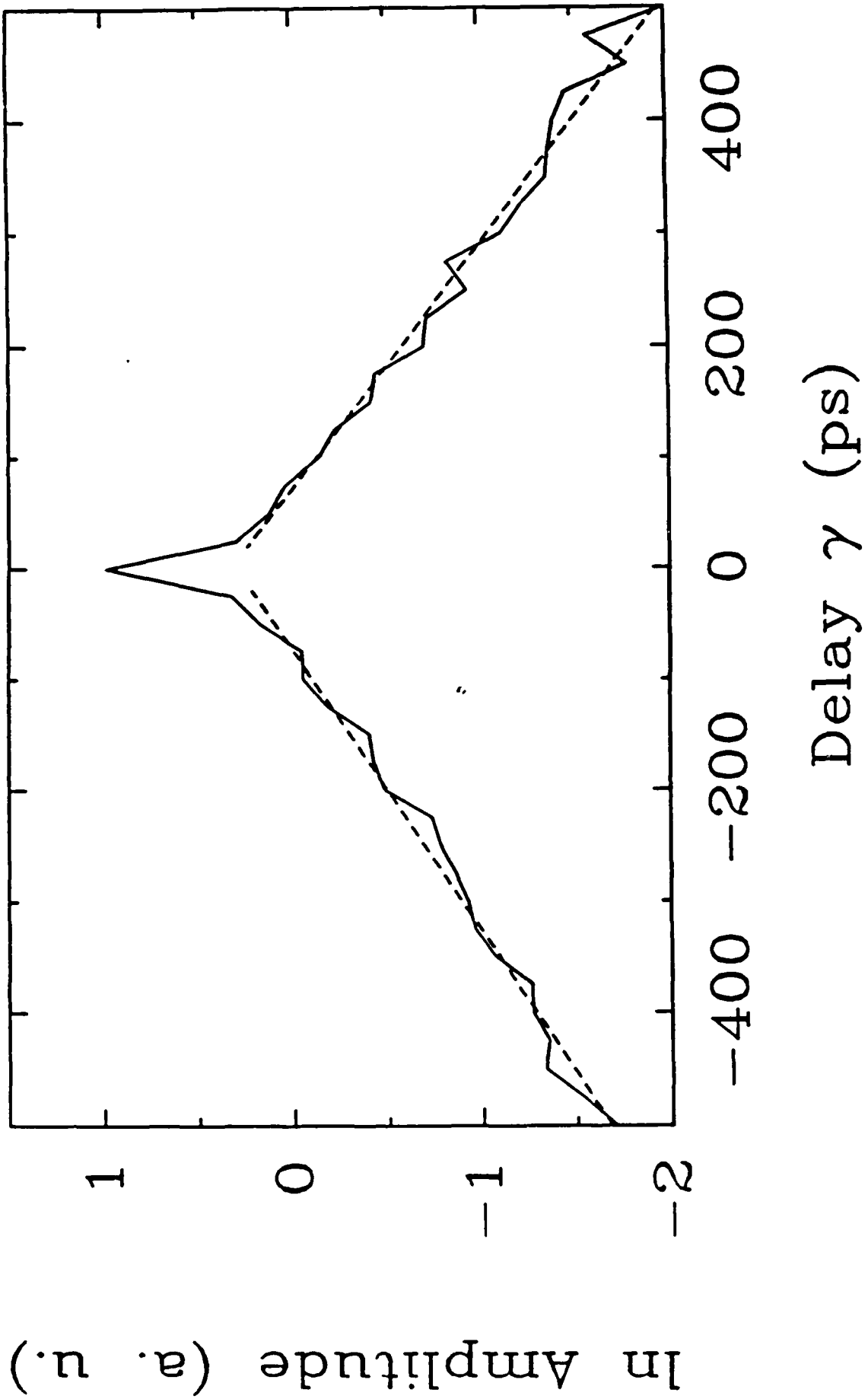


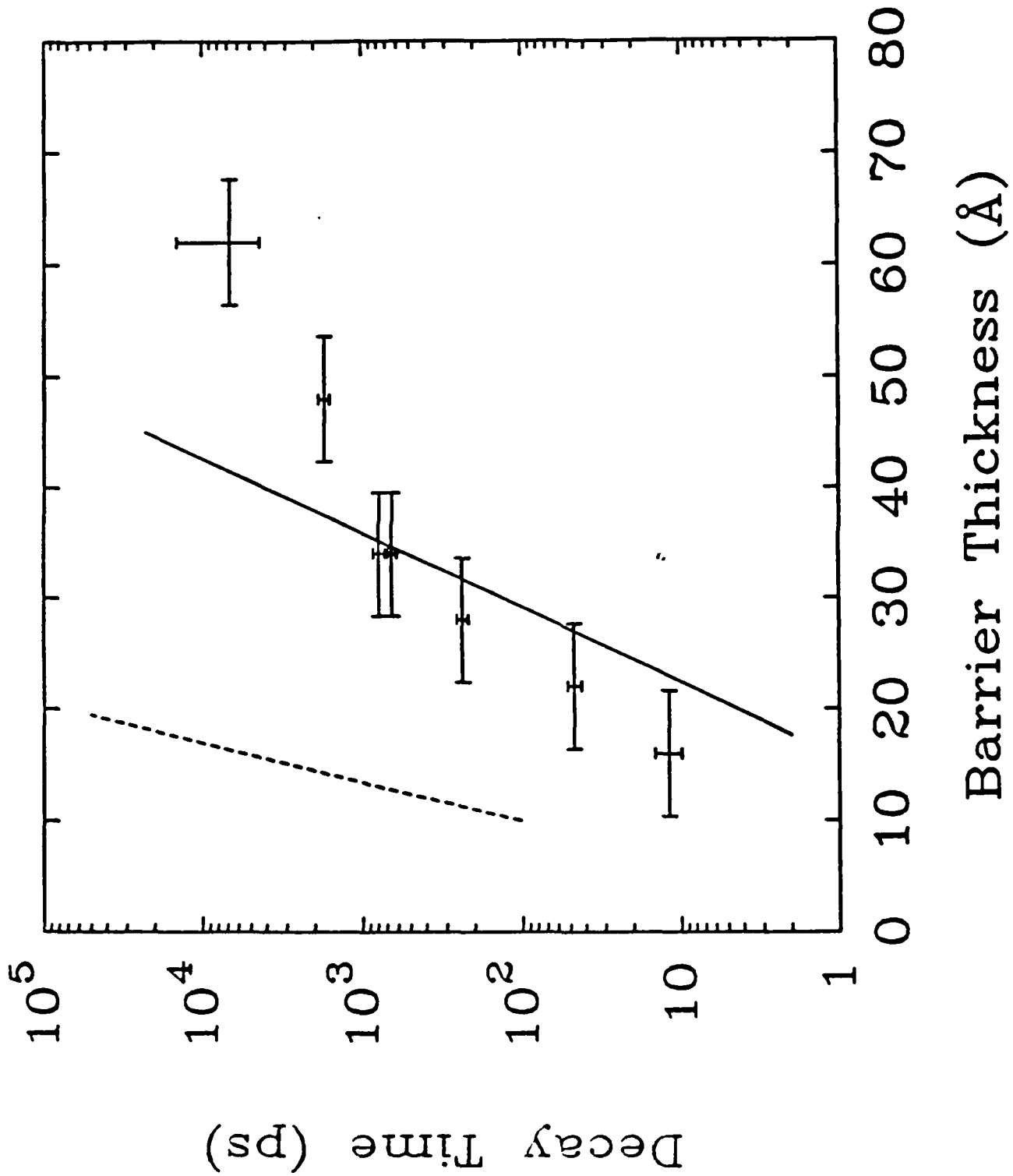




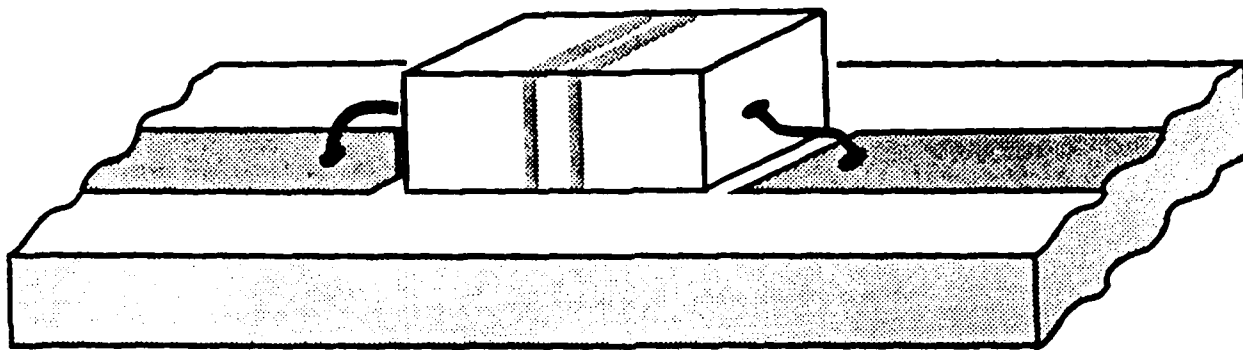
Amplitude (a. u.)



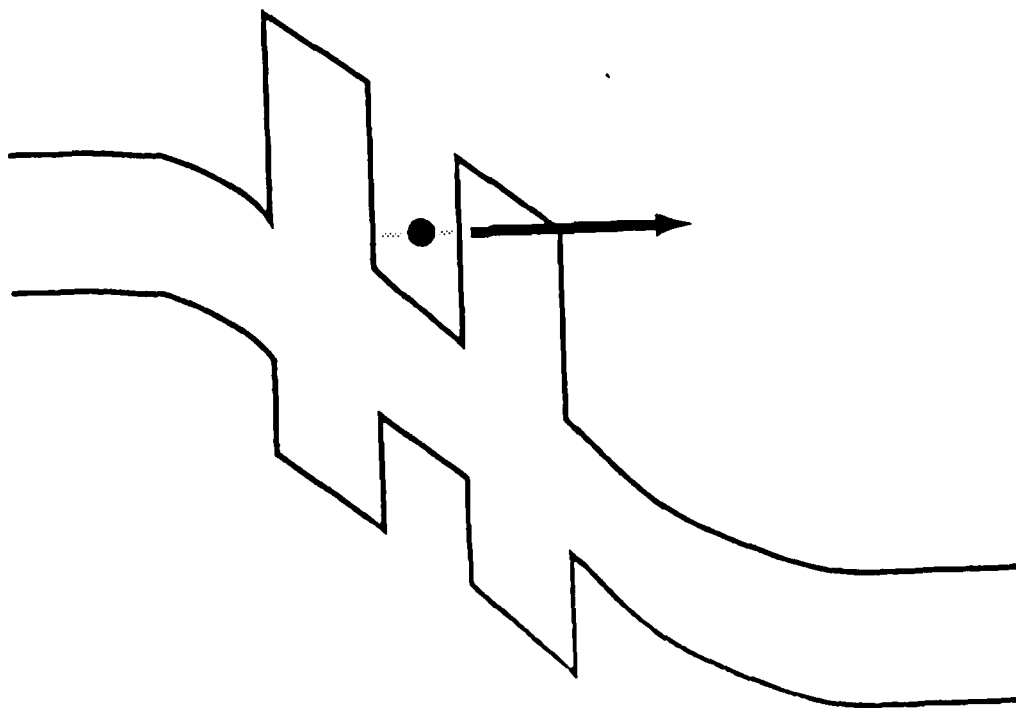


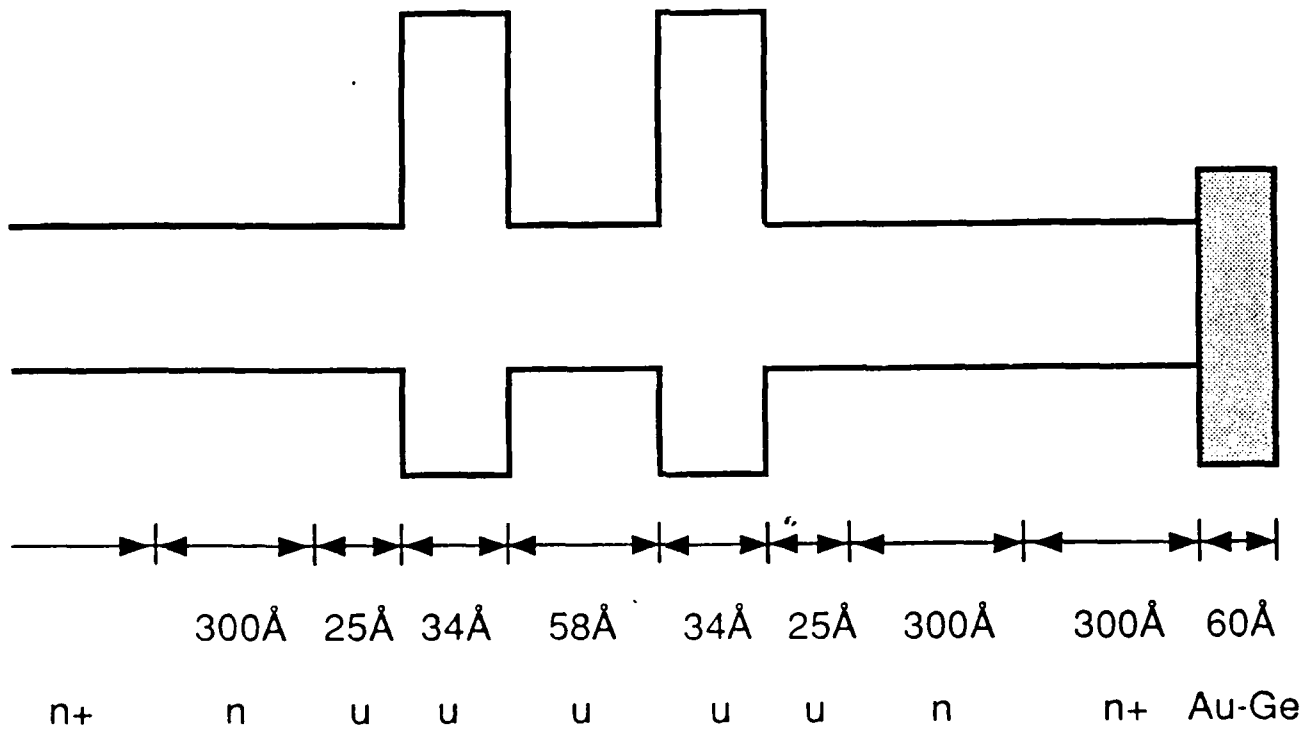


Real Device



Effect





Resonant tunneling through quantum wells at frequencies up to 2.5 THz

T. C. L. G. Sollner, W. D. Goodhue, P. E. Tannenwald, C. D. Parker, and D. D. Peck
 Lincoln Laboratory, Massachusetts Institute of Technology, Lexington, Massachusetts 02173

(Received 9 May 1983; accepted for publication 1 July 1983)

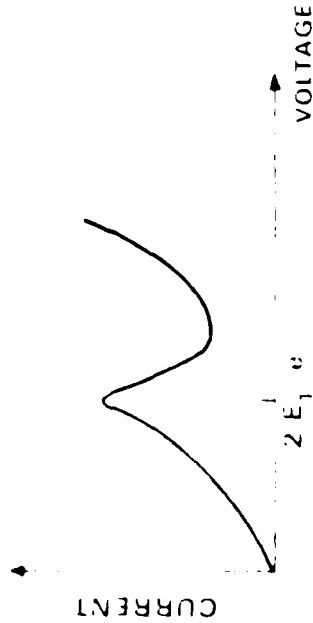
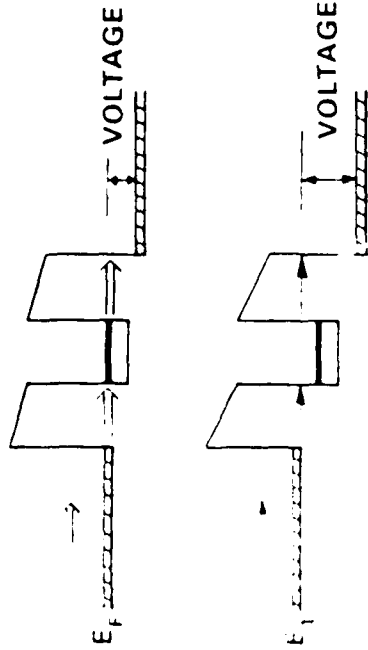
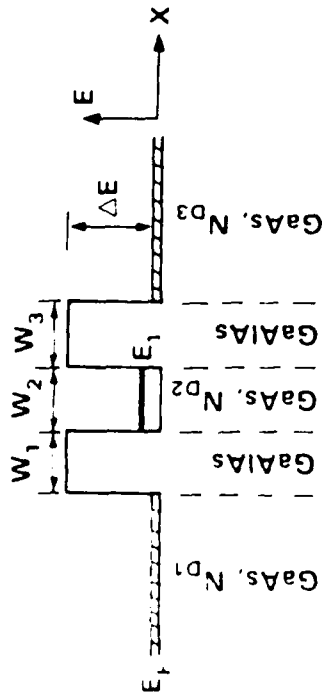


FIG. 1. Electron energy as a function of position in the quantum well structure. The parameters are $N_{D1} = N_{D2} = 10^{18} \text{ cm}^{-3}$, $N_{D3} = 10^{17} \text{ cm}^{-3}$, and $B_1 = B_2 = B_3 = 50 \text{ \AA}$. The doping level in the well center is an average value achieved by placing a layer of 10^{18} cm^{-3} material in the central 10% of the well. The energy level E_1 occurs above the bottom of the bulk conduction band because of confinement in the x direction. From the aluminum concentration ($\sim 2\%$, 30%) we estimate $\Delta E = 0.23 \text{ eV}$.

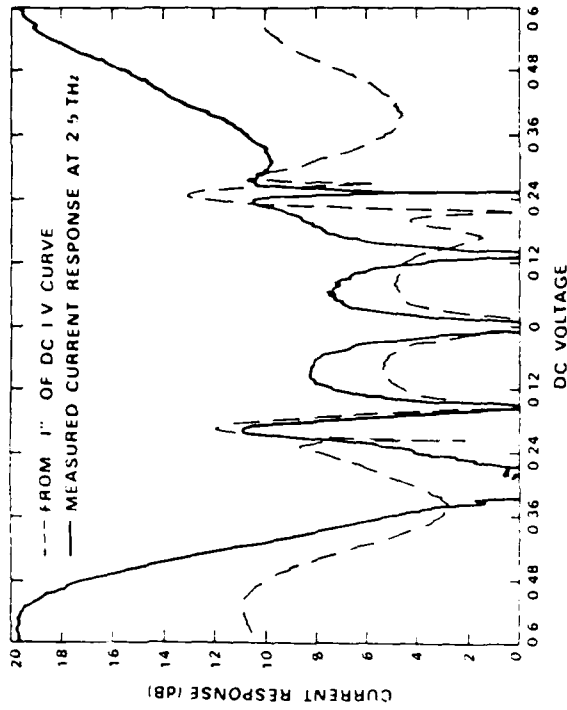
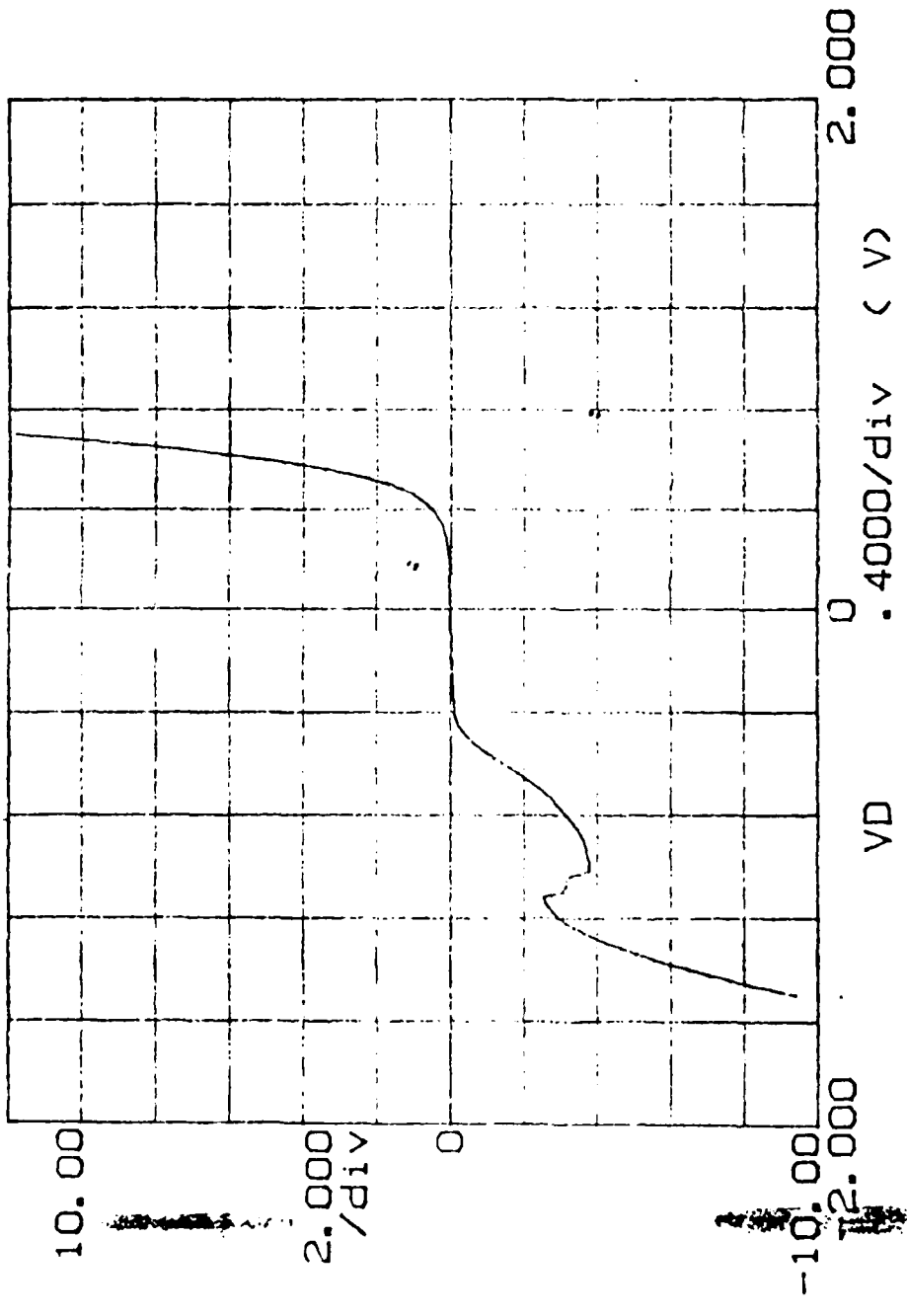


FIG. 3. Current response at 2.5 THz as a function of dc bias voltage. (Sample is at 25 K.) The dashed curve is calculated on the basis of the dc I - V curve. Zero decibels corresponds to $0.3 \mu\text{A/W}$ and 10 dB is $3 \mu\text{A/W}$. The general agreement shows that the I - V curve at 2.5 THz is very similar to the dc curve, and thus the charge transport is fast.

ID (mA) 247U $\frac{2}{3}$

T=77K



250 μ m device
60 Ω AuGe

SUMMARY OF OUR MEASUREMENTS

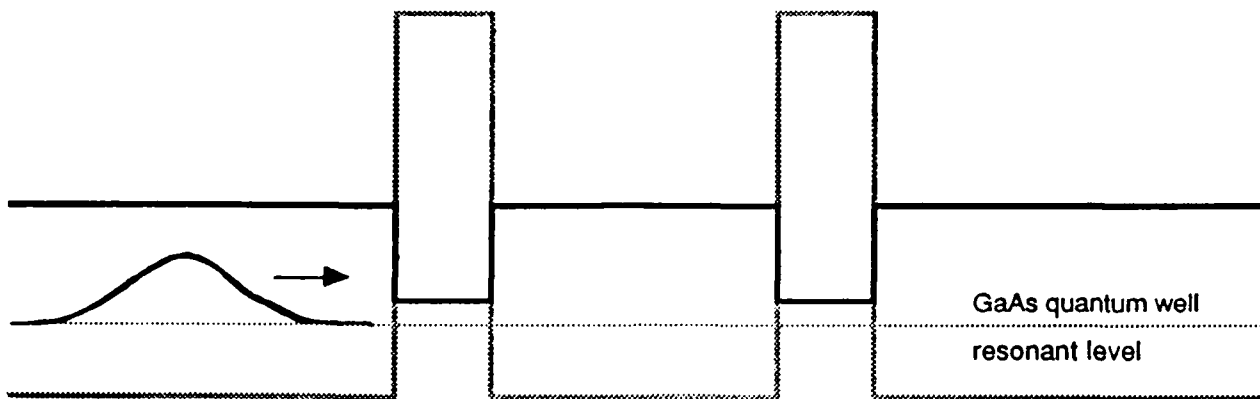
- A. CARRIED OUT PL DECAY MEASUREMENTS ON TUNNEL STRUCTURES
- B. MEASUREMENTS TO SHORTER TIMES THAN SAKAKI TO 10ps
- C. MEASURED A SINGLE DECAY TIME AT 80K
- D. ROLE OF DIFFERENCES IN ELECTRON AND HOLE DECAY TIMES UNCLEAR
- E. BEGINNING BIAS DEPENDENCE MEASUREMENTS

SUMMARY OF TUNNELING TIMES

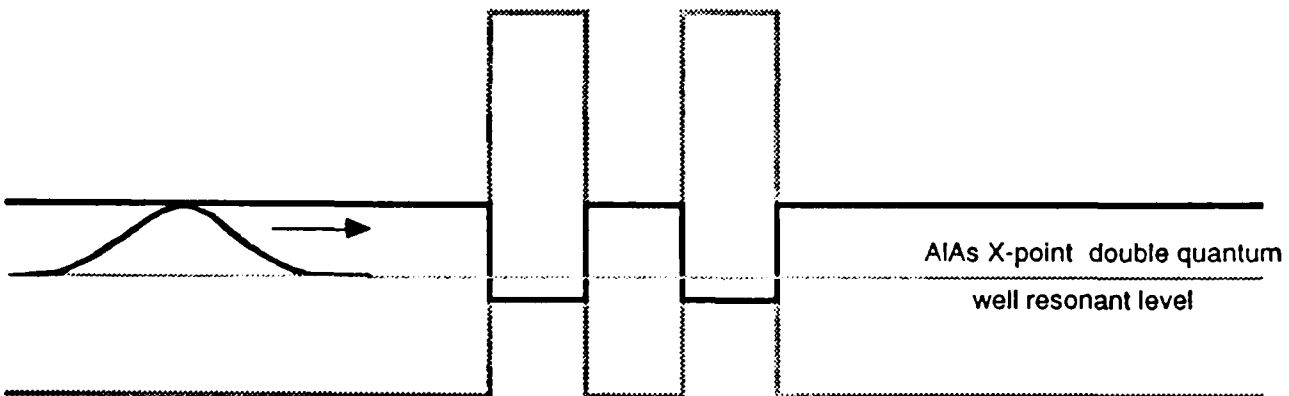
Source	Prediction for 16Å	Thickness for 2ps
Our Experiments; T=80K $\tau_T = 0.203e^{0.255L_B}$	12ps	9Å
2 Band Theory $\tau_T =$ $0.0047e^{0.342L_B}$	1.1ps	18Å
Sakaki and Co-workers: T=20K $\tau_T = 0.670e^{0.158L_B}$; T=90K $\tau_T = 0.229e^{0.201L_B}$	8.4ps (T=20K); 5.7ps (T=90K)	6.9Å (T=20K); 11Å (T=90K)

Resonant Tunneling

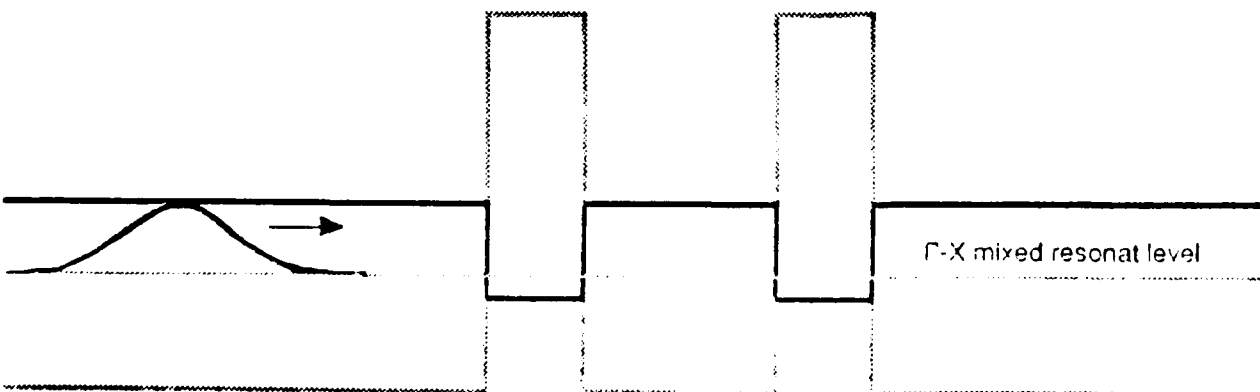
1. Γ -point resonant tunneling



2. X-point resonant tunneling



3. Resonant tunneling through Γ -X mixed state



Tunneling escape time of electrons from a quantum well under the influence of an electric field

T. B. Norris
Laboratory for Laser Energetics, and Department of Physics and Astronomy, University of Rochester, 250 East River Road, Rochester, New York 14623-1299

X. J. Song, W. J. Schaff, and L. F. Eastman
The School of Electrical Engineering, Cornell University, Ithaca, New York 14850

G. Wicks
The Institute of Optics, University of Rochester, Rochester, New York 14627

G. A. MOUROU^{a1}
Laboratory for Laser Energetics, University of Rochester, 250 East River Road, Rochester, New York 14623-1299

(Received 22 July 1988; accepted for publication 21 October 1988)

60 *Appl. Phys. Lett.* **54** (1), 2 January 1989

p ⁺	Al _x Ga _{1-x} As	2000 Å
i	Al _x Ga _{1-x} As	2000 Å
i	GaAs	30 Å
i	Al _x Ga _{1-x} As	b
i	GaAs	1000 Å
n ⁺	GaAs	1 μm

S.I. Substrate

FIG. 1. Structure of the single QW samples used in width b was varied to study the effect on the tunnel

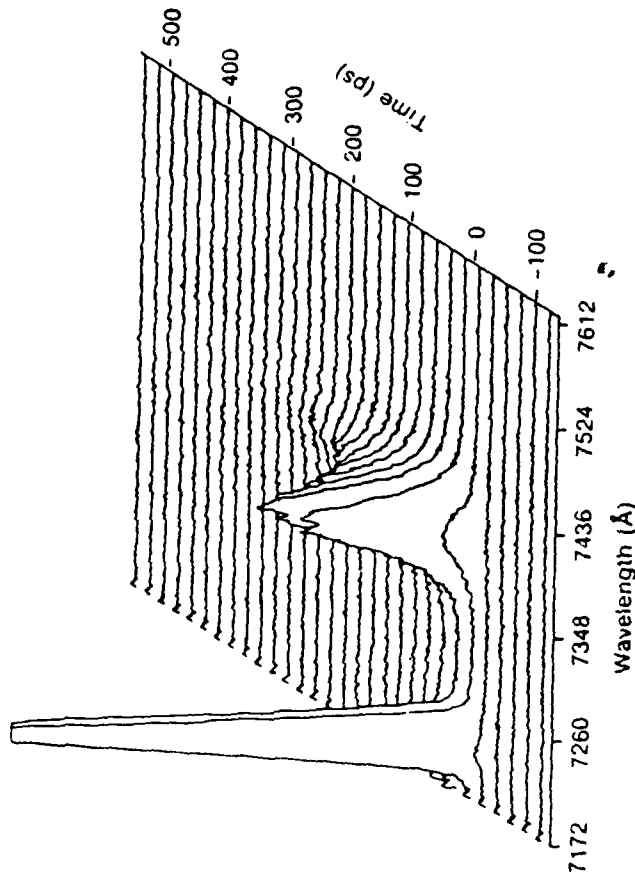


FIG. 2. Time-resolved PL spectrum from sample with $x = 30\%$, $b = 85$ Å at zero bias. The peak at 740 nm is the QW PL; the peak at 722 nm is scattered laser pump light.

Tunneling escape time of electrons from a quantum well under the influence of an electric field

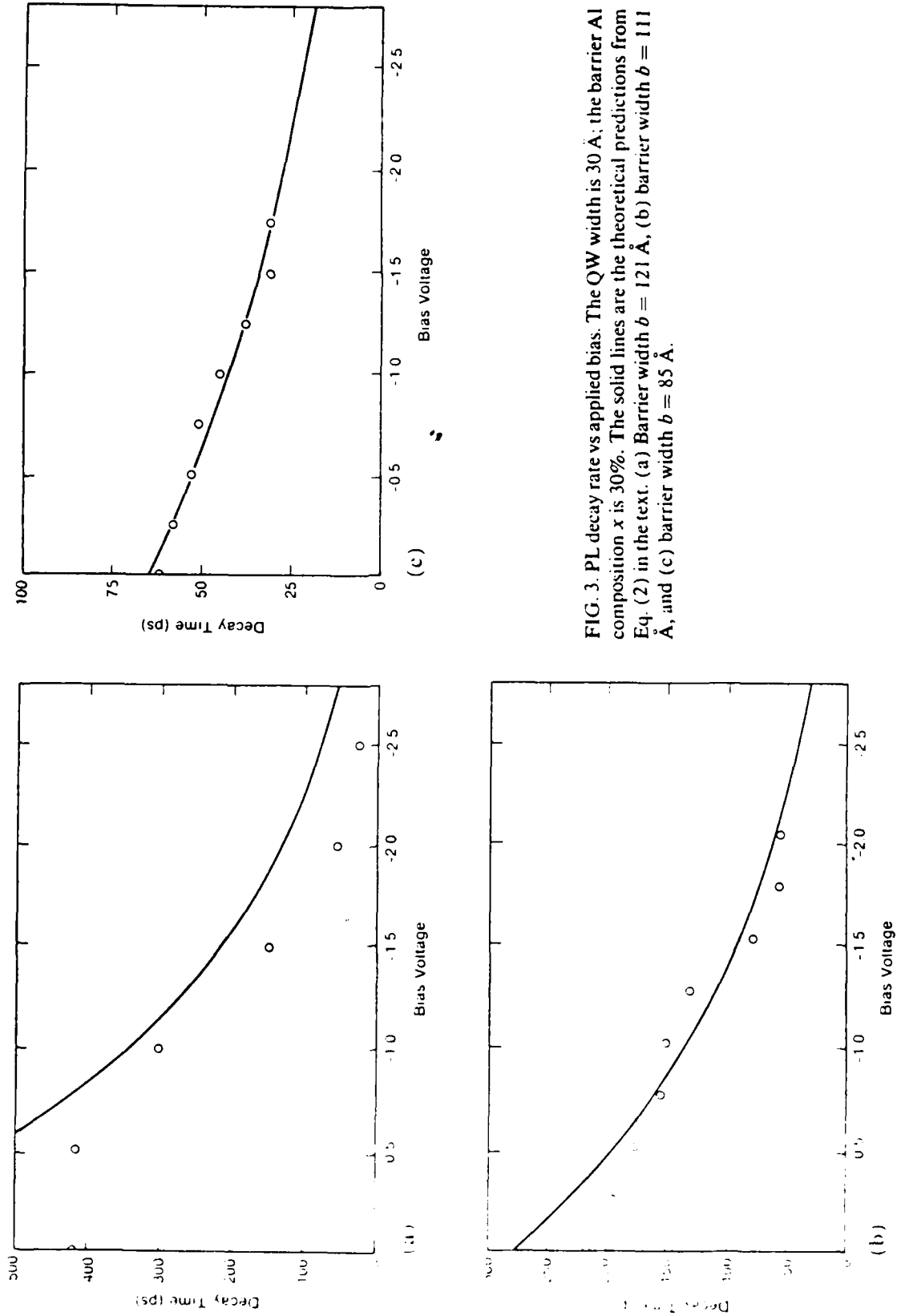


FIG. 3. PL decay rate vs applied bias. The QW width is 30 Å; the barrier Al composition x is 30%. The solid lines are the theoretical predictions from Eq. (2) in the text. (a) Barrier width $b = 121 \text{ \AA}$, (b) barrier width $b = 111 \text{ \AA}$, and (c) barrier width $b = 85 \text{ \AA}$.

MEASUREMENTS OF BIAS DEPENDENCE OF PL DECAY

- A. STRUCTURE NOT REALISTIC BARRIER WIDTH $>85\text{\AA}$
- B. DECAY TIMES MEASURED GREATER THAN 30-50ps
- C. SUBSTANTIAL DISAGREEMENT BETWEEN THEORY AND EXPERIMENT FOR THINNER BARRIERS

FUTURE PLANS

- A. MAKE BIAS DEPENDENCE MEASUREMENTS OF PL DECAY

- B. MAKE SIMULATIONS OF MEASUREMENT
 - DIFFERENCE IN BEHAVIOR OF ELECTRONS AND HOLES
 - ROLE OF BANDSTRUCTURE
 - COMPARE IN DETAIL THEORY AND EXPERIMENT

- C. INVESTIGATE THE USE OF OTHER TECHNIQUES
 - PCE STRIP LINE METHOD
 - ELECTRO-OPTIC READOUT

- D. MEASURE NEW TUNNEL STRUCTURES

EHF HBT Development

B. Bayraktaroglu

*Texas Instruments
Dallas, TX*



CENTRAL RESEARCH LABORATORIES

EHF HBT DEVELOPMENT

AGENDA

- PROGRAM GOALS
- APPROACH
- DEVICE STRUCTURE
- FABRICATION
- CHARACTERIZATION AND MODELING
- SUMMARY



EHF HETEROJUNCTION BIPOLAR TRANSISTOR

OBJECTIVE

DEVELOPMENT OF InGaAs/InP(InAlAs) HETEROJUNCTION BIPOLAR TRANSISTOR ON A GaAs SUBSTRATE FOR POWER AMPLIFICATION AT EHF BAND.

GOALS

FREQUENCY (GZ)	OUTPUT POWER (W)	GAIN (dB)	EFFICIENCY (%)
44	1.0	6	40
60	0.5	6	30
94	0.25	6	20



SCOPE

- DEVELOPMENT OF MATERIALS TECHNOLOGY TO PREPARE InGaAs/InP(InAlAs) HBT STRUCTURES ON GaAs SUBSTRATES BY MBE (MOMBE) AND MOCVD.
- DEVELOPMENT OF COMPLEMENTARY DEVICE STRUCTURES FOR HIGH POWER AND EFFICIENCY.
- SMALL AND LARGE SIGNAL DEVICE MODELING.



APPROACH

- PREPARE InGaAs/InAlAs HBT STRUCTURE ON InP SUBSTRATES BY MBE. OPTIMIZE DEVICE STRUCTURE.
- PREPARE InGaAs/InP HBT STRUCTURE ON InP SUBSTRATES BY MOCVD. OPTIMIZE DEVICE STRUCTURE
- GROW OPTIMIZED STRUCTURE ON GaAs SUBSTRATE BY MBE AND/OR MOCVD.
- USE 1 μm WIDTH EMITTER FINGERS AND SELF-ALIGNED EMITTER-BASE-COLLECTOR FABRICATION.
- OPTIMIZE npn AND pnp DEVICE PERFORMANCE ON SEPARATE SUBSTRATES. INTEGRATE OPTIMIZED STRUCTURES ON THE SAME SUBSTRATE.



Design: EHF-1
Emitter-up structure

LAYER	Doping (cm^{-3})	Thickness (μm)
n^+ -InAs	1×10^{19}	0.05
Grading InP \rightarrow InAs	5×10^{18}	0.05
n -InP	2×10^{17}	0.1
Grading InP \rightarrow InGaAs	2×10^{17}	0.01
p^+ -In _{0.53} Ga _{0.47} As	1×10^{19}	0.1
Grading InGaAs \rightarrow InP	5×10^{16}	0.01
n -InP	5×10^{16}	0.8
n^+ -In _{0.53} Ga _{0.47} As	5×10^{18}	1.0
InP buffer	SI	2.0
GaAs SUBSTRATE	Undoped	500(nom.)



CENTRAL RESEARCH LABORATORIES

Initial HBT Structure on InP

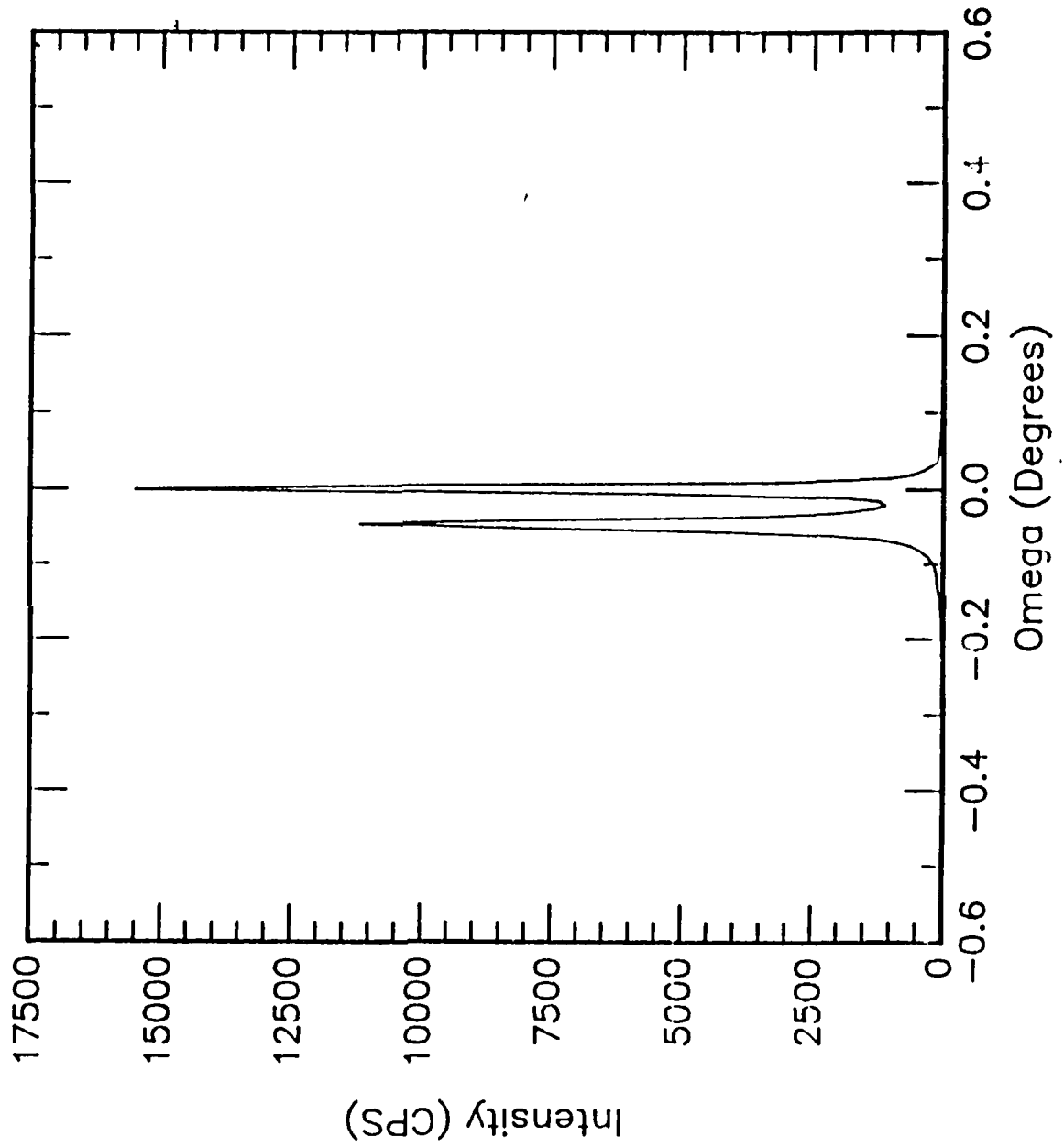
LAYER	Doping (cm^{-3})	Thickness (μm)
n^+ -InAs	1×10^{19}	0.05
Grading InAs \rightarrow InAlAs	1×10^{19}	0.05
n -In _{.52} Al _{.48} As	2×10^{17}	0.1
Grading InAlAs \rightarrow InGaAs	2×10^{17}	0.01
p^+ -In _{.53} Ga _{.47} As	1×10^{19}	0.1
n -In _{.53} Ga _{.47} As	1×10^{17}	0.5
n^+ -In _{.53} Ga _{.47} As	5×10^{18}	1.0
SI InP SUBSTRATE	Undoped	500(nom.)

Design: HBT-34
Strained-layer structure

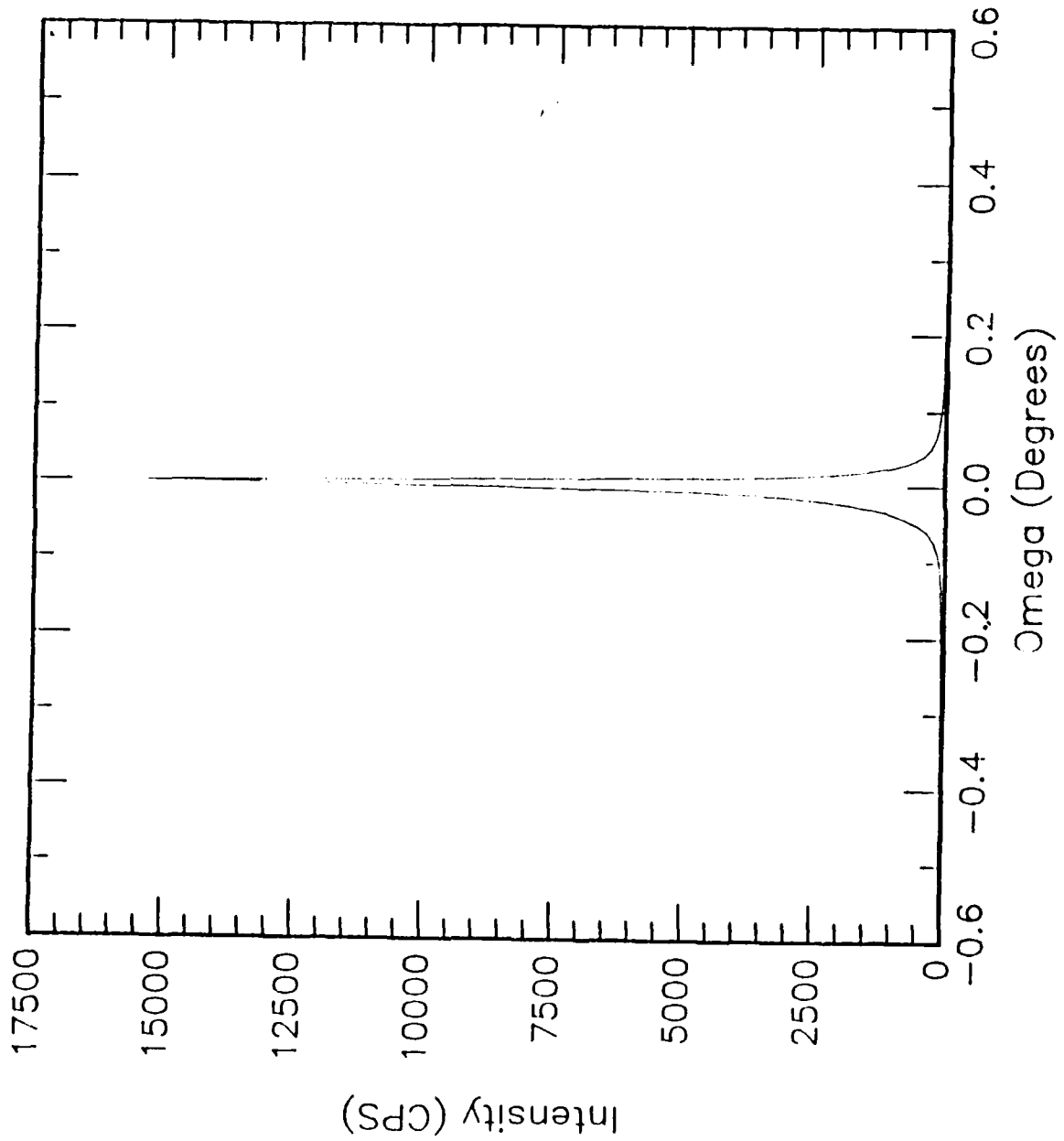
LAYER	Doping (cm^{-3})	Thickness (μm)
$\text{n}^+ - \text{InGaAs}$	5×10^{18}	0.02
$\text{n}^+ - \text{GaAs}$	5×10^{18}	0.05
n-grading	1×10^{18}	0.03
$\text{n} - \text{Al}_{0.3}\text{Ga}_{0.7}\text{As}$	3×10^{17}	0.1
$\text{n} - \text{GaAs}$	1×10^{18}	0.01
$\text{p}^+ - \text{In}_{0.1}\text{Ga}_{0.9}\text{As}$	1×10^{19}	0.02
$\text{p}^+ - \text{GaAs}$	1×10^{19}	0.04
$\text{p}^+ - \text{In}_{0.1}\text{Ga}_{0.9}\text{As}$	1×10^{19}	0.02
$\text{p}^+ - \text{GaAs}$	1×10^{19}	0.04
$\text{n} - \text{GaAs}$	3×10^{16}	1.0
$\text{n}^+ - \text{GaAs}$	5×10^{18}	0.5
SI SUBSTRATE	Undoped	500



InGaAs ON InP WITH LATTICE MISMATCH



LATTICE MATCHED InGaAs ON InP





TEXAS
INSTRUMENTS

008:0260

CENTRAL RESEARCH LABORATORIES

HETEROJUNCTION BIPOLAR TRANSISTOR ON-WAFER PROBE CIRCUIT



CENTRAL RESEARCH LABORATORIES

HETEROJUNCTION BIPOLAR TRANSISTOR 1 W CW UNIT CELL



EMITTER

BASE

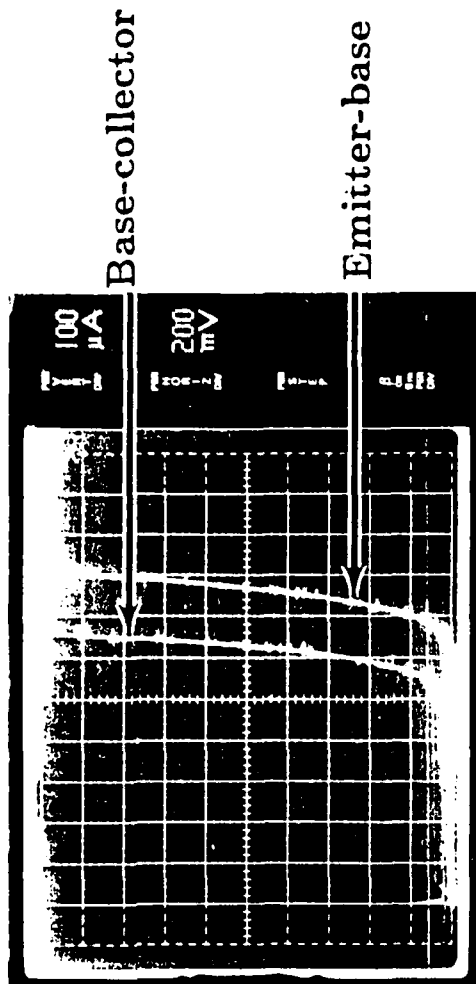
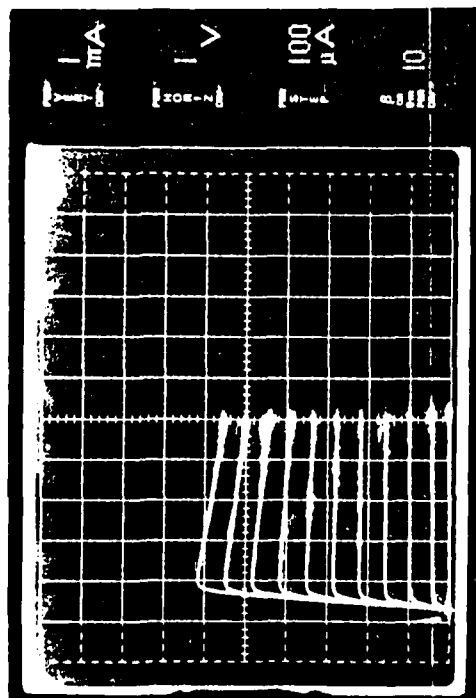
COLLECTOR

Emitter/base
fingers

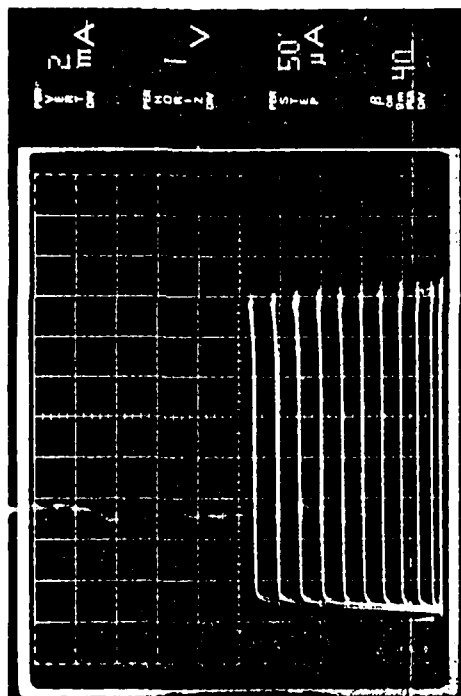
EMITTER



MBE GROWN STRUCTURE



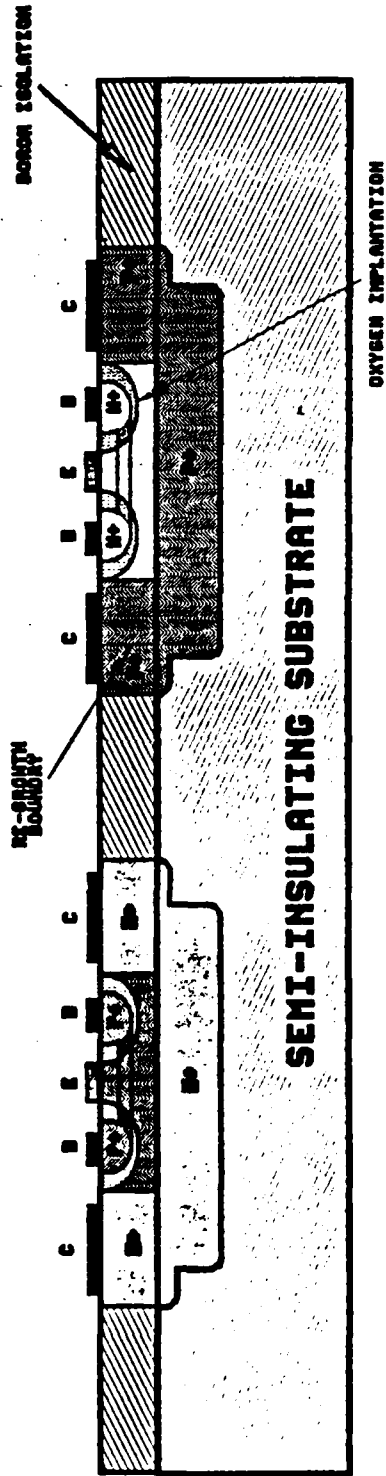
MOCVD GROWN STRUCTURE

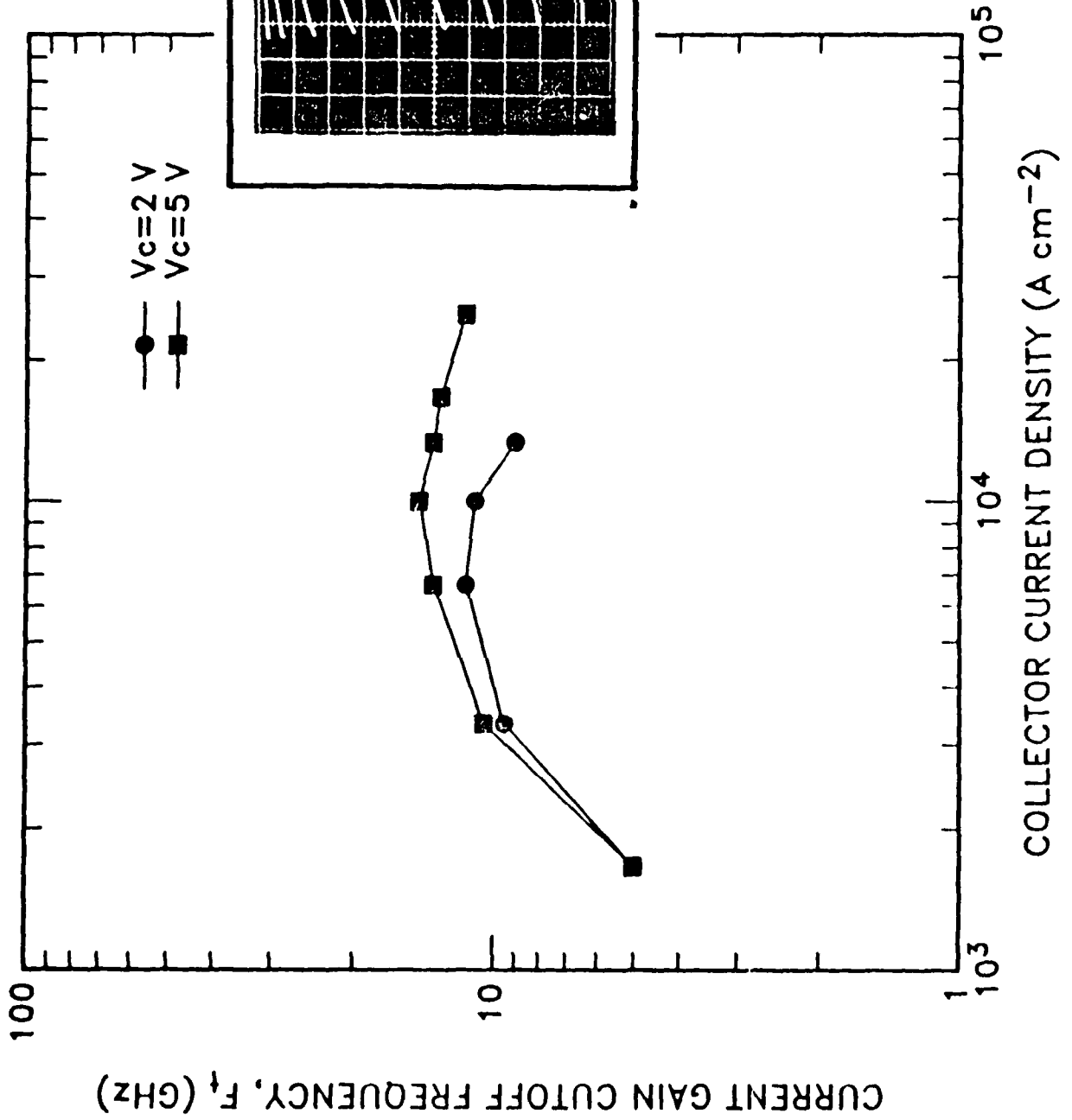


TEXAS
INSTRUMENTS



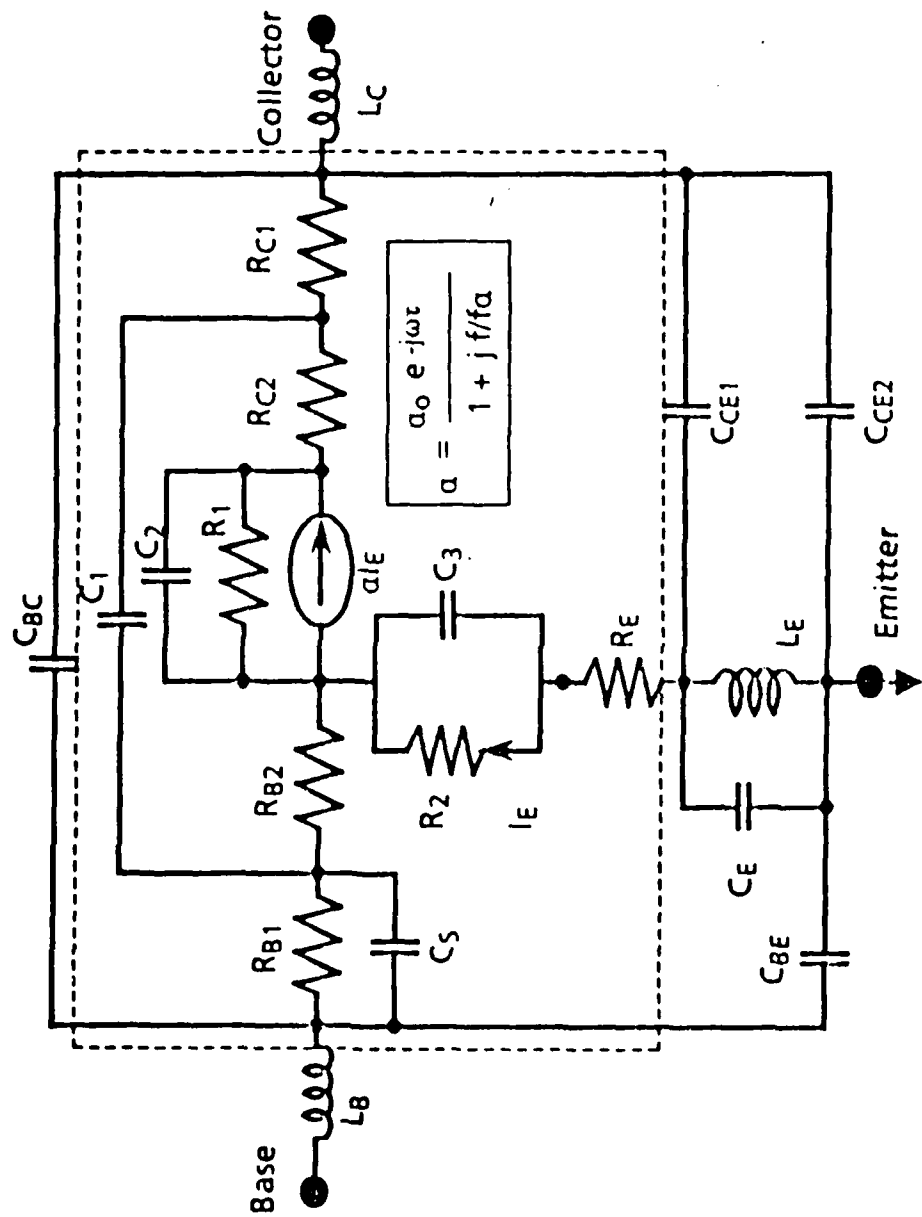
PLANAR COMPLEMENTARY HBT STRUCTURE





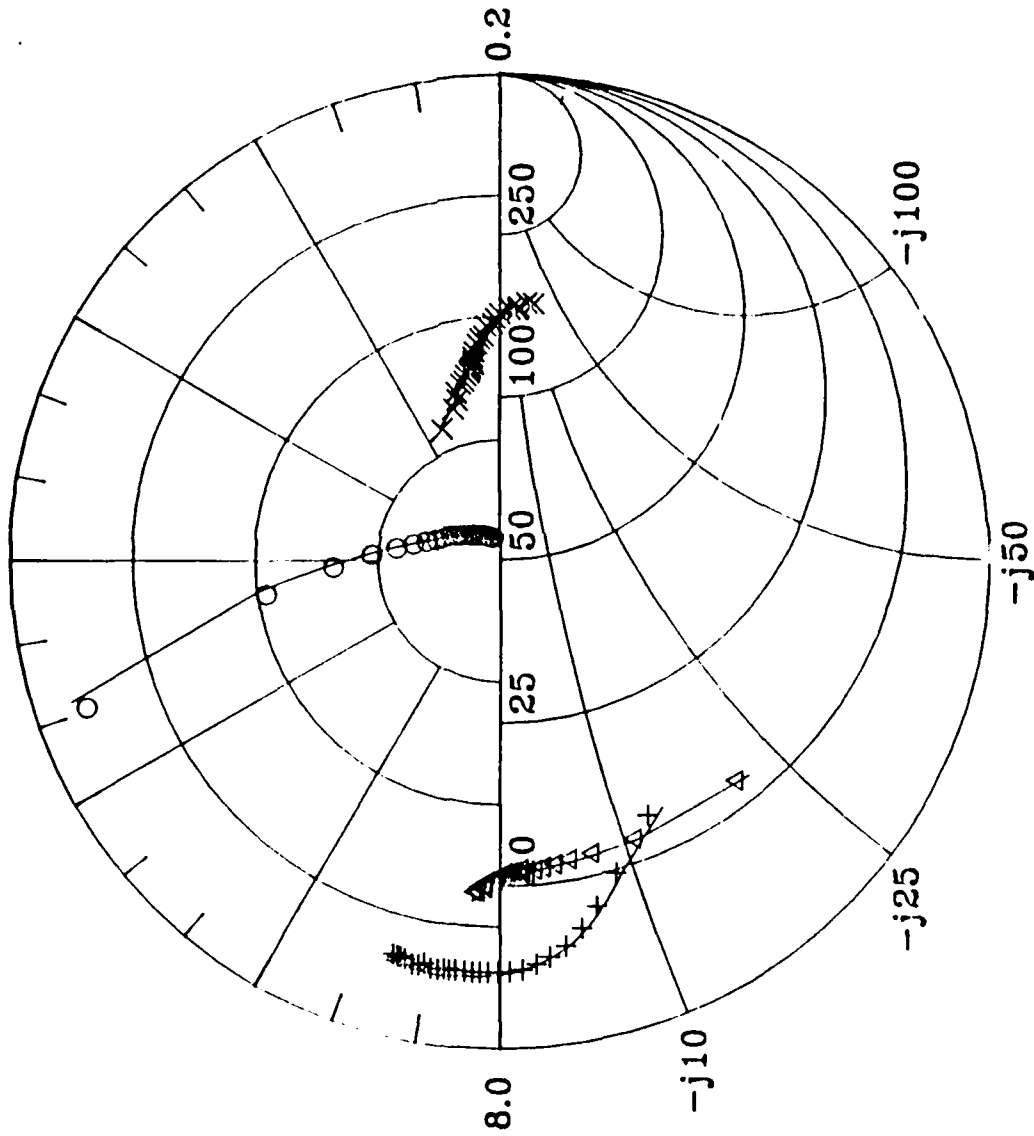


THE EQUIVALENT CIRCUIT



NPN HBT (138B-B5)

- + S11
- Δ S22
- S21
- × S12
- MODEL

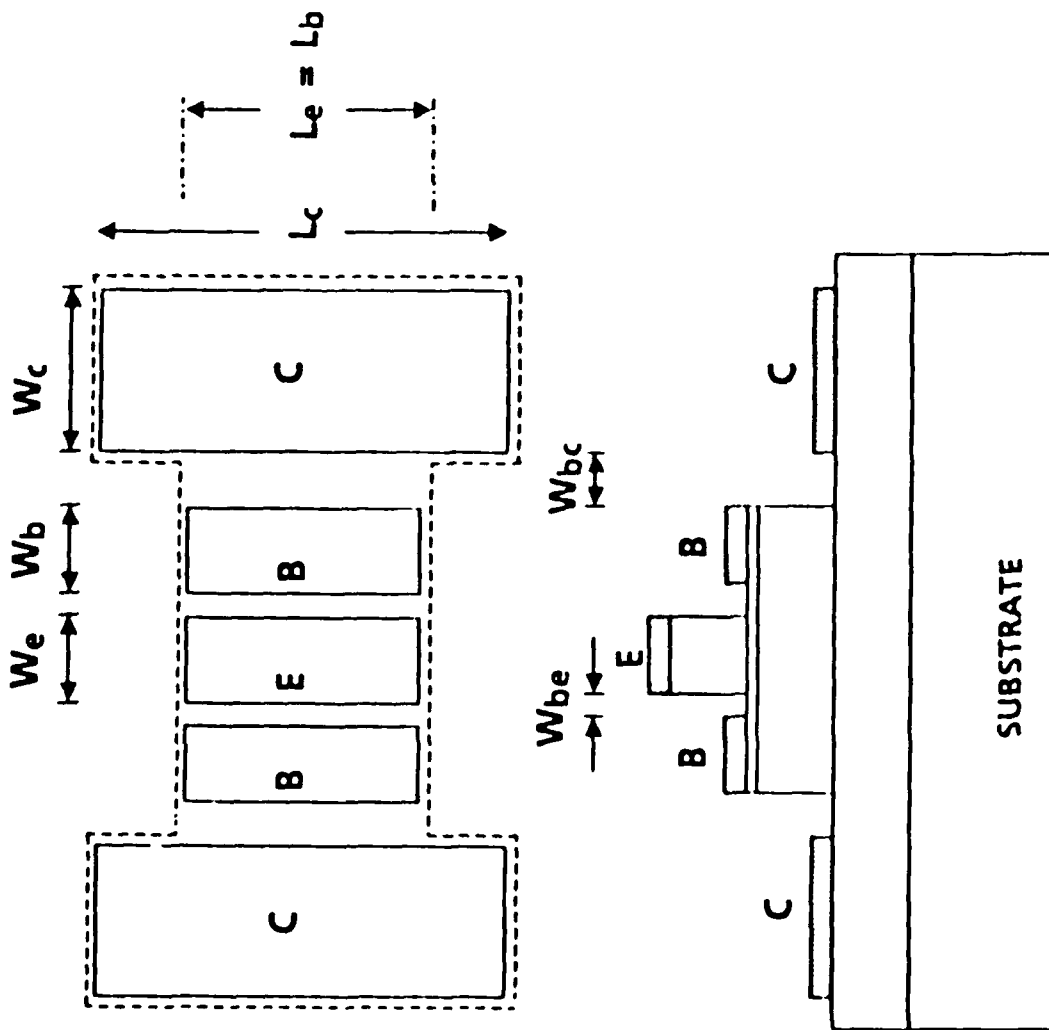


COMMON-EMITTER





PARAMETERS FOR SMALL-SIGNAL HBT MODEL

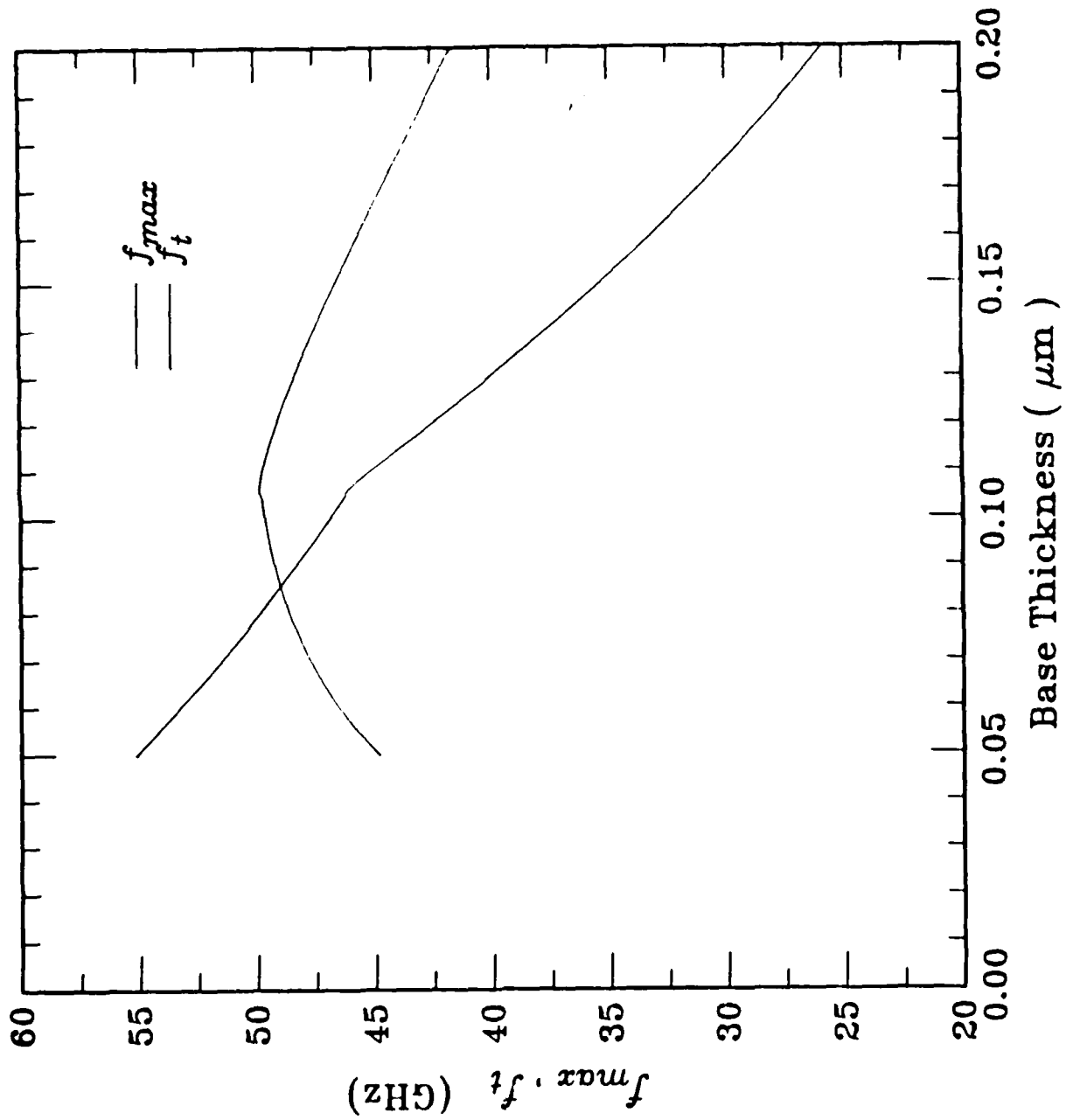


EMITTER CONTACT	t'_e, N'_e
EMITTER (Al, Ga, As)	t_e, N_e, χ
BASE	t_b, N_b
COLLECTOR	t_c, N_c
SUB-COLLECTOR	t_{sc}, N_{sc}
SUBSTRATE	

OTHER PARAMETERS

- = ρ_e EMITTER CONTACT RESISTIVITY
- = ρ_b BASE CONTACT RESISTIVITY
- = ρ_c COLLECTOR CONTACT RESISTIVITY
- = T TEMPERATURE
- = V_{bc}, I_c BIAS CONDITIONS

NPN Heterojunction Bipolar Transistor





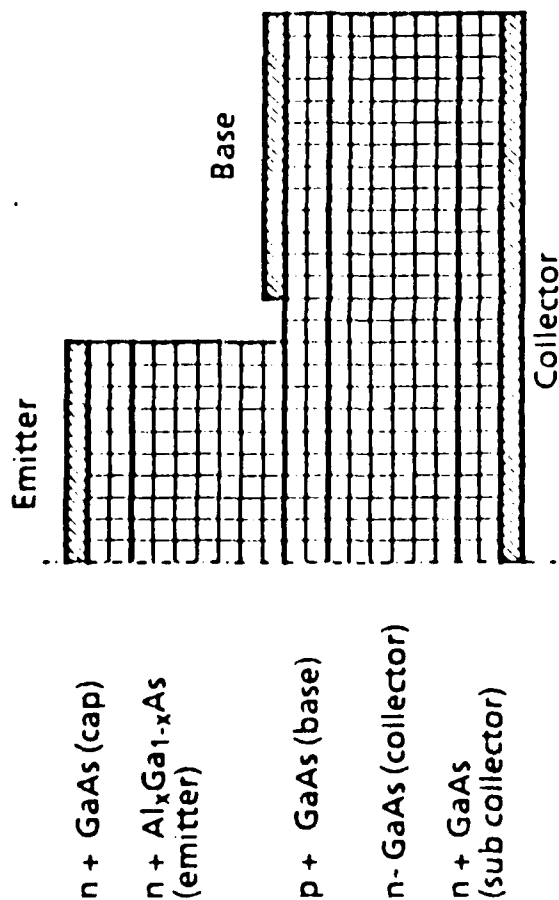
TWO - DIMENSIONAL NUMERICAL HBT MODEL

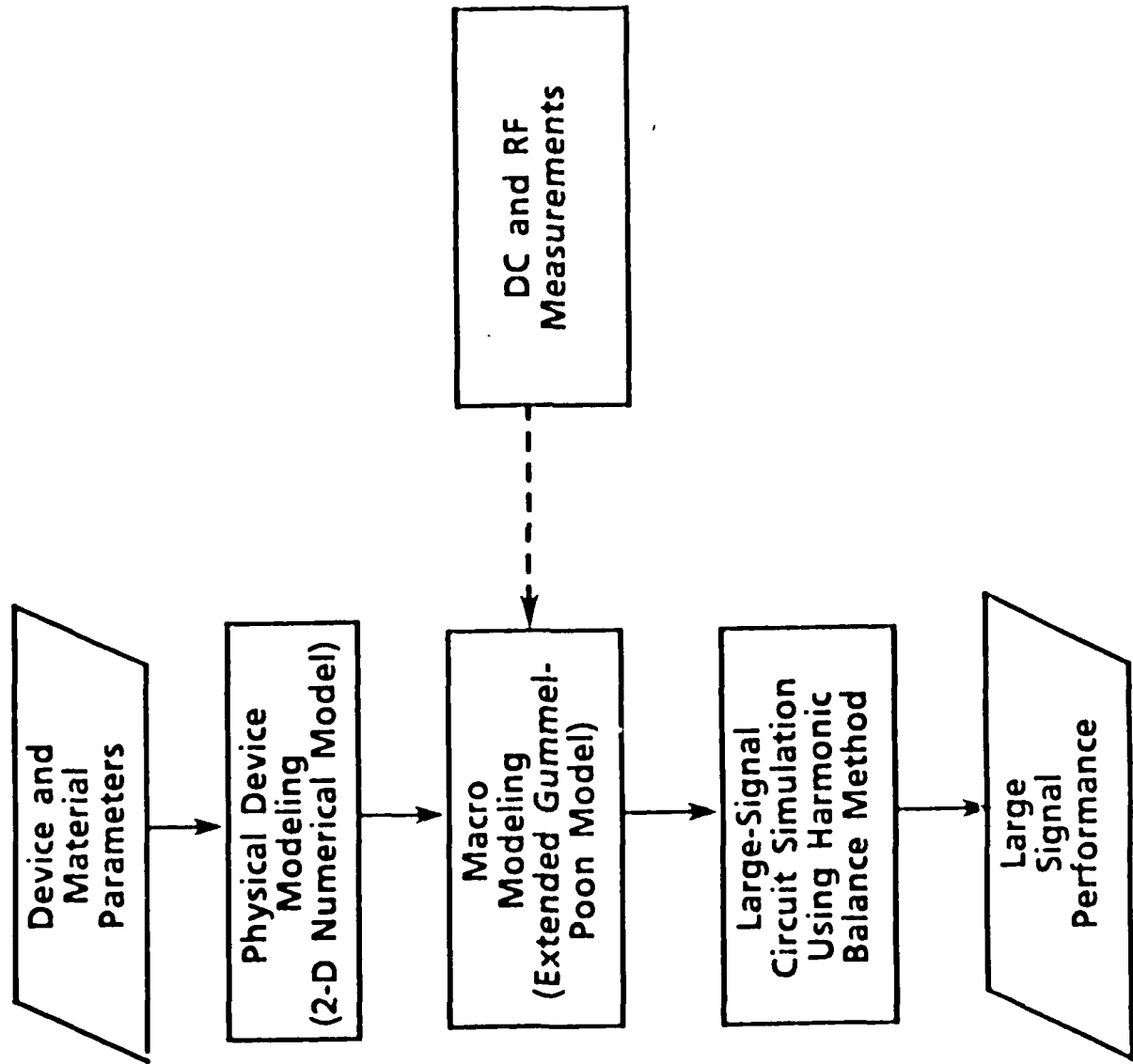
FEATURES:

- Finite difference model with variable mesh size.
- Drift and diffusion current transport model.
- Impact ionization generation and bulb and surface recombination considered.
- Arbitrary heterostructure layers (effects of bandgap grading in the base and at the base-emitter junction can be studied).

OUTPUT:

- Current and electric field distribution.
- Electrode currents and current gain (β).
- Breakdown voltage.
- Capacitances
- Transit time.
- Macromodel (Gummel-Poon) parameters for large signal circuit analysis.







CENTRAL RESEARCH LABORATORIES

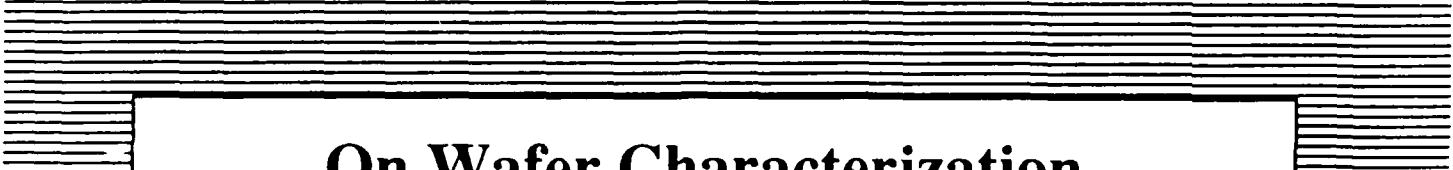
SUMMARY

- STRAINED-LAYER GaAs/InGaAs/AlGaAs HBT STRUCTURES WERE GROWN BY MBE AND MOCVD. DEVICE PERFORMANCE WAS EVALUATED.
- InGaAs/InAlAs HBT STRUCTURE WAS GROWN ON InP SUBSTRATE
- A COMPREHENSIVE SMALL-SIGNAL DEVICE MODEL WAS DEVELOPED.

On Wafer Characterization of High Speed Circuits

D. M. Bloom

*Stanford University
Stanford, CA*



**On Wafer Characterization
of
High Speed Circuits**

**D. M. Bloom
Edward L. Ginzton Laboratory
Stanford University**

**DARPA Joint Contractor Review of
EHF Monolithic Devices**

January 25, 1989



COST GOALS

MIMIC

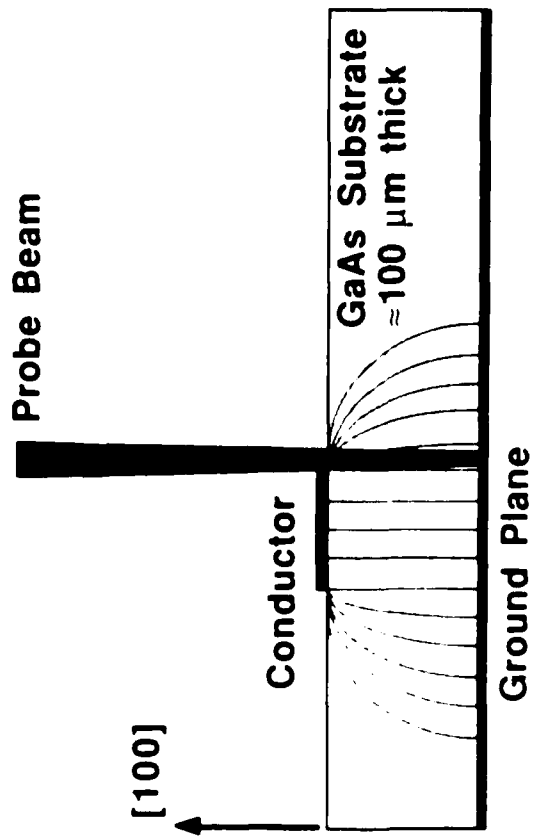
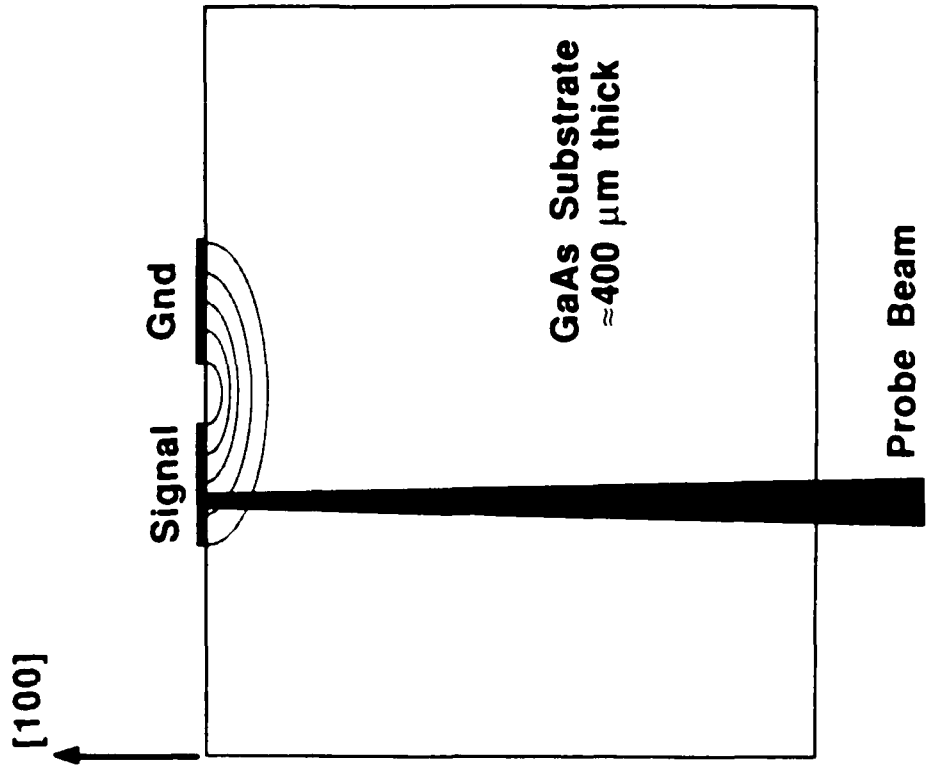
DEMONSTRATE THAT MONOLITHIC DEVICES CAN BE DELIVERED IN FUNCTIONAL MODULES AT:

- **\$2.50 CHIP COST, IN A**
- **\$25 PACKAGE, WITH LESS THAN**
- **\$250 OF TEST DATA**

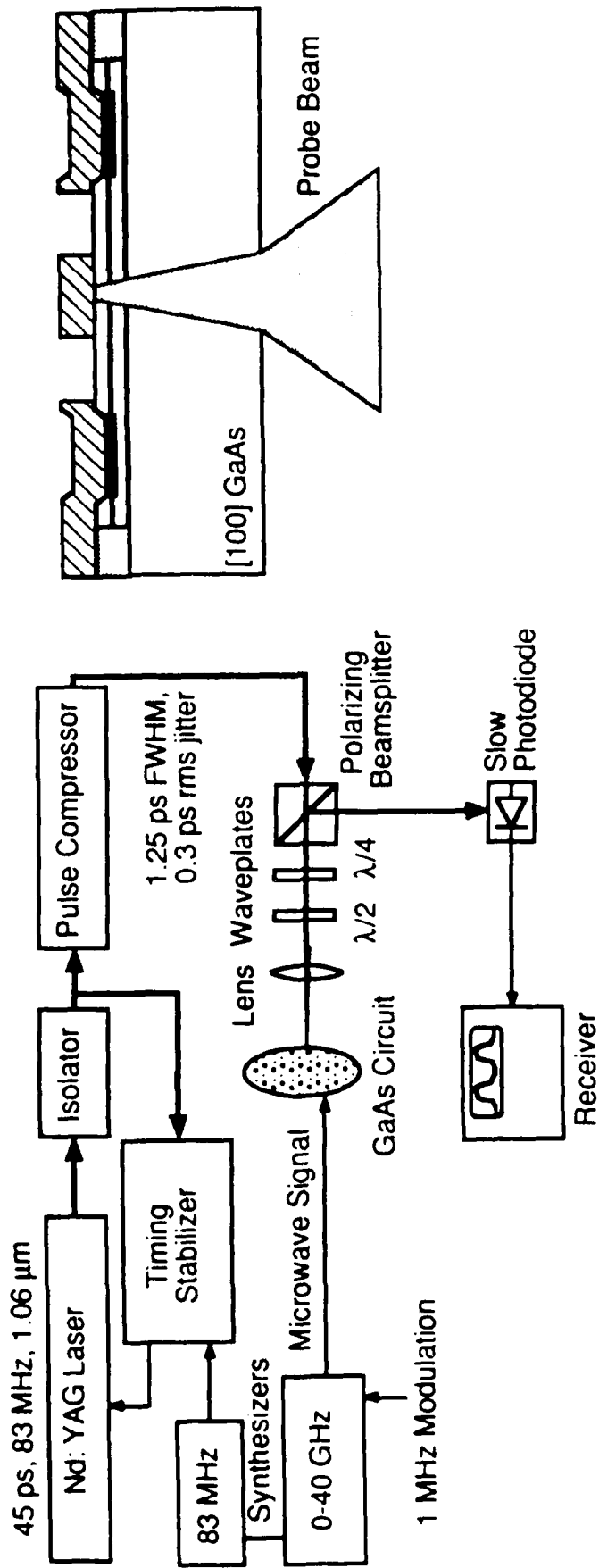
648 6

Frontside Probing

Backside Probing

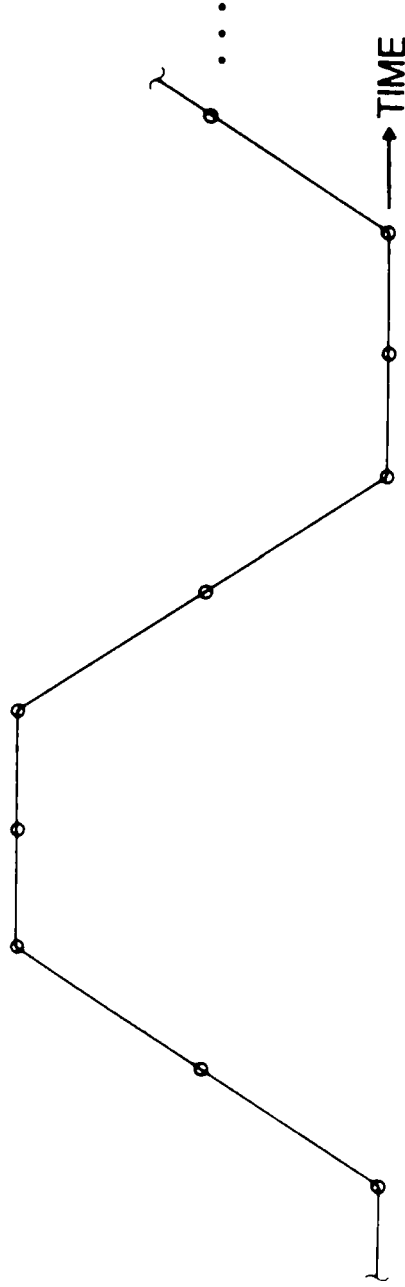
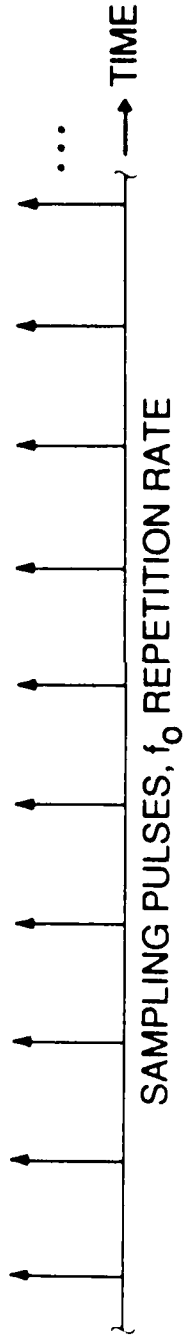
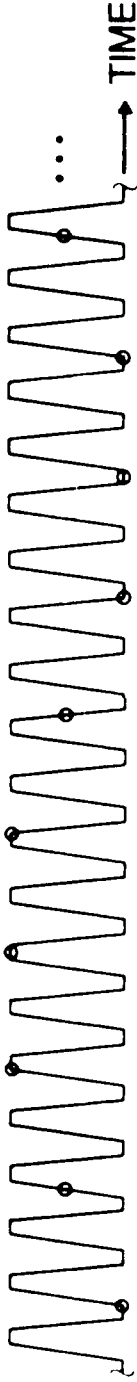


Electrooptic Sampling



Equivalent-time sampling

SIGNAL WAVEFORM, $N \cdot f_0 + \Delta f$ REPETITION RATE (N=2)

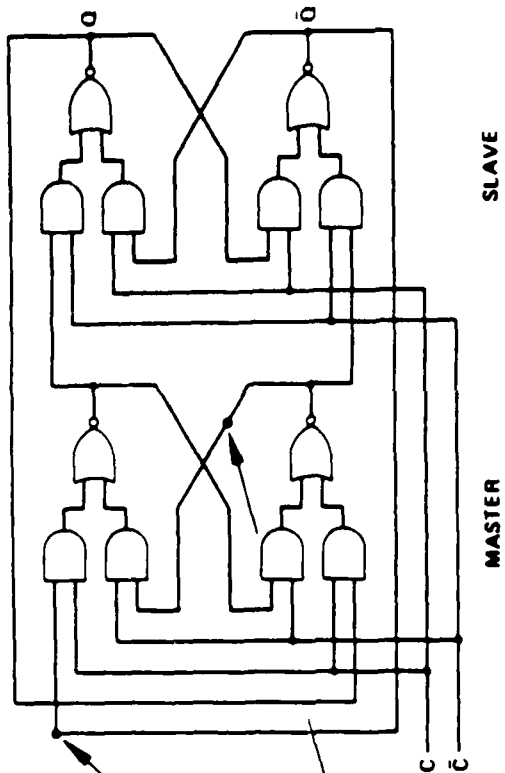
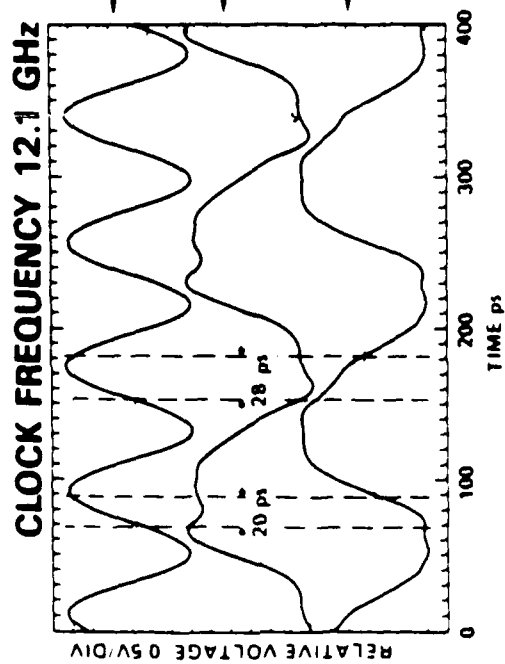


SAMPLED WAVEFORM, Δf REPETITION RATE

ULTRAFAST ELECTRONICS LABORATORY

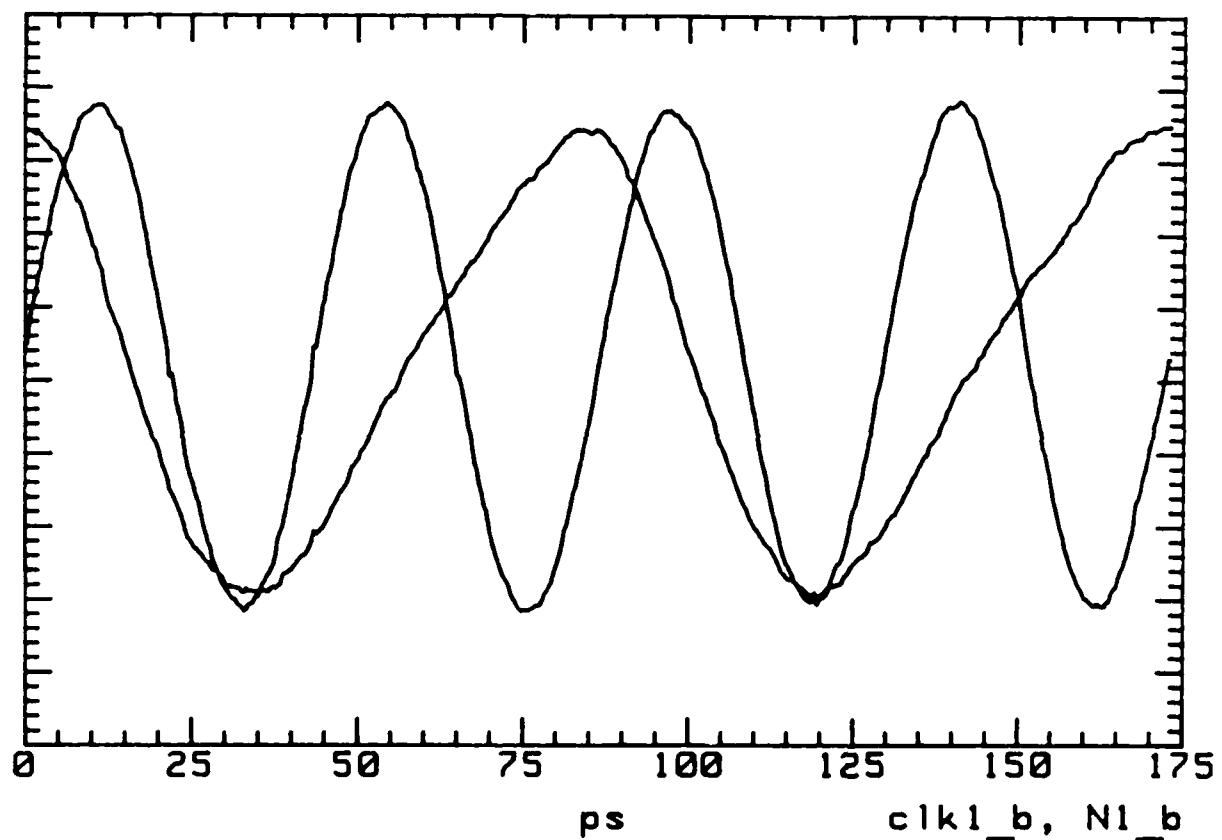
Stanford University

CEL DIVIDER ELECTROOPTIC SAMPLED WAVEFORMS

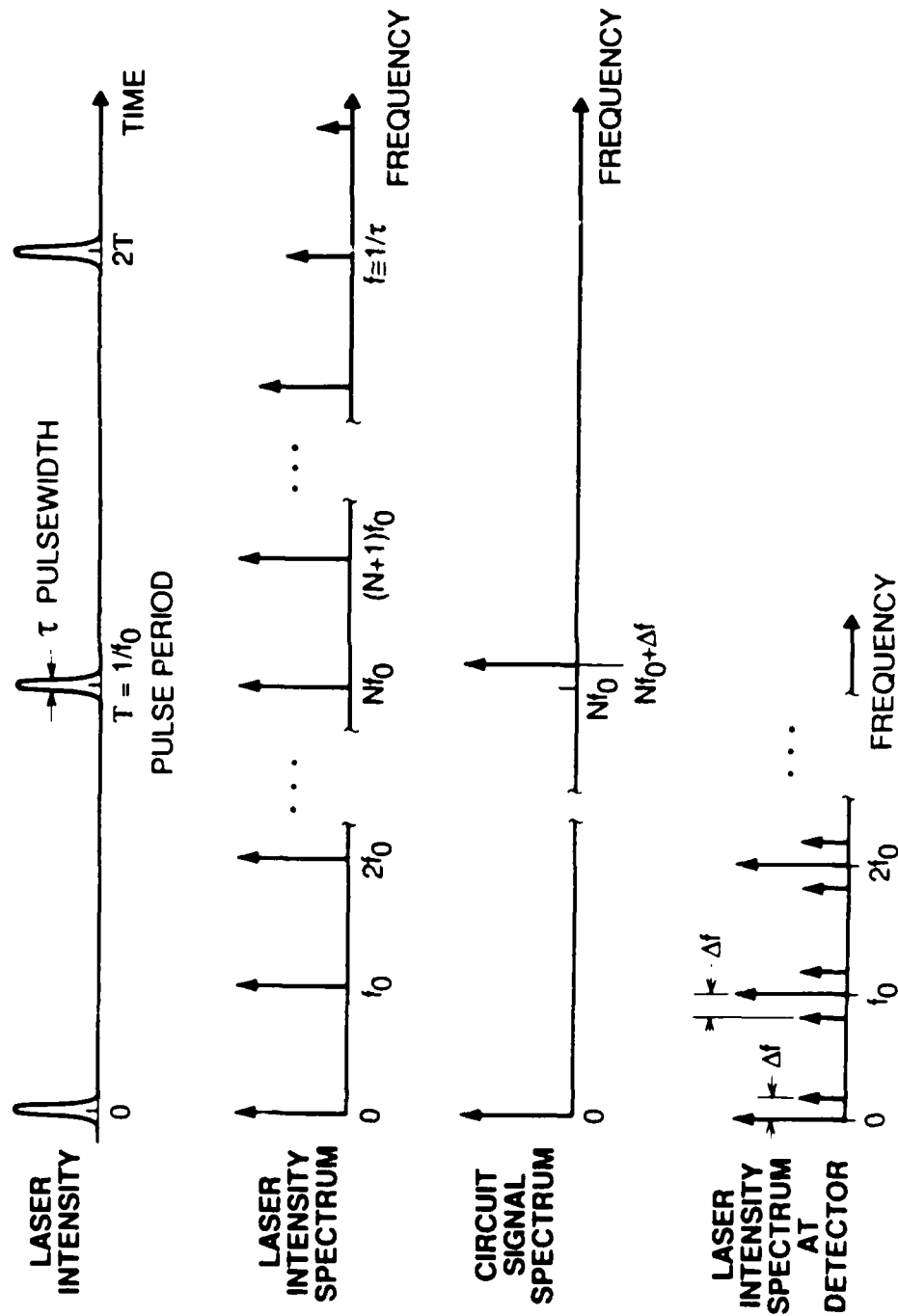


INDIRECT MEASUREMENT OF MAXIMUM CLOCK FREQUENCY = 17.9 GHz
 ELECTROOPTIC MEASUREMENT PREDICTS MAXIMUM CLOCK FREQUENCY = 17.9 GHz

BFL dynamic divider, 23 GHz operation



Harmonic mixing

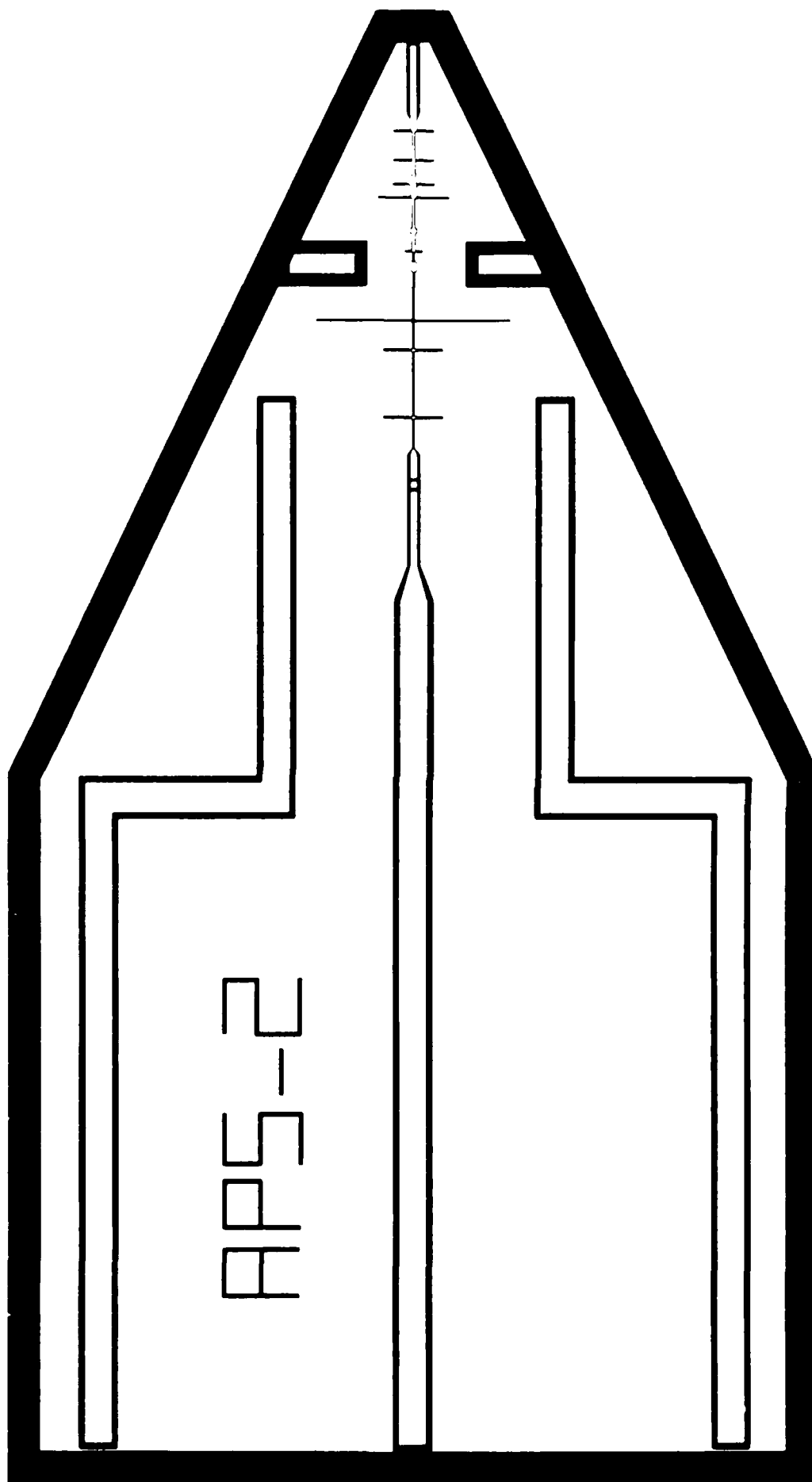


ULTRAFAST ELECTRONICS LABORATORY

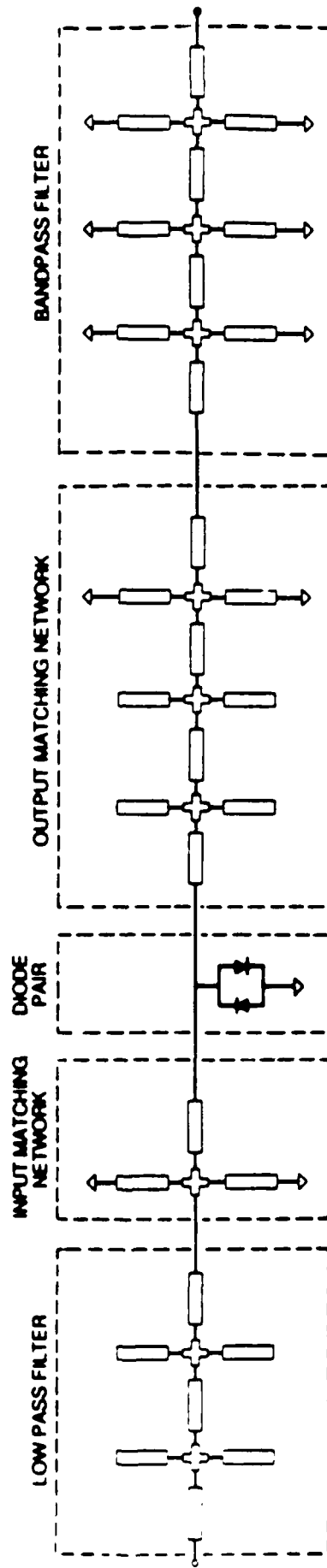
Stanford University

Millimeter-Wave Active Probe Quintupler

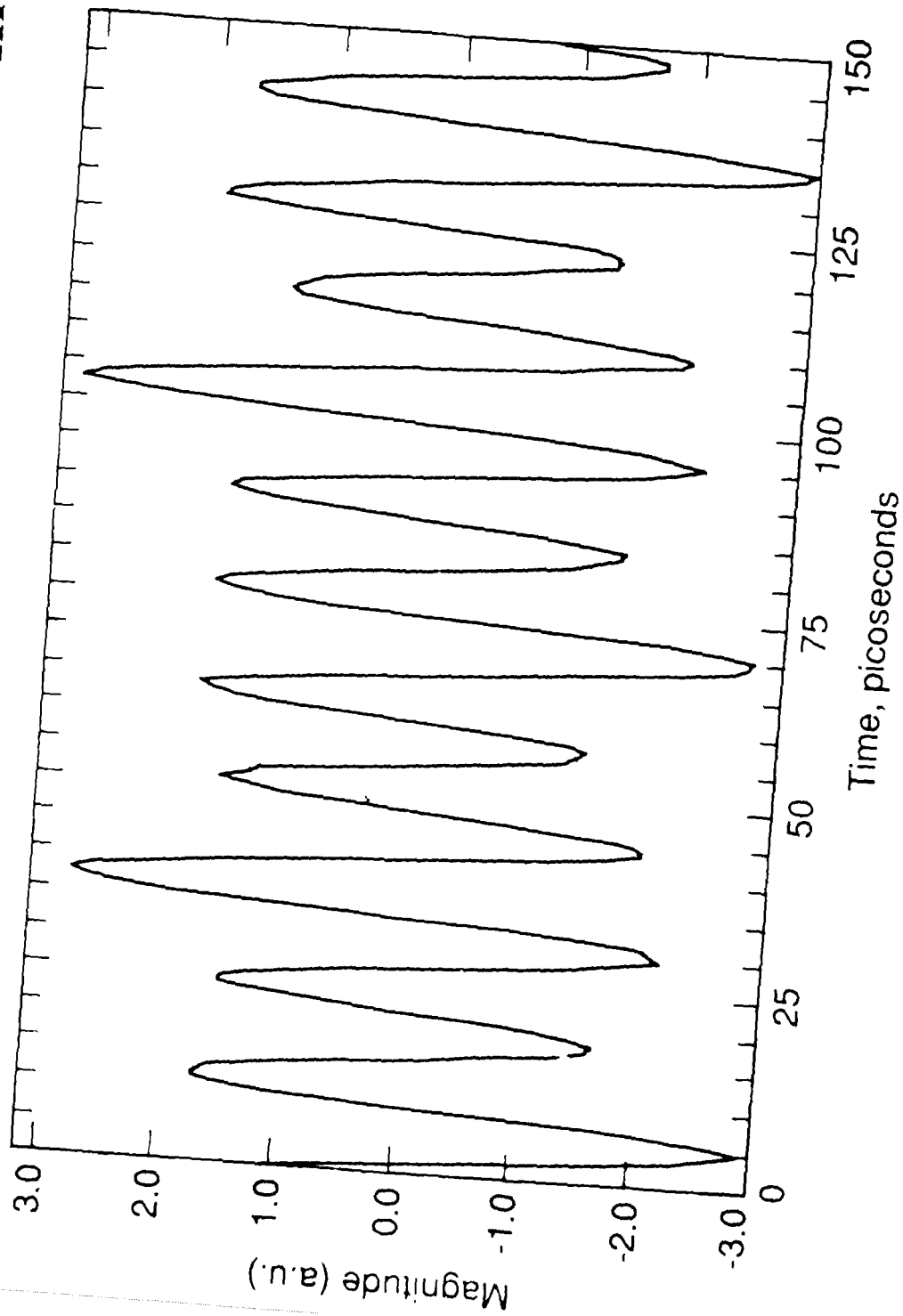
Output Frequency : 60-100 GHz



Active Probe Quintupler Schematic



77 GHz Active Probe Waveform



n + GaAs

n + Al_xGa
(emitter)

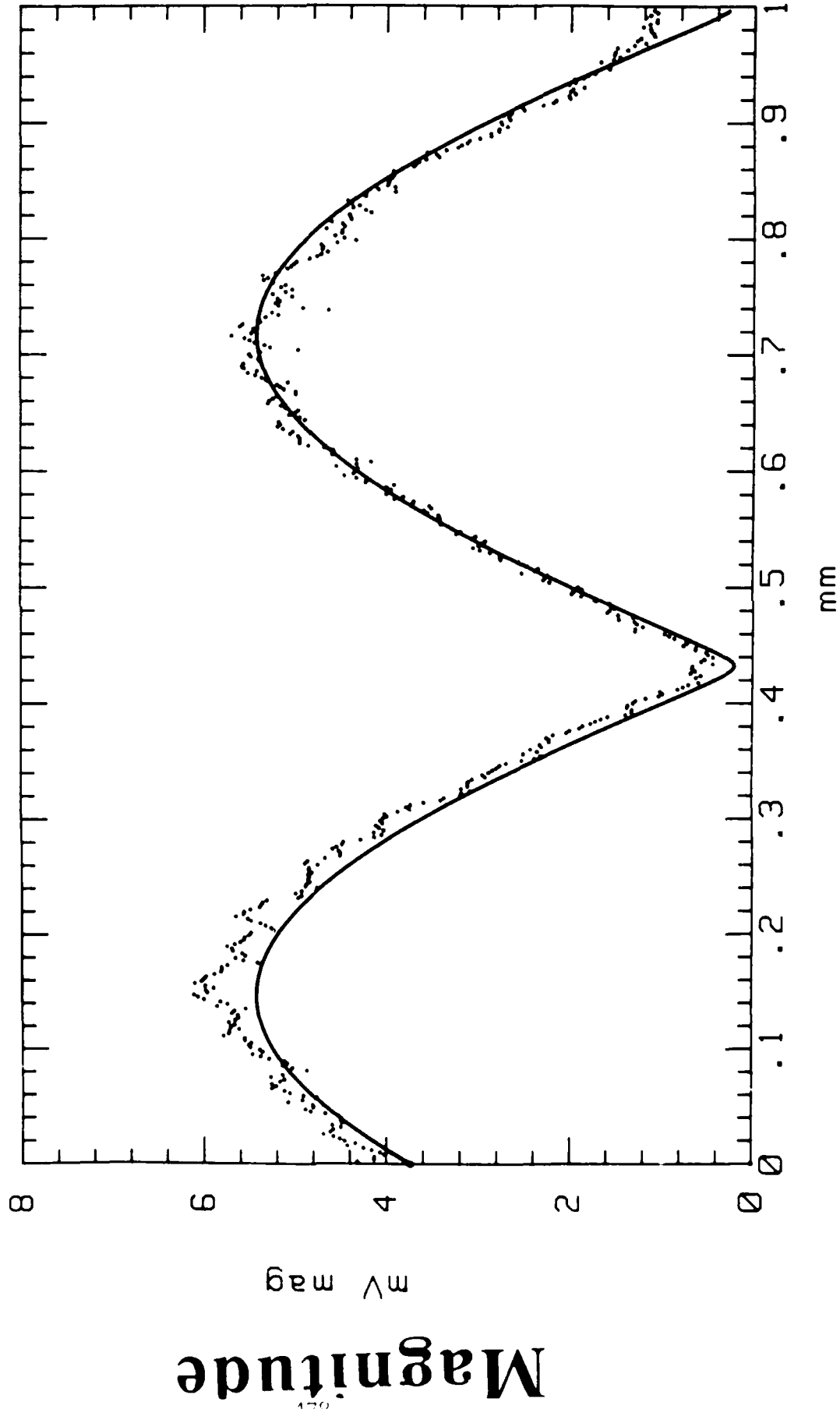
p + GaAs

n - GaAs (

n + GaAs
(sub colle

100 GHz CPW Standing Wave

$\Gamma = 0.93$ @ -94°



Distance

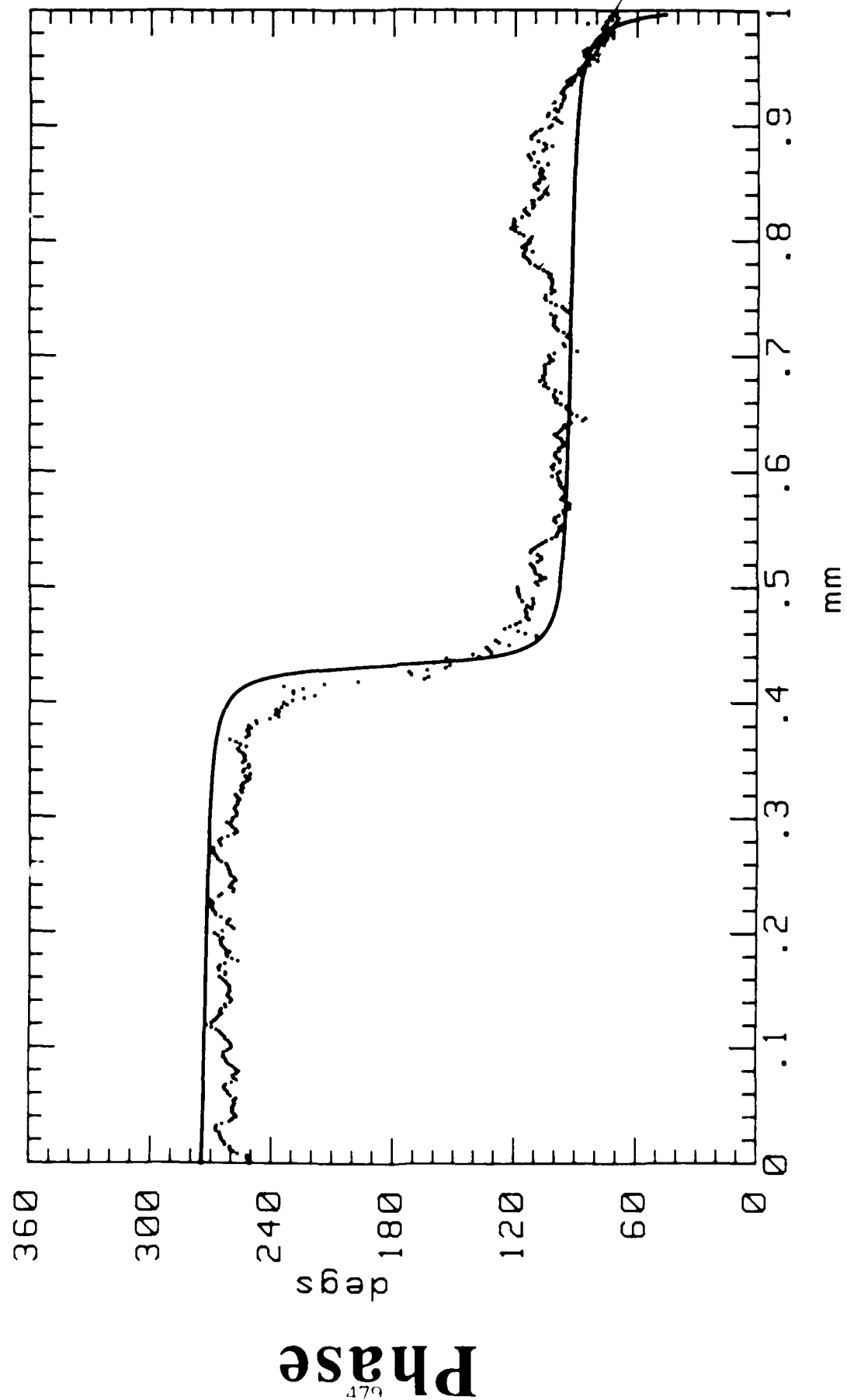
Magnitude

mV mag

mm

100 GHz CPW Standing Wave

$\Gamma = 0.93$ @ -94°

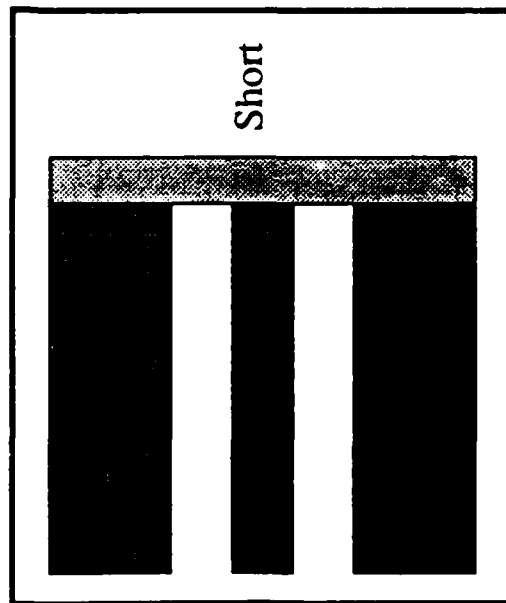


Distance

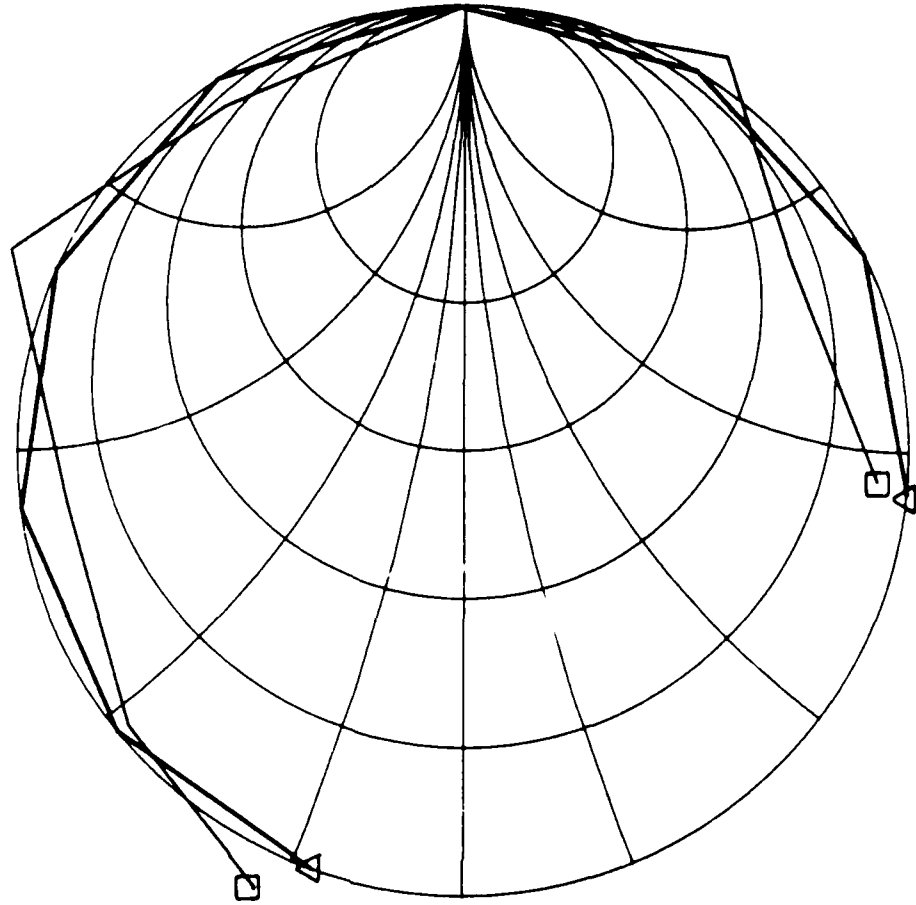
60-100 GHz S11 Measurements

△ S11
MODEL

□ S11
MEASURED



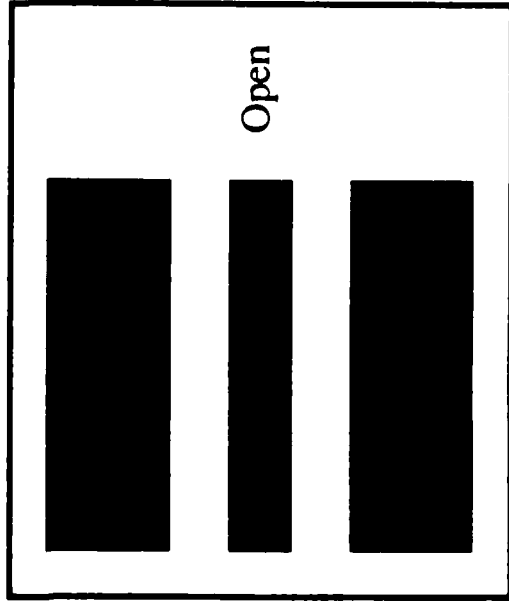
f1: 60.0000
f2: 100.0000



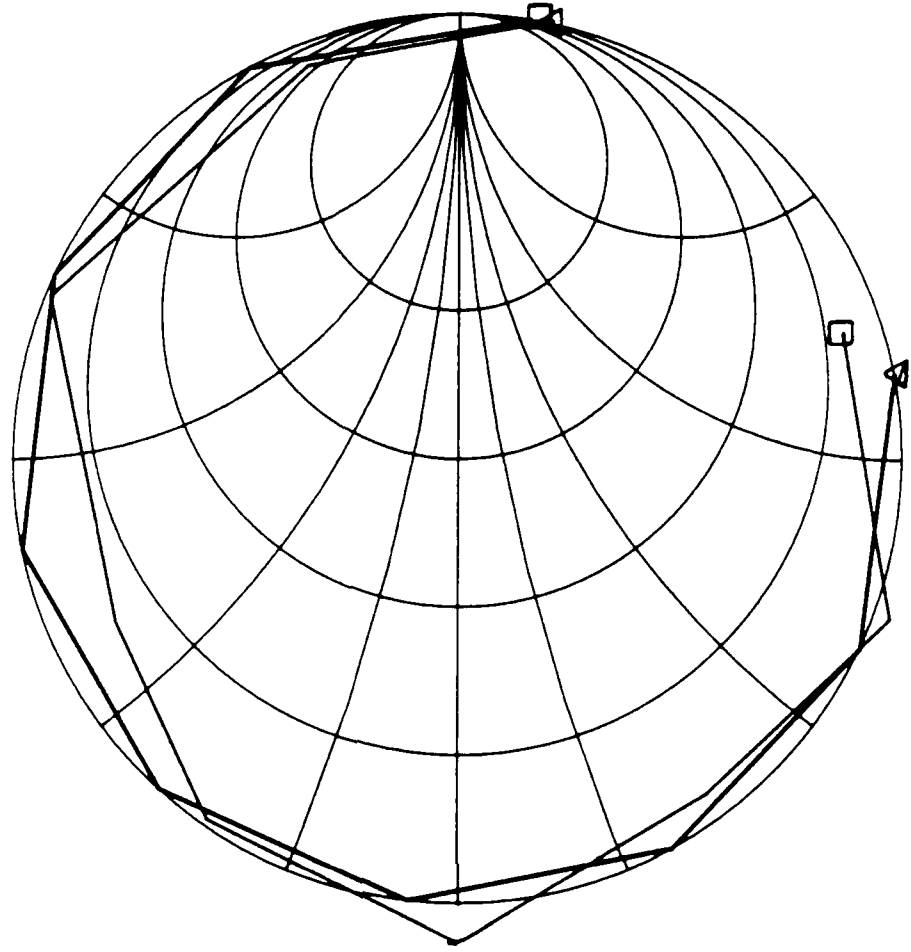
60-100 GHz S11 Measurements

△ S11
MODEL

□ S11
MEASURED

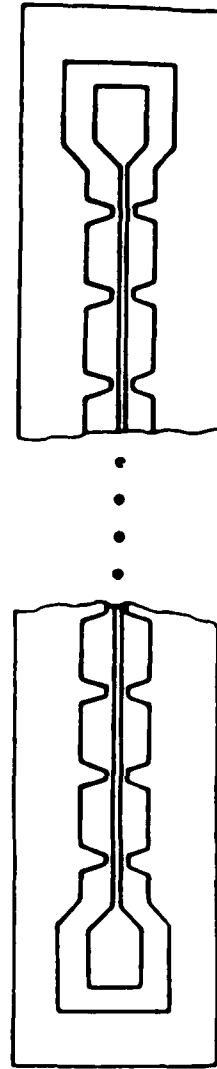
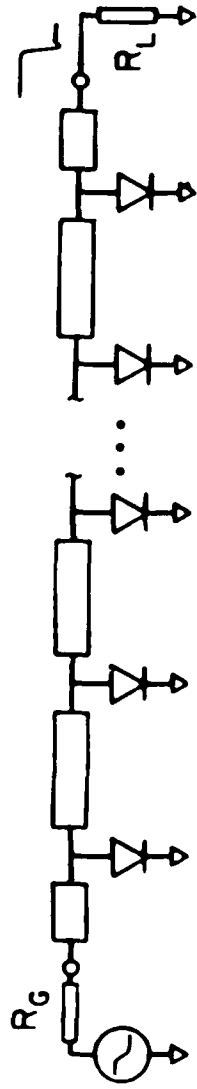


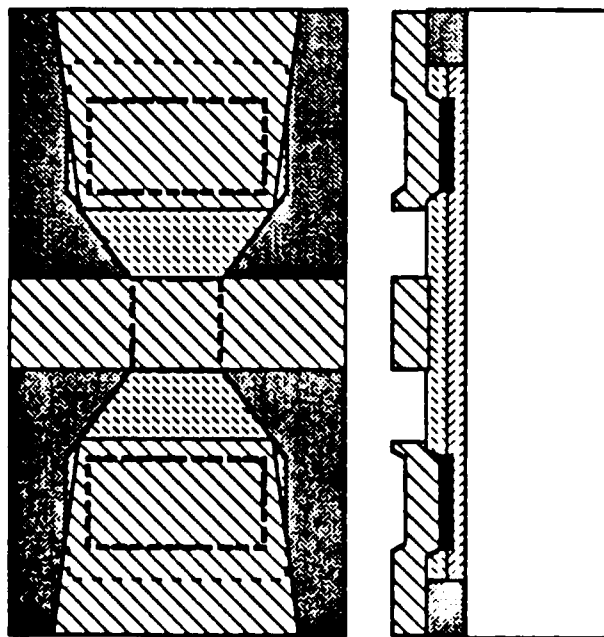
f1: 60.0000
f2: 100.0000












Nonlinear Transmission Line

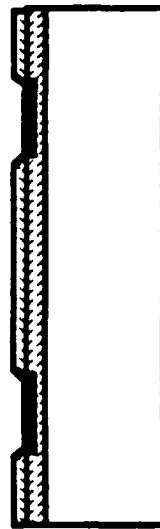
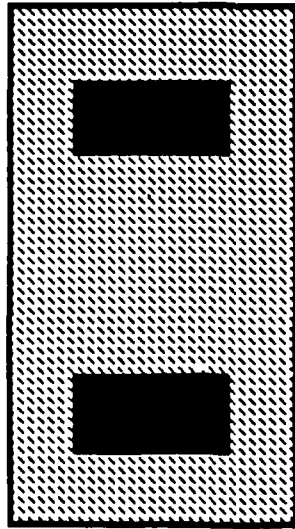




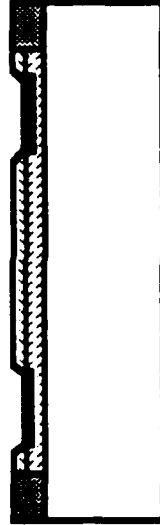
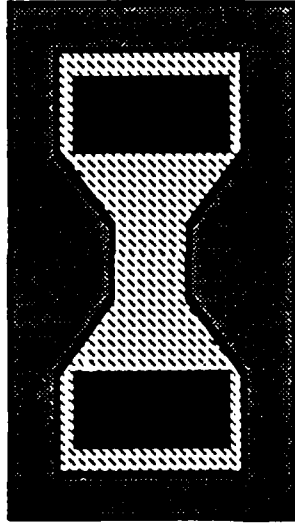
-  Schottky & Interconnect Metal
-  Ohmic Metal
-  N- Layer
-  N+ Layer
-  Semi-insulating GaAs
-  Proton Isolation Implant
-  Schottky and Ohmic Contact Regions

Fabrication Sequence

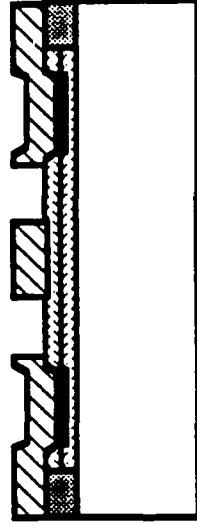
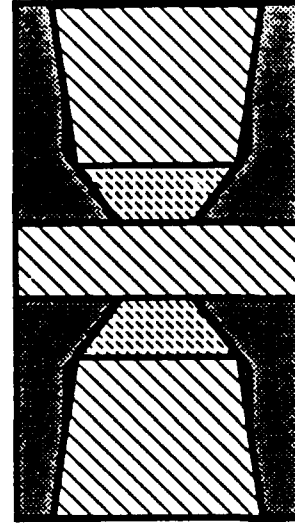
Ohmic Contacts



Isolation



Schottky Contacts
and Interconnect Metal



Schottky & Interconnect Metal



Ohmic Metal



N- Layer



N+ Layer

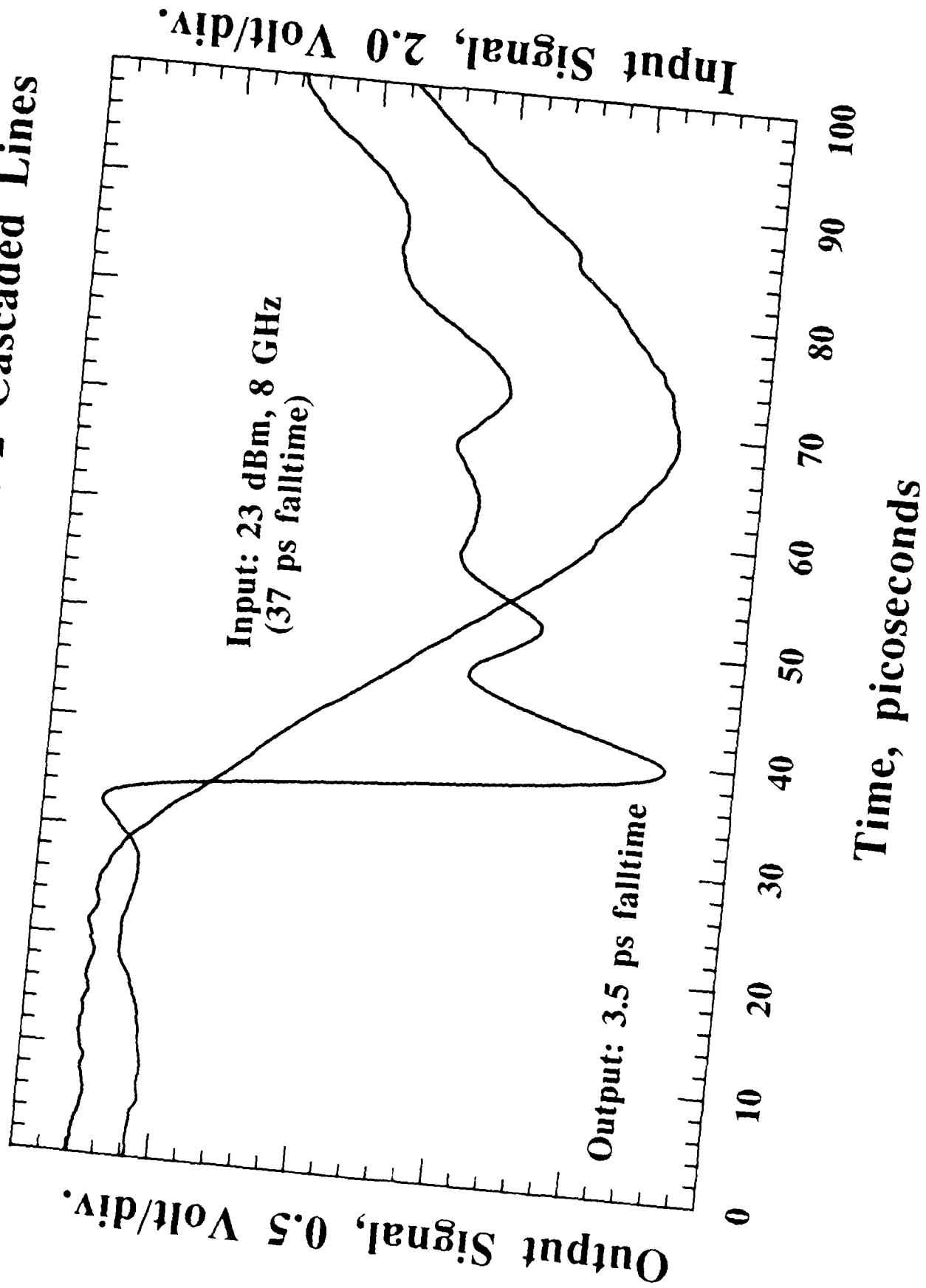


Semi-Insulating GaAs

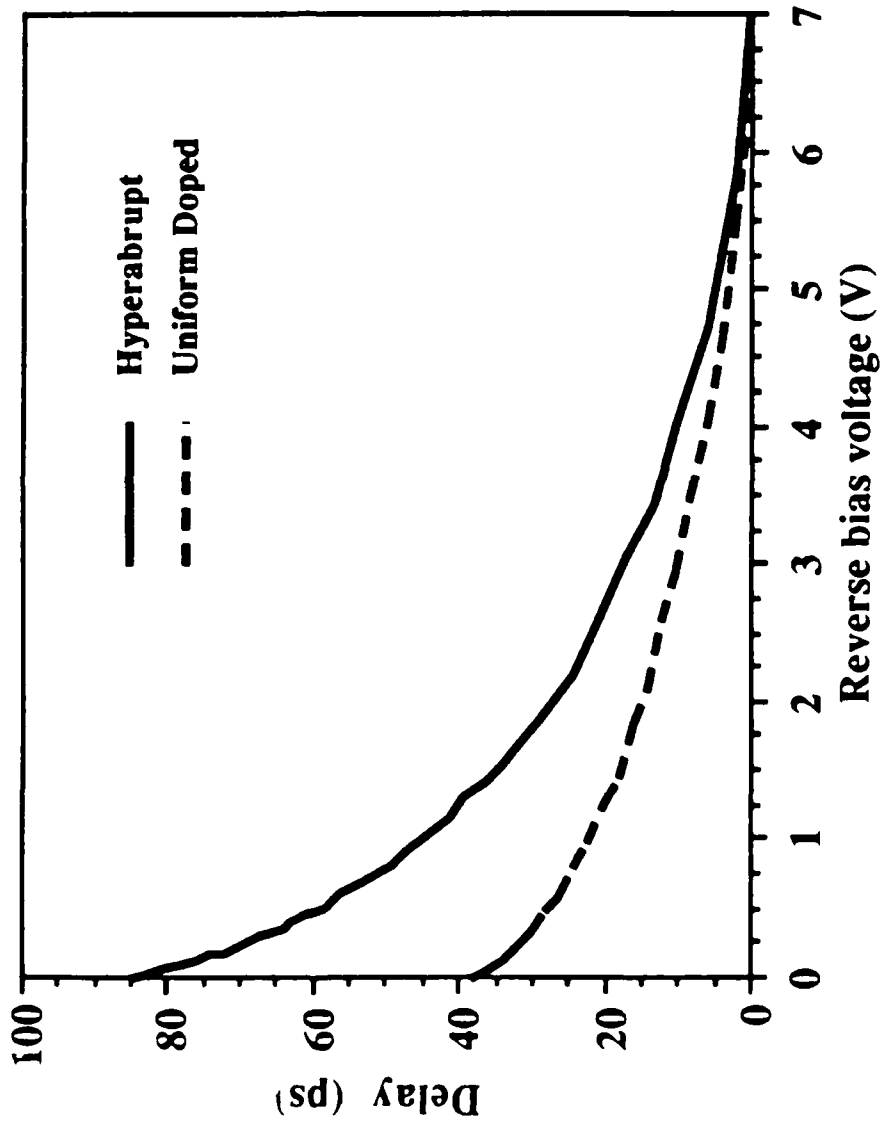


Proton Isolation Implant

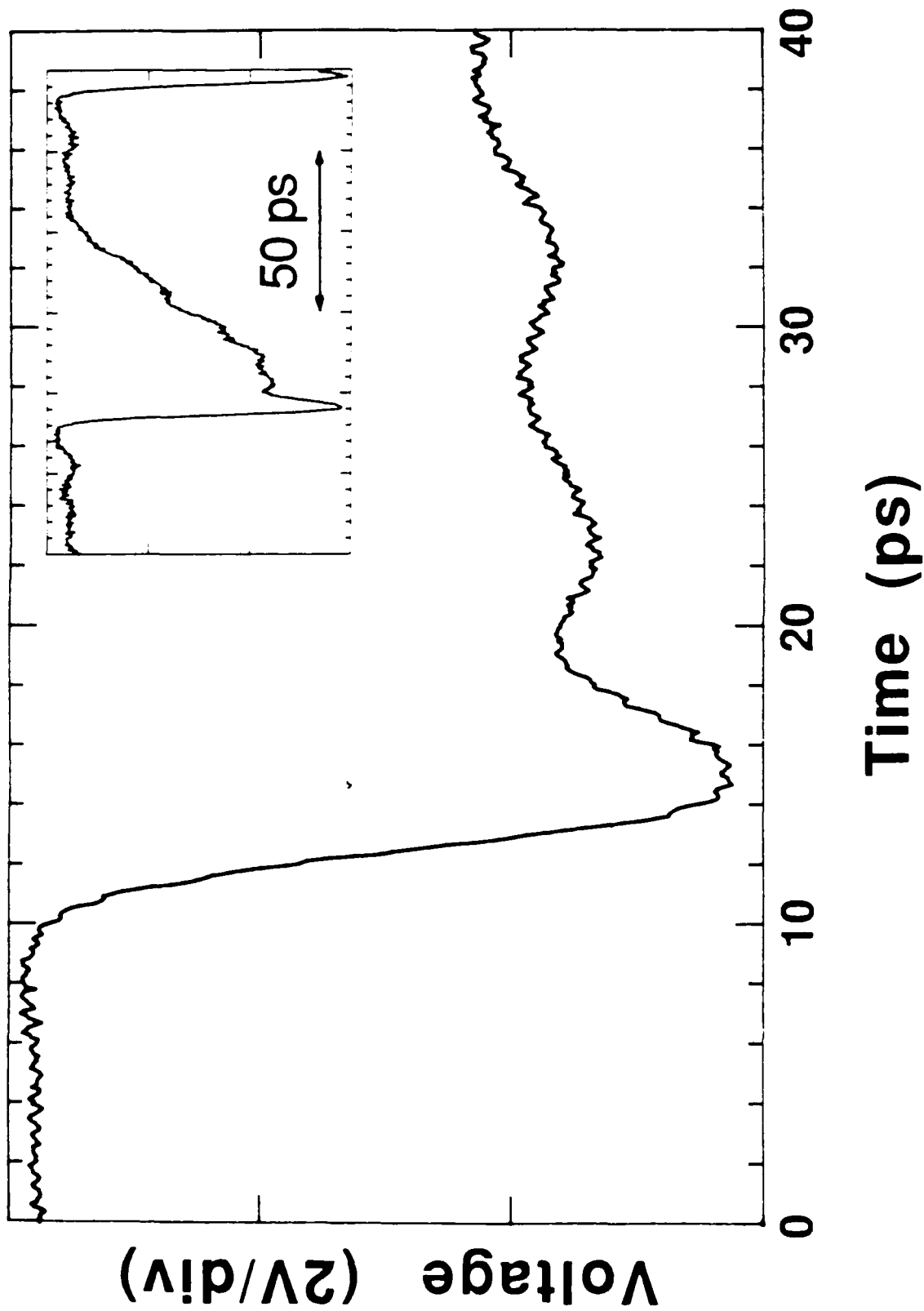
Falltime Compression with 2 Cascaded Lines



**Relative Change in Delay for Hyperabrupt
and Uniformly doped diode NLTTL's**



**Shock wave on a hyperabrupt
diode NLTL with sinusoidal drive**



Nonlinear Transmission Line

- Picosecond Shock-wave Generation
- Hyperabrupt Diode Design
 - 6 volt Signal Amplitude
 - Approx. 1.5 ps Falltime
- < 1 ps Output Falltime Possible in Future
 - Requires Improvement to Electrooptic Sampler
 - Investigate Circuit Applications

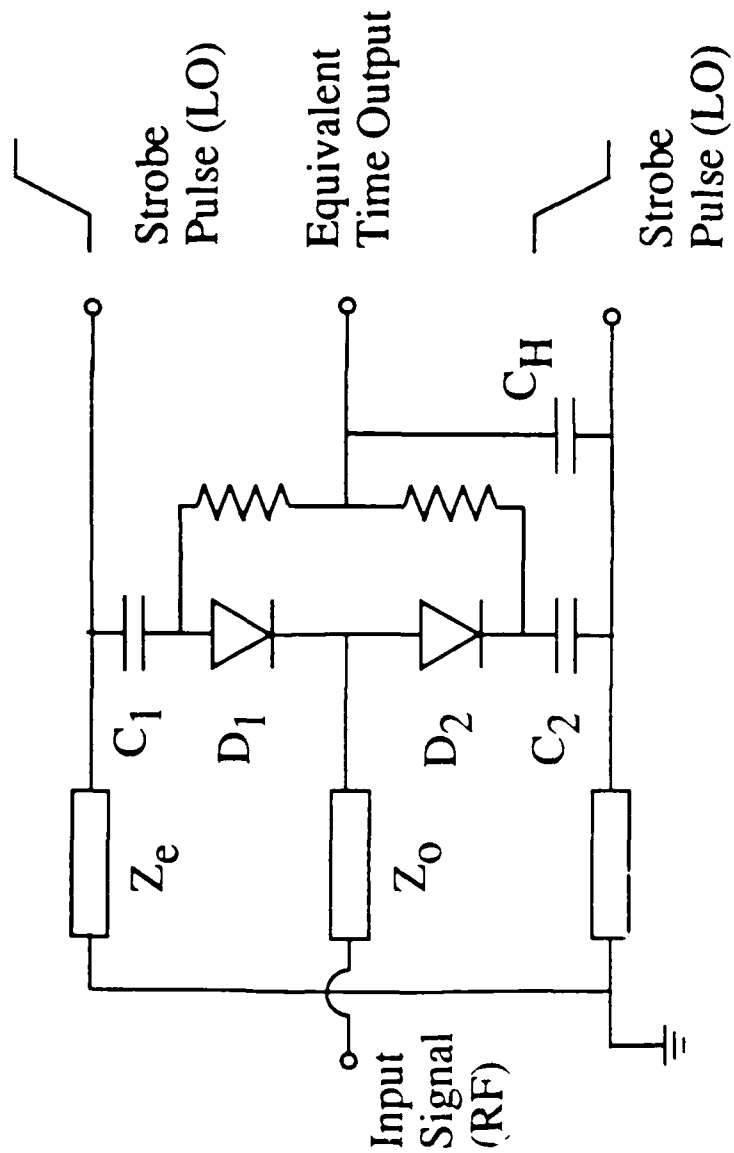


Prior Art in Threshold Devices and Pulsers

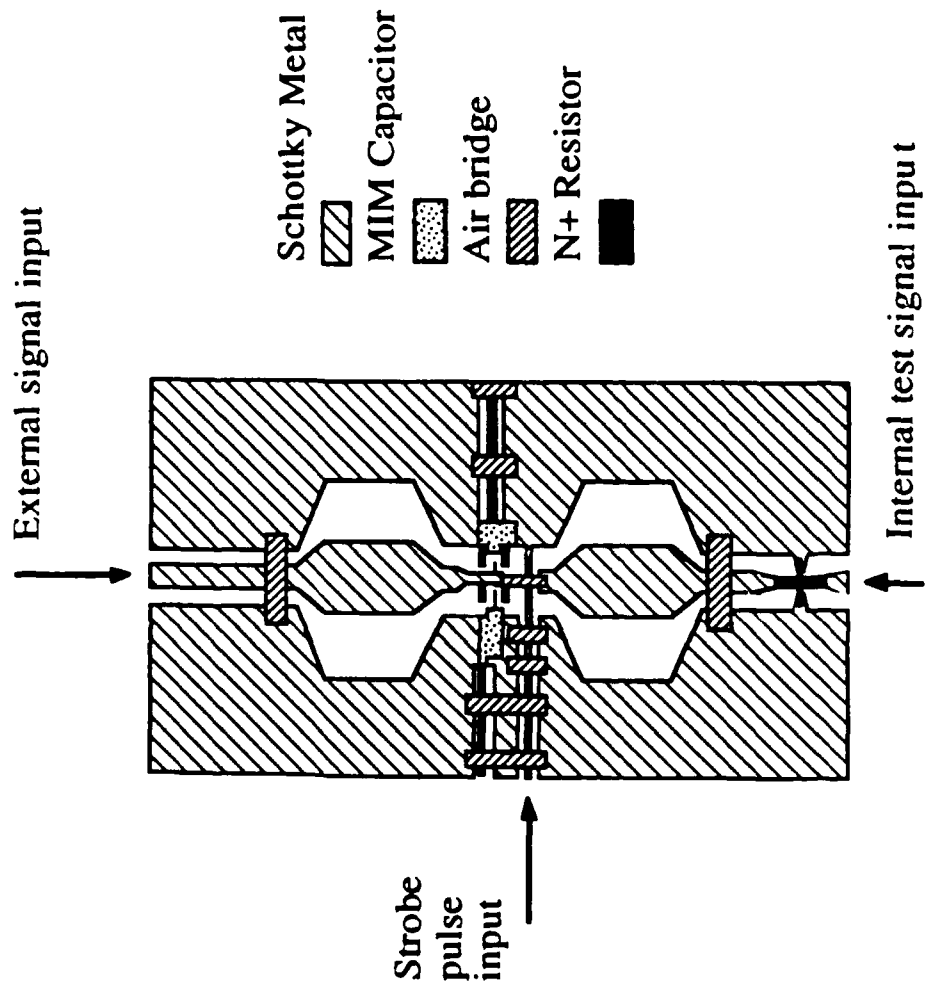
Threshold Device	Transition Time	Threshold
Josephson Junctions	2.1 ps	~ 5 mV
Schottky Diodes	0.2 ps	~ 800 mV

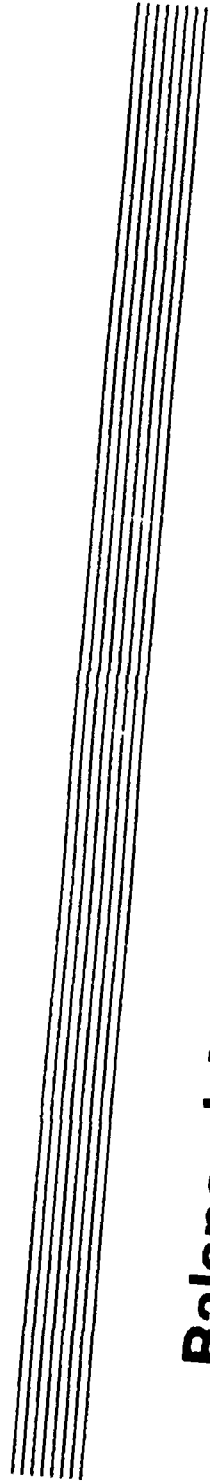
Pulsers	Transition Time	Amplitude
Josephson Junctions	2.1 ps	~ 5 mV
Step Recovery Diodes	35 ps	10 V
Nonlinear Line	3.5 ps	2 V

Two Diode Sampling Bridge

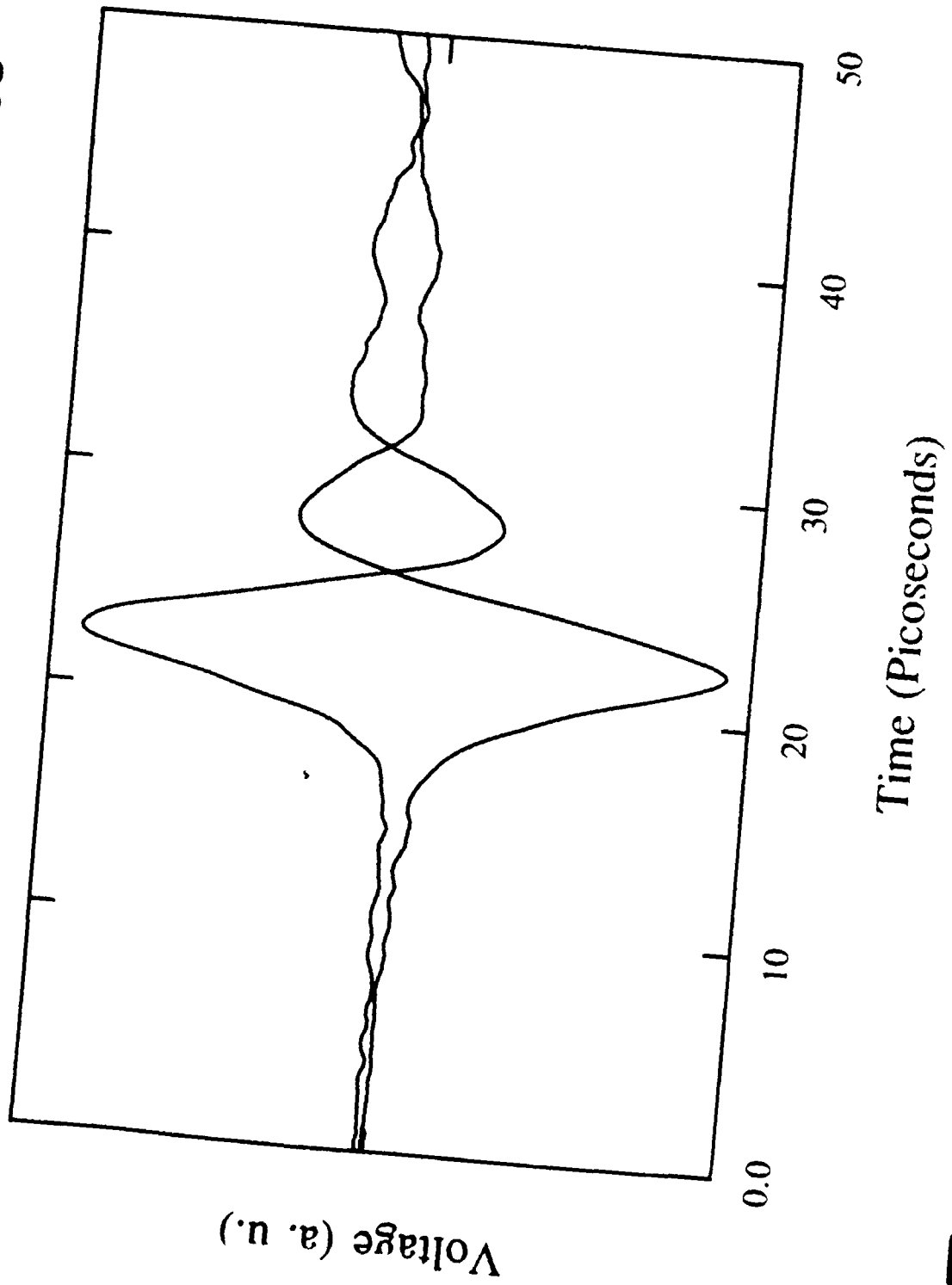


Layout of Diode Sampler



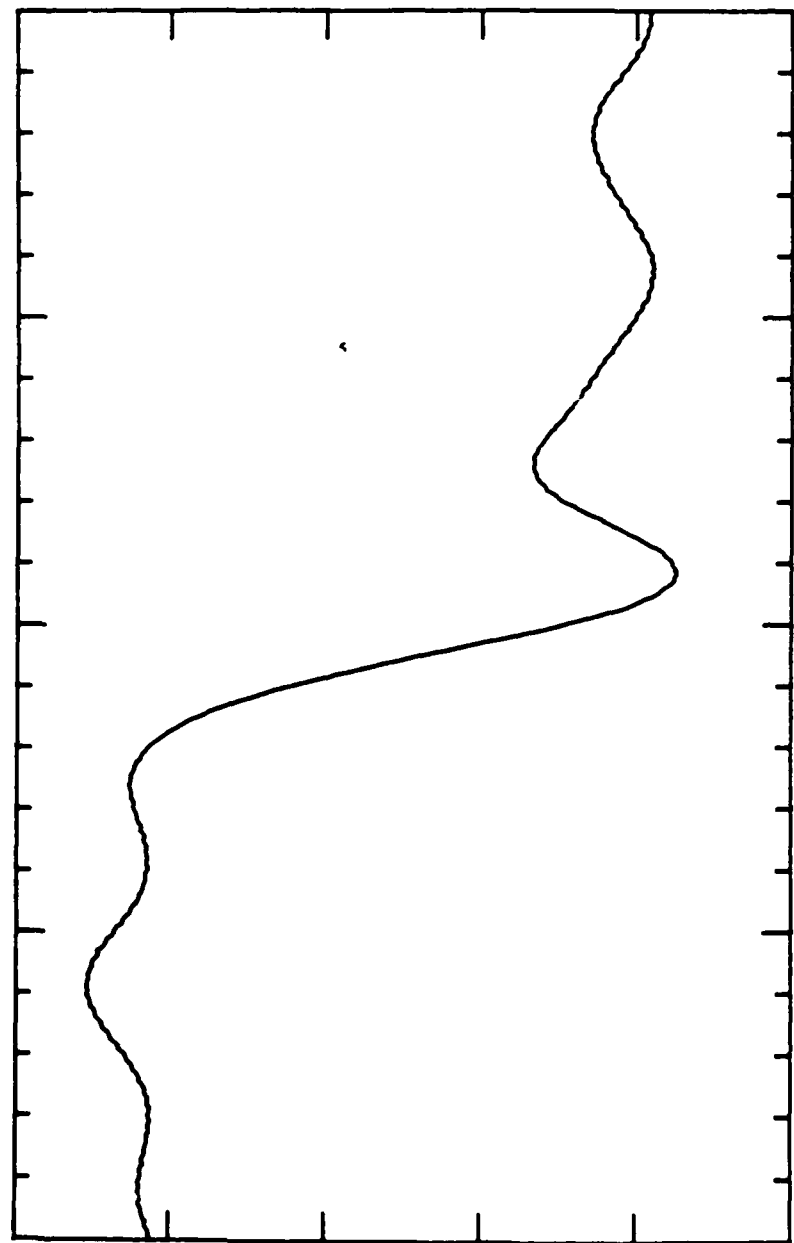


Balanced 4 ps FWHM Diode Gating Pulses





4.0 ps Falltime Measured with Diode Sampler

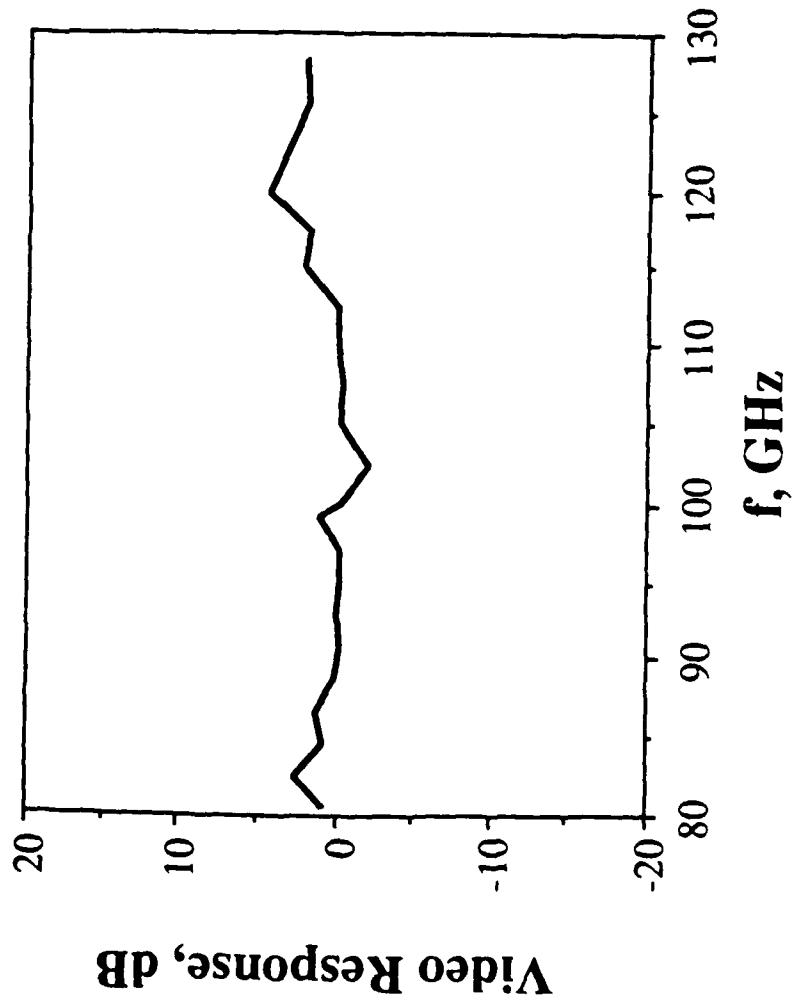


10 mV / Division

10 ps / Major Division



Frequency Response of Diode Sampling Bridge





Sampling Head Performance

RF Bandwidth	> 130 GHz	
Estimated Rise Time	2.7 ps	
Linearity to 400 mV	within 0.5%	
Sensitivity	90 nV/$\sqrt{\text{Hz}}$	
Isolation @ 5 GHz	LO to RF	68 dB
	RF to IF	55 dB
	LO to IF	63 dB